The Origin and Petrogenesis of the Ethiopian Flood Basalts

Thesis

UNRESTRICTED

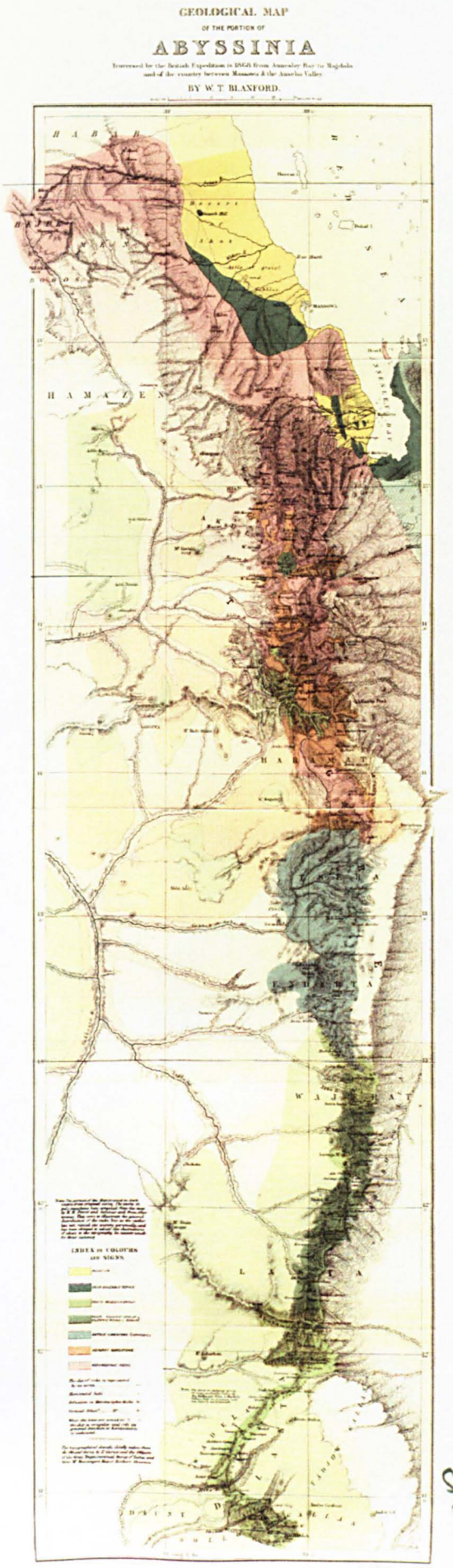

The Origin and Petrogenesis of the Ethiopian Flood Basalts

(Volume 1)

Marc Kerry Davies

B.Sc. (Hons) (College of St. Paul & St Mary, Cheltenham)

M.Sc. (Royal School of Mines, London)

D.I.C. (Imperial College, London)

P.G.C.E. (University of London)

Submitted for the
Degree of
Doctor of Philosophy
(Geochemistry)

Department of Earth and
Environmental Sciences
The Open University

Submission date: 23rd December, 2008
Date of award: 15 July 2009

CONTAINS PULLOUTS

MISSING PAGES ARE UNAVAILABLE

For my parents, my children and Jack.

ABSTRACT

The volcanic rocks of the Afro-Arabian volcanic province chart the nature and evolution of the mantle plume source responsible for a major continental flood basalt event and the manner in which it interacted with the lithosphere over the course of continental separation. The flood basalts of the Ethiopian Plateau constitute the larger part of this province and are associated with melting in the head of the Afar Plume. High-Ti picrites from the eastern part of the NW Plateau are among the earliest uncontaminated outpourings of flood volcanism; their compositions are therefore considered to be close to that of the primary melt. These are exposed in a stratigraphically coherent sequence with variably porphyritic high-Ti olivine-rich basalts and ankaramites, which together provide a continuous record of volcanism reflecting a transition from high- to low-flux magmatism. Phase-relations differ from those in other tholeiitic flood basalts in that clinopyroxene and magnetite crystallise before plagioclase. This is typical of ferropicrites and reflects a high-Fe-Ti-, and low Al-source. The olivine phenocrysts exhibit a range of morphologies and compositions which reflect fractionation and magma-mixing at varying depths prior to eruption, and the introduction of water into the magmas at shallow levels is evident from pervasive iddingsitization. The lavas have similar major element chemistry to MORB but show higher concentrations of incompatible elements inherited from a HIMU-type lithospheric component, and enrichments in LREE relative to HREE which reflect the presence of residual garnet in the source. The picrites and ankaramites have lower Al_2O_3 and higher K_2O, P_2O_5, TiO_2 and $Fe_2O_3^{(tot)}$ contents than any reported lavas with equivalent MgO content from other flood basalt provinces. These least evolved lavas were derived from oxidised (QFM+1), deep-seated magmas generated by different degrees of partial melting of the primary melt, whereas the olivine basalt magmas evolved by crystal fractionation at a shallow level from a melt similar in composition to the ankaramites. The MgO content of the primary melt calculated from the most Mg-rich olivines (Fo_{90}) is between 17 and 18 %, and it is likely that this ponded at the base of the crust where it evolved at pressures near to 1.2 GPa. Primary melt fractions of 3 - 6 % were generated in the plume at pressures of 4 - 5 GPa and temperatures in excess of 1600 °C, implying that melting occurred beneath thick (120 - 150 km) lithosphere prior to extension. Sub-chondritic initial $^{187}Os/^{188}Os$ ratios (0.125 - 0.126) indicate derivation from a depleted mantle source, and high $^{3}He/^{4}He$ (18.6 R_a) and solar-like Ne isotopic ratios imply an origin in undegassed mantle.

ACKNOWLEDGEMENTS

This thesis evolved over a long period and it has occupied an appreciable part of my life; consequently, different people contributed to its evolution at different stages and in different ways. Its inception I owe to my supervisors Ian Parkinson and Nick Rogers, and I am indebted to them for giving someone so long-in-the-tooth the opportunity to embark on such a fascinating project. First and foremost, I thank them for their encouragement and guidance, without which it would have been impossible, and for their time, humour, patience and faith. I am indebted also to Gezahegn Yirgu and Dereje Ayalew for their organisation and help in the field, which enabled me to collect some extraordinary rocks, see some truly remarkable places and taste some delightfully different food. On the analytical side I am grateful to John Watson for the XRF analyses, Andy Tindle for his introduction to world of the microprobe and capturing colours and contours reflected and refracted through the microscope, Mabs Gilmour for my apprenticeship in clean-room practices, and Mouhcine Gannoun for his encyclopaedic knowledge of osmium analysis and the Triton in negative mode. I thank also, Des Patterson for introducing the noble gas dimension and Masahiko Honda for measuring it.

I extend thanks to my early office-mates Steve Harding, Quintin Davies, Jason Harvey, Adela Fazel and Chris Pearce for sharing their stuff and enduring my digressions from work, and my animal companions. An undying debt of enchantment and hilarity is due to the Sopha People, Alex, Arun, Ed, Nik and Niall, and Ziggy, for the dimension outside – the musical collaborations, films, philosophical voyages, idiosyncratic observations on all manner of things, the hard laughter, and time well-spent together. Even less than perfect sandals are better than no sandals at all....! To Deborah also, for her companionship, understanding and fortitude, which sadly, but understandably, ran out.

Closer in time, I am thankful to Anthony Cohen, Peter van Calsteren and Louise Thomas for the opportunity to continue working in the laboratory so that I could stretch the substance of my research into something special. The continued buoyancy of the project I owe also in part to Steve Drury, for his enthusiasm for pioneering geologists and our shared critical opinions on roadside-research in Ethiopia; thanks are due too for his thorough and constructive review of Chapter 2. From inside and out, huge thanks are extended to Joachim for his sober encouragement and friendship, and additionally to Miquel for the music and expansive conversations, and his tolerance of my fanatical habits in the house; and,

to the residents of No. 10, Maria, Jen, Martin and Gaz, whose quirks, company and peculiar togetherness has been, and continues to be, a warmth to me. Sorry for the ridiculousness, and thanks for the fire and the fun!

I am grateful to have had two fantastic and unbelievably astute examiners, Sally Gibson, and Steve Blake. I can't begin to thank them enough for their thorough examination of the thesis and their detailed comments and constructive recommendations that prompted me to consolidate my thoughts on the content and wrap them up neatly in writing. Furthermore on this front, gratitude is extended to the Chair, Nigel Harris, and Paula Piggott of the Research School for their understanding and flexibility that allowed for some artistic license, which I believe greatly enhanced the thesis. I am appreciative too for the acknowledgement of the importance of that space for me from my current office-mates, Louise Thomas and Caroline Douglas, supervisor, Anthony Cohen, and laboratory associates, Pierre, Gaz, Alex and Cinzia (Queen of the Carius-tubes), who have had to put up with my shed of a head in the frenzied time before submitting the corrected thesis. Finally, a mountainous amount of appreciation is due to Janet Dryden and Jann Matela, who were there from the beginning to the end for all sorts of stuff that made it possible for me to finish the thesis.

CONTENTS

1. INTRODUCTION

1.1 Global perspective

1.1.1 Large igneous provinces

Large igneous provinces (LIP), originally defined by Coffin & Eldholm (1992), comprise massive crustal emplacements of predominantly mafic extrusive and intrusive igneous rock covering areas in excess of 0.1 million km^2 generated by processes other than those associated with normal plate tectonics. The original database used to formulate this definition included continental flood basalt provinces, volcanic passive margins, oceanic plateaus, submarine ridges, seamount groups and ocean basin flood basalts almost exclusively of Mesozoic and Cenozoic age. Substantial progress has since been made in extending the LIP record back to the Palaeozoic, Proterozoic and Archean (Ernst & Buchan, 1997, 2001, 2003; Tomlinson & Condie 2001; Arndt et al. 2001a; Isley & Abbott, 2002), and the reduced state of preservation of many of these older provinces has prompted proposed revisions to the original classification based on areal extent (Sheth, 2007). Moreover, the presence in many provinces of significant volumes of silicic extrusive and intrusive igneous rocks generated by processes other than those associated with normal plate tectonics has also led to the realisation that LIPs exhibit a greater variation in character, age and composition than first thought (Bryan et al. 2002). Such realisations have encouraged a restructuring of the classification to include a distinction between mafic and silicic LIPs (Bryan & Ernst, 2008) (Appendix 1.1.1). Nonetheless, the more recent, better preserved LIPs show a morphological record of their evolution which has important implications on their origins and timing (Fig. 1.1).

The key feature of these provinces is that they represent anomalously high magmatic fluxes, such that the majority of their volume is emplaced within a relatively short time-period of < 1 - 2 million years. They are often associated with continental break-up and are linked to active hotspots (Fig. 1.2) by linear chains of volcanic islands that can be related to persistent upwellings of anomalously hot mantle contentiously referred to as mantle plumes. These plumes represent a major component of heat-transfer within the mantle (Nataf, 2000). The initial voluminous outpourings of flood basalts are thought to be generated by melting in the hot head of a plume as it flattens on impact with the base of the lithosphere, and the younger chains of volcanic islands are thought to be generated by melting within its tail as the lithosphere moves across the remnant thermal anomaly in response to plate

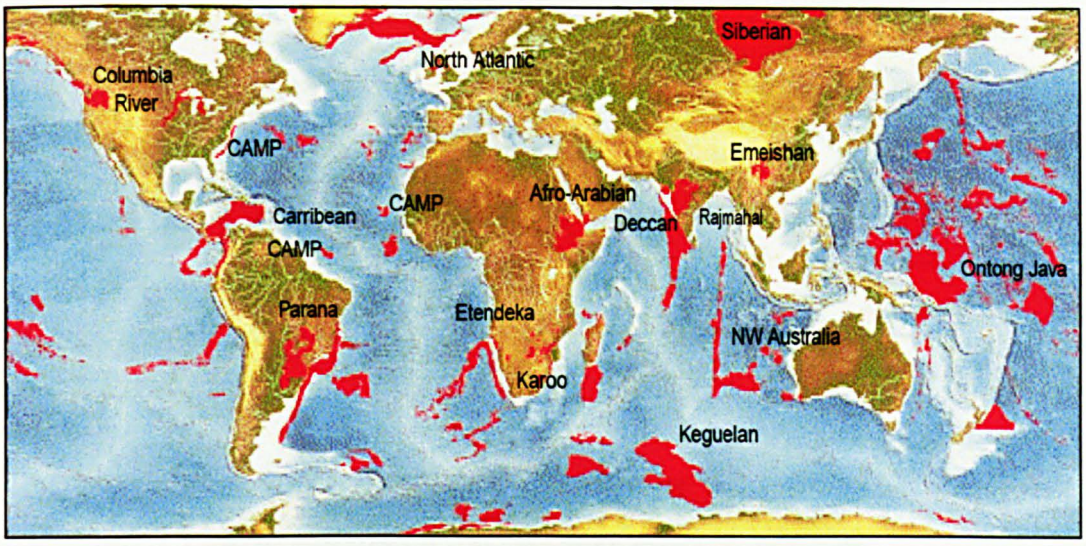

Figure 1.1 Geographical distribution of the large igneous provinces (LIPs). These include continental flood basalts and associated intrusive rocks, volcanic passive margins, oceanic plateaux, submarine ridges, ocean-basin flood basalts and sea-mount groups. The main provinces, including the remnants of the Central Atlantic Magmatic Provincve (CAMP), are labelled.

tectonics. Although the role of mantle plumes in continental break-up is still a matter for debate, it is argued that their impact on the base of the lithosphere is sufficient to initiate rifting which ultimately leads to continental separation and the formation of conjugate provinces on either side of an ocean basin (Hooper, 1990; Hill, 1991; Storey et al. 1992; Storey, 1995) as in the case of the Parana and Etendeka on opposite sides of the southern Atlantic Ocean (Fig. 1.1).

The huge volumes of material erupted during the emplacement of LIPs far exceeds any current eruptions and in this sense they are believed to mark major global events, some of which have been controversially linked to ocean anoxia and biotic extinctions (Courtillot et al. 1988, 1999; Duncan & Pyle, 1988; Wignall, 2001, 2005). It is suggested that the increase in gas and particulate emissions during such events can have a deleterious impact on the global environment, leading to substantial cooling as a result of atmospheric heat absorption. Submarine eruptions also can reduce the oxygen levels in seawater either by direct oxidation reactions with metals in hydrothermal fluids or by causing algal blooms that consume large amounts of oxygen (Kerr, 2005).

Alternative theories to the plume hypothesis have been proposed to explain intraplate volcanism and the formation of large igneous provinces (Anderson, 1994, 1995, 1998, 2000, 2002, 2003; Smith & Lewis, 1999; King & Anderson, 1995; Sheth, 1999;

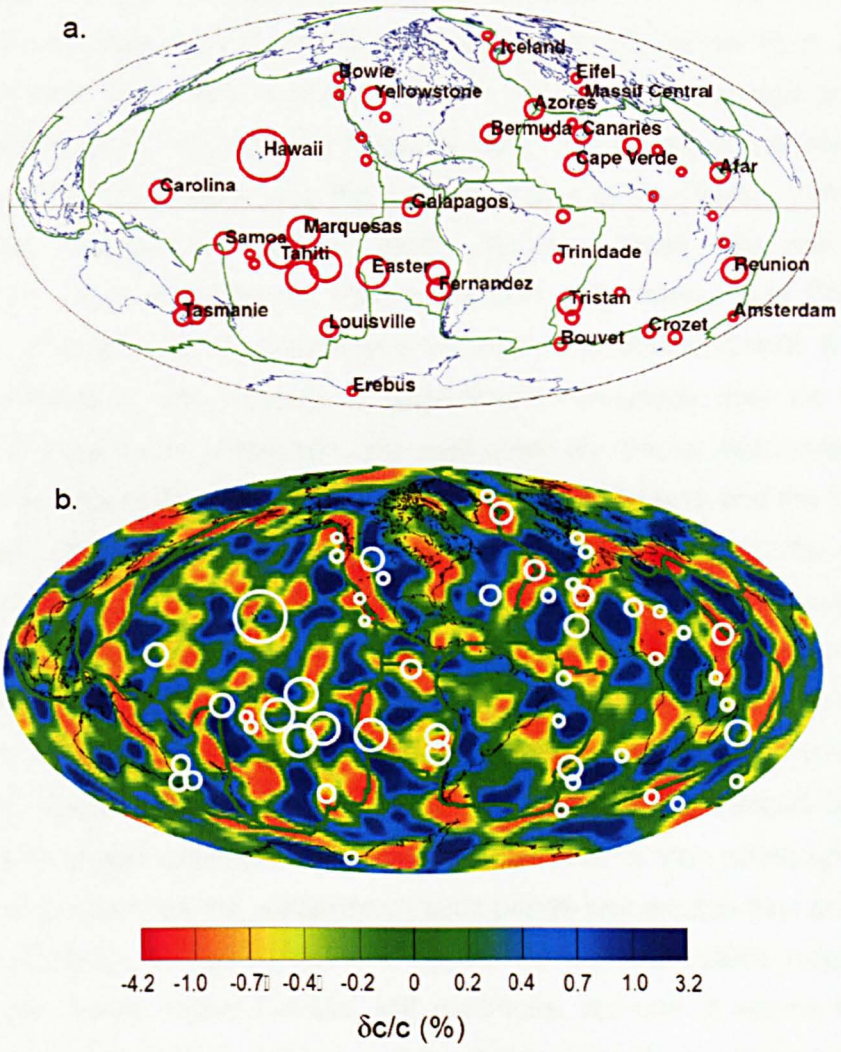

Figure 1.2 Comparison of bouyancy fluxes for named hotspots (estimated by Sleep, 1990) **(a)** with lateral heterogeneities in the upper mantle **(b)**. The red circles in are proportional to the plume bouyancy flux (Hawaii = 8.7 Mg s-1), and the heterogeneities are are synonymous with variations in the phase velocity c of 75 s-period Rayleigh waves as derived by Ekstrom et al. (1997). The waves are particularly sensitive to shear-velocity variations just below the lithosphere. The white circles in (b) match the named 'plumes' coincident with seismic slow regions in the upper mantle (Nataf, 2000).

King & Ritsema, 2000; Foulger, 2002; Foulger et al. 2005; Foulger & Jurdy, 2007), and although some of these theories may adequately explain some of the smaller scale intraplate volcanic phenomena, they cannot account for the huge volumes, high melting temperatures and rapid emplacement rates characteristic of large igneous provinces. Of course, it is unlikely that all volcanism other than that generated by normal plate tectonic processes can be attributed to mantle plumes. It is certainly apparent that structural features related to lithospheric architecture and stress can

play an important role in controlling intraplate volcanism, as for the Foundation and Juan Fernandez seamount chains in the South Pacific (O'Connor et al. 2001). It is also conceivable that many seamount chains that exhibit linear age progressions may be explained by propagating fractures as in the cases of the New England Seamounts (McHone, 2000), and the parallel chains in the Pacific, including Puka Puka Ridge (Natland & Winterer, 2005). Similarly, those with non-linear age progressions, such as Louisville, Marshall-Gilbert, Line Island, and Cook-Austral-Marquesas chains, may be interpreted as leaky transforms (Smith & Sandwell, 1997). Furthermore, the concept of edge-driven convection may be invoked to explain the voluminous volcanism and melt anomaly tracks associated with the margins of ancient cratons, such as the Columbia River Basalts and the Yellowstone hotspot trail (Christiansen et al. 2002), and possibly the Azores (King & Ritsema, 2000). Even if we accept that edge-driven convection generated by strong contrasts in lithospheric architecture is capable of producing large volumes of magma, oceanic plateaux and continental flood basalt provinces with no obvious cratonic association still remain unexplained without reference to plumes. If we go as far to accept that changes in lithospheric stress can release huge melt ponds trapped beneath the lithosphere to create large igneous provinces, we have to then come up with some evidence to substantiate the existence of such ponds and explain how such features can be maintained at sub-lithospheric depths for an appreciable length of time. Although the 'Great Plume Debate' still continues, for now it seems that mantle plumes are the most likely source and mechanism for the emplacement of large igneous provinces. There is still, however considerable uncertainty over where in the mantle these plumes originate, and this exacerbated by our uncertainty over the physical and compositional nature of the mantle itself.

1.1.2 Mantle convection

It is accepted that basaltic volcanism 'samples' the Earth's mantle, but the depth of the source for this volcanism, and the mechanisms whereby it is generated and transported to the surface remain enigmatic. This enigma is compounded by the fact that there is no definitive discriminatory index capable of characterising the source of volcanism. Fundamental differences in the geochemistry between mid-ocean-ridge basalts (MORB) and ocean-island basalts are suggestive of origins in depleted and less depleted (or enriched) mantle sources respectively. The implication of this is that convection within the mantle operates on different scales governed by thermal discontinuities, which may sub-divide the mantle according to its physical and chemical properties. This is inherent in most current models of mantle circulation

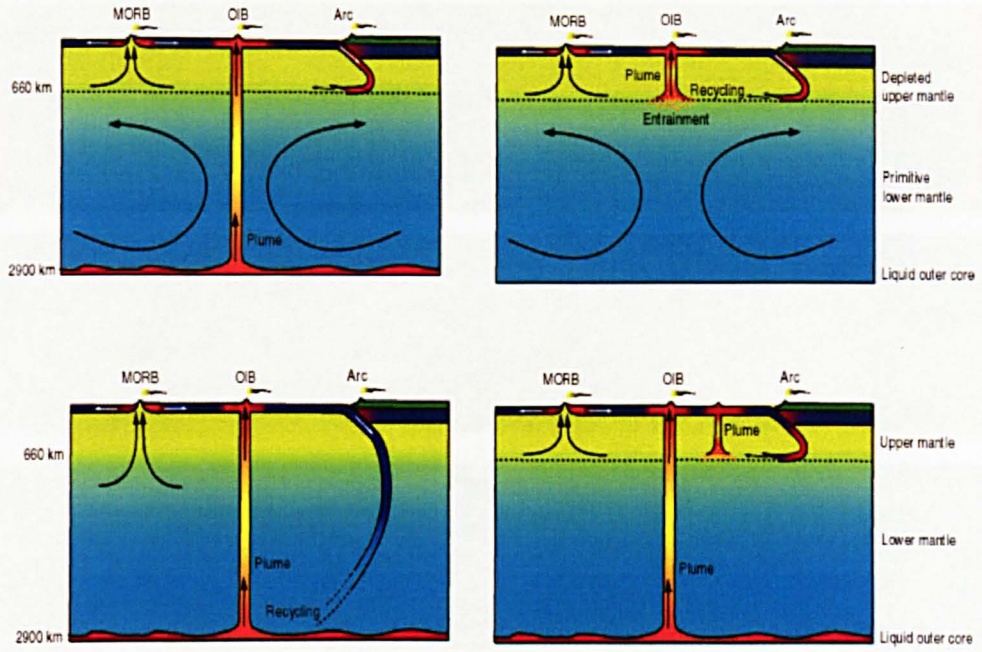

Figure 1.3 Models of mantle convection (adapted from Hofmann, 1997). **(a)** Standard two-layer convection comprising a well-mixed, trace element depleted upper layer and a less well-mixed, less depleted lower layer separated by an endothermic phase-chage boundary at 660 km. **(b)** Two -layer model with recycling of lithospheric components. Plumes rising at the base of the upper mantle may entrain material from the lower mantle. **(c)** Whole-mantle convection with plumes rising from the core-mantle boundary (CMB). **(d)** Hybrid model with most plumes sourced from the base of the upper mantle and occasional plumes sourced from the CMB.

(Fig. 1.3). On one scale, volcanism associated with normal plate tectonic processes is generated within the upper mantle, and on another scale volcanism associated with distinguishable upwellings of hot mantle, or 'mantle plumes', is sourced at greater depth. MORB is thought to be generated by decompression melting in response to crustal thinning associated with the separation of lithospheric plates at mid-ocean ridges, and island arc basalts are thought to be a product of melting in response to the addition of volatiles during subduction. The volcanism associated with mantle plumes, on the other hand, seems unrelated to current tectonism, and can occur in continental as well as oceanic settings.

1.1.3 Mantle Plumes

The location and dimensions of plumes that impinge on the base of the lithosphere may be inferred by simple observations of uplifted topography, which can be linked to thermal anomalies (White et al. 1995). Similarly, it is possible to estimate the extent of surface doming caused by thermal upwellings using combined gravity and topographic measurements (Crough, 1983). On a more detailed level, experimental

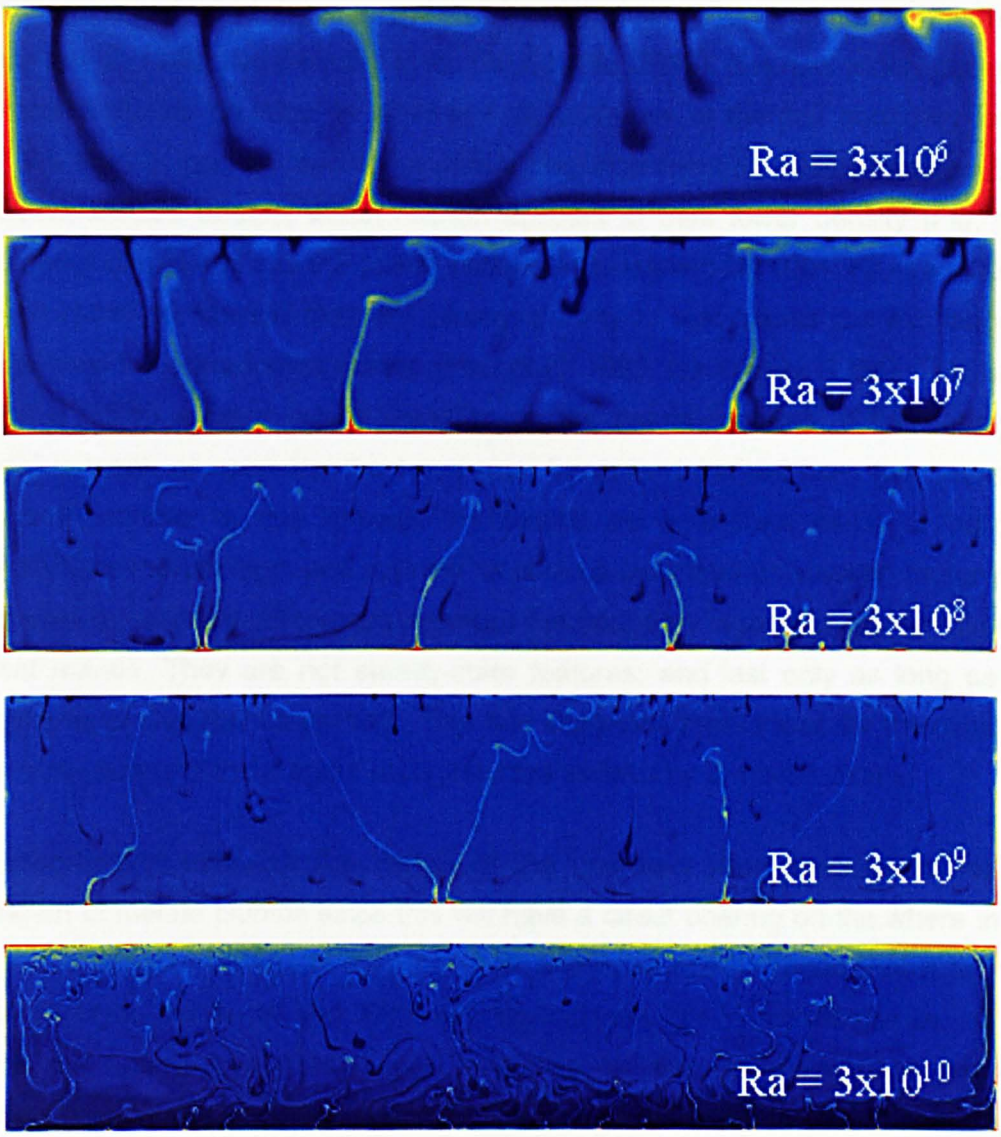

Figure 1.4 Two-dimensional axisymmetric modelling of thermal convection for varying Rayleigh number situations. At low Rayleigh numbers the pattern of convection is distinctly cellular and plumes tend to develop as large, widely-spaced spouts which mushroom-out on reaching the upper boundary. At high Rayleigh numbers, the pattern of convection tends to be more turbulent, and plumes are smaller, more closely spaced, and mushroom before reaching the upper boundary. Ra = (a x g x d^3 x T) / (k x V) where a = thermal expansivity, g = gravitational acceleration of Earth (10 m/s^2), d = depth of the mantle-layer, T = temperature difference across the mantle-layer, k = thermal diffusivity, and V = kinematic viscosity (Murphy et al 2000).

work with convective planforms using high viscosity fluids (reviewed by White & McKenzie, 1995), and computer generated numerical models (Zhang & Yuen, 1995; van Keken, 1997; Kiefer & Kellogg, 1998; Kellogg et al. 1999; Cserpes & Yuen, 2000; Hansen 2001; Murphy et al. 2000), attempt to describe the morphology and development of mantle plumes. Furthermore, seismic tomography has revealed plume-like structures in the mantle which have been interpreted as thermal

upwellings equivalent to those suggested by experimental and numerical modelling (Ritsema et al. 1999; van der Hilst et al. 1997; Nataf, 2000). It is now widely accepted that mantle plumes develop as wave-like disturbances at thermal boundary layers within the mantle, and on reaching a critical Rayleigh number, evolve into spouts or mushroom-shaped bodies, which rise on account of their lower density (Fig. 1.4). Entrainment of material into the plume occurs from below (Hill, 1991: Hansen, 2001), although radial conduction from the plume is likely to also cause the exchange of material from the surrounding mantle (Hart et al. 1992; Hauri et al. 1994). This is fed through a tail to a head, which enlarges as the plume matures. If the supply of material is weak or sporadic, the head may become detached from the boundary layer and continue to rise through the mantle as a discreet diapir or balloon. Generally, the morphology, and spacing of plumes, and their convection patterns, is determined by physical differences between the boundary layer and the surrounding ambient mantle. They are not steady-state features; and last only as long as the boundary layer disturbance persists. This has important implications for the evolution of the composition of the magma brought to the surface by a mantle plume.

It is important to establish the nature of the boundary layer responsible for the generation of mantle plumes since this will have a direct bearing on the where in the mantle it is likely to be found. Advocates of a layered mantle argue that a thermal boundary layer exists at the 660 km discontinuity as a consequence of the endothermic spinel-perovskite phase transition at this level. Another possible boundary layer at the 2900 km discontinuity (core-mantle-boundary) is considered to be a product of melting of the outer core by residual heat from the Earth's formation. With reference to the correlation of oceanic crust production and the timing of reversals in the Earth's magnetic field, Larson (1991) suggests that disturbances within this boundary layer may be created by protracted periods of magnetic normality. Controversially, on the other hand, Anderson (1992, 1995 and 1998) argues that thermal disturbances are produced by the insulating effect on the mantle of large and thick continental landmasses (edge effects), and that boundary layers are not a prerequisite for mantle upwelling. Irrespective of the mechanisms whereby mantle plumes are generated, or whether or not they exist, it is probable that the hot mantle upwellings responsible for the eruption of large igneous provinces are sourced within the deep mantle.

1.2 Source information

1.2.1 Ambiguity of depth

Information used to characterise the source regions for mantle plumes comes from five principal sources (listed below). This information will be explored in relation to the Ethiopian flood basalts throughout this thesis and will be covered in detail in the context of each chapter. A brief description of such sources is nevertheless outlined below to introduce the reader to the concepts and methodology used in this investigation. The way in which much of this information is interpreted is often conjectural. Despite this, generalisations may be made about the origins and evolution of magmatic rocks, particularly when complimentary information is available from several sources.

1.2.2 High pressure mineralogy experiments

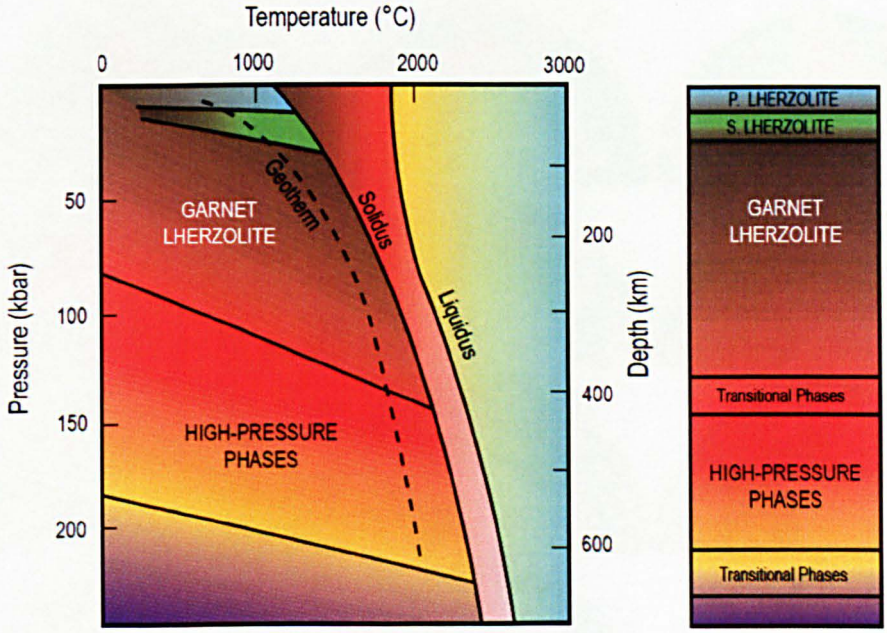

Figure 1.5 Subsolidus phase relations for anhydrous mantle lherzolite. The region of partial melting is represented by the space between the solidus and liquidus. P = plagioclase, S = spinel. The plotted geotherm is from Wyllie 1981.

The idea of a layered mantle and therefore the existence of related thermal boundary layers can to an extent be explained with reference to mineral phase changes inferred by comparisons between seismic data and synthetic experiments carried out on mantle rocks and minerals (Takahashi & Ito, 1987; Ito & Takahashi, 1987). Numerous model geotherms with the depth and nature of phase transitions have been proposed using such comparative studies (Fig. 1.5). More recent high pressure

and high temperature experiments on mantle materials (Fei, 2001; Ulmer et al. 2001; Pawley et al. 2001; Kohn et al. 2001), and quantum mechanical computer calculations, based on density functional theory (Ackland, 2001; Oganov et al. 2001), have placed more rigorous constraints on the stability of mantle minerals and the consequent phase boundaries within the mantle. These boundaries have been targeted by the 'model-makers' as potential source regions for mantle plumes.

1.2.3. Seismic tomography

Variations in seismic wave velocities have been used to image the mantle, and to identify structures interpreted as plumes (Nataf, 2000). Regional time travel tomography, for example, has provided clear evidence for plumes in the upper mantle beneath some hot spots (Fig. 1.6), and, although such structures are difficult to detect in the lower mantle, high resolution tomography has revealed meandering

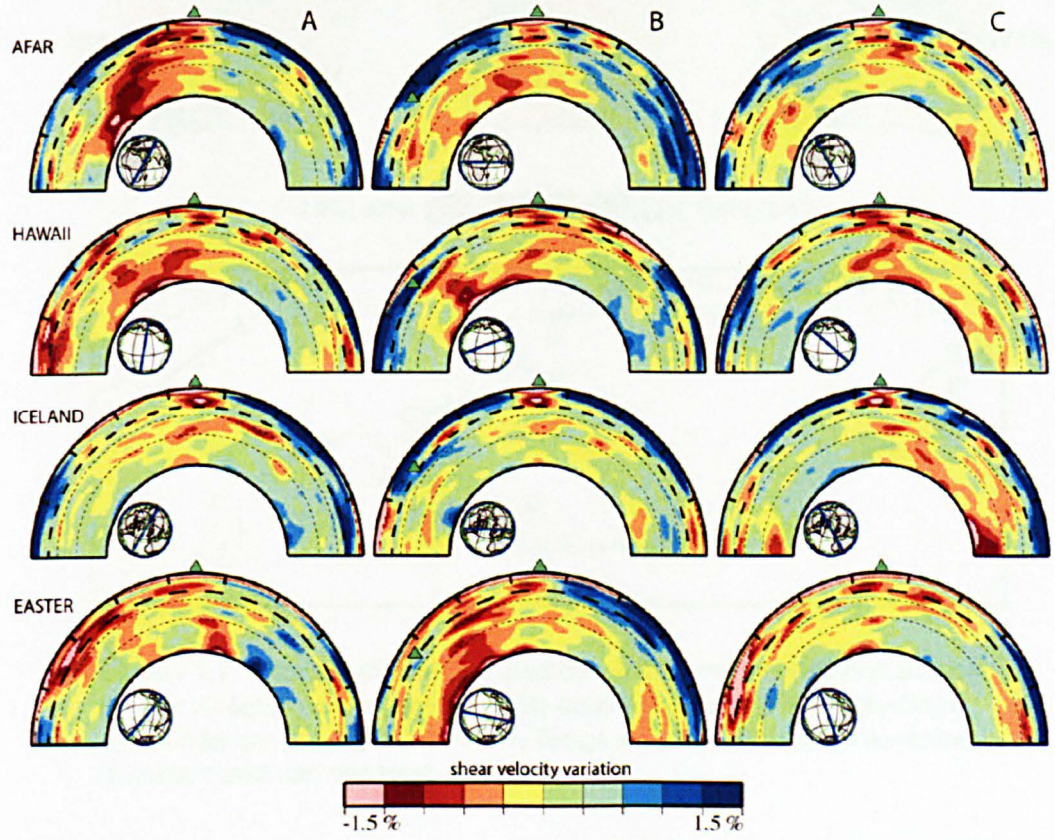

Figure 1.6 Shear velocity anomalies from model S20RTS in 180° wide cross-sections through the mantle. The triangles indicate the location of the Afar, Hawaii, Iceland, and Easter hotspots. The colour scale shows shear velocity anomalies between 31.5% and +1.5%. Shear velocity anomalies in the uppermost mantle (e.g. cratons and mid-ocean ridges) can be as high as 7%. The thicker dashed line marks the 670-km discontinuity. The thin dashed lines mark noticeable horizons at 1000 and 1700 km depth (Ritsema & Allen, 2003).

plume-like structures that extend down to the core-mantle boundary. Furthermore, tomographic models of three-dimensional shear wave velocities (Ritsema et al. 1999, van der Hilst & Karason, 1999), together with numerical models of thermochemical convection (Kellogg et al. 1999) suggest that compositional stratification of the

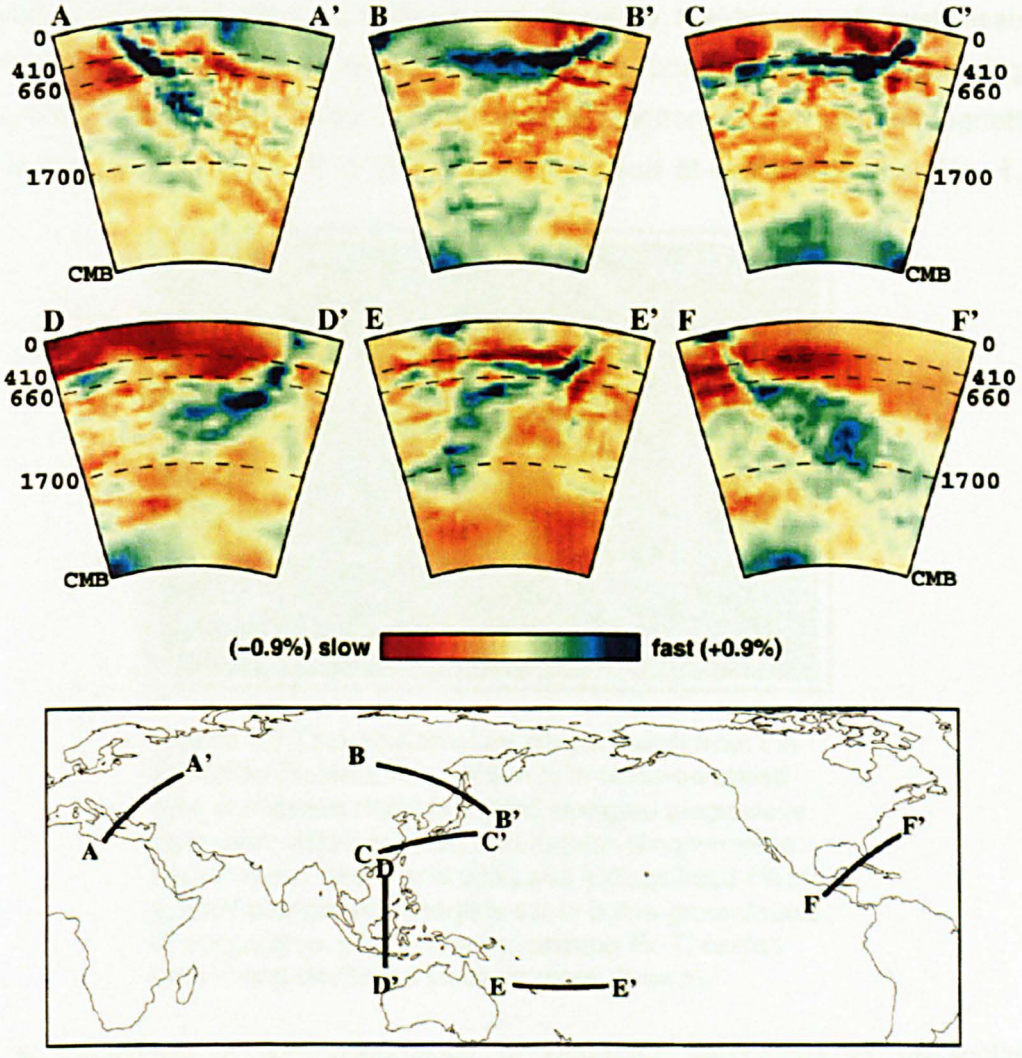

Figure 1.7 Slab structure illustrated by vertical mantle sections across: (A) the Hellenic (or Aegean) arc; (B) southern Kurile arc; (C) Izu Bonin; (D) Sunda arc (Java); (E) northern Tonga arc, and (F) central America (Karason and van der Hilst, 2000).

mantle creates source regions for plumes at distinct boundary layers giving rise to both shallow and deep sourced varieties. Seismic tomographic images showing sinking subducted slabs penetrating the 660 km discontinuity on the other hand suggest that although such compositional zoning may serve as boundary layers for the generation of plumes, they do not inhibit the transfer of material (hot or cold)

within the mantle (Fig. 1.7). Furthermore, such images are consistent with the concept of whole mantle convection.

1.2.4 Petrology of mantle derived rocks

The mineral associations and textures of plume derived lavas and intrusive rocks generally record the order, conditions and therefore the history of crystallisation (Wilson, 2000). Most flood basalts are variably porphyritic with assemblages (commonly plagioclase, rarely olivine, augite, pigeonite and titano-magnetite) indicative of low pressure (0 to 15 kbar) fractionation at shallow depths (Fig. 1.8).

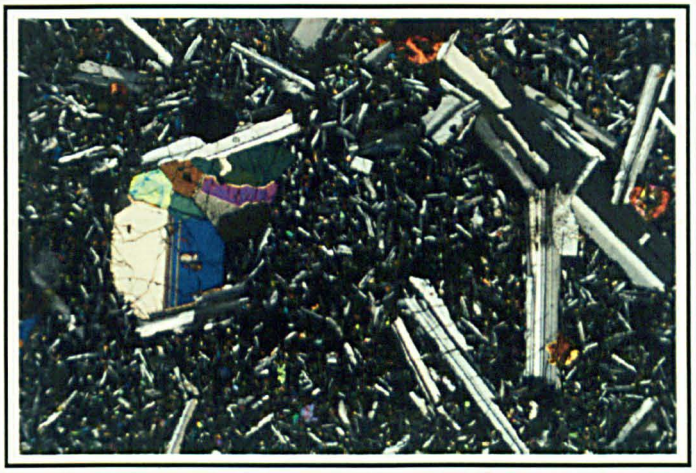

Figure 1.8 Thin section of an olivine basalt from the Ethiopian Plateau. The section is in cross-polarised light and shows multiple-twinnd elongate plagioclase (grey and white), twinned and regular clinopyroxene (blue, cream, green and pink) and iddingsitized olivine (rusted orange) phenocrysts set in a fine groundmass of plagioclase, clinopyroxene, opaque Fe-Ti oxides (black) and devitrified volcanic glass (brown).

This is supported by the occurrence of resorbed xenocrysts of plagioclase, clinopyroxene and olivine, which clearly crystallised at depth before rising to shallower levels where they were out of equilibrium with the ambient melt. The occurrence within flood basalt provinces of picritic basalts with glomerophyric forsteritic olivine (some with chromite inclusions) and orthopyroxene set in a groundmass of quenched clinopyroxene and opaques also suggests that initial crystallisation took place under high pressure at depth. Petrological evidence suggests then that the magmas responsible for the formation of flood basalt provinces are sourced deep within the mantle and evolve on reaching the base of the lithosphere. Subsequent evolution as a result of crustal contamination may further change equilibrium conditions to produce exotic mineral assemblages, the source of

which is difficult to ascertain. In order to determine the nature and composition of the melt sources it is therefore critical to examine those units of a lava sequence which are essentially uncontaminated. It is generally thought that the initial uncontaminated outpourings of flood basalts generated in the hot head of the impacting mantle plume are picritic in composition. These rocks are rare in occurrence, and in the provinces where they are found, they occur near the base of the sequence and close to the geographical centre (Campbell, 2005).

1.2.5 Geochemistry of mantle derived material

Major elements: Partial melting in a rising plume occurs as a consequence of adiabatic decompression and is thereby able to generate magmas ranging from tholeiitic to alkali basalt and nephelinite in composition depending on the depth and degree of partial melting and the mineralogy of the source (Fig. 1.9). The magmas

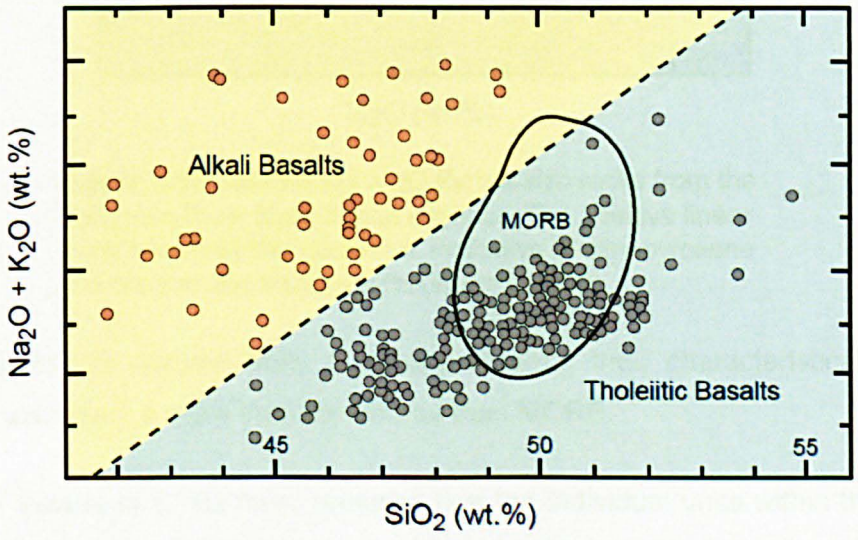

Figure 1.9 Variation in total alkalis and silica for basalts from Hawaii. The outlined field indicates the compostional space in which most mid-ocean ridge basalts (MORB) plot.

responsible for the generation of intracontinental volcanic provinces associated with crustal extension appear to evolve from alkalic to sub alkalic in composition with the production of large volumes of transitional to tholeiitic flood basalts as the rate of lithospheric extension increases. In rare cases such evolution culminates in the production of highly potassic lavas implying that the magma source becomes progressively metasomatically enriched by contamination from the sub-continental lithosphere. This variation in magma types exhibited by continental flood basalt provinces makes it difficult to use major element geochemistry as a reliable indicator of source. Generally continental flood basalts range from low-K tholeiites

(comparable to MORB) to sub-alkali basalts, although the majority are sub-alkali tholeiites with higher K_2O contents than MORB. Even though they exhibit considerable compositional variation, they often show marked trends in variation diagrams which reflect crystal fractionation, source heterogeneity and/or variable degrees of partial melting and crustal contamination (Fig. 1.10). If it is assumed that

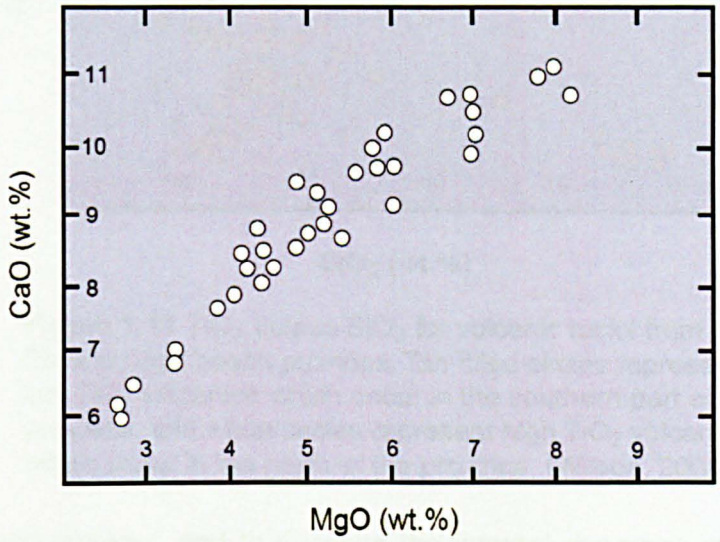

Figure 1.10 CaO versus MgO for basaltic rocks from the Columbia River flood basalt province. The positive linear trend shown by the dataset is indicative of clinopyroxene and plagioclase fractionation (Wilson, 2000).

flood basalts are derived from a primary magma, their characteristically low Mg values must reflect a more iron-rich source than MORB.

Intensive studies of CFBs have revealed that the individual units within the lava pile are not as laterally extensive as once thought. In fact many have geographically distinct areas with high and low TiO_2-basalts respectively (Fig. 1.11). In some cases these are interpreted as being derived from separate magmatic sources, whereas in others they may be explained by varying degrees of partial melting and crustal contamination. High TiO_2-basalts tend also to be Mg-rich, and are therefore likely to be more representative of a deep primary magma source. The fact that they are generally confined to the central regions of the provinces where they are found may be explained by the fact that they have tapped a least contaminated and fractionated portion of the plume-head.

There are wide-ranging opinions on the usefulness of trace elements and isotopic abundances as 'geochemical tracers' (White, 1995); nevertheless, geochemists have come to rely heavily on these in their efforts to characterise the source regions of

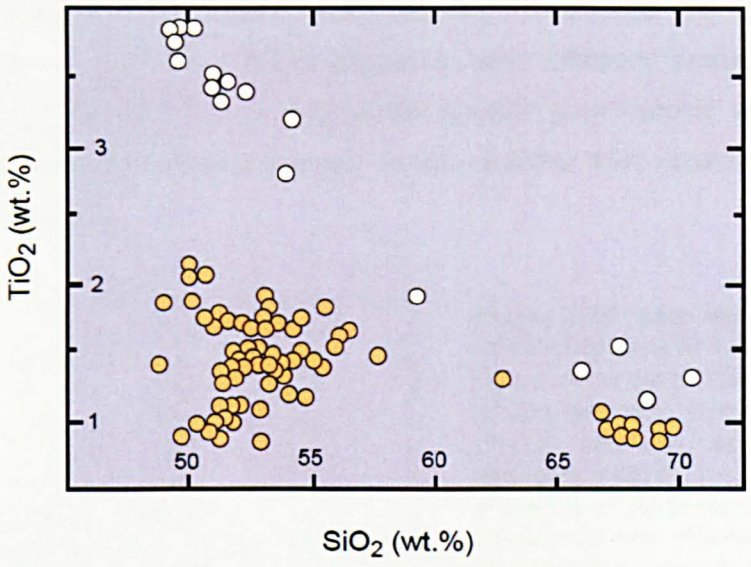

Figure 1.11 TiO_2 versus SiO_2 for volcanic rocks from the Parana flood basalt province. Tan-filled circles represent low TiO_2 volcanics which occur in the southern part of the province, and white circles represent high TiO_2 volcanics which occur in the north of the province (Wilson, 2000).

mantle-derived material, and to describe the internal dynamics of the mantle. Only those compositional features that are unaffected by magmatic processes are useful as tracers of mantle processes; these include ratios of incompatible trace elements or elements of similar incompatibility (such as Ba/Nb or Pb/Ce), radiogenic isotope ratios (such as those of He, Sr, Hf and Os), and stable isotope ratios (such as Oxygen).

Trace elements: During the evolution of magmas the partitioning of trace elements between the crystalline and liquid phases is controlled by the partition coefficients between them and the rock forming minerals and the composition of the magmatic liquid (Wilson, 2000). In most circumstances highly incompatible trace elements (those with partition coefficients of one or less) will partition entirely into the melt during crystallisation so that the ratio of two such elements in a basalt will be virtually identical to that ratio in its source (White,1995). Consequently the pattern of trace-element concentrations of a melt-derived rock can reflect its source (Fig. 1.12). When linked to mantle mineralogy and proposed phase boundaries, these patterns can also indicate the depth of source (Fig. 1.5). In addition, selected minerals have characteristic effects on the trace element pattern during crystallisation depending on their partition coefficients, thereby giving some insight into the role of these minerals in magmatic differentiation processes. In turn this may be linked to petrological observations to build up a picture of the evolution of a magma from source to

eruption. Likewise such patterns may be used to assess the degree of crustal contamination (Fig. 1.13). Spider-diagrams with different ordering of the trace elements can also be used to emphasise specific geochemical aspects of mantle derived melts thereby making it easier to characterise their source and subsequent magmatic evolution.

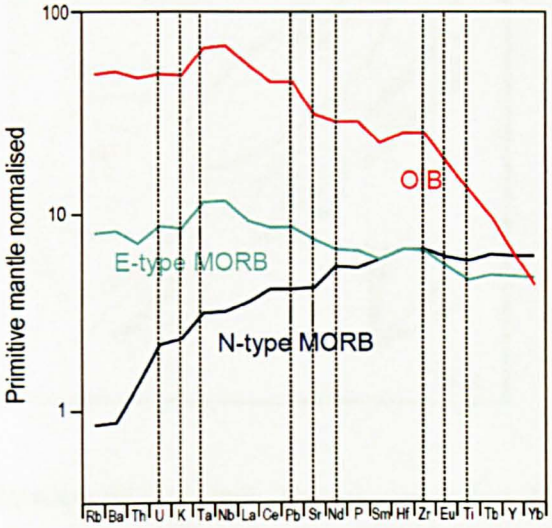

Figure 1.12 Trace element profiles or spider-diagrams for average OIB, E-type and N-type MORB. Enrichment of light rare earth elements (LREE - Nd, Ce, La) relative to heavy rare earth elements (HREE - Lu,Tb) for OIB is indicative of the presence of garnet in the source, and enrichment of very incompatible elements (VICE) imply derivation from undepleted mantle. In contrast, N-type MORB show depletion of LREE relative to HREE suggesting a garnet free source, and are depleted in VICE compared to OIB implying an origin in depleted mantle. Data is from Sun & McDonough (1989).

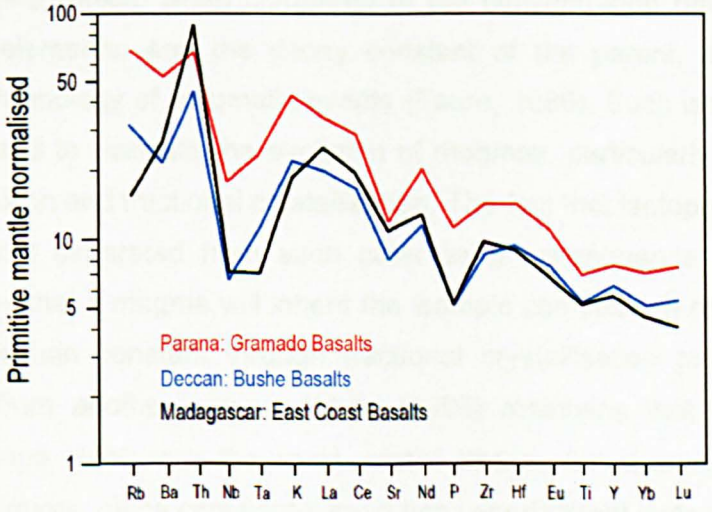

Figure 1.13 Spider-diagrams for basalts from selected flood basalt provinces. Pronounced negative anomalies for Nb and Ta is generally attributed crustal contamination although may also be explained by the retention of these elements in the source during partial melting (Saunders et al. 1992).

Continental flood basalts generally are characterised by low concentrations of compatible elements implying that they are not primary magmas but have undergone olivine fractionation en route to the surface. It is also evident from their trace element patterns that they have been contaminated as they ascend through the crust before

eruption. Above all, trace element data suggests that they are geochemically similar to OIB-tholeiites, although they show variable degrees of crustal contamination. Further information about the petrogenesis of plume-sourced melts may be obtained from trace-element data using variation diagrams (Fig. 1.14).

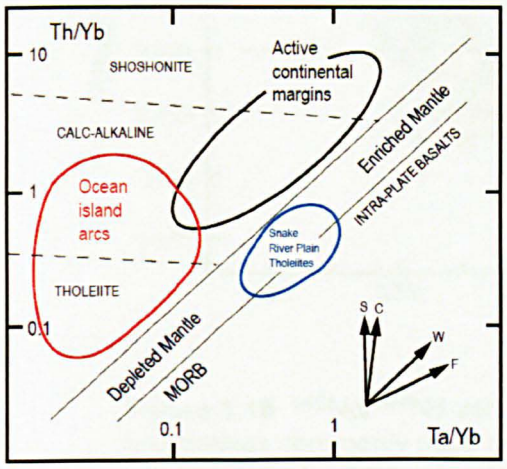

Figure 1.14 Th/Yb versus Ta/Yb showing the difference between subduction-related basalts, ocean island arcs compared to depleted mantle sources including MORB, and enriched mantle sources including OIB and CFBs. The vectors shown indicate the influence of subduction (S), crustal contamination (C), in-plate enrichment (W) and fractional crystallisation (F). Dashed lines separate the fields for shoshonitic, calc-alkaline and tholeiitic rocks (Pearce, 1983).

Radiogenic isotopes: The accumulation of radiogenic daughter elements relative to non-radiogenic isotopes of the same element caused by radio active decay results in isotopic variations, which, when compared to the concentration ratio of the parent and daughter elements, and the decay constant of the parent, can be used to establish the chronology of magmatic events (Faure, 1986). Such isotopic variations may also be used to evaluate the evolution of magmas, particularly with respect to source composition and fractional crystallisation. The fact that isotopes of the heavier elements are not separated from each other as a consequence of crystal-liquid equilibria means that a magma will inherit the isotopic composition of its source, and that this will remain constant through fractional crystallisation provided it is not contaminated from another source. White (1995) maintains that for this reason radiogenic isotope ratios are the most useful tracers for characterising magma sources. Furthermore, since continental crust has very different isotopic compositions to those of the mantle, appropriate isotopic data can provide significant constraints on crustal contamination.

The principal radiogenic isotopes used as geochemical tracers are those of strontium, neodymium, hafnium, lead and uranium (Hofmann, 1997). These are useful on their own or combined, and isotopic taxonomies derived from such data have been used to distinguish specific mantle components or species which are commonly referred to as the parental sources or end members (variably mixed or pure) for all basaltic rocks (Fig. 1.15) (Zindler & Hart, 1986). The fact that some

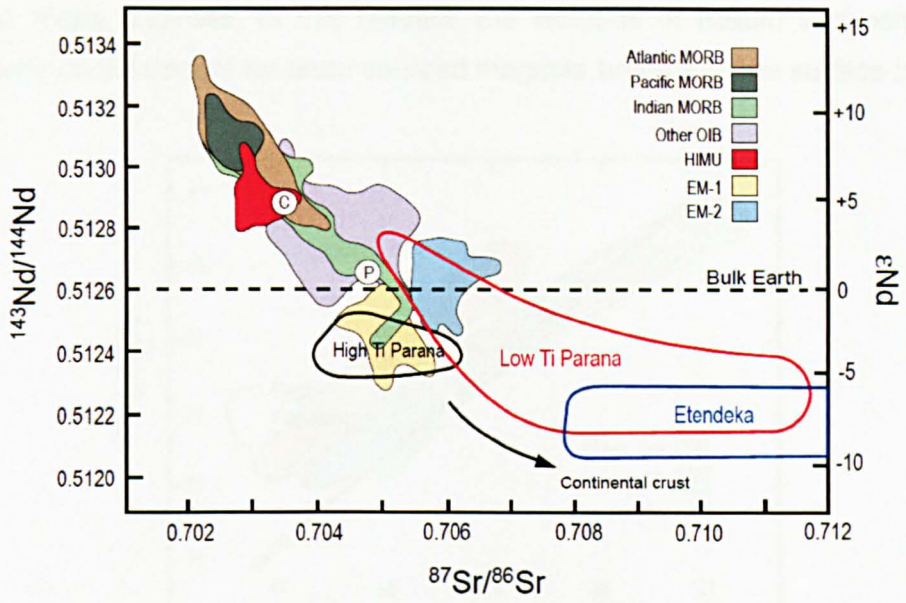

Figure 1.15 $^{143}Nd/^{144}Nd$ versus $^{87}Sr/^{86}Sr$ showing the isotopic taxonomies commonly used as potential parental sources or end -members for basaltic volcanism. P = PRIMA or primitive mantle based on the composition of meteorites, C is the composition for primitive mantle based on uncontaminated plume-derived rocks. Fields for the Parana-Etendeka province are shown to illustrate the influence of crustal contamination on the isotopic composition of the erupted lavas (Wilson, 2000).

continental flood basalts plot within the mantle array for uncontaminated oceanic basalts on a Nd-Sr diagram whereas others plot outside this field, has led to conflicting ideas on their origins. It is possible that those which plot within the MORB-OIB array represent uncontaminated magmas from isotopically heterogeneous sources, and those that plot outside show varying degrees of mantle mixing, partial melting and lithospheric contamination. Similar conclusions may be drawn from variation diagrams of selected isotopic and trace-element ratios. The strong affinity of flood basalt provinces with DUPAL-OIB shown by their lead isotope variations, on the other hand, suggests a significant link between continental and oceanic magmatism, and that the source for both evolved from remobilised continental lithosphere during continental breakup and extension (Fig. 1.16). In this model more-evolved components of flood basalts, such as the low-Ti series of the Parana province are interpreted as crustally contaminated variants of the same remobilised source.

Isotopic data of the nature described above emphasises the heterogeneity of the mantle and is only useful in constraining the compositional aspects of magma sources. When related to theoretical ideas on mantle evolution, however, such data can indicate the depth and characteristics of the boundary layers from which these

magmas might originate. In this respect, the isotopes of helium and osmium are particularly useful tracers for deep sourced magmas brought to the surface by mantle plumes.

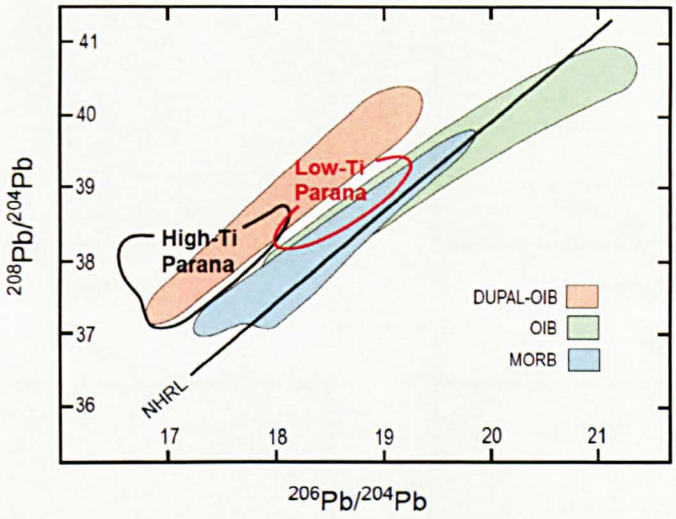

Figure 1.16 $^{208}Pb/^{204}Pb$ versus $^{206}Pb/^{204}Pb$ showing the variation in Pb isotopic compositions for the Parana flood basalts compared to DUPAL-OIB, other OIB and MORB (Wilson, 2000). The black line marked NHRL is the northern hemisphere reference line (Hart, 1984).

Noble gases: Atmospheric helium is not recycled into the mantle because it is continually lost to space, thus practically all ^{3}He generated from the mantle is primordial indicating that the Earth has not entirely degassed. The ratio (R_a) of this unradiogenic primordial helium to its radiogenic counterpart, ^{4}He (generated by the radioactive decay of ^{232}Th, ^{235}U and ^{238}U), in plume related basalts therefore provides a powerful tracer for source regions in the lower undegassed part of the mantle. R_a values for MORB generally range between 5 and 9, therefore this is taken to represent typical degassed upper mantle. Higher $^{3}He/^{4}He$ ratios (> R_a = 9) for basalts from Hawaii, Iceland, Galapagos, Easter, Juan Fernandez, Pitcairn, Samoa and Heard islands (Fig. 1.17) are consequently considered to reflect an undegassed primordial mantle source. Similarly, high R_a values identified in alkaline lavas from the Deccan and Siberian Traps (Basu et al. 1993 and Basu et al. 1995), and in picritic lavas from west Greenland (Graham et al. 1998) and the Ethiopian Highlands (Marty et al. 1996) have been interpreted as representative of a primordial lower mantle source. These observations are consistent with a layer mantle model (Hofmann, 1997). Low R_a values for the ocean islands, Tristan da Cunhna and Gough, suggest the involvement of recycled source components (Kurz et al. 1982).

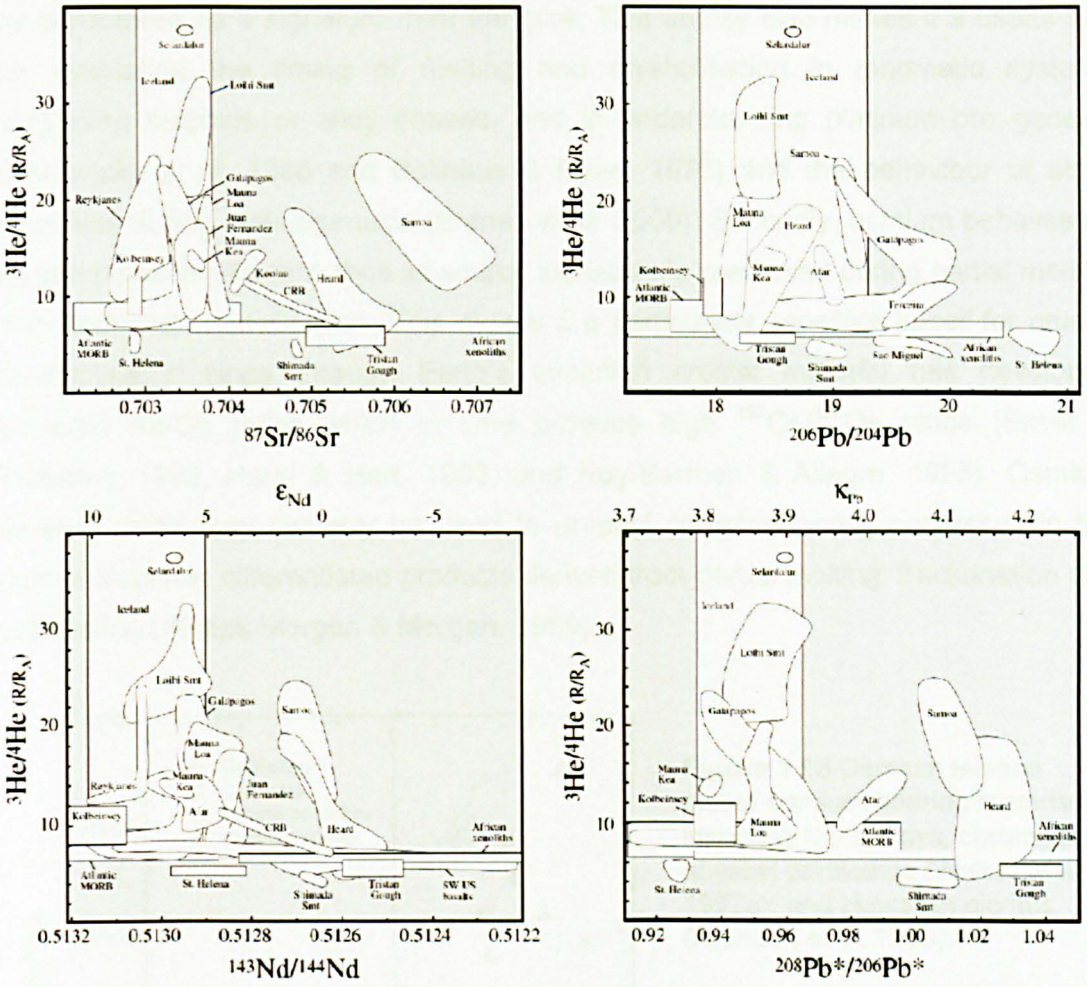

Figure 1.17 He - Sr, Nd, Pb isotopic relations for selected ocean island basalts (Graham et al. 2002).

With recent advances in isotopic analysis, some of the heavier noble gases including neon, argon, and xenon have been used alongside helium as geochemical tracers of primordial mantle. Our current understanding of the geochemistry of these gases is still in its infancy and some of their recent applications to the field are discussed in Chapter 6.

Osmium: Recent developments in analytical techniques have also made the determination of osmium in basalts feasible (Creaser et al. 1991). Osmium is a platinum group element (PGE) and its unique geochemical characteristics make it a potential tool in our understanding of the source and effects of melt migration of deep plume derived magmas. Firstly, both parent and daughter elements are siderophile and chalcophile and therefore both partitioned into the metallic or sulphide phases which became concentrated in the core during the formation of the Earth (Shirey & Walker, 1998). For this reason, osmium enrichment in plume-sourced magmas may

be considered as a signature from the core. This affinity also makes it a useful tool for evaluating the timing of melting and crystallisation in magmatic systems containing sulphide or alloy phases, and in understanding platinum ore genesis (Makovicky et al. 1986 and Ballhaus & Ryan, 1995) and the behaviour of other sulphides during metalogenesis (Brenan et al. 2000). Secondly, osmium behaves as an incompatible element, thus its source signature is preserved during partial melting and fractional crystallisation. This makes it a particularly sensitive tracer for crustal contamination since through Earth's evolution crustal material has developed elevated Re/Os ratios which in time produce high $^{187}Os/^{188}Os$ ratios (Esser & Turekian, 1993, Hauri & Hart, 1993, and Roy-Barman & Allegre, 1995). Osmium isotopic ratios may similarly be used to unravel complex mixing processes in the mantle involving differentiated products derived from partial melting, fractionation and subduction (Phipps-Morgan & Morgan, 1999).

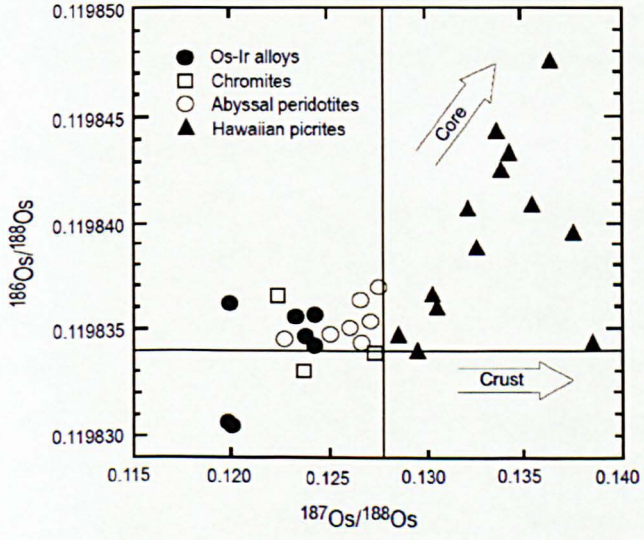

Figure 1.18 Osmium isotope plot of osmium-bearing materials including Os-Ir alloys, chromitites, abyssal peridotites (Walker et al. 1997a), and Hawaiian picrites (Brandon et al. 1998).

Since crustal contamination and mixing within the mantle are likely to mask the osmium signature of a plume's origin, it is critical to focus on plume derived material that is essentially uncontaminated in order to gain a true indicator of source. The anomalously hot material in the head of high-flux plumes represented by the picritic lavas from continental flood basalt provinces are the most likely to yield such a signature. It has already been revealed that picritic lavas from Hawaii show elevated $^{186}Os/^{188}Os$ and $^{187}Os/^{188}Os$ ratios indicating enrichment of ^{186}Os and ^{187}Os respectively (Fig. 1.18). This correlation of excess ^{186}Os and ^{187}Os has been interpreted by Brandon et al. 1998) as evidence of low and variable degrees of outer-core entrainment. Brandon et al. (2000) also have found similar excesses in abyssal peridotites which define a linear trend indicative of entrainment from the core. No

such excesses are evident in picritic lavas from West Greenland despite the fact that they contain high concentrations of Os and have high $^{3}He/^{4}He$ ratios (Schaefer et al. 2000a). This is attributed to high degrees of partial melting of mantle with no residual sulphide. The search for core contributions to mantle plumes thus continues.

Stable isotopes: Stable isotopes are generated by mass fractionation in chemical reactions and the effect of this process on their variation is small, (except for the lighter elements O, H, C and S) compared to that of their isotopic variation between the crust and the mantle. For this reason they are not useful in characterizing the source of deep mantle plumes, but they can be used to assess the importance of crustal contamination in volcanic rocks. The fact that the upper continental crust is enriched in ^{18}O relative to the mantle makes oxygen a useful indicator of crustal contamination, particularly when combined with ratios of incompatible elements such as Nd and Sr. Mahoney et al. (1985) suggest that $\delta^{18}O$ values of 8.3 ‰ for basalts from the Deccan coupled with strong correlations with their Nd and Sr ratios is strong evidence of upper crustal contamination in this province.

1.2.6 Numerical modelling

As well as describing the morphology of mantle plumes and patterns of convection, some of the numerical models referred to earlier also attempt to constrain the depth within the mantle from which they arise. This is done by relating the physical properties of plumes to temperature, pressure and phase transitions within the mantle (White & McKenzie, 1995). These relations apply equally to rising plumes and cold 'sinks' or mantle flushes (Yuen et al.1995). For example, as a consequence of these relations, viscosity increases and the thermal expansion coefficient decreases with depth in the mantle such that the buoyancy of rising plumes decreases, and the thickness of boundary layers increases with depth. Hansen et al. (1993) show that these effects create flow patterns dominated by a few large rising plumes which originate on the lower boundary and many small sinking plumes which 'fall' away from the upper boundary. This is confirmed by Murphy et al. (2000) as illustrated in Figure 1.4. With this basic premise in mind it is logical to assume that deep-sourced plumes emanate from thick boundary layers, and evolve as large, widely spaced bodies which make their way rapidly to the surface, whereas shallow sourced plumes emanate from relatively thin boundary layers as small, more closely spaced bodies which rise more slowly to the surface. This idea is supported by White & McKenzie (1995), who maintain that the size of plumes and their trailing channels are similar to the thickness of the thermal boundary from which they originate. Cserpes and Yuen,

(2000) have related these ideas to tomographic images created from seismic data to produce a schematic model of mantle convection which identifies the existence of different types of plume (Fig. 1.19). Both deep and shallow level plumes are

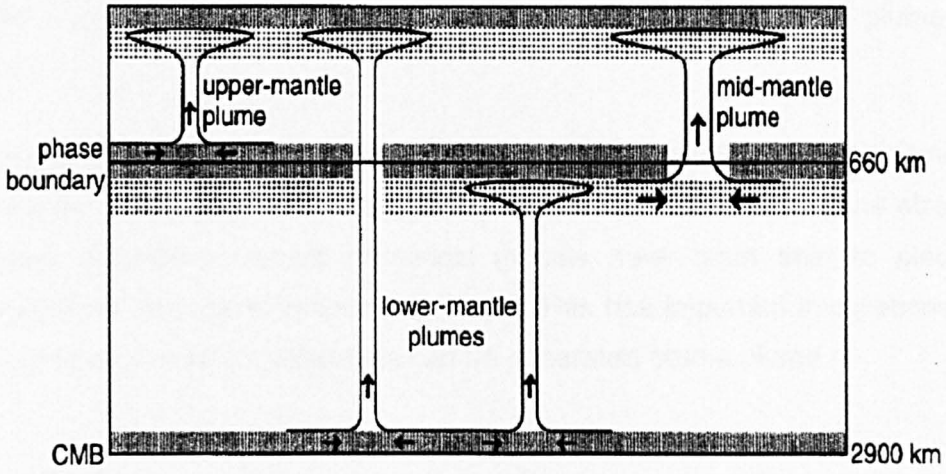

Figure 1.19 Two-layer mantle with a partially penetrable boundary at 660 km and a second asthenosphere beneath. Four kinds of plume can coexist in this model (Cserepes & Yuen, 2000).

generated from boundary layers at 660 km and 2900 km respectively. It is suggested that the 660 km discontinuity is a partially penetrable boundary, and, mid-mantle plume, with no root in the deep lower mantle can develop in a low viscosity zone or second asthenosphere just beneath this boundary. Cserpes and Yuen (2000) conclude that, because of the extreme physical differences between the compressed upwelling and the surrounding mantle, these mid-mantle plumes develop with an eruptive vigour much faster than boundary layer plumes, and can produce huge plume heads exceeding 1000 km in radius. Such plumes may account for the extensive episodic flood basalts associated with continental breakup, and the isotopically diverse signatures of hot spot volcanism. This model does not invoke the involvement of a core contribution in such cases since material from lower mantle plumes which fail to penetrate the 660 km boundary layer may be entrained into these mid-mantle plumes.

A similar model is presented by van Keken et al (2001) to explain the terrestrial heat-helium imbalance in terms of heat loss and degassing. It is postulated that both downwellings as well as upwellings are able to penetrate the 660 km discontinuity. This implies that in addition to material from the boundary layer plumes are likely to entrain differentiated portions of subducted and recycled mantle material as they

migrate toward the surface. The idea of a heterogeneous mantle has encouraged the use of descriptive terms such as marble cake, streaky or plum pudding mantle (Allegre & Turcotte, 1986; Phipps-Morgan & Morgan, 1998; Langmuir & Forsyth, 2007). This heterogeneity of the mantle may explain some of the variability in the isotopic composition and major and trace element geochemistry of plume related basalts.

With increased computer power, numerical models of mantle convection and plume development have become more complex. In addition to predicting the size, shape and form of plumes, recent numerical models have been able to place time-constraints on their development (Fig. 1.20). This has important implications for the length of time over which volcanism can be generated from a plume.

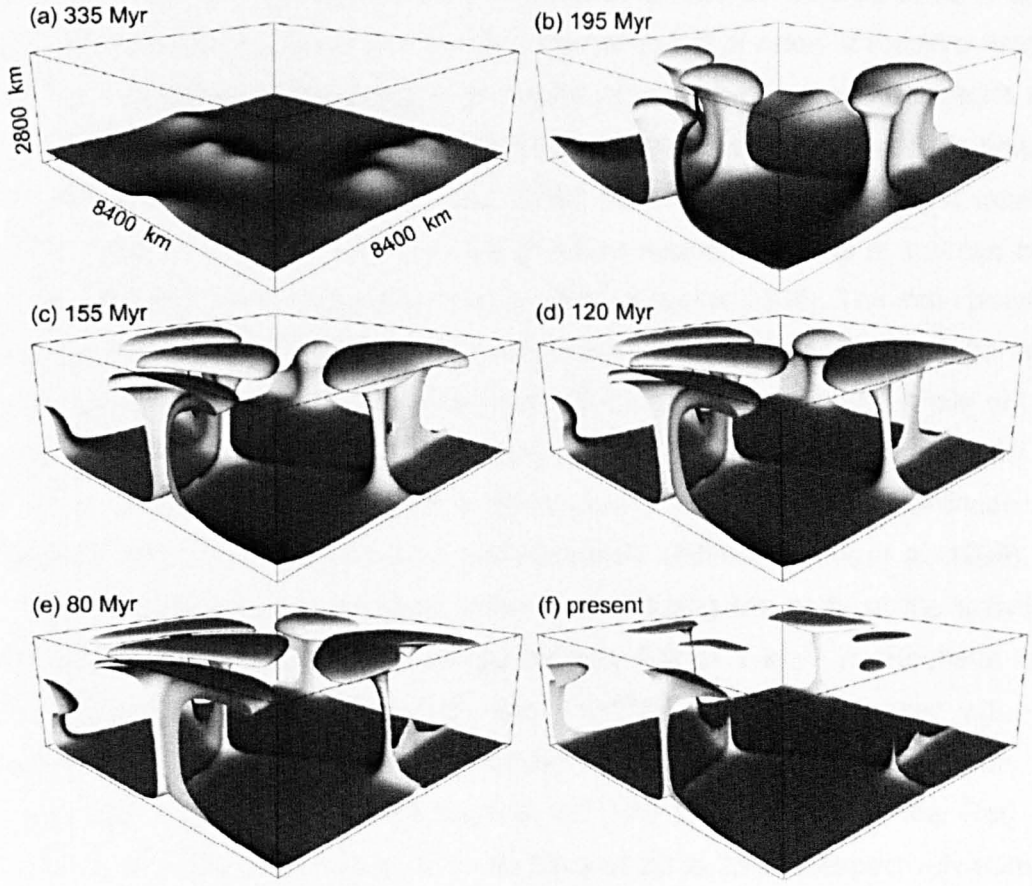

Figure 1.20 Mantle plumes in the forward modelling at successive diffusion times from (a) 335 Myr ago to (f) the present. The plumes are represented by isothermal surfaces at 3000 K (Ismail-Zadeh et al. 2006)

1.3 The thesis

1.3.1 Focus

This thesis focuses on the origin and petrogenesis of flood basalts (dominantly with Ti-rich, picritic compositions) from the Eastern Ethiopian Plateau in an attempt to address some of the issues discussed above relating to the nature and origin of mantle plumes, but also to provide an insight into the mechanics of flood basalt emplacement with the view of resolving the role of mantle plumes in the process of continental break-up. The Ethiopian Plateau forms the larger part of the Afro-Arabian continental flood basalt province, which, today, extends into Eritrea, Djibouti, Yemen and Somalia. The volcanic activity that formed the province is generally attributed to melting within the flattening head of the Afar Plume upon its impingement at the base of the lithosphere during the Oligocene (Pik et al. 1998; 1999). The tectonism and continuing volcanism associated with this initial event are considered to be in some way instrumental in the opening of the Red Sea and Gulf of Aden at the Afro Arabian triple junction. Tomographic images of mantle shear-wave velocities beneath Afar seem to confirm the existence of a low-velocity mantle anomaly that extends down to the core mantle boundary (Ritsema et al. 1999; Ritsema & Allen, 2003) and elevated $^{3}He/^{4}He$ ratios for high-Ti lavas from the province support that this is sourced in an undegassed part of the mantle (Marty et al. 1996; Pik et al 2006). The main phase of volcanism which formed the traps occurred between 30 Ma and 28 Ma (Baker et al. 1996a; Hofmann et al. 1997; Rochette et al. 1998). During this period, a pile of flood basalts with an estimated thickness of up to 2000 m, covering an area of 600 000 km^2 (Mohr & Zanettin, 1988) was erupted onto a basement of Pan-African arc-associated volcanics and intrusives, and Mesozoic sediments (Pik et al. 1999). 10^6 km^3 of this volume were emplaced within 1 myr during the peak of the activity at about 30 Ma; this indicates an average magma flux of 1 km^3/ yr (Rochette et al. 1998). Combined fission track data and $^{40}Ar/^{39}Ar$ age-data, together with field observations, suggest that uplift preceded volcanism and that extension was synchronous with volcanism (Menzies et al. 1997). Extension in the Red Sea occurred in two distinct pulses at 30 to 35 Ma and 20 to 25 Ma respectively (Omar & Streckler, 1995) and oceanic crust appeared around 10 to 13 Ma (Le Pichon & Gaulier, 1988), or more recently at 5 Ma (Izzeldin, 1987). Post-flood basaltic activity was marked by a transition from tholeiitc to alkaline volcanism (Arndt et al. 2001b; Kieffer et al. 2001, 2004) with the development of shield volcanoes on top of the flood basalts pile, and the eastward migration of central vent volcanism associated with trans-tensional structures perpendicular to the Main Ethiopian Rift (Abebe, 1998;

Korme et al. 1997). Volcanism continues today along the axial rift of the Red Sea and Gulf of Aden and in the Afar region where it remains controlled by trans-tensional east-west trending structures that intersect the main rift (Korme et al. 1997; Boccaletti et al. 1998; Acton, 2000).

On the basis of its size and mode of melt generation, the Afro-Arabian province is clearly defined as a large igneous province, and on the basis of its age, it represents the youngest example on the planet that can be directly related to continental break-up. The region encompasses a complete record of volcanism from the initial high-flux near-continuous flood volcanism during the Oligocene through the development of more sporadic low-flux shield volcanism during the Miocene and into the Pliocene with the onset of continental rifting and sea-floor spreading. In this sense the Afro-Arabian continental flood basalt province provides a unique natural museum of artefacts pertaining to the nature and evolution of the mantle source responsible for a major flood basalt event and the manner in which this source interacted with the lithosphere over the course of continental separation and the formation of a new ocean basin. It is hoped that by focusing the study on a stratigraphically coherent sequence of picritic lavas taken to represent some of the earliest uncontaminated outpourings generated by the plume, a clearer picture of its nature, composition and possible source-region will be obtained.

1.3.2 Outline

In Chapter 2 a description of the province gives context to the rocks reported in the thesis. A comprehensive account of the characteristics and stratigraphy of the rocks that make up the Afro-Arabian province is given together with current views on their petrogenesis. The sampled sections are documented in Chapter 3. The lava-types, their field relations and architecture are therein described and interpreted in the context of emplacement, and the implications of this are discussed with respect to evolution of the province. The subsequent chapters focus on two of the sample sections that can be related together, and the petrography, major and trace element geochemistry, and isotopic compositions of the laves from these sections are described and discussed in Chapter 4, 5 and 6 respectively. Reasons for concentrating on only two of the six sections sampled are explained at the beginning of Chapter 4. A summary of the findings of the research and a model for the origin and petrogenesis of the lavas are presented in Chapter 7. For the purposes of clarity, lengthy descriptions of analytical methods and data processing are not covered in the text; instead they are compiled in a fully comprehensive and referenced appendix in

Volume 2. All data-tables shown in the appendix, as well as all raw data and functional copies of the spreadsheets used throughout the thesis are contained in an electronic supplement on the accompanying compact disc attached to the inside back cover of Volume 2; these are referred to where appropriate in the text or in the appendices.

2. THE AFRO-ARABIAN VOLCANIC PROVINCE

2.1 Nature and extent of the province

2.1.1 Introduction

The volcanic and intrusive rocks of the Afro-Arabian Volcanic Province are believed to be related to asthenospheric upwelling during break-up of the Afro-Arabian plate and the subsequent separation of the component Nubian, Arabian and Somalian plates (Fig. 2.1). The full geographical extent of the province and the source of its magmatism remain debatable, but it is generally accepted that the focus of continuing associated activity today is centred on the Afar Depression. The initial pre-rift outpourings formed an extensive continental-flood-basalt province, which today is largely represented by the Ethiopian and Yemeni Traps. Volumetrically, these lavas constitute the larger part of the Afro-Arabian Volcanic Province, and it is thought that they were emplaced contemporaneously with uplift caused by the impingement of the Afar mantle plume on the base of the lithosphere around 30 Ma (early Oligocene), or possibly as early as 45 to 50 Ma (late Eocene). These initial outpourings, dominated by tholeiitic to transitional basalts, are taken to reflect the least differentiated and contaminated material from the plume.

Following the onset of rifting, volcanic activity became increasingly focused along the rift zones where a range of differentiated and variably contaminated lavas, dominantly alkaline in composition, were erupted, initially on the margins, and later in the axial regions of the developing rifts. This began in the Red Sea rift zone and western Gulf of Aden in the early Miocene during the early separation of the African and Arabian plates, and from the late Miocene in the Main Ethiopian Rift as the Nubian and Somalian plates began to separate. Early-rift development in the eastern and central Gulf of Aden and northern Red Sea appears to have been non-volcanic, which might suggest that these areas lay beyond the influence of the Afar upwelling, and that continental separation was primarily controlled by far-field tectonic stresses.

Actual continental separation (rather than crustal rifting) is marked by the transition from continental to oceanic volcanism and the subsequent generation of new oceanic crust. This occurred, from 10 Ma in the Gulf of Aden, from 5 Ma in the Red Sea, and is yet to occur in the Main Ethiopian Rift (Ebinger et al. 2004; Wolfenden et al. 2004). The range in compositions of the volcanic rocks of the Province from the continental flood basalts and rift related bimodal volcanics through to true oceanic MORB-type basalts provides a continuous record of the magmatic evolution associated with the

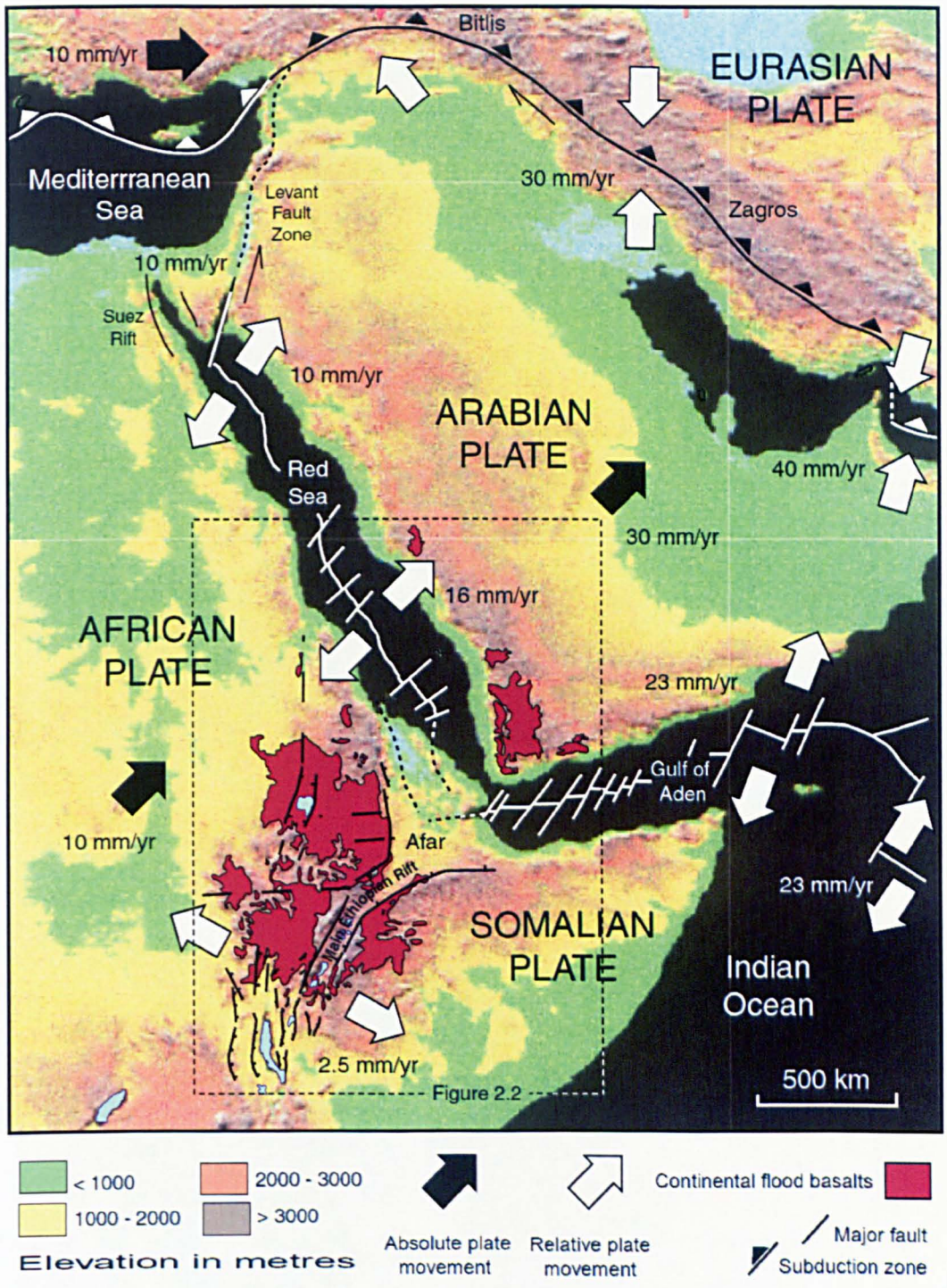

Figure 2.1 Tectonic framework of the Afro-Arabian triple-junction. Plate movements (Bellahsen et al. 2003), major faults and the extent of the Afro-Arabian Flood Basalt Province are overlain on a digital elevation model of the region.

process of continental break-up. In this sense the Afro-Arabian Volcanic Province represents one of the few regions in the World where we can study the nature of the interaction between upwelling mantle and the lithosphere coincident with continental break-up. The lavas are relatively unaltered by weathering and subsequent magmatic overprinting compared to older rifted margins such as the Deccan, the Parana-

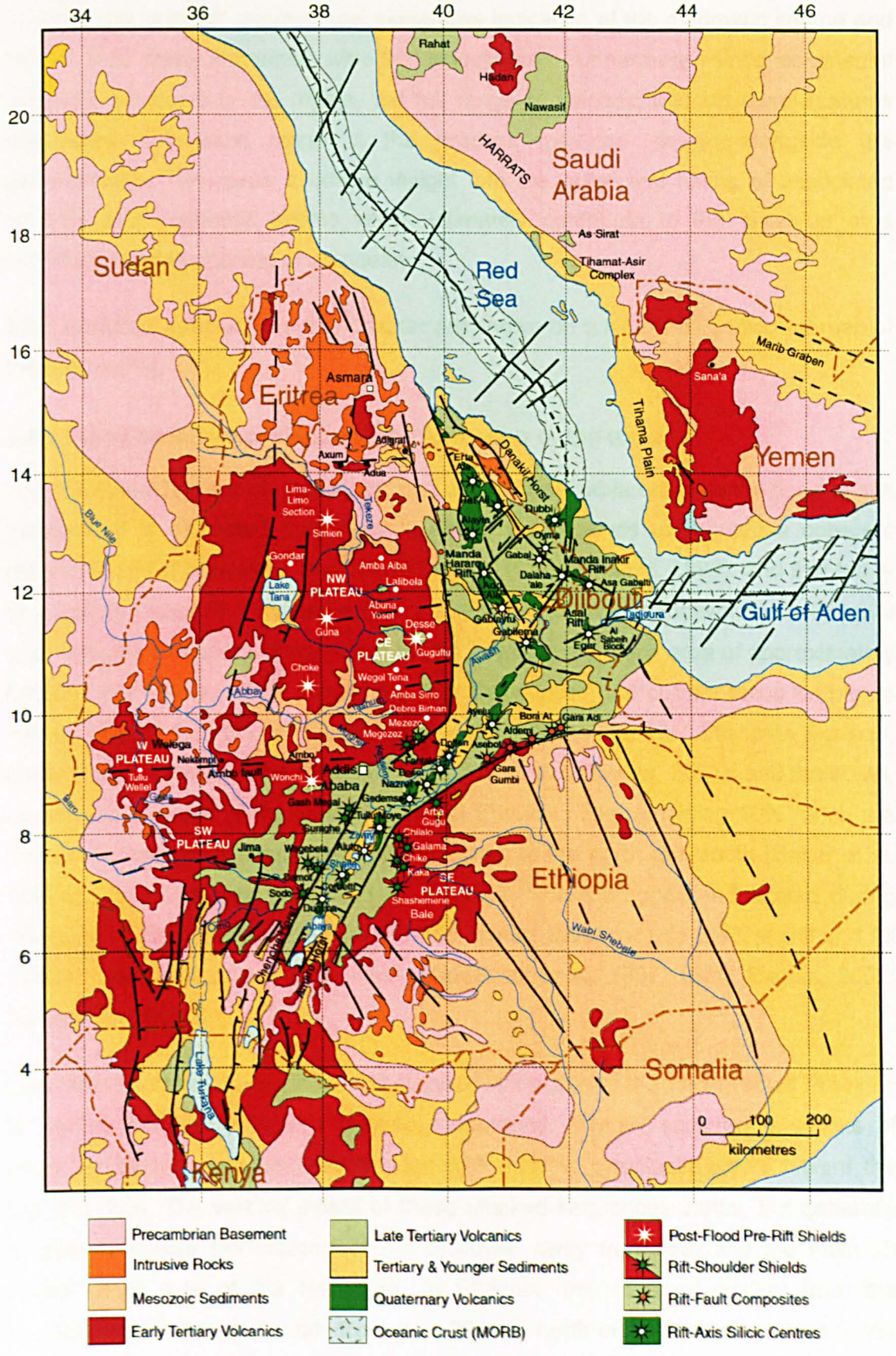

Figure 2.2 Simplified geological map of the Afro-Arabian volcanic province

Etendeka and the North Atlantic Volcanic Province; consequently they are more likely to retain the 'original' geochemical signatures indicative of the magmatic source and how it may have interacted with the lithosphere. Furthermore, since continental break-up continues in the region, the full range of volcanic and structural features associated with each stage in the process may be viewed alongside the geochemistry. This gives a unique insight into the order and timing of associated tectonic and magmatic events which ultimately contribute to the break-up of a continent and the opening of an ocean.

Most locations referred to in this chapter are shown on a simplified geological map of the region (Fig. 2.2).

2.1.2 Flood basalt volcanism and the formation of the traps

The Ethiopian Traps form the largest part of the Afro-Arabian continental-flood-basalt province. It is estimated that, prior to rifting, the province constituted a coherent magmatic pile of between 1 and 1.5 million km^3 (Courtillot et al. 1999), and that today, as a consequence of continued erosion, only a third of this original volume (~350,000 km^3) remains as variably fragmented blocks covering a surface area of approximately 600,000 km^2 (Mohr, 1983) around the Afar Depression, the current focus for plume activity (Fig. 2.1). 90% of this remnant volume forms the NW Ethiopian Plateau, partly disaggregated to the north in Eritrea and Sudan (Kenea, 2001), and the south, on the eastern side of the Ethiopian Rift in Somalia. The remaining 10% forms the Yemeni Traps with similarly fragmented outliers to the north and south (Baker et al. 1996a). Minor volumes, preserved as detached blocks dragged and rotated during rifting, have also been identified in the Afar region; these include the Danakil and Ali Sabieh Blocks (Courtillot et al, 1984, Manighetti et al. 1997, 1998, Eagles, 2002; Audin et al. 2004).

Like other flood basalt provinces the stepped landscape of the Afro-Arabian Province is typified by deeply incised plateau topography, fluvially sculpted in stacks of generally flat-lying basalts, inter-bedded with rhyolitic pyroclastic layers toward the top (Fig. 2.3). The vertical extent of these stacked sequences varies, but generally decreases toward the margins of the province, away from Afar and the main rift zones either side of the Red Sea. In Ethiopia, this is most evident from the progressive thinning of the pile from over 2000 m north of Addis Ababa, close to the rift escarpment, to 250 m at Yashum in the Abbay Basin on the western margins of the Central Plateau (Mohr, 1983); and from 1800 m at Ambo Sirro in the Central-

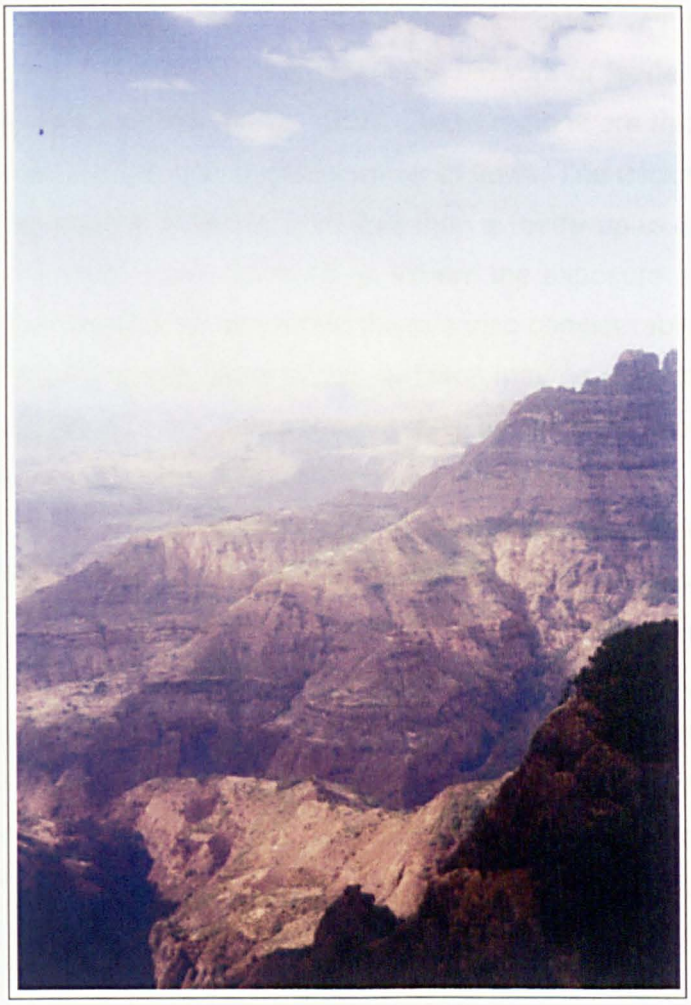

Figure 2.3 Deeply incised plateau topography of the NW Ethiopian Plateau - Simien Mountains.

Eastern Plateau, to 750 m at Ama Aiba on the north-east margin of the plateau (Berhe et al. 1987). Further to the south in the Kessem Gorge, the sequence thins from 1100 m to 800 m toward the Mugher River, and this trend continues toward the south up to the Ambo Fault which effectively forms a divide between the NW and SW Plateaus. Similarly, in Yemen the pile thins from over 1500 m between Wadi Lahima and Jubal Halash on the western rift margin to <300 m about 50 km north of Sana'a on the east rift shoulder (Baker et al. 1996b), and, in the SE Plateau, the thickness of the succession varies from 1000 m in Bale on the eastern rift margin to 800 m near Harar to the north east (Behre et al. 1987).

The away-from-rift thinning of the Ethiopian Traps is contested by Berhe et al. (1987) on account that the thickest part is represented in the Ari Highlands in the SW Ethiopian Plateau. This sequence, with a thickness of close to 3000 m, has since been attributed to an earlier phase of volcanism associated with the Kenyan Plume (George et al. 1998). Consequently, it is now generally accepted that the thickest

flood basalt sequences occur near the rift margins, coincident with the principal rift-parallel dyke swarms considered to represent the network of feeder-conduits for the volcanism that formed the traps (Mohr, 1983). These regions are thickest on account that they contain the thickest and largest number of flows. The thickness of individual flow-units varies across the province from less than a metre up to 20 m, whereas in the thickest regions some flows reach 40 m. Where the exposure allows formations to be traced along strike, it is apparent that there is also considerable lateral variation in the thickness of many flows. Some of this variation may be attributed to the infilling of localised irregularities in the palaeotopography by the still fluid lava. However, since the majority of flows were erupted onto an already infilled and flattened terrain, it is likely that most lateral variation in the thickness of individual flows is a consequence of thinning of the lava-fronts with distance from variably located feeder-conduits. This is confirmed where flows are clearly seen to overlap and interleave along strike. The lateral variation and discontinuity of the flows, and the large geographical extent of the flood basalts, strongly indicate that the volcanism that formed the Traps emanated from multiple fissures aligned along zones of maximum crustal warping induced by uplift, and that the location of these fissures shifted over time in response to the changing stress regime, coincident with the tectonic evolution of the province.

To an extent, the above observations dispel the myth that continental flood basalt provinces are typified by monotonous sequences of laterally extensive aphyric basalts. Not only are the lavas throughout the Afro-Arabian Province typically laterally discontinuous, they are also rarely aphyric. Aphyric basalts are common in the more evolved upper parts of the Traps where they alternate with rhyolitic ignimbrites and agglomerates, and, less commonly with trachytes and rhyolites. However, the majority of the flows which make up the main flood basalt succession, either side of the Red Sea, are dominantly pophyritic basalts with variable amounts of olivine and clinopyroxene phenocrysts, and less abundant plagioclase phenocrysts, set in an intergranular groundmass of plagioclase, olivine, clinopyroxene, Fe-Ti oxides and devitrified glass (Pik et al. 1998; Baker et al. 1996a).

Overall, the Traps constitute a stratigraphic sequence dominantly comprising tholeiitic to transitional basalts (Pik et al. 1998). Alkaline lavas occur less commonly in places near the base of the Traps (Kabeto et al. 2004), and in the upper reaches, where they merge with the more recent Miocene shield volcanics on the top of the pile (Kieffer et al. 2004). These upper reaches represent the transition from tholeiitic

to alkaline magmatism signifying the closing stages of high flux flood volcanism and the onset of continental rifting (Arnt et al. 2001 and Kieffer et al. 2004). The beginning of this closing phase is marked by a shift from exclusively basaltic volcanism to bimodal volcanism, evident from the appearance in the sequence of silicic extrusive rocks dominantly represented by rhyolitic ignimbrites which define prominent breaks of slope in the plateau escarpments across the province (Fig. 2.4). The vertical extent

Figure 2.4 Rhyolitic Ignimbrites of the Bimodal Upper Traps of the NW Ethiopian Plateau, seen along the plateau escarpment north of Gashena. The ignimbrite units are marked by the prominent breaks in slope indicated by the black arrows.

of these ignimbrite sequences across the Ethiopia Plateau is extremely variable. In the north at Wegel Tena it reaches 500 m, whereas in the southwest near Jima it is over 700 m and in the Central Plateau near Debre Birhan it is as low as 30 m (Ayalew et al. 2002). With an estimated volume of 43,000 km^3, covering an area of 70,000 km^2, they represent approximately 20% of the trappean pile in the Western Plateau. The thickness of individual ignimbrite flow units varies from 15 m to less than 3 m, and, texturally they range from massive, poorly consolidated porphyritic deposits to glassy, flow-banded, sparsely porphyritic welded flows. Detailed descriptions of the petrographic and geochemical characteristics of the Ethiopian ignimbrite deposits are given by Ayalew et al. (2002). In Yemen, the sequences of rhyolitic pyroclastic rocks are seen to thicken and coarsen toward the west, consistent with eruption from caldera centres marked by unroofed A-type granite plutons near the Red Sea rift margin (Baker et al. 1996a).

In addition to the silicic pyroclastic rocks in the upper bimodal section of the Traps, there are in places (more commonly in the Yemen) thick sequences of rhyolites (Menzies, 2001). In Ethiopia, rhyolites occur at Lima Limo in the northwest, at Wegel Tena in the east and at Jima in the southwest (Ayalew et al. 2002). Silicic volcanics also occur in the SE Plateau where they are seen to overlie stratoid basalts (Berhe et al. 1987); these have, however, been identified as Miocene in age and therefore post-trappean.

Within the bimodal succession across the province there are notable horizons of finely laminated felsic ash, infrequently interspersed with the basalts and ignimbrites. These vary in thickness from less than a centimetre to several metres, and in places they interfinger with the basalts and ignimbrites. It is likely that they represent distal airfall deposits. Furthermore, the fact that they interfinger in places with other volcanic units in the sequence suggests that some were emplaced simultaneously with these units. This supports the earlier stated premise that the trappean sequences emanated from multiple loci, some of which were at times contemporaneously active.

2.1.3 Post-flood pre-rift shield volcanism

In the NW Plateau the shift from fissure to central vent eruption, concomitant with the transition from tholeiitic to alkaline volcanism and increased activity in the rift during the Miocene, was evident from the development of broad, low-angled shield volcanoes which today sit conspicuously on top of the Traps (Fig. 2.5). These shields are unique to the Ethiopian Province and distinguish it from other less well preserved flood basalt provinces such as the Deccan, Siberian and the Karoo. The most prominent, Ras Dashen, the eerie summit of the Simien Shield, is the highest point in Ethiopia (4533 m), almost 2000 m above the top of the flood basalts. The summits of many of the other shields also rise above 4000 m even though their basal diameters are small in comparison to that of the Simien Shield. Mt Choke, for example, with a basal diameter of 100 km, rises to an altitude of 4052 m, 1200 m above the upper surface of the Traps. In the less dissected parts of the plateau the bases of these shields coalesce and it is thought that, prior to erosion, they collectively formed a continuous drape over 30 % of the area covered by the flood basalts. The Miocene sequences are typically bimodal, comprising variably alternating layers of basalts, rhyolites, tuffs and ignimbrites. In this respect they are similar to the underlying traps, so much so that the distinction between the two phases of volcanism is difficult to define clearly. The main distinction between the two is that the Miocene shield

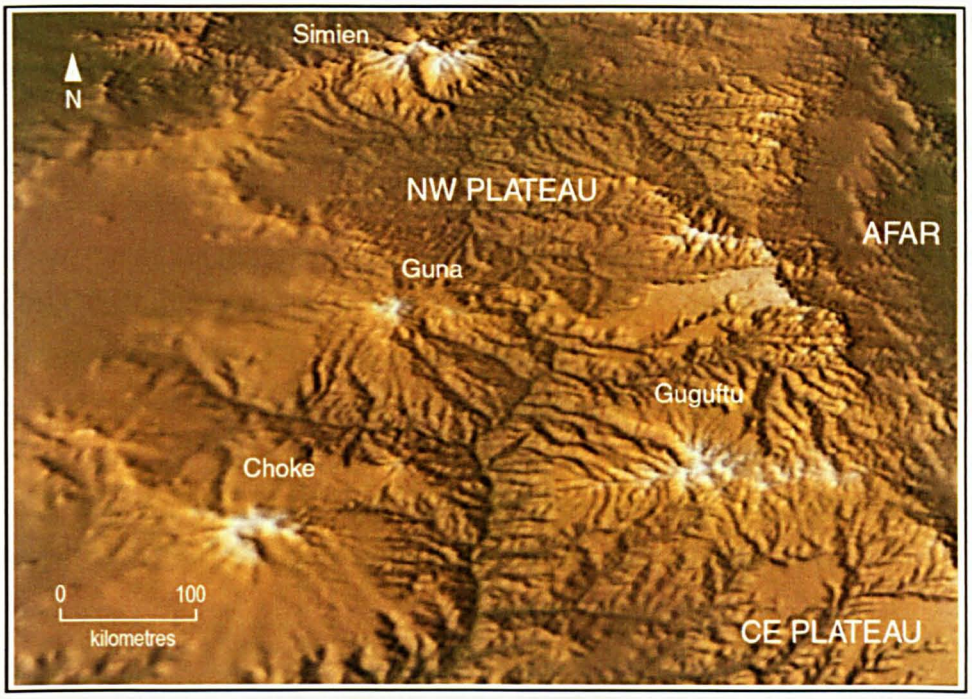

Figure 2.5 Digital elevation model showing post-flood pre-rift shields of the NW Plateau (modified Google image).

volcanics are dominantly alkaline in composition, whereas the Oligocene volcanics below are dominantly tholeiitic. Yet, in regions where alkaline lavas occur within the upper bimodal sections of the traps, the distinction between the two phases of volcanism remains vague. Detailed descriptions of the volcanic sequences of the Simien, Choke and Guguftu shields, and the respective underlying flood basalt formations, and the geochemical distinctions between the two phases of volcanism are given by Kieffer et al. (2004). Generally, the individual flow units which make up the shield sequences are thinner than those of the underlying flood basalt sequence, and at the highest points across the plateau, the shields have an average thickness of approximately 1500 m. Before erosion, the volume of the shield volcanics was therefore about 20% of that estimated for the flood basalts (Kieffer et al. 2004).

The distinctive Miocene shields of the NW Plateau are not evident in other parts of the province. The granitic plutons on the western margins of the Yemeni Plateau may represent the exposed roots of such structures, since they are of a similar age (20 - 26 Ma) and they have been identified as the source of the silicic volcanic and pyroclastic rocks in the upper part of the Yemeni volcanic pile (Davison et al 1994). Their alignment along the Yemen Great Escarpment strongly suggests that they are the remnants of a chain of calderas, possibly associated with the onset of rift-parallel faulting, and so may constitute a more evolved phase in the tectonomagmatic

evolution in the province than that represented by the Miocene shields of the NW Ethiopian Plateau.

The shield volcanoes of the SE Ethiopian Plateau (including Chike, Badda, Hunkuolo, Kaka, Chilalo and Kubsa) form prominent peaks of between 3700 and 4200 m. These have been related to a phase of volcanism which post-dates the shield events on the N.W Ethiopian Plateau (Woldegabriel et al. 1990). All except Mount Chike are of mid-Pliocene age. Mount Chike is late-Miocene in age (12 Ma – Woldegabriel et al. 1990)), and therefore belongs to an earlier phase of volcanism than that which formed the other SE Plateau shields. It is in fact of a similar age to the younger shield volcanoes of the NW Plateau such as Mount Guna (10 Ma – Kieffer et al. 2004), but is different only in that it is dominantly phonolitic in composition.

Shield volcanics of similar age to those of the NW Plateau do occur, together with fissural basalts and other central-vent volcanics, along well defined faulted lineaments associated with transtensional structures extending perpendicular away from the main rift zones. Such lineaments, described by Abebe et al. (1998) include the Axum-Adwa and Goba-Bongo lines and the Yerer-Tullu Wellel volcanotectonic lineament (YTVL), previously referred to by Mohr (1987), Wolde (1989) and Beyth (1991) as the Addis Ababa-Nekemt line. They constitute wide fault-bounded linear tracts of intense and complex fracturing with chains of variably spaced volcanic centres along their lengths. The YTVL, for example, is about 80 km wide and extends from the rift margin near Addis Ababa (Addis Ababa Rift Embayment) 700 km westward into Sudan. To the north it is bounded, for part of its length, by the Ambo Fault, although its southern margins are less well defined. Several central volcanoes occur along its length, each focussed at intersections between NW-SE and NE-SW trending fractures; these volcanic centres (including Tullu Wellel, Konchi, Gibat, Rogghe Badda, Wenchi, Dendi, Wechecha, and Yerer) become younger and progressively more alkaline eastward toward the rift and they are typified by silicic domes with bases predominantly of basaltic lavas. The observed riftward trend in the age and composition of the volcanic centres reflects an eastward migration in time of volcanism toward the rift - a trend which is inherent in the regional evolution of tectonically controlled volcanic activity across the province up to the present day. Activation of the east-west structural lineaments during the late Miocene has been interpreted as a response to accommodate movement along the Main Ethiopian Rift and, therefore, may be considered to represent the first amplified signals that, by this

time, the process of rifting was underway and was becoming more influential than uplift as a focus for volcanic activity.

There is an inherent difficulty in assigning volcanic features across the province to discreet phases of volcanism associated with defined tectonic events, since different parts of the province responded in different ways, and at different times, to changes in the regional stress regime imposed by the onset and progression of rifting. It is generally accepted, at least, that flood volcanism and subsequent bimodal volcanism in Ethiopia and Yemen are broadly coeval, and that in Ethiopia there is a progressive younging of volcanic activity along the rift escarpment from pre-rift in the north to syn-rift in the south (Ukstins et al. 2002). The sporadic outbursts of post-flood volcanism away from the rift are, however, more variable in age, and therefore more difficult to constrain in terms of a regional chronotectonic framework. Ages for the volcanic shields of the NW Plateau, for example, vary considerably between 30 Ma for the Simien shield and 10.7 Ma for the Mount Guna shield (Kieffer et al. 2004), and the more recent of these shields have similar ages to some of the volcanic centres along transtensional lineaments such as the YTVL (Abebe et al. 1998), even though their respective tectonic associations are distinctly different. This picture is further complicated by the contemporaneous occurrence of compositionally similar volcanism associated with fault reactivation in areas such as the Tana Basin (Chorowicz et al. 1998) and the Geba Rift Basin (Desissa, 2004).

2.1.4 Rifting and narrowing of the volcanic zone

Despite the somewhat random temporal and geographical distribution of post-trappean volcanism across the province, and the apparent variety of tectonic mechanisms controlling such volcanism, there was, from the Miocene through to the Quaternary, a general migration of volcanism toward Afar and the Main Ethiopian Rift, and a decline in activity elsewhere. This narrowing of the volcanic zone has been related to a progressive necking of the lithosphere below the African rifts (Mohr, 1983). The asymmetric position of the necked zone relative to the uplifted area, and to the distribution of volcanic cover, is more difficult to explain; Mohr (1983) maintains that it has persisted for at least the past 15 million years. It has been suggested that topographic factors may have played a role in directing volcanism westward (Williams, 1982). However, the greater volume of volcanic rocks along the western rift margin compared to the eastern rift margin is more likely to be a result of the magma supply to the east being cut off as the Arabian plate was pulled away from

the focus of plume activity beneath Afar as a result of subduction beneath the Zagros Mountains to the northeast (Ukstins et al. 2002).

As well as being progressively starved of magma, the Arabian margin has experienced a greater degree of uplift than the African margin since the onset of rifting. This is evident from the greater exposure of deep basement rocks in Yemen compared to Ethiopia, and from the fact that the eastern rift margin stands 500 m or so higher than the western margin thereby creating pronounced asymmetries in elevation across the Red Sea and Gulf of Aden (Doglioni et al. 2003). As a consequence, with the progression of rifting, denudational unloading became a more important process than magmatic accumulation in shaping the Yemeni margin (Ukstins et al. 2002); the fact there appears to be a relative absence of syn-rift volcanism in Yemen seems to support this. The asymmetry in elevation across the Red Sea rift axis appears to be a consequence of preferential uplift of the eastern flank compared to the western flank. This is attributed by Doglioni et al (2003) to an underlying density deficit created by the eastward shift of depleted asthenosphere from along the rift zone. The relative eastward motion of the mantle is assumed to be a result of its decoupling from the lithosphere, which is moving westward relative to it because of differential rotation between the two layers. The density deficit on the eastern margin may also be explained by lower density underplating.

Late Tertiary and Quaternary volcanic activity became concentrated in and immediately around Afar and the Main Ethiopian Rift where today it forms a complicated jigsaw of overlapping localised sequences built around central vents and fissures associated with discreet phases of tectonism. In places faulting and block-rotation associated with later tectonic phases has displaced earlier sequences, and later volcanics have been emplaced, sometimes unconformably, on top of these locally reorganised blocks (such as Danakil and Ali Sabieh). Frequent periods of inactivity are evident from the common occurrence of palaeosols in many sequences, and the more prominent of these are used by some authors to represent marker horizons between successive tectonomagmatic phases (Boccaletti et al. 1999). The occurrence of fluvial and lacustrine strata in some sequences also suggests that confined subsidence, uplift and erosion may have accompanied longer periods of inactivity in some areas (Woldegabriel et al. 1990).

2.1.5 Emergence of bimodal volcanic centres along rift-shoulders

Initial riftward migration of volcanism was marked by the emergence along the rift shoulders of bimodal volcanic centres, at first in the north associated with the Red Sea Rift, and later in the south, associated with the Main Ethiopian Rift. It is likely that such centres developed along rift-parallel flexural fractures related to crustal downwarping during extension, prior to the initial formation of the rifts (Mohr, 1983; Hart et al. 1989; Ebinger et al. 1993). Along the main Ethiopian Rift they are represented along the western shoulder by the Miocene shields of Megezez, Gash Megal, and Guraghe in the north and north-central sectors, and by the Pliocene shield, Mount Damot in the south-central sector. On the eastern shoulder they are represented, in the northern sector, by the Miocene shield Arba Gugu, and in the central sector by the Pliocene shields Chilalo, Badda, Hunkuolo, Kaka and Kubsa. Chilalo, Badda and Guraghe are located also along the Chilalo-Garaghe Tectonic Lineament, which may have influenced their development. Like the shields of the NW Plateau, the volcanic centres along the rift shoulders are built from alternating sequences of basalts, rhyolites and silicic pyroclastics. The general absence of detrital lithologies and erosional surfaces between the eruptive units suggests that the shields were built rapidly with little time for such features to develop between eruptions. Furthermore some of the older Miocene shields, such as Gash Megal and Guraghe, remained active for protracted periods of time through to, and during, the Pliocene. As a result, the bimodal sequences which constitute the basic form of these shields are blanketed by thick sequences of Pliocene pyroclastics with individual units of up to 40 m in thickness (Woldegabriel et al. 1990).

2.1.6 Rift-faulting and associated composite volcanism

The subsequent onset of rifting saw the development of high-angle rift-parallel border faults with associated dyke swarms and linear chains of composite volcanoes. Ebinger et al. (2004) and Wolfenden et al. (2004) suggest that this took place, first in the Red Sea rift during the Oligocene as a result of the separation of the Arabian and African plates, and later, during the Miocene, in response to the separation of the Nubian and Somalian plates. They conclude therefore that rifting in the Main Ethiopian Rift is not a primary feature of continental break-up associated with the Afar Plume, although the impact of the plume may have reactivated the northern extension of the East African Rift, causing it to propagate north-eastward into Ethiopia.

The process of rifting of the Red Sea is comprehensively reviewed by Ghebreab (1998). Initial extension and subsidence across the Red Sea rift was accommodated on both sides by N- to NW-trending, rift-parallel normal faults which served as conduits for pervasive dyke swarms and volcanic centres. In the Yemen, the tilted fault-blocks are typically between 2 to 6 km across with westward dipping displacements of between 0.5 and 2 km (Davison et al. 1994). To the north in Saudi Arabia these structures form foci for the extensive alkaline lava fields and volcanic cones known as the Harrats. Despite the general acceptance that there is an absence of syn-rift volcanism on the eastern side of the Red Sea, such alkaline volcanism contemporaneous with extension of the Red Sea was widespread in northern Yemen, Saudi Arabia, Jordan and Syria.

The Harrats, constitute one of the world's largest alkaline volcanic provinces, covering an area of approximately 180,000 km^2 (Coleman et al. 1983), and it is still debatable whether or not they are sourced from the Afar mantle upwelling and so an integral part of the Afro-Arabian Volcanic Province. Gass (1970) suggested that both the Red Sea and Arabian volcanism was related to the Afar Plume, with tholeiitic volcanism confined to the spreading-axis near the centre of the Afro-Arabian dome, and alkaline volcanism peppered along the flanking continental plateaus. More recently, however, since it has become established that most of the harrats are focussed along northerly trending fractures, oblique to the north-westerly trend of the Red Sea rift-axis (Almond, 1986a, 1986b; Camp & Roobol, 1989; Camp et al. 1991, 1992), it is generally thought that the two volcanic systems are separate. Subtle differences in the geochemistry of the lavas of the northern harrats compared to lavas from the Ethiopian and Yemen Plateaux seem to support this (Shaw et al. 2003).

Even so, Camp & Roobol (1989) maintain that the evolution of the harrats appears to have been in some way controlled by a regional stress regime inherently related to two phases of extension in Red Sea – one from 30 Ma to 15 Ma, and another from 5 Ma onward. They imply that the cessation in activity between these phases (marked by the accumulation of evaporite deposits in the Red Sea, and deposition of conglomerates along its flanking escarpments) coincides with the main phase of collision between the Arabian with the Eurasian plates along the Bitlis and Zagros suture, when the full thickness of the Arabian plate entered the convergent zone. Camp & Roobol suggest that the initial development of the harrats was a result of intracratonic rifting caused by crustal attenuation that coincided with subduction of

the Arabian plate beneath the Eurasian plate, and that this was contemporaneous with flood basalt eruption and the first phase of extension in the Red Sea. The older harrats and tholeiitic dyke swarms which trend north-west, parallel to the margins of the Red Sea are thought to have been erupted during this phase (Ilani et al. 2001). The second stage of extension in the Red Sea is considered by Camp & Roobol (1989) to be a result of the falling away of the rift flanks following uplift of the Afro-Arabian dome. This gave rise to more northerly fracture systems which formed the foci for alkaline volcanism of the younger harrats.

It seems that, although the evolution of the harrats may be structurally controlled by a similar regional stress regime to that imposed on the entire Afro-Arabian province, the source of their magmatism may be different from that which generated the flood basalts and rift-related lavas commonly attributed to the Afar Plume. Since the more southerly harrats lie within the proposed influence of the Afar Plume, they may be related to it, whereas those further to the north may be more related to localised asthenospheric upwelling associated with intracratonic rifting caused by subduction of the Arabian Plate beneath the Bitlis and Zagros suture zones.

On the western margins of the Red Sea, widely spaced rift-faults opposing those on the eastern margins also served as foci for dyke intrusion and surface volcanism. In Eritrea, for example, rift parallel dyke swarms controlled by northeast-dipping boundary faults have been described by Drury et al. (1994) and Ghebreab et al. (2002). Associated with these low-angle detachment faults are sets of younger domino-style, southwest-dipping normal and strike-slip faults which also served as conduits for dyke intrusion and surface volcanism. Similar structural features have also been identified along the north and south margins of the Gulf of Aden (Fantozzi, 1996; Manighetti et al. 1997, 1998; Leroy et al. 2004). The general trend of these, and other structures related to extension of the Red Sea and Gulf of Aden seem to follow that of the underlying tectonic fabric. In particular, the steeply dipping boundary faults of the western Red Sea have been linked to northwest-trending, high-angle shear-zones in the Pan African basement (Drury et al. 1994; Ghebreab and Talbot, 2000). This would suggest that the mantle processes associated with rifting in the Red Sea and Gulf of Aden were fundamentally controlled by existing rheological weaknesses in the lithosphere as suggested by Dixon et al. (1989). Alternatively, Bellahsen et al. (2003) argue that the geometry and kinematics of the both the Red Sea and the Gulf Aden rifts are principally related to intraplate stresses created by the weakening effect of the Afar Plume on the lithosphere, and oblique subduction of

the African plate beneath Eurasia; consequently, there is no need to invoke the presence of pre-existing structural weaknesses to explain the nature and orientation of rifting along these arms of the triple junction. They accept that such structures may define zones that are favourable to strain localization, but maintain that they have little control on where the plate boundary develops.

The southward propagation of rifting in the Red Sea became divided by the detachment of the Danakil Block from Ethiopian Plateau as the Arabian plate pulled away from the African plate. Down-faulting and subsidence associated with the continued southward propagation of the rift along this zone of detachment ultimately led to the formation of the Afar Depression (Lahitte et al. 2003a). This formative process was aided by extension of the Gulf of Aden rift and its westward propagation into Afar along the Gulf of Tadjoura (Manighetti et al. 1997; Audin et al. 2001). There are conflicting ideas on how exactly the depression opened and these have been summarised by Eagles et al. (2002). Souriot and Brun (1992) propose that fault patterns in SE Afar and the progressive widening southward of the rift zone are consistent with the counter-clockwise rotation of the Danakil Block about a fixed pole at the northwest extremity of the depression (crank-arm model). Tapponier et al. (1990) and Acton et al. (2000), on the other hand, suggest that both these features may be equally well explained by clockwise rotations associated with the interaction between the propagating arms of the Red Sea and Gulf of Aden rifts as they cut their respective ways into Afar. Northeast-directed extension of the Aden rift caused the counter-clockwise rotation of the Danakil Block, already moving eastward as a result of extension of the Red Sea rift. The formation of the Afar Depression was accompanied by widespread flood basalt eruption represented by the Afar Stratoid Formation, which filled the floor of the depression as it evolved (Chernet et al. 1998).

In the Main Ethiopian Rift (Fig. 2.6), sets of high-angle (> 60°) normal faults dipping both sides toward the rift axis became foci for minor fissure eruptions and the development of linear chains of composite volcanoes such as the Miocene centres of Gara Adi, Bora At, Afdem, Asebot and Gara Gumbi on the northeast margin of the northern sector (Chernet et al. 1998), and the Mid-Miocene syenitic plugs of the Mimo trachytes on the eastern and western margins of the southern sector (Ebinger et al. 1993). Many of these composite volcanic centres in the northern sector, such as those of the Gara Gumbi formation, grew on top of the flood basalts of Lower Afar Stratoid Series. The opposing half-graben structures of the rift margins are described in a series of cross-sections across the central and northern sectors of the rift

Figure 2.6 The northern Main Ethiopian Rift

respectively by Woldegabriel et al. (1990) and Boccaletti et al. (1998). Generally they are widely spaced with large vertical displacements, and form distinctive topographical staircases that step from the rift floor upward to the elevated flanks either side. Along the western margin of the northern sector they trend east-northeast and show vertical displacements of up to 1000 m, whereas further south they trend more north-south, are of smaller lateral extent, and show vertical displacements of only a few tens of metres. In contrast, the border faults along the eastern margins trend north-northeast and show greatest vertical displacements in the south (1000 m in the Dilla area).

In the southern sector, the Main Ethiopian Rift becomes segmented to form a series of north-trending horsts and grabens with huge vertical displacements. To the south of Lake Abaya, for example, the eastern rift margin drops westward into the Gelana Graben, which is bounded to the west by the Amaro Horst, which, in turn, drops westward into the Ganjuli Graben, itself bounded to the northwest by the Chencha Horst and the northwest-trending Gofa basin and range beyond. The vertical displacements between the Gelana Graben and the Amaro Horst, and the Amaro Horst and the Ganjuli Graben are 1200 m and 1700 m respectively. The uncharacteristic width-wise division of the rift in this region, and the unusually large vertical displacements between its component parts compared to those to the north suggest that the tectonic controls that influenced the development of the southern sector were in some way different from those that influenced the development of the

northern and central sectors. With reference to palaeogeographical evidence George et al. (1998) and Rogers et al. (2000) propose that during the initial phase of volcanism represented by the Amaro Basalts, the southern sector of the Main Ethiopian Rift was 1000 km to the south, within the region dynamically supported by the upwelling Kenyan Plume. With additional reference to the geochemical differences between these Eocene lavas and the Oligocene lavas of the NW Plateau, they therefore imply that this initial burst of volcanic activity during the Eocene was a product of the Kenyan Plume rather than of the Afar Plume as suggested by Ebinger et al. (2004). Furthermore, they suggest that the migration of magmatism southward from the Amaro Horst, as well as from the northern margin of the SW Plateau, is consistent with the north-eastward passage, since the Eocene, of the African plate over the Kenyan Plume. This draws a rather sharp line, irrespective of geological structure, between the Oligocene flood basalts to the north, and the Eocene flood basalts to the south. By the time of the onset of rifting, however, the southern sector would have migrated beyond the influence of the Kenyan Plume to within that of the Afar Plume, so it is unlikely that it would have experienced a significantly different stress regime to that experienced by the central and northern sectors. It is possible though that while subjected to the stress field associated with the Kenyan Dome, the basement beneath the southern sector may have developed structural weaknesses that were later exploited during rifting. Alternatively, the uncharacteristic style of rifting in this transitional region may simply be a result of the interplay between the stress fields of the both plumes.

Regardless of the complexity of the structural controls on the evolution of the Main Ethiopian Rift, the volcanism coincident with the development of the border faults along its entire length is similar both in style and composition. This period of tectonomagmatic activity, dominated by the eruption of alkaline silicic and basaltic volcanics, signified the second phase in the narrowing of the volcanic zone associated with the Afar plume. The progressive younging northward along the rift of the border fault volcanic centres representative of this period, from the Miocene through to the Pliocene, implies that rifting began in the south and propagated north-eastward as proposed by Ebinger et al. (2004) and Wolfenden et al. (2004). This is opposite to what would be expected if the rift was 'active'.

2.1.7 Development of rift-axis magmatic segments

Propagation of the Aden and Red Sea rifts into the Afar triangle continued through the Quaternary to Recent times in a series of rift-segment jumps which were

accompanied by fissure-fed basalt eruptions and the development of silicic central volcanoes. To the north and east, sea floor spreading had by this time become established in the Red Sea and Gulf of Aden respectively. Propagation of the not yet connected arms of the two rifts now defined a complex overlap zone within Afar characterised by a system of northwest to southeast trending normal faults with minor strike slip components (Abbate et al. 1995; Manighetti et al. 1998) and rotated blocks with clockwise rotation of between 13° and 3° (Courtillot et al. 1984; Acton et al. 2000; Manighetti et al. 2001; Kidane et al. 2003). Propagation of the Aden Ridge through the Gulf of Tadjoura became bent northward to form the Asal Rift Zone which subsequently divided along a north-south, left-slip fault zone (Tapponier and Varet, 1974; Audin et al. 1990) to form the parallel northwest trending Asal Ghoubbet and Manda Inakir Rifts. The southward propagating Red Sea Ridge also became divided to form an oceanic branch to the west of the Danakil Block (Manda Hararo Rift), and an on-land propagating rift to the east. A series of segmented roughly en-echelon linear rift axes subsequently developed along the principal rift zones associated with both ridges, and these became the focus for continued extension and volcanic activity within Afar from the Late-Pliocene onward. Volcanism along these axes was dominated by the development of large bimodal shield volcanoes, minor fissural basalts and silicic central volcanoes, which Lahitte et al. (2003) suggest were precursor features which directed future rift propagation. Central volcanic centres representative of this tectonomagmatic phase include Asa Alayta, Eger, Andabi Eale, Asa Gabalti, Data Gabalti, Dalaha'ale, Egersuwa, Humbab, Gabal, Didolli and Oyma, along the Asal and Manda Inakir rift zones of the Aden arm, and Erta Ale, Alayta, Boina, Ado'Ale, Gablaytu, Tat'Ali, Quarry, Dawa Ale and Gabilema, along the Manda Hararo rift of the Red Sea arm. These volcanoes and their relations with the propagation of the Red Sea and Gulf of Aden rifts are described by Lahitte et al. (2003). Generally the south and central centres range in composition from trachy-rhyolites to pantellerites, and vary in their morphology from simple silicic lava domes to more complex strato-volcanoes. The northern centres such as Erta Ale, Boina, and Tat'Ali, on the other hand, are large shield volcanoes built from a range of differentiated products from basalts to alkaline and peralkaline rhyolites.

The central volcanoes listed above, have grown on top of the Afar Stratoid Series, along well defined rift axes which have been interpreted as incipient spreading centres. They therefore represent the third phase in the narrowing of the volcanic zone associated with continental break-up and the opening of the Red Sea and Gulf of Aden.

In the Main Ethiopian Rift, this third phase of narrowing of the volcanic zone saw a decline in alkaline volcanism along the rift margin border faults and a concentration of peralkaline volcanism along narrow NNE-aligned en-echelon magmatic segments collectively referred to as the Wonji Fault Belt. This transition, during the Quaternary, was structurally manifested in the change from the development of rift parallel, widely spaced normal faults with large vertical displacements on the rift margins, to the development of dense swarms of N- to NNE-trending en-echelon, right-stepping extensional faults with throws of <100 m, on the rift floor (Boccaletti et al. 1998). The dense networks of faults that make up these swarms define the extent of the magmatic segments of the Wonji Fault Belt. The segments reach up to 50 km in length and 20 km in width, and at intervals along the rift they are offset along west- to northwest-aligned accommodation zones represented by faulted lineaments, some of which extend far beyond the margins of the rift. These linear fault zones include the Yerer-Gugu, Chilalo-Guraghe and Ambo lineaments. They are synonymous with the transtensional lineaments previously described, and most have remained as foci for sporadic tectonic and volcanic activity coincident with movements along the rift throughout its evolution.

Volcanism along the Wonji Fault Belt is, however, controlled by the N- to NE-trending extensional fractures which characterise the along-rift en-echelon magmatic segments. Fissural basalts and aligned scoria cones occur along the lengths of many of these structures, and large off-centre elongate silicic volcanoes have developed at the tips of the propagating fault segments (Boccaletti et al 1999; Kurz et al 2004). The silicic volcanoes, including Aluto, Tullu Moye, Boset, Ayelu and Doffen, form discreet chains along the fault belt, and many, such as Fantale, Gariboldi, Gedemsa, Kone and Corbetti have collapsed to form impressive sub-circular calderas (Acocella et al. 2003). Thick ignimbritic sheets and pyroclastic fall deposits described by Woldegabriel et al. (1990), Boccaletti et al. (1999) and Chernet et al. (1998) have been identified as products of such caldera collapse events, which Acocella et al. (2003) and Asfaw et al. (2004) have linked to subsidence as a result of magma withdrawal.

In a seismic study across the Boset magmatic segment, Keranen et al. (2004) have identified a high-velocity body which they interpret as an elongate mafic intrusion beneath the axial zone. They suggest that this may represent the magma chamber that fed the silicic centres along the Boset segment. Furthermore, they suggest that the segments are extensional features that behave as simple cracks, along which

basalt magmas can move easily from the magma chamber to erupt from fissures to form flows and cinder cones, but not calderas. Magma that becomes trapped in the complex stress-field at the tips of segments may then assimilate crustal material before erupting explosively to form large calderas. This simple explanation of the relationships between the extensional structures and the style of volcanism observed in the Wonji Fault Belt is based on the assumption that the direction of extension from the Quaternary onward was E - W to WNW - ESE (perpendicular to the orientation of the fractures and oblique to the rift margins). This would have entailed a shift, sometime at the beginning of the Quaternary, from the NW - SE direction of extension (orthogonal to the rift margins) responsible for the formation of the NNE- to NE-trending border faults as suggested by Chorowicz et al. (1994), Korme et al. (1997), Boccaletti et al. (1998, 1999); Acocella & Korme, 2002 and Wolfenden et al. (2004). Keranen et al. (2004) argue that such a rotation of the stress-field may account for the en-echelon geometry of adjacent magmatic segments. The variable lengths of the segments may then have been controlled by the variation in the angle of rotation of the stress-field along the length of the rift (Ebinger and Casey, 2001). The cause of this change in the stress-field at the beginning of the Quaternary is not really understood. With reference to the work of Chase (1978) and Jestin et al. (1994), Boccaletti et al. (1998) propose that the younger E - W to WNW - ESE direction of extension is related to the relative motion between the Nubian and Somalian plates, but why, after an already long period of movement between these plates, a change from NW - SE extension occurred at the beginning of the Quaternary, is uncertain.

Propagation of the younger N- to NNE-trending faults of the Wonji Fault Belt into the older NNE- to NE-trending border faults along the rift margins created rhomb-shaped structures described by Kurz et al. (2004). The younger faults have become curved at the point of capture with the older faults, particularly where they have propagated southward. As in the Red Sea, the orientation of the extensional faults systems throughout the Main Ethiopian Rift generally reflects that of the tectonic fabric of the underlying basement (Gashawbeza et al. 2004), thereby implying that, here too, the process of rifting was in some way controlled by the pre-existing lithospheric architecture.

Recent detailed seismic imaging across the Main Ethiopian Rift has revealed an underlying crustal asymmetry with thicker crust to the west than to the east (Mackenzie et al. 2004; Keller et al. 2004; Maguire et al. 2004). The thicker crust

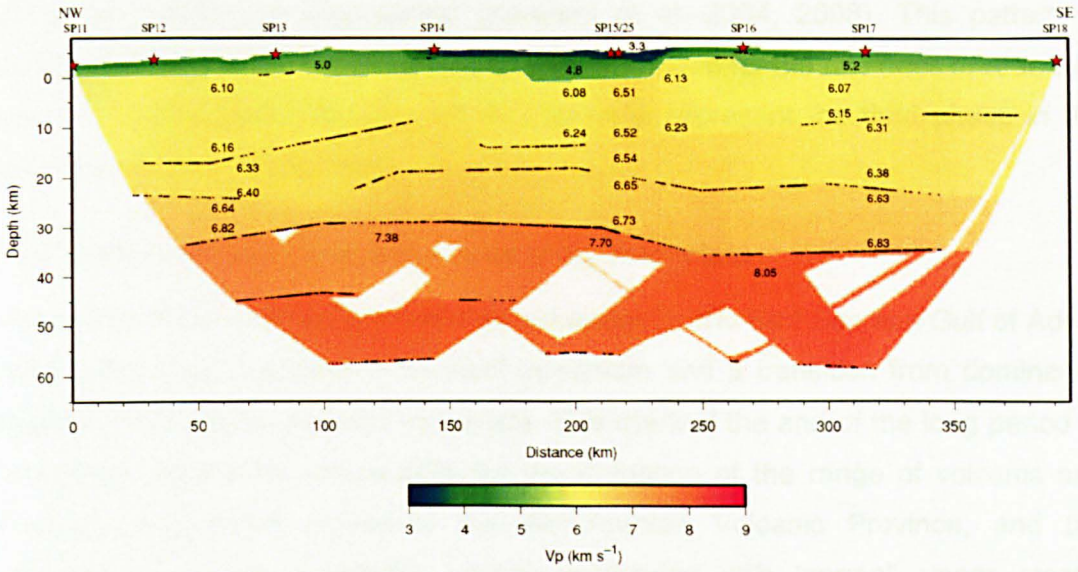

Figure 2.7 2-D P-wave velocity across the northern Main Ethiopian Rift. Red stars indicate shot points and black lines indicate bounce points (MacKenzie et al. 2005).

beneath the western edge is attributed to the presence, in the lower crust there, of a high-velocity layer which is absent beneath the eastern edge (Fig. 2.7). The margin of this additional lower crustal component defines, at depth, the extensional axis of the rift, therefore suggesting that it acted as a pre-existing boundary which was exploited during rifting. One of the possible explanations for this extra layer proposed by Mackenzie et al. (2004) is that it is part of the Lower Proterozoic basement, in which case, it would support the idea that rifting was controlled by existing structural weaknesses in the crust. Mackenzie et al. (2004), however, favour the interpretation that the layer represents underplated material associated with the Oligocene flood basalts, although they do not account for the fact that the layer is present only beneath the western side of the province. They suggest that the edge of this underplated region corresponds to the area of maximum thickness of the flood basalts, and that it influenced the location of rifting by directing it along the boundary between thick underplated crust and thinner crust. Furthermore, they suggest that the change in orientation of the rift from NNE to NE as it opens into the Afar depression is a consequence rifting being directed in this way along the proposed boundary of the underplated material.

The seismic studies referred to above seem to confirm that the Wonji Fault Belt represents the extensional axis of the Main Ethiopian Rift, as proposed by Boccaletti et al. (1999), and Wolfenden et al. (2004). It may be assumed therefore that the extensional structures along its length represent incipient spreading centres, and that the silicic central volcanoes and calderas at their tips mark the direction in which the

spreading centres are propagating (Keranen et al. 2004, 2008). This pattern of faulting and volcanism resembles that already described for the rift zones in Afar, and here too, in the Main Ethiopian Rift it is taken to represent the third phase in the narrowing of the volcanic zone.

2.1.8 Transition from continental to oceanic volcanism

The change from continental to oceanic volcanism (in the Red Sea and Gulf of Aden) was evident from a decline in bimodal volcanism and a transition from dominantly alkaline to exclusively tholeiitic volcanism. This marked the end of the long period of continental magmatism responsible for the formation of the range of volcanic and intrusive rocks which constitute the Afro-Arabian Volcanic Province, and the beginning of a new magmatic regime associated with 'normal' upper mantle convection and sea-floor spreading. In this respect the tholeiitic basalts and associated intrusive rocks which constitute new oceanic crust along the axial ridges of the Red Sea and Gulf of Aden are not considered part of the Afro-Arabian Volcanic Province, therefore they are not dealt with further in this thesis and instead the reader is referred to the published work of Girdler (1970, 1971); Bonatti et al. (1984); Bonatti (1985); Girdler & Southren (1987); Fantozzi (1996); Antonini et al. (1998).

2.1.9 Recent volcanism

During Recent times and up to the present day, volcanism in the Afro-Arabian Province has become almost entirely restricted to the axial-rift zones, although minor sporadic activity has continued along some of the transtensional lineaments that extend across and away from the rifts. A catalogue of most reported recent activity is presented in Appendix 2.1.1. The latitude and longitude of the numbered entries are given so that each may be approximately located on Figure 2.2. Furthermore, to facilitate easy referencing of the entries, they have been arranged firstly according to the country in which they occur and secondly according to their latitude from north to south. The numbers in brackets below refer the reader to specific volcanic features recorded in Appendix 2.1.1; for further details on these features the reader is referred to the website of the Global Volcanism Program (www.volcano.si.edu).

In the Red Sea, besides ongoing seafloor spreading activity along the already developed axial rift, on-land volcanic activity has continued along the southward propagating rifts in Afar, and less frequently along the eastern margins in Saudi Arabia and Yemen. Volcanism along the western oceanic branch of the Red Sea rift within the Danakil Depression (Afar) is evident from north to south in the Erta Ale

(20 – 28), Tat Ali (29- 35), Alayta (36 – 38), and Manda Hararo (39 - 45) volcanic ranges respectively. Dallol (21), Erta Ale (26) and Alayta (34) are the only centres which have erupted along this western branch within the last 100 years, although fumarolic and hydrothermal activity is seen in many of the other centres along its length. Erta Ale is one of the few volcanoes on Earth to have a permanently active lava lake (Oppenheimer and Francis, 1997, 1998; Burgi et al. 2002). Volcanism along the eastern on-land propagator is represented by the stratovolcanoes and Nabro (79) Dubbi (78) (Wiart & Oppenheimer, 2005). The last eruption of Dubbi in May, 861 was reported to have killed 175 people (Wiart et al. 2000).

Along the eastern margins of the Red Sea, sporadic volcanism has continued in the harrats and harras of Saudi Arabia (1 - 8) and Yemen (9 – 19). There are documented accounts for the eruption of many of these volcanoes, some of which have been woven into local legends. The eruption of Harrat Rahah, for example, has been linked to the Israelite account, in the book of Exodus (Chapter 19, verses 16 - 18), of the manifestation of God prior to the announcement of the Ten Commandments (Neumann van Pandang, 1963). The more northerly harrats in Saudi Arabia and into Jordan have been distinguished as different from those to the south on the basis on their geochemistry (Shaw et al. 2003). They are therefore considered not to be genetically related to the volcanism associated with the Afar plume. Many of the more southerly harras in the Yemen are located far inland, and it is likely that these are related more to transtensional fracture zones perpendicular to the Red Sea and Gulf of Aden rifts, than to extensional structures associated with rifting. In fact, of those listed in Appendix 2.1.1, only the shield volcanoes Jebel Zubair (13), Zukur (17) and Hanish (18) lie on the coastal margins of the Red Sea.

Today seafloor spreading also continues in the Gulf of Aden and current on-land volcanic activity in this arm has focussed along the north-westward propagating Asal (84) and Manda Inakir (82, 83) rift zones. Kammourta (82) in the Manda Inakir volcanic range last erupted between 1928 and 1929, and Ardoukôba (84) in the Asal Rift last erupted in 1978 (Audin et al. 1990).

In the Main Ethiopian Rift recent volcanism has been confined to along the magmatic segments of the Wonji Fault Belt (46 -76). Although the continental crust within the rift has been thinned to 70% of its original thickness (Mackenzie et al. 2004; Keller et al. 2004; Bastow et al. 2004, 2005, 2008), seafloor spreading is yet to begin in the Main Ethiopian Rift (Wolfeneden et al. 2004). Of all the volcanic centres located along the Wonji Fault Belt, only Fantale (53), Kone (55) and Tulle Moje (62) have

erupted within the last 200 years. Fumarolic and hydrothermal activity are however widespread along the entire length of the axial zone of the Main Ethiopian Rift, as well as along the transtensional lineaments that cut across, and away from the rift. In addition to the this activity associated with the volcanic centres listed in Appendix 2.1.1, hot springs occur within the rift at Sodore Awash, Arba Minch, Anno, Abaje Filwoha, and Wolliso, and away from the rift along the Addis Ababa - Nekempt Line (YTVL) at Addis Ababa (Filwoha) and Ambo.

2.2 Stratigraphy of the province

2.2.1 Introduction

The laterally discontinuous nature of the lithological units constituting the Afro-Arabian Volcanic Province, and the lack of consistent marker-horizons and unconformities between, make it difficult to construct a meaningful regional stratigraphy for the entire province. Compiling a time-relative stratigraphy is also made more difficult by the fact that many lithological sequences throughout the province are commonly segmented, offset and displaced by faulting and large-scale slumping. Understandably, stratigraphic studies of the province have tended to focus on those sections of the province, particularly along the rim of the Western Plateau into Afar, where the exposed lithological sequences are intact and readily accessible by road; as a consequence detailed coverage of the stratigraphy elsewhere in the province is scant. This unevenness of stratigraphic cover exacerbates the already difficult problem of compiling a realistic regional stratigraphy for the Province, and it has meant that when compiling the current geological maps of the region, the stratigraphy has been extrapolated for hundreds of kilometres from the few localities where it is known. Such extrapolation has led to contradictions raised by subsequent work and it has meant that, in some cases, the names of formations and other stratigraphic units have been changed in a rather piecemeal manner, thereby making cross-correlation of units between localities sometimes confusing.

It is only recently that reliable age data from precision dating techniques for selected stratigraphic units have become available. As a result, a cross-correlative stratigraphy for the entire volcanic province has not yet been fully developed. The majority of age data that exist for volcanic sequences throughout the province is mainly whole-rock K-Ar ages measured during the early 1970s through to the early 1990s (Fig. 2.8). In the last decade, however, more precise age data from $^{40}Ar/^{39}Ar$ dating studies have revealed that many of these early K-Ar ages show excessively

dispersed age-spectra, such that they are, today, discredited by many authors (Baker et al. 1996a). Recent $^{40}Ar/^{39}Ar$ dating studies have, in particular, concentrated on confining the timing of flood basalt volcanism (Baker et al. 1996a; Hofmann et al, 1997; Ukstins et al. 2002; Coulie et al. 2003). These show unequivocally that the duration of main phase flood volcanism lasted for no more than 4 million years, rather than tens of millions of years as suggested by early K-Ar measurements.

Despite their imprecision, the early K-Ar dates define broad stratigraphic units corresponding to the tectonomagmatic phases which mark the progressive evolution of the province from flood volcanism through to the development of the axial rift zones (Fig. 2.8). Furthermore, the collated stratigraphic columns constructed from available radiometric data show broad trends that reflect the variation in timing of these tectonomagmatic phases along the length of each arm of the triple junction and across the Ethiopian Plateau. The timing of flood, shield, rift-shoulder, and border fault volcanism, for example, appears to have occurred later from north to south in the Red Sea, and from south to north in the Main Ethiopian Rift - thus reflecting the respective directions of rift propagation along each arm. Similarly, shield volcanism appears to have occurred later from northwest to south-east across the Ethiopian Plateau. In this respect, the compiled stratigraphies illustrate the relative timing of events across the Province as described in Section 2.1.

The K-Ar data for the many of the younger (< 15 Ma) rift- zone formations are not as misleading as the those for the older lavas of the flood basalt pile, since they are less altered and more commonly contain well preserved feldspars suitable for dating. $^{40}Ar/^{39}Ar$ dates published for these younger formations (Zumbo et al. 1995a, 1995b; Chernet et al. 1998; Renne et al. 1999; Woldegabriel et al. 2001; Wolfenden et al. 2004) closely match the earlier respective K-Ar dates; however there are still too few data to reliably redefine the stratigraphy for the Province as a whole, and some authors (Ukstins et al. 2002) choose not to relate new $^{40}Ar/^{39}Ar$ ages for selected formations to earlier published K-Ar dates. Nevertheless, the current compiled stratigraphies still reflect the distinction between the older Trap Series and the younger Rift (or Aden) Series first described by Blanford (1869) in his original classification of the volcanic rocks of northern Ethiopia. The transition between the two series, dated in the north by Zanettin et al (1980) at about 14 Ma, marks the onset of rifting in the southern Red Sea and Afar Depression, and in the Main Ethiopian and Kenyan Rift, and so separates flood and shield volcanism associated

Figure 2.8 Compiled Stratigraphy for the Afro-Arabian Volcanic Province

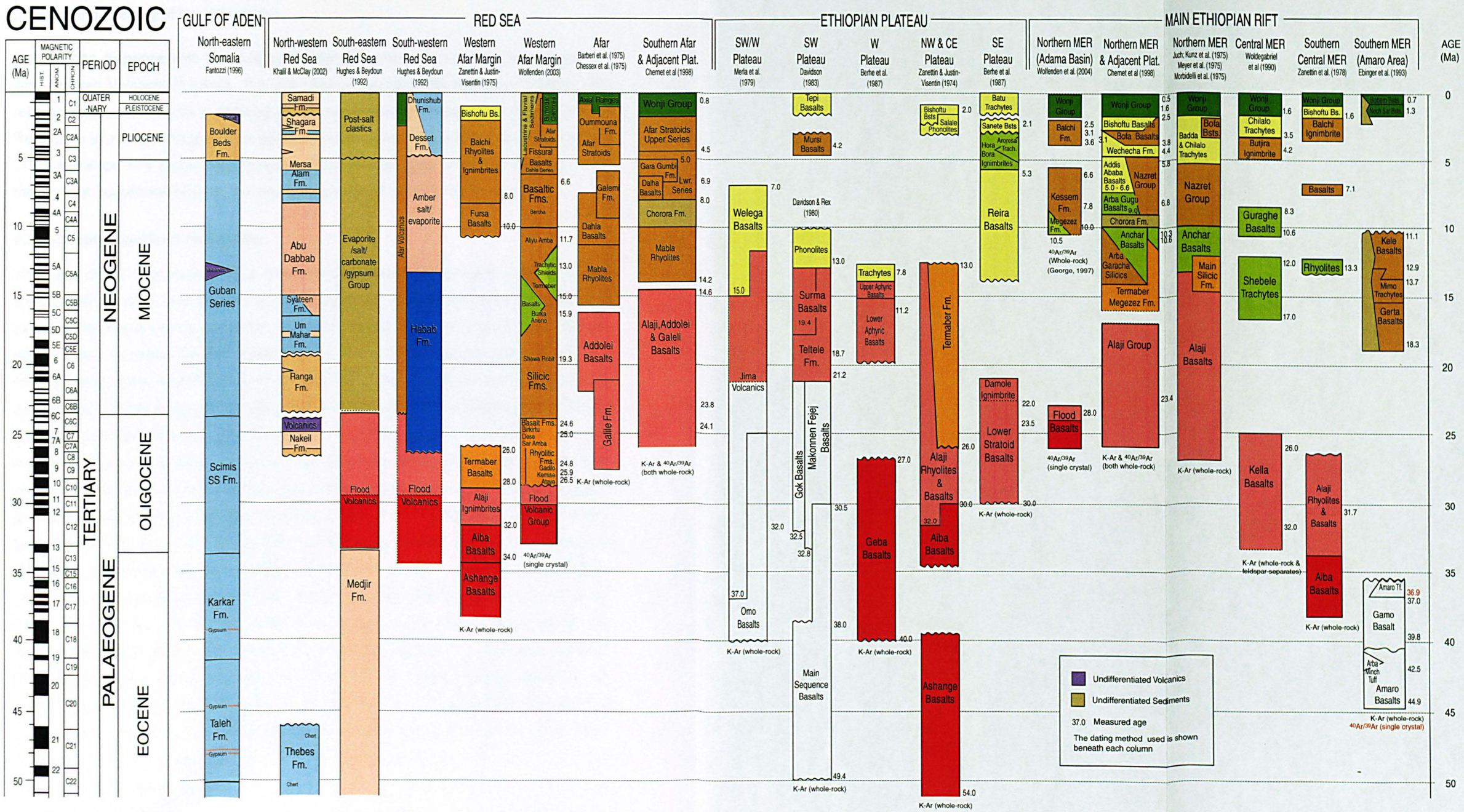

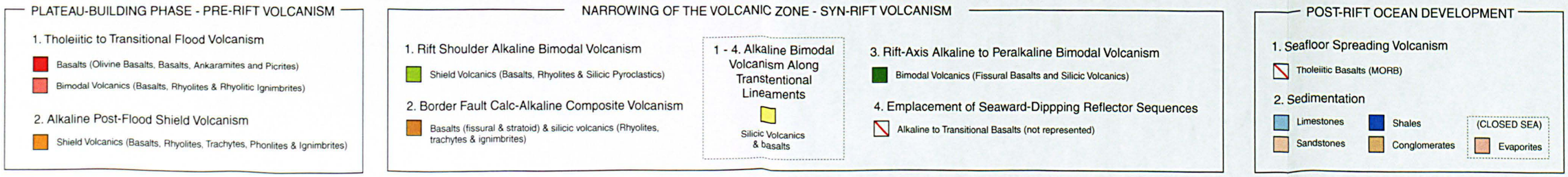

with plateau-building from rift-related volcanism associated with the progressive thinning and necking of the lithosphere.

Rather than dispense with the existing stratigraphic records for various parts of the Afro-Arabian Volcanic Province, it is intended in the following sections to clarify the relevance of such records in defining distinct evolutionary phases in its development. Reference is made, throughout, to selected published stratigraphies for various parts of the Province, and in this respect the reader is encouraged to refer to Figure 2.8 for the ages of quoted formations, and the dating method used to determine them.

2.2.2 Continental flood-volcanism

The base of the flood basalt pile is rarely represented in stratigraphic studies of the province since most have focused on stratigraphically extensive sections in which the base of the sequence is not seen. It is only really exposed around the plateau margins and in deeply incised gorges where the Central Plateau and uplifted and faulted flanks of the Afar Depression and Main Ethiopian Rift have been dissected by river erosion. Generally, in the western and southern parts of the plateau the volcanic pile sits unconformably on basement rocks comprised mainly of metamorphosed Pan-African arc-associated volcanics and intrusives, whereas in the central and northern parts of the Main Plateau, and eastern parts of the SE Plateau, it rests unconformably on the Mesozoic sediments that lie unconformably above these basement rocks (Fig. 2.2). In northern Ethiopia and Eritrea, the upper surface of Mesozoic sediments has been regionally laterized, thereby marking an extensive period of palaeosol development prior to the eruption of flood basalts (Drury et al. 1994). Similarly, in Yemen, the base of the flood basalts rests unconformably on lateritic palaeosols (ferricretes) which form the upper surface of Cretaceous to early Palaoecene marine and terrestrial sandstones of the Tawilah Group (Baker et al. 1996; Davison et al. 1994; Menzies et al. 2001). The unconformities between the flood basalts, the Mesozoic sediments and the underlying crystalline basement may be seen in a few locations along the Main Ethiopian rift, and dating of the flood basalts in these areas has revealed that they are just as old there as elsewhere in the Province (Woldegabriel et al. 1990). This is contrary to the opinion that flood volcanism migrated from the NW Plateau to the rift (Zanettin et al. 1980). In the light of this, it may be more true to say that post-flood volcanism migrated toward the rift, and that the timing of flood volcanism was more or less contemporaneous across the entire Province around 30 Ma, as recently confirmed by Ukstins et al. (2002) and Coulie et al. (2003).

Much of the confusion that has led to a misapprehension that the focus of flood volcanism migrated riftward from the NW Plateau, comes from the inappropriate assignment of age data to stratigraphically ambiguous formations. For example, basalts with younger ages of between 23.8 and 24.1 Ma (Chernet et al. 1998), and between 26 and 23.4 Ma (George, 1997), overlying Mesozoic strata on the eastern and western margins of the northern Main Ethiopian Rift respectively, may easily be (and have been) misinterpreted as basal components of the flood basalt pile on account of their relative stratigraphic position. Such data may then be used to support the premise that these basal units are younger than others elsewhere in the Province, and that this may be explained by the fact that the focus of flood basalt volcanism migrated over time. These younger basalts are however, alkaline in composition rather than tholeiitic like rest of the basal units of the flood basalt pile; they are therefore likely to belong to a much later phase of volcanism that has perhaps overlapped the margins of earlier volcanic units. The logical development of theory from such misinterpretations can ultimately become self-sustaining, until it begins to develop at odds with other more robust observations. This is one of the grave dangers of adopting a geographically limited view, or by confining an investigation to one method of approach in isolation from others.

In Ethiopia, flood volcanism falls into three, not always distinctive, stratigraphic units, namely the Ashange, Aiba and Alaji formations. The original distinction between the basal Ashange Formation and the Aiba Formation above was based on the presence, between the two formations, of an angular unconformity observed by Blanford (1869). The existence of this unconformity has since been disputed by some authors (Merla and Minucci, 1938) and accepted by others (Zanettin & Justin-Visentin, 1974 and 1975; Zanettin et al. 1980). Despite the fact that Merla & Minucci (1938) dispute the existence of Blanford's unconformity, they do identify that, in the vicinity of its proposed existence, there is a region of intense faulting of both a compressional and extensional nature. Zanettin et al. (1980) suggest that this deformation event was responsible for tilting and folding the Ashange Formation prior to the eruption of the Aiba Basalts, and for resetting the K-Ar age-systematics of the Ashange Basalts such that their reported ages in this deformed region were younger than those reported for the overlying Aiba Basalts. On the strength of these observations Zanettin et al. (1980) support the existence of Blanford's unconformity, even though they report that it is not identifiable further west beyond Mt. Abuna Yoseph, as well as further south toward Addis Ababa. The fact that the unconformity is not everywhere present across the Ethiopian Plateau, and that there are no clearly distinguishable mineralogical and

geochemical differences between the Ashange and Aiba basalts, has meant that, today, the distinction between these respective formations has become somewhat out-dated. Both formations are dominantly composed of tholeiitic basalts, and it is this characteristic which unifies the two more than the presence of the local unconformity divides them.

The greater part of the Ethiopian Flood Basalt sequence is represented by the Aiba Formation, and together with the Ashange Formation, where it is recognised, both constitute the main phase of flood volcanism most recently estimated by $^{40}Ar/^{39}Ar$ dating to have erupted within a period of 1 Myr around 30 Ma (Hofmann et al. 1997, Ukstins et al. 2002; Coulie et al. 2003), rather than over a much more protracted period of time as suggested by earlier less precise K-Ar age data (Fig. 2.8). The Ashange and Aiba Formations take their name from type-locations in northern Ethiopia (Fig. 2.2), and although these names have been adopted for the basal sequences in some other parts of the Province such as in Western Afar (Zanettin & Justin-Visentin, 1975) and in the Main Ethiopian Rift (Zanettin et al. 1978), they are not used everywhere in the Province. Other basal and lower trap formations which correlate, temporally and geochemically, with the Ashange and Aiba Formations include the Geba Basalts and the Lower Abbay Lavas in Western Ethiopia, and the Lower Stratoid Series in SE Ethiopia (Berhe et al. 1987), and possibly the Gok, Makonnen and Fejej Basalts (Davidson and Rex, 1980) and part of the Jima Volcanic Group (Merla et al. 1979), in SW Ethiopia. Older Eocene basalt formations considered to represent the initial stages of flood volcanism in southern and south-western Ethiopia by Berhe et al. (1987) and Ebinger et al. (1993) are here considered to represent an earlier phase of volcanism associated with the Kenyan Plume as suggested by George et al. (1998); these include the Akobo, Main Sequence and Omo Basalts in SW Ethiopia (Davidson & Rex, 1980; Merla et al. 1979), and the Amaro and Gamo Basalts in southern Ethiopia (Ebinger et al. 1993).

The Alaji Formation, conformably overlying the Aiba Formation, represents the bimodal upper trap sequence which reflects the transition from tholeiitic to alkaline volcanism coincident with the closing stages of flood volcanism. The base of the Alaji is generally defined by the first appearance, in the volcanic pile, of rhyolitic ignimbrites; however where these are absent the distinction between it and the underlying Aiba Formation is impossible to ascertain precisely. For this reason, Zanettin et al. (1980) represent the transition between the two formations as a broad overlap, spanning approximately 3 million years between 30 and 27 Ma (Mohr, 1983).

The Alaji Formation is recognised almost everywhere across Ethiopia except in the south where it appears to be absent (Ebinger et al. 1993). Other formations correlated with the Alaji Formation on the grounds of their relative stratigraphy, timing, lithology and geochemistry include the Addolei and Galeli Basalts in SW Afar (Barberi et al. 1975; Chessex et al. 1975; Chernet et al. 1998), the Kella Basalts in the central Main Ethiopian Rift (Woldegabriel et al. 1990), the Teltele Formation and Surma Basalts in the SW Plateau (Davidson & Rex, 1980), the Damole Ignimbrite in the SE Plateau (Berhe et al 1987), the Blue Nile Formation in the Western Plateau (George, 1997), and possibly the upper part of the Jima Volcanic Group in the SW Plateau (Merla et al. 1979). K-Ar dates for the age range of the Alaji Formation and its correlatives vary across the Plateau from 4 myr (28 - 32 Ma) on the western Afar Margin (Zanettin & Justin-Visentin, 1975) to 19 myr (13 - 32 Ma) in the NW and Central Plateau (Zanettin & Justin-Visentin, 1974). This range has been narrowed considerably by more recent $^{40}Ar/^{39}Ar$ data to less than 3 myr (26.9 - 29.4 Ma) on the Western Plateau margin (Blue Nile Fm. - Hofmann, 1997), 2 myr (28.2 - 30.2 Ma) at Wegal Tena in the Central Eastern Plateau, and 0.3 myr (29.4 - 29.7 Ma) on the NW Plateau margin (Lima Limo Section - Hofmann et al. 1997; Rochette et al. 1998).

The most complete slice through the Ethiopian flood basalt pile so far documented is exposed in the Lima Limo Section on the margin of the NW Plateau, 450 km to the north of Addis Ababa. Both lower trap (Ashange and Aiba) and upper trap (Alaji) formations are represented in this 2000 m thick sequence of lavas which constitutes the entire flood basalt pile in this region, from the basement unconformity through to the post-flood shield volcanics on top (Fig. 2.9). This section, together with another, constituting the upper 500 m of the flood basalt pile in the central eastern Ethiopian Plateau, at Wegel Tena, have been the foci for co-ordinated $^{40}Ar/^{39}Ar$ dating and palaeomagnetic studies aimed at constraining the timing and duration of flood volcanism in Ethiopia (Hofmann et al 1997; Rochette et al. 1998). $^{40}Ar/^{39}Ar$ dates from two other sections were also included in this initiative - one from a section near Adigrat on the northern margin of an outlier of the volcanic pile to the north of the Main Ethiopian Plateau, and two from along the main road between Weldya and Woreta (Chinese Road) in the NE Plateau. The correlated palaeomagnetic and $^{40}Ar/^{39}Ar$ data, alongside petrological and geochemical evidence (Pik et al. 1998) from the respective sections strongly support that the entire flood basalt pile was emplaced over a short period of between 1.9 and 0.8 myr (including a hiatus in activity of ~ 0.4 Myr), during Chron 11 at around 30 Ma (Rochette et al. 1998). Hofmann et al. (1997) confirm that emplacement occurred in two pulses, the first

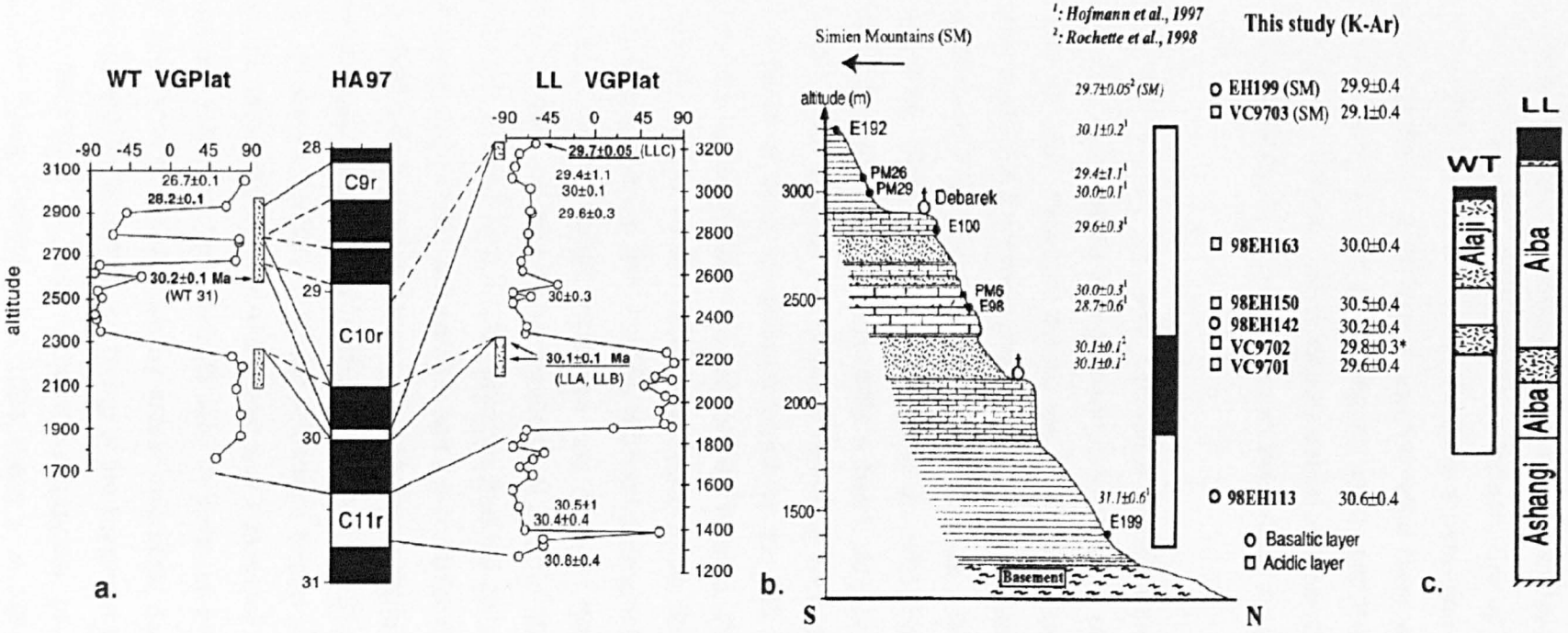

Figure 2.9 Compiled data for the Lima-Limo Section. **(a)** Vertical log of paleomagnetic polarity (shown by VGP latitude) in the Lima-Limo (LL) and Wegel Tena (WT) sections, with $^{40}Ar/^{39}Ar$ ages, correlated with the HA97 reversal timescale (Rochette et al. 1998). (b) $^{40}Ar/^{39}Ar$ ages and stratigraphic log for Lima-Limo Section (Coulie et al. 2003). (c) Simplified stratigraphic sections of Lima-Limo (LL) and Wegel Tena (WT), showing lithological units (Rochette et al. 1998).

beginning just prior to 30 Ma in Chron 11r, and the second ending before 29 Ma in Chron 10r. This is suggestively evident in the Lima Limo Section where there are two discreet sequences of basaltic lavas separated by a thick layer of differentiated felsic material which forms a regionally extensive terrace, the upper surface of which is proposed to represent an unconformity marking a cessation in activity between the two respective cycles of volcanism. A second felsic layer with an erosional upper surface similarly marks the end of the second cycle, and therefore the end of flood volcanism in the NW Plateau. The quiescent period between the two proposed cycles of differentiation appears to coincide with an episode of magnetic normality marked by Chron 11n.

$^{40}Ar/^{39}Ar$ ages reported for the basal formations of less extensive sections through the volcanic pile in other parts of the Province (both sides of the Red Sea) support that the onset of flood volcanism across the Province occurred between 29.5 and 30.5 Ma, as is evident in the Lima Limo Section. These include age data for sections in the Blue Nile and Adigrat areas of Ethiopia (George, 1997; Hofmann, 1997), in Eritrea (Drury et al. 1994), in Yemen (Zumbo et al. 1995; Baker et al. 1996) and in the As Sarat volcanic field in south-western Saudi Arabia (Kellogs et al. 1983). Rochette et al. (1998) suggest that on the strength of such correlations, the relative timing and duration of flood volcanism inferred for the NW Plateau from the Lima Limo Section may be extended to the rest of the Province. This has been confirmed more recently by Ukstins et al. (2002) and Coulie et al. (2003) in $^{40}Ar/^{39}Ar$ dating studies comparing the timing and duration of flood volcanism in Ethiopia and Yemen. Both conclude that flood basalt volcanism was more or less contemporaneous in Ethiopia and Yemen, and that it was initiated just prior to 30 Ma, and lasted for no more than 1 myr. Ukstins et al. (2002) propose that the onset of flood volcanism in Ethiopia occurred at 30.9 Ma, between 0.2 and 2 myr earlier than in Yemen, whereas Coulie et al. (2003) maintain that there is little distinguishable difference between the onset times for flood volcanism both sides of the Red Sea (30.6 ± 0.4 Ma in Ethiopia and 30.2 ± 0.4 Ma in Yemen). Bimodal volcanism began at about 30 Ma, and is thought to have continued in parts of Ethiopia and Yemen for 5 myr or so up until the onset of syn-rift volcanism at about 25 Ma. In parts of Ethiopia, where bimodal sequences are conformably overlain by shield volcanics, the division between the two is indistinguishable, therefore the timing of the transition from one to the other is impossible to determine. In Yemen, the entire trappean pile is referred to as the Yemen Volcanic Group (Davison et al. 1994; Baker et al. 1996; Menzies et al. 2001) and, although there are similar lithological distinctions there between the upper and

lower traps to those found in Ethiopia, it is not sub-divided into stratigraphic units that reflect such distinctions in the same way as in Ethiopia.

2.2.3 Post-flood pre-rift shield volcanism

The shield volcanics on top of the Ethiopian flood basalt pile (i.e. above the Alaji Formation) belong to the Termaber Formation. This phase of volcanism, dominated by alkaline lavas and related pyroclastics, is largely confined to the north-western and central eastern Ethiopian Plateau (Zanettin & Justin-Visentin, 1974). Its age range varies enormously, partly because its constituent sequences are products of individual central volcanoes which developed on top of the flood basalts at different times in different parts of the province. In the NW Plateau, alone, the age range for the Termaber shield volcanics is between 25 and 13 Ma (Zanettin & Justin-Visentin, 1974). This is not inconsistent with more recent $^{40}Ar/^{39}Ar$ age determinations reported by Kieffer et al. (2004) for the Simien (30.4 - 18.7 Ma), Guguftu (23.3 Ma), Choke (22.4 Ma) and Mt. Guna (10.7 Ma) shields on the NW Plateau.

As already implied, the fact that post-flood pre-rift shields are today confined to the NW and CE Ethiopian Plateau does not necessarily mean that they were not more widespread previously, since they may have been removed by erosion. The unroofed plutons along the Great Escarpment in Yemen, for example, may represent the remnant magma chambers of such features, and if indeed they are, this would strongly support the premise that eastern Red Sea margin experienced a greater degree of uplift than its western counterpart (Doglioni et al. 2003).

2.2.4 Rift-shoulder shield volcanism

Some of the younger shields (< 13 Ma), previously ascribed to the Termaber Formation, along the western margins of the Afar Depression and northern Main Ethiopian Rift (Jones & Rex, 1974; Zanettin & Justin-Visentin, 1975; Jones, 1976; Chernet et al. 1998) may, more appropriately, be assigned to a more recent tectonomagmatic phase than that with which the Termaber is fundamentally associated. Although these shields, such as Megezez (George, 1997; Chernet et al. 1998; Wolfenden et al. 2004), are morphologically and compositionally similar to the shields of the NW Plateau and may similarly be associated with plateau-building, they appear to have developed later along the rift shoulders above flexural rift-parallel fractures caused by crustal down-warping just prior to rifting. It is likely therefore that they are associated with the narrowing of the volcanic zone. This might explain the unexpected young ages measured by George (1997) and Chernet et al.

(1998) for the Megezez Formation (10 Ma) compared to previous age estimates for the Termaber Basalts elsewhere on the eastern edge of the Ethiopian Plateau. Similar ages are obtained for the Termaber trachytic shields (13 Ma - Wolfenden, 2003) and Marbla Rhyolites (14 -10 Ma – Barberi et al, 1975; Chernet et al, 1998), along the rift-shoulders of western and southern Afar respectively. The Guraghe Basalts (10.6 - 8.3 Ma) and the Gash Megal rhyolites (10 Ma), along the western shoulder of the central Main Ethiopian Rift (Woldegabriel et al. 1990), and the Anchar Basalts and Arba Guracha Silicics (14 - 10 Ma) along the shoulders of the northern Main Ethiopian Rift (Chernet et al. 1998), also yield similar ages. All these stratigraphic units have been related to bimodal alkaline shield volcanoes associated with rift-parallel faulting along the rift shoulders; it is probable then that, like Megezez, they are related to crustal down-warping prior to, or coincident with, rifting. Younger shield volcanoes with similar compositions and structural associations are found along the eastern shoulder of the central Main Ethiopian Rift; these include the Pliocene shields, Chilalo, Asela, Badda, Hunkuolo, Kaka, Kubsa, Shashemene and the Galama linear volcanic range described by Woldegabriel et al. (1990), and the Aroresa Trachytes and Hora Bora Ignimbrites described by Berhe et al. (1987). Such features might indicate that down-warping of the SE Plateau margins occurred much later than along the eastern margins of the Main Ethiopian Plateau. This is consistent with the premise that the principal focus of uplift prior to flood volcanism was in the NW Plateau, and that extension was first initiated in the Red Sea during the Oligocene in response to the separation of African and Arabian plates, and later, during the Miocene, in the Main Ethiopian Rift in response to the separation of the Nubian and Somalian plates. Down-warping would first have occurred in the Red Sea Rift and would later have been initiated in the Main Ethiopian Rift. Furthermore, a longer period of extension would have been necessary for down-warping to occur along the riftward margins of the SE Plateau, compared to the NW Plateau, because of its lower palaeo-elevation.

2.2.5 Volcanism along transtensional lineaments

Other shield volcanoes occur along the transtensional lineaments and accommodation zones which cut across, and away from, the rifts. As already explained, these lineaments were periodically reactivated in response to structural readjustments during the development of the rifts, and as a consequence, the timing of associated volcanism varies accordingly. Since some of the shields along these lineaments are therefore comparable in age, and morphologically and compositionally similar to the Termaber and Rift Shoulder shield-volcanics, they may

easily be misinterpreted as such. In fact, those that occur near the intersections of the faulted lineaments with the topographic trace of the rift-shoulders may, in the absence of detailed structural and geochemical analyses, be interpreted either way if their age matches that proposed for rift-shoulder volcanism in that region. The Yerer and Arba Gugu Mio-Pliocene shields along the Yerer-Gugu lineament and the Badda and Chilalo Pliocene shields along the Chilalo-Guraghe lineament are examples of such ambiguities (Chernet et al.1998). Equally ambiguous, are the Miocene Shebele Trachytes and Mount Chike Phonolites, similarly located on the eastern shoulder of the central Main Ethiopian Rift along an undefined lineament which appears to offset the rift just to the south of Lake Ziway (Woldegabriel et al. 1990). Further south, in the Bale area of the SE Plateau on the eastern rift shoulder, the Sanete Basalts and Batu Trachytes, representative of volcanic shields which form the second highest volcanic edifices in Ethiopia (Berhe et al. 1987), occur within the complexly faulted lineament referred to as the Goba - Bongo Line by Abebe et al. (1998). It has furthermore been suggested by Berhe et al. (1987) that the Reira Basalts, which also outcrop in the Bale area, represent the earliest volcanics emitted by the Sanete and Batu shields.

The only shield volcanoes that exist in SW Ethiopia are those associated with the Ambo or Addis Ababa - Nekempt Line referred to as the Yerer - Tellu Wellel volcanotectonic lineament (YTVL) by Abbate et al. (1998). They belong to the Welega Volcanic Group (Merla et al. 1979) and include the Tulu Wollel and Sayi shields as well as an undefined number of minor trachytic and phonolitic plugs. Berhe et al. (1987) suggest that the Welega Volcanic Group may be assigned to the Termaber Formation despite its younger age (15 - 7 Ma) and contrasting structural associations. Here, however, it is emphasised that the tectonic association of the group is more meaningful than its morphology and relative stratigraphic position above the main flood basalt pile in the SW Plateau. This distinction is supported by subtle differences in the geochemistry between the shield-volcanism along the transtensional lineaments and that represented by the Termaber and rift-shoulder shields that are not associated with cross-rift lineaments. In particular, phonolitic lavas are common in the volcanic shields located along the transtensional lineaments, and are rare in other parts of the Province. Berhe et al. (1987) suggests that this seems also to be a general feature of the difference between the magmatic centres of NW Ethiopia and SW Ethiopia. In the NW compared to in the SW, there are more silicic volcanics within and on top of the flood basalts, and phonolitic lavas are not at all common. Whether or not this is related to the presence in the NW, and absence in

the SW, of Mesozoic sediments between the basement and the base of the flood basalt pile (Fig. 2.2), remains to be investigated. Abbate & Sagri (1980) attribute the absence of Mesozoic sediments in SW Ethiopia to the possibility that the area formed a structural high during Mesozoic times.

The transtensional lineaments are geographically extensive structures that are the focus for volcanism with a range of compositions. Since they cut across other pervasive structures which may also serve as conduits for volcanic activity, it is sometimes impossible to determine which volcanic centres are primarily a result of transtensional tectonics as opposed to either uplift or extension. What is significant, however (in terms of the evolutionary stratigraphy of the Province) is the progressive younging, and decrease in alkalinity and silica undersaturation of volcanism along their length toward the rift zones. Formations, other than those already mentioned above, that may possibly be linked to such transtensional tectonism related to periodic adjustments in the stress field coincident with rifting include the Late Miocene Addis Ababa Basalts, the Pliocene Wechecha Formation and Bishoftu Basalts (Chernet et al. 1998), the Mid-Pliocene Salale Phonolites (Zanettin & Justin-Visentin, 1974), and the bimodal volcanics of the Wonchi Caldera (Woldegabriel et al. 1990) - all within the Addis Ababa Rift Embayment at the riftward end of the YTVL. It is possible also that the Tepi Basalts in SW Ethiopia (Davidson & Rex, 1980) are a result of transtensional stresses along the Tepi Fault Belt which cuts WSW obliquely across the western end of the Goba - Bongo Line (Fig. 2.2).

2.2.6 Border- and rift-fault volcanism

As described in Section 2.1.5, volcanic activity associated with the early stages of rifting became focused along extensional rift-parallel faults which today delineate the margins of the Southern Red Sea, Main Ethiopian rifts and the western sector of the Gulf of Aden. Similar fault structures are seen along the margins of the east and central Gulf of Aden and Northern Red Sea, but there is no significant reported volcanic activity associated with such structures in these areas. This is evident from the limited occurrence of volcanic lithologies in stratigraphic sequences reported for these parts of the Province (Fig. 2.8), and as a consequence they have been interpreted as non-volcanic rifted margins (Leroy et al. 2004). The volcanism associated with rift-faulting confined to the Western Gulf of Aden, Southern Red Sea and the Main Ethiopian Rift may then be related to the proximity of these parts of the intersecting arms of the triple junction, above the asthenospheric upwelling interpreted to be the Afar Plume. Such volcanism was responsible for the formation

of bimodal composite volcanoes and caldera complexes, and the extensive eruption of fissural and stratoid basalts which covered large area of the rift floors. Along the western and southern margins of Afar, the silicic volcanics erupted from the bimodal composite centres are represented by the Balchi Formation (Zanettin & Justin-Visentin, 1975), the Aliyu Amba and Shewa Robit Silicic Formations (Wolfenden, 2003), the Galemi Formation (Barberi et al. 1975; Chessex et al. 1975) and the Gara Gumbi Formation (Chernet et al. 1998). The silicic volcanics from the Mio-Pliocene shields Asebot, Afdem, Bora At and Gara Adi, in the Southern Afar marginal graben are also representative of such rift margin composite centres (Chernet et al. 1998). Pliocene basalts erupted along the Southern and Western Afar margins are nominally represented by the fissural basalts of the Bercha Basaltic Formation (Wolfenden, 2003) and the Dahla Basalts, and the stratoid basalts of the Afar Stratoid Series (Barberi et al. 1975; Chessex et al. 1975; Chernet et al. 1998; Wolfenden, 2003).

A stratigraphy for post-flood, syn-rift volcanism has not really been documented for the opposing eastern rift margins of the Red Sea in Yemen, to the same extent as it has been for the western margins as above. Ukstins et al. (2002) in fact maintain that, with the exception of two sets of dyke swarms along the southern Red Sea margins (Zumbo et al. 1995b), syn-rift volcanism is practically absent in Yemen. These dyke swarms, dated at 25.5 Ma and 18.5 – 16 Ma respectively by Zumbo et al (1995b), may represent feeder conduits for syn-rift lava sequences that have been removed by preferential erosion on the eastern side of the continental split.

In the Main Ethiopian Rift, equivalent rift-parallel, and border fault silicics, are represented by the Balchi and Butajira Ignimbrites in the central sector (Zanettin et al. 1974; Woldegabriel et al. 1990), and the Nazret Group (Juch, 1975; Kunz et al. 1975; Meyer et al. 1975; Morbidelli et al. 1975; Chernet et al. 1998), and the Kessem and Balchi Formations (Wolfenden et al. 2004) in the northern sector. Basaltic formations in the Main Ethiopian Rift with similar tectonomagmatic associations include the Bofa Basalts (Juch, 1975; Kunz et al. 1975; Meyer et al. 1975; Morbidelli et al. 1975; Chernet et al. 1998).

In the southern sector rift-fault volcanism appears to have occurred much earlier than in the central and northern sectors. It is represented by the Mid-Miocene Gerta and Kele Basalts and Mimo Trachytes, and since the rift is longitudinally segmented in the southern sector these formations occur across the rift repeatedly in association with the principal faults which segment the rift (Ebinger et al. 1993). It is still

questionable whether or not this volcanism can be linked to the Afar mantle upwelling and therefore be compared to similar volcanism further north. It is likely, however, that by the Mid- Miocene, the African plate would have moved sufficiently far north-eastward to place the southern sector of the Main Ethiopian Rift within the proposed influence of the Afar upwelling (George et al. 1998); in which case it may be assumed that all volcanism in this part of the rift, from this time onward was generated by the same mechanisms responsible for the equivalent volcanism to the north. Similarities in the trace element geochemistry of the Gerta and Kele Basalts, and picro-basalts and basanites from the Maichew area in the NW Plateau (Kabeto et al. 2004) seem to support this. Furthermore, the older ages for such syn-rift volcanism in the southern sector of the Main Ethiopian Rift are consistent with the assumption that rifting began in the south and propagated northward with time.

2.2.7 Rift-axis volcanism

The change in the stress field at the Pliocene-Quaternary boundary marked in the Main Ethiopian Rift by the decline in activity along the widely spaced faults of the rift margins, and the development of the densely fractured rift-axial magmatic segments of the Wonji Belt, was accompanied by a shift from predominantly alkaline to predominantly peralkaline volcanism (Boccaletti et al. 1999). This was manifested in the development of the aligned off-centre elongate silicic centres and scoria cones, and the eruption of fissural basalts, related to extensional fracture systems along the rift axis (Section 3.1.6). Almost everywhere the volcanism associated with these axial ranges is assigned to the Wonji Group (Fig. 2.8), apart from in the southern sector where it is represented by the Bobem and Nech Sar Basalts (Ebinger et al. 1993), and the Tosa Sucha Volcanics (George, 1997). In Afar, a similar shift from rift margin to axial range volcanism occurred during the from the Late Pliocene onward, and here it is generally assigned to the volcanic groups of the Axial Ranges (Barberi et al (1975); Chessex et al. 1975) and Bimodal Centres (Wolfenden, 2003). Volcanic formations representative of the axial ranges of southern Afar have been assigned by Chernet et al. (1998) to the Wonji Group since they are similar in age and composition to the equivalent formations further to the south in the Main Ethiopian Rift. Most are assigned to the magmatic segments in which they occur, and these generally take their name from the most prominent associated volcanic centre. These volcanic centres, referred to earlier in Section 2.1.7, include Erta Ale, Tat Ali, Ado Ale, Gablaytu, Gabilema, Dubbi, Dalaha'ale, Asa Gabalti and Eger. They occupy the principal rift zones within Afar, and like their counterparts in the Main Ethiopian Rift they have been interpreted as incipient spreading centres.

2.3 Timing of events

2.3.1 Introduction

As is evident from the previous section, it seems that, with the exception of continental flood volcanism which appears to be coeval across the Province, all subsequent phases of tectonomagmatic activity associated with the continuing process of continental break-up occurred at different times in different parts of the province. In this sense a time correlative stratigraphy is of limited use in defining a generalised chronology for the timing of related events across the Province. Instead, it is more meaningful to clarify when these events occurred in different parts of the province relative to one another. Here it is proposed that there are eight overlapping but distinctive phases of tectonomagmatic activity characterised by varying styles of volcanism attributable to discernable changes in the stress regime associated with the various stages of continental break-up concomitant with the evolution of the Afro-Arabian Volcanic Province. These phases may be related also to discernable changes in the geochemistry of the volcanism which reflect the changing nature of the interaction between the upwelling mantle and the continental lithosphere. Eight sequential tectonomagmatic phases are presented in Figure 2.10, and the timing of these for the Red Sea–Gulf of Aden and Main Ethiopian rifts is documented in Figure 2.11. Each phase is colour-matched between the figures and with the stratigraphic sections in Figure 2.8. The tectonic development of the triple junction relating to these phases is shown in Figure 2.12. With the exception of a few younger K-Ar ages which were considered reliable because of their consistent stratigraphic relationship with more recent $^{40}Ar/^{39}Ar$ dates, all age data for the timing of events shown in Figure 2.11 were determined by $^{40}Ar/^{39}Ar$ dating; in this respect it represents the most up-to-date chronology for the events that shaped the Afro-Arabian Volcanic Province. Each phase is described below.

2.3.2 Uplift and lithospheric attenuation

Combined fission track and $^{40}Ar/^{39}Ar$ data, together with field observations, suggest that, in Yemen, uplift preceded the initial stages of flood volcanism, and that there was no extension of the crust prior to this (Menzies et al. 1997). This would suggest that uplift was a direct result of the impingement of already buoyant mantle at the base of the continental lithosphere. Furthermore, it suggests that buoyancy of the mantle was not induced by decompression melting beneath lithosphere thinned by extension. Pre-volcanic (> 31 Ma) surface uplift is estimated to be in the order of tens of metres as indicated by the change shallow from marine to fluvial conditions

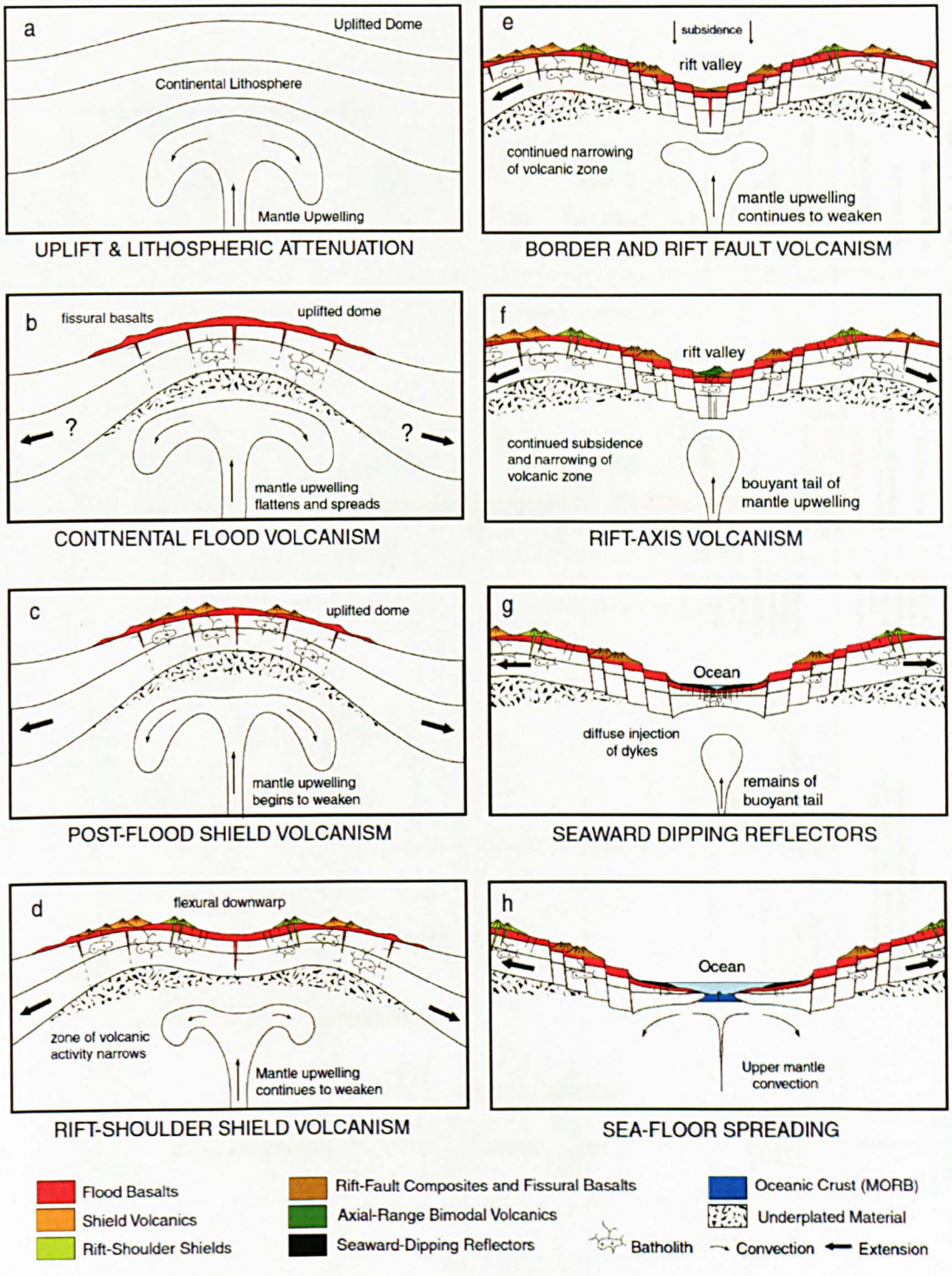

Figure 2.10 Tectonomagmatic phases in the evolution of the Afro-Arabian volcanic province

(evident in the sedimentary record of the upper part of the Tawilah Formation), and the subsequent subaerial development of palaeosols laterites, silicretes, and saprolites, prior to eruption of the Tertiary volcanics (Overstreet et al. 1977; Al'Kadasi, 1995; Al'Subbary, 1996). Uplift is thought to have continued contemporaneous with flood volcanism (31 - 26 Ma), and during this time no significant denudation or

Figure 2.11 Timing of events that shaped the Afro Arabian Volcanic Province

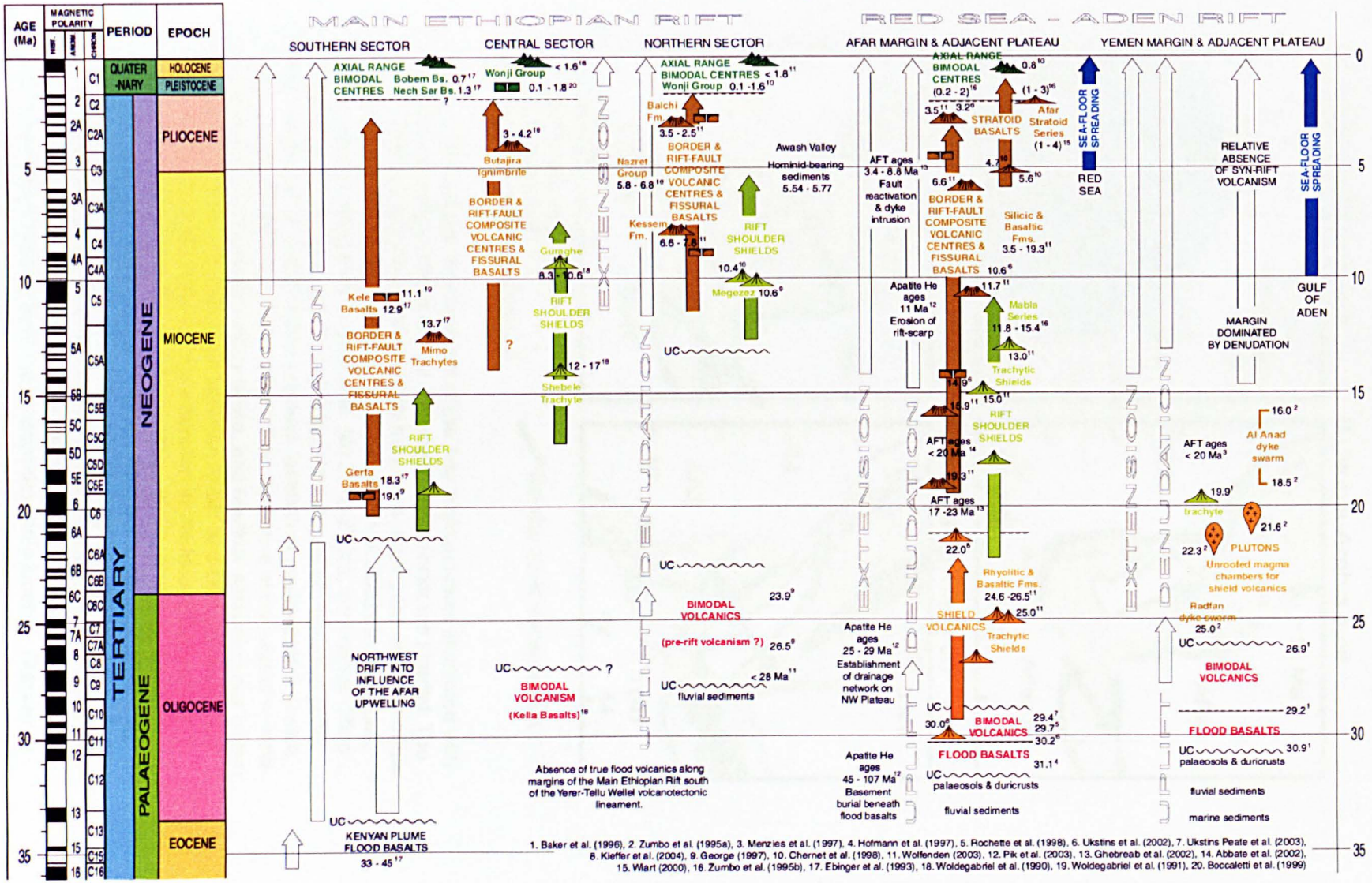

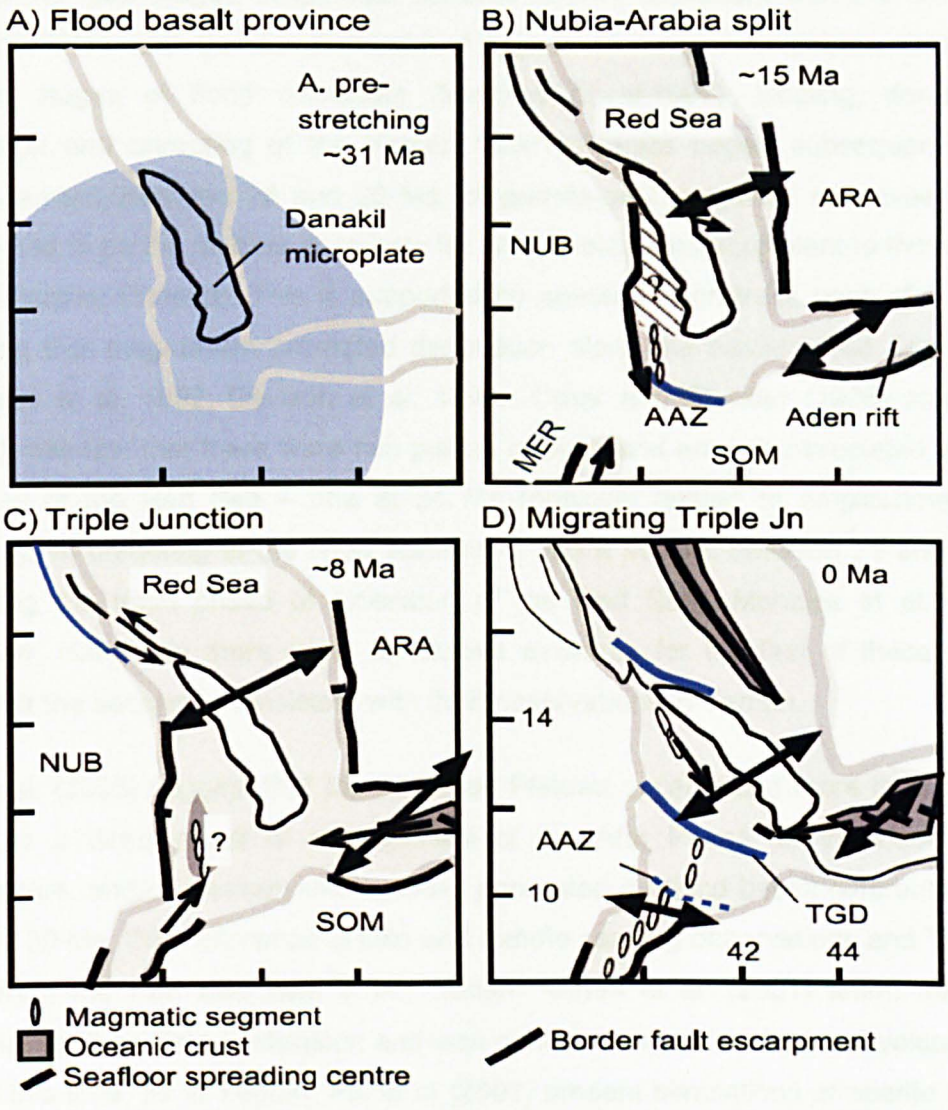

Figure 2.12 Tectonic development of the Afar triple junction, illustrated with snapshots of representative stages. Relatively rigid blocks are shaded. The lighter stippling indicates regions which may have undergone small amounts of extension. Plate reconstructions from (Eagles et al. 2002). In all stages, arrows indicate along-axis propagation. **(A)** 35 to 27 Ma, continental rifting commences in Red Sea and Gulf of Aden. Arcuate accommodation zone (AAZ -Tesfaye et al. 2003) marks previous location of southwestern Arabia. (B) By 15 Ma, rift basins in the southern Red Sea have accumulated several kilometers of volcano-sedimentary strata, and seafloor spreading has begun in the eastern Aden rift. Extension between Nubia and Danakil microplate may have initiated. **(C)** After 11 Ma, extension in the Main Ethiopian rift propagates northward to form a triple junction for the first time. Greatest stretching has occurred in southern Afar, where some oceanic crust may have been created by 8 Ma. **(D)** Along-axis propagation of the Gulf of Aden and Red Sea spreading centres induced renewed extension and volcanism between 4 and 2 Ma. Magmatic segments form in the Main Ethiopian rift as it propagates northward to form the present-day triple junction. Diagram is from Wolfenden et al. (2004).

extension took place. There is evidence for only minor syn-volcanic denudation toward the later stages of bimodal volcanic activity coincident with the decline in eruption rates and the development of high-level magma chambers during the closing stages of flood volcanism (Menzies et al.1997). Cooling, denudation, extension and unroofing of the Yemen flood volcanics began subsequent to the emplacement, between 26 and 20 Ma, of granite-gabbro-syenite intrusives (earlier suggested to be the magma chambers for shield volcanoes equivalent to those of the NW Ethiopian Plateau). This is supported by apatite fission track ages of < 20 Ma implying that magmatism pre-dated denudation along the eastern Red Sea margin (Menzies et al. 1992; Davison et al. 1994). Omar and Steckler (1995) and Omar (2001) maintain that there were two pulses of uplift and erosion associated with the opening of the Red Sea – one at 34 Ma (possibly related to emplacement and subsequent unroofing of the flood volcanics), and a second between 21 and 25 Ma (marking the main phase of extension of the Red Sea). Menzies et al. (1997), however, claim that there is no conclusive evidence for the first of these pulses, whereas the second is consistent with their observations in Yemen.

Pik et al. (2003) suggest that the Ethiopian Plateau experienced more than 1 km of uplift as a direct result of impingement of the Afar Plume on the base of the lithosphere, and/or massive underplating generated by flood basalt differentiation at around 30 Ma. With reference to field and remote sensing observations and $^{40}Ar/^{39}Ar$ data from the Red Sea Hills in NE Sudan, Kenea et al. (2001) affirm that such regional uplift predated extension and was contemporaneous with flood volcanism at about this time, as in Yemen. Pik et al (2003) present simulations of apatite He age partial resetting to support the implication that by 25 – 23 Ma erosion of the north-western flanks of the uplifted Ethiopian Dome had already begun, and that the elevated plateau topography, which today determines the drainage pattern for the whole of the Upper Nile catchment, was already well established by this time. Similarly, if it assumed that drainage off the dome was radial, then it likely that the catchment areas for rivers draining the southward and eastward off the SW Ethiopian and Yemeni Plateaux were also established at this time. Erosion of the rift scarp on the western Afar margin is estimated to have begun much later at about 11 Ma (Pik et al. 2003). It may be assumed therefore that much of the drainage pattern of the NW Plateau existed, as it does today, for more than 10 million years before the onset of rifting in the Red Sea. Crustal extension of the western Red Sea margin prior to rifting must have started at around 25 Ma contemporaneous with extension of the eastern margin. Apatite fission track ages for the Eritrean margin that indicate a

regional crustal cooling event attributable to an accelerated phase of denudation at around 20 Ma appear to confirm this (Abbate et al. 2002; Ghebreab et al. 2002). Ghebreab et al. (2002) also identify a second cooling event between 8.8 and 3.4 Ma; this may be attributable to localised age-resetting along faults reactivated and injected with dykes coincident with the rotation of the Danakil Block caused by sea-floor spreading in the Gulf of Aden, rather than to a period of accelerated erosion. Abbate et al. (2002) estimate overall rates of denudation along the Eritrean border-fault at 190 -200 m/myr compared to 60 -70 m/myr on the Ethiopian Plateau.

It is assumed that, since the main focus of the Afro-Arabian uplift was centred on the NW Plateau (Pik et al. 2003); uplift further south, adjacent to Main Ethiopian Rift would have been less pronounced, and would have occurred later than 30 Ma. An earlier phase of uplift associated with the Kenyan Dome may, however, have left the southern sector of the Rift relatively more elevated than the north before this time.

2.3.3 Continental flood volcanism

It is now generally accepted that Afro-Arabian flood volcanism occurred contemporaneous with uplift within a few million years around 30 Ma, and that it was more or less coeval across the province (Section 2.2.2). This is supported by a number of recent studies which have independently reached similar conclusions (Zumbo et al. 1995a; Zumbo et al. 1995b; Baker et al. 1996a; Hofmann et al. 1997; Rochette et al. 1998; Ukstins et al. 2002; Coulie et al. 2003). On account of its timing and duration, (beginning before 30 Ma in Chron C11r and ending before 29 Ma in Chron C10r), and its erupted volume (10^6 km^3 at a rate of 1 km^3/yr), the event has been correlated with a major δO^{18} excursion (Oi2) and an associated period of global cooling and sea-level change that brought about an extinction event that defines the Eocene – Oligocene boundary (Hofmann et al. 1997; Rochette et al. 1998). The huge input into the atmosphere of sulphur-rich aerosols and fine ash from the trappean eruptions coincident with long-term cooling may have accelerated global cooling and aridity, thereby leading to a major advance in the Antarctic ice-sheet, and a consequent drop in global sea-level of between 40 – 80 m (Rochette et al. 1998). Such environmental change may have led to a significant reduction in biological productivity which, in turn, brought about the extinction of many species (Hofmann et al. 1997; Courtillot et al. 1999; Wignall, 2001). The main phase of flood volcanism was dominated by tholeiitic to transitional basalts which are thought to represent the initial, relatively uncontaminated, and undifferentiated outpourings from the hot head of the mantle upwelling responsible for the uplift of the Afro-Arabian Dome. This

material is likely to have burnt its way through the uplifted, thinned, and fractured continental lithosphere to erupt on the surface through multiple fissures controlled by the diffuse stress regime associated with doming (Mohr, 1983). Successive eruptions from such fissures built up layer upon layer to form the stacked sequences which characterise the trappean landscape described in Section 2.1.2.

The transition from tholeiitic to alkaline magmatism marked by the switch from exclusively basaltic to bimodal volcanism, and the appearance in the sequence of rhyolitic ignimbrites, signified the waning of the mantle upwelling and the development of high level magma chambers in which ascending magma was trapped and allowed to differentiate before eruption. Ukstins-Peate et al. (2003) suggest that the silicic pyroclastics, which occur toward the top of the flood basalt pile, make up 20% of the total volume of the Afro Arabian Flood Basalt Province. The thickness of the larger ignimbrite units vary between 15 and 100 m and their volumes range from 150 km^3 to over 2000 km^3 - making them among the largest magnitude silicic pyroclastic eruptions on Earth. Some of these huge ignimbrite eruptions have been correlated with deep-sea tephra layers, marked by prominent magnetic susceptibility peaks, in the Oligocene section of ODP Leg 115 in the Southern Indian Ocean near the Madingley Rise, 2700 km to the southeast of the Ethiopian Traps (Ukstins-Peate et al. 2003; Touchard et al. 2003). Touchard et al. (2003) report that the tephra layers occur in the interval spanning Chrons C11n.2n to C11n.1n, and, on this basis they support the observations of Hofmann et al. (1997) and Rochette et al. (1998), that the trap-related emissions are synchronous with the Oi2 global cooling event. On the contrary, with reference to inherent errors in the chronostratigraphic timescale, Ukstins-Peate et al. (2003) argue that while the trappean emissions probably exacerbated global cooling they in fact marginally post-date the Oi2 cooling event.

Bimodal flood volcanism is estimated to have begun at about 30 Ma both sides of the Red Sea, although thereafter this transitional phase of volcanism seems to have continued for longer in Yemen (29.2 to 26.9 Ma – Baker et al. 1996a) than on the Ethiopian Plateau (30.2 to 29.4 Ma – Hofmann et al. 1997; Ukstins-Peate et al. 2003). The occurrence of alkaline flood basalts with ages of 26.5 and 23.9 (George, 1997) in the Kessem and Mugher Gorges respectively may suggest that bimodal flood volcanism continued for longer south of the CE Ethiopian Plateau adjacent to the Main Ethiopian Rift. However, although these basalts are seen to directly overlie Mesozoic strata, it is debatable whether or not they are, in fact, an integral part of the flood volcanic pile. An age of 28 Ma for the plateau basalts just to the north of the

Kessem Gorge (Wolfenden, 2003) may be more realistically ascribed to bimodal flood volcanism in this region.

With the exception of the flood basalts of the SW Plateau, which are here attributed to Eocene flood volcanism associated with the Kenyan Plume (George et al. 1998), there seems to be a relative absence of 'true' tholeiitic flood basalts south of the Central Ethiopian Plateau. The Ambo Fault, which marks the northern margin of the Yerer-Tellu Wellel volcanotectonic lineament, appears to form a natural limit for the Oligocene tholeiitic flood volcanism (Fig. 2.2). South of this divide all reported flood volcanics are dominantly alkaline in composition and they are characteristically bimodal.

It is likely that, coincident with flood basalt volcanism, huge volumes of differentiated material accumulated at the base of the crust, and that this contributed to the uplift of the Afro-Arabian Dome (Pik et al. 2003). This is implied by recent seismic studies which have identified the presence of a high velocity layer beneath the western margin of the Main Ethiopian Rift (Fig. 2.7) (Mackenzie et al. 2004; Keller et al. 2004; Maguire et al. 2004).

2.3.4 Post-flood pre-rift shield volcanism

The initial weakening of the Afar mantle-upwelling and the consequent slowing in the rate of uplift during the Oligocene through to the early Miocene saw the widespread development of volcanic shields across the NW Ethiopian and western Yemen plateaux within a broad area around the apex of uplift (Section 2.1.3). The remnants of these shields still sit conspicuously on top of the NW Ethiopian Traps whereas in the Yemen they have been removed by erosion; their absence in other parts of the province may be because these regions were not sufficiently affected by the stress regime associated with uplift and extension to generate the conditions necessary for their formation. The post-flood pre-rift shields were built from the range of differentiated products allowed to evolve in high-level magma chambers periodically recharged with material from the mantle upwelling; the bimodal character of their constituent lava sequences are testimony to this process. New influxes of material from the mantle-upwelling may have been encouraged by early periods of extension which may have further stretched and thinned the lithosphere thereby accelerating melting as a result of decompression, and/or opening fractures that served as conduits for passage of magma into the magma chambers and upward toward the surface.

The bimodal volcanics of the post-flood pre-rift shields are not dissimilar to those of the upper bimodal trap sequences in that they comprise alternating layers of alkaline basalts and interbedded silicic volcanics. This similarity, together with the fact that many of the shields grew seamlessly on top of the traps and probably were initially fed by the same fissures, makes the transition between the two difficult to define (Kieffer et al. 2004). Although not always apparent from field observations, the distinction between the two phases is more typically characterised by a shift from fissural to central-vent volcanism rather than by a discernable change in the composition of the lavas.

2.3.5 Rift-shoulder shield volcanism

Crustal extension together with the continued weakening of mantle upwelling caused a down-warping of the crust to create the embryonic conditions for the subsequent formation of the rift zones (Mohr, 1983). Flexural fissures dipping away from the axis of down-warping developed on the adjacent shoulders of the downwarp as a consequence. These away-from-rift-dipping fractures described in Section 2.1.6 have been identified on both sides of the Red Sea and Gulf of Aden (Drury et al. 1994; Fantozzi, 1996). Some appear to have served as conduits for dyke intrusion and surface volcanism, and so became the focus for the development of the rift shoulder shields described in Section 2.1.5. Like the post-flood pre-rift shields, the rift-shoulder shields were probably fed by similar high-level magma chambers which allowed the generation of the same range of differentiated products; as a consequence, morphologically and compositionally they are indistinguishable from the post-flood pre-rift shields. They are told apart from the post-flood pre-rift shields only by their relatively younger age (< 20 Ma) and structural association with flexural fissures on the rift-shoulders.

Rift-shoulder volcanism represents the initial phase in the narrowing of the volcanic zone. The ages of rift-shoulder volcanics along the Red Sea rift extend roughly from 20 to 10 Ma. Shields within a similar age range on the adjacent plateau, not located along the rift shoulders, are likely to be associated with transtensional structures similar to the Axum Adua Line and Yerer-Tullu Wellel volcanotectonic lineament.

Although there are no documented rift-shoulder shields along the Southern Main Ethiopian Rift, the fact that rift-fault volcanism in the area was already established by 19.1 Ma (George et al. 1997) and 18.3 Ma (Ebinger et al. 1993) suggests that by this time such shields might already have been emplaced. Age determinations for rift-

shoulder volcanics in the central sector of the Main Ethiopian Rift span from 17 to 8.3 Ma (Woldegabriel et al. 1990); whereas in the northern sector, they cluster around 10 Ma (George, 1997; Chernet et al. 1998). Overall, there appears to be a progressive younging of rift-shoulder volcanism from south to north in the Main Ethiopian Rift. This suggests that propagation of the rift was, likewise, south to north as proposed by Ebinger et al. (2004) and Wolfenden et al. (2004), rather than from north to south, as would be expected if the rifting was initiated by the same mechanisms as along the Red Sea and Gulf of Aden Rifts. The time gap between the initiation of rift-shoulder volcanism along the western Afar margin and the adjacent northern Main Ethiopian Rift, together with the overall south to north direction of propagation of the rift, might suggest that the Main Ethiopian Rift is not a primary feature of continental break-up above the Afar mantle upwelling (Ebinger et al. 2004).

2.3.6 Border and rift-fault volcanism

Further weakening of the Afar mantle upwelling, continued lithospheric extension, and the consequent accelerated subsidence, led to the brittle fracture of the crust and the development of widely-spaced, riftward-dipping normal faults which controlled the initial formation of the rifts. These rift-faults became the foci for sporadic eruptions of fissural basalts and the development of large bimodal composite volcanic centres fed by shallow-seated magma chambers (Section 2.1.6). Although the composition of the volcanics associated with this phase in the development of the rift remained dominantly alkaline, the stress regime that controlled the volcanism had shifted from one dominated by uplift and subsidence to one dominated by extension. This served to focus volcanism in and immediately adjacent to the rifts, thereby further narrowing the volcanic zone.

Rift-fault fissural and composite volcanism on the western Red Sea margin began in the early Miocene as early as 19.3 Ma and continued in the Afar region well into the Quaternary period (Wolfenden, 2003). Although syn-rift volcanism is considered to be virtually absent along the eastern Red Sea margin, the presence of the two phases of dyke intrusion at 25 Ma, and between 18.5 and 16 Ma respectively in southern Yemen suggest that rift-fault volcanism was at one time present in the region, but has since been removed by erosion (Zumbo et al. 1995a). It is debatable also whether or not the contemporaneous alkaline volcanism that formed the Harrats further to the north in Saudi Arabia is representative of this period of rift development (Section 2.1.6). In the Main Ethiopian Rift, rift-fault volcanism shows a similar south to north younging in age to rift-shoulder volcanism.

2.3.7 Rift-axis volcanism

Continued crustal attenuation as a result of ongoing extension, and a relative relaxation in the rate of subsidence and mantle upwelling, gave rise to a third phase in the narrowing of the volcanic zone marked by a decline in alkaline volcanism along the widely-spaced rift-faults, and a concentration of alkaline to peralkaline volcanism along the narrow densely-faulted magmatic segments of the rift-axis. Recent seismic imaging (Mackenzie et al. 2004; Keller et al. 2004; Maguire et al. 2004) has confirmed that these magmatic segments represent the extensional axis of the rifts as proposed by Boccaletti et al. (1999) and Wolfenden et al. (2004). It is further suggested by Lahitte et al. (2003a-b) and Kernanen (2004) that the extensional fractures along the lengths of the magmatic segments in fact represent incipient spreading centres. The volcanism associated with the magmatic segments has led to the development of distinctive axial ranges characterised by prominent silicic volcanic centres and fields of fissural basalts (Section 2.1.7). The axial ranges developed through the profuse injection of dykes, and the periodic explosive eruptions of silicic volcanics fed from shallow seated magma chambers beneath the rift axis.

The development of the axial ranges began at the beginning of the Quaternary period at about 2 Ma in the Afar region (Zumbo et al. 1995b), slightly later at 1.8 Ma in the Main Ethiopian Rift. Such development is still ongoing today in both these active rifts, and it must have occurred sometime much earlier in the central Red Sea and the western Gulf of Aden prior to the initiation of seafloor spreading in these regions.

2.3.8 Seaward-dipping reflectors

Extreme crustal thinning as a result of continued extension and the progressive replacement of upwelling mantle by normal mantle convection marks the decline of silicic volcanism and the subsequent profuse injection of dykes into thinned and thermally weaken crust together with the widespread eruption of layer upon layer of associated alkaline to transitional fissural basalts. These lavas are subsequently tilted riftward to form seaward dipping reflector sequences which become submerged beneath the developing ocean as a result of continued subsidence and extension. The emplacement of seaward dipping reflectors represents the final stage in the narrowing of the volcanic zone prior to the onset of seafloor spreading. However, since no age data for this tectonomagmatic phase is presented here, it does not feature in Figures 2.8 and 2.11. It is assumed that seaward-dipping reflector sequences were emplaced prior to the advent of seafloor spreading at about 5 and 10 Ma in the Red Sea and Gulf of Aden respectively although there is no evidence of

this. Ebinger et al. (2004) suggests that the emplacement of seaward dipping reflectors is ongoing in the Main Ethiopian Rift.

2.3.9 Sea-floor spreading

The transition from continental to oceanic rifting and the initiation of seafloor represents the final separation of continental crust and the subsequent generation of new oceanic crust coincident with the establishment of 'normal' upper mantle convection. True seafloor spreading had become established by the Middle to late Miocene at about 10 Ma in the Gulf of Aden and later during the Pliocene at about 5 Ma in the Red Sea. The current extent of new ocean crust in these regions is shown in Figure 2.2.

2.3.10 Tectonic development

Recent geochemical and geophysical data for the propagating rift zones of the Red Sea and Gulf of Aden suggest that the two arms are becoming connected through Afar rather than joining through the Straits of Bab el Mandeb as might be expected. This deviation from the expected course was probably controlled by structural weaknesses in the crust (Manighetti et al. 1997). Ayele et al. (2004, 2007) suggest also that a possible coupling of the Danakil micro-plate with the Arabian plate forced the Aden and Red Sea rifts along the respective continental margins into Afar. This is in good agreement with the ideas that rifting occurs close to the boundary between continental and oceanic crust, and that it will exploit existing weaknesses that are preferentially developed in the continental crust. If it is accepted that the Afar Plume impinged on the lithosphere prior to rifting, the thermal impact of such impingement may have further weakened the crust beneath the Afar Depression, thereby making more it susceptible to rift propagation.

The rate of rift propagation along both the Red Sea and Aden arms, and the associated opening of the respective Afro-Arabian Ocean seem fundamentally controlled by the relative plate motions of the Nubian and Somalian plates and the Arabian plate. Current estimates for the rates of plate movement between these plates vary enormously (DeMets et al. 1990; Argus and Gordon, 1991; DeMets et al. 1994a-b; Kreemer et al. 2003). Predictions of the NE movement of the Arabian Plate relative to the Eurasian Plate vary between 30.5 mm/yr (DeMets et al. 1994) and 22.1 mm/yr (Kreemer et al. 2003), whereas predictions for the more NNE movement of the Nubian Plate relative to the Eurasian Plate vary between 10 mm/yr (DeMets et al. 1994a) and 6 mm/yr (Kreemer et al. 2003). Most importantly, all estimates of plate

motion show that Arabia is moving north-eastward faster than Africa, and it is this preferential movement, as a result of subduction beneath the Eurasian Plate, that is primarily responsible for the opening of the Afro-Arabian Ocean (Fig. 2.1). The maximum extent to which this ocean will be able to open will be limited to the space between it and the convergent margin to the northeast along the Zagros Mountains, before the ridge itself is subducted and the ocean is subsequently closed by the continued northeast advancement of the Nubian Plate.

Despite the fact that the axial zones of the magmatic segments of the Wonji Fault Belt have been interpreted as incipient spreading centres (Keranen et al. 2004), it is still debatable whether or not the Main Ethiopian Rift will develop as an ocean spreading centre. The current E – W extension of the rift has been related to the relative motion between the Nubian and Somalian plates, but south of 20° S there is little (if any) expression of deformation and seismicity to mark relative motion between these plates. In order for an ocean to open between the Nubian and Somalian plates the boundary between the two must extend southward until it intersects another plate boundary. Chu and Gordon (1999) and Lemaux et al. (2002) argue that this boundary cuts along the East African Rift and continues southward until it intersects the Southwest Indian Ridge along the Andrew Bain Fracture Zone, which is interpreted to have been slowly spreading (2 mm/yr) over the past 11 million years. If this is the case, then oceanization of the Main Ethiopian Rift may occur, but the extent to which the resultant ocean will be allowed to open will be restricted by the absence, between it and the Central Indian Ridge, of an active convergent margin, necessary to accommodate the eastward movement of the Somalian Plate. Current estimates of extension across the East African Rift range from between 4 mm/yr (Bilham et al. 1999) and 6 mm/yr (Chu & Gordon, 1999; Sella et al. 2002) to 1.6 mm/yr (Kreemer et al. 2003). Kreemer et al. (2003) dispute that there is any discernable movement further south along the extension of the boundary between the Somalian and Nubian plates as proposed by Chu & Gordon (1999) and Lemaux et al (2002). This might suggest that any movement still ongoing in the East African and Main Ethiopian rifts is a result of intraplate stresses associated with localised uplift caused by the upwelling of the Afar and Kenyan plumes (Coblenz & Sandiford, 1994), and that as these stresses relax, extension will slow and ultimately cease, leaving the rifts as a failed arm. In this respect the role of plumes, or at least of upwelling thermally buoyant mantle, appears to be a fundamental influence on the process of rifting, however, the contributory role of such phenomena in the process of continental break-up still remains poorly understood.

It seems more likely that the over-riding control on the geometry of continental break-up between Africa and Arabia is principally attributable to far-field stresses arising from plate tectonic processes; the Afar mantle upwelling seems to have played a secondary role in the process by weakening the lithosphere in the region around the current position of the triple junction. The current position of the triple junction has been identified by Wolfenden (2003) as a broad sub-circular area, of about 300 km in diameter, centred on the intersection of the Main Ethiopian Rift with the Tendaho Goba' ad Discontinuity which marks the southern boundary of the Afar Depression. The three rift arms are evidently propagating toward this point of intersection rather than away from it, as would be if the Afar Plume had initiated the process of continental break-up as in the conventional model of active rifting. The fact that the earliest phase of opening of the Afro-Arabian Ocean along the eastern section of the Gulf of Aden appears to have been a passive process (Leroy et al. 2004) is also at odds with the model of active rifting. On the other hand it is generally accepted that the uplift of the Ethiopian and Yemeni Plateaux and the synchronous eruption of the flood basalts which formed the plateaus are attributable to the upwelling of the Afar Plume, and that these events predated rifting and continental break-up. This might suggest that the impingement of the plume at the base of the lithosphere played a more active role in continental break-up than suggested by the structural evidence previously described. Within the framework of current ideas on rifting and continental break-up, it is difficult to equate these contradictions. We cannot discount the fact that the origin and evolution of the Afar Plume may have been entirely independent of the processes that have led to continental separation; however, it is inescapably circumstantial that the focus of the plume is centred on the region defined by the triple junction. This raises the question, of what came first - the plume or the split? More aptly, did upwelling of the mantle stretch and thin the lithosphere prior to rifting? Or, did thinning of the lithosphere, as a result of tectonically driven extension, lead to the decompression melting and consequent upwelling of the mantle? If the lithosphere was thinned by the impact of an upwelling plume, then we have to look for a possible boundary layer from which the plume originated. Moreover, we have then to explain how the boundary layer disturbance that generated the plume happened to have occurred directly below a lithospheric suture, the geometry of which may be easily explained in terms of surface tectonics.

In order to address the above questions it is essential to characterise the source of the upwelling and establish the depth at which melting of the mantle occurred. From this, inferences may be then made regarding the nature of the source region and the

relative timing of interaction between the lithosphere and upwelling mantle; furthermore, by comparing the trace element and isotopic characteristics of the primary source material (represented by the more primitive uncontaminated flood basalts) with the more evolved products from more recent volcanism, inferences may be made on the how this interaction changed over time as the process of continental break-up progressed. Such fundamental issues are addressed in this thesis.

2.4 Source of the magmatism

2.4.1 Introduction

Like other continental flood basalt provinces, the Afro-Arabian province comprises a great diversity of volcanic rocks which are variably fractionated and modified by magma mixing and crustal contamination. As much as this diversity allows us to unravel the processes that have affected the evolution of the magmatism through time, the degree to which such processes have modified the magmas that feed the volcanism often obscures any signature of the source. The majority of geochemical studies have concentrated on recent volcanic rocks in the rifts and Afar (Barberi et al. 1980; Brotzu et al. 1981; Betton & Civetta, 1984; Hart et al. 1989; Barrat et al. 1990, 1993; Vidal et al. 1991; Gasparon et al., 1993; Marty et al. 1993, 1996; Deniel et al. 1994; Barrat et al. 1998; Trua et al. 1999, Peccerillo et al. 2003, Furman et al. 2006), and most propose the involvement of the Afar mantle plume variably mixed with HIMU-like lithospheric mantle and depleted (DM and PREMA), and/or enriched (EM-like) mantle components. The number of studies on the Oligocene flood basalts is somewhat more limited. Hart et al. 1989; Vidal et al. 1991, Deniel et al. 1994 analysed some lavas which were contemporaneous with the flood basalts. These basalts have trace element and isotopic (Sr, Nd, and Pb) characteristics intermediate between EM I and EM II mantle, and such compositions are attributed to old enriched lithospheric mantle. Similar conclusions were reached for the flood basalts from Yemen (Chazot and Bertrand, 1993; Baker et al. 1996a-b) and southern Ethiopia (Stewart and Rogers, 1996). Baker et al. (1996) suggest that the EM signature recognized in the Oligocene basalts of western Yemen also reflects upper and lower crustal contamination of Afar plume-derived magmas. The possible role of the Afar mantle plume modified by both lithospheric and crustal components has also been recognised in the flood basalts from the NW Ethiopian Plateau (Pik et al. 1998, 1999).

2.4.2 Flood basalts from the NW Ethiopian Plateau

The lavas of the NW Plateau form three distinct groups referred to by Pik et al. (1998) as the LT, HT1 and HT2 basalts. The groups are classified according to their TiO_2 content and this is expressed geographically rather than temporally (Fig. 2.13). The LT basalts, which occupy the northwest part of the plateau, are transitional to tholeiitic and show consistently low TiO_2, P_2O_5, and Fe_2O_3* and high SiO_2 contents, and considerable heterogeneity in their trace element geochemistry. The HT2 basalts, which occur in the southeast part of the plateau, on the other hand are generally sub-alkaline and have consistently high TiO_2, P_2O_5, and Fe_2O_3* and low SiO_2 contents, and relatively homogeneous trace element signatures compared to the LT basalts. The HT1 basalts display characteristics between the other two groups, and occur stratigraphically above and below the HT2 basalts within the southern-central part of the plateau. Marked troughs for Th and Ta-Nb, and variable LREE enrichment in the LT basalts suggest that they have undergone significant crustal contamination, and that they were possibly derived from a LREE-depleted garnet-free source. In contrast, consistent enrichment of LREE and a relative depletion of HREE in the HT2 basalts suggest the presence of residual garnet in their source, and that they have experienced little, if any, contamination with crustal material. These observations, together with consistent differences in the petrography and mineral chemistry of the two lava groups imply that, whereas the LT basalts have undergone shallow level fractionation and contain a significant lithospheric component, the HT2 basalts fractionated at a much deeper level and made their way directly to the surface with little or no interaction with the crust en route (Pik et al. 1998, 1999). This is supported by distinctive geochemical trends for both lava groups which are difficult to relate to one another through differentiation. The HT1 basalts show characteristics of shallow level fractionation and lithospheric interaction similar to the LT basalts and source characteristics similar to the HT2 basalts; their geochemical trends are also difficult to relate to the other lava groups through differentiation. On this basis, Pik et al. (1998, 1999) propose that all three groups were derived from different parental magmas even though they suggest that the geochemical differences between the HT1 and HT2 basalts may reflect the variable involvement in their genesis of a deep mantle component.

Despite the wide variation in major and trace element compositions for the three lava types, their Sr, Nd and Pb isotopic ratios show a restricted range ($^{87}Sr/^{86}Sr$ = 0.70304–0.70429, $^{143}Nd/^{144}Nd$ = 0.51271–0.51298, $^{206}Pb/^{204}Pb$ = 18.00–18.86) which is suggestive of a common origin. Pik et al. (1999) suggest that, within this

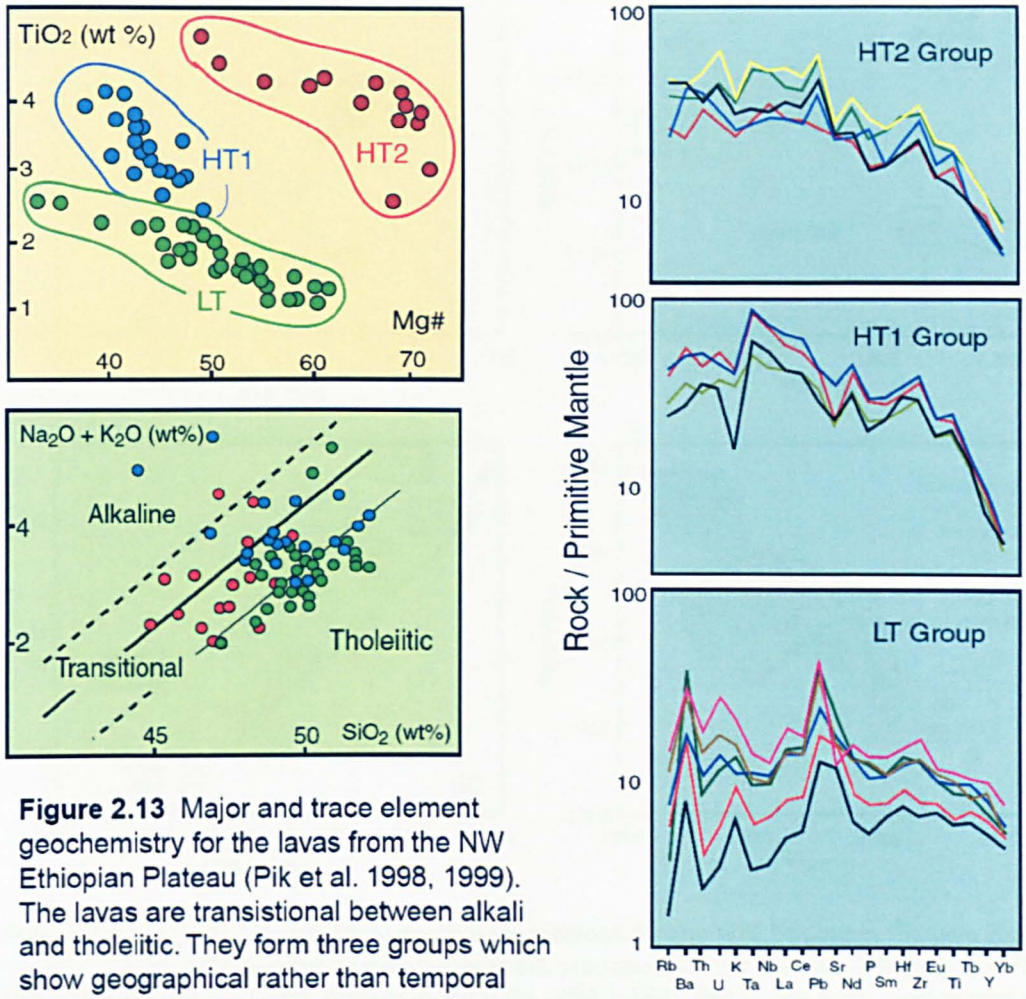

Figure 2.13 Major and trace element geochemistry for the lavas from the NW Ethiopian Plateau (Pik et al. 1998, 1999). The lavas are transistional between alkali and tholeiitic. They form three groups which show geographical rather than temporal variation (see map below).

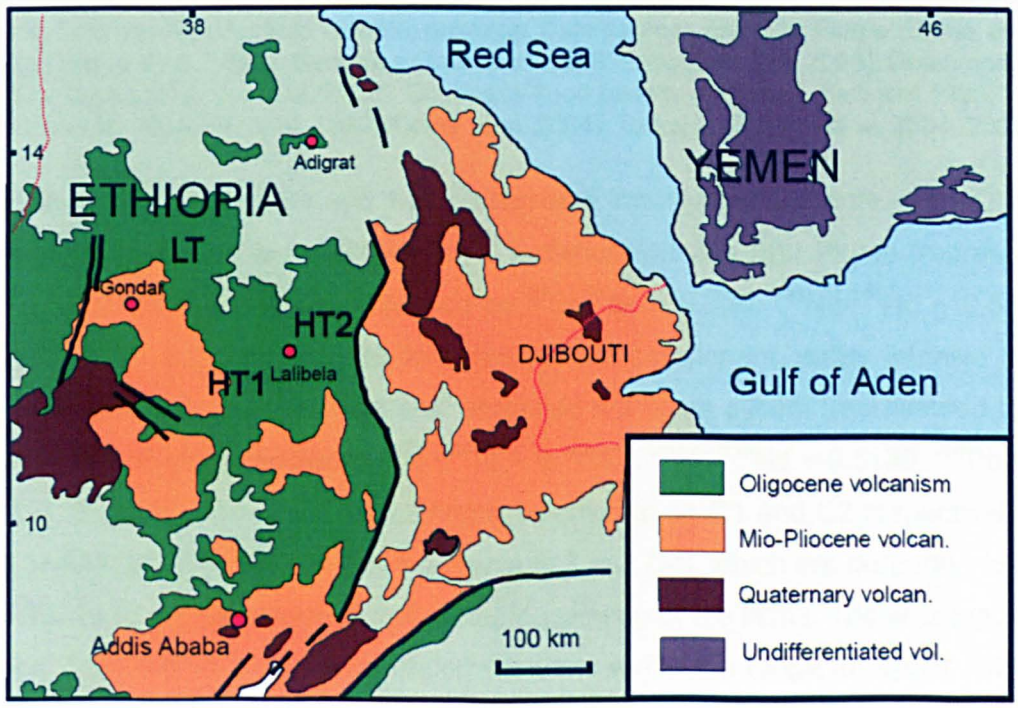

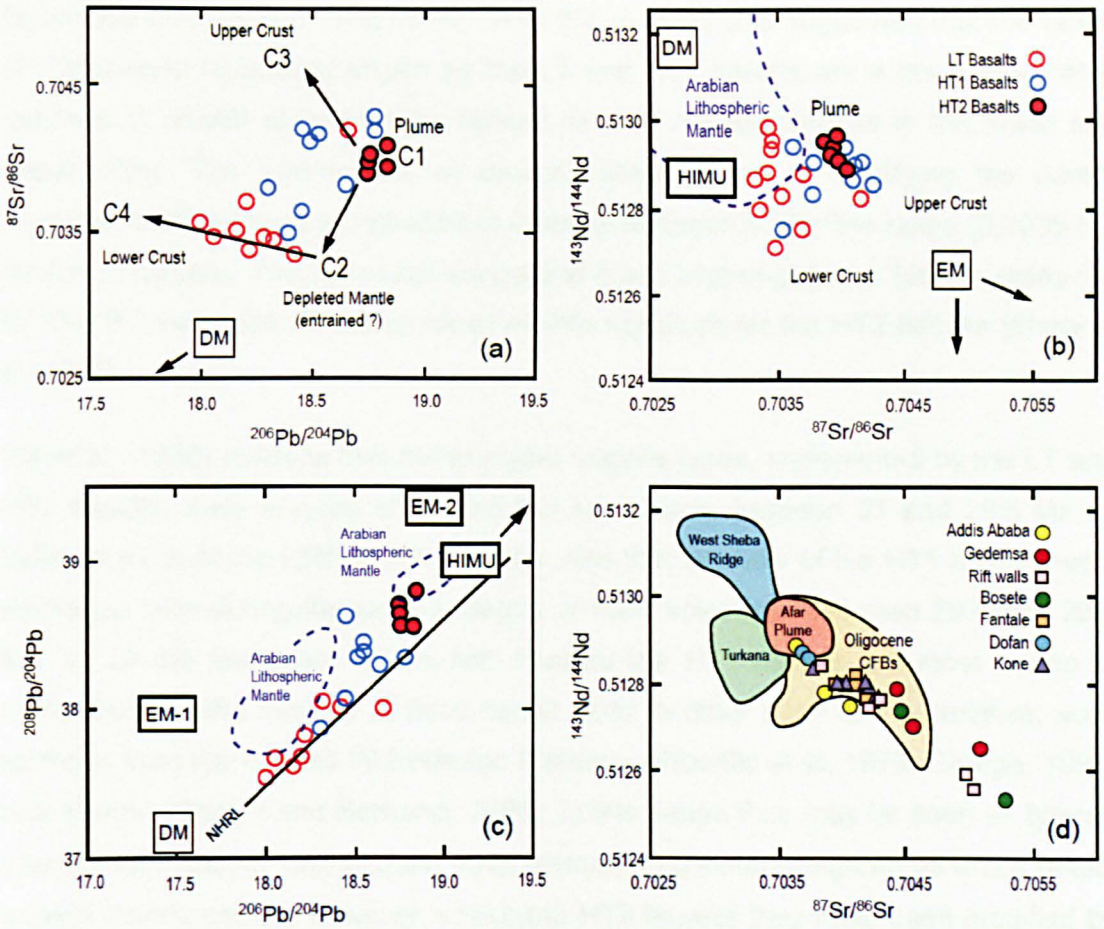

Figure 2.14 (a) - (c) Sr-Nd-Pb isotopic compositions for the NW Ethiopian Plateau basalts. C1, C2, C3, and C4 are the four end-members proposed for the basalts (Pik et al. 1999). The main mantle reservoir compositions (DM, HIMU, EMI, EM II) are from Zindler and Hart (1986), and the Arabian lithospheric mantle fields are from Henjes–Kunst et al. (1990), Bluztajn et al. (1995) and Baker et al. (1998). **(d)** $^{87}Sr/^{86}Sr$ vs $^{143}Nd/^{144}$ Nd for basaltic lavas from the Afro-Arabian volcanic province. Data sources are: Afar Plume (Deniel et al. 1994; Barrat et al. 1998); Gedemsa (Trua et al. 1999; Peccerillo et al. 2003); Dofan and Addis Ababa (Furman et al. 2006); Oligocene flood basalts (Chazot & Bertrand 1993; Baker et al. 1996; Pik et al. 1999; Kieffer et al. 2004); Turkana (Furman et al. 2004, 2006).

restricted range, there are still two discernable mantle components – an OIB-like component proposed to reflect the initial material from the Afar Plume (represented by the HT2 basalts and characterised by $^{87}Sr/^{86}Sr$ ~ 0.704, $^{143}Nd/^{144}Nd$ ~ 0.51295, $^{206}Pb/^{204}Pb$ ~ 18.8) and a more depleted mantle component, either intrinsic to the plume itself or inherited from material entrained during its ascent (represented by the LT basalts and characterised by $^{87}Sr/^{86}Sr$ ~ 0.7033, $^{143}Nd/^{144}Nd$ ~ 0.5130, $^{206}Pb/^{204}Pb$ ~ 18.6). In addition to these components, referred to as C1 and C2 respectively, Pik et al. (1999) identify two other components (C3 and C4), which are purported to have contributed to the geochemical and isotopic variation of the lavas. These components display trace element and isotopic compositions within the range for upper (C3) and lower (C4) Pan-African crust with unradiogenic Pb isotopic compositions and variable

Sr isotope compositions (Fig. 2.14). With this in mind, it is suggested that the range of lithospheric signatures shown by the LT and HT1 basalts are a result of variable degrees of crustal contamination related to their residence-times in the lower and upper crust. The involvement of crustal contamination in modifying the parent magmas of these lavas is reflected in strongly radiogenic $^{3}He/^{4}He$ ratios (0.0035 R_a) for the LT basalts. This is in stark contrast to much less radiogenic $^{3}He/^{4}He$ ratios (up to 19.6 R_a) indicative of a deep lower mantle signature for the HT2 basalts (Marty et al. 1996).

Pik et al. (1998) propose that the principal magma types, represented by the LT and HT2 basalts, were erupted at around the same time, between 31 and 29.5 Ma, in different parts of the uplifted NW Plateau, and that the bulk of the HT1 basalts were emplaced later during the closing stages of flood volcanism between 29.4 and 26.4 Ma. Of all the lava-types of the NW Plateau the HT1 basalts are most similar in composition to the majority of flood basalt lavas in other parts of the province, such as those from the CE and W Ethiopian Plateaux (Piccirillo et al. 1979; George, 1997) and Yemen (Chazot and Bertrand, 1993); in this sense they may be seen as typical. Like the HT2 basalts they contain trace element and isotopic signatures which reflect a deep mantle source, however, unlike the HT2 basalts they have been modified by variable degrees of deep- and shallow-level fractionation, and crustal contamination, and therefore cannot be considered as representative of a primary magma. Likewise, the LT basalts have been modified by a series of high-level processes such that signatures of the origins of their primary source material have become indecipherable. Pik et al. (1998) further maintain that because of their elevated MgO contents the HT2 basalts also cannot be considered as representative of the primary magma since such elevated MgO contents are a consequence of olivine accumulation. Nevertheless, whereas the LT and HT1 basalts have compositional ranges similar to low-Ti and high-Ti basalts from other continental flood basalt provinces such as the Deccan (Lightfoot et al. 1993), Parana (Peate et al. 1999) and the Siberian Traps (Lightfoot et al. 1990; Wooden et al. 1993), the HT2 basalts exhibit limited extreme OIB-like compositions which are quite unusual and isotopically close to a depleted primitive mantle end member component (PREMA, FOZO, PHEM or C – Fig. 1.15). Such a composition is indicative of a deep mantle origin, and in this sense the HT2 basalts can at least be regarded to reflect the nature of this origin despite the fact that their compositions may, in part, have been determined by variable degrees of differentiation. Compared to the compositionally diverse lavas from across the

province (Fig. 2.14d), the HT2 basalts at least represent a relatively unmodified analogue of the parent source.

2.4.3 Seismic tomography

Seismic tomographic images for the mantle beneath Afar show a plume-like structure extending upward from the core-mantle boundary (Ritsema et al. 1999, Gurnis et al. 2000; Nyblade, 2000; Nyblade et al. 2000a-b; Montager 2001; Ritsema & Allen, 2003) (Fig. 1.6). This might suggest that the origins of the Afar mantle plume are rooted at the core-mantle boundary. More recent finite frequency tomographic images, however, show that the mantle upwelling beneath Afar extends no deeper than the 660 km discontinuity (Nolet et al. 2003, 2007). If indeed there is a contribution from the core in the origin of the Afar mantle upwelling, there is a possibility that it will be reflected in the osmium isotopic composition of the uncontaminated HT2 basalts.

3. LAVA SEQUENCES OF THE NW ETHIOPIAN PLATEAU

3.1 The NW Ethiopian Plateau

3.1.1 Geography

The NW Ethiopian Plateau is the most elevated part of the Afro-Arabian Volcanic Province, and is generally considered to have been the principal focus for uplift associated with the Afar mantle upwelling during the Oligocene through to the early Miocene. It forms a deeply incised, expanse of tableland that fans broadly westward from the northeast plateau rift-escarpment, which drops over a kilometre into the Danakil Depression (Fig. 3.1). Its northern and southern margins are defined respectively by the Tekeze and Blue Nile river canyons, and its western margin descends gently from the lip of the Tana Graben into the deserts of Sudan. The average elevation of the NW Plateau is over 2000 m, and its tableland commonly flattens at levels in excess of 3000 m. The prominent volcanic shields which sit on top of this tableland, including Ras Dashen (4623 m) in the Simien Mountains, Mt Guna (4231 m) and Mt Choke (4100 m) are among the highest peaks in Africa, and as a consequence the region is often referred to the Ethiopian Highlands.

The climate of the NW Plateau, like the rest of Ethiopia, varies according to its elevation. Below 1830 m it is tropical with an average temperature of 27 °C and an annual rainfall of 510 mm, however, for most of the Plateau (between 1830 and 2440 m) it is sub-tropical, with an average temperature of 22 °C and an annual rainfall between 510 and 1525 mm. Above 2440 m the climate becomes temperate, with an average temperature of 16 °C and an annual rainfall between 1270 and 1780 mm. The main rainy season extends from mid June through to September following a long dry season sometimes interrupted by a short rainy season in February or March.

The main surfaced roads which cut across the NW Plateau are shown in Figure 3.3. Other than these, the majority of roads in the region are not surfaced and as a consequence they can become difficult to navigate during the rainy season. The region is also served by local airports at Dessie, Bahar Dar, Gondar, Lalibela and Mekele, and internal flights run daily between these destinations from the main international airport at Addis Ababa.

3.1.2 Geology

The lavas of the NW Plateau have traditionally been sub-divided into three formations – the Ashange, which forms the base and lower portion of the Oligocene

Figure 3.1 Composite Thematic Mapper Image of the NW Ethiopian Plateau

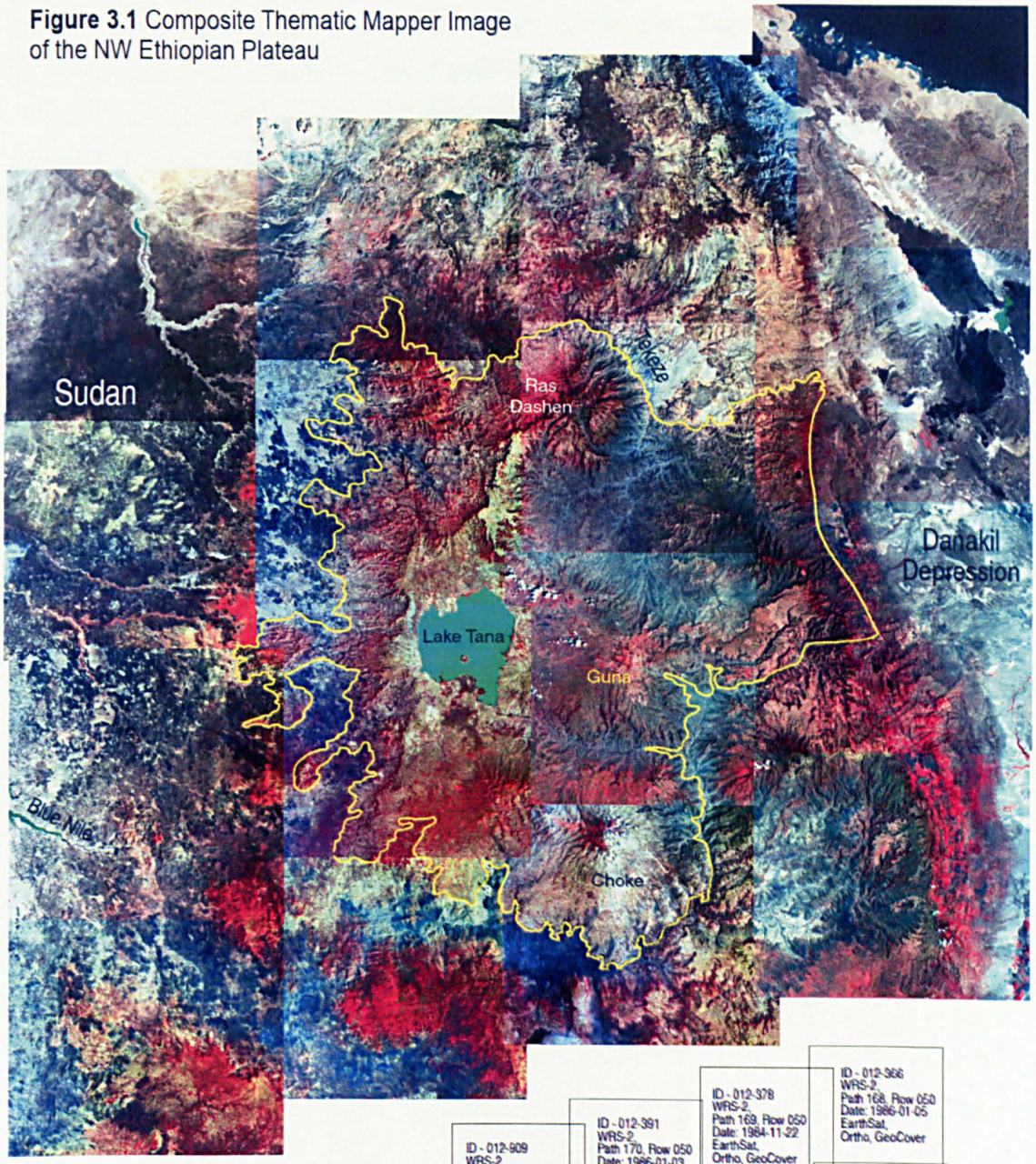

The above images were downloaded from Earth Science Data Interface at the Global Land Cover Facility, University of Maryland. They are colour composite images of Thematic Mapper Data taken from a standardized, high resolution, orthorectified dataset. The online identification number, the path and row numbers, and the date of aquisition for each image is shown in the grid to the right. The approximate outline of the NW Ethiopian Plateau is marked by the yellow line. Red - vegetation, Blue - water, Green/Brown - bare ground.

http://glcf.umiacs.umd.edu/index.shtml

flood basalt pile, the Aiba, which forms the main, and greater part of the pile, and the Alaji, which forms the upper bimodal portion of the pile. Together these formations represent the entire Oligocene flood basalt sequence in the area, and this has so far been best documented in the Lima Limo section (Section 2.2.2). The shield volcanics on top of the flood basalt pile belong to the Termaber Formation (Section 2.2.3).

The individual lava flows which make up the flood volcanic pile are typically tiered, with dense, vaguely columnar lower bodies, and chaotically-structured scoriaceous upper sections. They are generally near to flat-lying and laterally discontinuous, and comprise mainly tholeiitic to transitional olivine basalts and ankaramites, both of which are variably pophyritic and rarely aphyric (Section 2.1.2). In the upper bimodal part of the pile these become interbedded with rhyolitic ignimbrites, and it is the first appearance in the sequence of these silicic volcanics that marks the base of the Alaji Formation.

The basaltic lavas of the NW Plateau are today more commonly described with reference to the three fold classification into LT, HT1 and HT2 basalts after Pik et al. (1998) and little reference is made to their established stratigraphic taxonomy. The lavas described in this thesis are analogous to the HT2 basalts and are exposed within high-Ti sub-province (Fig. 3.2).

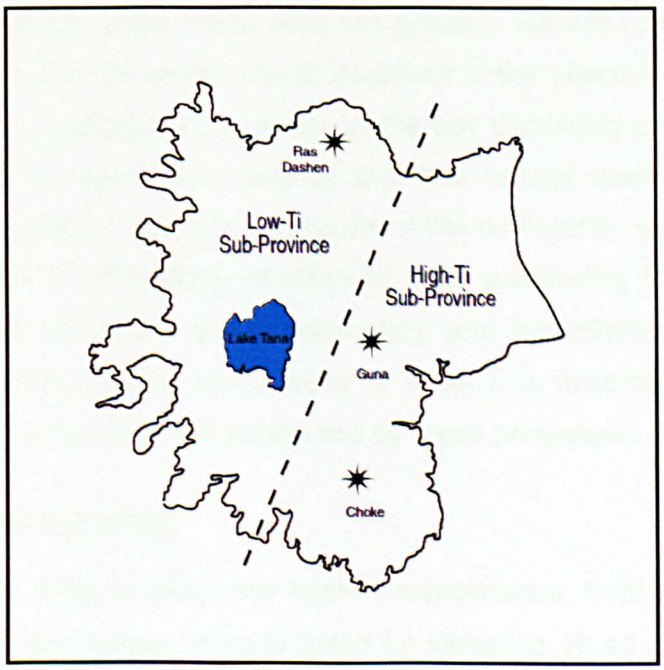

Figure 3.2 Proposed divide between the low-Ti and high Ti sub-provinces of the NW Ethiopian Plateau (Pik et al.1998).

3.2 Location of sampled sections

3.2.1 Rationale

It is generally accepted that all volcanism associated with the process of continental break-up between the Africa and Arabia is in some way linked to the Afar mantle plume (Chapter 2). The HT2 basalts of the NW Ethiopian Plateau represent the most primitive material related to this upwelling so far found anywhere in the Afro-Arabian volcanic province. The high MgO, FeO and TiO_2 contents of these lavas suggest that they represent the least contaminated magma generated by melting in the head of the upwelling, and their pronounced OIB-like trace-element signature reflects an origin in the deep mantle (Pik et al. 1999). If this signature is coupled with enrichments of $^{186}Os/^{188}Os$ and $^{187}Os/^{188}Os$, as in the picrites from Hawaii (Brandon et al. 1998), and Siberia (Walker et al. 1997b), then it may be further suggested that the Afar plume originated at the core-mantle boundary. This would be consistent with the seismic tomographic images which show a plume-like structure beneath Afar extending upward from the core-mantle boundary (Ritsema et al. 1999, Gurnis et al. 2000, Nyblade et al. 2001 and Montager 2001).

The deeply incised valleys which dissect the NW Plateau within the high-Ti sub-province expose coherent unbroken sections of the flood basalt pile which in this region is dominantly composed of HT2 basalts. These are more accessible where roads zig-zag up steep valley-sides onto the plateau. Recent road cuttings which expose relatively fresh lava sequences in particular make effective sampling easier, as sometimes older roadsides have slumped thereby displacing sequences, or they may be obscured by weathered material that has moved down-slope. Chemical weathering on the plateau is intense because of the dominantly sub-tropical climate and because basalt is particularly affected by such weathering fresh samples are sometimes difficult to obtain. Since weathering and hydrothermal alteration can dramatically alter the isotopic composition of lavas it is important to ensure that samples collected for analysis are unaffected by these processes.

3.2.2 Location and sampling

A number of road sections within the high-Ti sub-province, from low points on the traps to the top of the plateau, were targeted for sampling. Road sections that climb steeply up the edges of the escarpment were identified from 1:50 000 maps of areas to the northwest of Weldiya, and to the north of Lalibela, and, of these, six were selected subsequent to reconnaissance to assess the suitability of roadside

Figure 3.3 Location map for the six sampled sections within the High-Ti Sub-Province

exposures (Fig. 3.3). Sampling was carried out from 24th March, 2001 to 31st March, 2001, just prior to the beginning of the short rainy season when conditions were not too hot and dry, or too wet. Where practicable, every flow-unit in the selected sequences was sampled with a view to constructing a detailed picture of the temporal

evolution of the traps and relationships between units. Where significant intra-unit variation was apparent, flows were sampled in more detail to highlight any textural, mineralogical and geochemical differences produced by differentiation during emplacement and cooling. Samples of no less than approximately 20 cm^3 were collected from each lava flow and transferred to sealable plastic bags labelled with a sample number prefixed with the date on which the sample was collected (eg. 01.03.24.02 denotes the second sample collected on 24th March, 2001). Joint surfaces and highly fractured areas of the flows were avoided for sampling, and care was taken to remove the weathered rind and any discoloured mantle from each sample before it was transferred to the labelled bags. A GPS and altitude reading were taken at each sample location using a Garmin eTrex 12 channel personal navigator, and these were recorded in a field-notebook alongside field-sketches and brief notes describing salient features of the rock-types and their field-relations. Photographs of specific features were taken at selected locations, and these were indexed accordingly in the field-notebook.

3.3 Sampled Sections

3.3.1 Introduction

The sampled sequences are described in the following sections. Hand-specimen descriptions of the lavas and descriptions of their field relations are tabulated in Appendix 3.1 together with the latitude, longitude and altitude of the locations from which they were collected. All entries are in top-down stratigraphic order rather than in the order that the samples were collected. The listed rock-types were classified retrospectively using hand-specimen and thin-section descriptions, and geochemical analyses.

3.3.2 Dilb Section

The sequence of lavas that constitute the Dilb Section are exposed along the Weldiya to Debre Tabor road from just north of a bridge over the Tekle Haymanot river (2649 m) through the village of Dilb and along the northern margins of the Alech Ber Ridge onto the plateau to a tor-like exposure (3543 m) near a group of abandoned stone tukuls (Figs 3.4 & 3.5). The road was built by Chinese engineers, and for this reason it is sometimes referred to as the Chinese Road. Although unsurfaced, it is well constructed from compacted gravel, and in numerous places it has been cut by blasting to expose relatively fresh, easily accessible sections of the lava sequence. Only in a few places, where decomposition of the exposed lavas has

been accelerated by moist conditions in some of the deep gullies that descend from the plateau and intersect the road, are the rocks too weathered to yield suitably fresh samples. The entire section comprises an essentially unbroken sequence typified by laterally discontinuous picritic, ankaramitic and olivine basalt pahoehoe-like lava flows with massive, widely jointed bodies and chaotically structured scoriaceous upper sections. The continuity of the lava pile along the road is broken only toward the north by a normal fault, which displaces the sequence downward toward the northeast by an undefined amount. The lavas beyond this discontinuity, on the downthrown side of the fault, were not sampled because it was not possible to establish their relationship with the lavas of the main sequence in the hanging wall, and since, at this point, the road swings in a tight loop north-eastward away from the main sequence, a large part of the section (between locations 28 and 30) was not sampled.

Much of the lava pile (below location 11) is dominated by compound flows comprising interleaved and coalesced pahoehoe flow-lobes and sheets similar to those described in the Columbia River Basalts (Long & Wood, 1986, 1987) and in other continental flood basalt provinces such as the Deccan (Keszthelyi et al. 1999; Bondre et al. 2004) and the British Tertiary Province (Kent et al. 1998; Lyle, 2000). Such compound flows, typified by those exposed in a prominent road cutting between locations 23 and 28, are commonly over 30 m thick, and comprise numerous well defined variably-sized pahoehoe sheet flows, up to 3 m thick, characterised by well-jointed lower bodies and scoriaceous upper profiles (Fig. 3.5, Location 25). They are likely to have developed on flat to gently sloping topography as a result of the gradual inflation and coalescence of multiple flow-lobes. The column-bounding fractures or vertical joints of the individual sheets are truncated at the boundaries with the scoriaceous upper flow-sections, and their spacing is evidently wider in the larger thicker flows than in the smaller thinner flows. This supports the proposition that the distribution of such fractures, caused by contraction during cooling, is related to the aspect ratio (width/height) of the flow-units (Schaefer & Katterhorn, 2004). The denser hackly fracture of the scoriaceous upper sections implies that these parts of the flow-sheets cooled more rapidly than the main well jointed bodies. It may be assumed therefore that cooling of the upper sections of the flows occurred as a result of rapid radiation loss to the atmosphere aided by localised convective overturning, whereas cooling of the lower main body of the flows occurred more slowly as a result of conduction with the already cooled upper surface of the flow below. Column-normal fractures, which are thought to propagate along vesicle layers (Schaeffer &

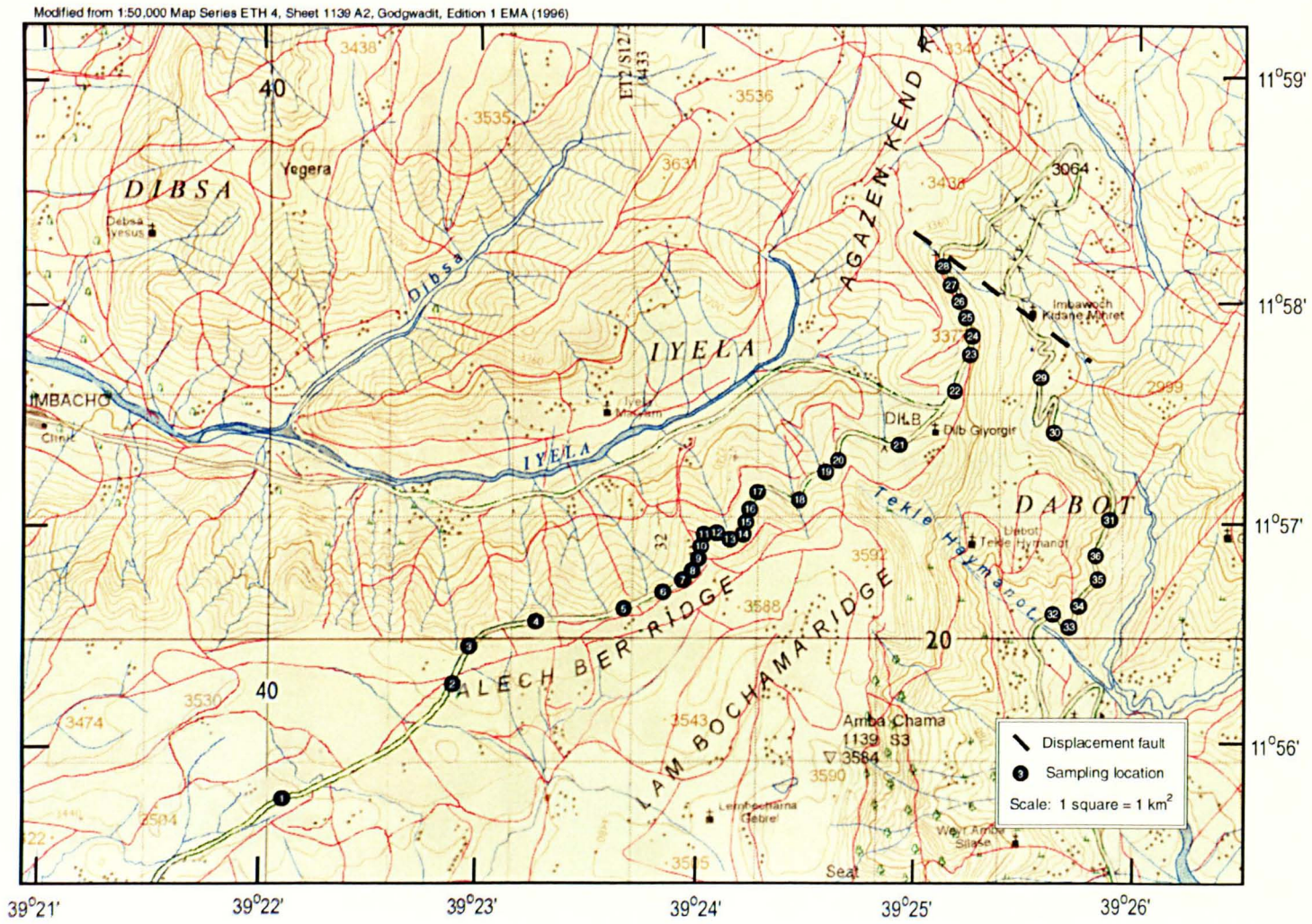

Figure 3.4 Sampling locations for the Dilb Section

Location 1 Ignimbrite on top of the Plateau

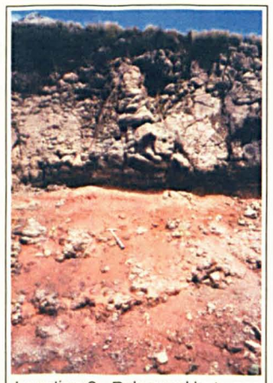

Location 2 Palaeosol between 01.03.24.03 and 01.03.24.04

Location 5 Interfingering of scoriacious lava flow with more a dense columnar jointed unit represented by 01.03.24.07

Location 9 Vesicle sheet in 01.03.24.13

Location 18 Pahoe hoe flow structures in 01.03.25.03

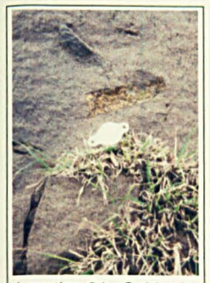

Location 24 Gabbroic xenolith in 01.03.25.10

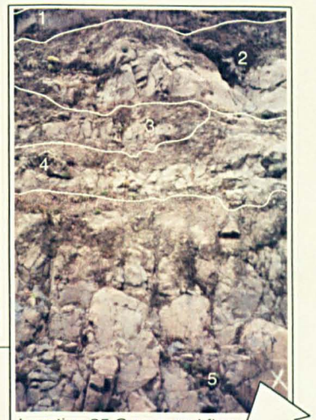

Location 25 Compound flow comprising interleaved jointed sheet flows with scoriacious upper sections

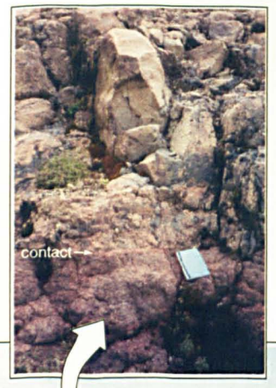

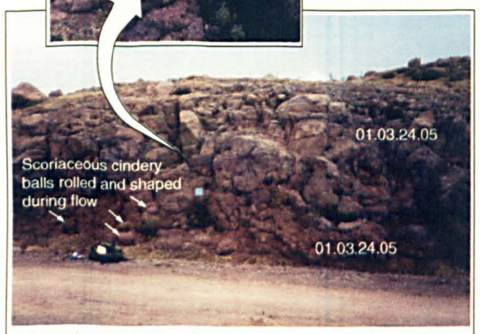

Location 3 Oxidised contact between 01.03.24.04 and 01.03.24.05.

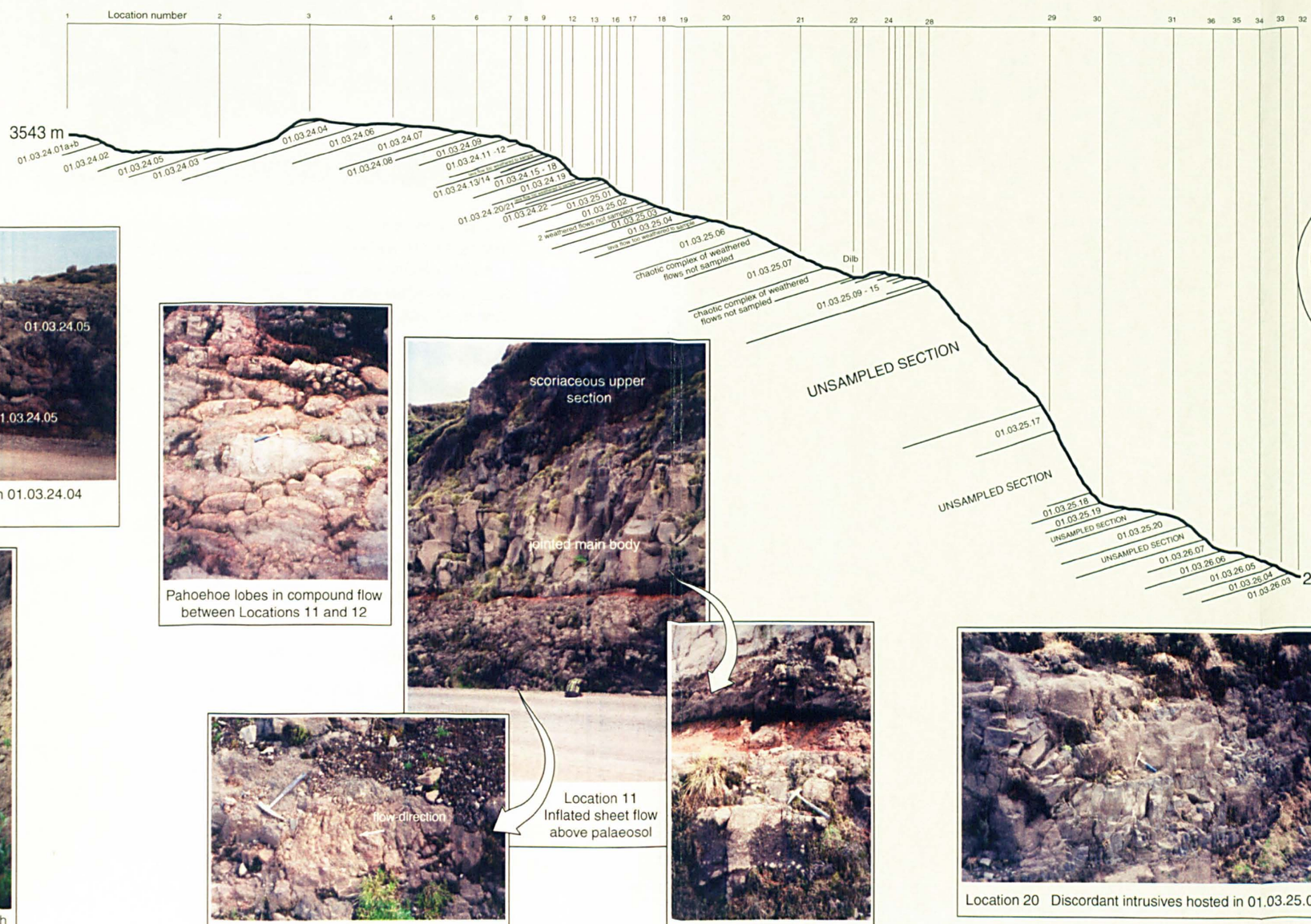

Location 23 Sill with distinctive chilled margins within compound flow

Pahoehoe lobes in compound flow between Locations 11 and 12

Location 11 Inflated sheet flow above palaeosol

Pahoe hoe flow structures on upper surface of flow beneath 01.03.24.18

Palaeosol between 01.03.24.16 and 01.03.24.17

Location 20 Discordant intrusives hosted in 01.03.25.06

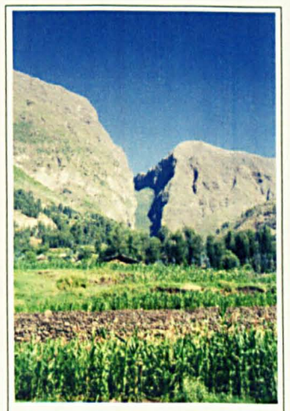

Rift fault which offsets the pile to south of the Dilb Section

Location 29 Dyke (01.03.25.16) with well defined chilled margin cross-cutting flow 01.03.25.17

Figure 3.5 Topographic cross section of the Dilb Lava Sequence

Katterhorn, 2004) are not well developed in the flow-units which make up the compound flow-fields suggesting that the lava flows in these compound flows were not particularly charged with volatiles.

Further up the sequence, between locations 14 and 15, similar compound flows to those described above between locations 22 and 28 occur, sandwiched between two sheet flows with a more simple form (Fig. 3.6). Since these compound flows are

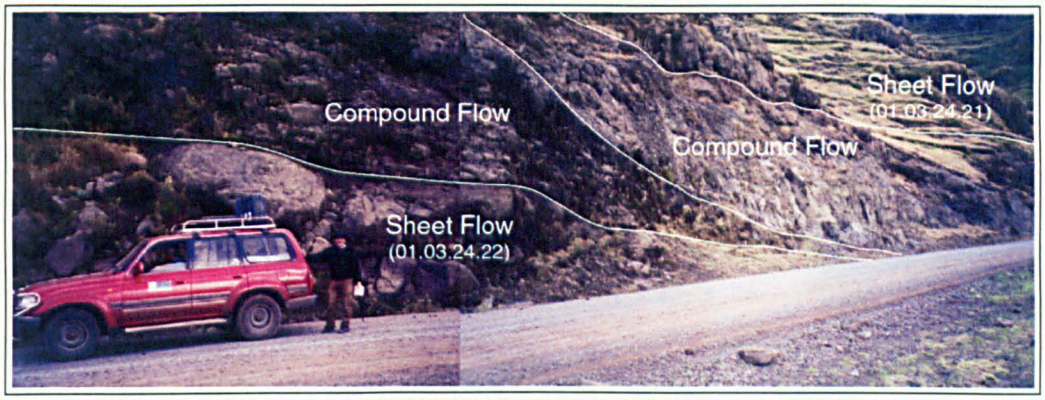

Figure 3.6 Two compound flows or flow fields sandwiched between sheet flows between locations 14 and 15. The flow fields are a complex jumble of pahoehoe lobes and thin laterally discontinuous inflated sheets. The upper surface of the lower compound flow has been oxidised to form a thin red divide between it and the upper compound flow. The variable thickness and lateral discontinuity of the flows is quite apparent at this location.

much thinner than those lower down the sequence, the variable thickness and laterally discontinuity which is typical of such flows, is seen more clearly here. The lower compound flow can be seen to pinch out from left to right (roughly NNE – SSW from location 15 to location 14) almost entirely beneath the upper compound flow so that both effectively interleave. The aspect of both flows together with the jumbled interleaved arrangement of their constituent flow-units strongly suggests the lavas emanated from multiple point sources which periodically migrated overtime.

The mechanisms of emplacement of pahoehoe lava flows are reviewed by Self et al (1998); the typical stages in their development are illustrated in Figure 3.7. Most basaltic eruptions of this nature initiate as fissure eruptions, often with fountains of incandescent lava along the lengths of the open fissures leading to the development of spatter ramparts and scoria fields. The open fissures seal quickly within hours or days on account of their thermal inefficiency, and the remaining lava is issued from point sources or vents. Pahoehoe lavas are typically the first to erupt from such vents. Lava is fed from the vents into the bodies of flow lobes and continues to flow underneath their rapidly cooled plastic skins in such a way that much of the lava is

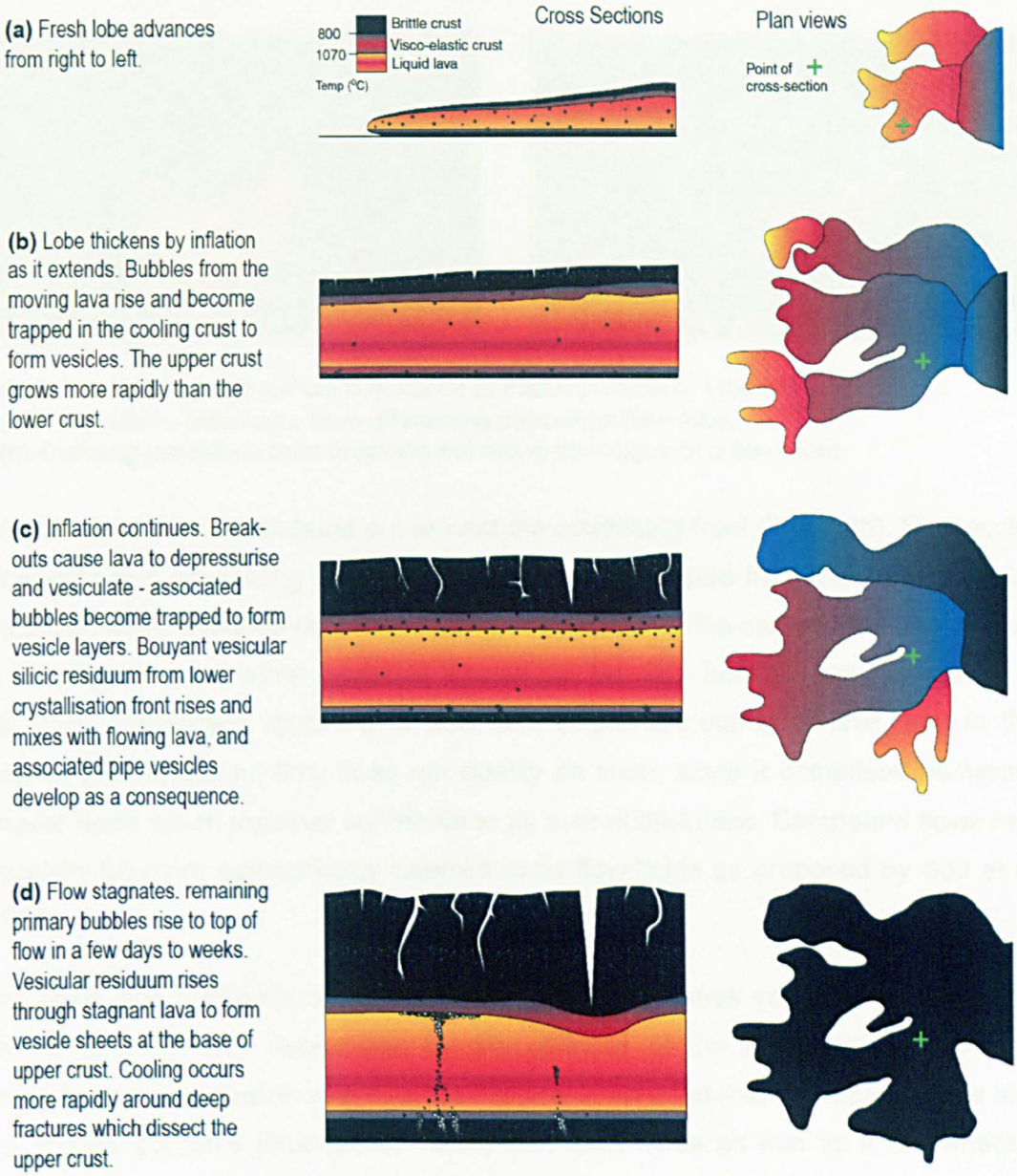

Figure 3.7 Development of an inflated pahoehoe sheet flow (after Self et al. 1998)

never exposed at the surface. As flow continues, the skin may become bellied and wrinkled to form a ropey surface which may be used to infer the direction of flow – indicated by the orientation of the bellying of the surface (Fig. 3.5, Locations 11 & 18). The flow-lobes themselves are initially relatively thin (< 50 cm) and have such low viscosities that they are able to advance in a smooth rolling motion. The flow-fronts normally advance as thin incandescent lobes that chill and crust over after 1 - 2 m of flow. Further pulses of lava into the lobe may cause the front to inflate and burst thereby forming a breakout which allows the flow to propagate downslope (Fig. 3.8a); alternatively as the front slows it may be over-run by a subsequent flow. Slow moving flows tend to propagate by the protrusion of numerous small bulbous appendages

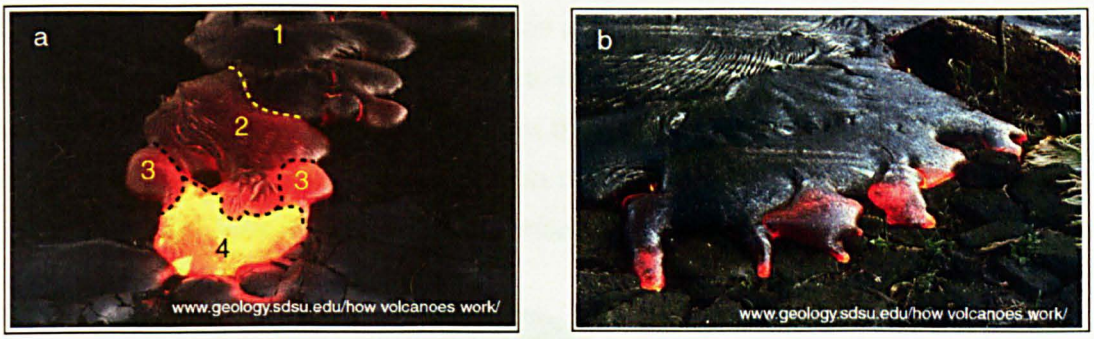

Figure 3.8 Active pahoehoe flow-fronts at Kilauea Volcano, Hawaii.
(a) Progressive breakouts from advancing pahoehoe flow-lobe.
(b) Budding pahoehoe toes breaking out along the edges of a flow-front.

referred to as toes which burst out around the advancing front (Fig. 3.8b). Successive breakouts and over-riding flow-lobes which have originated from the same ongoing magmatic event produce compound flows. It is likely that the compound flows evident at Location 25, and other locations throughout the Dilb Section, were emplaced in this way. Technically speaking, a flow is a single outpouring of lava, and in this respect the compound flow does not qualify as such, since it comprises numerous smaller flows which together contribute to its overall thickness. Compound flows may therefore be more appropriately referred to as flow-fields as proposed by Self et al. (1998).

The scale and thickness of individual pahoehoe flow-lobes varies enormously and seems to be initially determined by the stiffness of the bubble-laden lava, and thereafter on the effusion rate and the volume of lava fed into the lobes. Lavas with low volatile contents (blue-glassy flows) can form lobes as thin as 2 cm whereas lavas with high volatile contents of up to 50% (silvery flows) can form lobes as thick as a couple of metres (Self et al. 1998). Furthermore, with continued inflation, metre-scale lobes can coalesce laterally to form extensive sheet flows up to tens of metres thick and several tens of kilometres in length (Hon et al. 1994; Self et al. 1996). All such scales of flow architecture referred to above are, to an extent, represented in the Dilb Section.

Between locations 11 and 12, and locations 20 and 21, there are flow fields of comparable thickness (< 20 m) to those already described between locations 23 and 28. These however comprise numerous chaotically stacked, pillow-like, pahoehoe flow-lobes generally less than 50 cm thick and no more than a metre long (Fig. 3.5, Locations 11 - 12), rather than well formed sheet flows. The lobes are characterised by massive scoriaceous interiors and well-defined red oxidised rinds where

weathering has penetrated the fine-grained fractured fabric of the rapidly cooled skins. They may, on account of their size and shape, be mistaken for pillow lavas, however, the evidently elongate profiles of the majority of lobes and the limited amount of hyaloclastite between, suggest that they more likely to be flow-lobes than pillows. The size, shape and organisation of the lobes are indicative of low effusion rates (Fig. 3.9). Their dimensions are similar to typical advancing pahoehoe lobes in

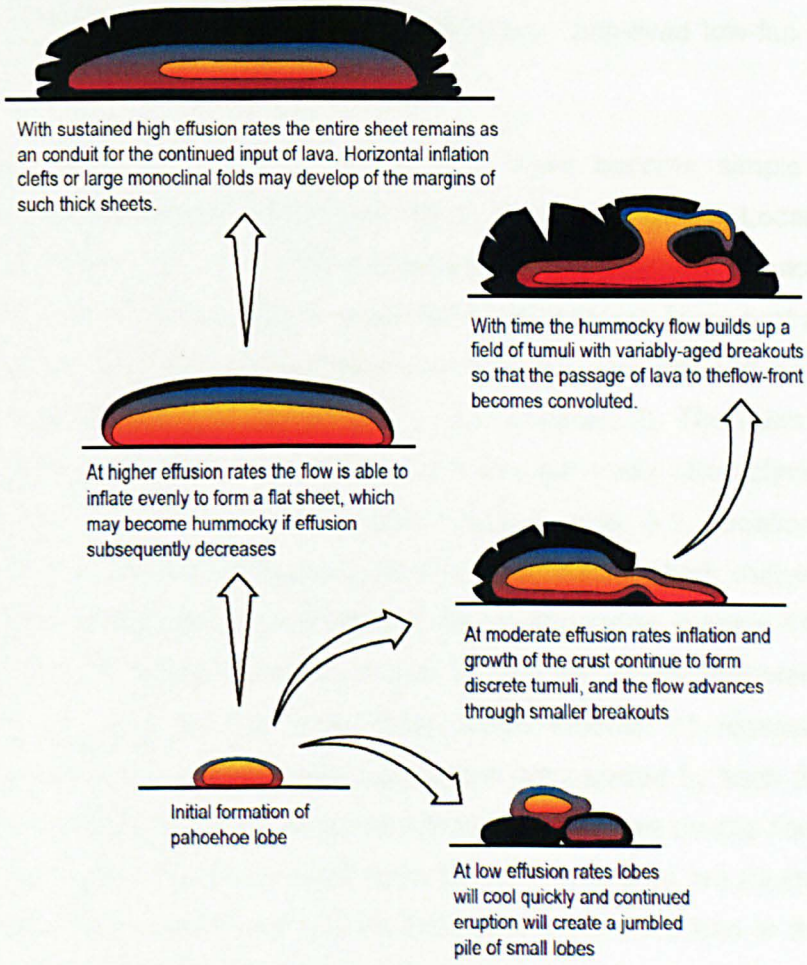

Figure 3.9 Effusion rates and flow morphology (adapted from Self et al. 1998) In addition to effusion rate, the morphology of a flow is dependent the viscosity of the lava, the slope and roughness of the surface, moisture conditions and temperature.

Hawaii where effusion rates have been measured at < 1 m^3s^{-1} (Blake & Bruno, 2000). It may be assumed therefore, that effusion rates for the flows which constitute the flow-fields between locations 11 and 12, and locations 20 and 21 were similar to those observed in Hawaii today. Moreover, the great thicknesses of both of these flow fields suggest that such conditions were sustained for an appreciable length of time during their emplacement. The low effusion rates for the constituent flows suggest that, at the time of their emplacement there was slowing in the supply of

magma to the surface. This is supported by the fact that the lobes have not propagated and coalesced to form inflated sheets as in the compound flows or flow fields lower in the section. The presence of a well-defined palaeosol (Fig. 3.5, Location 11) on the upper surface of the flow field between locations 11 and 12 furthermore implies that, at this point, following a long period of low and slowing effusion rates, volcanic activity ceased for long enough to allow for a soil to develop. This is the first palaeosol encountered in the Dilb Section, and it seems to mark a change in the nature of volcanism from continuous, long-lived low-flux eruptions to sporadic short-lived high-flux eruptions.

Above the palaeosol at location 11 the lava flows become simple rather than compound, with discernable red oxidised upper surfaces (Fig. 3.5, Location 3) which signify short breaks in volcanic activity between the emplacement of each flow, when the upper surface of the flows were subjected to weathering. More protracted breaks in effusive activity are evident at a few locations where there are well-developed vivid red paleaosols between the flow-units (Fig. 3.5, Location 2). The flows are laterally discontinuous and variable in thickness, and are generally characterised by well-jointed main bodies and scoriaceous upper sections (Fig. 3.5, Location 11); in this sense they are similar in structure to thicker sheet flows which make up the flow fields already described in the lower part of the section below location 11. They differ from the flow-fields below, however, mainly in that each flow represents an entire effusive episode, whereas the sheet flows below location 11 represent separate outpourings related to ongoing effusive episodes represented by each flow field; it is on this basis that they are considered as simple flows. These simple flows also differ from the sheets within the compound flows below in that they are much thicker (2 – 12 m) and laterally more extensive. Like the flow-sheets described in the lower flow fields, they were formed by the progressive inflation and coalescence of pahoehoe lobes. Higher effusion rates during their emplacement, however, encouraged the development of much thicker and more laterally extensive sheets than are seen in the flow fields below. It is suggested that, at such high effusion rates, inflation or endogenous growth can convert lobes of between 20 and 50 cm thick into sheets many metres thick within a period of weeks (Self et al. 1998).

The regularly spacing of the joints in the main bodies of the simple sheet flows implies that they cooled as discreet units prior to the emplacement of each successive flow. Their scoriaceous upper parts, which generally constitute near to a third of the total thickness of each flow, display a dense hackly fracture which implies

more rapid cooling. In some flows this more rapidly cooled upper section appears to have been deformed and broken up during the advancement of the flow, so that parts have been rolled into small cindery balls and pillows generally less than 30 cm in diameter (Fig. 3.5, Location 3). Where the ends of flows are visible they can be seen to interleave with other flows in much the same way as seen in the compound flows below (Fig. 3.5, Location 5).

Vesicle sheets and pods of varying dimensions (< 20 cm thick) are common in many of the simple flows in the upper part of the section, and in some of the thicker sheets in the compound flows in the lower part of the section. The majority of these are likely to have formed when bubbles produced by depressurisation of the lava, become trapped in the cooling crust of the flows (Fig. 3.7c). Some of the larger vesicle pods, however, show sharp boundaries with the host, and discernable trails of vesicles that extend downward into the body of the flows (Fig. 3.5, Location 9) suggesting that they were formed, during the period between the cessation of lava movement and the deep penetration of columnar joints, by rising plumes of bubble-rich differentiated liquid originating at the lower crystallisation fronts of the flows (Fig. 3.7d). Such features, referred to as vesicle cylinders, have been reported to show marked enrichments in elements, such as Fe, Mn, Ti, Na, K, P and many incompatible trace, not removed by initial crystallization of the host basalts (Goff, 1996, Caroff et al. 1997, 2000; Greenough et al. 1999). Whether or not the features here interpreted as vesicle cylinders show such compositional differences compared to their hosts, remains to be investigated since they were not sampled because, more often than not, they were severely weathered. Their occurrence in the lavas nevertheless implies an unusually high water-content for the magma prior to eruption, and this is supported by the consistent presence in all the lavas of olivine phenocrysts that have been altered, to one degree or another, to iddingsite. High temperature iddingsite alteration has been noted as a common feature of lavas with vesicle cylinders (Goff, 1996; Caroff et al. 1997, 2000; Greenough et al. 1999).

With reference to geothermometry data generated from the compositions of minerals and glasses from a number of alkaline and tholeiitic lava-flows containing vesicle cylinders across the western USA, Goff (1996) reports that vesicle cylinders begin to form at ~ 1100 - 1075 °C and cease crystallising at ~ 950 °C. Field relations and cooling profiles suggest that in flows of between 3 and 10 m thick, vesicle cylinders form within 1 - 5 days after cessation of flow. The temperature of cylinder formation

varies between flows depending on their chemistry, water-content, eruption temperature and nucleation rate of bubbles (Goff, 1996).

Although vesicular features are common in most of the lava flows in the Dilb Section, thick pods and cylinders are only seen in the olivine basalts (Fig. 3.5, Location 9) which form the thickest individual flows of the pile. This consistent association of high degrees of iddingsitization with thick simple vesicle-cylinder-bearing sheet flows with evolved compositions has important implications for the evolution and emplacement of the lavas throughout the Section. Thick olivine basalt flows occur in the lower part of the section (below Location 11) between locations 32 and 35, and at locations 30, 16 and 14, interspersed with compound flows dominated by ankaramitic lavas, between locations 23 and 28, and 14 and 15, and simple sheet flows of dominantly picritic composition at locations 32, 36, 30, 31, 29, 19 18 and 17. There is no systematic evolutionary trend shown in this lower part of the sequence as the stratigraphic distribution of the different lava-types is somewhat random reflecting periodic pulses of magma into oxidising shallow-seated reservoirs and variable residence times in these reservoirs. The absence of paleasols and erosion surfaces between the lavas suggest that they were erupted in quick succession although the variable thicknesses of the flows suggest that effusion rates varied throughout. The gradual slowing of effusion rates up to the first palaeosol at Location 11 is evident from the decreasing dimensions of the flow units in the compound flows which begin to dominate the section from Location 28 up to the palaeosol at Location 11. Continued pulsing of the magma supply, although on a smaller scale in the compound flows is still evident from the variation in composition of each constituent flow-unit (Locations 23 - 28).

Breaks in volcanic activity, evident from the oxidised surfaces and occasional palaeosols between the simple sheet flows above the first palaeosol at Location 11, imply that at from this point onward the supply of magma into the magma chamber began to wane, and as a consequence volcanic activity became more sporadic and effusive. It is likely that pressure in the magma chamber became too low to sustain a continuous flux of material to the surface and as a result active conduits for the lava were effectively sealed between eruptions. This would have meant that, during periods of inactivity, magma was trapped in the magma chamber where continued fractionation led to the crystallisation of low pressure clinopyroxene and plagioclase phenocrysts, and extensive iddingsitization of the olivine phenocrysts occurred under the elevated oxidising conditions generated by the inflow of meteoric water into the

magma chamber. Subsequent influxes of new magma into the magma chamber, and the release of volatiles during oxidation, would have led to the progressive increase in pressure in the magma chamber ultimately leading to the sudden eruption and rapid outpouring of large volumes of evolved and oxidised lava through newly breached conduits to the surface. This episodic process can be considered to be responsible for the formation of thick olivine basalt and ankaramitic sheet flows which typify the lava sequence above the palaeosol at Location 11.

The reduction in the supply of magma from the underlying upwelling mantle into the crust inferred from the morphology of the lavas in the upper part of the section is also suggested by the absence of picritic lavas above Location 17. The emplacement of these lavas requires the input of magma into lower crustal reservoirs, where fractionation of olivine and possibly high-pressure clinopyroxene can occur, in sufficient volumes and with sufficient rapidity to displace the partially crystallised magma upward into the upper crust with such force that it rises, relatively unimpeded, directly to the surface. The uppermost picritic sheet flows at locations 19, 18 and 17 respectively represent the last manifestations of this process before the onset of more sporadic volcanism above the palaeosol at location 11.

There are numerous examples throughout the Dilb Section, of intrusive bodies which cut through and between the lavas. These are generally recognised by their pronounced chilled margins, their sharp contact with, and slight colour difference, and contrasting joint spacing and orientation, compared to, their hosts (Fig. 3.5, Locations 29, 23 and 20). Although the compositions of these intrusives are slightly different from those of their hosts, they are similar to lavas elsewhere in the section; it may be assumed therefore that they represent feeders for the lavas above. Ankaramitic dykes occur at locations 29 and 7, hosted in picritic and ankaramitic flows respectively, and olivine basalt dykes occur at locations 32 and 22, hosted in picritic and ankaramitic flows respectively. The morphologies of the intrusives vary from simple dykes (Fig. 3.5, Location 29) and sills (Fig. 3.5, Location 23), generally less than a metre in thickness, to more complex but similarly-scaled discordant features (Fig. 3.5, Location 20), which have been evidently controlled by the internal features of the host lavas. The intrusives at Location 20, for example, appear to have been intruded along the margins of metre-scale flow lobes thereby giving them the appearance of discordant features when in fact they are concordant. Concordant intrusive features of this nature may have been formed when large volumes of molten

lava from breakouts were forced through piles of already cooled flow-lobes, and in this sense they might not necessarily represent feeders for lava flows above.

Hydrothermal alteration of the lavas in the Dilb Section is widespread and there are few flows that do not show signs of its effects (Appendix 3.1.1). In most flows the vesicles and fracture surfaces are lined with a pale blue powdery zeolite which imparts a blue tinge to freshly exposed surfaces. This is evident also in more dense sections of the flows where there are no vesicles suggesting that interstitial glass in the matrix of the lavas has been replaced by the same pervasive mineralisation. Some flows also show secondary infillings of a white mammilated zeolite (possibly analcime) which appears to have been deposited on top of the more pervasive bluish zeolite. Zeolites are low-temperature (< 200°C) minerals typically formed during the waning stages of volcanic activity in near-surface water-saturated environments. Slightly higher temperature hydrothermal alteration (< 400°C) is also evident in a number of flows above Location 28 where many of the olivine phenocrysts have been variably pseudomorphed by a bright yellow-green mineral identified in thin section as serpentine (Chapter 4). As with zeolitization, this style of alteration is indicative of water-saturated conditions, and the common occurrence of serpentinized olivines and low-temperature zeolites in the same lavas suggests that both products were produced from the same hydrothermal fluids but at different temperatures. Serpentinization of the olivine must first have occurred at higher temperatures, then, as the temperature of the hydrothermal fluids dropped, zeolites replaced the interstial glasses of the lavas, and were precipitated on the inner surfaces of vesicles and fractures.

From the above observations it may be assumed that the post-eruptive-alteration of the Dilb lavas was a result of large-scale hydrothermal upflow rather than localised hydrothermal activity associated with individual eruptions and intrusions. The main source of the water is therefore likely to have been meteoric rather than juvenile. This is consistent with the source for the water suggested earlier to be responsible for the iddingsitization of olivine phenocrysts in the magma chamber prior to eruption of the lavas. The nature of both the pre-eruptive and post-eruptive alteration of the lavas suggests, then, that the climate prevailing during the eruption of the flood basalts in the region was such that it was able to maintain a high water-table.

The top of the Dilb Section is marked by the occurrence of thick rhyolitic ignimbrites which form prominent tor-like outcrops across the top of the plateau (Fig. 3.5, Location 1). These deposits signify further slowing in the supply of magma into the

crust in that they were given time to evolve in closed high-level magma chambers for an appreciable amount of time before being erupted explosively at the surface. Their origins have been attributed to low-pressure fractional crystallisation of basaltic magmas (similar in composition to those from which the flood basalts below were derived) and variable amounts of assimilation of crustal material, mainly of mafic composition (Ayalew & Yirgu, 2003). The unsorted and poorly compacted nature of most of these deposits, consisting of glass shards, crystals and lithic fragments of a variety of sizes and compositions, suggests that they were deposited by hot rapidly-expanding turbulent gases following explosive eruptions of volatile-saturated magma generated by strong differentiation. The mechanisms for the emplacement of such deposits are reviewed by Branney and Kokelaar (2003). At Location 1 there are two ignimbritic units of 5 - 8 m in thickness separated by a layer of fine felsic ash of variable thickness (< 16 cm). The lower unit, which directly overlies a thick aphyric olivine basalt sheet-flow, is a welded ignimbrite with flattened glass shards and rounded quartz in a glassy matrix, whereas the upper unit is poorly consolidated with lithic fragments, small euhedral feldspars and rounded quartz in a fine earth-like matrix (Appendix 2a). For similar deposits at Wegel Tena, 50 km or so to the south, it is estimated that emplacement temperatures are < 750 °C, water contents are < 2 wt.%, fO_2 conditions are close to FMQ, and liquidus temperatures are between 900 and 950°C (Ayalew et al. 2002).

The first appearance of ignimbrites in the flood basalt sequence is generally considered to mark the onset of bimodal volcanism, and this respect they may be here taken to represent the base of the Alaji Formation (Section 2.2.2). All the lavas, below this point, which constitute the Dilb Section, may therefore be assumed to belong to the Aiba Formation, since there is no apparent unconformity, lower in the section, to distingiush them from the Ashange Formation below. It cannot be assumed, however, that the Ashange Formation is not represented in this region since the base of the sequence and the contact with the underlying basement is not exposed, and there may be, near enough, another 1000 m of lavas below the lowermost unit sampled in the Dilb Section.

3.3.3 Iyela Section

Before the construction of the Chinese Road, the narrow unsurfaced road that runs roughly parallel with the Iyela River westward from Dilb was the main road between Weldiya and Lalibela. The lavas which constitute the Iyela section are exposed in several low cuttings along the length of this road between altitudes of 3178 and 2599

metres, from 0.5 km west of Dilb to approximately 5 km west of Imbacho (Figs 3.10 & 3.11). These lavas effectively form the lower flanks of the northern escarpment which steps progressively downward from the Alech Ber Ridge (Fig. 3.4); it is likely, therefore, that they are part of the same sequence of lavas represented in the Dilb Section. Many of the road-cuttings along the 'old road' have, since its construction, become severely weathered, and some are almost entirely buried beneath material that has moved down-slope over time. Also, where small streams descend from the escarpment, the bedrock is covered by thick alluvial soils which are intensively cultivated, and in these places, the road veers away from, rather than toward, the exposed escarpment. Consequently there are large parts of the Iyela Section that were not sampled (Fig. 3.11), and where sampling was possible, fresh samples were difficult to obtain because of the poor state of preservation of the exposed rocks. In total, only 11 samples (Appendix 3.1.2) were collected along 15 km stretch of the section - of these, nine were lavas and two were dykes.

The Iyela lavas are all inflated sheet flows of variable lateral extent and thickness (< 5 m) with distinctive red to yellow oxidised upper surfaces which may be used to distinguish one flow from another (Fig. 3.11, Location 37). They are similar in their morphology and composition to the thick sheet flows in the lower part of the Dilb Section, with jointed main bodies, and scoriaceous upper sections, and picritic to ankaramitic compositions, and in this respect they are indicative of high effusion rates. The reddened flow-tops evident in most of the lavas also indicate that they were products of sporadic activity, and that the periods between eruptions were sufficiently long enough for weathering to appreciably oxidise the surface crust of the lava before being covered by the next flow.

The average southwest dip (< 5°) of the lava pile (Fig. 3.11) suggests that the lavas in the Iyela Section may be stratigraphically correlated with lavas in the Dilb Section at slightly higher altitudes. In which case, the lavas in the upper part of the Iyela Section between locations 37 and 87 may be correlated with lavas in the unsampled part of the Dilb Section between locations 28 and 29, and those that are exposed in the lower part of the Iyela Section, between locations 88 and 91, may be correlated with lavas between locations 29 and 32 in the Dilb Section. It is almost impossible to confirm such correlations 'flow for flow', particularly since the flows are typically laterally discontinuous and more so since post-eruptive differentiation can create significant chemical variations in a single flow unit. It is notable, however, that the major- and trace-element compositions of all the lavas from the Iyela Section are

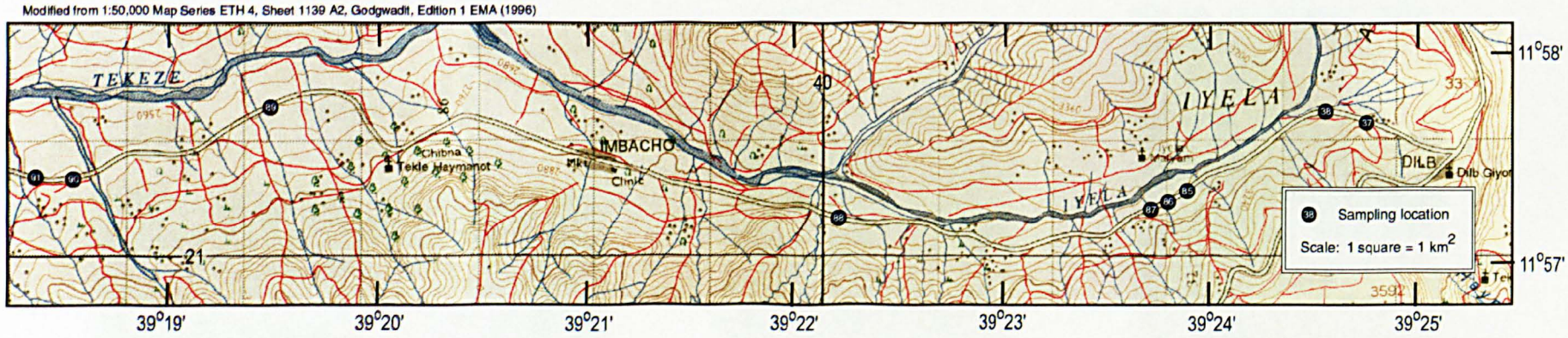

Figure 3.10 Map showing sampling locations for the Iyela Section

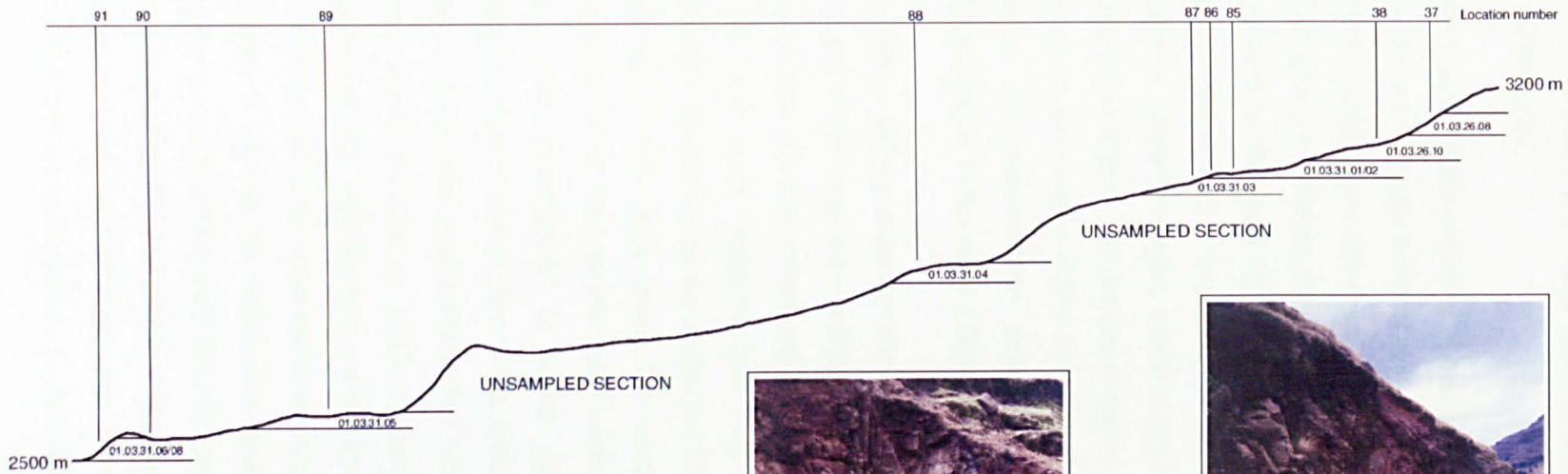

View westward from Location 38 along the Iyela Valley showing the traps gently dipping (~ 5°) toward the south-west. The northern escarpment which descends from the Alech Ber Ridge (Fig. 3.4) is shown on the left of the photograph.

Location 38 Dyke (01.03.26.09) intruded into picritic flow represented by 01.03.26.10

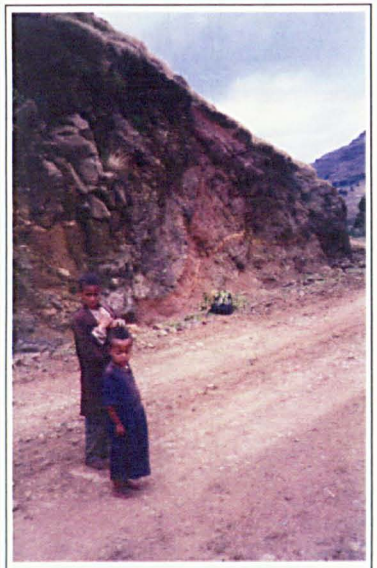

Location 37 Massive flow (01.03.26.08) above heavily oxidised flow top

Figure 3.11 Cross-section of the Iyela Lava Sequence

similar to those for the picrites and ankaramites from the lower part of the Dilb Section below the first palaeosol at location 11, and markedly different from those of the ankaramites in the upper part of the Dilb Section above the palaeosol at location 11 (Chapter 5).

The intrusive rocks exposed in the Iyela Section include two picritic dykes which are seen to cut through ankaramitic flows at locations 38 and 91 respectively. These vertical features are between 1.5 and 2 m wide, and are recognised by their slight colour and compositional differences, and contrasting joint spacing and orientation, compared to the host lavas (Fig. 3.11, Location 38). They are likely to represent material that cooled in situ in feeder conduits for the picritic flows above. Both show distinctive chilled margins which suggest that they were intruded into the already cooled host lavas. The baked margins are darkened and relatively more oxidised than the main bodies of the host flows, and have been preferentially weathered to expose the near-surface sides of the intrusions, so that they are clearly distinguishable in the road cuttings where they occur.

The effects of hydrothermal alteration in the Iyela lavas are similar to those reported for many of the lavas from the Dilb Section (Appendix 3.1.2). The pervasive presence of pale-blue and white mammilated zeolites in the groundmass and vesicles of most of the Iyela lavas suggests that they were affected by the same regional-scale hydrothermal activity as described for the Dilb Section. There is, however, no visible evidence in the Iyela lavas for serpentinization, which may indicate that the temperatures of the hydrothermal waters in this part of the lava pile were slightly lower than experienced in some parts of the Dilb section. The degree of iddingsitization of the olivines in the lavas from the Iyela Section is also similar to that seen in the picrites and ankaramites from the Dilb Section, suggesting that they too were variably affected by oxidising conditions in the crust en route to the surface. Nowhere in the Iyela Section are the olivines totally pseudomorphed by iddingsite to the extent commonly observed in the olivine basalts in the Dilb Section. Furthermore, although it cannot be discounted that olivine basalts might be present in the unsampled parts of the Iyela Section, the fact that there are none observed along its length suggests that the entire sequence of lavas which constitute the Iyela Section are representative of relatively unmodified partially crystallised magmas that rapidly rose through the crust directly to the surface from a deep-seated reservoir.

3.3.4 Bilbala Section

The Bilbala Section is one of three sections sampled in the region around Lalibela, 70 km or so northwest of the area represented by the Dilb and Iyela Sections. It undulates between altitudes of 2172 m (Location 39) and 2378 m (Location 40) along the surfaced road between Lalibela and Sekota, from 4 km southeast of a bridge over the T'eda Shet, to about 2 km southwest of the village of Bilbala approximately 20 km north of Lalibela (Figs 3.12 & 3.13). The gradient of the topography here is considerably gentler than in the Dilb Section, and in places the road appears to dip in and out of the same lava flows for sometimes more than a kilometre. As a consequence only seven lavas were collected along the 6 km length of the section between locations 40 and 43; five dykes were also sampled between these locations (Appendix 3.1.3). A boulder of basaltic composition containing wehrlite mantle xenoliths up to 8cm in diameter was also collected from the river bed of the Yimra Shet at location 44, and although this cannot be considered part of the lava sequence in the immediate area, it has recorded as part of the sampled section only to mark the location from where it was collected (Fig. 3.12, Location 44).

The lava flows exposed along the Bilbala Section are, invariably, inflated pahoehoe sheets indicative of high effusion rates, and they are characterised by well jointed bodies and scoriaceous upper sections. They vary in thickness from 3 m to over 15 m, and it may be inferred, from field observations, that they extend laterally for several kilometres. The composition and thickness of the individual lava flows seem to vary randomly throughout the section. Picritic flows in excess of 15 m thick occur at locations, 39, 40 and 43 (Fig. 3.13, Location 40), and in between these, there are ankaramitic flows of comparable thickness at locations 41, 42 and 43 (Fig. 3.13, Location 42). At location 41 there is also a 3m thick olivine-phyric basalt flow sandwiched between two considerably thicker ankaramitic flows (Appendix 3.1.3). Generally the flow units seem relatively homogeneous in their composition; however, the thick ankaramitic unit at Location 43 (01.03.27.10) shows a marked increase in the size and abundance of clinopyroxene phenocrysts (up to 2 cm in length) toward the top of the flow. This may be explained by the possibility that the clinopyroxene phenocrysts floated toward the top of the flow during and after its emplacement because of their lower density compared to that of the remaining melt. Furthermore, it is possible also that the olivine-enriched picrite at Location 43 (01.03.27.12) may represent the base of the picritic flow seen at Location 39 (01.03.27.01) since there is no discernable contact between the two flows evident anywhere along the stretch of road between the two locations. Such enrichment may be attributed to the possibility

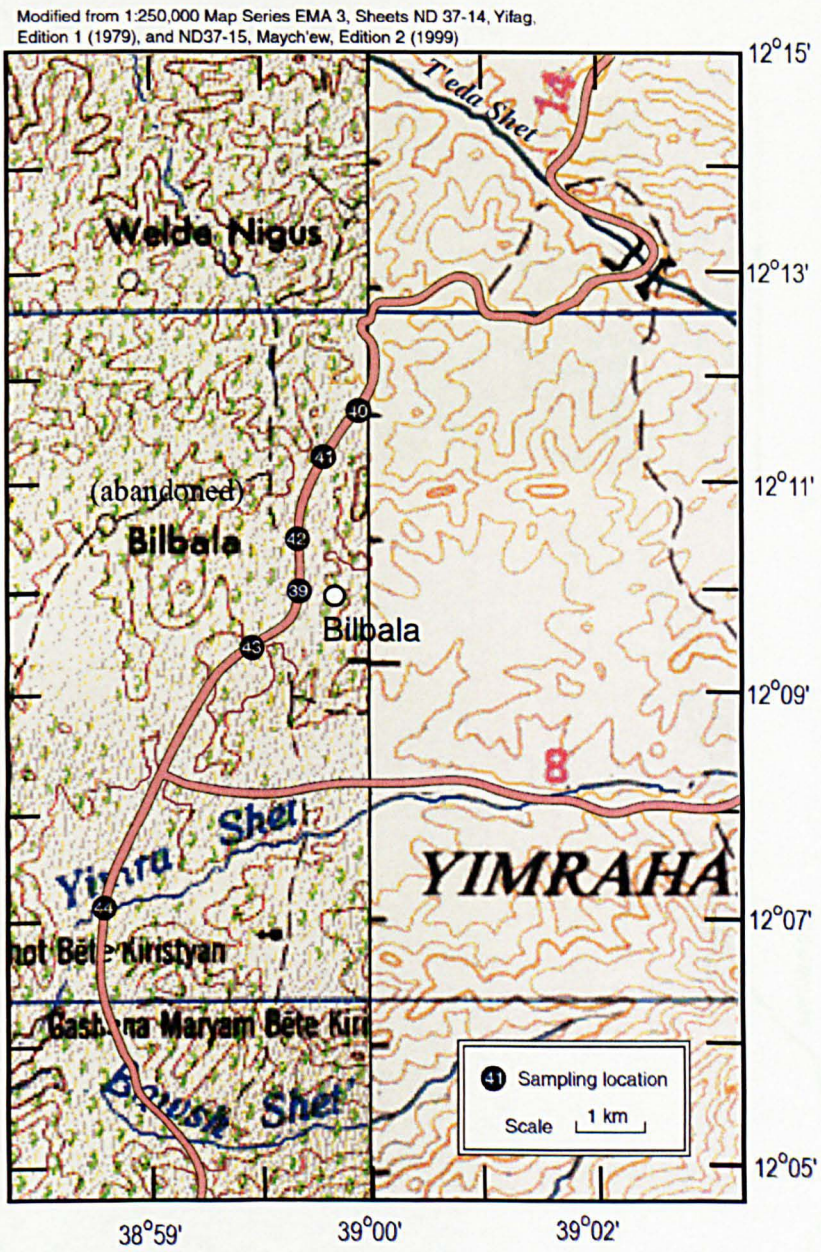

Figure 3.12 Sampling locations for the Bilbala Section

that olivine phenocrysts were able to sink to the base of the flow, after its emplacement, because of their relatively higher density compared to the remaining hot melt.

The upper surfaces of many of the flows are reddened by oxidation indicating that effusive activity was often sporadic and separated by long periods of no volcanic activity when weathering was able to partially decompose the surface of the lava flows. The presence of a fine, felsic distal ash-layer of approximately 20 cm thick between lava flows at Location 41 (Appendix 3.1.3) suggests also that more

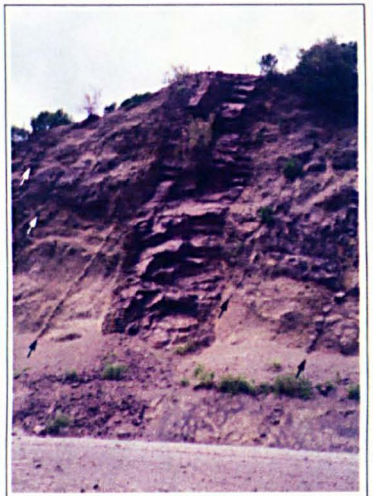

Location 42 Basanitic dyke (01.03.27.08) with stringers (arrowed), hosted in ankaramitic flow 01.03.27.09

Location 40 Parallel mafic dykes (01.03.27.03) hosted in picritic flow (01.03.27.02) approximately 15 m thick. The dykes (arrowed) are stretched and discontiuous, and vary in thickness from a few cms up to 75 cm. They are steeply inclined and trend roughly north-east to south west.

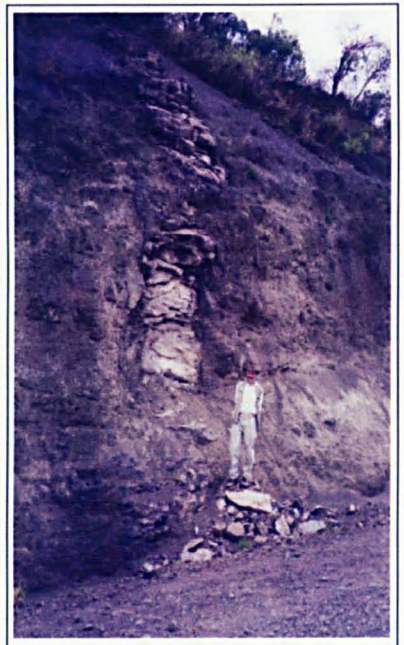

Location 40 Evolved dyke (01.03.27.04) hosted in picritic flow (01.03.27.02). This dyke trends north-west to south-east

Basalt containing mantle xenoliths collected from the river-bed of the Yimra Shet at Location 44.

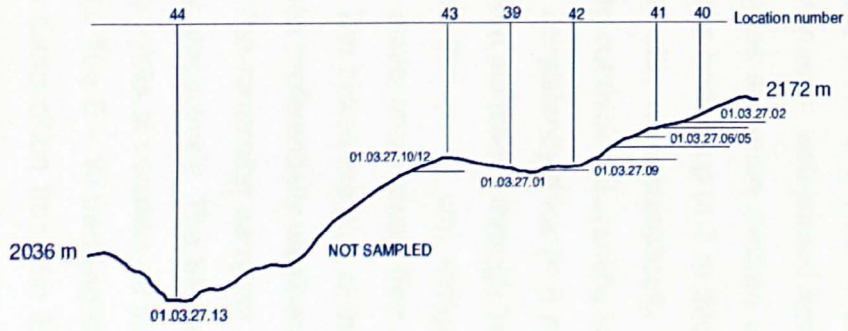

Figure 3.13 Topographic cross-section of the Bilbala Lava Sequence

explosive rhyolitic volcanic activity was occurring elsewhere at the time when the lavas of the Bilbala section were emplaced.

Throughout the Bilbala Section there are swarms of dykes which are seen to cut through the lava sequence at almost every location where it is exposed. On account of their obvious compositional differences from the host lavas, most of these dykes are assumed to be unrelated to the volcanism responsible for the emplacement of the lavas. Three distinct trends for the dykes are discernable between the locations where they are observed. Two perpendicular sets of dykes trending NE and SE respectively can be seen cutting through the thick picritic flow at Location 40 (Fig. 3.13, Location 40). The NE-trending dykes are typically mafic and occur within the host flow as parallel to sub-parallel, stretched, discontinuous, well-jointed lenses of generally < 75 cm thick, where as the SE-trending dykes are more evolved in their composition and occur as more well-defined, continuous bodies up to 2 m thick with pronounced chilled margins. A third set of dykes with characteristically mafic compositions and a consistent E – W trend are seen to cut thick ankaramitic flows in the vicinity of Location 42. These dykes are typically consistently thick (< 3 m) with well-jointed intrusive bodies which form distinctive broken staircases through the host lavas. They exhibit well-defined chilled margins, and thin (< 10 cm) stringers of differentiated material can be seen to extend at an acute angle away from these margins into the host lava both sides of the intrusion. The baked margins of the host have been reddened by oxidation, and these have been preferentially weathered out to expose the near-surface sides of the intrusions. The remaining sampled dykes exposed at Locations 41 and 43 trend SE and E – W respectively. The SE-trending dyke at Location 41 may be related to the SE trending dykes at Location 40 since its composition as well as trend is similar to these dykes. The E – W trending dyke at Location 43, on the other hand, is quite different in composition from the E – W-trending dykes at Location 42; it is in fact more similar to the composition of the some of the lavas elsewhere in the section, so it may represent a feeder for a lava flow emplaced somewhere above.

All the dykes in the Bilbala Section were recorded in the field as olivine basalts. Subsequent geochemical analysis has, however, revealed that they are basanites with enormously variable chemical compositions (Chapter 5), and so they have been documented as such in Appendix 3.1.3. The olivine basalt flow at Location 41 has been documented as a basanite for the same reason. On the other hand, even though the ankaramitic lava at Location 42 is basanitic in its composition, its label of

ankaramite has been retained from the field records because it contains a high percentage of clinopyroxene phenocrysts. The other ankaramites at Locations 41 and 43 are typically basaltic although they are much more alkaline in their composition compared to the ankaramites of the Dilb and Iyela Sections. In fact, all the rocks sampled in the region around Lalibela, including the picrites from the Bilbala Section, are alkaline, and in this respect they are fundamentally different from the tholeiitiic lavas and intrusives from the Dilb and Iyela sections (Chapter 5).

The lavas (and intrusives) in the Bilbala Section are also different from those in the Dilb and Iyela Sections in that they show little or no evidence of iddingsitization, and have not been significantly altered by hydrothermal activity. This might suggest that, during the emplacement of the Bilbala Lavas, conditions in the crust for that region at least were relatively dry compared with those in the Dilb region during the emplacement of the lavas there. This may have been due to differences between the regions in the drainage networks and/or the underlying geology, or there may been some change in the climate between the times when both lava sequences were emplaced. Regardless of the cause, the absence of iddingsitized olivines in the Bilbala Lavas suggest that conditions in the magma chamber from which they were derived are likely to have been relatively dry, with an oxygen fugacity close to FMQ. Nevertheless, the broadly similar Fe and Mg contents of the lavas from the Bilbala area compared with those from the Dilb area suggest that the eruption temperatures for both are likely to have been roughly comparable. It may in fact be assumed that this is the case for majority of lavas with similar compositions throughout the Lalibela region.

The stratigraphic position of the Bilbala lava sequence relative to that represented in the Dilb and Iyela Sections is indeterminable, without further field-evidence. The fact there is a layer of felsic ash (similar to ash-layers seen at the top of the Dilb Section, Location 1; and in the Gashena Section, Locations 74 - 76) between at least two of the lava flows in the sequence suggests that explosive activity elsewhere in the Province may have already began sometime during the emplacement of the Bilbala Lavas. This would imply that the Bilbala sequence may be correlated (in terms of time) to the lower part of the Alaji Formation, and, if this was the case, it would be representative of a later stage of flood volcanism than that represented by the Dilb and Iyela sections, despite its lower altitude. Its close proximity to the huge ignimbrite sequences in and around Lalibela, and the alkaline compositions of its constituent

lavas, elsewhere interpreted to be characteristic of the later bimodal stage of flood volcanism generally ascribed to the Alaji Formation, would seem to support this.

3.3.5 Lalibela North Section

The surfaced road that winds steeply down, north-westward, from Lalibela to the Simeno river, 400 m below, cuts into a sequence of lava flows which exhibit considerable variation in both their morphology and composition. The upper part of this sequence exposed in a series of road-cuttings between altitudes of 2210 and 2478 m, from locations 45 to 49, forms the Lalibela North Section (Figs 3.14 & 3.15). The lower part of the sequence, below location 45, was not sampled since the gradient of the road beyond this point becomes less steep and the lavas are generally concealed beneath a broad spread of top soil and loose material that has been washed down-slope by intense seasonal run-off. Even in the upper part of the sequence many of the lava flows are obscured by loose soil and scree, and many of the exposures that are accessible are severely weathered; consequently only the more prominent thicker flows which have been less degraded by weathering were sampled.

Four out of the five sampled flow units in the section (Appendix 3.1.4) are sheet flows of several metres thick with massive, jointed main bodies, and scoriaceous upper profiles. These include a picritic flow at Location 45, an ankaramitic flow at Location 47, and two olivine basalt flows at locations 48 and 49 respectively. In between these, partially obscured by loose material washed down-slope in the unsampled parts of the section, there are, what seem to be, a jumble of compound flows consisting of piles of metre-scale pahoehoe lobes and sheets of generally < 3 m. The ankaramitic flow sampled at Location 46 represents the upper flow unit of one these compound flows exposed between Locations 45 and 46.

The pattern of volcanic activity evident in the lava sequence of the Lalibela North Section, up to the thick ignimbrites that form the plateau on which the town of Lalibela is built, is suggestive of alternating periods of high and low effusivity, and the presence of oxidised flow surfaces between some of the units indicates that this activity was, at times, sporadic. Some degree of iddingsitization of olivine is evident in all of the lavas (Appendix 3.1.4), which might suggest that the fO_2 of the magma may have been elevated prior to the eruption of the lavas, as described for the lavas from the Dilb Section. The fact, however, that the iddingsitization here is not so pervasive as seen in the Dilb Lavas, might suggest in this case it is a product of post

eruptive alteration and weathering. The absence of zeolites and other obvious effects of hydrothermal alteration in the Lalibela North Lavas suggest, at least that there may not have been as much water around during their emplacement as there might have been during the emplacement of the Dilb Lavas.

The lava sequence represented in the Lalibela North Section appears to have been locally displaced in places by rotational slumping. This has caused the apparent dip of the flows to vary from near-horizontal to up to 45° roughly southward into the escarpment (Fig. 3.15). The slump structures are developed in the less competent compound flows, and their lower limits are marked by the more competent massive flow units over which they seem to have moved. It is possible that the thicker more massive sheet flows are more impervious than the complex jumbled piles of lavas which form the compound flows; therefore in times of heavy rainfall their upper surfaces may have acted as glide-planes lubricated by an excess of water that had percolated down through the compound flows and accumulated there. Rotational slumps of this nature normally occur rapidly in a catastrophic manner on steep unstable slopes following periods of heavy rainfall when the ground is saturated with water. Where they rip away from the hillside, they leave arctuate scars, which may subsequently become infilled with weathered material and soil from slopes above. These features are recognisable in cross-section as V-shaped infills which effectively mark the upper surface of the slumped block. The V-shaped infill consisting of loosely-compacted soil above an inclined oxidised surface of a disaggregated lava flow overlying the roughly horizontal olivine basalt flow at Location 48 may be interpreted as the upper surface of such a slumped block (Fig. 3.15, Location 48).

Rotational slump structures similar to those seen in the Lalibela North Section occur throughout the Lalibela region. They are particularly evident along the southern fringes of the Mesgeja and Mashela Meda Ridges, south of Lalibela (Fig. 3.15), where they are seen to displace numerous segments of the lava sequence to form a series of rotated blocks with varying dip-angles, one to another, for their constituent lavas (Fig. 3.15 - View of the Mesgeja and Mashela Meda Ridges). When these slumps occurred is debatable. It is most likely however, that they occurred relatively recently after prolonged periods of erosion during which the drainage system was able to cut deeply into the plateau, thereby destabilising the steepening slopes of the incised valleys and escarpment edges. This process is ongoing as erosion continues to cut into the plateau, and it is evident today in the common occurrence across

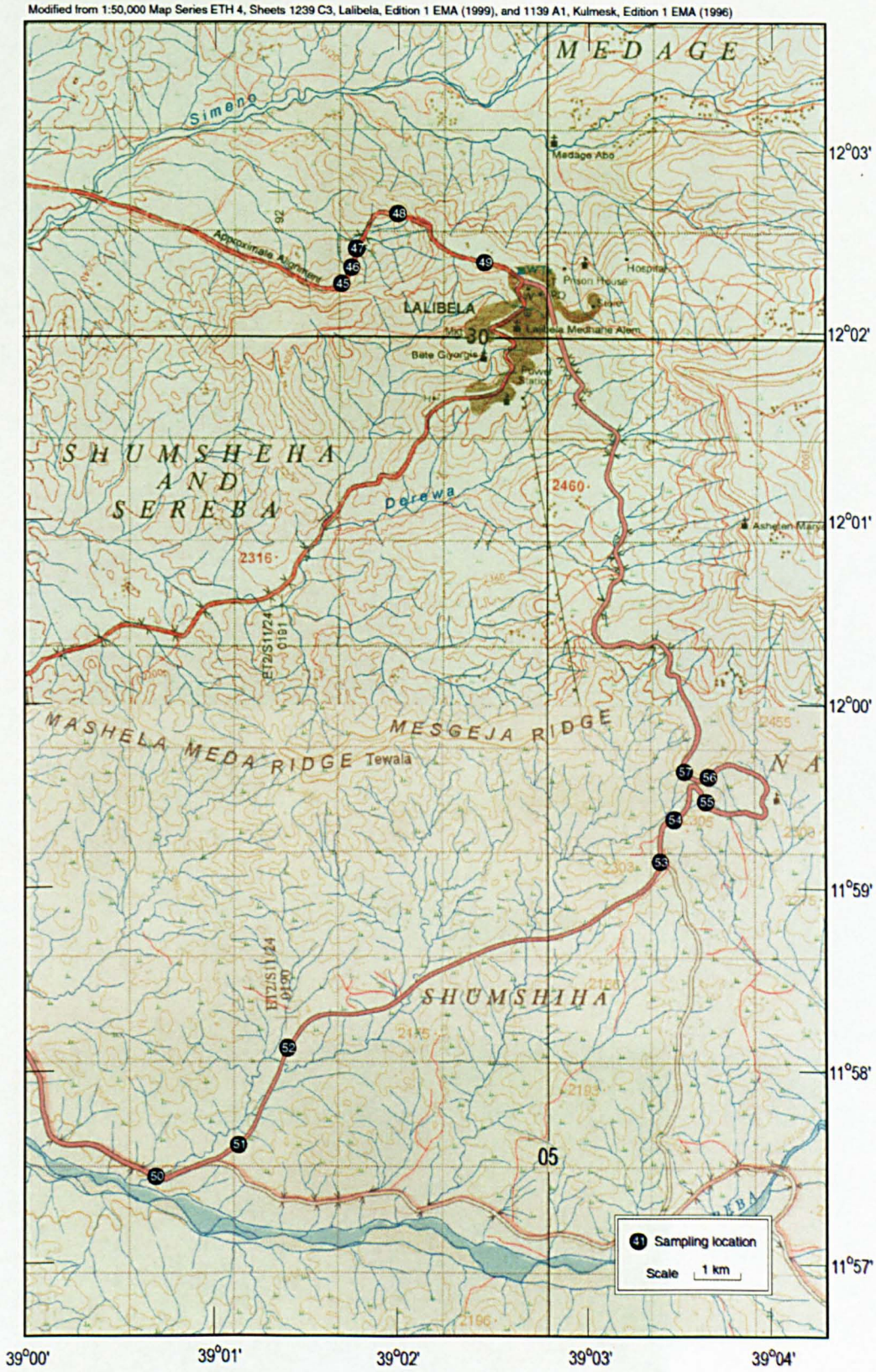

Figure 3.14 Sampling locations for the Lalibela North and Lalibela Airport Sections

Figure 3.15 Topographic cross-sections of the Lalibela North and Lalibela Airport Lava Sequences

Inter-trappean conglomerate between Locations 53 and 54

Location 48 V-shaped infill above tilted slump-block overlying undisturbed near-horizontal olivine basalt flow 01.03.27.18. The dashed line marks the hanging wall, and the arrow indicates the rotational movement ot the slumped block.

View of the Mesgeja and Mashela Meda Ridges from the roadside just north of Location 57, showing a series of slumped blocks which have tilted the otherwise flat layers of the traps around the Lalibela region. The white arrows show the rotational movement of the slumps.

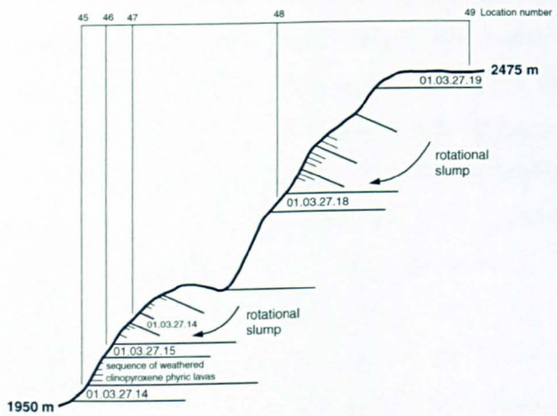

One of the many churches carved out of the ignimbrite sequences in Lalibela

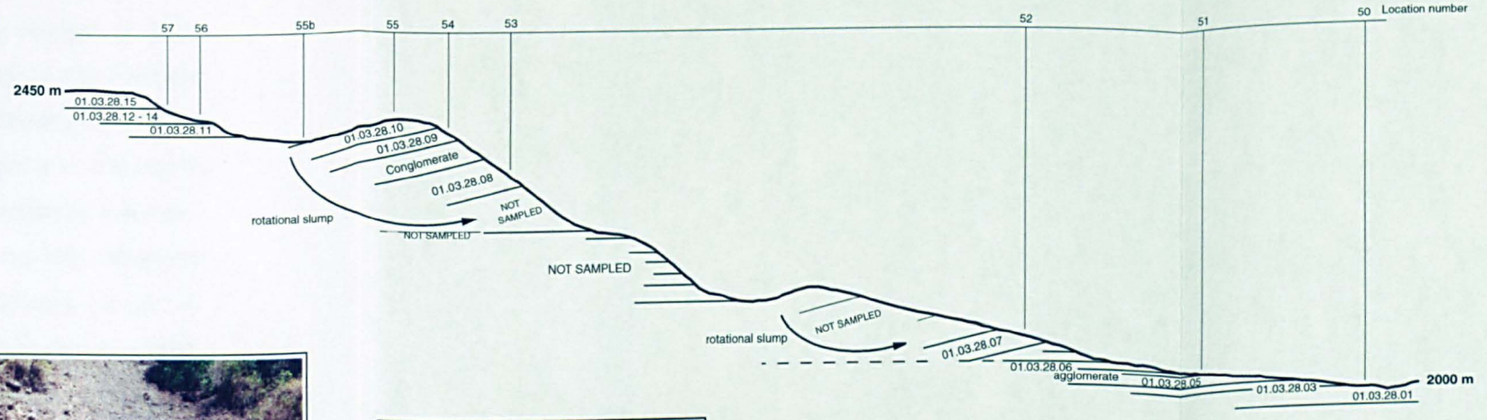

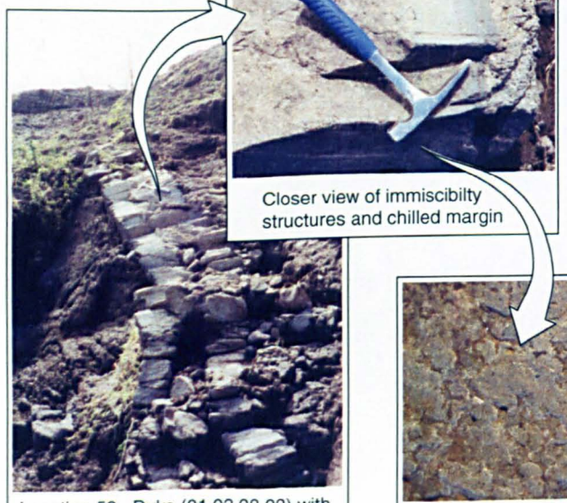

Location 50 Dyke (01.03.28.02) with unusual immiscibility structures and distinctive chilled margins

Closer view of immiscibilty structures and chilled margin

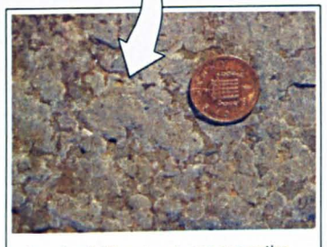

Immiscibility structures near the core of the dyke

Location 52 Oxidised paleaosol beneath picritic flow 01.03.28.07

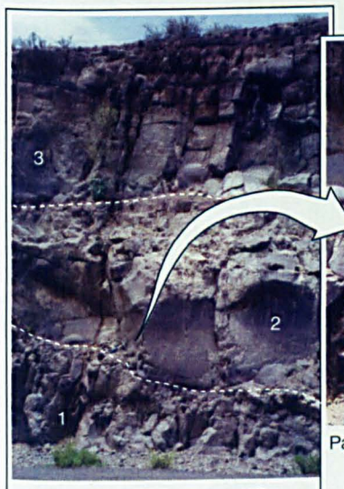

Location 57 Compound flow comprising three flow units (numbered) with dense massive lower parts (01.03.28.13) and scoriacious upper parts (01.03.28.14).

Pahoehoe structures on upper surface of flow beneath 01.03.28.13

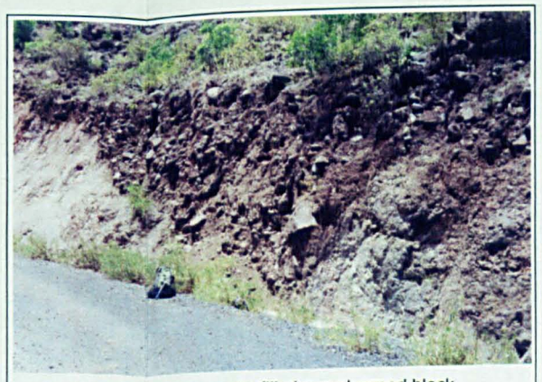

Location 55b V-shaped infill above slumped block

plateau of similar types of mass movement which are triggered by heavy rainfall during the rainy season.

The only intrusive body sampled in the Lalibela North Section was a dyke seen cutting through an ankaramitic flow sheet at Location 47, in the slumped section between locations 46 and 48. The dyke is approximately a metre wide with well developed cooling joints and pronounced chilled margins. It has an E – W trend and a basanitic composition very similar to the dyke encountered in the Bilbala Section at Location 43 (Chapter 5). It is unlikely that slumping has dramatically changed the orientation of the dyke, since the slumped block has shifted vertically rather than at an angle relative to the undisturbed sequence.

3.3.6 Lalibela Airport Section

From field observations it may be implied that the Lalibela Airport Section represents the more southerly and lower exposures of the same lava pile represented by the Lalibela North Section. The lavas along its length are similarly varied in their composition (Appendix 3.1.5) and morphology to those encountered in the Lalibela North Section, and they are similarly displaced by rotational slump structures evident in the field from V-shaped infills (Fig. 3.15, Location 55b) and variations in the dip of the lavas at different levels in the section (Fig. 3.15). The section extends between altitudes of 1988 and 2435 metres from locations 50 to 57, along the relatively recently constructed surfaced road from the town of Lalibela to its local airport at Shumshiha about 8 km to the southwest (Fig. 3.14). Its upper part reaches similar altitudes to the Lalibela North Section, and therefore, if the sequence between was not so broken and displaced by slumping, it might be expected that some of the thicker individual lava flows could be correlated between the two sections.

The lower part of the Lalibela Airport Section below Location 52 is made up of undisturbed, roughly horizontal, massive, jointed, laterally extensive sheet flows in excess of several metres thick with scoriaceous upper sections. The lowermost unit, exposed in the bed of a tributary of the Kechm Areba River beneath a low bridge at Location 50, is typically ankaramitic, and this is overlain by a distinctive trachybasalt flow which can be followed along the road for half a kilometre toward Location 51 before it disappears beneath the topsoil. Above this a series of flows including an aphyric basalt, an ankarmitic and a picritic flow, each near to 10 m thick, are exposed in a small quarried clearing and the hillside above at Location 51. Between the aphyric basalt and the ankaramitic flows there is also an agglomerate comprising a

variety of basaltic and trachytic fragments up to 30 cm or more across set in a fine ashy yellow-brown heavily decomposed matrix. Between locations 51 and 53 the topography becomes gently undulating with a thick soil cover and the lava sequence is rarely exposed, except at Location 52 where a picritic flow of an undefined thickness (> 2 m) can be seen, in a low road cutting, dipping at an angle of approximately 15° toward the northeast, suggesting that it may be part of a slumped block. Beneath this flow there is a distinctive red palaeosol with an approximate thickness of between 20 and 30 cm (Fig. 3.15, Location 52). The scoriaceous flow beneath this was too weathered to sample.

Beyond Location 53 the road begins to climb more steeply up toward the plateau, and the lava sequence from here up becomes better exposed in the numerous cuttings along its length up to Location 57. The olivine basalt and picritic flows exposed here, up to Location 56 form massive sheeted flows of up to 15 m thick with well-defined oxidised flow-tops. The flow units can be seen to vary in thickness laterally and in places they appear braided, suggesting that some are in fact part of compound flows. Between locations 53 and 54 there is, sandwiched between two lava flows, a 3.5 m thick conglomeratic unit with well-rounded boulders and cobbles (< 30 cm in diameter) of similar composition set in a light coloured friable matrix (Fig. 3.15, Locations 53 – 54). It exhibits rough cyclical grading with the majority of large clasts concentrated near the base, and at a second horizon 0.5 m from the top. The coarser horizons tend to be dominantly clast-supported whereas the intermediate sections between tend to be matrix supported. The upper surface of the unit is reddened by oxidation with some evidence of palaeosol development above. The rounded clasts and graded nature of the deposit suggest that it might be alluvial in origin, and in this respect it may represent a series of flood deposits washed onto the surface of the flow below. Alternatively it may be an agglomerate in which the ejecta were somehow rolled along during deposition. Since the unit was not studied in the field in sufficient detail, it was not possible to ascertain which of these alternatives was more probable.

The top of the sampled section is marked by a pronounced road-cutting through the brow of the hill at Location 57. This exposes part of a compound flow consisting of three massive jointed flow sheets with scoriaceous upper and lower margins (Fig. 3.15, Location 57). Good examples of pahoehoe flow structures are evident on the upper surfaces of the lower flow unit, and in the thicker upper scoriaceous section of the flow above, there are large vesicular cavities (20 cm in diameter) with drusy

linings of a white precipitate. The three flow sheets that make up this compound flow exposure are all olivine basalts with similar major- and trace-element compositions (Chapter 5). Above Location 57 the gradient of the topography becomes less steep again and the road rises steadily through a series of compound flows similar to that described above before reaching the vast ignimbrite sequences on the top of the plateau. None of these compound flows were sampled, and so they have not been included in the section.

E – W trending dykes similar to the one sampled in the Lalibela North Section are evident along the Lalibela Airport Section at locations 50, 51 and 53. On account of their appearance and orientation it may be suggested that the dykes from both sections are related, but since the chemistry of these dykes was not analysed, it cannot be concluded confidently that they are part of the same swarm. The dyke seen cutting the ankaramitic and trachytic flows exposed at Location 50 shows strange immiscibility structures which suggest that some sort of mixing between two melts of different composition took place during its emplacement (Fig. 3.15, Location 50). These structures are rounded globules (up to 7 mm in diameter), which are commonly agglomerated and partially coalesced to form larger globular clusters (up to 2 cm across). The spaces between the globules and the globular clusters are infilled with a fine-grained material similar in appearance to the globules themselves, such that, in places, the globules are only recognisable by the presence of a lighter coloured rim which seems to be some sort of reaction rim. On close examination of the dyke it can be seen that its entire is made up from this globular material. The average dimensions of the globules become smaller toward the chilled margins of the dyke where they are no more than 2mm in diameter. In places, the core of the dyke, where the globules are largest has been preferentially weathered out to leave hollow the central section of the dyke. The dyke itself, at its thickest, is no more than a metre wide.

Overall, the pattern of volcanic activity reflected in the Lalibela Airport Section, shows a gradual change from highly effusive sporadic activity, apparent from the thick sheet flows separated by oxidized flow tops and occasional palaeosols in the lower part of the section, to more continuous but lower effusive activity evident from the compound flows in the upper part of the section. The ignimbrites toward the top of the plateau furthermore mark a subsequent change to much more sporadic explosive volcanic activity. It is in these ignimbrites that the numerous and quite spectacular rock-hewn churches of Lalibela and the surrounding region have been crafted.

Like the lavas from the Lalibela North Section, the majority of lavas sampled in the Lalibela Airport Section show at least some signs of iddingsitization possibly indicative of high fO_2 conditions in the magma chamber from which they were derived. Unlike the lavas from the Lalibela North Section, however, those from the Lalibela Airport Section all show evidence for hydrothermal alteration of one kind or another, although it is not as pervasive as seen in the Dilb and Iyela sections. Most of the lavas contain zeolites, which generally can be seen lining the interior surfaces of vesicles and fracture surfaces, and some contain olivines which have been partially serpentinised.

As in the case of the Bilbala Section, all the lavas and intrusives, from the Lalibela North and Lalibela Airport sections, with the exception of two picrites from the Airport Section (01.03.28.09 & 01.03.28.10), are alkaline in composition, suggesting they too are representative of the later bimodal stage of flood volcanism generally assigned to the Alaji Formation. This is supported by the occurrence in the sequences of lavas with trachybasalt compositions and agglomerates indicative of explosive volcanism typical of more evolved magmatic activity than is generally associated with the generation of exclusively basaltic lavas.

3.3.7 Gashena Section

The Gashena Section represents the most varied of all the sampled sections, in terms of both the composition and the morphology of its constituent lithologies (Appendix 3.1.6). It extends in a long undulating path along the recently constructed surfaced Lalibela to Gashena road, between altitudes of 1906 and 2981 metres, from Location 58 on the southern side of the Koga River to Location 84 on the top of the plateau, half a kilometre or so north of Gashena (Figs. 3.16 & 3.17). The alkaline lavas and felsic pyroclastic deposits exposed along the length of the section truly reflect the bimodal character of the later stages of flood volcanism generally assigned to the Alaji Formation. Repetitive alternating sequences of thick sheet and compound flows of varying basaltic compositions and felsic pyroclastic deposits including ash-layers, agglomerates and ignimbrites, occur throughout the section signifying repeated cycles of differentiation and crustal contamination following successive influxes of partially crystallised source material into shallow-seated magma chambers (Pik et al. 1998 & 1999; Ayalew et al, 2002; Ayalew & Yirgu, 2003). Variations in the dip of the lavas along the lower flatter part of the section between locations 58 and 70 suggest that the sequence of lavas and pyroclastic deposits in this part of the section have been displaced either by faulting or by slump structures similar to those

seen in the region around Lalibela (Fig. 3.17). The series of low escarpments between these locations, with gentle northeast-facing dip-slopes and steeper southwest-facing scarp-slopes are typical of such faulted or slumped terrain, and the larger tributary rivers such as the Tiku Telef and Serdo Wiha, which cut north-westward across the area to join the northward flowing Deremo River (Fig. 3.16), seem to mark the inferred lines of displacement between each tilted block (Fig. 3.17). The upper part of the section, between locations 70 and 84 seems relatively intact, with the lavas and pyroclastics dipping consistently at an angle of ~ 5° toward the southwest, as in the Dilb and Iyela Sections 50 km or so to the east.

The lower part of the lowermost block, between locations 58 and 60 comprises a number of massive, relatively evolved basalt sheet flows in excess of 10 m thick (Fig. 3.17, Location 58) separated by polymict agglomerates containing a variety of basaltic ejecta (< 45 cm in diameter) set in a light coloured friable, ashy matrix. Similar agglomerates (Fig. 3.17, Location 61) are seen in the upper part of the block between well-jointed ankaramitic sheet flows several metres in thickness. Most of the flows throughout the lowermost block can be seen to vary in thickness laterally, and where there the surfaces of the flows are reddened by oxidation some of the flows can be seen to interleave.

In the series of titled blocks between locations 61 and 70, a number of near-horizontal, laterally extensive (> 2 km) sheet and compound flows of ankaramitic composition, generally < 10 m thick, separated by oxidised flow surfaces (Fig. 3.17, Location 62), occur in sequence with aphyric basalt flows of similar thickness and lateral extent. The top of this sequence is marked by the only picrite in the Gashena section at Location 69. Above this there is an unusual basaltic agglomerate which appears to have been deformed by faulting (Fig. 3.18, Location 70). It is probable that the fault zone immediately to the north of this agglomerate represents the northern limit of the tilted block between locations 64 and 70 (Fig. 3.17). At Location 63, one of the aphyric basalt flows in the sequence below is seen to be overlain by an ignimbrite with angular embayed lithic fragments of varying compositions, several centimetres in length, set in a fine partially-vitrified purple matrix.

It is notable that there are no picrites, ankaramites or olivine basalts in the upper part of the Gashean Section above Location 70, and that all the basalts above this point are aphyric. Furthermore, most of these aphyric basalts exhibit well-defined columnar colonnades and scoriaceous, intensely fractured upper entablatures (Fig. 3.17, Location 79), which are characteristic of lava flows in which the cooling regime has

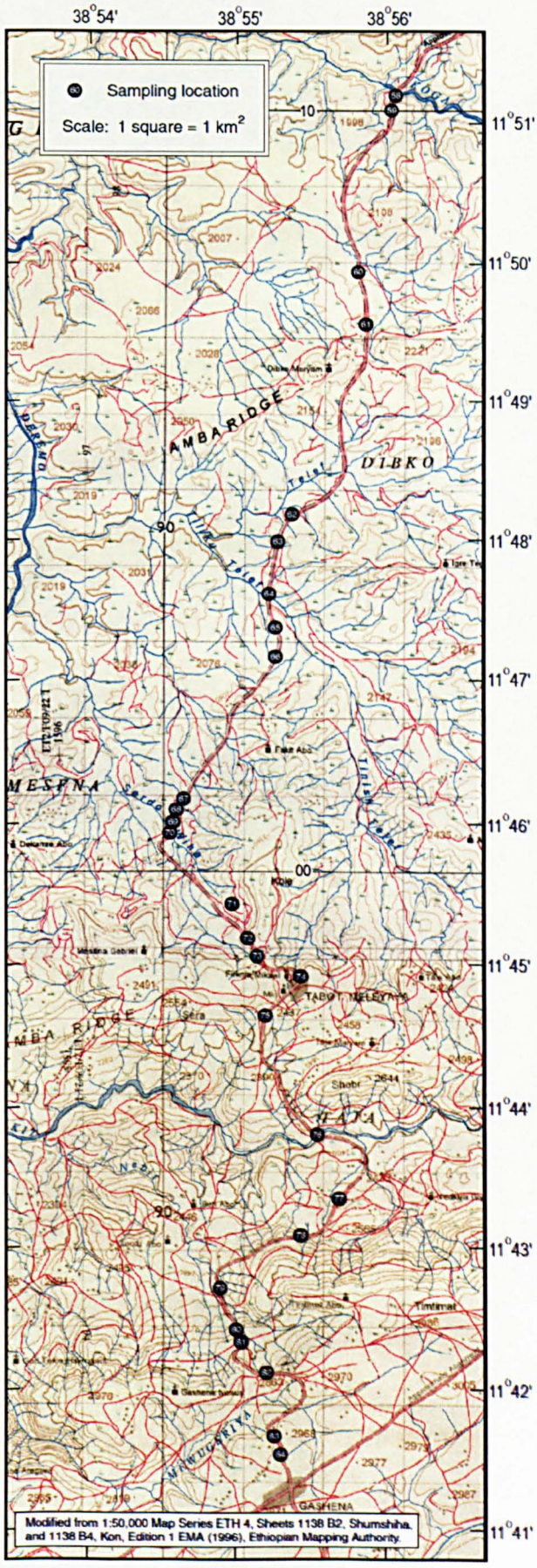

Figure 3.16 Sampling locations for the Gashena Section

Figure 3.17 Topographic cross-section of the Gashena Lava Sequence

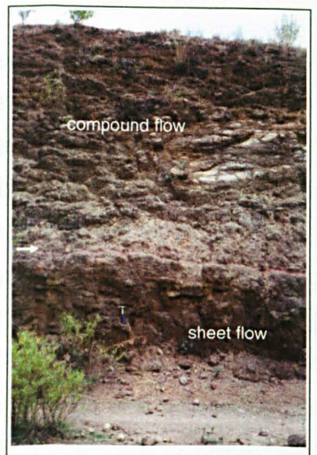

Location 62 Compound flow above sheet flow with oxidised flow-top. The flow top is shown by the white arrow.

Location 70 Basaltic agglomerate/breccia (01.03.30.01) marking possible narrow fault zone following the Serdo Wiha River

Location 74 Finely laminated felsic ash (01.03.30.05) at Tabot Meleyaya

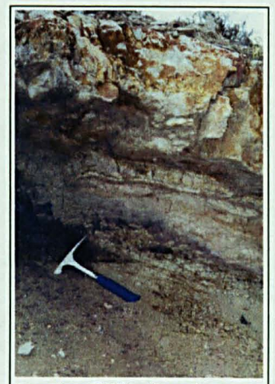

Location 75 Weathered contact between felsic ash and basalt

Location 75 Fingers of baslt within the felsic ash

Location 77 Ignimbrite (01.03.30.07) overlying basalt (01.03.30.08). The basalt is masked by weathered ignimbrite

Location 61 Agglomerate beneath 01.03.29.04

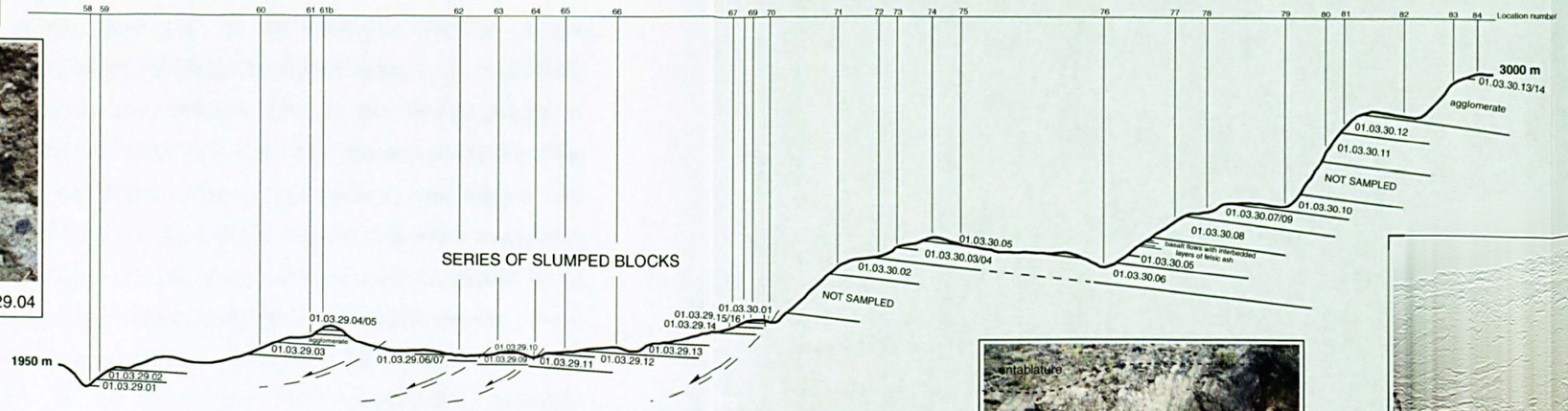

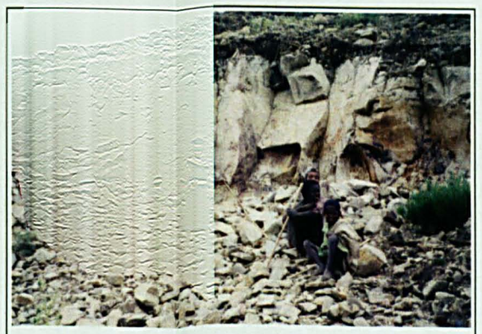

Location 80 Jointed ignimbrite exposure (01.03.30.11)

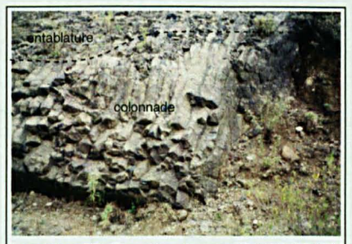

Location 79 Basalt columns (01.03.30.10)

Location 58 Massive basalt flow (01.03.29.01) above oxidised flow top level with Koga River bridge

Location 72 Columns of aphyric basalt (01.03.30.03) protruding from road-cutting

Location 84 Basalt on the top of the plateau (01.03.30.14)

Location 73 Curved columns of ahyric basalt (01.03.30.04)

Location 82 Agglomerate above 01.03.30.12

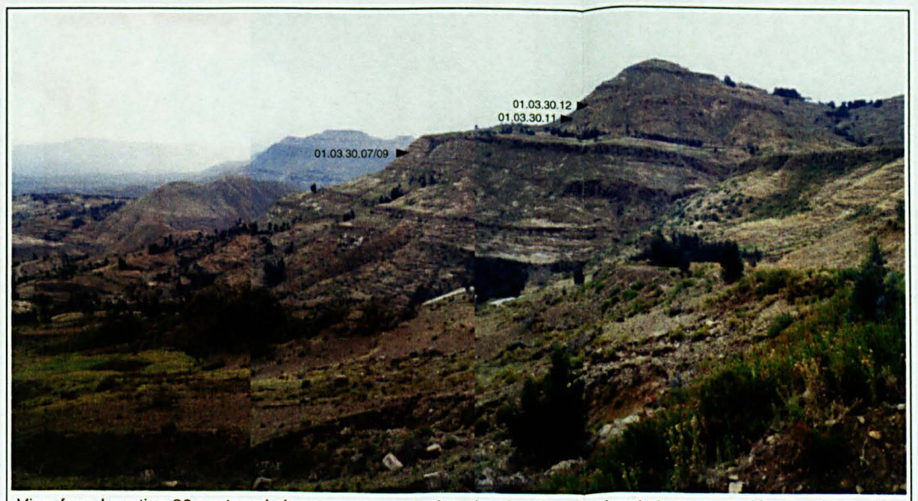

View from Location 80 eastward along escarpment edge showing the prominent steps created by the alternating layers of basalt and ignimbrite in the upper bimodal section of the Traps.

been modified in some way by their interaction with surface water (Lyle, 2000). This is supported by the fact that in some of the basalt flows, the columns are seen to extend horizontally (Fig. 3.17, Location 72) suggesting that cooling propagated through the lava away from a standing bodies of water. Similarly, the curvi-columnar jointing evident in other similar flows (Fig. 3.17, Location 73) may be attributed to the inundation of the cooling lava-surfaces by displaced drainage, which subsequently penetrated along the master joints thereby modifying the internal isotherms (Lyle, 2000). These cooling features therefore indicate that, during the emplacement of the lavas, there was an abundance of surface water in the region, and that the prevailing climate was able to sustain such hydrological conditions.

Between the aphyric basalts in the upper part of the Gashena Section (above Location 70), there occur a variety of felsic pyroclastics. A thick layer (> 3 m) of finely laminated felsic ash is exposed along the roadside through the hill-top village of Tabot Meleyaya (Fig. 3.17, Location 74). This layer can be followed along the road for half a kilometre to the south of the village where it can be seen interleaved with aphyric basalt (Fig. 3.17, location 75). It is also seen in several roadside exposures between locations 76 and 77 where it is interspersed with the aphyric basalt lavas suggesting that it was deposited contemporaneously with their emplacement. Above Location 77, between the aphyric basalt flows, a series of thick massive rhyolitic ignimbrites occur at locations 77, 78, 80 and 81 (Fig. 3.17, Locations 77 and 80). These ignimbrite units, similar to those seen at the top of the Dilb Section, form prominent breaks-of-slope, which can be traced for several kilometres along the escarpment (Fig. 3.17 - View from Location 80 eastward along escarpment). They reach up to 20 m in thickness, and are composed of light grey to beige coloured, earthy to sinter-like deposits with numerous euhedral crystals of feldspar, pyroxene and amphibole, lithic fragments of dominantly basaltic composition, and rounded quartz (Appendix 3.1.6). In some of the units, the crystal assemblage is often present as glomerophyric aggregates, which may have amassed under turbulent conditions during deposition. In others, some of the lithic fragments have been stretched into thin wisps, suggesting that they were pliable when they were deposited. The evolution and mode of deposition of these ignimbrites would have been similar to that described for the similar deposits seen at the top of the Dilb Section (Section 3.3.2). The correlation of similar rhyolitic ignimbrites, described elsewhere in the Province, with tephra-layers in the Indian Ocean is testimony at least to the magnitude and highly explosive nature of the eruptions responsible for their emplacement (Touchard et al. 2003; Ukstins Peate et al. 2003). Toward the top of the Section at Location 82

there is thick (> 8 m) agglomerate unit which is sandwiched between the uppermost ignimbrite exposed at Location 81 and the columnar basalts exposed at locations 83 and 84 on the top of the plateau. This agglomerate is similar both in terms of its composition and thickness to those previously encountered in the lower part of the Gashena Section at Location 61 and in the lower part of the Lalibela Airport Section at Location 51. It is a polymict agglomerate with a variety of mainly basaltic ejecta, and some felsic ignimbritic ejecta set in a light beige fine friable matrix (Fig. 3.17, Location 82). The unit is matrix supported, and the diameter of some of the constituent ejecta reach up to 70 cm, or more. As for the lithic fragments in the ignimbrites, it is likely that the ejecta seen in the agglomerates represent fragments of the lithological units beneath, broken off during eruption.

No intrusive rocks were sampled in the Gashena Section. As in the other sections, the extrusive rocks of the Gashena Section show variable effects of hydrothermal alteration, and iddingsitization. These effects are more noticeable in the porphyritic basalts and ignimbrites than they are in the aphyric basalts (Appendix 3.1.6). Like the other sections, the nature of the alteration seen in the Gashena Section is pervasive, suggesting that it too was a result of large-scale hydrothermal upflow rather than localised hydrothermal activity associated with individual eruptions and intrusions. This suggests that during the emplacement of the Gashena lavas and pyroclastic deposits the ground was saturated with water; this is consistent with the inference that there was an abundance of surface water as suggested by the columnar features in the aphyric basalts described above.

4. PETROGRAPHY AND MINERAL CHEMISTRY

4.1. Introduction

4.1.1 Focus on the Dilb and Iyela sections

The Dilb and Iyela sections together are stratigraphically more coherent and contain more picrites than the other sections. Furthermore, $^{40}Ar/^{39}Ar$ ages for selected lavas in the sequence (31 - 30 Ma) and for the ignimbrite marking the base of the Alaji Formation at the top of the Dilb Section (28.2 - 30.2 Ma) (Hofmann et al. 1995; Hofmann, 1997) place temporal constraints on the emplacement of the sequence that allow it to be related to other documented lava sequences elsewhere in the province (Fig. 2.8). In the other sampled sections, picrites are rare, and the lava sequences are not so clearly related stratigraphically because of their more sporadic exposure and the apparent presence of structural discontinuities that apparently displace them relative to one another. Also, the fact that there are no reliable age data for these other sections makes it difficult to relate them one to another and to other documented lava sequences elsewhere in the province. Moreover, the lavas and pyroclastic deposits in these other sections are petrographically and geochemically more diverse and consequently not so obviously genetically related compared with those in the Dilb and Iyela sections. For these reasons, and because of time constraints in compiling this thesis, it was decided to focus on the Dilb and Iyela sections. By documenting the petrography and geochemistry of the dominantly picritic lavas from these sections in detail, rather than presenting an overview of the petrography and geochemistry of the more diverse rocks from all the sections, it is envisaged that a more coherent picture of the petrogenesis and evolution of the magmatism responsible for the formation of the traps will be revealed.

4.1.2 Petrography

Polished sections approximately 30 µm thick were made of all the samples collected, with the exception of samples 01.03.29.08 and 01.03.29.15 (which were lost in transit) and 01.03.29.02 and 01.03.27.13 (which were kept intact for photographs). Polished sections rather than thin-sections were made so that the mineralogy of the cut sections could be examined by electron microprobe as well as with a standard polarising microscope. Petrographic descriptions of the polished sections of all the rocks from the Dilb and Iyela sections are compiled in Appendix 4.1 and as with the sample details tabulated in Appendix 3.1 these are documented in stratigraphic order rather than in the order in which the samples were collected. The characteristics of

the phenocryst and groundmass assemblages are described together with visual estimates of their percentage proportions, and the nature and percentage-content of vesicles present in section. The phenocryst and vesicle percentages are recorded as proportionate to the whole rock, whereas the percentages of groundmass minerals are recorded as proportionate to a representative area of the groundmass only. The nomenclature used to describe the morphology of the olivine phenocrysts is adapted from Donaldson (1976) (Appendix 4.2.1), and the classification and grouping of the rock-types is based, retrospectively, on combined petrographic and geochemical analyses. The terminology used to classify the rock-types is loosely based on the TAS classification scheme (Fig. 5.1), adapted from Cox et al. (1979), although the more descriptive terms, are adopted to emphasise their principal mineralogical differences. The term picrite is here, however, used to describe lavas with more than 12% MgO - as proposed in the more recent IGUS reclassification of high-Mg and picritic volcanic rocks (Le Bas, 2000). The use of the term komatiite for rocks above 18% MgO, proposed in the same reclassification, is, on the other hand, not used here, on the grounds that it is a textural term referring to rocks characterised by the presence of spinifex olivine (Kerr and Arndt, 2001) - it was therefore considered inappropriate for the rocks described in this thesis. According to this revised classification, all of the rocks classified as ankaramites are technically picrites, although they are not referred to as such because the notable dominance of clinopyroxene in their phenocryst assemblages.

4.1.3 Mineral chemistry

The mineral chemistry of representative phenocrysts and groundmass microlites from each lava-group in the Dilb Section, and from picrites in the other sections (except Gashena) were determined by electron microprobe analysis. All microprobe analyses were carried out on a Cameca SX100 electron microprobe at the Open University, using an accelerating voltage of 20 kV, a beam current of 20 nA and a spot size of 10 μm. Analytical precision was estimated from repeated analyses of Olivine Standard 131292 (Appendix 4.3.1), and analytical accuracy was measured against published values for this standard reported by McGuire et al. (1992). On the basis of 55 analyses of the standard, the percentage uncertainties calculated from 100 x 1σ/mean for SiO_2, FeO, MgO, CaO and NiO are 0.6%, 0.8%, 0.3%, 28.8% and 2.2% respectively; the percentage errors for these oxides compared to the published values (McGuire et al. 1992) are -0.8, 0.6, -0.4, -2.2 and -10.1 respectively. Analytical precision was also estimated from repeated analyses of a selected olivine phenocryst from Sample 01.03.31.05 (Appendix 4.3.2). On the basis of 11 analyses of this

phenocryst, the percentage uncertainties for SiO_2, FeO, MgO, CaO and NiO are 0.6%, 0.4%, 0.2%, 4.5% and 2.5% respectively. Control charts for the above oxides, and for Fo content calculated directly from the cation contents for Mg and Fe^{2+} ($Mg/(Mg+Fe^{2+})$, are presented for the standard and duplicate data at the end of Appendix 4.3.1 and 4.3.2 respectively to illustrate the accuracy and precision of the analyses. It can be seen from these charts that the majority of data for the represented oxides for both the standard and the duplicate plot well within the confidence limits set at plus and minus 2σ from the mean, thereby confirming an acceptable degree of precision for the analyses. Similarly, with the exception of NiO, an acceptable degree of accuracy for all other represented oxides may be assumed since their published values, plotted on the control charts for the standard data, also plot comfortably within the 2σ confidence limits. This is true even for CaO with an initially alarming percentage uncertainty of 28.8%. With the exception of FeO, the average values for all other represented oxides plot can be seen to plot marginally below the respective published values as confirmed by the percentage errors quoted above.

Microprobe analyses of the phenocrysts and groundmass minerals of representative samples from the main lava-types were carried out to illustrate the range of compositions present within and between the sampled sections, and to support observations made during petrographic examination of the polished sections. The bulk of the analyses are of the core compositions of the main phenocrysts, and these were carried out primarily to evaluate whether or not the phenocrysts were in equilibrium with the whole-rock composition of their hosts. Since olivine is the first mineral to crystallise in basaltic magmas, its core composition may be assumed to reflect the composition of the parental liquid (Ford et al. 1983; Beattie et al. 1991, 1993; Thompson and Gibson, 2000), which in turn may be used to estimate its potential temperature and degree of mantle melting from which it was generated (McKenzie and Bickle, 1988, Gill et al. 1992; Nisbet et al. 1993). For these reasons the olivine phenocrysts, particularly those in the more Mg-rich picrites from each section, were targeted for analysis. Core-to-rim traverses of selected phenocrysts were also analysed to check for compositional zoning which may reflect evolutionary changes in the temperature, pressure, redox state or bulk composition of the melt during crystallisation (Simonetti et al. 1996). Clinopyroxene is particularly useful in monitoring such evolutionary changes since it remains on the liquidus over a wide range of temperatures (1100°C - 1600°C - Bultitude and Green, 1971; Thompson, 1974) and melt compositions, it readily incorporates measurable concentrations of

minor and trace elements, and is relatively slow to re-equilibrate through diffusion (Shimuzu, 1990). Consequently, as well as a number of potentially zoned olivine phenocrysts, several large, zoned clinopyroxene phenocrysts identified as such under the microscope were selected for core-to-rim analysis. Core compositions of clinopyroxenes were also analysed to gain some insight into the composition, temperature and oxygen fugacity of the melts from which they formed. In addition, a number of Cr spinels and their host olivines from selected samples from each section were analysed to estimate the temperature and oxygen fugacity (fO_2) of the magmas from which the olivine phenocrysts crystallised.

All raw microprobe data are compiled, together with the dates and order of analyses, in Supplement 1. This data has been sorted on the basis of the minerals analysed and compiled in Appendix 4.4 in ascending sample-number for each section. The oxide contents for olivine, pyroxene and feldspar analyses have been copied to this appendix from the raw data, and to avoid possible discrepancies arising from differences in the atomic masses used in the software to automatically calculate cation contents, the respective cation contents were recalculated using the atomic masses listed on the title page of the Appendix 4.4. Fe^{3+} contents for the pyroxene analyses were calculated stoichiometrically (Droop, 1987) using an interactive spreadsheet PX-NOM (Sturm, 2002), and the recalculated pyroxene analyses (together with calculated vales for Al^{IV} and Al^{VI}) generated from this spreadsheet have been included in the appendix in addition to the raw analyses. Canil & O'Neill (1996) argue that the calculation of accurate Fe^{3+} contents from electron microprobe analyses by such stoichiometrically based methods is unreliable for pyroxenes; therefore, the iron-corrected pyroxene analyses have been included for speculative purposes, primarily to give some indication of the Fe_2O_3 content of the pyroxenes. Such speculative data, when viewed alongside more robust data from spinel analyses, may be usefully employed as a proxy for fO_2. The Fe^{3+} contents for spinels and other Fe-Ti oxides were calculated from their total iron values (FeO) using the method outlined in Appendix 4.5 after Lucas et al. (1989). This method of calculating Fe^{3+} contents for Fe-Ti oxides is similar to that used for the pyroxenes in that it is stoichiometrically based. It is suggested by Canil & O'Neill (1996), however, that such methods yield more precise estimates of Fe^{3+} for Fe-Ti oxides than they do for pyroxenes because of their comparatively higher total Fe, and much lower contents of SiO_2, which is particularly prone to vary with subtle changes in operating conditions of the microprobe. Furthermore, recent doubts over the accuracy of such

stoichiometric calculations of the ferric iron content of spinels from electron microprobe analyses were reported to be unfounded by Ballhaus et al. (1991).

With the exception of a few Fe-Ti oxide analyses for which no other representative data was available, all analyses with oxide totals below 98 % or above 102 %, or those with spurious stoichiometric totals, were omitted from the appendix. Those Fe-Ti oxide analyses with uncharacteristically high SiO_2 contents were also omitted despite the fact their oxide and stoichiometric totals were within acceptable limits, since it is likely that some of the matrix in which the targeted grains were set contributed to such analyses. For each analysis in the appendix, a reference for the mineral grain analysed, and the position or order in which it was analysed have been included so that the treated data may be traced back to the raw analyses compiled in Supplement 1. In addition, the morphology of the analysed grains and a description of the type of analysis (indicated by the abbreviated references listed on the title page) are also included in the appendix, along with useful elemental exchange indices and end-member compositions calculated directly from the cation contents of each analysis.

4.2 Petrography of the rocks from the Dilb Section

4.2.1 Preface

Detailed petrographic descriptions of the lavas, ignimbrites and intrusive rocks from the Dilb section are documented in Appendix 4.1.2. On the basis of these descriptions and the geochemical analyses presented in Chapter 5, the lavas have been grouped as picrites, ankaramites or olivine basalts as shown in Figures 4.1 - 4.3. The ignimbrites and intrusive rocks have been grouped separately as shown in Figures 4.23 and 4.24.

4.2.2 Lavas from the Dilb Section

Classification: The lava groups are presented in Figures 4.1, 4.2 and 4.3, from left to right, in order of increasing grain size of the groundmass, and micrographs of three representative samples are shown therein to illustrate the textural range for each group. From the visual estimates of the percentage proportions of phenocrysts and groundmass minerals shown for each sample, it can be seen that there are consistent and significant variations in both the phenocryst and groundmass assemblages between the lava groups. The picrites are characterised by phenocryst assemblages dominated by olivine (15 – 33 %) with subsidiary amounts of

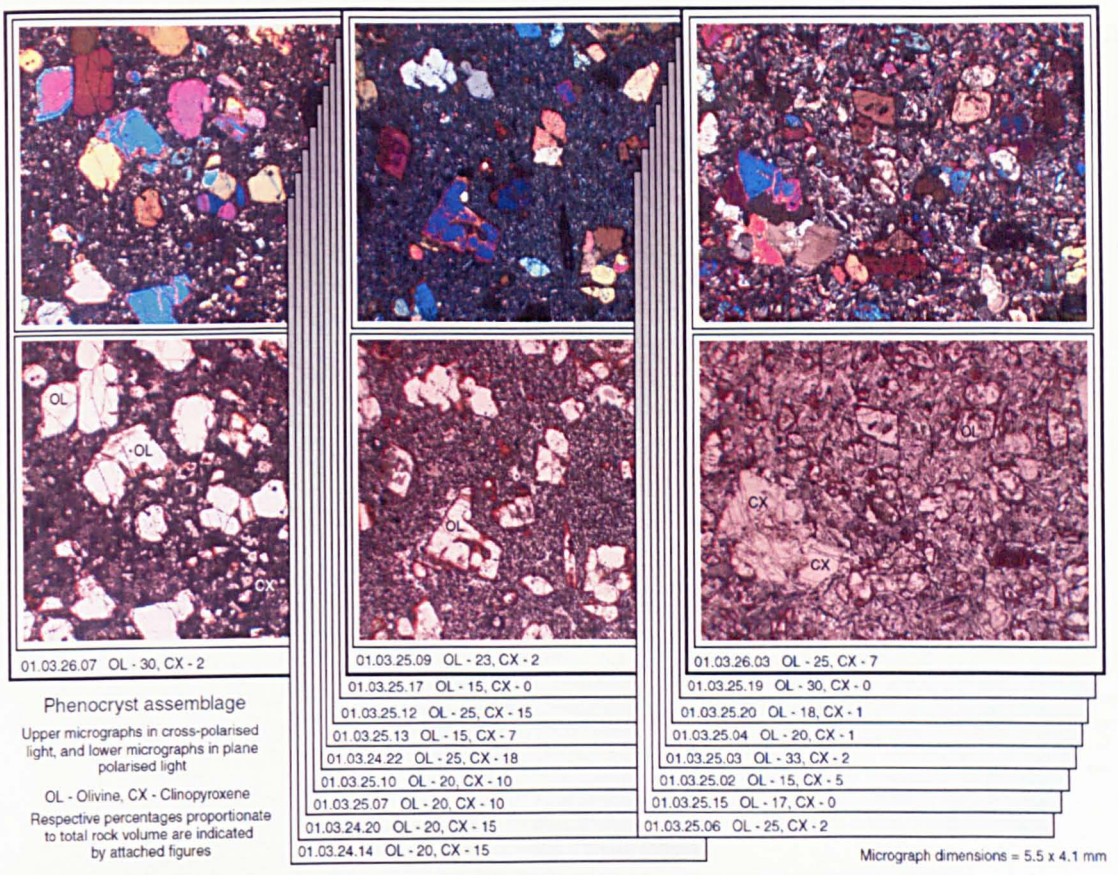

Phenocryst assemblage

Upper micrographs in cross-polarised light, and lower micrographs in plane polarised light

OL - Olivine, CX - Clinopyroxene

Respective percentages proportionate to total rock volume are indicated by attached figures

Micrograph dimensions = 5.5 x 4.1 mm

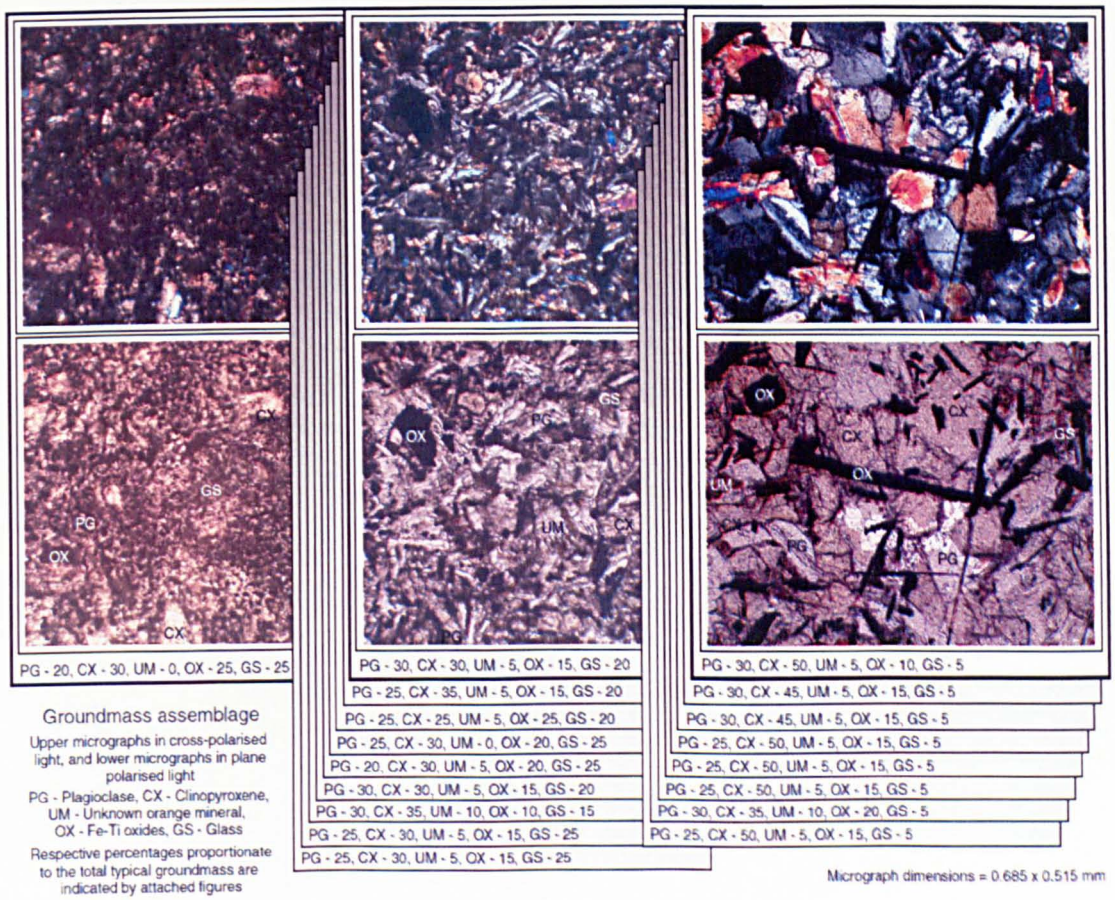

Groundmass assemblage

Upper micrographs in cross-polarised light, and lower micrographs in plane polarised light

PG - Plagioclase, CX - Clinopyroxene, UM - Unknown orange mineral, OX - Fe-Ti oxides, GS - Glass

Respective percentages proportionate to the total typical groundmass are indicated by attached figures

Micrograph dimensions = 0.685 x 0.515 mm

Figure 4.1 Picrites from the Dilb Section (see text for description of micrographs)

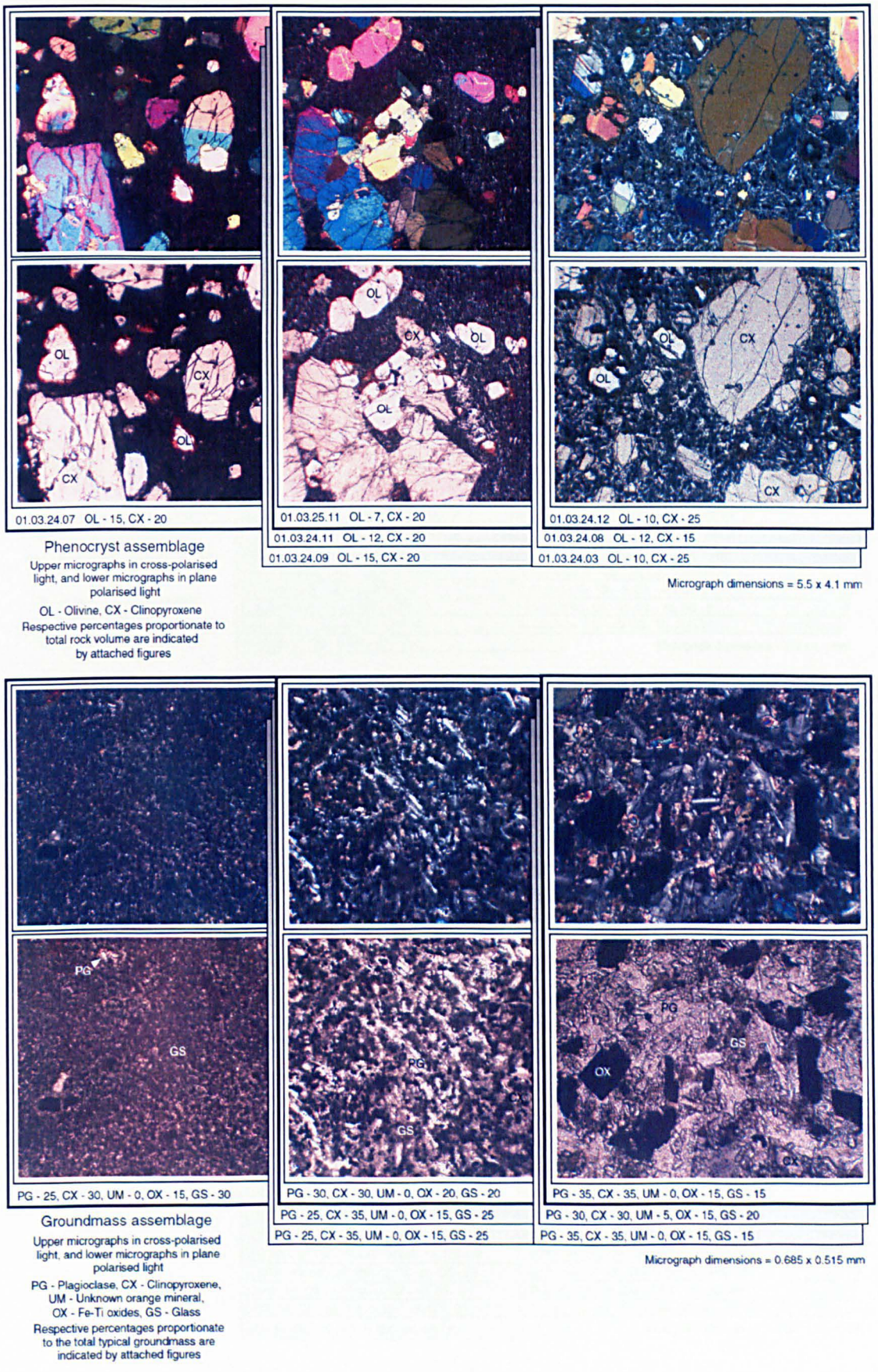

Figure 4.2 Ankaramites from the Dilb Section (see text for description of micrographs)

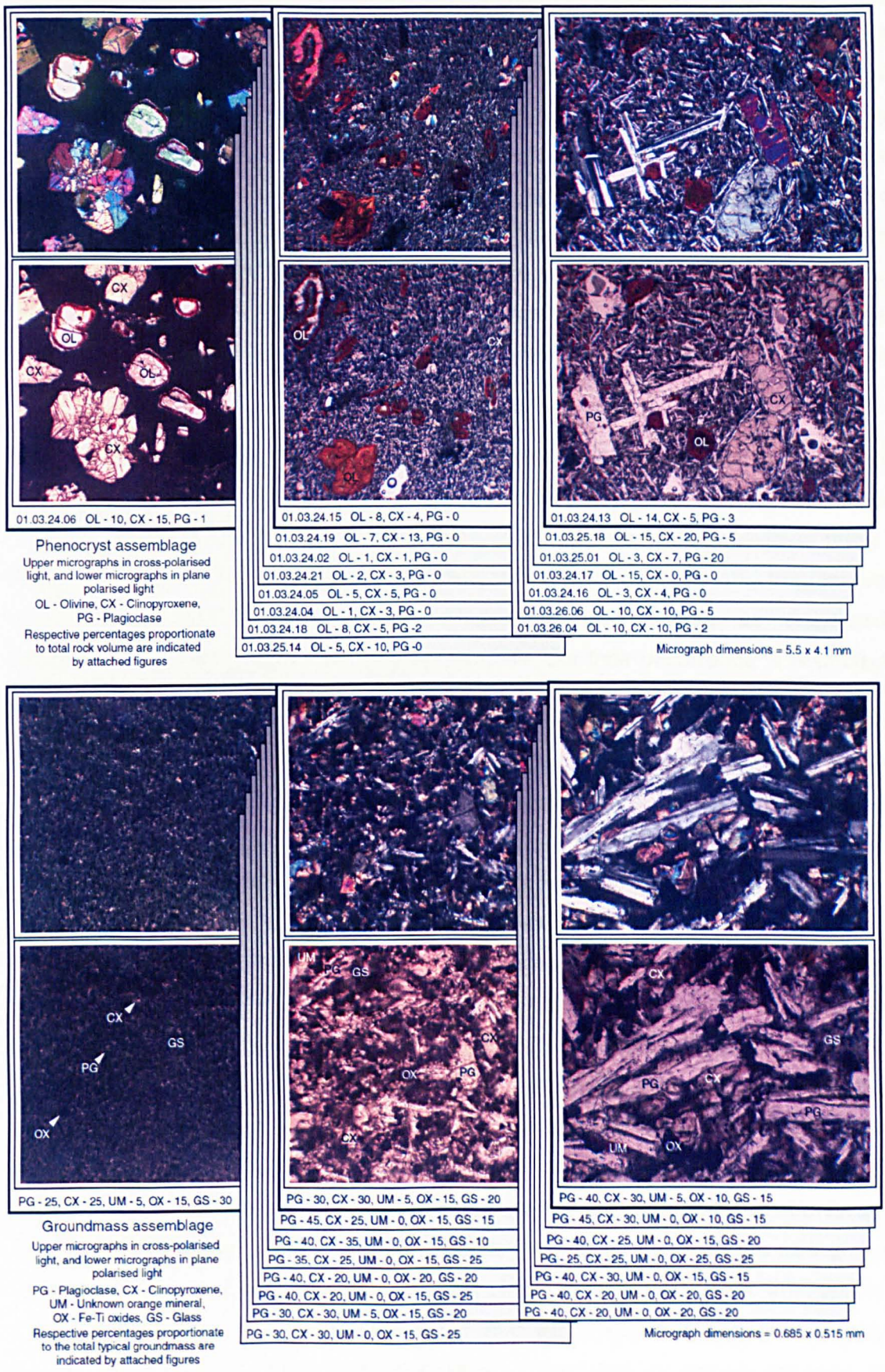

Figure 4.3 Olivine Basalts from the Dilb Section (see text for description of micrographs)

clinopyroxene (0 – 18 %), whereas the ankaramites are characterised by phenocryst assemblages dominated by clinopyroxene (15 – 25 %), with subsidiary amounts of olivine (7 – 15 %). Generally, both these groups show a characteristic dominance of clinopyroxene over plagioclase in their groundmass assemblages, although this is less pronounced in the ankaramites than in the picrites. The olivine basalts have a variable mix of phenocrysts, but are more so characterised by a dominance of plagioclase over clinopyroxene in their groundmasses, and by the occurrence of plagioclase phenocrysts (1 – 20 %) in the more coarse-grained samples. It is generally the case, also, that most olivine phenocrysts in the olivine basalts are extensively or entirely replaced by iddingsite, and are almost all overgrown with fresh olivine.

Phenocrysts: The textural relations, morphology and optical properties of the olivine and clinopyroxene phenocrysts are similar in all three lava groups, although there are slight but significant differences in the olivine morphology between individual lavas. Both minerals occur in most of the lavas as randomly dispersed, variably fragmented phenocrysts, and as glomerocrysts. Plagioclase also occurs as dispersed phenocrysts and as components in glomerocrysts, but their occurrence is restricted to the more coarsely grained olivine basalts.

Olivine: Morphologically, the olivine phenocrysts have been grouped into five distinct types (Large Polyhedral, Small Polyhedral, Striated, Elongate and Skeletal) as described and illustrated in Appendix 4.2.1. The occurrence of these different morphological types in each of the sampled lavas, together with their characteristics and habits are recorded in Table 4.1 – illustrated examples are shown in Figure 4.4. The large polyhedral olivines range in size between 1 and 4 mm across, small polyhedrals are invariably < 1 mm, striated are rarely > 2 mm across, and the elongate and skeletal are generally no more than 2 mm long. All varieties range in form from euhedral to anhedral, and are characteristically clear and cracked. They are generally non-pleochroic and exhibit a range of vivid third order interference colours from grey to white, yellow, orange, pink and blue, typical for Mg-rich olivine. Representatives of each of the morphological types, occur in most of the lavas, irrespective of their group, however it is notable that skeletal olivines are rare in the olivine basalts and absent in the ankaramites (Table 4.1). Most olivines, irrespective of their morphology, are variably rounded and embayed, and almost invariably rimmed with iddingsite. Many, are extensively iddingsitized, or entirely replaced by iddingsite, and/or serpentine, particularly those of the striated, elongate and skeletal

Table 4.1 Olivine morphology of the lavas from the Dilb section

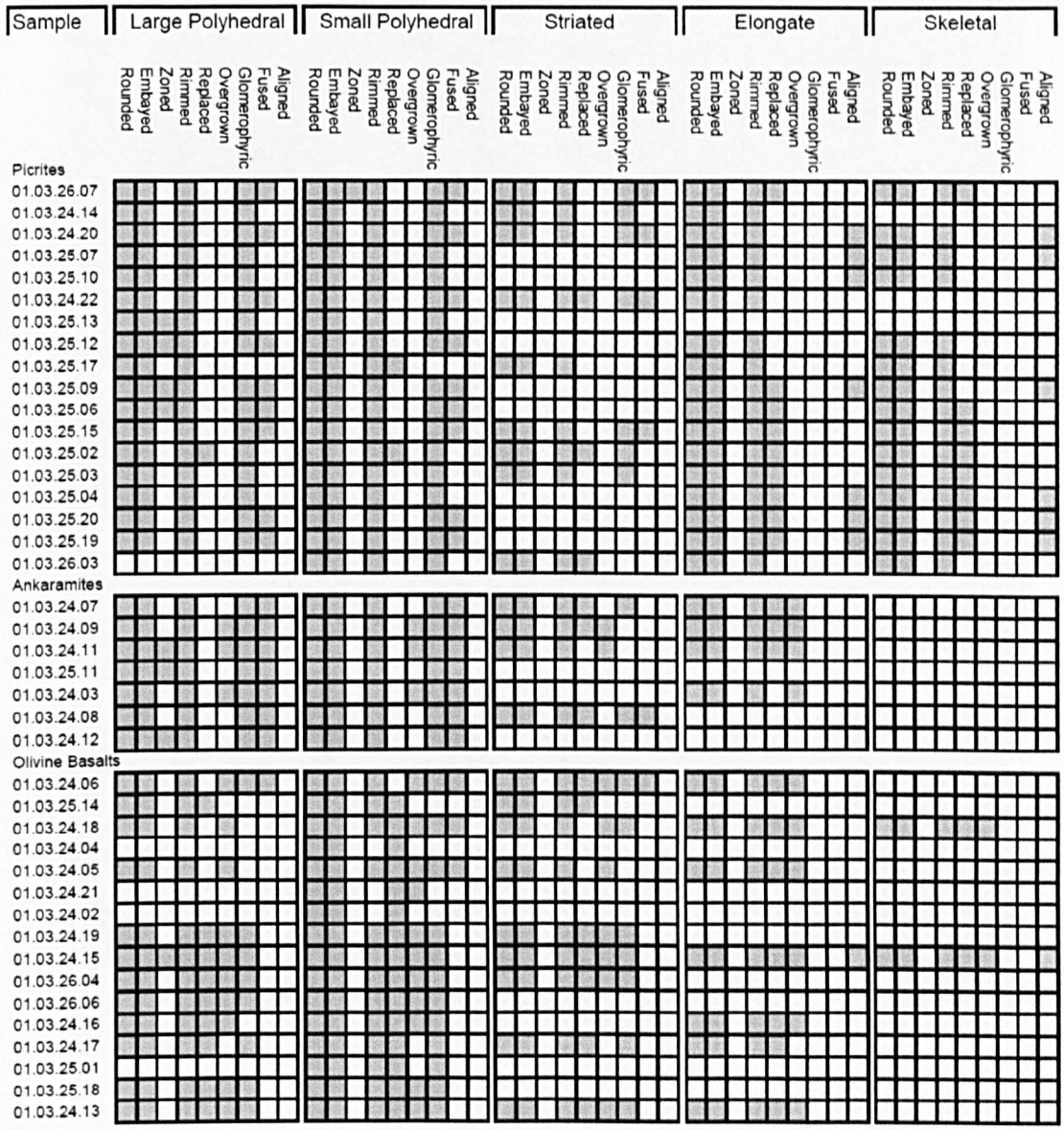

Note: Samples in each group are arranged in order of increasing grain size of the groundmass.

varieties. As previously mentioned, almost all of the olivines in many of the olivine basalts, including the polyhedral varieties, are largely replaced or entirely pseudomorphed by idddingsite and/or serpentine (Fig. 4.3). It is notable also that many of these are overgrown or rimmed with fresh highly birefringent olivine (Fig. 4.5). Such overgrowths are often thin and only visible at high magnification. They do not occur in the picrites and they are rare in the ankaramites. Strain features and zoning are rare in the olivines and seem confined to the polyhedral varieties. The tendency to occur as glomerocrysts also seems confined to the polyhedral and striated varieties. In fact, the elongate and skeletal olivines are never glomerophyric, whereas they are often aligned and chained (Fig. 4.6).

LP - Large polyhedral, SP - Small polyhedral, ST - Striated, E - Elongate, SK - Skeletal (Micrograph dimensions = 7 x 4.5 mm)

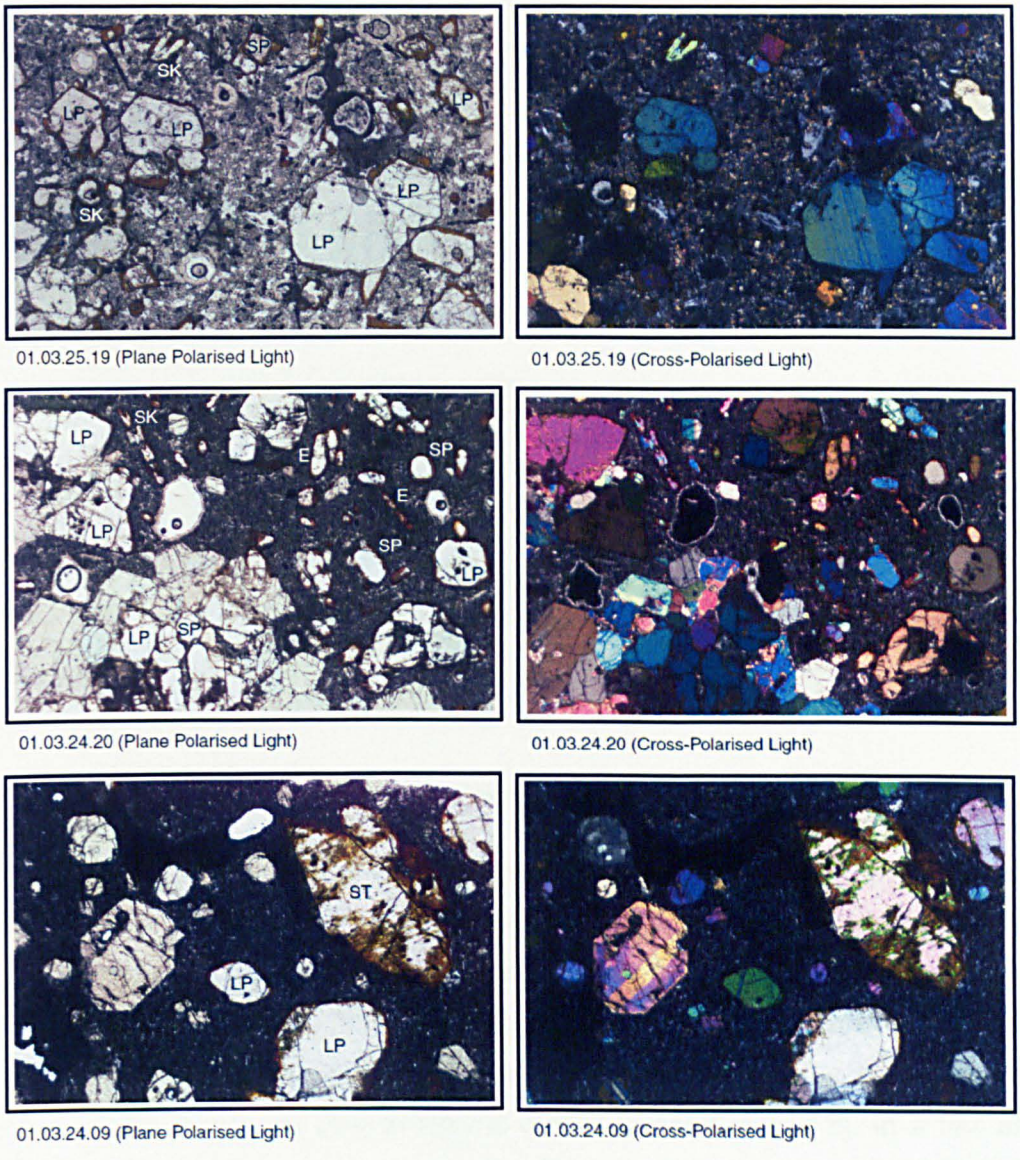

Figure 4.4 Morphology of olivine phenocrysts typically found in the Dilb lavas.

Clinopyroxene: Clinopyroxene phenocrysts occur in all the lavas with the exception of a few picrites. They range in form from euhedral to anhedral, but are dominantly subhedral and cracked, with sharp and sometimes splintered edges, and they vary in size from < 0.05 mm up to 6 mm in length (Figs 4.1 – 4.3). In plane polarised light, they are pale brown to pale green in colour, and invariably exhibit weak pleochroism between these colours. In cross-polarised light, they show a range of crisp second order interference colours from grey to white, to yellow, orange, pink and blue, and extinction angles of between 40 and 48° typical for augite. The more elongate crystal sections (010 and 100) show well developed cleavages, and in rare basal sections these can be seen to intersect at characteristic angles of approximately 87° (Fig. 4.7). Simple and multiple twinned crystals with vivid and contrasting interference colours

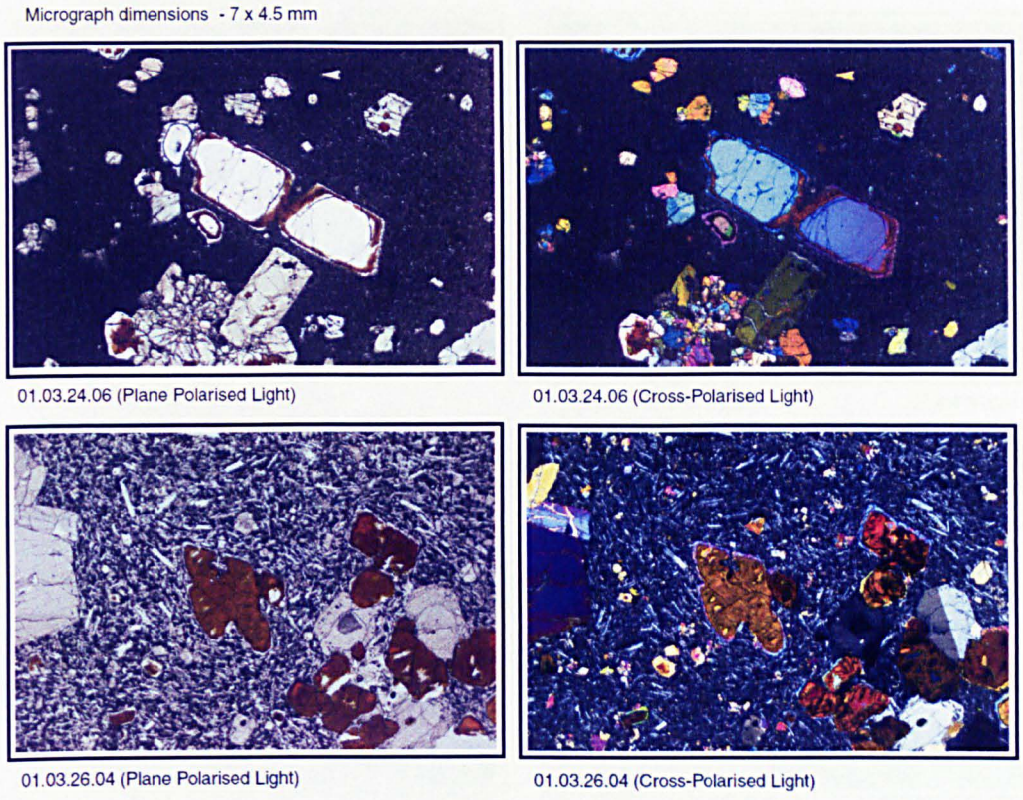

Figure 4.5 Rimmed and replaced olivines overgrown with fresh olivine

are common in many of the lavas, and in some, there are phenocrysts which exhibit oscillatory and (more rarely) hour-glass zoning. Such exotic crystals are often fragmented, and occur both as isolated phenocrysts, and as components in glomerocrysts (Fig. 4.11b). Strain features such as bent, zig-zagged and faulted twin-planes, kink-bands and irregular undulose extinction patterns are also common in both the phenocrystic and glomerophyric clinopyroxenes (Fig. 4.8). In a few of the olivine basalts and ankaramites (eg. 01.03.24.13, 01.03.25.01 and 01.03.24.03), some of the larger clinopyroxene phenocrysts contain inclusions of olivine, around which they seem to have grown (Fig. 4.9). There are some rare examples (in 01.03.25.07) of clinopyroxene phenocrysts which are host to numerous randomly orientated opaque to reddish brown translucent needles of either ilmenite, rutile or spinel. The needles are similar to those seen in the groundmass of some of the lavas; they are mainly encased in the outer growth zones, and appear not to occur in the core of the phenocrysts. Good examples of these needle-bearing clinopyroxenes occur in the ankaramite (01.03.31.04) from the Iyela Section (Fig. 4.34).

Plagioclase: The occurrence of plagioclase phenocrysts is largely confined to the coarser grained (> 0.3 mm) olivine basalts (Fig. 4.3). Some small isolated laths (< 1 mm in length) do occur in two finer grained olivine basalts (01.03.24.06 and

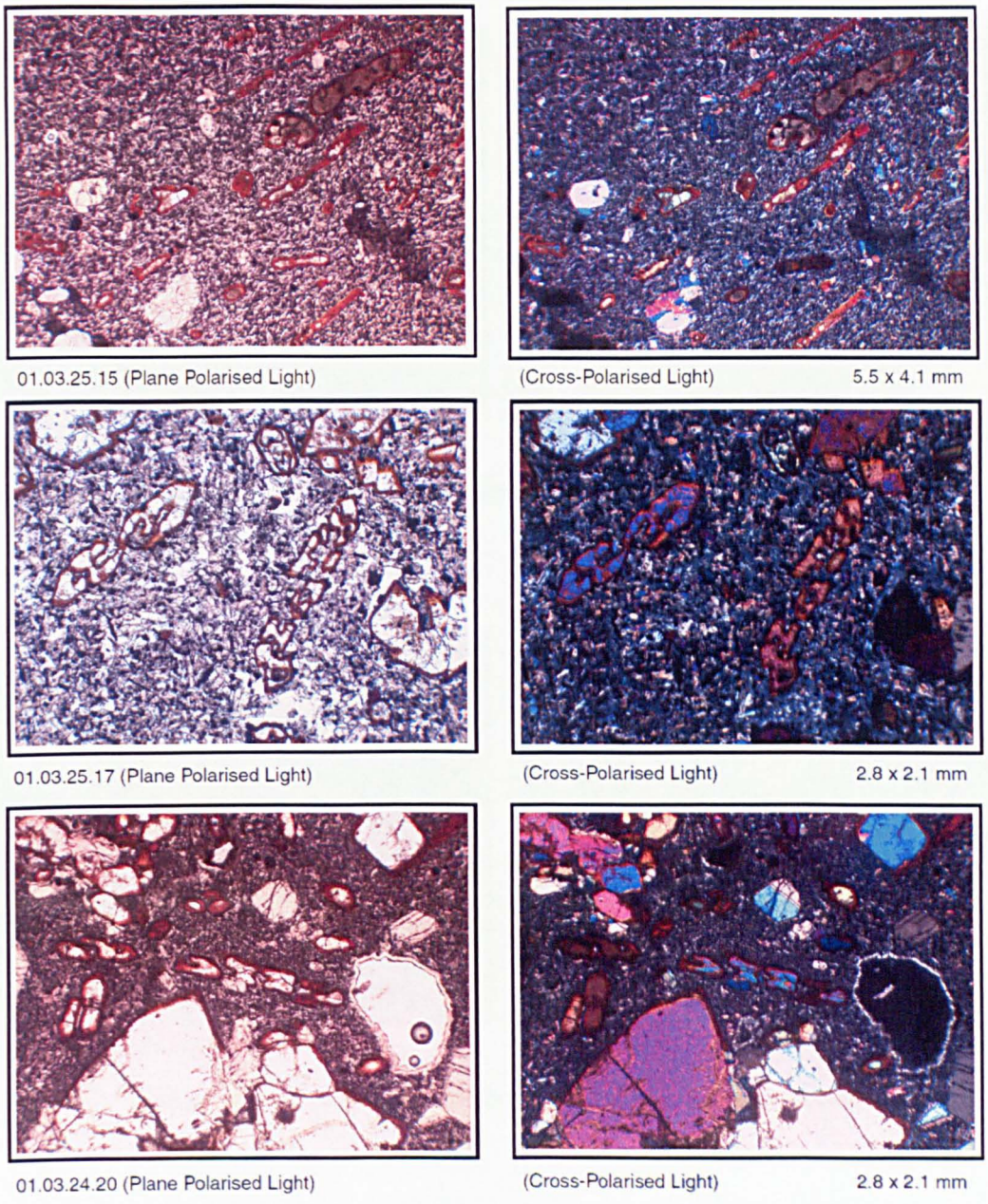

Figure 4.6 Chained, aligned, elongate and skeletal olivines in the Dilb lavas

01.03.24.18), but these may only be regarded as phenocrysts on account of their difference in size from the rest of the groundmass constituents in these samples. In every other respect they are more similar to the groundmass plagioclase crystals than the plagioclase phenocrysts in the coarser olivine basalts. Even in the lavas in which plagioclase phenocrysts do occur, their percentage proportions are low (< 5%, with the exception of 01.03.25.01 with 20%), and their occurrence is limited to a few loose glomerophyric clusters of rarely more than ten individual crystals. Despite this, the morphology, habit, and optical properties of the phenocrysts are consistently similar in each of the lavas in which they occur. Two distinct populations can be recognised (Fig. 4.10). The first is characterised by long (up to 5 mm), slender,

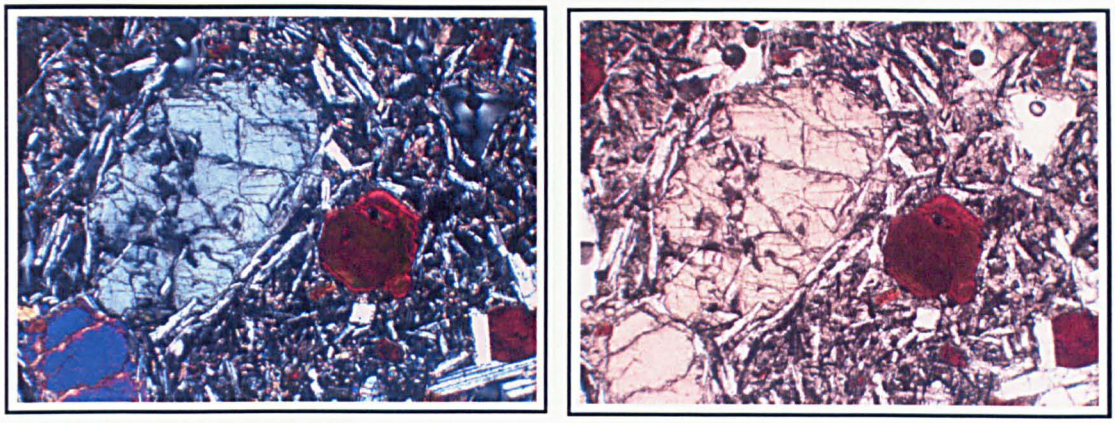

01.03.24.13 (Plane Polarised Light) (Cross-Polarised Light) 2.8 x 2.1 mm

Figure 4.7 Basal section of clinopyroxene showing intersecting cleavage planes

Both micrographs are in cross-polarised light

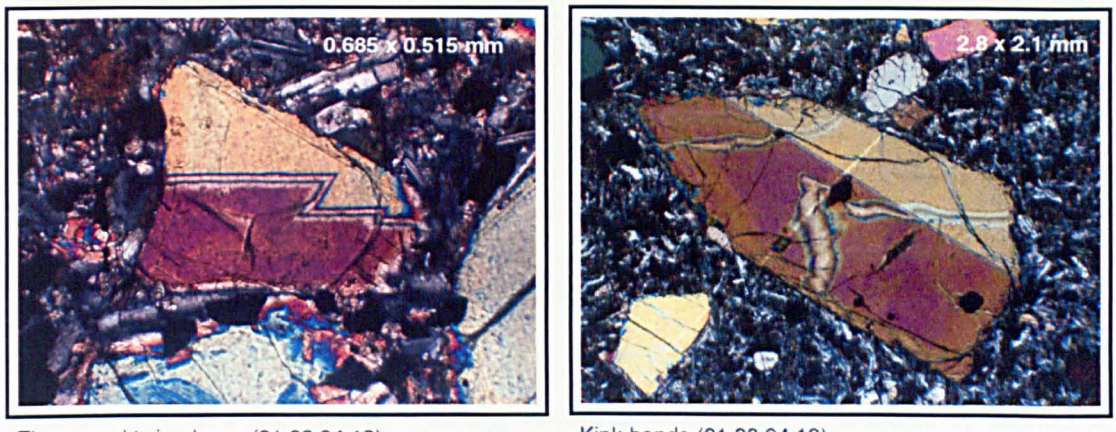

Zig-zagged twin-planes (01.03.24.12) Kink-bands (01.03.24.12)

Figure 4.8 Typical strain features present in the clinopyroxene phenocrysts

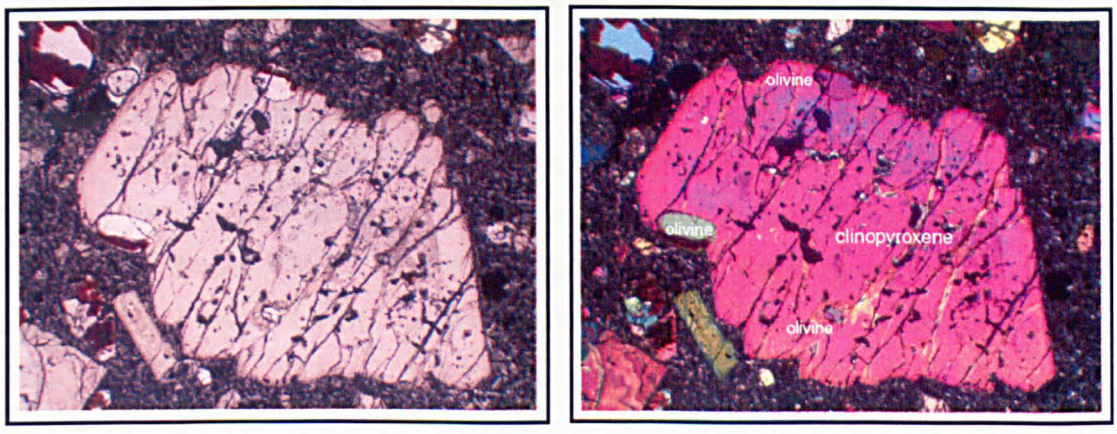

01.03.24.03 (Plane polarised light) (Cross-polarised light) 5.5 x 4.1 mm

Figure 4.9 Olivine inclusions in a dissolving clinopyroxene phenocryst. Note that only the exposed edges of the olivines are iddingsitized.

PG1 - Andesine, PG2 - Labradorite, CX - Clinopyroxene, OL - Olivine

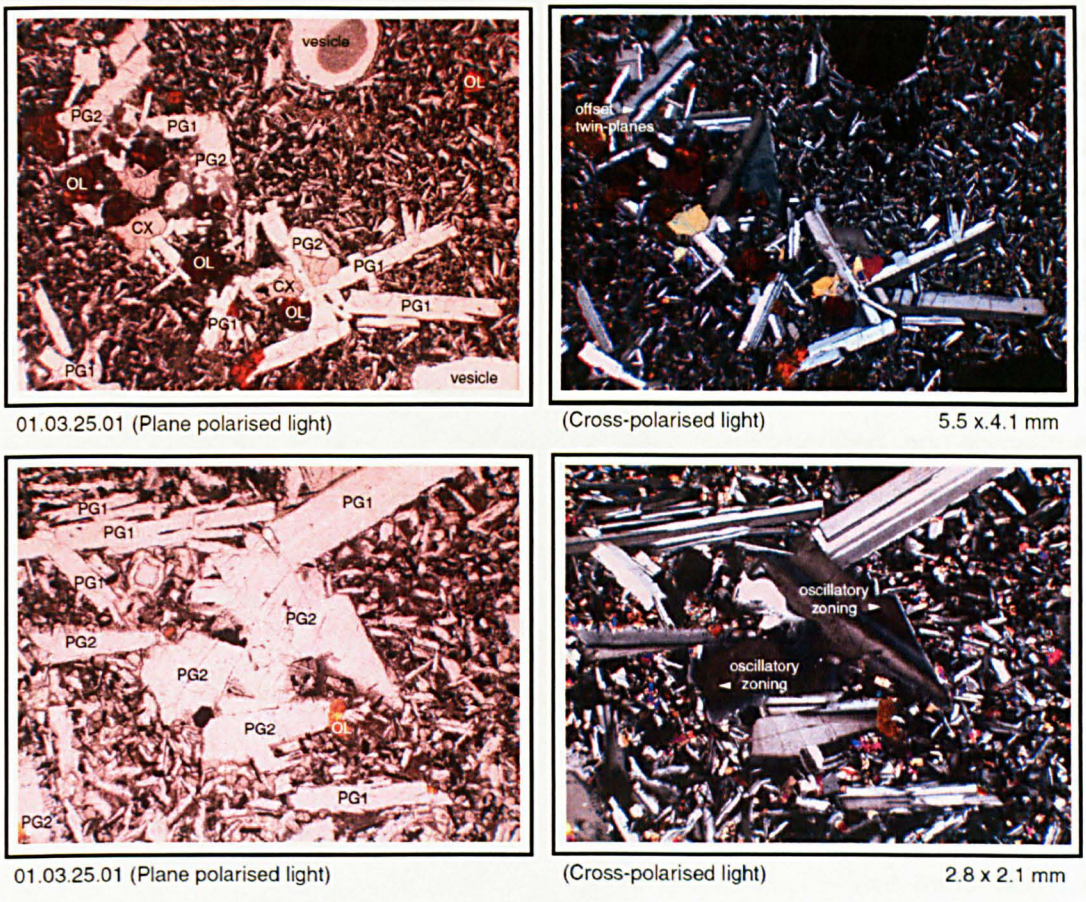

01.03.25.01 (Plane polarised light) (Cross-polarised light) 5.5 x.4.1 mm

01.03.25.01 (Plane polarised light) (Cross-polarised light) 2.8 x 2.1 mm

Figure 4.10 Morphology of the plagioclase phenocrysts in the olivine basalts

euhedral to subhedral, simple and multiple twinned laths with extinction angles between 18° and 36° (An_{38} – An_{58}), and the second by subhedral to anhedral, cracked and strained, twinned crystal fragments and fat laths (up to 2 mm long) with extinction angles between 35° and 45° (An_{57} – An_{75}). On the basis of their range in extinction angles, the first population may be identified as andesine, and the second as labradorite. The two populations are immediately distinguishable in that the long slender phenocrysts appear new and unworn, with sharply defined twin-planes and crisp crystal edges, whereas the strained ones appear old and blurred with indistinct phased edges. In addition, some of the strained phenocrysts exhibit oscillatory zoning, and most have twin-planes that are buckled, blurred and/or faulted (Fig. 4.10). Extinction angles for the slender variety are not dissimilar to those of the groundmass plagioclase crystals in some of the olivine basalts; however they are consistently higher than those for the plagioclase in the groundmass in which they occur. Extinction angles for the strained variety, on the other hand, are invariably much higher than those for any of the groundmass plagioclase crystals for any of the lavas.

Glomerocrysts: Glomerocysts are common in most of the lavas from each group. They range in size from < 1 mm to 7 mm across, and comprise numerous fragmented, and sometimes complete, crystals, either exclusively of olivine or clinopyroxene, or of variable proportions of olivine, clinopyroxene and very rarely, plagioclase. The glomerocrysts that consist exclusively of olivine are often fused so that in plane polarised light they appear as large single crystals (Fig. 4.11a), whereas the glomerocrysts consisting exclusively of clinopyroxene (Fig. 4.11b) or of both clinopyroxene and olivine (Fig. 4.11c), are never fused, but instead are either compacted or loosely agglomerated. In many of the glomerocrysts with mixed mineralogy, the core is often made up from previously agglomerated, and sometimes iddingsitized, olivine crystals, which are surrounded or fringed by later agglomerated clinopyroxene (Fig. 4.11c). In some cases, particularly in the olivine basalts, these core olivines are entirely replaced by iddingsite (Fig. 4.11d). In most fused olivine glomerocrysts that occur in the picrites and ankaramites, on the other hand, those crystals encased within the interiors of the glomerocrysts are generally unaltered and free from iddingsite.

Glomerocrysts exclusively composed of clinopyroxene show a greater variation in size than those composed exclusively of olivine, or those of mixed mineralogy. In some lavas (mainly olivine basalts) they occur both as large and often stellate masses up to 5 mm across, as well as showers of smaller masses no more than 0.075 mm in diameter composed of countless tiny crystal fragments together exhibiting a kaleidoscopic play of interference colours in cross-polarised light (Fig. 4.11e). These tiny fragmented crystals, where they are dissagregated from the glomerophyic masses, are often difficult to tell apart from the groundmass clinopyroxenes. Although the plagioclase phenocrysts in the olivine basalts distinctively show glomerophyic tendencies, they rarely form compacted glomerocrysts. The only instance in which they do is in sample 01.03.26.06, where plagioclase phenocrysts occur in a few compacted glomerocrysts together with a jumble of variably sized and fragmented phenocrysts of clinopyroxene and iddingsitized olivine (Fig. 4.11f).

Xenoliths: As well as phenocrysts and glomerocrysts, there are also xenoliths observed in one of the lavas (01.03.26.07), and it may be assumed, on the strength of this, that they occur at least in some of the other lavas. Those that are observed in thin section comprise scattered rounded inclusions of lava, sometimes seen attached to olivine phenocrysts or glomerocrysts (Fig. 4.12). It is notable that these inclusions

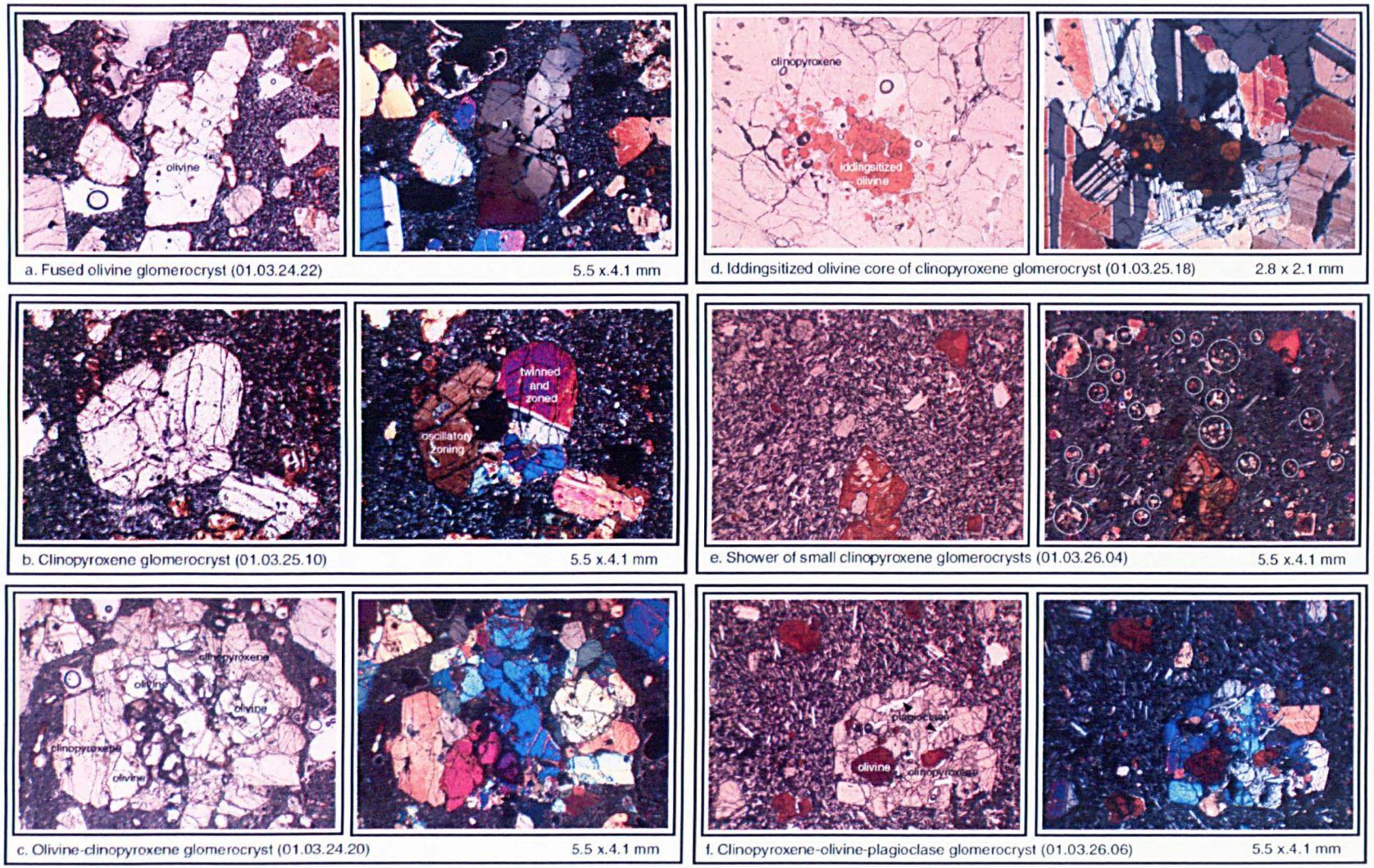

Figure 4.11 Variation in the types of glomerocryst present in the lavas from the Dilb Section.

Micrograph dimensions - 1.4 x 1 mm (plane polarised light on left and cross-polarised light on right)

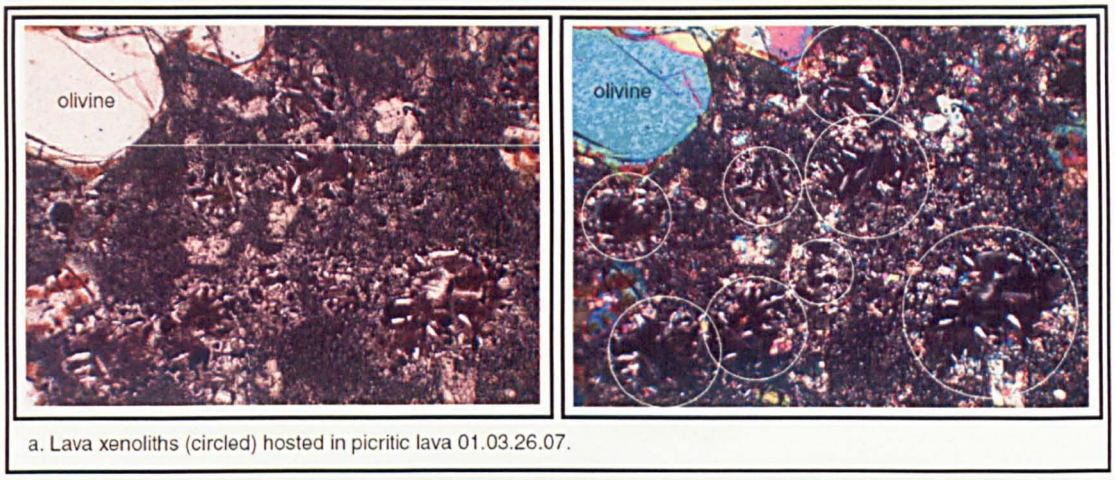

a. Lava xenoliths (circled) hosted in picritic lava 01.03.26.07.

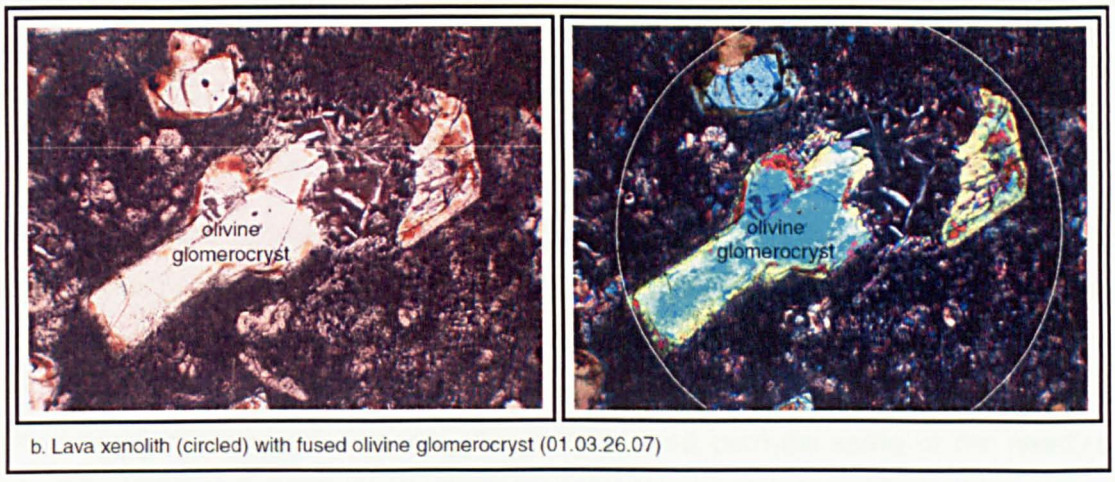

b. Lava xenolith (circled) with fused olivine glomerocryst (01.03.26.07)

Figure 4.12 Xenoliths in the lavas from the Dilb Section.

have a similar mineralogy and texture to some of the olivine basalts that occur stratigraphically below.

Groundmass: The groundmass mineralogy in all the Dilb lavas is remarkably similar, although, as previously mentioned, there are significant variations in the ratio of clinopyroxene to plagioclase which are broadly distinguishable between the three lava groups. Essentially, it comprises variable proportions of plagioclase, clinopyroxene, Fe-Ti oxides, and devitrified glass. In some of the lavas, there are also variable amounts of an unidentified high relief, orange mineral, which occurs mainly as well-formed needles, and sometimes as irregularly shaped patches. The two forms may represent different minerals but they have been recorded here as one (Appendix 4.1). Further microprobe analyses are required to properly establish the compositions of the two forms since the analyses presented in Supplement 1 are inconclusive. In plane and cross-polarised light, the two forms appear identical to the iddingsite which forms the altered rims of the olivine phenocrysts; however, in reflected light, the needles are seen to be highly reflective (Fig. 4.13), and are

Micrograph dimensions - 0.685 x 0.515 mm

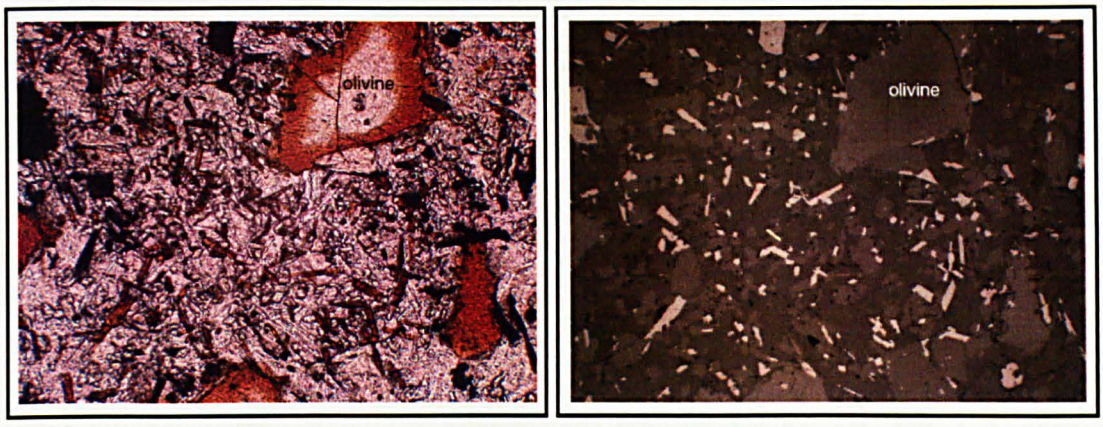

01.03.25.07 (plane polarised light) (reflected light)

Figure 4.13 Unidentified orange needles found in the groundmass of some of the Dilb lavas. In transmitted light the needles have similar optical properties to iddingsite, which is seen here as a replacement rim around olivine just right of centre in the upper part of the micrographs, and as a pseudomorph after olivine in the lower right. In reflected light, the unidentified needles are highly reflective and appear white, whereas the iddingsite is non-reflective and grey.

therefore possibly a product (may be rutile) associated with the alteration of acicular ilmentite, with which they almost invariably occur (Table 4.2). Alternatively, they may be skeletal spinels; their low range, and occasional absence of interference colours in cross-polarised light suggests that his may be more so the case since rutile is often highly birefringent. The irregular patches, and perhaps some of the needles, may be groundmass, or small phenocrystic, olivines that have been replaced by iddingsite.

Grain size: The range in grain-size of the groundmass for the lavas in each group is illustrated in Figures 4.1, 4.2 and 4.3 respectively, together with rounded visual estimates for the percentage proportions of the groundmass-constituents in each of the lavas. Maximum sizes typical for the various morphologies of groundmass minerals, extinction angles for plagioclase and clinopyroxene microlites, the condition of the interstitial glass, and the percentage content and maximum size of vesicles, for all the lavas are shown in Table 4.2. Using plagioclase as an index, since it tends to be the largest mineral in the groundmass of most of the lavas, it can be seen that the variation in the typical coarseness of the groundmass is relatively similar in both the picrites (0.03 – 0.3 mm) and olivine basalts (0.08 – 0.5 mm), whereas the variation in the ankaramites it is more limited (0.03 – 0.1 mm).

Plagioclase: Irrespective of the coarseness of the groundmass, plagioclase is present in the groundmass of the lavas, mainly as randomly orientated, clear, subhedral to euhedral, simple and multiple-twinned laths, which are occasionally feather-edged,

Table 4.2 Groundmass mineralogy of the lavas from the Dilb section

Sample	Plagioclase					Clinopyroxene					Unknown		Fe-Ti Oxides				Glass		Vesicles		
	Laths	Irregular	Twinned	Zoned	Extinction	Polyhedral	Irregular	Twinned	Zoned	Extinction	Acicular	Irregular	Prismatic	Globular	Acicular	Granular	Devitrified	Zeolitized	% content	Max. size	Lined
Picrites																					
01.03.26.07	0.03	0.03	indeterminab			0.08	0.08	indeterminable					0.05	0.15		0.03					
01.03.24.14	0.08	0.08			26	0.08	0.08			44	0.05		0.05	0.10	0.10	0.03			1	0.5	
01.03.24.20	0.08	0.08			24	0.15				46	0.40		0.05	0.05	0.08				5	1.0	
01.03.25.07	0.08	0.08			32	0.10	0.10			46	0.05		0.05	0.10	0.08						
01.03.25.10	0.10	0.10			31	0.10	0.10			45	0.08		0.05	0.10	0.08				6	5.0	
01.03.24.22	0.10	0.10			32	0.15	0.15			46	0.08		0.10	0.15	0.08				2	0.3	
01.03.25.13	0.10	0.10			28	0.15	0.15			46			0.05	0.10	0.08						
01.03.25.12	0.10	0.10			30	0.10	0.10			45		0.10	0.05	0.10		0.03					
01.03.25.17	0.10	0.10			30	0.10	0.10			45	0.15	0.10	0.05	0.10	0.30	0.03			3	3.0	
01.03.25.09	0.10	0.10			32	0.10	0.10			47	0.05	0.08	0.05	0.10	0.08	0.05			2	0.5	
01.03.25.06	0.20	0.20			29	0.15	0.15			46	0.15		0.10	0.10	0.15	0.05			10	5.0	
01.03.25.15	0.20	0.20			30	0.15	0.15			46	0.15		0.10	0.10	0.15	0.05			20	6.0	
01.03.25.02	0.20	0.20			22	0.15	0.15			46	0.15		0.05	0.10	0.08	0.05			1	1.5	
01.03.25.03	0.25	0.25			25	0.20	0.20			43	0.30		0.05	0.10	0.30	0.05			40	4.0	
01.03.25.04	0.25	0.25			24	0.15				46	0.40		0.05	0.05	0.08				5	2.5	
01.03.25.20	0.30	0.30			24	0.15				46	0.40		0.05	0.05	0.08				7	8.0	
01.03.25.19	0.30	0.30			31	0.15				46	0.60		0.05	0.05	0.10				5	0.1	
01.03.26.03	0.30	0.30			29	0.15				44	0.05		0.05	0.10	0.08				3	6.0	
Average	0.16	0.16			28	0.13	0.12			45	0.20	0.09	0.06	0.09	0.12	0.04			8	3.1	
Ankaramites																					
01.03.24.07	0.03	0.03	indeterminab			0.08	0.08	indeterminable					0.05	0.15		0.03			4	1.0	
01.03.24.09	0.08	0.08			30	0.08	0.05			45			0.05	0.08		0.03			1	0.5	
01.03.24.11	0.08	0.08			25	0.08	0.05			44			0.05	0.08		0.03			1	0.5	
01.03.25.11	0.08	0.08			24	0.08	0.05			46			0.05	0.08		0.03			2	0.1	
01.03.24.03	0.08	0.08			25	0.05	0.05			45			0.10	0.15		0.03			6	0.3	
01.03.24.08	0.10	0.10			22	0.10	0.10			45	0.08		0.05	0.05	0.40	0.03			2	1.5	
01.03.24.12	0.10	0.10			22	0.10	0.10			46			0.10			0.15					
Average	0.08	0.08			25	0.08	0.07			45	0.08		0.06	0.10	0.40	0.04			3	0.7	
Olivine Basalts																					
01.03.24.06	0.08	0.08			26		0.08			44	0.05		0.05	0.10		0.03					
01.03.25.14	0.08	0.08			25	0.08	0.05			45			0.05	0.08		0.03			3	3.0	
01.03.24.18	0.08	0.08			26	0.10	0.08			43	0.08		0.05	0.10		0.03			3	1.6	
01.03.24.04	0.08	0.08			28		0.08			43						0.03			4	0.8	
01.03.24.05	0.08	0.08			27		0.08			43				0.05		0.03			6	0.3	
01.03.24.21	0.08	0.08			27		0.08			46						0.03			1	0.8	
01.03.24.02	0.10	0.10			22		0.08			46			0.20			0.03					
01.03.24.19	0.10	0.10			23	0.08	0.08			47			0.20			0.03			2	2.0	
01.03.24.15	0.15	0.15			27	0.10	0.10			45	0.15	0.10	0.05	0.05		0.05			3	2.5	
01.03.26.04	0.15	0.15			20	0.10	0.10			45			0.05	0.05		0.03			2	2.0	
01.03.26.06	0.15	0.15			20	0.10	0.10			45			0.05	0.05		0.03			10	3.0	
01.03.24.16	0.20	0.20			22	0.10	0.10			43			0.05		0.30	0.03			20	4.0	
01.03.24.17	0.30	0.30			25	0.10	0.10			45					0.25				40	6.0	
01.03.25.01	0.30	0.30			19	0.10	0.10			46			0.08		0.20	0.03			15	2.0	
01.03.25.18	0.30	0.30			22	0.10	0.10			45			0.05		0.10	0.03					
01.03.24.13	0.50	0.50			26	0.10	0.10			43	0.20	0.05	0.05		0.10	0.03			5	1.2	
Average	0.17	0.17			24	0.10	0.09			45	0.12	0.08	0.08	0.07	0.19	0.03			9	2.2	

Note: Samples in each group are arranged in order of increasing grain size of the groundmass. Grain size (mm) is shown as the maximum for a representative area of groundmass (Appendix 4.1). Extinction angles are in degrees.

and as irregular amorphous infill, sometimes showing ghost-like twinning. Average extinction angles for the mineral vary between 22° and 32° (An_{43} – An_{53}) in the picrites, 21° – 30° (An_{42} – An_{51}) in the ankaramites, and 19° – 28° (An_{40} – An_{50}) in the olivine basalts. At low magnification, the plagioclase laths in some of the lavas from each group can be seen to be vaguely aligned between, and around, the edges of some of the larger phenocrysts and glomerocrysts (Fig. 4.14). This feature, indicative of flow, is not as evident in the coarser grained lavas as it is in the finer grained ones. In some of the lavas there are areas of the groundmass infilled with an irregular mosaic of exceptionally clear plagioclase riddled with randomly orientated fine, clear

Micrograph dimensions - 5.5 x 4.1 mm (plane polarised light)

Figure 4.14 Alignment of groundmass plagioclase laths around glomerocrysts in picritic lava 01.03.25.12.

to pale green, high relief needles with grey interference colours typical of apatite. These are most prominent in some of the lavas of the Iyela Section (Fig. 4.35).

Clinopyroxene: Clinopyroxene is present in the groundmass of the lavas as anhedral to euhedral, but mainly subhedral, pale green to pale yellow-brown, elongate prismatic crystals showing random orientation, except sometimes along the edges of large phenocrysts where they are sometimes aligned. Extinction angles for the mineral show little variation within and between groups (43° – 47°), and they are notably similar to the clinopyroxene phenocrysts. The more well-formed crystals are often twinned and occasionally zoned (oscillatory and hour-glass), and in some lavas, the more fragmented crystals sometimes occur as glomerocrysts, which are often stellate in form. In the coarser grained picrites with the highest percentages of clinopyroxene, the groundmass clinopyroxene forms an impressive mosaic of pristine, clear, pale green subhedral to euhedral stumpy laths and polyhedral crystals which show a spectacular play of colours in cross-polarised light (Fig. 4.15). In contrast, in the finer-grained lavas in all three groups, much of the clinopyroxene in the groundmass is too small to distinguish, and its presence is marked only by a mottled play of typical interference colours.

Fe-Ti oxides: Opaque Fe-Ti oxides occur in the groundmass of the Dilb lavas in four distinct forms – prismatic, globular, acicular and granular. All forms show a limited variation in size between the lavas, and their distribution and occurrence in the lavas

PG - Plagioclase, CX - Clinopyroxene, UM - Unknown orange mineral, OX - Fe-Ti oxides, GS - Glass. Micrograph dimensions - 0.685 x 0.515 mm

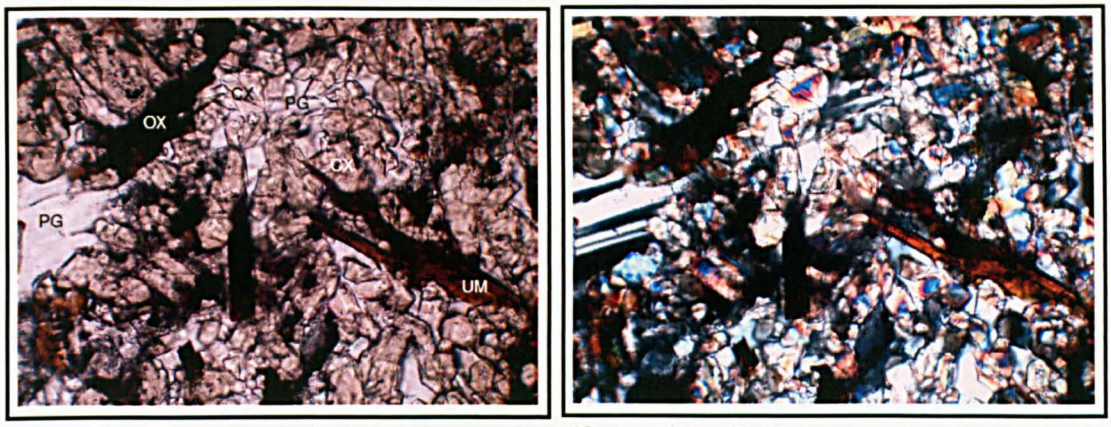

01.03.25.04 (Plane polarised light) (Cross-polarised light)

Figure 4.15 Clinopyroxene-rich groundmass in some of the coarse-grained picrites from the Dilb Section

does not appear to conform to any discernable pattern in terms of grain-size, mineralogical composition, or stratigraphic order (Table 4.2). Prismatic forms, comprising mainly anhedral to subheral, and rarely euhedral, cubic and hexagonal crystals of probably magnetite and titanomagnetite, occur randomly spread in all the lavas except for in four olivine basalts, which are either almost exclusively dominated by granular or acicular Fe-Ti oxides. Some of the largest of these prismatic crystals (0.2 mm in 01.03.24.02 & 01.03.24.19) might be considered phenocrysts on account of their difference in size compared the rest of the groundmass minerals with which they occur. The fact they occasionally occur agglomerated with other phenocrystic minerals such as olivine would support this (Fig. 4.16). Rounded or globular Fe-Ti

Micrograph dimensions - 3.3 x 2.4 mm

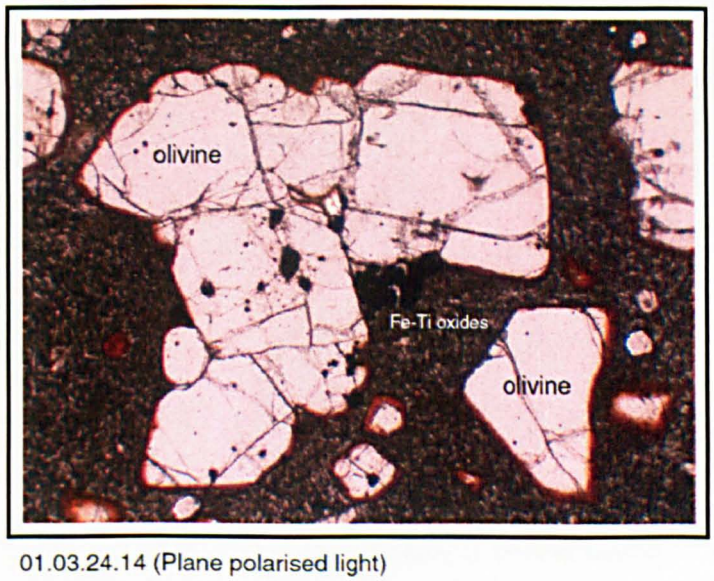

01.03.24.14 (Plane polarised light)

Figure 4.16 Glomerophyric Fe-Ti oxides. Prismatic Fe-Ti oxides (black) agglomerated with olivine.

oxides (probably magnetite), are less plentiful than the prismatic Fe-Ti oxides, and they are more plentiful in the picrites and ankaramites than they are in the olivine basalts. They commonly occupy indentations along the iddingsitized edges of olivine phenocrysts, and in such cases may be associated in some way with the alteration of olivine. Some Fe-Ti oxides also occur within composite material infilling of vesicles sometimes confined to distinct horizons or thin vesicle sheets (Fig. 4.17).

Micrograph dimensions - 5.5 x 4.1 mm

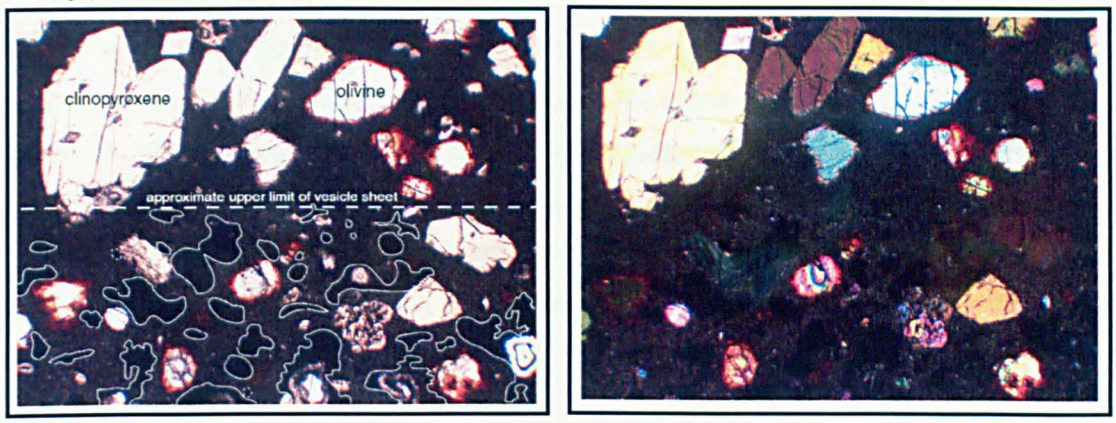

01.03.24.07 (Plane polarised light) (Cross polarised light)

Figure 4.17 Vesicle layer in which the vesicles have been infilled with a composite material rich in Fe-Ti oxides.

Acicular ilmenite (distinguished by its characteristic shape and slight brownish tinge in reflected light) is most common in the picrites, although it does occur in some olivine basalts and in one ankaramite (Table 4.2). Unsually, in one olivine basalt (01.03.24.17), it is the only type of Fe-Ti oxide present, and it forms near to 25 % of the groundmass (Fig. 4.18). Generally, however, it occurs, as randomly orientated,

Micrograph dimensions - 0.685 x 0.515 mm

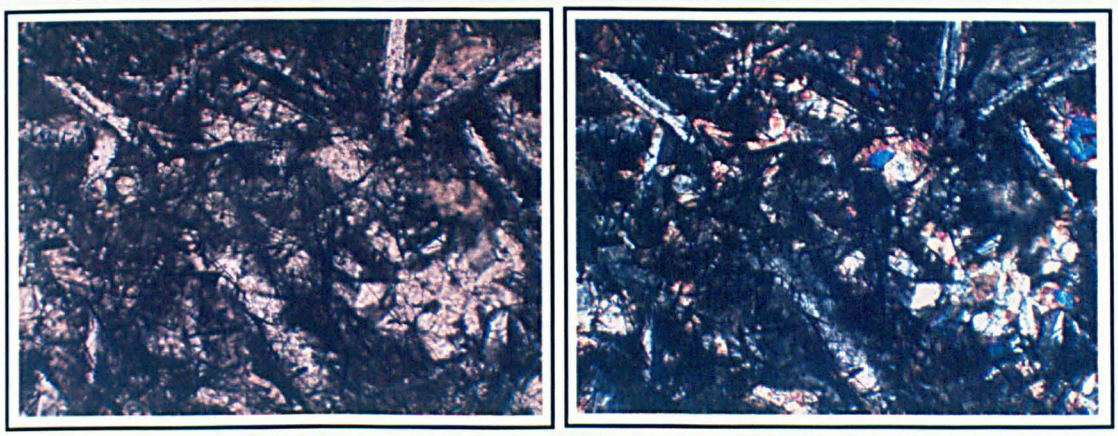

01.03.24.17 (Plane polarised light) (Cross-polarised light)

Figure 4.18 Acicular ilmenite in the groundmass of olivine basalt 01.03.24.17

sparsely dispersed, euhedral to subhedral needles < 0.3 mm in length, together with other forms of Fe-Ti oxides. In some lavas, some needles can be seen to be hollow

with prismatic cross-sections, and in others, they appear to be made up from chains of coalesced prismatic crystals sometimes as long as 0.4 mm. The highest proportion of Fe-Ti oxides in most of the lavas is probably made up from granular magnetite. This occurs mainly as relatively even, but variably dense stubble comprising irregularly shaped granules of < 0.05 mm in diameter. In a few of the finer grained olivine basalts it is the only form of Fe-Ti oxide present in the groundmass, but in most lavas is occurs together with variable proportions of other forms of Fe-Ti oxides.

Glass: Variable proportions of devitrified volcanic glass occur in all of the lavas as dirty brown infill between the mineral components of the groundmass (Figs 4.1 – 4.3). In some of the finer grained lavas it is sometimes difficult to distinguish from clinopyroxene, which sometimes is pale brown with dark grey interference colours not dissimilar to the near isotropic grey of the glass in cross-polarised light. In most of the lavas, the distribution of devitrified glass coincides with that for the Fe-Ti oxides, since they appear to be set within it.

Textural variations: Although the mineralogy and texture of the groundmass in most of the lavas is relatively uniform, mineralogical and textural variations do occur in the groundmass of a few of the lavas. This is most apparent in the olivine basalt, 01.03.24.06, in which there occurs a well defined mixing front between two lava types marked by an abrupt change in both the texture and composition of the groundmass (Fig. 4.19). Similar but less pronounced features, more likely to represent internal

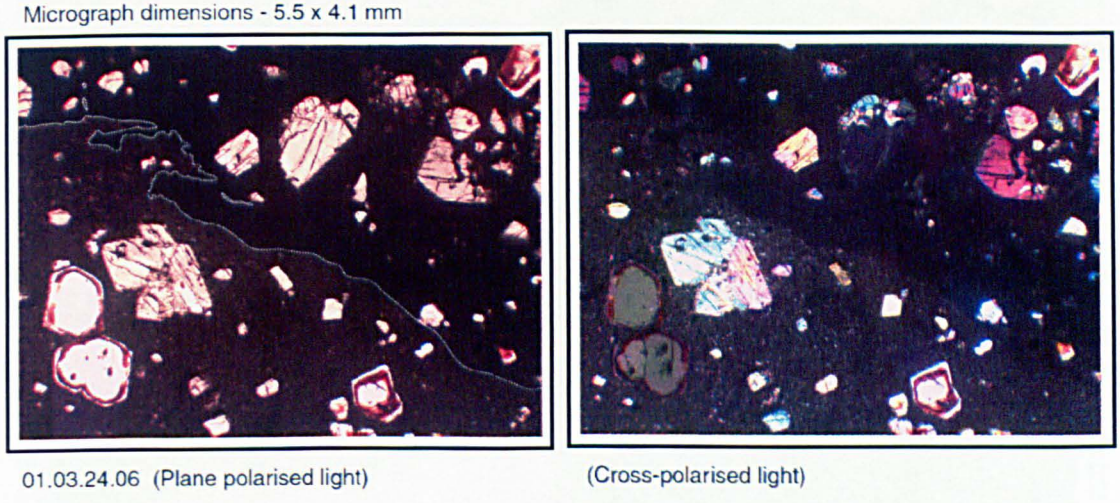

Figure 4.19 Mixing front between different lava-types in olivine basalt 01.03.24.06. The front (indicated by the dotted line) is defined by a marked change in the composition and texture of the groundmass.

differentiation rather than mixing between lavas, also occur in a number of the lavas. The coarser grain-size and more noticeable presence of plagioclase laths in the

groundmass of the vesicle sheet described above (Fig. 4.17) compared to the groundmass for the lava in which the sheet occurs, is an example of such a feature.

Vesicles: Vesicles are present in most of the lavas although few are wholly vesicular in thin-section partly because vesicular portions of the lava flows were purposely avoided for sampling since often they were intensely weathered (Section 3.2.2). In some samples the vesicles are discreet and rounded, and sometimes coalesced (Fig. 4.20a), whereas in others they form irregular and often elongate cavities, some of which may have been formed by crumpling of the lava while still plastic, rather than by gases rising through the lava. The maximum size for the vesicles and/or cavities in each of the lavas are shown in Table 4.2 together with their percentage contents (proportionate to the volume of the whole rock) and an indication of whether or not they are lined or infilled. In most cases the vesicles and cavities are lined with a colourless to pale yellow zeolitic crust with a mammilated surface. At high magnification, this crust can sometimes be seen to consist of tightly packed radiating crystals with growth layers that alternate from black to grey to white in cross-polarised light (Fig. 4.20b). In some samples the vesicles and/or cavities are neither lined nor infilled.

Figure 4.20 Vesicles in the Dilb Lavas

(a) Rounded and coalesced vesicles in vesicular olivine basalt 01.03.24.17. Some are lined with a zeolitic crust and others are not.

(b) Highly magnified view of a vesicle in picrite 01.03.25.17 showing features of its zeolitic lining. The crust has a mammilated surface, and in cross-polarised light there are growth rings with grey to white interference colours.

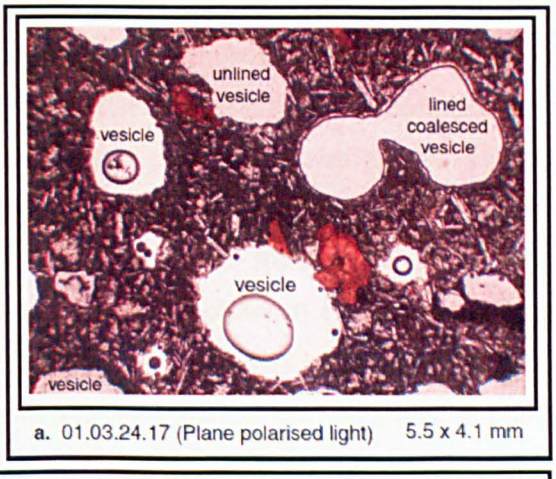

a. 01.03.24.17 (Plane polarised light) 5.5 x 4.1 mm

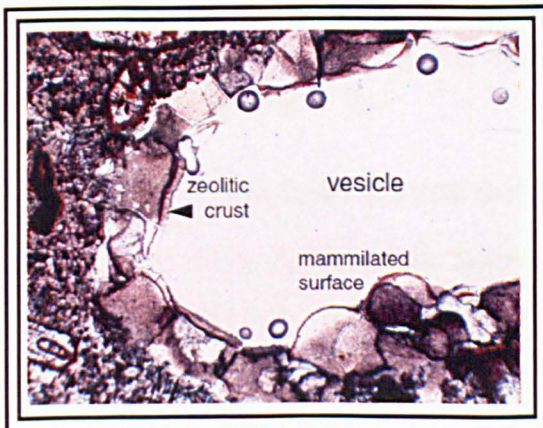

b. 01.03.25.17 (Plane polarised light)

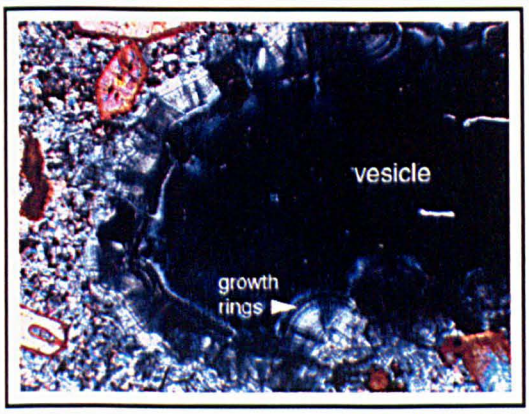

(Cross-polarised light) 0.685 x 0.515 mm

Alteration: All the lavas, to one degree or another, are altered in some way. As already described above, few olivines are not affected by iddingsitization. In all the lavas, most are rimmed by iddingsite, and many, particularly in the olivine basalts, are extensively or entirely replaced by iddingsite (Figs 4.1 – 4.3). The iddingsite is characteristically reddish-brown to bright orange in both pale and cross-polarised light, and in some instances where it has not entirely replaced the olivine, it sometimes shows a mottled subdued play of interference colours reminiscent of the olivine. Pseudomorphs of iddingsite also show straight extinction reminiscent of the olivine that has been replaced. Some lavas from each group are serpentinized as well iddingsitized, and in such cases the olivines are variably rimmed or replaced by serpentine. The serpentine is generally clear to dirty pale brown, with subdued interference colours ranging from grey to yellow to green, orange, pink and blue. Complete pseudomorphs are not common. In the lavas where they do occur, there are rare examples which exhibit mesh and hour glass textures. There is no consistent pattern in the order of alteration between the serpentinized lavas. In some, the olivines are rimmed and/or replaced with iddingsite, which is in turn rimmed with serpentine (Fig. 4.21a), in others, they are rimmed and/or replaced with serpentine, which is in turn rimmed with iddingsite (Fig. 4.21b), and in others, the olivines may be rimmed or replaced by serpentine only (Fig. 4.21c). Whereas the effects of iddingsitization are pervasive in the sense that they seen in all the lavas and are not confined to specific areas within them, the effects of serpentinization are more localised in that they are seen only in some lavas, and are sometimes evidently confined to specific areas within these lavas. In addition to the effects of iddingsitization and serpentinization, most of the lavas from each group show evidence of zeolitization. This is most commonly confined to the widespread deposition of zeolites in vesicles and in cavities as described above (Fig. 4.20). In some of the lavas, however, the glass within the groundmass can be seen, in places, to be replaced by pale brown zeolitic material with interference colours indistinguishable from those of the unaltered groundmass plagioclase laths that remain set within it (Fig. 4.22).

4.2.3 Intrusive rocks from the Dilb Section

The intrusive rocks from the Dilb Section are petrographically similar to the lavas, and in this respect they may be assumed to represent either feeder conduits for lava flows above, or they may be lavas that have been channelled by structural weaknesses or topographic irregularities in the surface lavas during eruption (Section 3.3.2). With the exception of 01.03.25.05, which is aphyric, all the intrusives are

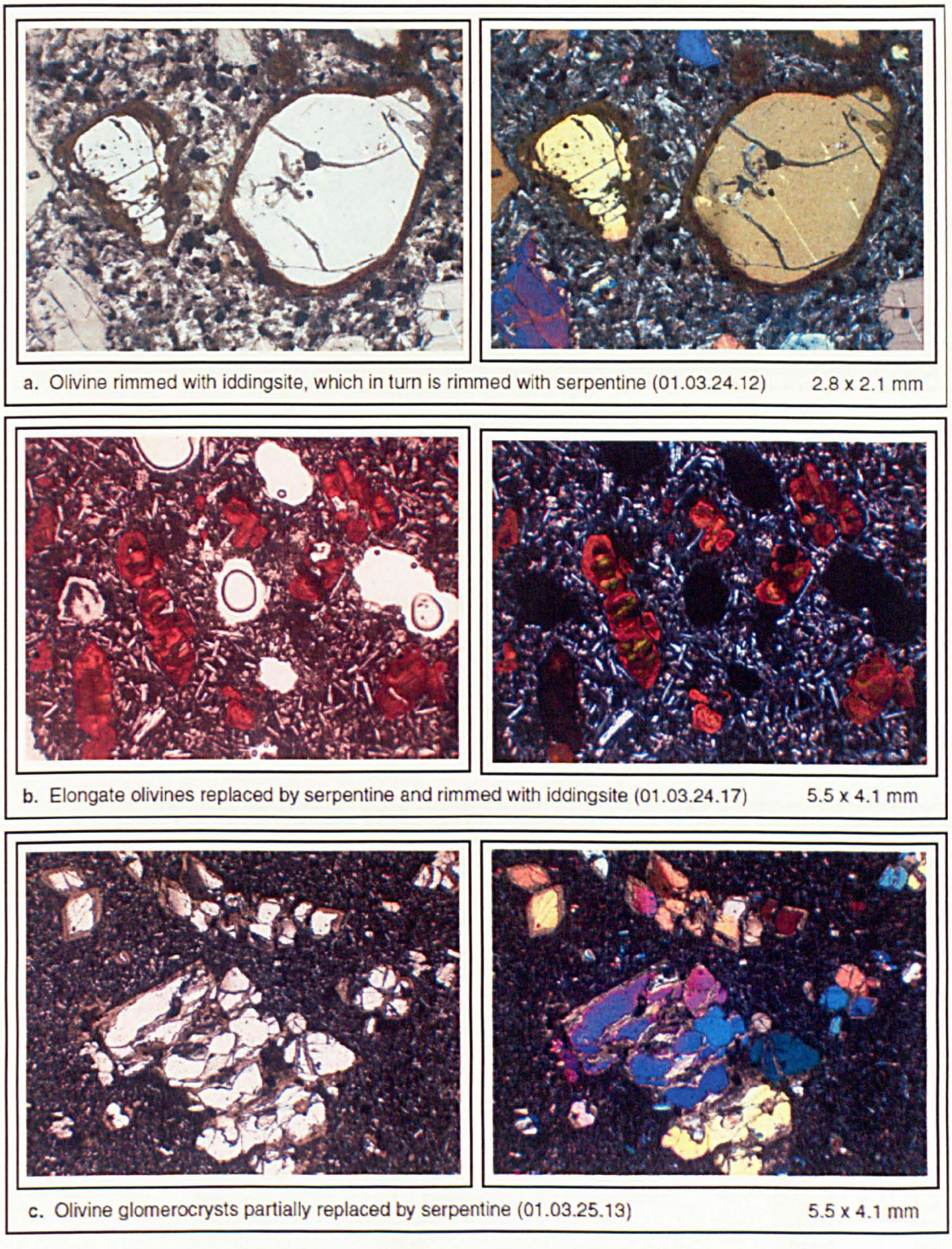

a. Olivine rimmed with iddingsite, which in turn is rimmed with serpentine (01.03.24.12) 2.8 x 2.1 mm

b. Elongate olivines replaced by serpentine and rimmed with iddingsite (01.03.24.17) 5.5 x 4.1 mm

c. Olivine glomerocrysts partially replaced by serpentine (01.03.25.13) 5.5 x 4.1 mm

Figure 4.21 Serpentinization in the lavas from the Dilb Section

variably porphyritic. As in the lavas, the phenocrystic minerals including olivine and clinopyroxene occur both as isolated phenocrysts and as glomerocrysts, and the groundmasses comprise variable proportions of plagioclase, clinopyroxene, Fe-Ti oxides, devitrified glass and an unidentified orange mineral (Fig. 4.23). The characteristics of the different olivine morphologies in each of the intrusive rocks are recorded in Table 4.3, and details of the groundmass constituents are shown in Table

Micrograph dimensions - 0.685 x 0.515 mm

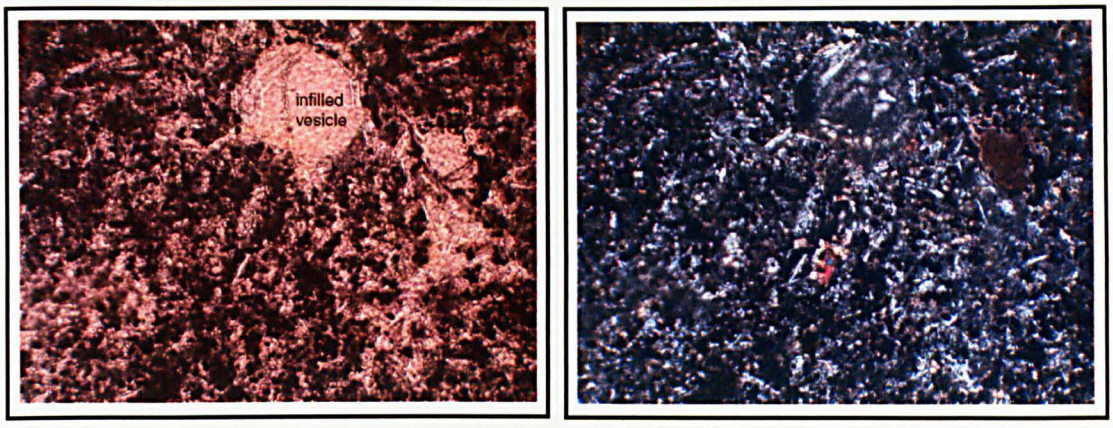

01.03.24.05 (Plane polarised light) (Cross-polarised light)

Figure 4.22 Zeolitization in the Dilb Lavas. Here a veicle is seen to be infilled with a pale brown zeolite with white to grey interference colours similar to the plagioclase in the ground-mass. Much of the glass within the groundmass has also been replaced by the same mineral.

Table 4.3 Olivine morphology of the intrusive rocks from the Dilb section

Sample	Large Polyhedral							Small Polyhedral							Striated							Elongate							Skeletal						
	Rounded	Embayed	Zoned	Rimmed	Replaced	Overgrown	Glomerophyric	Fused	Aligned	Rounded	Embayed	Zoned	Rimmed	Replaced	Overgrown	Glomerophyric	Fused	Aligned	Rounded	Embayed	Zoned	Rimmed	Replaced	Overgrown	Glomerophyric	Fused	Aligned	Rounded	Embayed	Zoned	Rimmed	Replaced	Overgrown	Glomerophyric	Fused	Aligned
01.03.24.10																																			
01.03.26.01																																			
01.03.25.08																																			
01.03.25.16																																			
01.03.26.02																																			
01.03.25.05																																			

Table 4.4 Groundmass mineralogy of the intrusive rocks from the Dilb section

Sample	Plagioclase						Clinopyroxene					Unknown		Fe-Ti Oxides				Glass	Vesicles		
	Laths	Irregular	Twinned	Zoned	Extinction		Polyhedral	Irregular	Twinned	Zoned	Extinction	Acicular	Irregular	Prismatic	Globular	Acicular	Granular	Devitrified	Zeolitized	% content	Max. size	Lined
01.03.24.10	0.03	0.03	indeterminable				0.08	0.08	indeterminable					0.05	0.08		0.03					
01.03.26.01	0.10				26		0.08	0.05			45			0.05	0.08		0.03					
01.03.25.08	0.08	0.08			24			0.05			45			0.10		0.70	0.03			2	0.5	
01.03.25.16	0.20	0.20			26			0.05			45			0.10		0.80	0.03					
01.03.26.02	0.40	0.40			23		0.10	0.10			45	0.15	0.10	0.05		0.30				3	0.6	
01.03.25.05	0.10	0.10			26		0.10	0.10			46			0.05		0.60	0.03			3	0.8	
Average	0.15	0.16			25		0.09	0.07			45	0.15	0.10	0.07	0.08	0.60	0.03			3	0.6	

Note: Samples in each group are arranged in order of increasing grain size of the groundmass. Extinction is in degrees. Grain size (mm) for microlites are shown as the maximum for a representative area of groundmass (Appendix 4.1).

4.4. As far as was possible, the intrusive rocks were classified in the same way as the lavas. All, except 01.03.24.10 are classified as olivine basalts on the basis that they contain < 12% MgO. 01.03.24.10 is classed as an ankaramite since it has > 12% MgO and has a phenocrysts assemblage dominated by clinopyroxene.

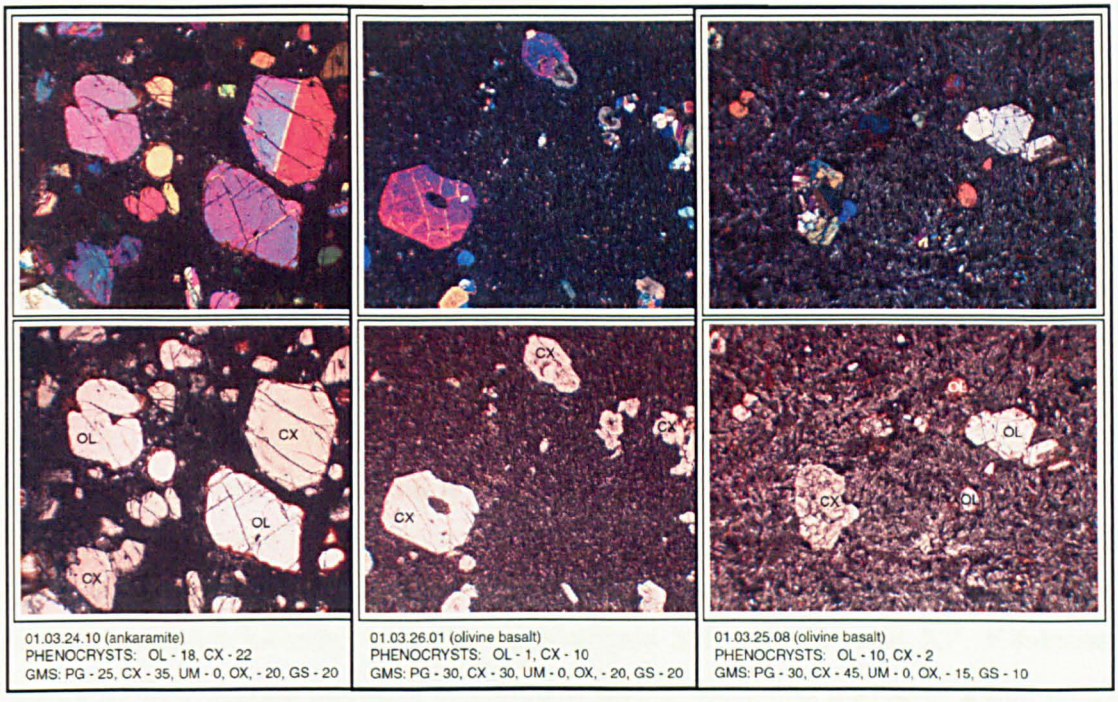

01.03.24.10 (ankaramite)
PHENOCRYSTS: OL - 18, CX - 22
GMS: PG - 25, CX - 35, UM - 0, OX, - 20, GS - 20

01.03.26.01 (olivine basalt)
PHENOCRYSTS: OL - 1, CX - 10
GMS: PG - 30, CX - 30, UM - 0, OX, - 20, GS - 20

01.03.25.08 (olivine basalt)
PHENOCRYSTS: OL - 10, CX - 2
GMS: PG - 30, CX - 45, UM - 0, OX, - 15, GS - 10

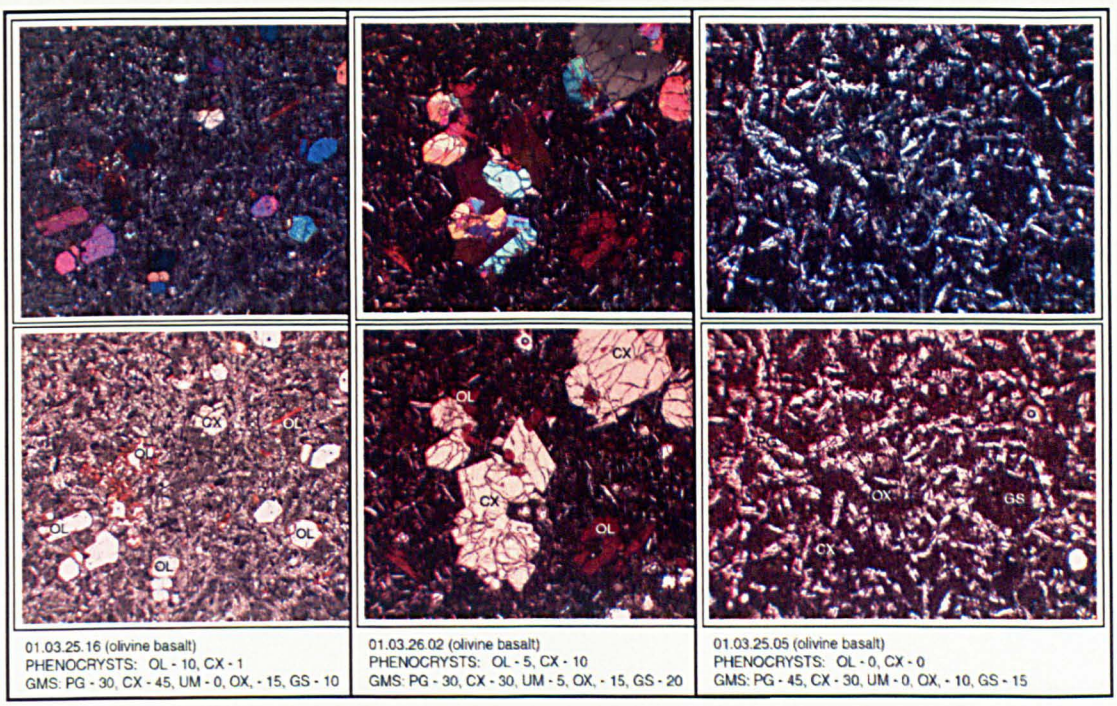

01.03.25.16 (olivine basalt)
PHENOCRYSTS: OL - 10, CX - 1
GMS: PG - 30, CX - 45, UM - 0, OX, - 15, GS - 10

01.03.26.02 (olivine basalt)
PHENOCRYSTS: OL - 5, CX - 10
GMS: PG - 30, CX - 30, UM - 5, OX, - 15, GS - 20

01.03.25.05 (olivine basalt)
PHENOCRYSTS: OL - 0, CX - 0
GMS: PG - 45, CX - 30, UM - 0, OX, - 10, GS - 15

Micrograph dimensions (shown fully on right) = 5.5 x 4.1 mm. Upper micrographs are in cross-polarised light, and lower micrographs are in plane-polarised light.
GMS - Groundmass, OL - Olivine, CX - Clinopyroxene, PG - Plagioclase, UM - Unknown orange mineral, OX - Fe-Ti oxides, GS - glass (respective percentages indicated by attached figures). The percentage of phenocryst phases are proportionate to the total volume of the rock, whereas the percentages of groundmass minerals are proportionate only to the groundmass, typical for the rock. The micrographs are arranged in order of increasing grain size of the groundmass, and the rocks have been classified as closely as was possible in accordance with the main lava groups.

Figure 4.23 Intrusives from the Dilb Section (see text for description of micrographs)

01.03.25.08 and 01.03.25.16 are petrographically and geochemically almost identical; consequently it may be suggested that they represent the same intrusive body. Despite the fact that they have a groundmass dominated by clinopyroxene, they have been classified as olivine basalts on the basis of their geochemistry.

4.2.4 Ignimbrites from the Dilb Section

Micrographs of the ignimbrites that occur at the top of the Dilb Section are shown in Figure 4.24 together with visual estimates of the percentage proportions of phenocrysts, inclusions, and groundmass constituents present in each sample. It is apparent that both samples are mineralogically very similar, but texturally quite different. Both have phenocryst assemblages consisting of quartz (5 %), plagioclase (2 %), K-feldspar (10 %), clinopyroxene (4 %), hornblende (1 – 2 %), and Fe-Ti oxides (1 %), and both contain lithic fragments dominantly of ignimbritic material (Fig. 4.25). Quartz is present as rounded anhedral crystals, pyramids and splinters (< 1 mm long), commonly exhibiting a pale yellow interference in cross-polarised light. Plagioclase is present as rare subhedral laths and fragments (< 0.5 mm long), generally heavily resorbed with crenulated margins, deteriorated interiors and remnant lamellar twinning with extinction angles between 16° and 23°. K-feldspar occurs as flow-aligned euhedral to anhedral tabular laths and prisms (< 2 mm long), often partially resorbed with rounded and embayed edges. Few crystals show simple twinning and, at high magnification, some can be seen to contain perthitic intergrowths of sodic feldspar (Fig. 4.26). There are also present, rare examples of K-feldspar which exhibit cross-hatched lamellar twinning. Clinopyroxene is present as moderately pleochroic, pale green to pale brown, euhedral to subhedral, variably fragmented crystals (< 1.5 mm long) with well-developed cleavage, and inclined extinction. The crystals show a subdued range of interference colours from yellow through to orange, pink and blue, and are often pitted and partially resorbed, and sometimes twinned. Hornblende is rare in both samples, but is more common in 01.03.24.01b. It is present in both as moderately pleochroic, green, stumpy, lath-like crystals (< 0.5 mm long) with pronounced cleavage. Fe-Ti oxides are also rare, but present in both samples as isolated, euhedral hexagonal prisms and short elongate stumps (< 0.3 mm long).

The matrix in both of the ignimbrites is consists of turbulent tangle of glass shards interleaved with thin wisps and irregular clumps of an unidentified opaque composite material. In 01.03.24.01a it is partially welded, and dominantly eutaxitic, composed of variably compressed devitrified glass shards, many of which have retained their structure (Fig. 4.27). Some shards are axiolitic, with fine radiating acicular microlites (probably of cristobalite and alkali feldspar) lining the inner walls (Fig. 4.28), whilst others have been squashed flat and re-crystallized so that their original morphology is not discernable. In 01.03.24.01b the matrix is characteristically more welded than in 01.03.24.01a. It is typically eutaxitic, composed dominantly of compressed and

Phenocryst assemblage

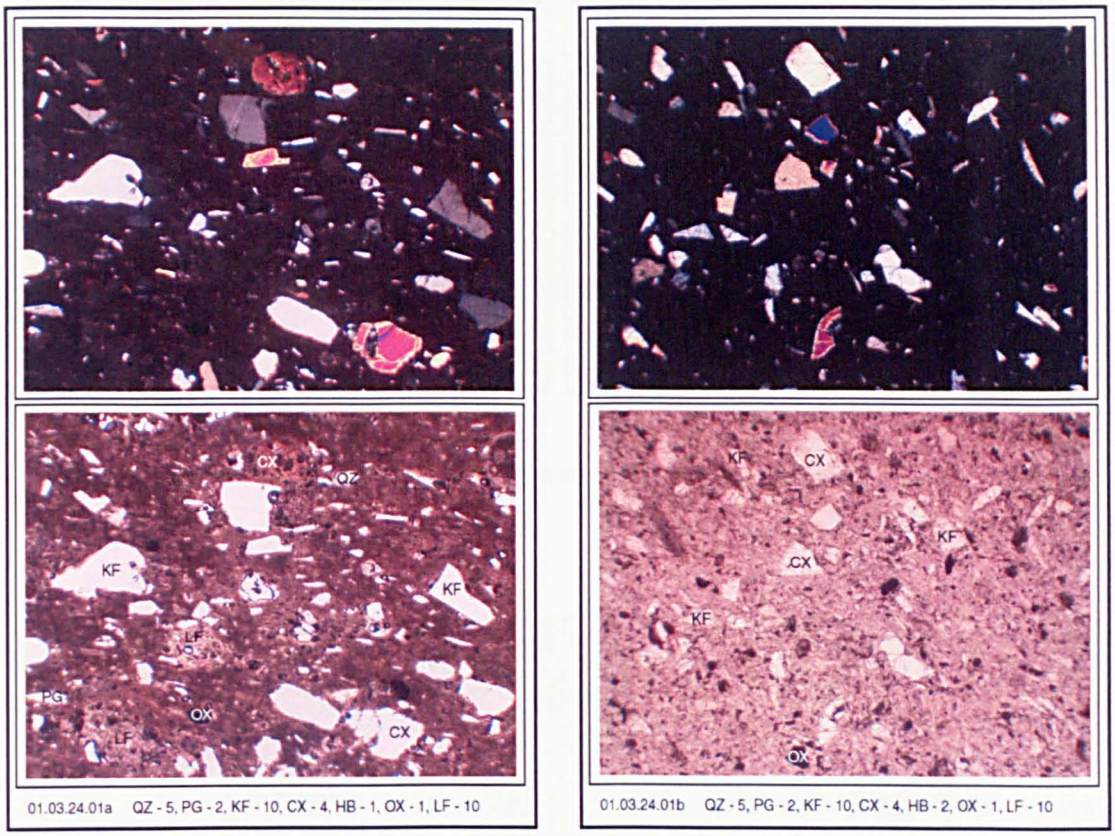

01.03.24.01a QZ - 5, PG - 2, KF - 10, CX - 4, HB - 1, OX - 1, LF - 10

01.03.24.01b QZ - 5, PG - 2, KF - 10, CX - 4, HB - 2, OX - 1, LF - 10

Micrograph dimensions = 5.5 x 4.1 mm. Upper micrographs are in cross-polarised light, and lower micrographs are in plane-polarised light.
QZ - Quartz, PG - Plagioclase, KF - K-feldspar, CX - Clinopyroxene, HB - Hornblende, OX - Fe-Ti oxides, LF - Lithic fragments (respective percentages are given as proportionate to the total volume of the rock and are indicated by the attached figures).

Groundmass assemblage

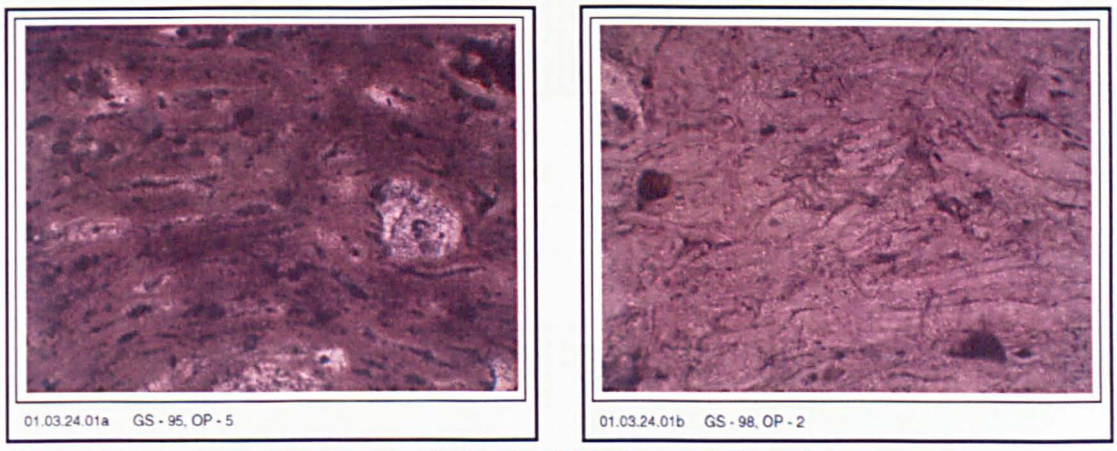

01.03.24.01a GS - 95, OP - 5

01.03.24.01b GS - 98, OP - 2

Micrograph dimensions = 0.685 x 0.515 mm. Micrographs are in plane-polarised light (sections are dominantly isotropic in cross-polarised light).
GS - Glass, OP - Opaque infill (respective percentages are proportionate only to the groundmass typical for the rock, and are indicated by the attached figures).

Figure 4.24 Ignimbrites from the Dilb Section (see text for description of micrographs)

folded glass shards, few of which have retained their structure. The glass is only partially devitrified and so appears almost clear in plane polarised light, and almost entirely extinct in cross-polarised light. In 01.03.24.01a there are countless rounded and irregular cavities within the matrix, whereas in 01.03.24.01b there are only a few; most are unlined, but some have a thin lumpy lining of an unidentified opaque composite material.

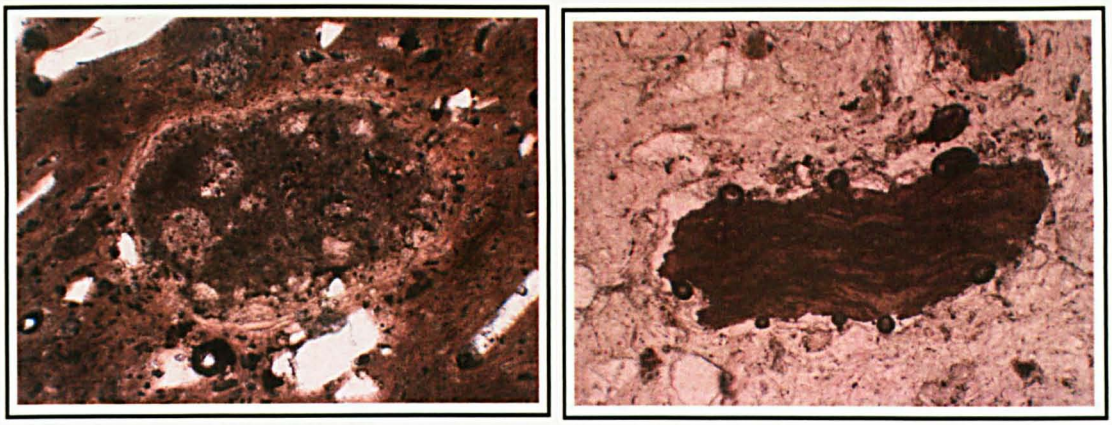

01.03.24.01a (Plane Polarised Light) 1.4 x 1 mm 01.03.24.01b (Plane Polarised Light) 1.4 x 1 mm

Figure 4.25 Ignimbritic lithic fragments present in the ignimbrites.

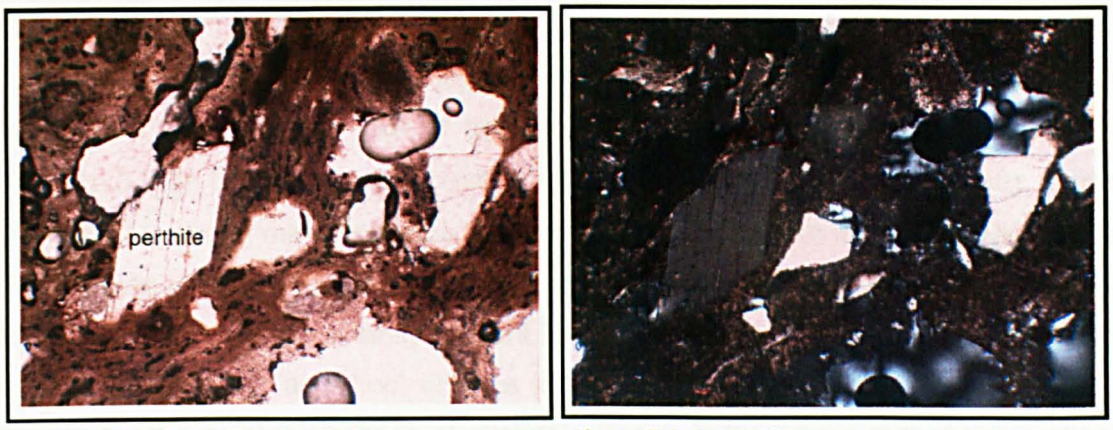

01.03.24.01a (Plane Polarised Light) (Cross-Polarised Light) 1.4 x 1 mm

Figure 4.26 Perthite present in the ignimbrite 01.03.24.01a

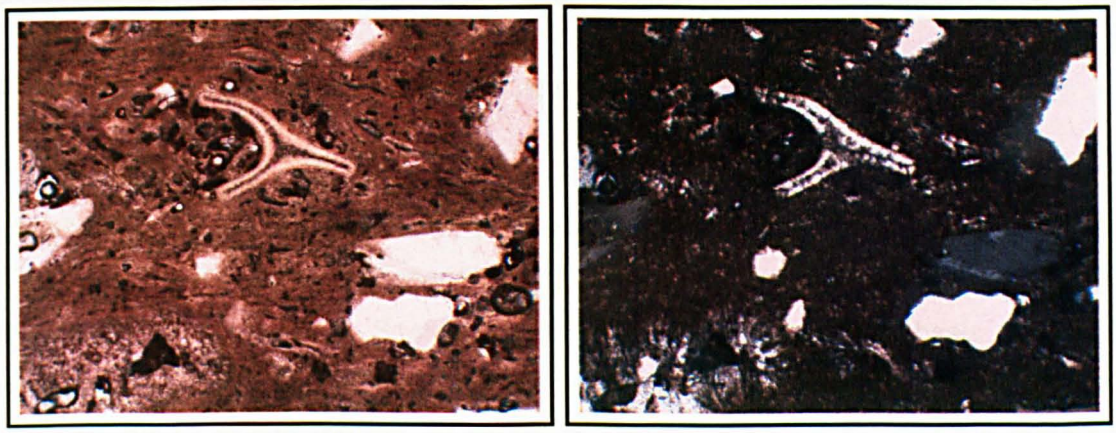

01.03.24.01a (Plane Polarised Light) (Cross-Polarised Light) 1.4 x 1 mm

Figure 4.27 Cuspate glass shard in ignimbrite 01.03.24.01a. The shard is a classic triple-junction,bubble-wall from shattered pumice.

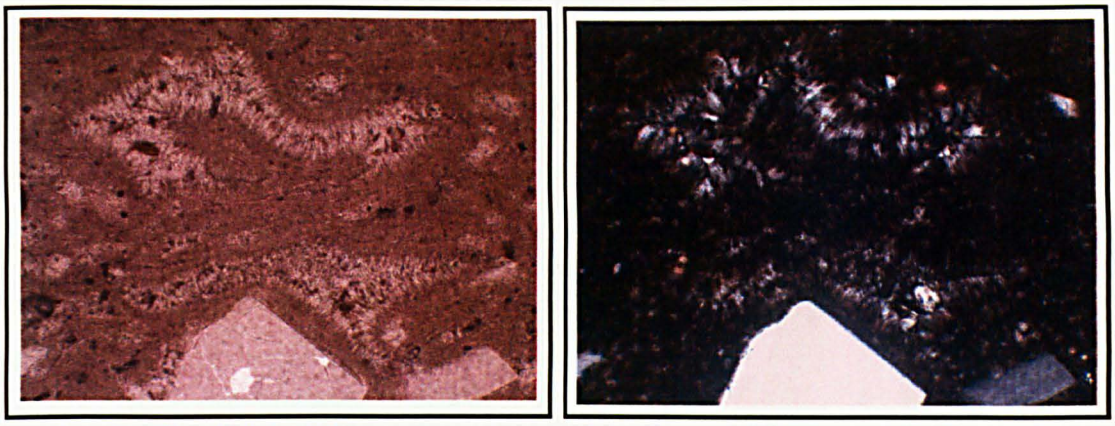

01.03.24.01a (Plane Polarised Light) (Cross-Polarised Light) 0.685 x 0.515 mm

Figure 4.28 Axiolitic shards in ignimbrite 01.03.24.01a. The shards have been devitrified and recrystallised as intergrowths of fine radiating acicular microlites (alkali feldspar and cristobalite) which extend inward from the shard-walls.

4.2.5 Stratigraphic relations

The stratigraphic relations of the lavas and ignimbrites in the Dilb Section are shown in Figure 4.29. The lower part of the section, below the paleaosol at Location 11 (Section 3.3.2), is dominated by picrites. Only one picrite (01.03.24.14) occurs above Location 11, and in many respects this sample is as much like an ankaramite as it is like a picrite. Although ankaramites and olivine basalts do occur in the lower part of the section, they are dominantly present in the upper part. The ignimbrites at the top of the section mark a distinct change in the nature of volcanism (Section 3.3.2). Except for the notable absence of skeletal olivines in the upper part of the section, above 01.03.24.15, and striated olivines between 01.03.25.14 and 01.03.25.03 (Table 4.5), there is no apparent systematic variation in phenocryst size, content and morphology with height in the section (Fig. 4.30b). Similarly, there is no systematic altitudinal variation in the coarseness and mineralogy of the groundmass (Fig. 4.30a).

4.3 Petrography of the rocks from the Iyela Section

4.3.1 Preface

Detailed petrographic descriptions of the lavas and intrusive rocks from the Iyela Section are documented in Appendix 4.1.3. As with the lavas from the Dilb Section, the lavas from the Iyela Section have been grouped, on the basis of these descriptions and geochemical analyses presented in Chapter 5 as picrites, ankaramites or olivine basalts as shown in Figures 4.31 - 4.33, and the intrusive rocks have been grouped separately as shown in Figure 4.39.

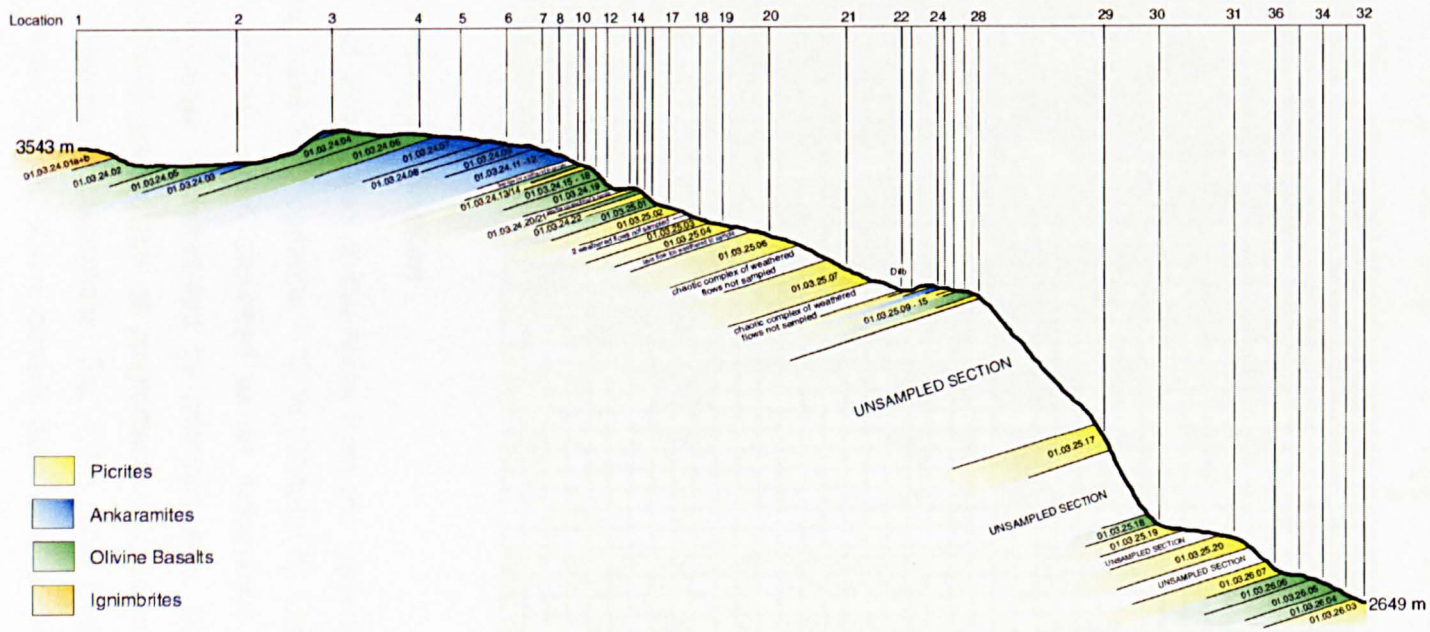

Figure 4.29 Stratigraphic relations of the lava groups and ignimbrites in the Dilb Section. The dip of the lavas is exaggerated for the purpose of representation. The dip of the lavas in the field is more shallow (< 5^{O} toward the south-west).

Table 4.5 Stratigraphic variation in olivine morphology of the Dilb lavas

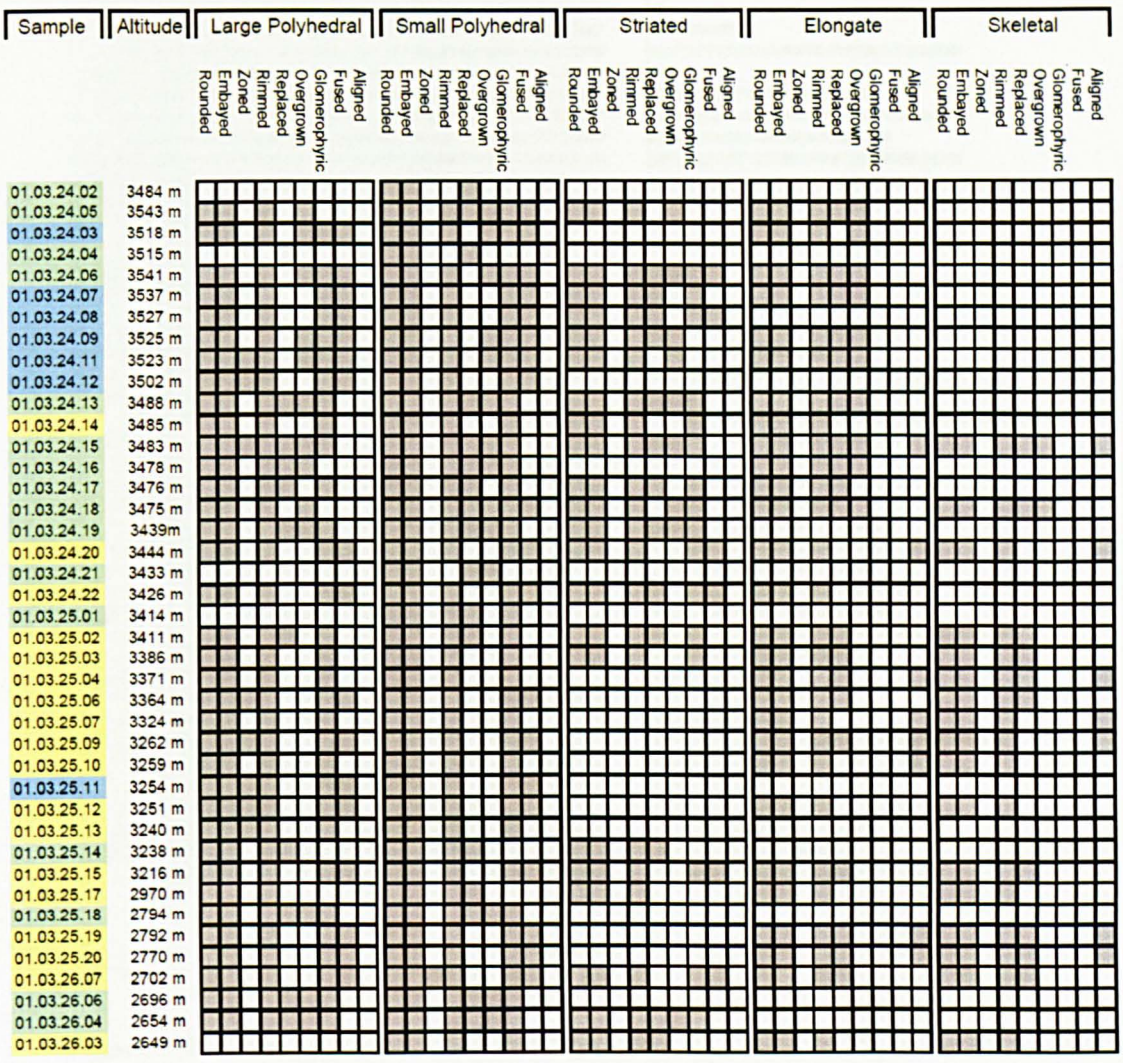

4.3.2 Lavas from the Iyela Section

Classification: All except one of the lavas from the Iyela Section are technically picritic since they have MgO contents > 12 % (Chapter 5). Only one of these picritic lavas (01.03.31.04) has been classified as an ankaramite on the basis that its phenocryst assemblage is dominated by clinopyroxene, despite the fact that it contains a significant percentage of plagioclase phenocrysts, and that it has a groundmass dominated by plagioclase (Fig. 4.32). This lava is in, most respects, similar to the coarser grained olivine basalts from the Dilb Section, but it has been classified otherwise on account of its higher MgO content. The rest of the picritic lavas are typically similar to picrites from the Dilb Section with phenocryst assemblages dominated by olivine (15 – 40 %), and groundmass assemblages dominated by clinopyroxene, and so have been classified accordingly (Fig. 4.31). The only lava from the Iyela Section with < 12 % MgO (01.03.31.02) is similar to the

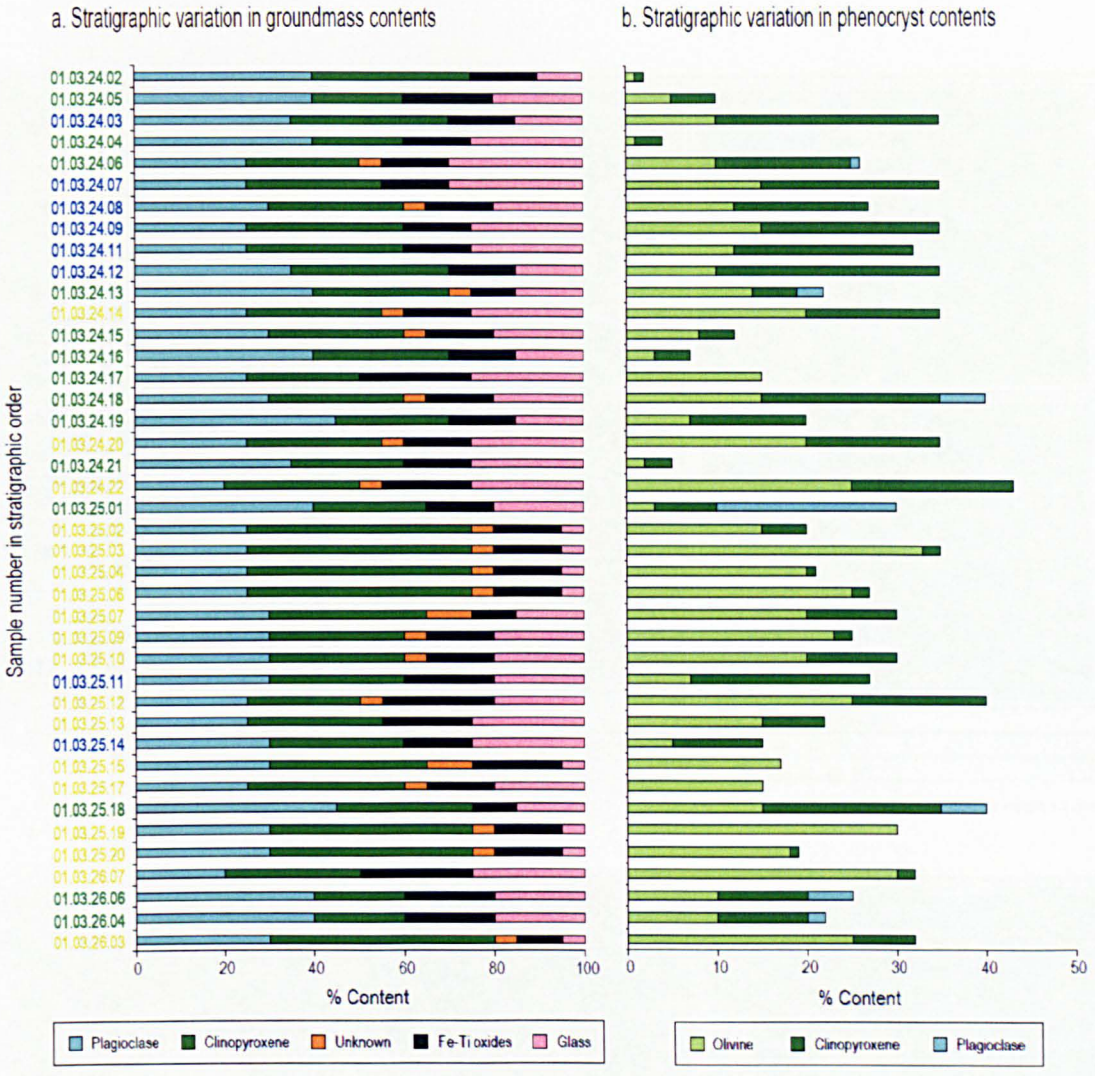

Figure 4.30 Stratigraphic variation in the groundmass and phenocryst contents of the lavas from the Dilb Section. The lava groups are denoted by the colour of the sample number - yellow for picrites, blue for ankaramites and green for olivine basalts.

olivine basalts from the Dilb Section, with extensively iddingsitized olivine phenocrysts and a groundmass assemblage dominated by plagioclase (Fig. 4.33), and in this respect it has been classified as such.

Phenocrysts: Textural relations, size, morphology and optical properties of the phenocryst phases within the Iyela lavas are similar to those seen in the Dilb lavas. The phenocryst assemblage for each lava group is characterised by a varied mix of randomly dispersed, variably rounded and fragmented olivine and clinopyroxene phenocrysts and glomerocrysts. Plagioclase phenocrysts are present only in the ankaramite (01.03.31.04).

Olivine: All varieties of olivine (Appendix 4.2) are represented in the picrites, though skeletal forms only occur in two of the lavas (Table 4.6). As is generally the case in

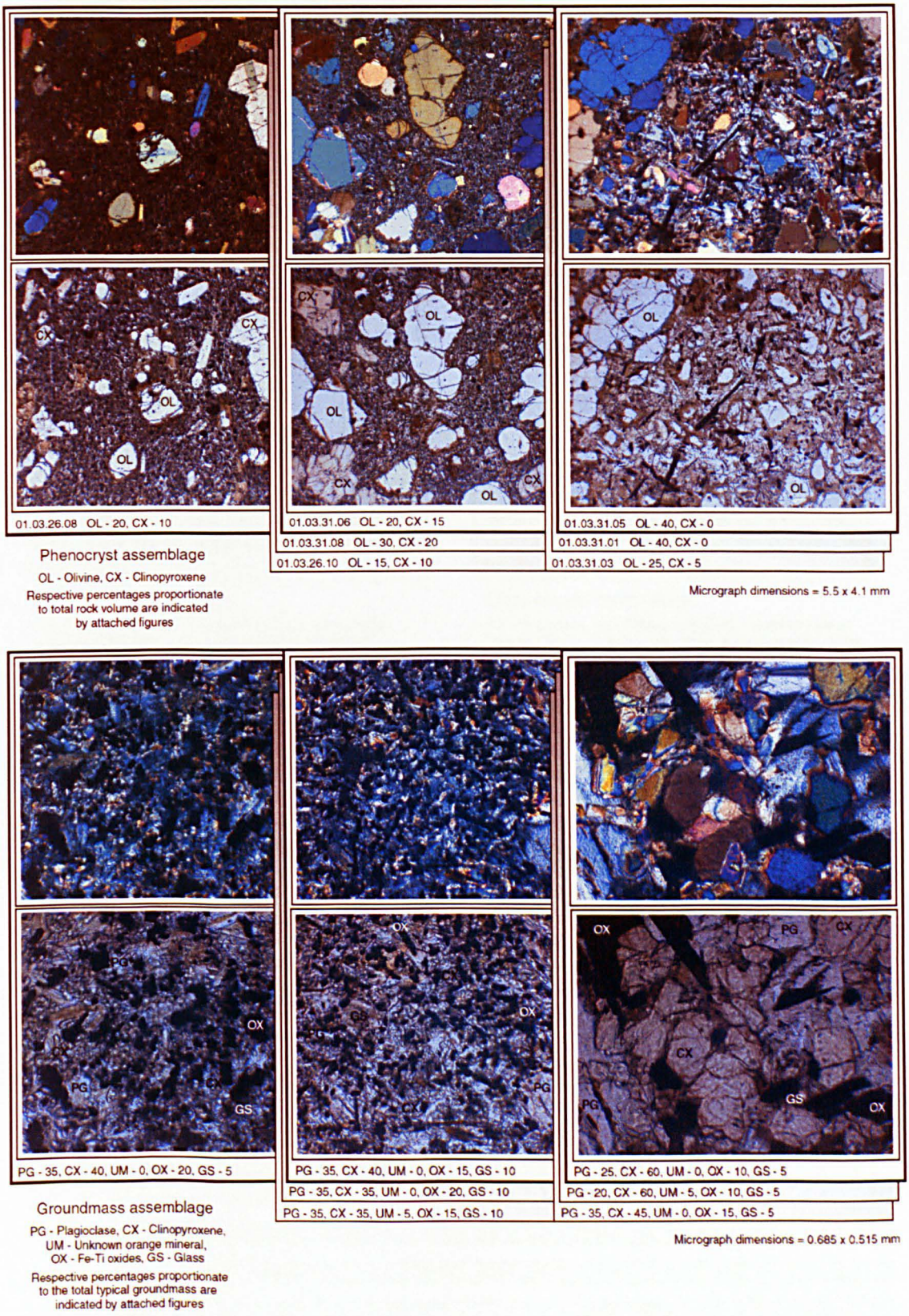

Figure 4.31 Picrites from the Iyela Section. Upper and lower micrographs for phenocryst and groundmass assemblages are in cross and plane polarised light respectively.

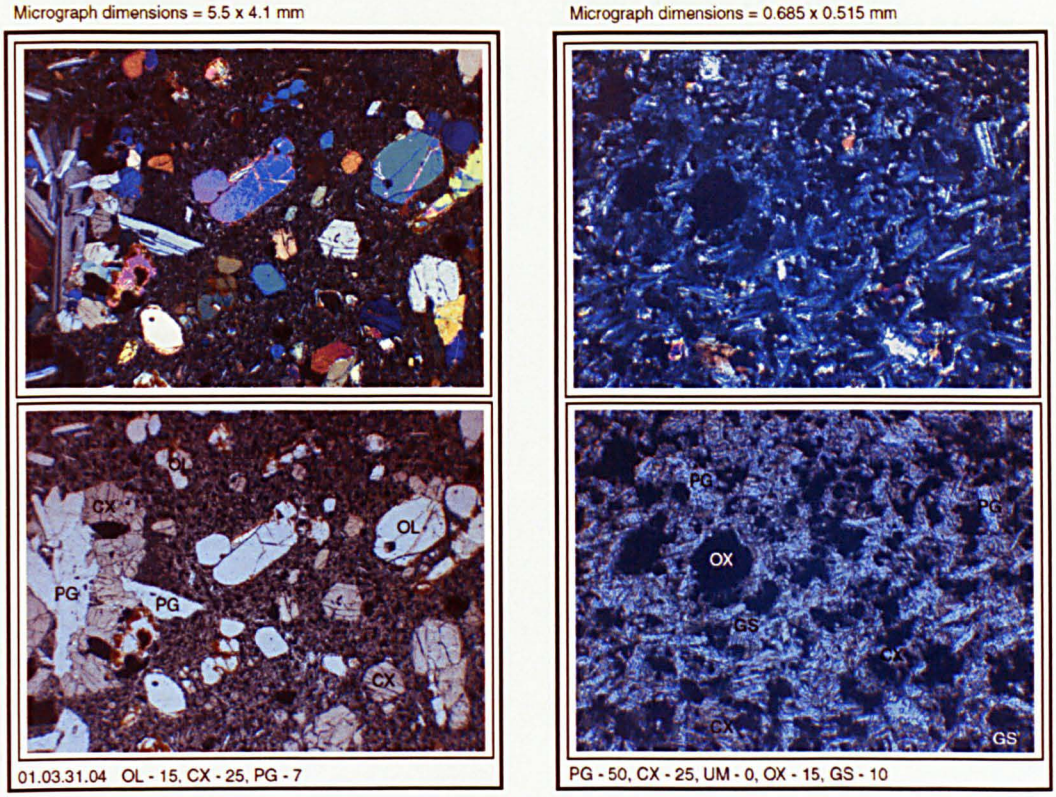

Figure 4.32 Ankaramite lava from the Iyela Section. Upper and lower micrographs for the phenocryst and groundmass assemblages are in cross and plane polarised light respectively (see text for description of micrographs).

Table 4.6 Olivine morphology of the lavas and intrusives from the Iyela section

Sample	Large Polyhedral								Small Polyhedral								Striated								Elongate								Skeletal							
	Rounded	Embayed	Zoned	Rimmed	Replaced	Overgrown	Glomerophyric	Fused	Aligned	Rounded	Embayed	Zoned	Rimmed	Replaced	Overgrown	Glomerophyric	Fused	Aligned	Rounded	Embayed	Zoned	Rimmed	Replaced	Overgrown	Glomerophyric	Fused	Aligned	Rounded	Embayed	Zoned	Rimmed	Replaced	Overgrown	Glomerophyric	Fused	Aligned	Rounded	Embayed	Zoned	Rimmed	Replaced	Overgrown	Glomerophyric	Fused	Aligned
Picrites																																										
01.03.26.08																																										
01.03.26.10																																										
01.03.31.08																																										
01.03.31.06																																										
01.03.31.03																																										
01.03.31.01																																										
01.03.31.05																																										
Ankaramites																																										
01.03.31.04																																										
Olivine Basalts																																										
01.03.31.02																																										
Intrusives																																										
01.03.31.07																																										
01.03.26.09																																										

Note: Samples in each group are arranged in order of increasing grain size of the groundmass

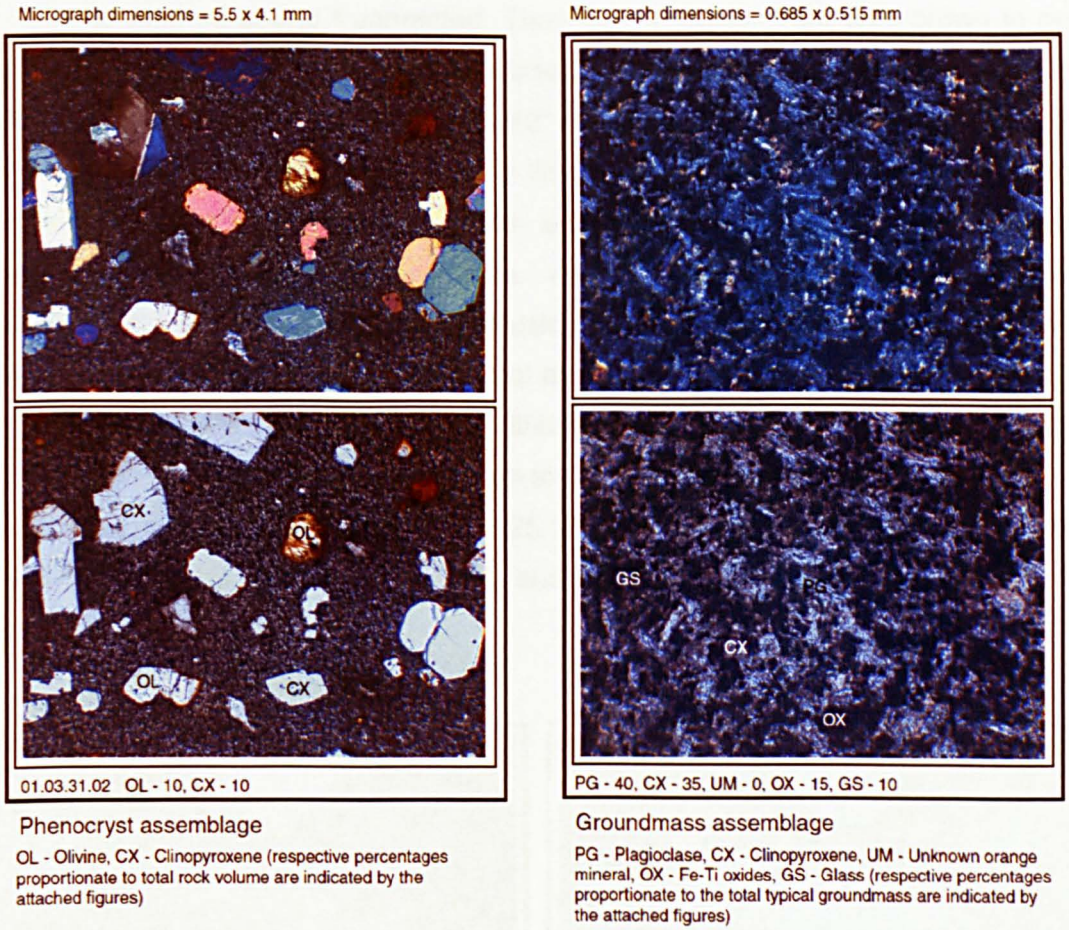

Figure 3.33 Olivine Basalt from the Iyela Section. Upper and lower micrographs for the phenocryst and groundmass assemblages are in cross and plane polarised light respectively (see text for description of micrographs).

the Dilb lavas, skeletal olivines are absent in the ankaramite and olivine basalt. All varieties are characteristically clear and cracked, and variably rounded and embayed, and strain features are rare (an example of a strained olivine is shown in the centre of the micrograph of 01.03.26.08 in Figure 4.31). In most of the lavas, the olivines are rimmed and, to one degree or another, replaced by iddingsite, though in some (01.03.26.08, 01.03.31.05 and 01.03.31.06) they are rimmed and variably replaced with serpentine, and rarely with chlorite (01.03.26.08). Olivine overgrowths similar to those seen in the olivine basalts and ankaramites from the Dilb Section (Fig. 4.5) also occur around the majority of olivine phenocrysts in the ankaramite 01.03.31.04. As noted in the Dilb lavas, glomerophyric tendencies are only exhibited by the large, small and striated polyhedral olivines, and although the elongate and skeletal olivines are never glomerophyric, they are sometimes chained and/or aligned.

Clinopyroxene: Clinopyroxene phenocrysts occur both as individual phenocrysts and as glomerocrysts in all the lavas except the two most coarsely grained picrites (Fig. 4.31). As in the Dilb lavas, they range in form from euhedral to anhedral, but are

dominantly subhedral and fragmented. They vary in colour from pale brown to pale greenish or greyish brown and are commonly twinned and sometimes zoned. The range of extinction angles between 42° and 46° is slightly smaller than for clinopyroxene phenocrysts from the Dilb Section, but is still within the range typical for augite. Strain features such as kink bands, offset and bent twin-planes, and irregular undulose extinction patterns occur in both the phenocrystic and glomerophyric clinopyroxenes, and inclusions of unaltered olivine are common in many of the larger well-preserved euheral phenocrysts. There are isolated examples in the ankaramite 01.03.31.04 of clinopyroxene phenocrysts with numerous inclusions of randomly orientated opaque to reddish-brown, acicular oxides similar to those seen in one of the picrites (01.03.25.07) from the Dilb Section (Fig. 4.34). The inclusions are bright in reflected light, and have high relief, and low interference colours typical of spinel.

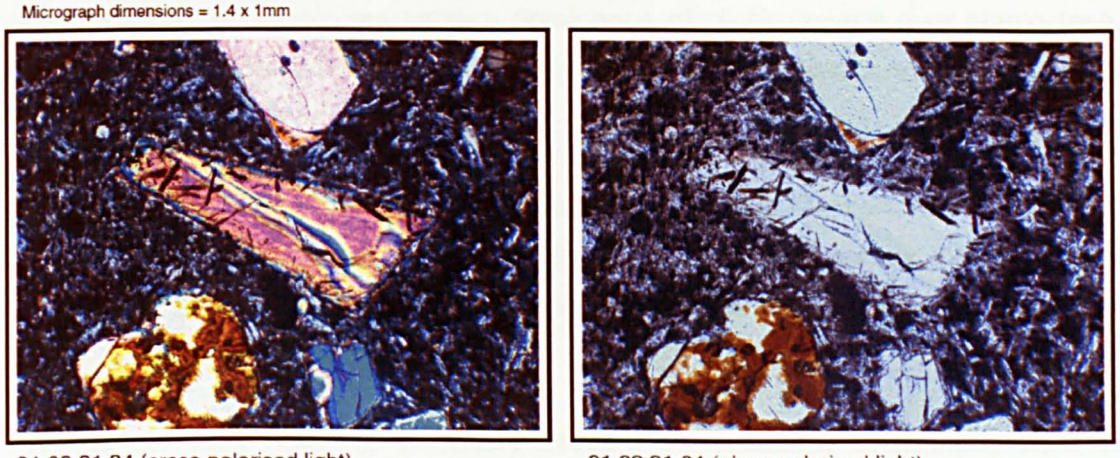

Figure 4.34 Acicular oxide inclusions in clinopyroxene (ankaramite 01.03.31.04)

Plagioclase: The plagioclase phenocrysts in the ankaramite (Fig. 4.32) are similar to the long slender variety seen in the coarser grained olivine basalts from the Dilb Section (Fig. 4.10). They occur mainly in glomerophyric clusters with clinopyroxene and olivine, and are characterised by long (< 3mm) slender euhedral to subhedral laths with sharply defined simple and lamellar twinning, and extinction angles between 18° and 36° (An_{57} – An_{58}). The range of extinction angles for the phenocrysts is only marginally lower than that for the plagioclase microlites in the groundmass, and is similar to that for plagioclase microlites in other lavas from both the Iyela and Dilb sections (eg. 01.03.26.10).

Glomerocrysts: The lavas from the Iyela Section contain a variety of glomerocryst types similar to those seen in the Dilb lavas (Fig. 4.11), including fused and loosely

clustered masses exclusively of olivine, and variably compacted mosaics of olivine, clinopyroxene. As described above, plagioclase is also present with clinopyroxene and olivine in glomerocrysts in the ankaramite 01.03.31.04. It is notable that in the glomerocrysts of mixed mineralogy, olivine tends to form the core of the agglomerations, and that in some cases this is unaltered, and in others it is variably rimmed and/or replaced by iddingsite. As in the lavas from the Dilb Section, the glomerocrysts composed exclusively of clinopyroxene show a greater variation in size than those composed exclusively of olivine, or those of mixed mineralogy, and often they are stellate in form.

Groundmass: The groundmass of the Iyela lavas comprises variable proportions of plagioclase, clinopyroxene, Fe-Ti oxides and devitrified glass; two of the picrites also contain an unidentified orange mineral (possibly spinel) similar to that seen in the groundmass of selected lavas from the Dilb Section (Fig. 4.13). Generally, the groundmasses of the picrites show a dominance of clinopyroxene over plagioclase, whereas those of the ankaramite and olivine basalt show a dominance of plagioclase over clinopyroxene (Figs 4.31 – 33).

Grain size: Although there are a few lavas in the Dilb Section with much finer groundmasses than any of the lavas in the Iyela Section, generally the lavas from both sections show a similar variation in the size of the groundmass microlites between flows (Tables. 4.2 & 4.7).

Plagioclase: Plagioclase is invariably present as randomly orientated, clear to clouded, subhedral to euhedral, simple and multiple twinned laths, and as irregular clear infill occasionally exhibiting ghost-like twinning. Flow alignment of plagioclase laths around larger phenocrysts and glomerocrysts is only evident in the ankaramite. Average extinction angles for the mineral vary between 19° and 24° (An_{40} – An_{44}) in the picrites, 19° (An_{40}) in the ankaramite, and 24° (An_{44}) in the olivine basalt. In some of the lavas, areas of irregular plagioclase infill are shot through with randomly orientated clear to pale green needles with high relief and grey interference colours typical of apatite (Fig. 4.35).

Clinopyroxene: Clinopyroxene is present in the groundmass of the Iyela lavas, mainly as randomly orientated, subhedral pale green to pale brown, elongate, prismatic microlites, and irregular flakes and infill. As in the Dilb lavas, extinction angles for the mineral show little variation within and between flows (45° - 46°). The more well-formed microlites are often twinned and occasionally exhibit oscillatory and hour-

Table 4.7 Groundmass mineralogy of the lavas and intrusive rocks from the Iyela section

Sample	Plagioclase				Clinopyroxene				Unknown		Fe-Ti Oxides				Glass	Vesicles		
	Laths	Irregular	Twinned	Extinction	Polyhedral	Irregular	Twinned	Extinction	Acicular	Irregular	Prismatic	Globular	Acicular	Granular	Devitrified	% content	Max. size	Lined
Picrites																		
01.03.26.08	0.10	0.10		25	0.10	0.08		46			0.10	0.20	0.20	0.05				
01.03.26.10	0.10	0.10		21	0.10	0.08		45	0.20		0.10	0.20	0.20	0.05		10	5.0	
01.03.31.08	0.20	0.20		22	0.05	0.05		45			0.10		0.10	0.05				
01.03.31.06	0.20	0.20		23	0.10	0.10		45			0.20	0.15	0.30	0.05				
01.03.31.03	0.20	0.20		19	0.20	0.15		46			0.08		0.20	0.05		3	1.0	
01.03.31.01	0.30	0.40		23	0.30	0.20		45	0.50		0.20		0.40	0.08		15	2.0	
01.03.31.05	0.50	0.50		24	0.40	0.20		45			0.20		0.50	0.05		5	1.2	
Average	0.23	0.24		22	0.18	0.12		45	0.35		0.14	0.18	0.27	0.05		8	2.3	
Ankaramites																		
01.03.31.04	0.20	0.20		19	0.10	0.10		46			0.25			0.50				
Olivine Basalts																		
01.03.31.02	0.10	0.10		24	0.10	0.08		46			0.10			0.05				
Intrusives																		
01.03.26.09	0.40	0.40		23	0.20	0.20		45	0.10		0.10		0.20	0.05				
01.03.31.07	0.15	0.15	indeterminable		0.20	0.20	indeterminable						0.20			10	0.2	
Average	0.28	0.28		23	0.20	0.20		45	0.10		0.10		0.20	0.05		10	0.2	

Note: Samples in each group are arranged in order of increasing grain size of the groundmass. Grain size (mm) is shown as the maximum for a representative area of groundmass (Appendix 4.1). Extinction angles are in degrees.

Micrograph dimensions = 0.685 x 0.515 mm

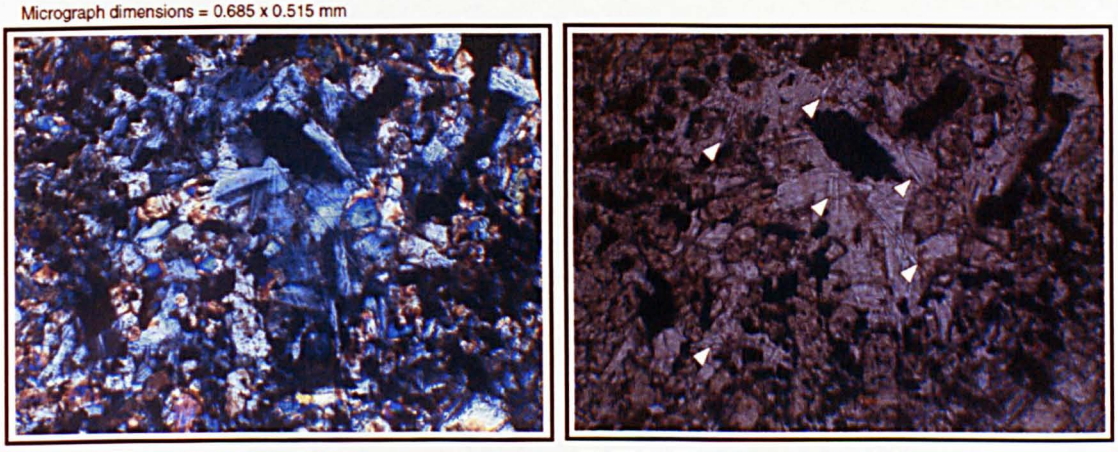

01.03.31.03 (cross-polarised light) 01.03.31.03 (plane polarised light)

Figure 4.35 Apatite needles in the groundmass plagioclase of picrite 01.03.31.03. The more prominent needles are indicated by the white infilled arrows.

glass zoning. In some of the coarser grained lavas, the clinopyroxene is sometimes glomerophyric, and forms striking stellate rosettes of radiating microlites with bright and contrasting interference colours (Fig. 4.36).

Fe-Ti oxides: All varieties of opaque Fe-Ti oxides seen in the groundmass of the Dilb lavas are represented in the Iyela lavas. They show a similar distribution between lava-types, and, likewise, show no discernable pattern in their size and morphology with respect to average groundmass grain size, mineralogical composition and stratigraphic order (Table 4.7). Variably sized euhedral to anhedral, cubic and hexagonal prisms, and granules of probably magnetite and titano-magnetite are

Micrograph dimensions = 1.4 x 1mm

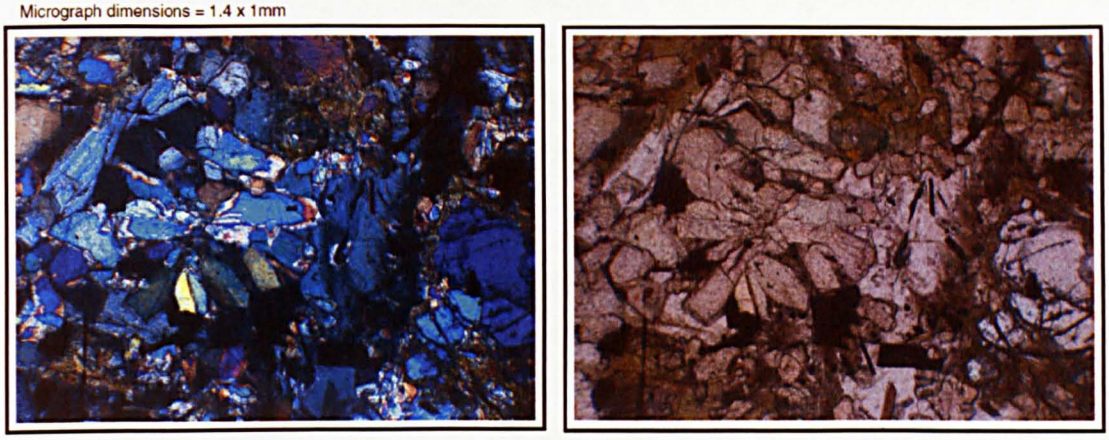

01.03.31.05 (cross-polarised light)

01.03.31.05 (plane polarised light)

Figure 4.36 Glomerophyric clinopyroxene in the groundmass of picrite 01.03.31.05. A rosette of elongate clinopyroxenes is shown just left of the centre of the micrographs

common in all the lavas. The prismatic forms are present both as evenly distributed groundmass microlites, and as larger isolated phenocrysts (up to 0.3 mm across), often nestled in embayments along the margins of iddingsitized olivines. Acicular ilmenite and globular magnetite are confined to the groundmasses of the picrites. In few of the coarser grained picrites some of the acicular oxides can be seen to be made up of strings of tiny coalesced prisms that appear to have used fine hair-like oxides as nuclei for their growth (Fig. 4.37). The unidentified orange to reddish brown

Micrograph dimensions = 0.685 x 0.515 mm

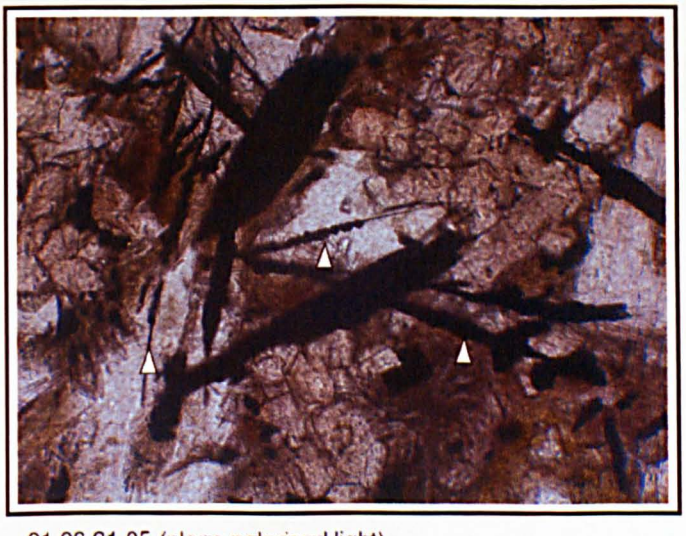

01.03.31.05 (plane polarised light)

Figure 4.37 Strings of tiny prismatic opaque Fe-Ti oxides (indicated by white arrows) nucleated on pre-existing hair-like opaque oxides.

acicular mineral, previously suggested to be spinel or rutile is present in the two picrites, 01.03.26.10 and 01.03.31.01, and is therefore included as an additional oxide mineral within the groundmass of these two lavas.

Glass: Greyish brown devitrified glass occurs in varying proportions in all the Iyela lavas. Generally, it forms less of a proportion of the total groundmass in the more coarse grained lavas, and in the finer grained lavas, it is sometimes difficult to distinguish from the mush of tiny pale brown clinopyroxene microlites also present in the groundmass.

Textural variations: As noted for the Dilb lavas, although the mineralogy and texture of the groundmass in most the Iyela lavas is, on the whole, relatively uniform, there are a few lavas in which there are significant textural and minerlogical variations within the groundmass that might suggest that differentiation and/or mixing took place during and/or after emplacement. This is most noticeable in the picrite, 01.03.31.03, in which there are discernable regions with larger proportions of plagioclase, opaque oxides and acicular apatite compared to the main fabric of the groundmass. The plagioclase, oxide and apatite microlites in these differentiated regions are generally much larger than those in the typical groundmass (Fig. 4.38).

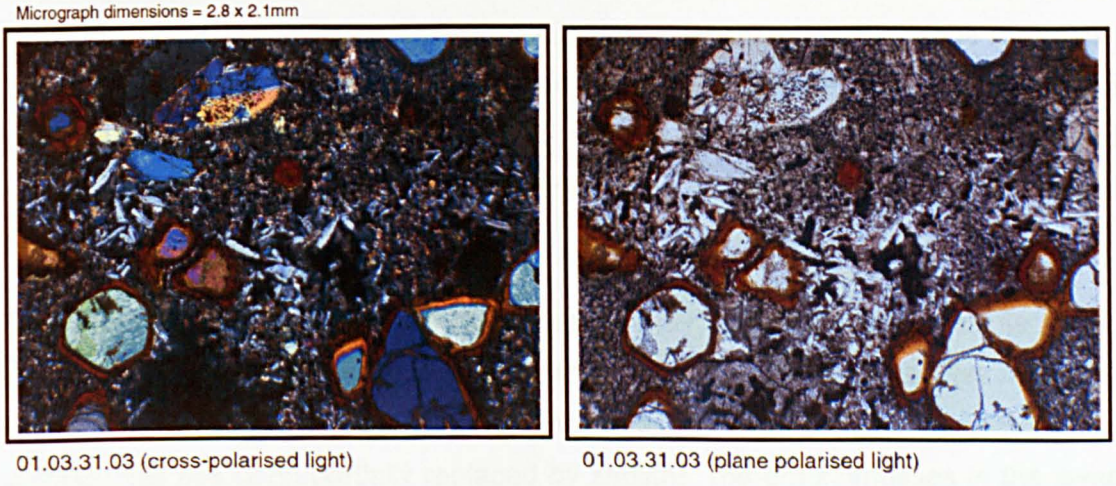

Figure 4.38 Differentiated areas of the groundmass in the picrite 01.03.31.03. These are evident as areas of larger plagioclase microlites and a higher proportion of opaque oxides compared to the main fabric of the groundmass. The differentiated zone shown extends in a meandering band across the centre of the micrographs.

Vesicles: Vesicles are present only in four of the picrites from the Iyela Section (Table 4.7). Generally, the vesicles show a random but dispersed distribution in the lavas in which they occur, and are spherical to slightly flat in form. There are no irregular cavities like those seen in some of the Dilb lavas. In the picrite, 01.03.31.01, however, the concentration of vesicles is such that some have coalesced to form irregular globular shaped cavities. Most of the vesicles that occur in the Iyela lavas are lined with a thin zeolitic crust similar to that seen lining vesicles in the Dilb lavas. Few are unlined. In the picrite 01.03.31.05 there occur numerous spherical vesicles

invariably encrusted with a pale-green mammilated mineral, and infilled with a pale olive-green to brown, slightly birefringent mineral, possibly associated with serpentinization (see below).

Alteration: As in the Dilb Section, all the lavas in the Iyela Section are, to one degree or another, altered in some way. Few olivines have escaped iddingsitization or serpentinization - most are rimmed, and some are psuedomorphed by either iddingsite or serpentine as a result. The styles of alteration are similar to those seen in the Dilb lavas (Fig. 4.21). In most of the Iyela lavas the olivines are rimmed and variably replaced by iddingsite, whereas in the picrites, 01.03.26.08 and 01.03.31.05, they are rimmed, crack-lined, and variably replaced with serpentine. In 01.03.31.05 the effects of serpentinization appear to have permeated the groundmass, which in places has been replaced and infilled by an amorphous olive green to pale brown, almost isotropic serpentine. These zones of replacement run away from the serpentinized margins of altered olivines, and where they extend into vesicular areas of the groundmass, the inner walls of the vesicles are encrusted in the same amorphous material. In the peripheral regions around the altered olivines the green replacement material is more fibrous and exhibits a delicate play of interference colours more typical of serpentine. The olivines in 01.03.31.06 are rimmed and variably replaced by a mixture of serpentine and iddingsite, but the sequence of alteration is difficult to ascertain.

The effects of zeolitization in the Iyela lavas is only apparent in the vesicular units, where the vesicles are lined and infilled with pale brown and clear zeolites with grey interference colours. Unlike some of the lavas in the Dilb Section where the groundmass has been partially replaced by zeolites, the groundmasses in the lavas of the Iyela Section show little evidence of zeolitization.

4.3.3 Intrusive rocks from the Iyela Section

The two intrusive bodies in the Iyela Section are petrologically and geochemically similar to the lavas, and therefore, like the intrusives encountered in the Dilb Section, they may be assumed to be either feeder conduits for lava flows above or lavas that have been channelled by structural weaknesses or topographic irregularities in the surface lavas during eruption (Section 3.3.2). They are both picritic in composition with MgO contents > 12% and phenocryst assemblages dominated by olivine (Fig. 4.39). 01.03.31.07 is unusual in that most of its olivine phenocrysts have sharp edges and are not rimmed with iddingsite, despite the fact that their interiors are partially

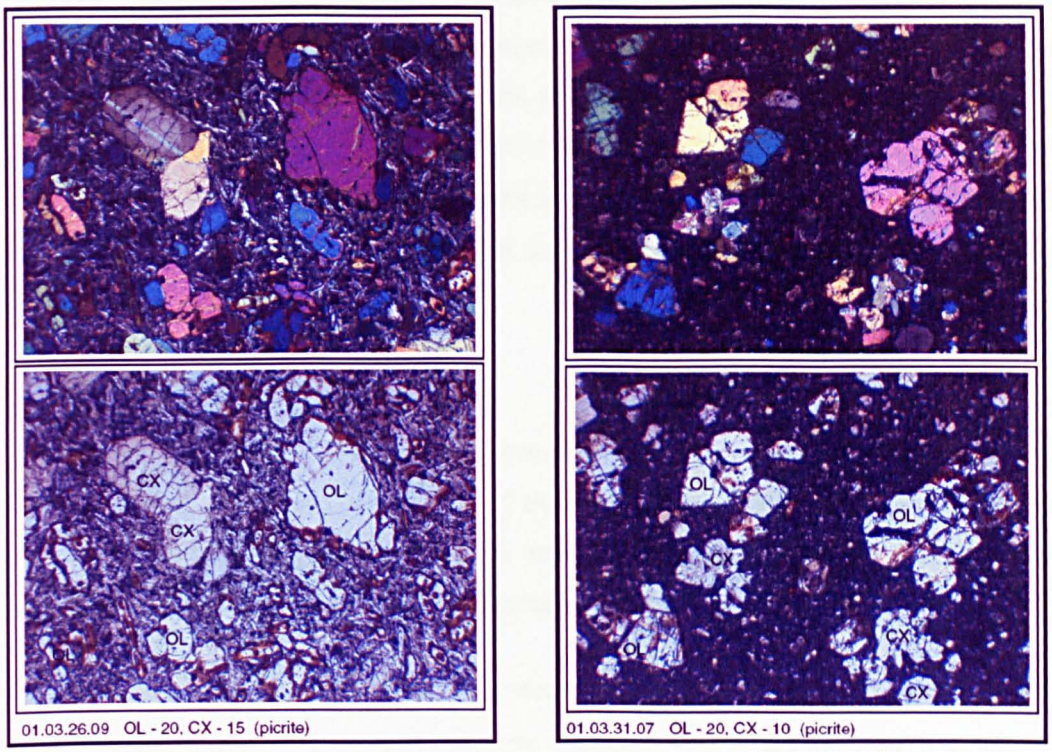

01.03.26.09 OL - 20, CX - 15 (picrite)

01.03.31.07 OL - 20, CX - 10 (picrite)

Micrograph dimensions = 5.5 x 4.1 mm

Phenocryst assemblage

OL - Olivine, CX - Clinopyroxene (respective percentages proportionate to total rock volume are indicated by attached figures)

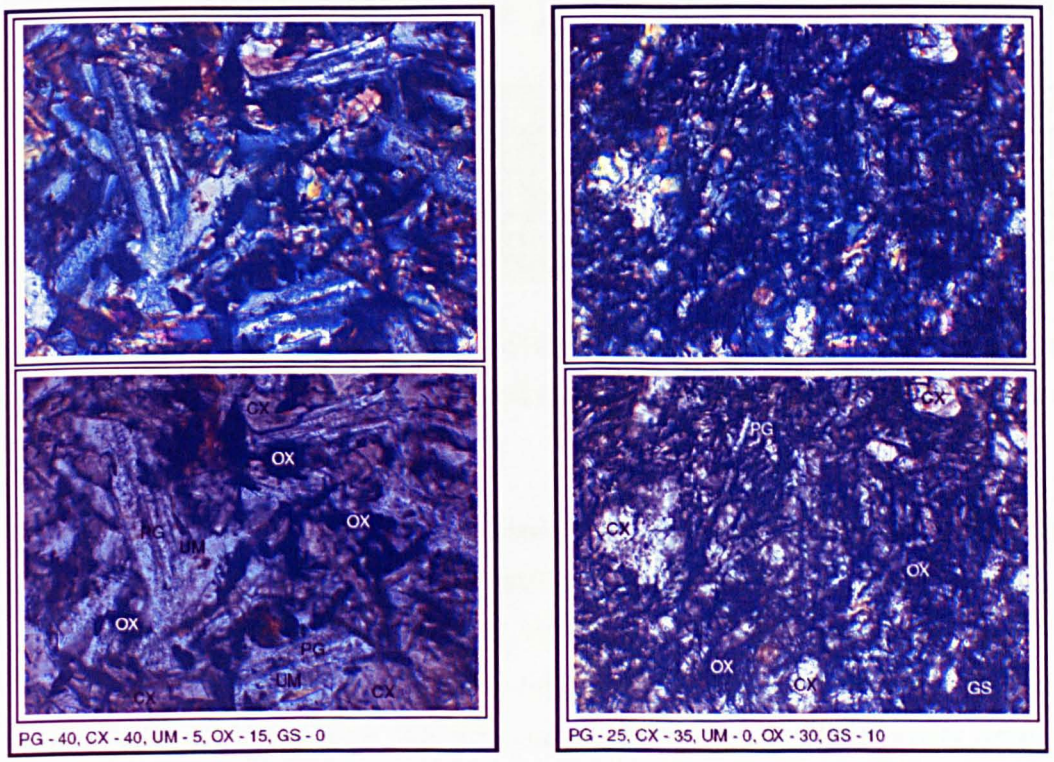

PG - 40, CX - 40, UM - 5, OX - 15, GS - 0

PG - 25, CX - 35, UM - 0, OX - 30, GS - 10

Micrograph dimensions = 0.685 x 0.515 mm

Groundmass assemblage

PG - Plagioclase, CX - Clinopyroxene, UM - Unknown orange mineral, OX - Fe-Ti oxides, GS - Glass (respective percentages proportionate to the total typical groundmass are indicated by attached figures)

Figure 4.39 Intrusive rocks from the Iyela Section. Upper and lower micrographs for the phenocryst and groundmass assemblages are in cross and plane polarised light respectively (see text for description of micrographs).

iddingsitized; the few olivines that are rimmed are rimmed with a composite mixture of serpentine and iddingsite. It is also unusual in that it has groundmass with a very high percentage of Fe-Ti oxides which are exclusively acicular ilmenite. This forms a dense mesh of needles giving the groundmass an exceptionally dark appearance (Fig. 4.39). The characteristics of the various olivine morphologies present in both the intrusives are recorded in Table 4.6, and details of the groundmass constituents are shown in Table 4.7.

4.3.4 Stratigraphic relations

The stratigraphic relations of the lavas in the Iyela Section are shown in Figure 4.40. Picrites form the upper and lower part of the section and the ankaramite and olivine basalt are sandwiched between. As in the Dilb Section, there is no systematic stratigraphic variation in the olivine morphology (Table 4.8), or in the content of the

Table 4.8 Stratigraphic variation in olivine morphology of the lavas from the Iyela section

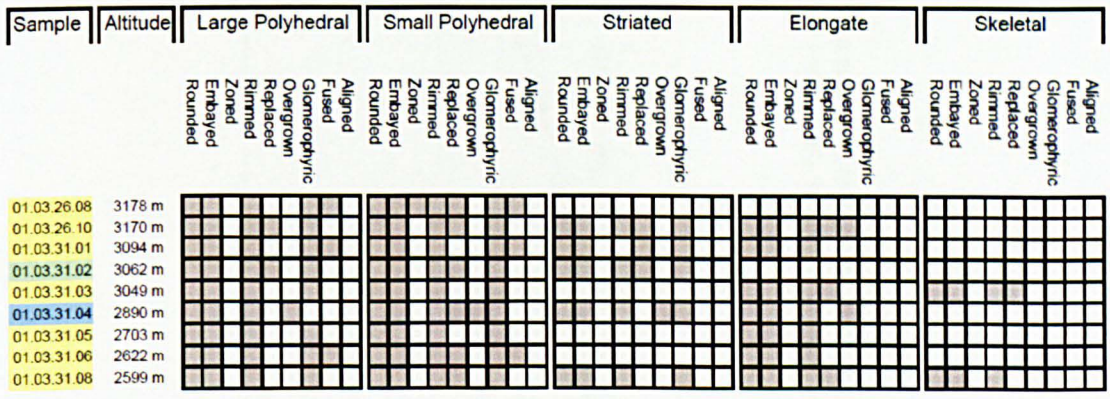

phenocryst assemblage (Fig. 4.41b). Similarly there is no systematic stratigraphic variation in the grain size, mineralogy and morphology of the groundmass (Table 4.7 & Fig. 4.41a).

It is apparent in the field that the sequences of lavas represented by the Dilb and Iyela sections are part of the same fault-block (Chapter 3). It may therefore be assumed that the two sequences are in some way stratigraphically related. By extrapolating the approximate dip of the Iyela lavas eastward to intersect the line of the Dilb Section it can be seen that, if the lavas are assumed to be laterally extensive, the extent of the entire sequence would outcrop in the part of the Dilb Section not sampled between lava flows 01.03.25.15 and 01.03.25.17 (Fig. 4.42). Evidence from field relations, on the contrary, suggests that individual flows vary in thickness and are laterally discontinuous over several kilometres such that they interleave with one another to form flow fields (Chapter 3); therefore it may not necessarily be expected

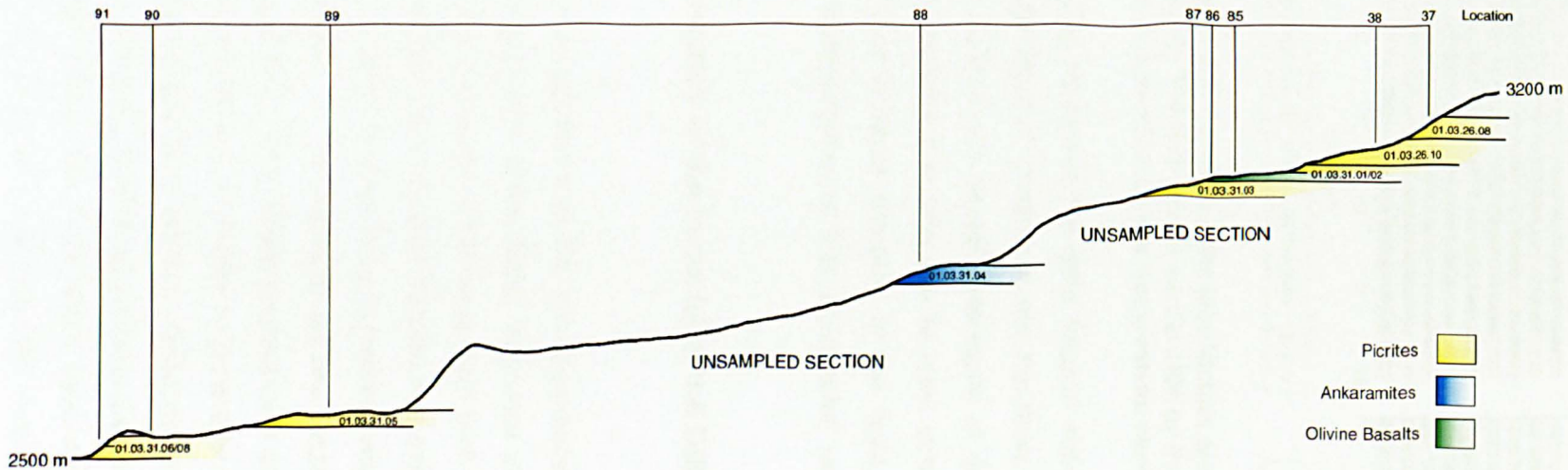

Figure 4.40 Stratigraphic relations of the lava groups in the Iyela Section. For the convenience of representation the lava flows are shown as horizontal units. In the field, they are laterally discontinuous with variable dip and thickness, and the sequence dips slightly south-west (< 5°) - right to left in section.

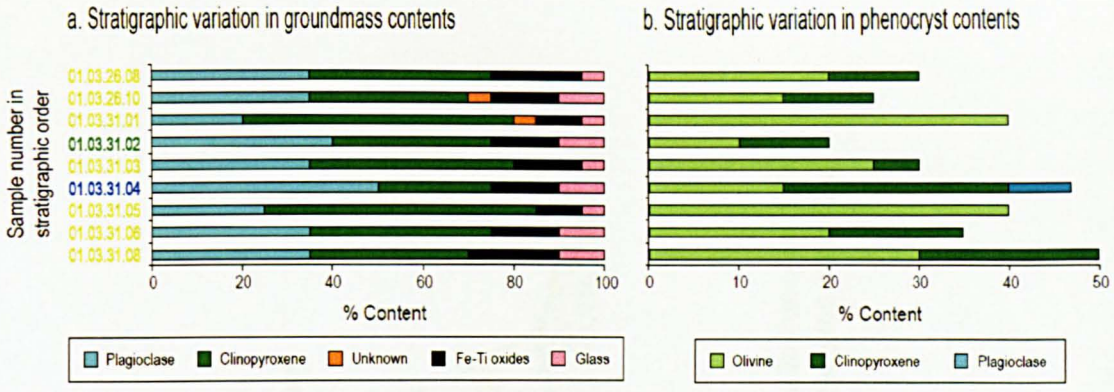

Figure 4.41 Stratigraphic variation in the groundmass and phenocryst content of the lavas from the Iyela Section. The lava groups are denoted by the colour of the sample number - yellow for picrites, blue for ankaramites and green for olivine basalts.

that the same flows we see in the Iyela Section should outcrop in the Dilb section. Nevertheless, regardless of whether or not, the flows that outcrop in the unsampled part of the Dilb Section are lateral extensions of those that outcrop in the Iyela Section, we may assume that they are at least stratigraphically correlated. In this sense the sequence of lavas exposed in the Iyela Section may be taken to be statigraphically representative of that unsampled part of Dilb Section referred to above.

4.4 Mineral chemistry of the lavas from the Dilb and Iyela sections

4.4.1 Preface

Since it has been suggested that the lava sequence exposed in the Iyela Section constitutes an integral part of the larger sequence of lavas represented in the Dilb Section, the mineral chemistry of the lavas from both sections is dealt with together. Only one of the picrites from the Iyela Section was examined by electron microprobe, and its mineral chemistry is seen to be consistent with that for picrites from the Dilb Section. Nevertheless, in the following figures, analyses for the phenocrysts and groundmass microlites in this lava are marked by a different symbol from that for the phenocrysts and groundmass microlites in picrites from the Dilb Section so that they may be distinguished one from another. Although phenocrysts and microlites from the ankaramite and olivine basalt from the Iyela Section were not analysed, it may be assumed that, like the picrites, they would have similar chemistry to those in the anakramites and olivine basalts from the Dilb Section. This is certainly the case for their whole-rock geochemistry (Chapter 5).

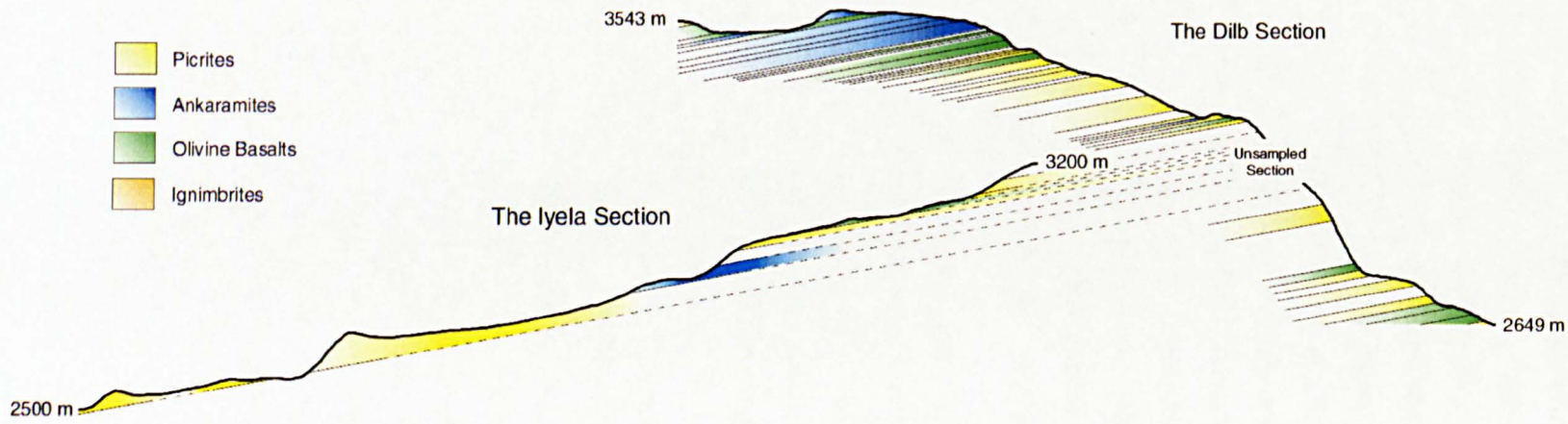

Figure 4.42 Diagrammatic cross-section showing the relationship of the lava sequence of the Iyela Section with that of the Dilb Section. The dotted lines represent the extrapolated dip of the Iyela lavas (Fig. 4.39); these intersect the unsampled part of the Dilb Section between lavas 01.03.25.15 and 01.03.25.16 (Fig. 4.29).

4.4.2 Olivines

Microprobe analyses of olivine phenocrysts from representative samples for the three lava groups from the Dilb and Iyela sections are compiled in Appendix 4.4.2. Average core compositions for the different olivine morphologies from each lava group, together with their maximum, minimum and median values for each oxide analysed are shown in Table 4.9. Overall, the olivine phenocrysts have a wide range in Mg# (68.2 - 89.9). The picrites show a more restricted range, and more similar mean values (~ 84) for all morphologies, than the ankaramites and olivine basalts (Fig. 4.43). The large polyhedral phenocrysts in each group have the highest Mg#, and, although some large and small polyhedral phenocrysts do yield low Mg#, more consistently low values for Mg# occur in the striated and elongate phenocrysts of the ankaramites and olivine basalts. This difference in Mg# between the large and small polyhedral, and striated and elongate phenocrysts in the ankaramites and olivine basalts (apparent from their offset range-bars – Fig. 4.43) is not evident in the picrites.

There are significant variations in the major and minor element compositions of the analysed olivines. Both SiO_2 and NiO are positively correlated with Mg#, although there appear to be two distinct parallel arrays which are most apparent from the variation in SiO_2 (Fig. 4.44 a - b). CaO exhibits more scatter than SiO_2 and NiO, but is still positively correlated, with respect to Mg# (Fig. 4.44c) - this scatter is more noticeable in relation to other oxides such as NiO (Fig. 4.45). The same distinction between the striated and elongate, and polyhedral phenocrysts in the ankaramites and olivine basalts, and the phenocrysts in the picrites referred to above is evident in Figures 4.44 and 4.45, and is indicated therein by a dotted line separating the two compositional domains. It is likely that the two parallel arrays are a result of inconsistent operating conditions of the microprobe between analyses, since, without exception, all phenocrysts which plot in the upper array in the SiO_2 diagram were analysed during the first and second microprobe sessions, whereas the phenocrysts which plot in the lower array plot on the same diagram were analysed during the third microprobe session. The measurement of SiO_2 by electron microprobe is particularly affected by subtle changes in operating conditions, more so than other routinely measured oxides. This is partly, because it forms a much larger percentage of the typically analysed silicate minerals than other constituent oxides; therefore any percentage variation in SiO_2 induced by differences in the machine conditions are amplified compared to other oxides present in smaller percentage concentrations. For this reason, the two arrays are not as discreet on other variation diagrams as they are on the SiO_2 diagram. If the data was corrected for the inconsistencies in

Table 4.9 Averaged compositions, and compositional ranges for the different olivine morphologies in the Dilb and Iyela lavas.

Group	Picrites *				Picrites *				Picrites	Picrites *				Picrites			
Morph.	Large Polyhedral				Small Polyhedral				Striated	Elongate				Skeletal			
Anal.	80				21				1	18				6			
Stat.	Mean	Max	Min	Median	Mean	Max	Min	Median	Mean	Mean	Max	Min	Median	Mean	Max	Min	Median
SiO_2	38.71	40.84	36.54	38.60	38.83	40.66	37.66	38.72	41.05	38.91	41.19	37.86	38.69	38.32	38.98	37.47	38.48
TiO_2	0.025	0.073	0.000	0.024	0.034	0.064	0.000	0.035	0.020	0.027	0.061	0.009	0.025	0.029	0.041	0.012	0.032
Al_2O_3	0.025	0.097	0.000	0.023	0.040	0.130	0.010	0.036	0.170	0.026	0.046	0.010	0.023	0.034	0.048	0.012	0.040
Cr_2O_3	0.045	0.087	0.009	0.046	0.051	0.075	0.018	0.053	0.070	0.038	0.070	0.008	0.041	0.040	0.050	0.019	0.043
FeO	15.39	19.53	10.49	15.22	15.51	19.02	12.27	15.37	15.09	15.71	18.46	13.95	15.54	15.68	16.79	15.03	15.47
MnO	0.229	0.284	0.150	0.229	0.223	0.245	0.188	0.228	0.200	0.226	0.271	0.190	0.229	0.238	0.249	0.229	0.237
MgO	44.59	48.45	41.26	44.70	44.25	46.57	40.54	44.28	43.69	44.46	45.75	42.70	44.58	44.13	45.04	42.61	44.25
CaO	0.328	0.406	0.260	0.327	0.341	0.426	0.283	0.340	0.330	0.326	0.395	0.282	0.320	0.343	0.358	0.326	0.341
Na_2O	0.016	0.058	0.000	0.016	0.016	0.037	0.000	0.013	0.000	0.019	0.050	0.000	0.017	0.025	0.052	0.011	0.023
K_2O	0.002	0.015	0.000	0.000	0.004	0.015	0.000	0.002	0.000	0.004	0.020	0.000	0.003	0.004	0.007	0.000	0.005
P_2O_5	0.017	0.072	0.000	0.015	0.035	0.173	0.000	0.027	0.000	0.023	0.085	0.000	0.021	0.028	0.057	0.000	0.026
NiO	0.338	0.458	0.274	0.350	0.322	0.380	0.265	0.342	0.340	0.345	0.384	0.266	0.344	0.296	0.330	0.265	0.292
Mg#	83.78	89.17	79.01	84.00	83.56	87.12	79.16	83.78	83.77	83.46	85.40	80.48	83.67	83.37	84.21	82.34	83.40

Group	Ankaramite				Ankaramite				Ankaramite				Ankaramite			
Morph.	Large Polyhedral				Small Polyheral				Striated				Elongate			
Anal.	9				5				3				4			
Stat.	Mean	Max	Min	Median	Mean	Max	Min	Median	Mean	Max	Min	Median	Mean	Max	Min	Median
SiO_2	38.79	41.14	37.00	38.16	39.77	41.14	37.21	40.18	38.88	39.08	38.73	38.84	38.43	40.03	37.15	38.26
TiO_2	0.020	0.037	0.002	0.019	0.024	0.049	0.006	0.017	0.029	0.029	0.028	0.029	0.013	0.017	0.010	0.012
Al_2O_3	0.025	0.041	0.003	0.027	0.039	0.072	0.014	0.034	0.161	0.326	0.004	0.152	0.022	0.039	0.013	0.019
Cr_2O_3	0.041	0.108	0.000	0.036	0.038	0.083	0.009	0.028	0.014	0.028	0.000	0.015	0.026	0.029	0.023	0.025
FeO	17.96	26.71	9.81	18.72	18.30	27.59	13.97	16.23	23.39	26.56	20.13	23.49	20.31	22.87	17.68	20.35
MnO	0.258	0.420	0.151	0.249	0.260	0.447	0.176	0.214	0.308	0.348	0.270	0.306	0.291	0.338	0.249	0.289
MgO	42.58	49.11	36.05	42.24	41.62	45.16	35.32	42.95	36.09	38.77	32.01	37.49	40.76	42.98	39.00	40.52
CaO	0.265	0.316	0.229	0.248	0.297	0.387	0.219	0.280	0.318	0.471	0.193	0.291	0.255	0.317	0.217	0.243
Na_2O	0.031	0.107	0.003	0.024	0.044	0.114	0.005	0.022	0.037	0.079	0.016	0.017	0.013	0.031	0.004	0.008
K_2O	0.001	0.003	0.000	0.000	0.013	0.037	0.000	0.012	0.016	0.038	0.000	0.011	0.001	0.002	0.000	0.000
P_2O_5	0.009	0.021	0.000	0.007	0.001	0.003	0.000	0.000	0.000	0.000	0.000	0.000	0.004	0.008	0.000	0.003
NiO	0.297	0.460	0.186	0.289	0.266	0.306	0.174	0.291	0.214	0.276	0.162	0.203	0.276	0.291	0.237	0.287
Mg#	80.78	89.92	70.63	80.08	80.15	85.21	69.53	82.51	73.22	77.44	68.24	74.00	78.13	81.25	75.33	77.98

Group	Olivine Basalts				Olivine Basalts				Olivine Basalts				Olivine Basalts			
Morph.	Large Polyhedral				Small Polyhedral				Striated				Elongate			
Anal.	16				13				3				8			
Stat.	Mean	Max	Min	Median	Mean	Max	Min	Median	Mean	Max	Min	Median	Mean	Max	Min	Median
SiO_2	40.48	41.56	39.58	40.44	40.16	41.72	38.44	40.21	39.61	39.75	39.48	39.60	40.07	40.23	39.90	40.08
TiO_2	0.024	0.050	0.008	0.023	0.019	0.035	0.000	0.019	0.030	0.040	0.013	0.037	0.024	0.040	0.010	0.025
Al_2O_3	0.026	0.056	0.010	0.020	0.024	0.051	0.000	0.020	0.014	0.017	0.010	0.016	0.028	0.110	0.000	0.010
Cr_2O_3	0.053	0.093	0.030	0.046	0.033	0.079	0.006	0.030	0.019	0.040	0.008	0.009	0.037	0.050	0.020	0.035
FeO	15.13	17.27	10.41	16.52	17.75	27.88	11.31	17.19	20.93	22.65	18.91	21.24	17.54	18.58	16.92	17.59
MnO	0.207	0.250	0.153	0.210	0.241	0.393	0.177	0.230	0.282	0.302	0.265	0.280	0.232	0.250	0.220	0.230
MgO	44.02	48.25	41.68	42.63	42.13	47.88	33.99	42.25	39.86	40.91	38.78	39.90	42.04	42.63	40.93	42.19
CaO	0.397	1.850	0.260	0.290	0.322	0.412	0.250	0.300	0.261	0.280	0.246	0.258	0.308	0.400	0.280	0.290
Na_2O	0.018	0.060	0.000	0.018	0.012	0.030	0.000	0.011	0.011	0.016	0.006	0.010	0.018	0.030	0.010	0.018
K_2O	0.002	0.020	0.000	0.000	0.002	0.010	0.000	0.000	0.000	0.000	0.000	0.000	0.001	0.010	0.000	0.000
P_2O_5	0.000	0.000	0.000	0.000	0.000	0.000	0.000	0.000	0.000	0.000	0.000	0.000	0.000	0.000	0.000	0.000
NiO	0.305	0.372	0.210	0.300	0.268	0.326	0.158	0.280	0.241	0.280	0.213	0.231	0.278	0.300	0.230	0.282
Mg#	83.79	89.20	81.35	81.97	80.81	88.30	68.49	81.55	77.25	79.41	75.32	77.01	81.03	81.76	79.70	81.04

Averaged values were calculated from the compiled analyses of phenocryst cores (including the first analysis in core-to-rim traverses). Averaged values for large and small polyhedral, and elongate olivines from the picritic lavas included analyses from the only lava analysed from the Iyela Section - these are marked with a star. The values in red are included only to give an idea of the respective olivine compositions - errors on these values are unreliable. Oxide values are in weight %. Mg# = 100x Mg/(Mg+Fe2+).

machine conditions, the correlations referred to above would be more tightly constrained than illustrated in the respective variation diagrams. It is important to note however, that since Fe and Mg are least affected by such inconsistencies (evident from the closeness of the two arrays in Figure 4.46), the Mg# would be only marginally changed by correcting the data. This is apparent from the fact that there is little discernable variation in the Mg# between the clusters of analyses for the phenocrysts from the picrites in both arrays (Fig. 4.44).

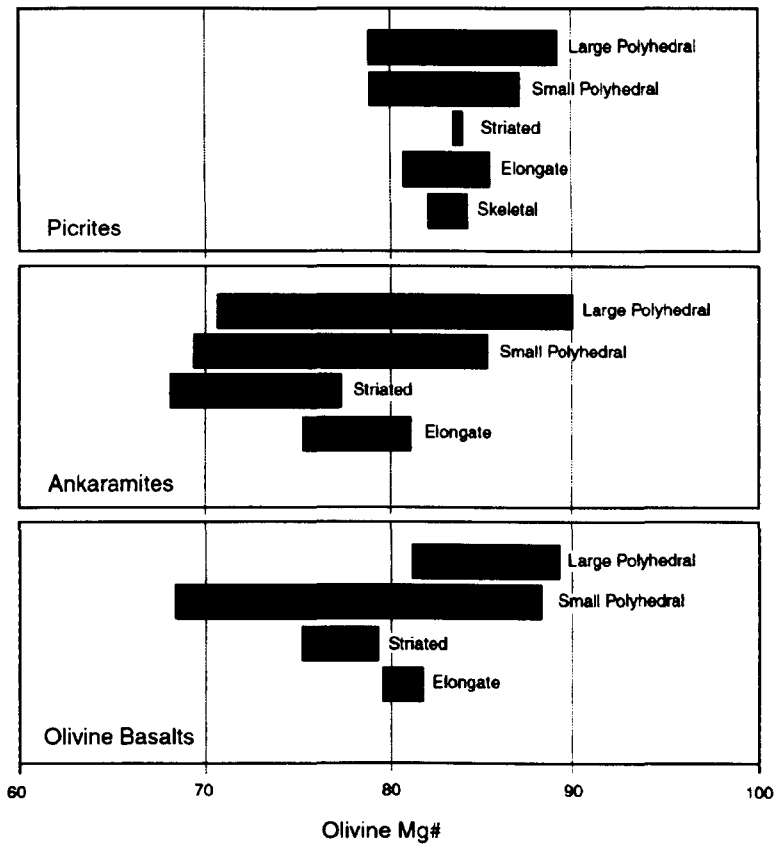

Figure 4.43 Ranges in Mg# for olivine morphologies in the Dilb and Iyela lavas.

In most respects, the major and minor element compositions of the olivines from the Dilb and Iyela lavas are similar to those of olivines from other plume-related lavas such as those from the Hawaiian Islands, the Deccan, Kerguelan, Iceland, Greenland and Etendeka (Fig. 4.47). They have a similar range and trend in SiO_2 with respect to Mg# (Fig. 4.47a), and they have a similar CaO contents which are generally elevated relative to those for olivines from subduction arc-related lavas such as those from Honshu (Fig. 4.47c). They differ only slightly in that their NiO contents are higher relative to Mg# compared to the majority of the olivine data for the plume-related provinces (Fig. 4.47b), and in this respect they are more specifically similar to the compositions of olivines from iron-enriched basaltic lavas from these provinces. In particular, these include picrites from the Hawaiian Islands (Garcia, 1996; Garcia et al. 1995; Nicholls & Stout, 1988) and the Deccan (Krishnamurthy et al. 2000), and ferropicrites from Etendeka (Gibson et al. 2000; Thompson & Gibson, 2000; Thompson et al. 2001).

Although examples of optically-zoned olivines were rarely encountered in the thin sections of the lavas from both sections, most of the olivines analysed by microprobe show some degree of normal zoning with steepening compositional gradients

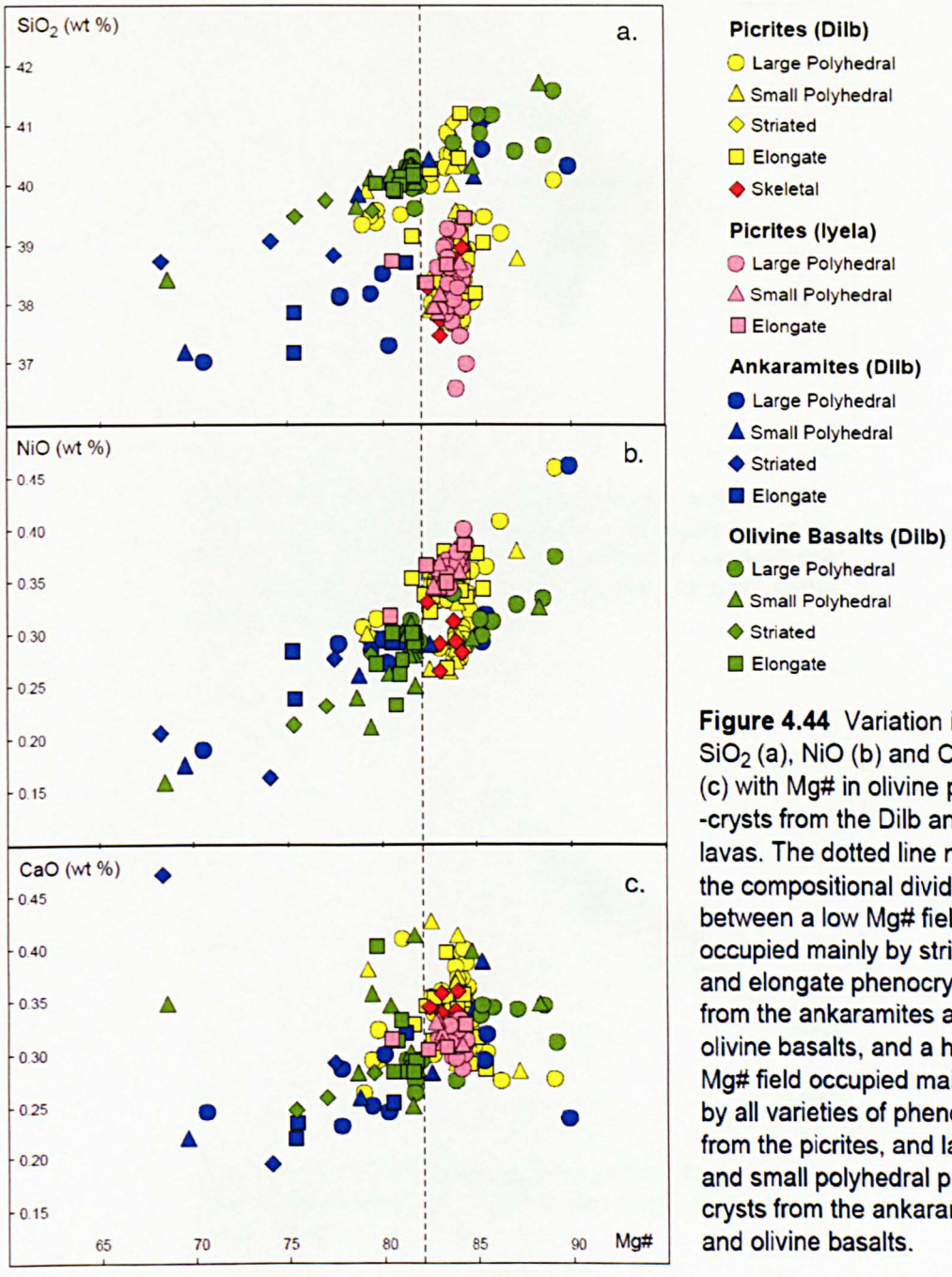

Figure 4.44 Variation in SiO_2 (a), NiO (b) and CaO (c) with Mg# in olivine pheno-crysts from the Dilb and Iyela lavas. The dotted line marks the compositional divide between a low Mg# field, occupied mainly by striated and elongate phenocrysts from the ankaramites and olivine basalts, and a high Mg# field occupied mainly by all varieties of phenocryst from the picrites, and large and small polyhedral pheno-crysts from the ankaramites and olivine basalts.

towards their margins (Fig. 4.48). The large polyhedral olivines with high Mg#, which plot above the compositional divide referred to above, commonly show little or no compositional variation from core to rim, and those that are zoned show flat-topped profiles and only narrow zoned margins, except where they are overgrown with fresh olivine with significantly higher iron contents and therefore much lower Mg# than the core of the phenocrysts. The small and striated polyhedral, and elongate phenocrysts, and the large polyhedral phenocrysts which plot below the compositional divide, generally show more progressively zoned profiles. The pattern of zonation is generally marked by a decrease in Fo content, and a concomitant increase in CaO

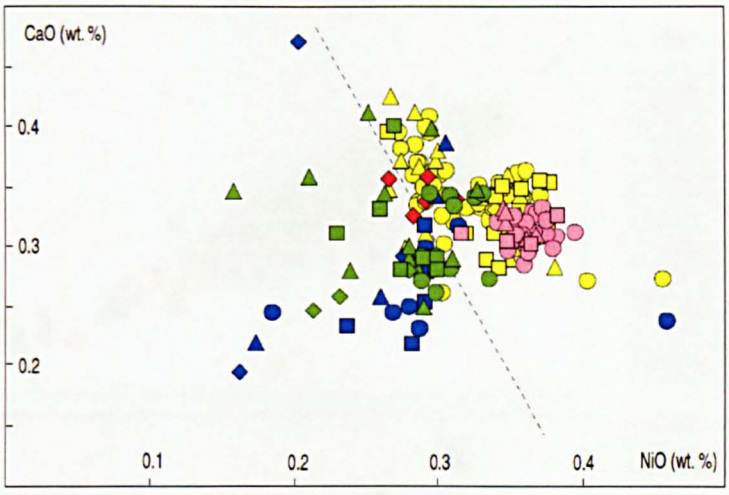

Figure 4.45 NiO versus CaO for olivine phenocrysts in lavas from the Dilb and Iyela sections. Symbols are as in Figure 4.44. The dashed line represents the compositional divide between the olivines in the picrites and those in the ankaramites and olivine basalts.

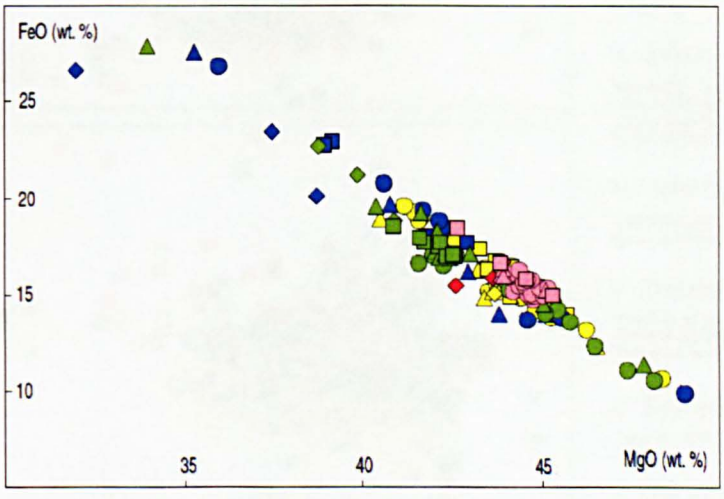

Figure 4.46 FeO versus MgO for olivine phenocrysts in lavas from the Dilb and Iyela sections. Symbols are as in Figure 4.44.

and decrease in NiO toward the margins of the phenocrysts. In some phenocrysts, however, both CaO and NiO decrease with Fo content toward the rim, particularly where they are overgrown with fresh olivine. The olivine overgrowths show considerable variation in their composition between samples, and in comparison with the only groundmass olivine found in the lavas, although their variation in Mg# (60 - 70) is consistently much lower than their host-phenocrysts (Table 4.10).

4.4.3 Pyroxenes

Microprobe analyses of pyroxene phenocrysts from representative samples for the three lava groups from the Dilb and Iyela sections are compiled in Appendix 4.4.3 & 4.

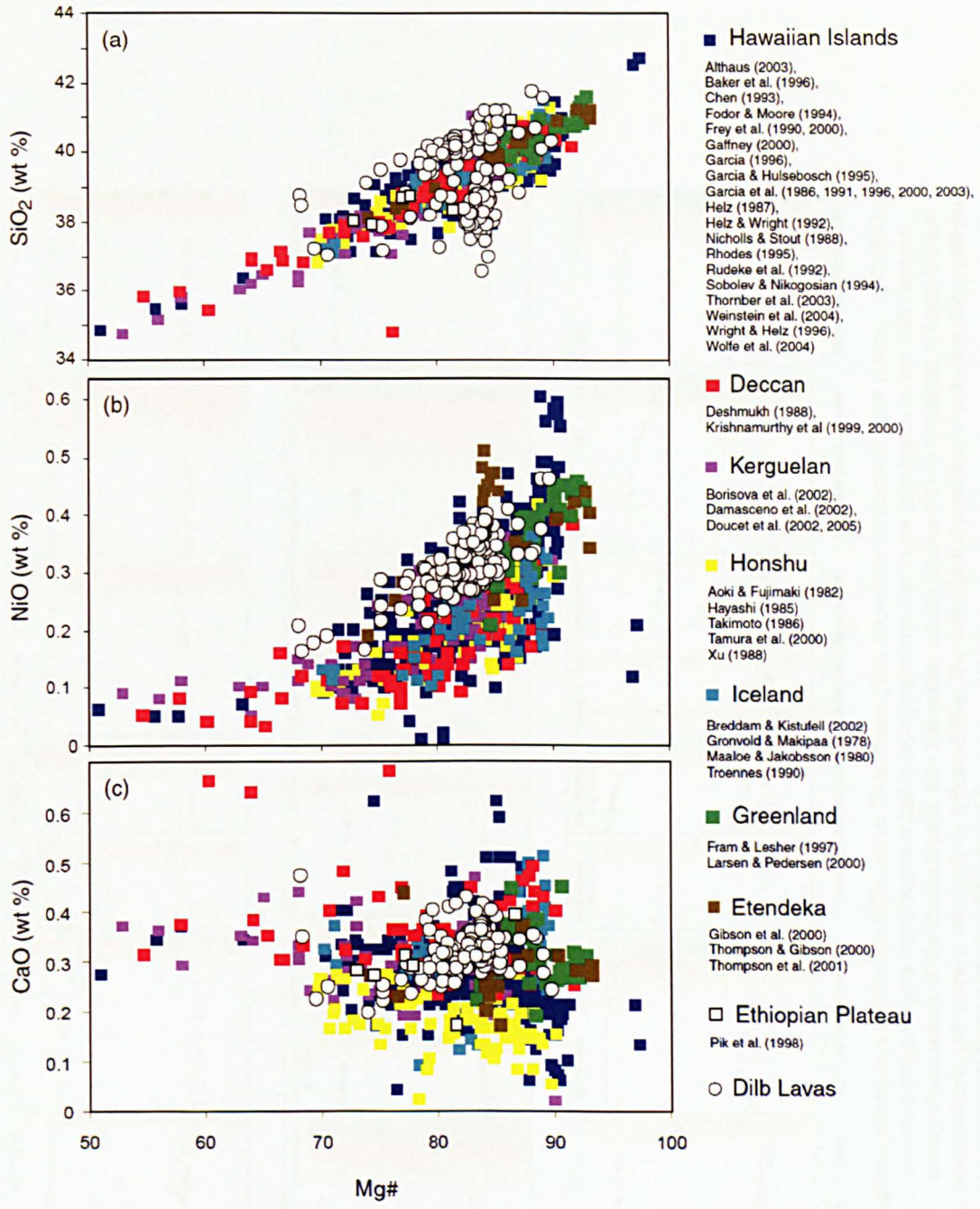

Figure 4.47 Comparison of the variation in SiO_2 (a), NiO (b) and CaO (c) with Mg# for olivines from the Dilb and Iyela lavas with that for olivines from similar and contrasting tectonic environments. All analyses in the compilation are for olivines from basalts and picrites only. Analyses for the Ethiopian Plateau include a pair from each of the magma types described by Pik et al. (1998). The pair with the highest Mg# are from the HT2 basalts, those with the lowest Mg# are from the HT1 basalts, and the pair with Mg# between these are from the LT basalts. NiO values for these basalts were not published, and therefore have not been included in this compilation. Data compilation is from GEOROC database.

Average raw and iron-corrected core compositions for pyroxene phenocrysts from each lava group, together with their maximum, minimum and median values for all analysed oxides are shown in Table 4.11. For comparative purposes, both averaged end member compositions calculated from the raw and recalculated analyses

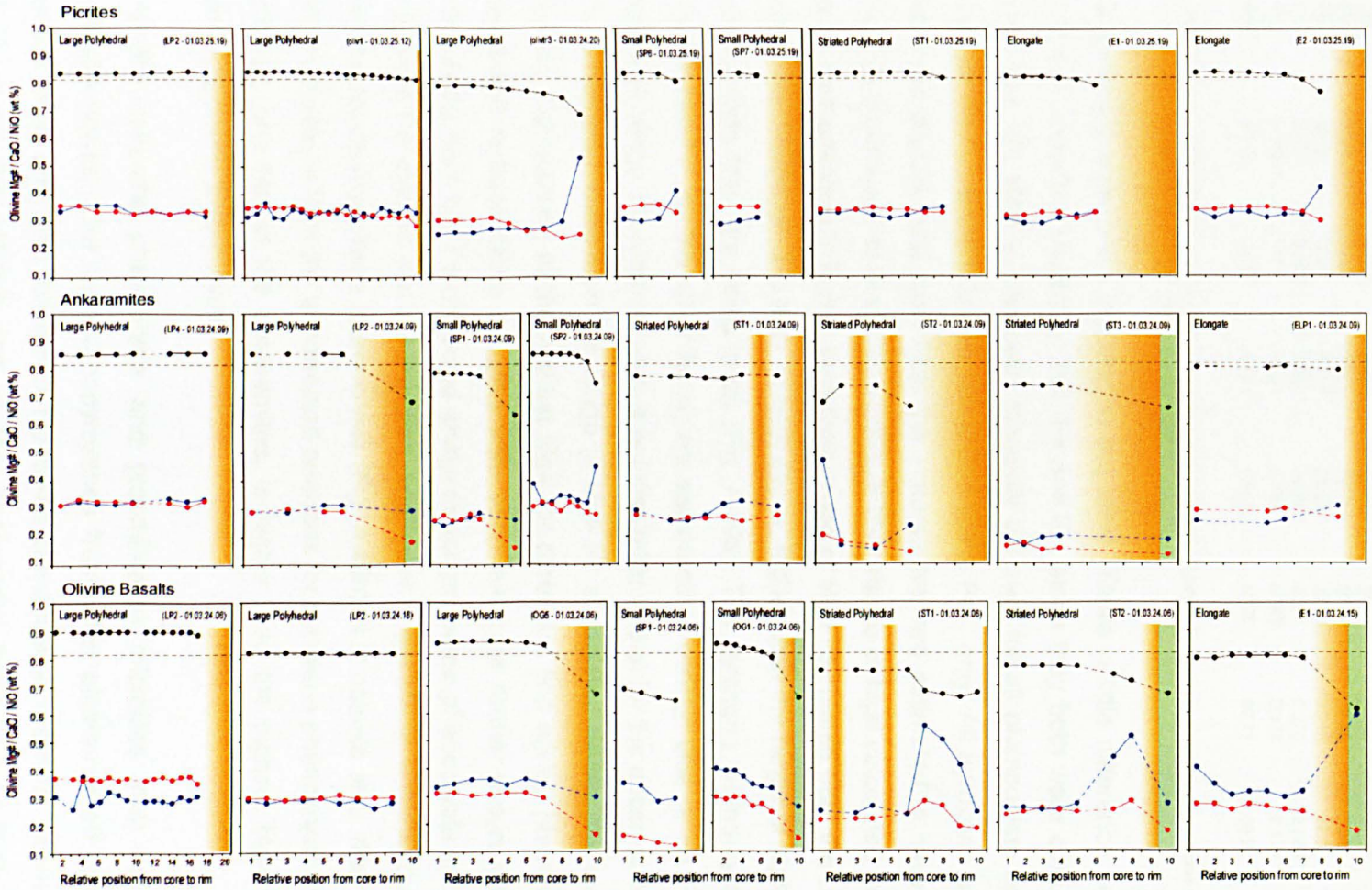

Figure 4.48 Zoning trends in olivine phenocrysts from the Dilb Lavas. The above plots show the variation in Mg# (black), CaO (blue) and NiO (red) from core to rim in selected phenocrysts from representative samples of the the three lava-types in the Dilb Section. The orange zones represent the iddingsitized areas of the phenocrysts, and the green zones represent overgrowths of fresh olivine. Where spurious analyses have been omitted, the trace is inferrred by a dotted line. The fine black dotted line marks the compositional divide at Fo_{82} between the low and high Mg# fields shown in Figure 4.44.

Table 4.10 Representative microprobe analyses for olivine overgrowths in the Dilb lavas

Group	Ankaramite	Ankaramite	Ankaramite	Olivine Basalt	Olivine Basalt	Olivine Basalt	Olivine Basalt	Olivine Basalt
Sample	01.03.24.09	01.03.24.09	01.03.24.09	01.03.24.06	01.03.24.06	01.03.24.06	01.03.24.15	01.03.24.06
Morph.	Large Polyhedral	Small Polyhedral	Striated	Large Polyhedral	Small Polyhedral	Striated	Elongate	Groundmass
Ref.	LP2	SP1	ST3	OG5	OG1	ST2	E1	OLGMS
SiO_2	38.04	37.33	37.27	38.31	37.93	38.34	38.87	36.67
FeO	27.66	31.65	29.61	29.56	30.59	29.49	30.90	33.56
MgO	33.32	30.54	31.87	32.93	32.26	33.15	27.02	28.74
CaO	0.293	0.260	0.184	0.297	0.261	0.270	0.590	0.397
NiO	0.182	0.162	0.131	0.161	0.148	0.173	0.170	0.072
Mg#	68.22	63.23	65.73	66.51	65.28	66.71	60.92	60.42

Note: The above analyses are for the olivine overgrowths shown in green in Figure 4.36. Analysis of the only groundmass olivine found is shown in the right-hand column. Oxide values are in weight %.

respectively have been included in the table. There is little difference between the raw and corrected values for Wo, Fs and En, since they both were calculated from total iron; the Mg# is, however, markedly different for all phenocrysts estimated to contain Fe_2O_3, since this was calculated using Fe^{2+} only. All pyroxene phenocrysts from the picrites, and most from the ankaramites, are estimated to have significant Fe_2O_3 contents (up to 6 wt. %), such that their range of Mg# calculated from the Fe-corrected analyses is higher than their range of Mg# calculated from the uncorrected analyses. Moreover, it is also, in both cases, higher than the range of Mg# for olivine phenocrysts from the same lavas (Fig. 4.49a). The pyroxene phenocrysts from the olivine basalts, on the other hand, are estimated to contain little or no Fe_2O_3, such that their range of corrected Mg# is not dissimilar to that for the uncorrected Mg# and is consistently lower than the range of Mg# for associated olivine phenocrysts (Fig. 4.49a). Comparison of the highest Mg# for pyroxene and olivine phenocrysts from the same representative samples from each lava-type further shows that the Mg# calculated from the Fe-corrected analyses for pyroxene phenocrysts is consistently higher in the picrites and ankaramites, and lower in the olivine basalts, than the Mg# for the respective olivine phenocrysts (Fig. 4.49b). It is notable also, that the highest Mg# calculated from the uncorrected analyses for pyroxene phenocrysts in one of the picrites, and two of the ankaramites, is higher than the highest Mg# for the co-existing olivine phenocrysts.

All the pyroxene phenocrysts and groundmasss microlites from the lavas are clinopyroxenes. Like most clinopyroxenes from other plume-related provinces and island arcs, they plot, on the Di-Hd-En-Fs classification diagram, within the augite field, along the Mg-rich end of the Skaergaard trend (Fig. 4.50a). This is in agreement with the classification determined from their extinction angles evident in thin section (Section 4.2.2). Together, they display a short trend of decreasing MgO and CaO and increasing FeO similar to that shown by pyroxenes from the HT1, HT2

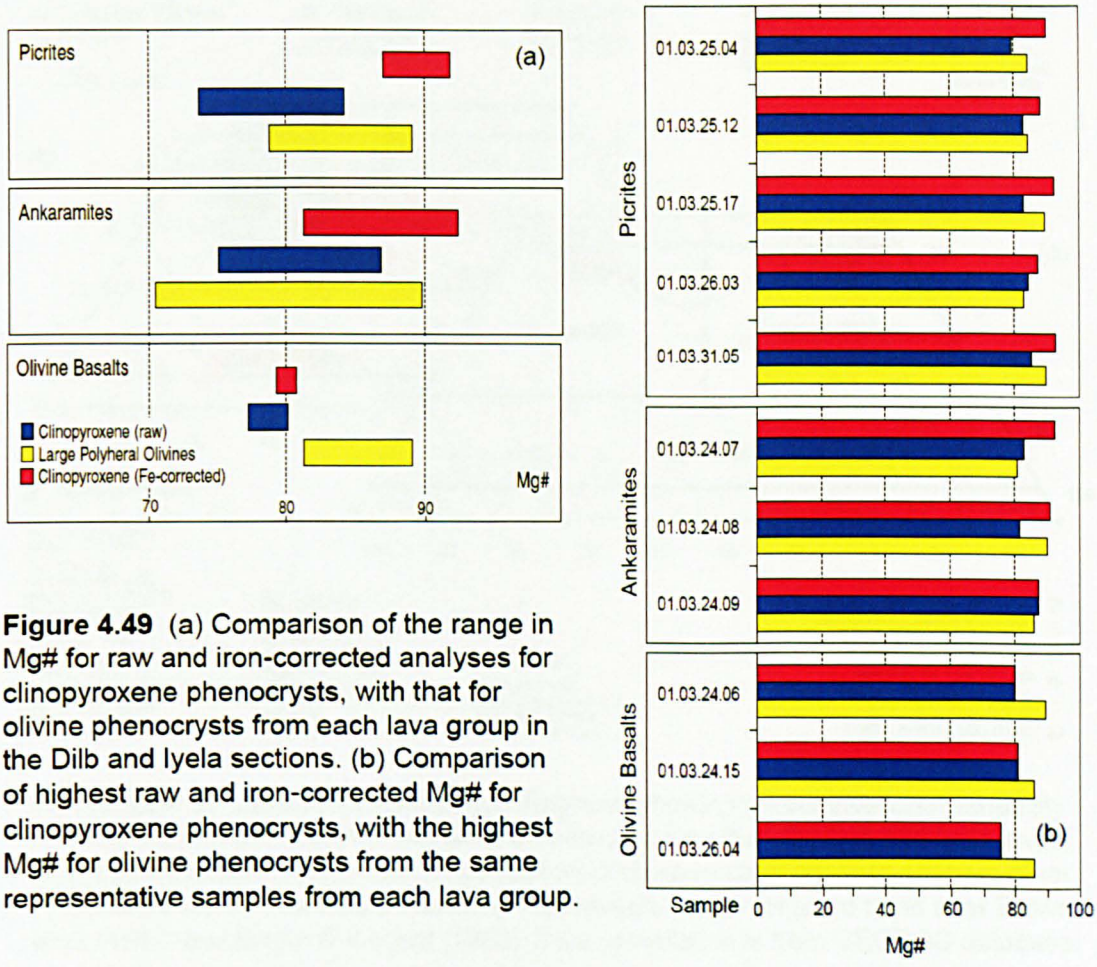

Figure 4.49 (a) Comparison of the range in Mg# for raw and iron-corrected analyses for clinopyroxene phenocrysts, with that for olivine phenocrysts from each lava group in the Dilb and Iyela sections. (b) Comparison of highest raw and iron-corrected Mg# for clinopyroxene phenocrysts, with the highest Mg# for olivine phenocrysts from the same representative samples from each lava group.

and LT lavas from the Ethiopian Plateau reported by Pik et al. (1998), and as with these lavas, they do not exhibit the usual augite-pigeonite association typical of tholeiitic magmas (Fig. 4.50b). The groundmass microlites plot at the more Fe-rich, Ca-poor end of the trend in relation to the phenocrysts. The differences in composition between the clinopyroxene phenocrysts from the picrites ($Wo_{40-45}\,En_{41-48}\,Fs_{9-15}$), ankaramites ($Wo_{41-44}\,En_{43-49}\,Fs_{7-14}$) and the olivine basalts ($Wo_{40-42}\,En_{45-48}\,Fs_{12-13}$), on the other hand, are reflected across rather along this trend. This is evident from a loose linear array for the phenocrysts from each lava group, at progressively lower CaO contents, sub-parallel to the Skaergaard trend (Fig. 4.50a). More pronounced differences in the composition of the phenocrysts between groups are apparent from their variation in Al_2O_3, Na_2O and MgO with respect Cr_2O_3 (Fig. 4.51a-c). The clinopyroxene phenocrysts from the picrites generally show higher Al_2O_3 and Na_2O and lower MgO than the ankaramites and olivine basalts. Also, at higher Cr_2O_3 contents, the Mg/(Mg+Fe(tot)) ratios for the clinopyroxene phenocrysts from the picrites become progressively lower in comparison with those for the ankaramites because of their comparatively higher Fe(tot) and lower Mg contents (Fig. 4.51d). Despite these differences, the range in Al_2O_3, Na_2O, MgO and Cr_2O_3 contents for the

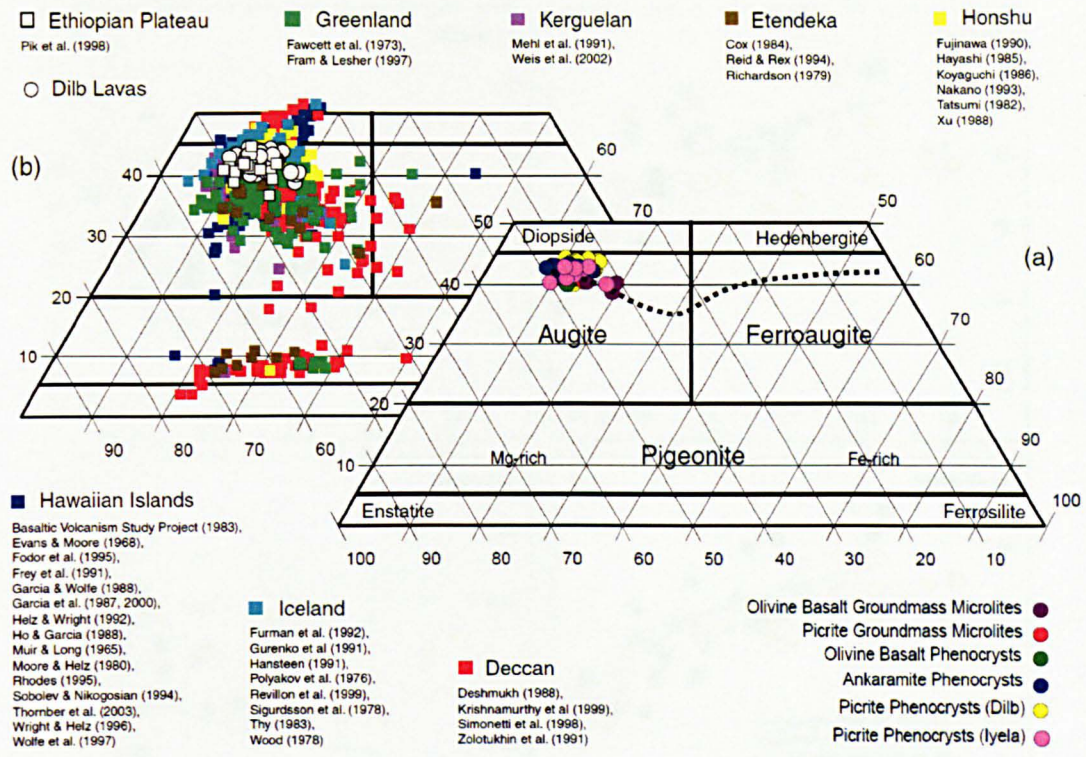

Figure 4.50 Di -Hd-En-Fs classification diagrams showing **(a)** compostional variability of clinopyroxene phenocrysts and groundmass microlites from the Dilb and Iyela lavas, and **(b)** their range of compositions compared to clinopyroxene phenocrysts from other volcanic provinces. The dashed line in (a) represents the Skaergaard trend after Brown et al. (1957) and Brown & Vincent (1963). Data compilation is from GEOROC database.

clinopyroxene phenocrysts from all three lava groups is, together, typical of magmatic clinopyroxenes from other plume-related and island arc lavas, even though the Al_2O_3 contents for the ankaramites and olivine basalts are low in comparison to the majority of respective data for such lavas (Fig. 4.52). On a tectono-magmatic discrimination ternary diagram of $SiO_2/100 - TiO_2 - Na_2O$, they all plot within the MORB field (Fig. 4.53a), suggesting that they are typical of clinopyroxenes from tholeiitic basalts; however the higher Ti, Ca and Na contents of most of the clinopyroxene phenocrysts from the picrites and some of the ankaramites are more typical of clinopyroxenes from alkali basalts (Fig. 4.53b).

Despite the differences described above, most clinopyroxene phenocrysts from the Dilb and Iyela sections show similar Al:Si and Al:Ti ratios (Fig. 4.54). The variation in Al, Si and Ti imply that their Al contents are generally sufficient to balance the deficiency in the tetrahedral site (Al > or = 2-Si), but insufficient to balance the deficiency in the octahedral site (Al:Ti < 6:1). Only those phenocrysts and groundmass microlites, estimated not to contain Fe^{3+} (Appendix 4.4.3) lie off the gradient-line for Si + Al = 2 (Fig. 4.54a); these include clinopyroxene phenocrysts and

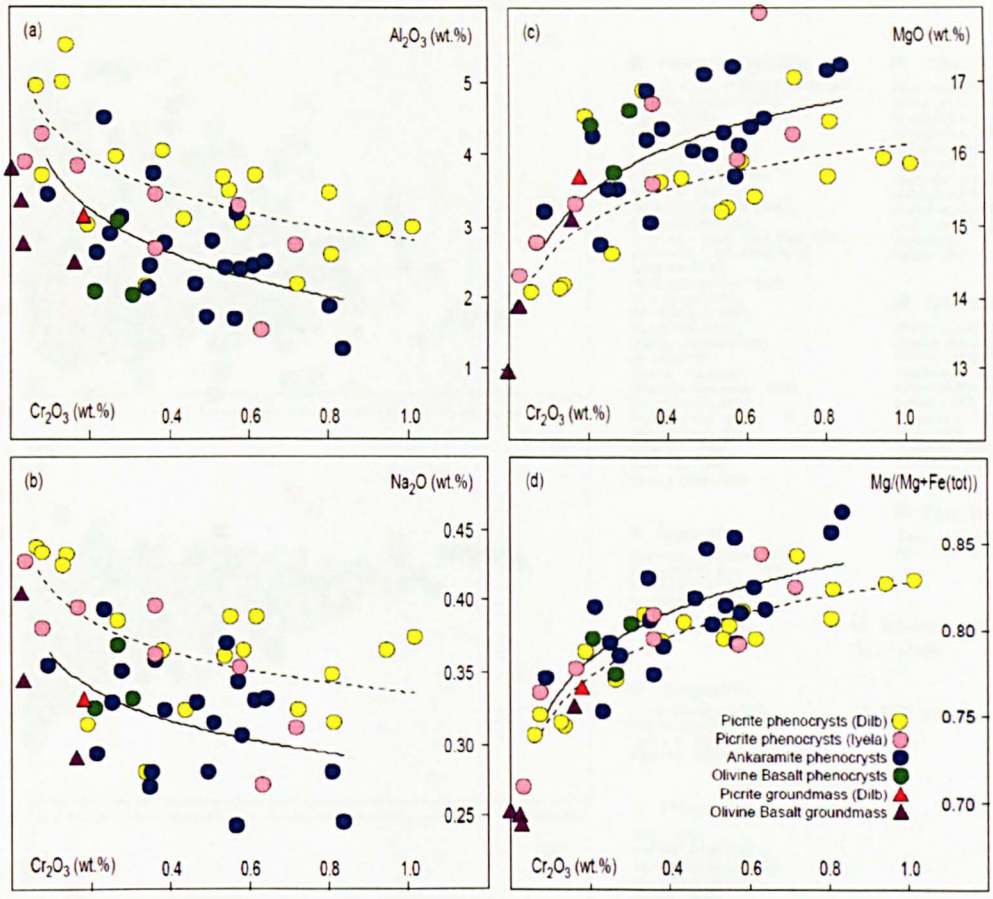

Figure 4.51 Variation of **(a)** Al_2O_3, **(b)** Na_2O, **(c)** MgO and **(d)** $Mg/(Mg+Fe^{(tot)})$ with Cr_2O_3 for clinopyroxene phenocrysts and groundmass microlites in lavas from the Dilb and Iyela sections. Logarithmic trend-lines for the picrites and ankaramites from the Dilb section are shown to illustrate the trends for these lavas (indicated by the dashed and solid curves respectively). The curves were plotted using Excel, which calculates the least squares fit through the points using the equation y = c(lnx)+b, where c and b are constants, and ln is the natural log-function.

groundmass microlites from the olivine basalts, 01.03.24.06 and 01.03.24.15, and phenocrysts from the ankaramite 01.03.24.09. These plot to the right of the gradient-line for Si + Al = 2, indicating that they have more than enough Al to balance the deficiency in the tetrahedral site, and although this excess Al has been assigned, by the recalculation process, to the octahedral (M1) site (Appendix 4.4.4), it is, in each case, still insufficient to balance the deficiency there (ie. their Al:Ti ratios are < 6:1 - Fig. 4.54b). The absence of Fe^{3+} and the coincident presence of $Al^{(vi)}$ in these phenocrysts and groundmass microlites sets them apart from the majority of the clinopyroxene phenocrysts which show good negative correlations between Fe^{2+} + Si, Fe^{3+} + $Al^{(iv)}$ and Mg indicative of increasing fO_2 coincident with decreasing Mg and increasing Al contents (Fig. 4.55).

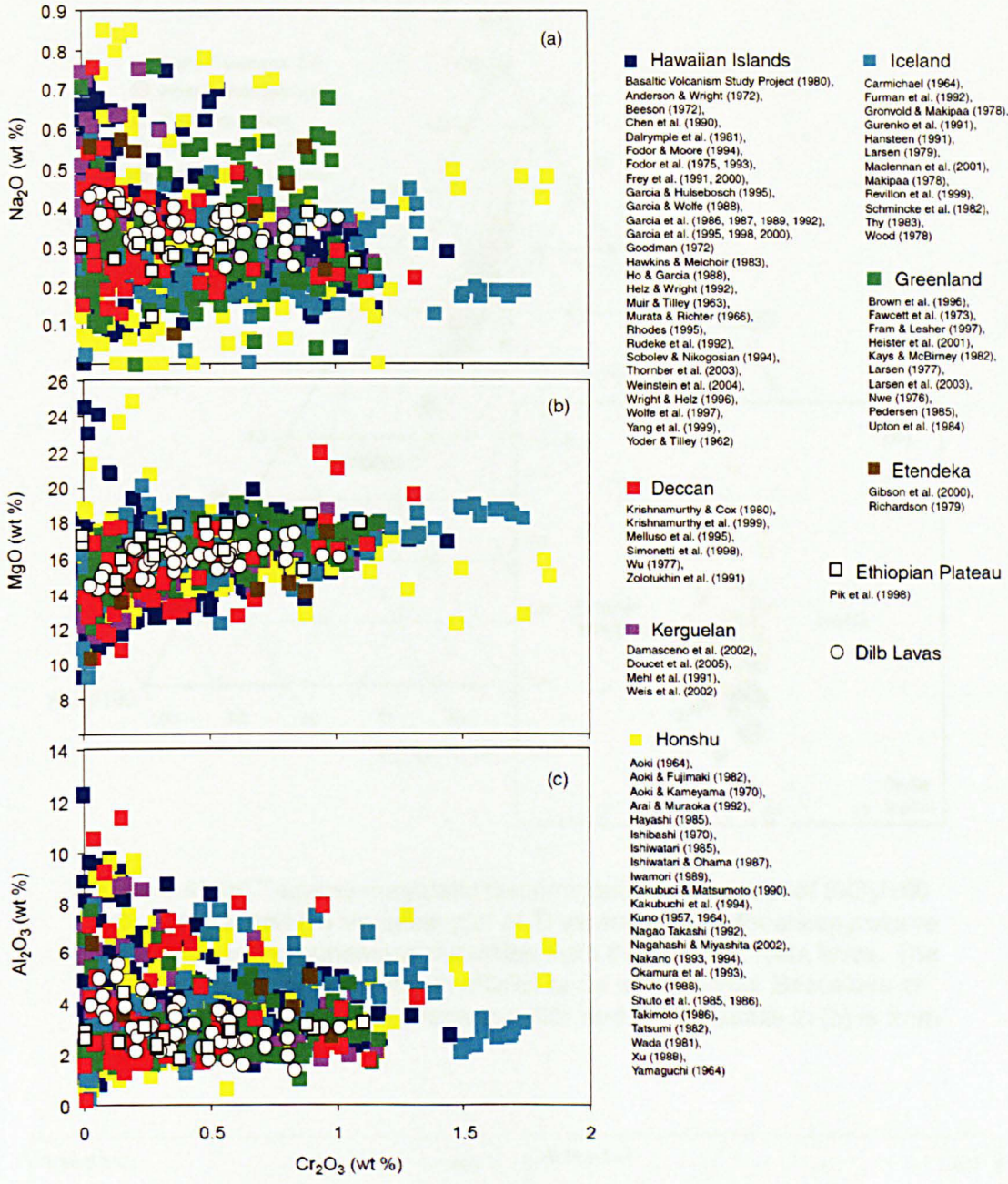

Figure 4.52 Comparison of the variation in Na_2O (a), MgO (b) and Al_2O_3 (c) with Cr_2O_3 for clinopyroxene phenocrysts from the Dilb and Iyela lavas with that for clinopyroxene phenocrysts from similar and contrasting tectonic environments. All data in the compilation (from GEOROC database) are for clinopyroxenes from basalts and picrites only. There is no systematic variation in the oxide contents shown above for the clinopyroxene phenocrysts from other lavas from the Ethiopian Plateau reported by Pik et al. (1998).

Oscillatory zoning is common in clinopyroxene phenocrysts from all three lava groups (Section 4.2.2); this is reflected in the variation in composition from core to rim in representative phenocrysts from the ankaramites and olivine basalts (Fig. 4.56). The composition and pattern of zoning in the clinopyroxene phenocrysts from these two lava groups is broadly similar. They all show normal zoning with a progressive, but

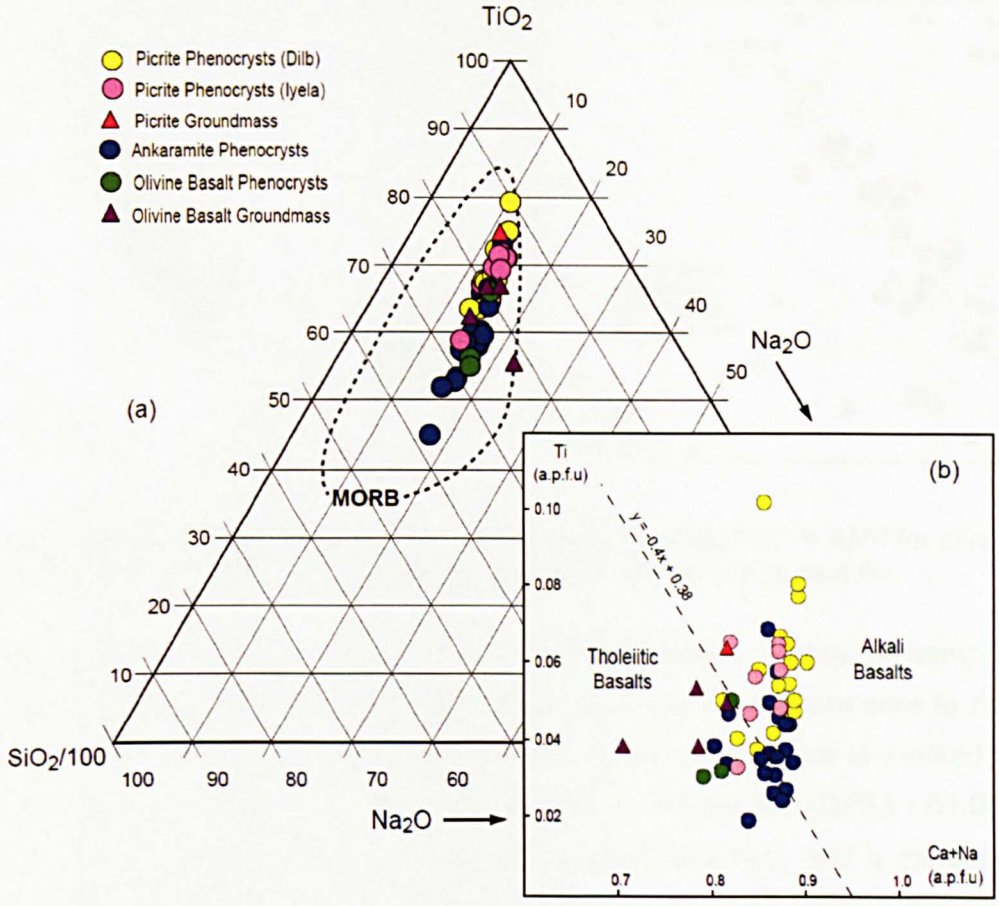

Figure 4.53 (a) Tectono-magmatic discrimination ternary plot of $SiO_2/100$ - TiO_2 - Na_2O, and **(b)** Variation plot of Ti versus Ca+Na for clinopyroxene phenocrysts and groundmass microlites from the Dilb and Iyela lavas. The field for pyroxene phenocrysts in MORB lavas in (a) is from Beccaluva et al. (1989), and the divide between tholeiitic and alkali basalts in (b) is from Letterier et al. (1982).

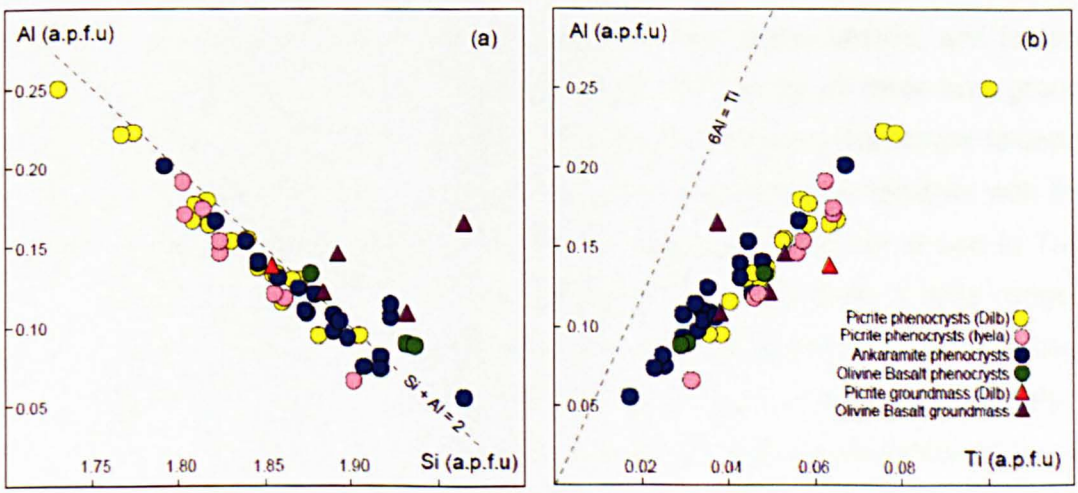

Figure 4.54 Variation of **(a)** Si and **(b)** Ti with total Al for clinopyroxene from representative samples of the Dilb and Iyela lavas.

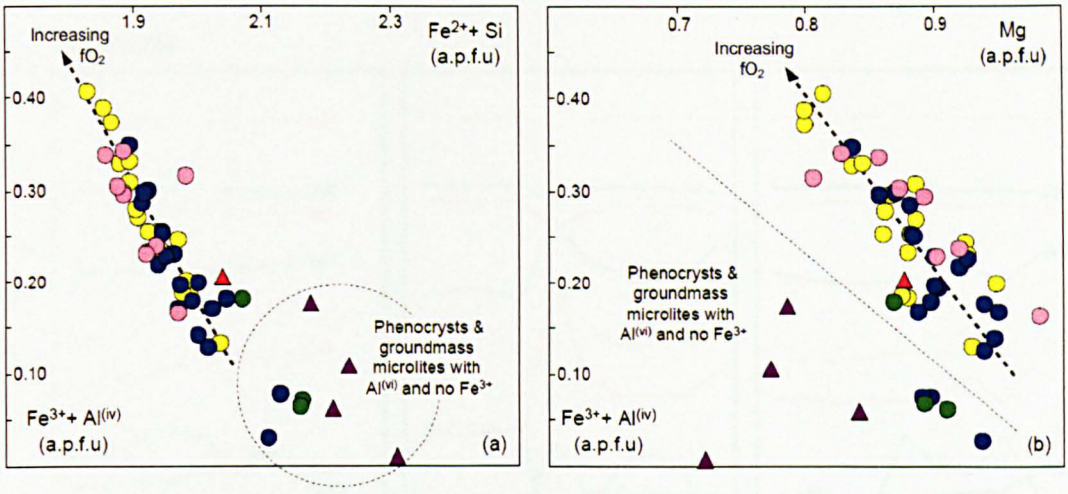

Figure 4.55 Variation of **(a)** Fe^{2+} + Si and **(b)** Mg with Fe^{3+} + $Al^{(iv)}$ for clino-pyroxene in the Dilb and Iyela lavas. Symbols are as in Figure 4.54.

general increase in FeO, Al_2O_3, TiO_2, Na_2O and Fe_2O_3 (where present), and a corresponding decrease in SiO_2, CaO, MgO, Cr_2O_3 and NiO from core to rim. The presence of a well-defined rim around each of the phenocrysts is marked by the same, but more pronounced, antithetic variation in composition (CPX1 - 01.03.24.09 differs slightly in that it shows an increase in CaO and NiO, and a corresponding decrease in Al_2O_3 and Na_2O at its rim). Marked peaks and troughs exhibiting the same compositional contrasts occur midway between the core and rim in CPX4 – 01.03.24.09, and these are coincident with the appearance of Fe_2O_3 in the profile. Similar, but less acute, variations in composition are also evident in association with Fe_2O_3 at a similar point in the profile of CPX1 – 01.03.24.09.

4.4.4 Feldspars

Microprobe analyses of feldspar phenocrysts from the olivine basalts, and feldspar microlites from the groundmass of representative samples for all three lava groups, are compiled in Appendix 4.4.5. Average compositions for the groundmass feldspars for each lava group, and for phenocrysts from the olivine basalts, together with their maximum, minimum and median values for all analysed oxides are shown in Table 4.12. The feldspar microlites from the picrites (An_7 – An_{52}) show a wide range in composition compared to the ankaramites (An_{39} – An_{47}) and olivine basalts (An_{39} – An_{47}), though this may simply be because a greater number and variety of groundmass feldspars from these lavas were analysed. With the exception of the one microlite from the picrites, which plots in the sanidine field (Fig. 4.57a), the groundmass feldspars from each lava group range from andesine to labradorite as indicated by their extinction angles in thin section (Section 4.2.2). The presence of

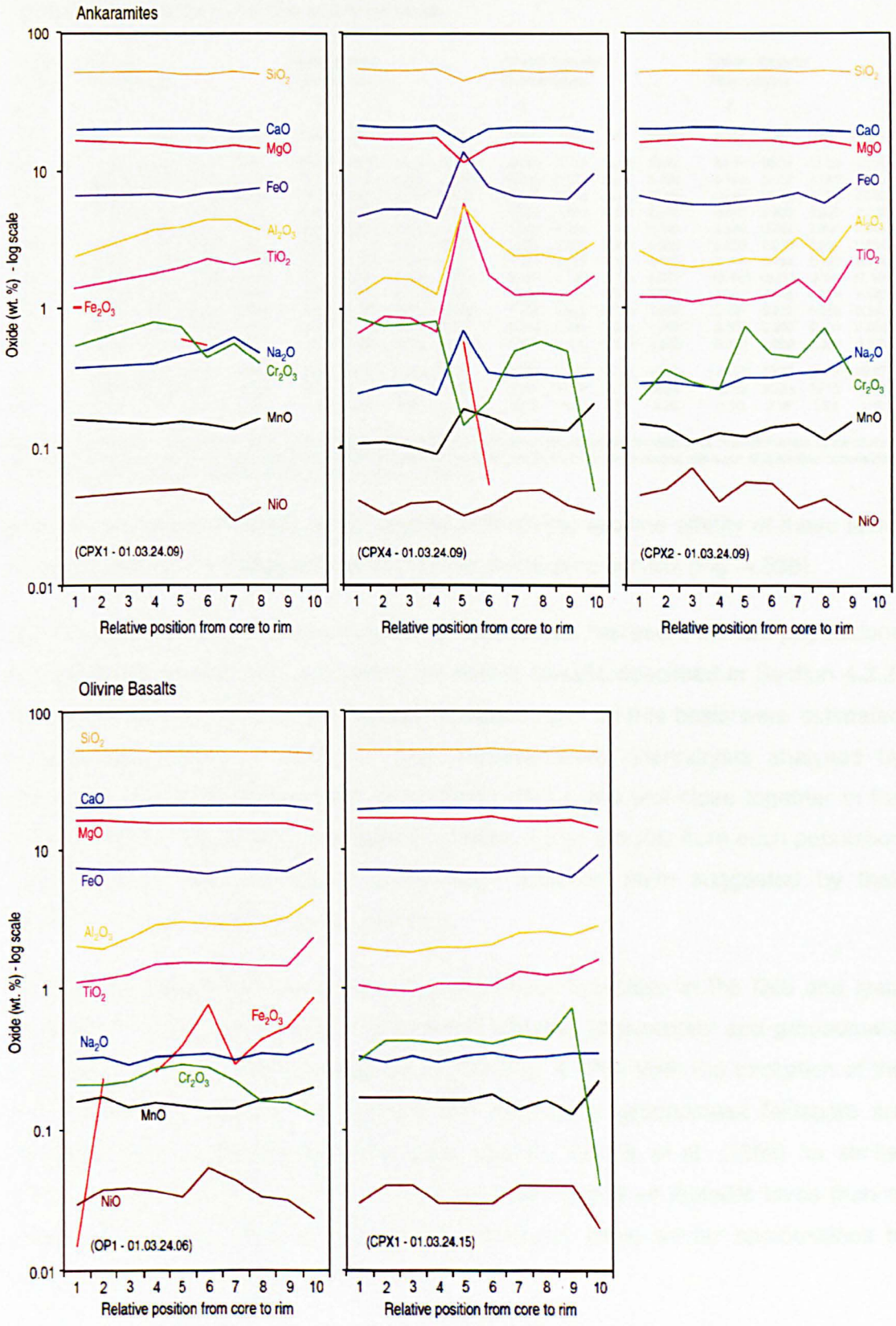

Figure 4.56 Zoning trends in clinopyroxene phenocrysts from the Dilb lavas. Analyses for the rims of CPX1 and CPX2 from 01.03.24.09 are not shown as their stoichiometric totals were unreliable. Fe_2O_3 is absent where there is no trace in the profile.

Table 4.12 Averaged compositions, and compositional ranges for feldspar phenocrysts and groundmassmicrolites in the Dilb and Iyela lavas

Group	Picrites *				Ankaramites				Olivine Basalts				Olivine Basalts			
Morph.	Groundmass				Groundmass				Groundmass				Phenocrysts			
Anal.	11				2				3				2			
Stat.	Mean	Max	Min	Median	Mean	Max	Min	Median	Mean	Max	Min	Median	Mean	Max	Min	Median
SiO_2	54.97	62.49	51.99	53.91	56.22	58.16	54.29	56.22	56.50	57.13	55.66	56.72	53.34	53.39	53.29	53.34
TiO_2	0.483	2.119	0.144	0.178	0.139	0.151	0.127	0.139	0.310	0.374	0.257	0.300	0.149	0.152	0.145	0.149
Al_2O_3	25.29	27.54	18.85	26.48	25.78	26.69	24.88	25.78	24.82	25.48	24.04	24.93	28.82	28.89	28.75	28.82
Cr_2O_3	0.004	0.021	0.000	0.000	0.009	0.017	0.000	0.009	0.000	0.000	0.000	0.000	0.000	0.000	0.000	0.000
FeO	1.481	3.079	0.658	0.975	0.829	0.884	0.773	0.829	1.555	1.985	1.301	1.380	0.548	0.552	0.544	0.548
MnO	0.008	0.041	0.000	0.004	0.009	0.017	0.001	0.009	0.000	0.000	0.000	0.000	0.000	0.000	0.000	0.000
MgO	0.840	3.368	0.095	0.150	0.231	0.270	0.192	0.231	0.214	0.220	0.205	0.218	0.146	0.154	0.137	0.146
CaO	8.633	10.572	1.315	10.139	8.771	9.658	7.883	8.771	8.837	9.500	7.703	9.307	12.166	12.183	12.149	12.166
Na_2O	5.346	6.177	4.758	5.260	5.920	6.315	5.524	5.920	5.438	5.604	5.340	5.370	4.392	4.414	4.369	4.392
K_2O	1.176	6.320	0.000	0.572	0.766	0.851	0.680	0.766	1.158	1.692	0.710	1.067	0.191	0.372	0.010	0.191
P_2O_5	0.021	0.053	0.000	0.019	0.023	0.026	0.019	0.023	0.000	0.000	0.000	0.000	0.000	0.000	0.000	0.000
NiO	0.001	0.015	0.000	0.000	0.000	0.000	0.000	0.000	0.000	0.000	0.000	0.000	0.000	0.000	0.000	0.000
Ab	49.22	55.98	45.11	47.50	52.54	56.23	48.85	52.54	49.08	51.07	47.88	48.29	39.07	39.40	38.75	39.07
An	43.66	52.07	6.57	49.20	42.99	47.20	38.79	42.99	44.04	47.48	38.79	45.86	59.82	60.54	59.10	59.82
Or	7.12	37.59	0.00	3.30	4.47	4.99	3.96	4.47	6.88	10.14	4.23	6.26	1.10	2.15	0.06	1.10

Note: Oxides are given in wt %. Averaged values were calculated from the compiled analyses of phenocryst and microlite cores. Averaged values for the picrite groundmass included analyses of feldspar microlites from the only lava analysed from the Iyela Section - these are marked with a star. End member compositions are calculated as follows: Ab=Na/(Ca+Na+K), An=Ca/(Ca+Na+K), Or=K/(Ca+Na+K).

sanidine in the groundmass of the picrites reflects the alkaline affinity of these lavas as suggested by the compositions of their pyroxene phenocrysts (Fig. 4.53b).

The two feldspar phenocrysts analysed by microprobe represent the two populations of plagioclase phenocrysts present in the olivine basalts described in Section 4.2.2. Although these populations are optically different, and on this basis were estimated to have contrasting An contents, both representative phenocrysts analysed by electron microprobe show similar An contents (An_{60}) and plot close together in the labradorite field (Fig. 4.57a). If a greater number of phenocrysts from each population were analysed, the contrast in composition between them suggested by their extinction angles, might be more apparent.

Overall, the feldspar phenocrysts and groundmass microlites in the Dilb and Iyela lavas show similar compositions to those of feldspar phenocrysts and groundmass microlites from other plume-related provinces (Fig. 4.57b). With the exception of the one sanidine analysed in the picrites, the majority of groundmass feldspars are compositionally quite different from those reported by Pik et al. (1998) for similar lavas from the Ethiopian Plateau – they are more typical of tholeiitic lavas than of alkaline lavas. The feldspar phenocrysts, however, show similar compositions to those reported by Pik et al. (1998).

4.4.5 Fe-Ti oxides

Fe-Ti oxides are present in the Dilb and Iyela lavas both as inclusions in olivine and clinopyroxene phenocrysts, and as microlites of variable morphology within the

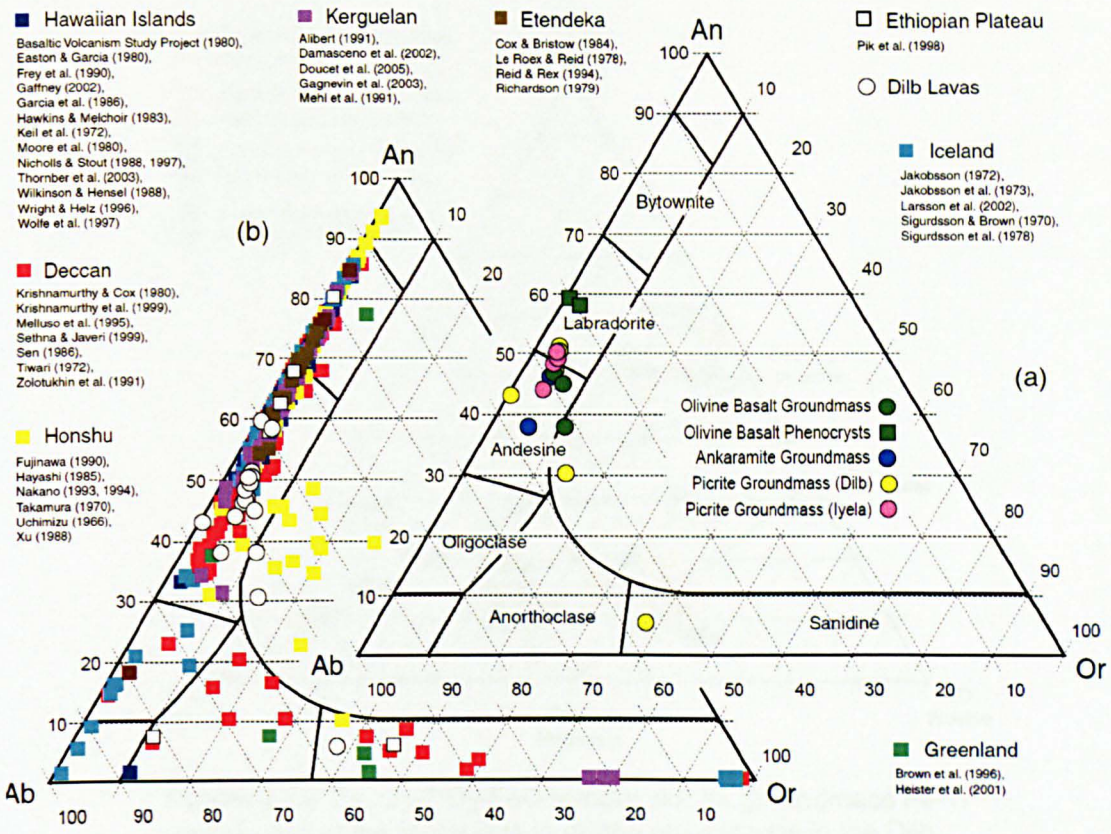

Figure 4.57 Ab-An-Or ternary plots showing **(a)** the compositional variability of feldspar phenocrysts and groundmass microlites in the Dilb and Iyela lavas, and **(b)** their range of compositions compared to feldspars from similar and contrasting tectonic environments. The feldspar phenocrysts and groundmass microlites from the Ethiopian Plateau (Pik et al. 1998) shown in (b) include two phenocrysts from the LT Basalts (those with the highest An contents), two phenocrysts from the HT1 Basalts (those with intermediate An contents), and groundmass microlites from the HT1 and HT2 Basalts (those with low An, and high and intermediate Ab contents respectively). Data compilation is from GEOROC database.

groundmass (Section 4.2.2). Representative microprobe analyses of these are compiled in Appendix 4.4.6. They include chromian spinels, present both in olivine phenocrysts and in the groundmass, and magnetites, titano-magnetites, ilmenites and hematites present in the groundmass only (Fig. 4.58). The subhedral prismatic spinels in the groundmass are likely to be relic inclusions in decomposed olivines. The compositions of the spinels, magnetites and ilmenites are similar to those of Ti-rich Fe-oxides found in comparable lavas from other plume related provinces, particularly those from Hawaii, the Deccan, and Etendeka (Fig. 4.59). The presence of hematite, however, is indicative of oxidising conditions less typical of the lavas from such provinces. Average compositions for spinel inclusions in olivine phenocrysts from the lavas, together with their maximum, minimum and median values for all analysed oxides are shown in Table 4.13. There is no apparent systematic variation in the composition of the inclusions between the lava-types

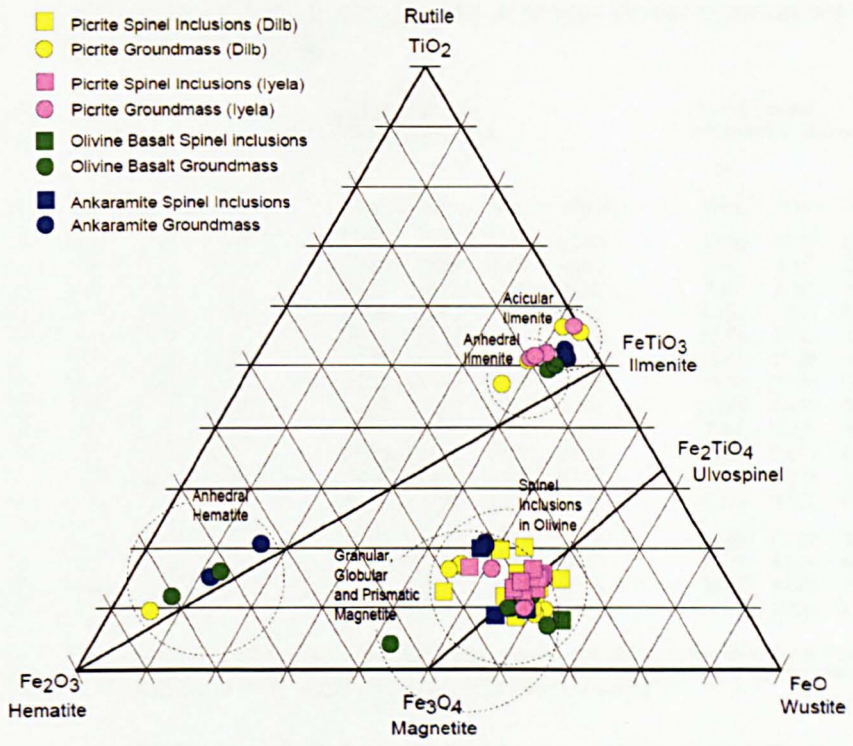

Figure 4.58 Fe_2O_3-TiO_2-FeO ternary plot for groundmass Fe-Ti oxides, and spinel inclusions in olivine phenocrysts in the Dilb and Iyela lavas.

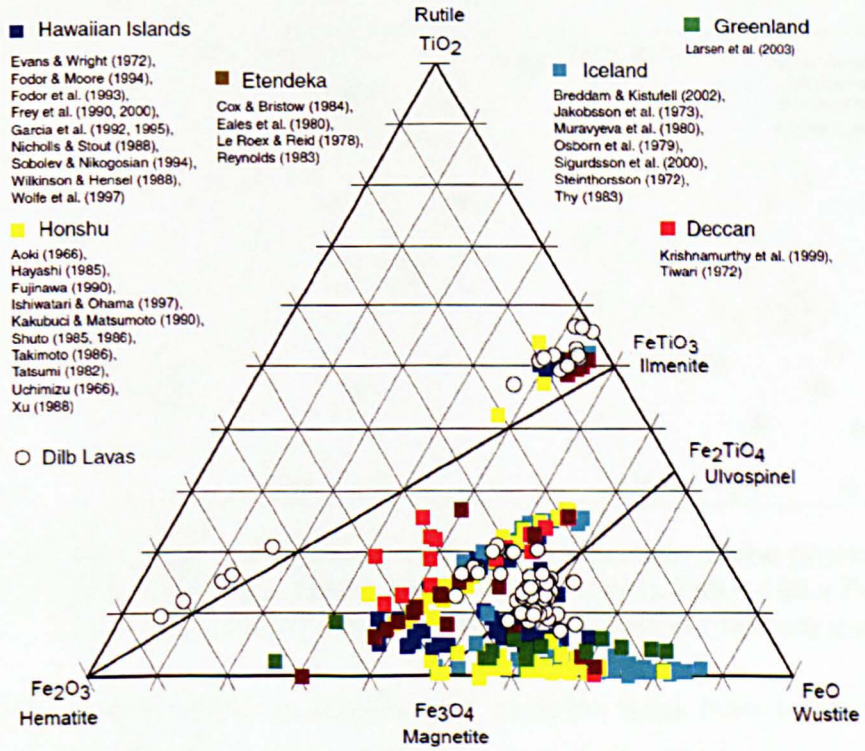

Figure 4.59 Fe_2O_3-TiO_2-FeO ternary plot showing the compositional range of Fe-Ti oxides from the Dilb and Iyela lavas compared to those for Fe-Ti oxides from similar and contrasting tectonic environments. Data compilation is from GEOROC database.

Table 4.13 Averaged compositions, and compositional ranges for spinel inclusions in olivine phenocrysts in the Dilb and Iyela lavas

Group	Picrites *				Ankaramites				Olivine Basalts			
Morph.	Inclusions in olivine				Inclusions in olivine				Inclusions in olivine			
Anal.	22				3				6			
Stat.	Mean	Max	Min	Median	Mean	Max	Min	Median	Mean	Max	Min	Median
SiO_2	0.115	0.205	0.068	0.110	0.086	0.102	0.069	0.087	0.110	0.131	0.098	0.103
TiO_2	7.46	13.41	4.43	7.07	7.58	14.79	3.76	4.20	3.98	5.17	2.69	4.00
Al_2O_3	7.53	8.67	4.83	7.54	8.45	10.84	7.17	7.33	7.31	9.37	6.66	6.91
V_2O_3	0.000	0.000	0.000	0.000	0.000	0.000	0.000	0.000	0.492	0.597	0.308	0.559
Cr_2O_3	33.27	42.24	18.80	35.17	31.26	46.96	11.18	35.64	38.70	49.63	23.51	37.09
Fe_2O_3	14.91	25.30	10.46	14.42	16.80	23.47	11.19	15.74	16.46	31.25	8.75	16.21
FeO	27.34	34.10	23.99	27.06	26.32	33.80	21.15	23.99	24.90	27.60	20.92	25.98
MnO	0.398	0.499	0.330	0.396	0.350	0.368	0.327	0.355	0.376	0.409	0.285	0.392
MgO	7.53	9.15	5.09	8.01	8.46	9.62	7.49	8.28	7.13	9.12	6.13	6.42
CaO	0.016	0.105	0.000	0.007	0.025	0.074	0.000	0.001	0.020	0.061	0.002	0.013
NiO	0.214	0.407	0.000	0.253	0.249	0.366	0.171	0.210	0.170	0.213	0.154	0.165
ZnO	0.000	0.000	0.000	0.000	0.000	0.000	0.000	0.000	0.285	0.334	0.165	0.306
Mg#	32.91	39.34	23.63	34.89	37.05	44.77	28.31	38.07	33.88	43.73	28.35	30.60
Cr#	74.32	78.63	60.99	75.58	66.95	81.45	50.58	68.81	77.16	81.96	62.73	78.83
Fe#	24.55	43.19	16.85	22.61	29.43	50.27	15.59	22.44	24.10	44.25	12.09	24.70
$Fe^{3+}/\Sigma Fe$	0.3265	0.4509	0.2582	0.3243	0.3594	0.3845	0.3224	0.3712	0.3574	0.532	0.2734	0.347

Note: Oxides are given in wt %. Averaged values were calculated from the compiled analyses of inclusions in olivine phenocrysts. Averaged values for inclusions in the picrites included analyses from the only lava analysed from the Iyela Section - these are marked with a star. End member compositions have been calculated as follows: Mg#=100xMg/(Mg+Fe^{2+}), Cr#= 100xCr/(Al+Cr), Fe#= Fe^{3+}/(Al+Cr+Fe^{3+}).

except that those from the picrites are generally more Ti-rich, and show less of a compositional range, than those from the ankaramites and olivine basalts (Fig. 4.60). Overall, they are enriched in TiO_2, Fe_2O_3 and FeO, and depleted in Al_2O_3, compared to chromites in picrites from West Greenland (Fig. 4.61), and they are

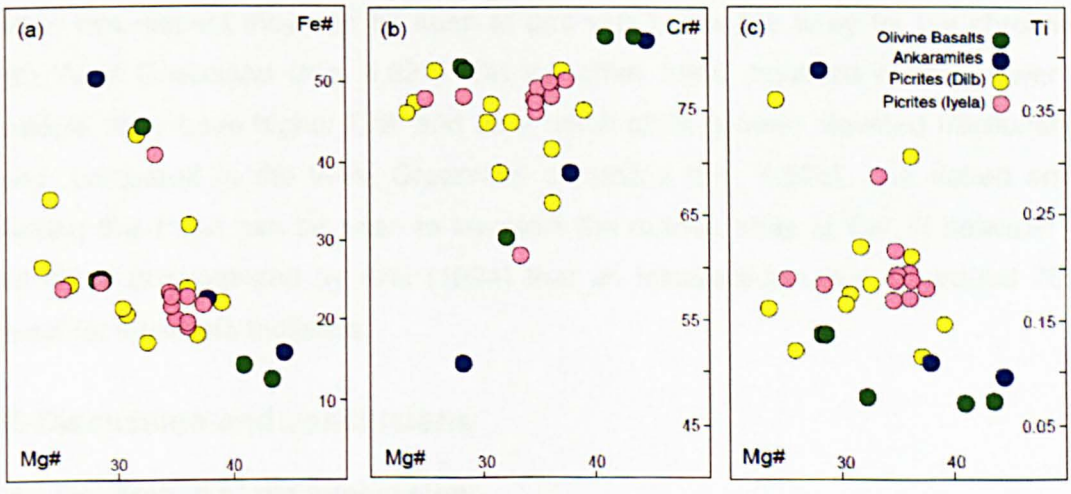

Figure 4.60 Compositional variations of spinel inclusions in olivine phenocrysts from the Dilb and Iyela lavas. Mg# = 100 x Mg/(Mg+Fe^{2+}), Fe# = 100 x Fe^{3+}/(Cr +Al+Fe^{3+}), Cr# = 100 x Cr/(Cr + Al). Ti is shown as atoms per formula unit.

compositionally more similar to spinels from tholeiitic lavas from Hawaii (Basaltic Volcanism Study Project, 1981, Wilkinson & Hensel, 1988) and the Deccan (Krishnamurthy & Cox, 1977, Krishnamurthy et al. 1999). The Mg# of the spinels and their host olivines are not correlated in the same way as other suites of coexisting

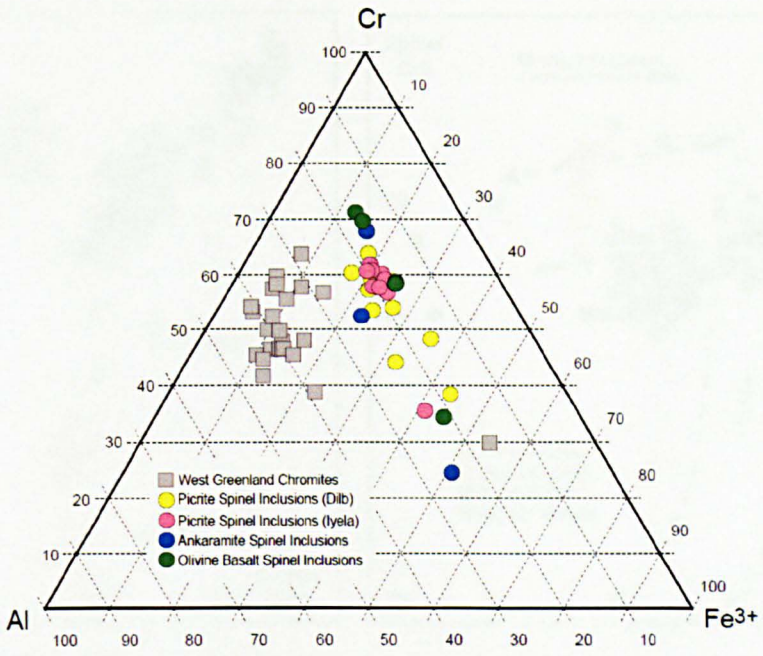

Figure 4.61 Ternary plot of trivalent cations for spinel inclusions in olivine phenocrysts from the Dilb and Iyela lavas. Analyses for chromites in olivine phenocrysts from the Vaigat Formation, W. Greenland (Larsen & Pedersen, 2000) are shown for comparison.

spinels and olivines, such as those from West Greenland. As a result of their high Fe-contents, the Dilb and Iyela spinels have low Mg# compared to their host olivines, and in this respect they can be seen to plot well below the array for the chromites from West Greenland (Fig. 4.62a). On the other hand, because of their lower Al contents, they have higher Cr#, and as a result show a more elevated fractionation trend, compared to the West Greenland chromites (Fig. 4.62b). The dotted arrow marking this trend can be seen to intersect the mantle array at Cr# of between 70 and 80; it is suggested by Arai (1994) that an intersection value of around 70 is typical for intraplate tholeiites.

4.5 Discussion and conclusions

4.5.1 Coherence of the succession

The lavas of the Dilb and Iyela sections together form a coherent pile near to 1000 m thick comprising a sequence of basaltic lavas (Figs 4.29, 4.40 & 4.42) estimated to have been emplaced between 30 and 28 Ma ago (Hofmann et al. 1997, Pik et al. 1998). Since the rhyolitic ignimbrite which caps the sequence marks the base of the Alaji Formation; it can be assumed at least that they represent the upper part of the Aiba Formation (Chapters 2 & 3). It is likely that, beneath the Dilb Section, there may be another 1000 m or so of similar basaltic lavas which constitute the lower part of

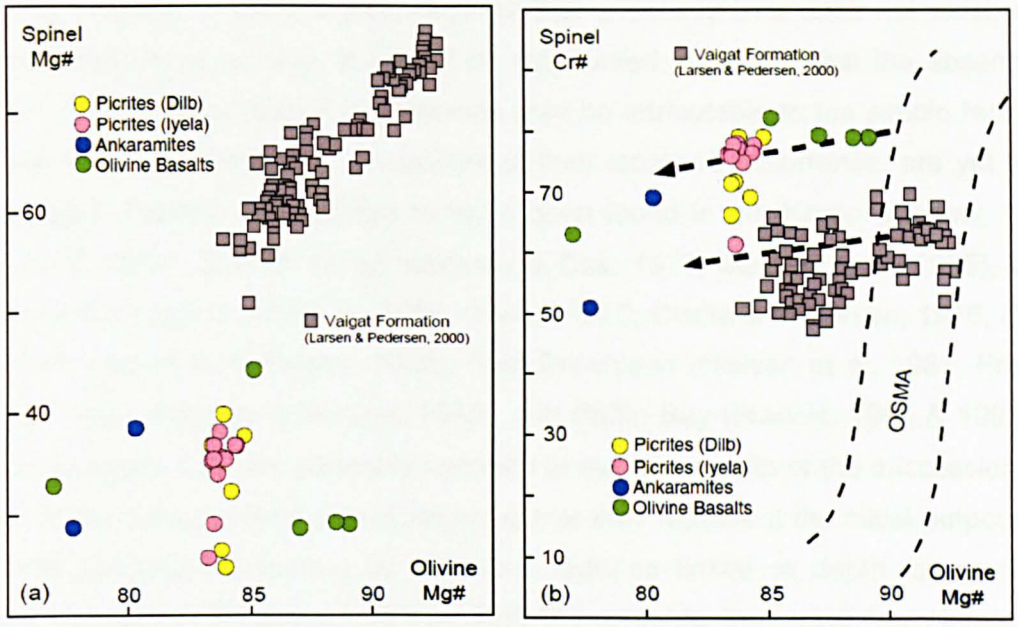

Figure 4.62 Variation of Mg# and Cr# of spinel inclusions with Mg# of host olivines from the Dilb and Iyela lavas. Data for coexisting spinels and olivines from the Vaigat Formation, West Greenland are shown for comparison. The dashed arrows in (b) indicate fractional crystallisation trends, away from the mantle array toward lower Mg# (Larsen & Pedersen, 2000). OSMA = olivine-spinel-mantle array (Arai, 1994).

the Aiba Formation and possibly the whole of the Ashange Formation. Despite the fact that the base of the pile is not seen, the Dilb and Iyela sections together provide a continuous, albeit localised, record of flood volcanism from some point in its high flux stage thought to be associated with melting in the hot head of the Afar mantle plume, through to the onset of lower flux bimodal volcanism signalling the closing stages flood volcanism thought to be associated with the initial decline in plume-head activity.

4.5.2 Nature and significance of the lavas

Like most flood basalts in continental and oceanic provinces, the lavas exposed in the Dilb and Iyela sections are variably porphyritic (Figs 4.1 – 4.3 & 4.31 – 4.33). They are unusual, however, in that they rarely contain phenocrysts of plagioclase. The virtual absence of aphyric lavas and the abundance of picrites in the sections similarly reflect the unusual character of the succession compared to successions in other flood basalt provinces, and elsewhere in the Ethiopian province. Sequences with such an abundance of picrites are rare in most flood basalt provinces. This has generally been ascribed to density trapping of the primary magma at the base of the crust where olivines are precipitated to form ultramafic cumulates, and only the evolved basaltic melts are erupted (Cox, 1980). Larsen & Pedersen (2000) suggest

that the eruption of picrites then requires that a density trap does not exist, or is circumvented in some way. It cannot be discounted, however, that the absence of picrites in many flood basalt successions may be attributable to the simple fact they are yet to be uncovered or, on account of their localised occurrence, are yet to be discovered. Picrites are reported to have been found in the Karoo (Bristow, 1984; Cox et al. 1984), Deccan (Krishnamurthy & Cox, 1977; Melluso et al. 1995), West Greenland (Drever & Johnston, 1957; Clarke, 1970; Clarke & Pedersen, 1976, Gill et al. 1992; Larsen & Pedersen, 2000), East Greenland (Nielsen et al. 1981; Fram & Lesher, 1997; Hansen & Nielsen, 1999), and Baffin Bay (Francis, 1985 & 1995). In these provinces they are generally confined to the lower parts of the succession and show limited geographical extent, implying that they represent the initial outpourings of flood volcanism focussed by structural features linked at depth to a primary magmatic source. On account of their high Mg contents, they have been inferred to be products of partial melting in the hottest parts of the upwelling mantle at temperatures significantly higher than the ambient mantle (McKenzie & Bickle, 1988; Campbell & Griffiths, 1990); therefore their composition may be assumed to be close to that of the primary mantle-derived melt. The localised occurrence of such an abundance of picrites in the Dilb and Iyela sections implies then that the region was the structural focus for the some of the earliest outpourings of the Ethiopian flood volcanics derived from partial melting in the convecting head of the Afar mantle upwelling.

On the basis of their petrography and geochemistry, the Dilb and Iyela lavas have been classified as picrites, ankaramites and olivine basalts (Section 4.2.2). This three-fold classification is similar to that used by Krishnamurthy and Cox (1977) to sub-divide the flood basalts of the Deccan. They subdivide picrites, originally classified as such by West (1958), into oceanitic types characterised by phenocryst assemblages dominated by olivine, and ankaramitic types characterised by phenocryst assemblages dominated by clinopyroxene. These are distinct from the basalts and three-phenocryst basalts both reported by West (1958) to contain phenocrysts of plagioclase in addition to olivine and clinopyroxene. In these respects the lavas from the Dilb and Iyela sections are similar to those from the Deccan; however they differ in that they show a range of olivine morphologies not seen in the lavas from the Deccan (Fig. 4.4). In addition to the equant polyhedral and tabular olivines typically seen in the Deccan lavas, the lavas from the Dilb and Iyela sections contain elongate and skeletal olivines (Fig. 4.6) similar to those seen in picrites from the North Atlantic province (Drever and Johnston, 1957; Larsen and Pedersen, 2000),

the Karoo (Cox et al. 1965), Etendeka (Thompson et al. 2001) and Hawaii (Baker et al. 1996). Such forms of olivine are interpreted by Donaldson (1976) not to be a result of rapid cooling, but of rapid olivine growth caused by a high normative olivine content of the magma. The presence of water in the melt can also contribute to a greater variety of olivine shapes, particularly during rapid cooling (Donaldson, 1976). Most of the Dilb and Iyela lavas contain elongate olivines (Table 4.1) which suggest then that they were derived from Mg-rich magmas with high normative olivine contents, and in this respect their compositions might in some way reflect that of the primary melt even though they may not strictly be considered as primary magmas. The fact that most of the olivines in the lavas are rimmed and variably replaced by iddingsite, and that in ankaramites and olivine basalts this is almost invariably overgrown with fresh fayalitic olivine furthermore suggests that the magmas had high water contents (Goff, 1996; Furgal & McMillan, 2001), and that this may have aided the growth of such diverse olivine morphologies. High water contents in the magmas have already been inferred from the occurrence of vesicle cylinders in some of the lavas (Section 3.3.2). It cannot be discounted that in the ankaramites and olivine basalts with a dominance of plagioclase in the groundmass indicative of more evolved compositions than in the picrites, elongate olivines may have been acquired by mixing with more primitive partially crystallised magmas. It is generally the case that there is an absence of elongate olivines in those olivine basalts that contain phenocrysts of plagioclase, and in this respect it may be assumed that these lavas at least were derived from a shallower, less Mg-rich magma than the picrites, even though they may contain remnant signatures of a deeper common parent.

Skeletal olivines, which are more acutely indicative of melts with high normative olivine contents, are almost entirely confined to the picrites (Table 4.1). This suggests that the picrites were derived from magmas with significantly higher normative olivine contents than those from which the ankaramites and olivine basalts were derived. In this respect it can be assumed that the picrites were sourced at depth and that their ascent to the surface was not punctuated by prolonged periods of shallow level fractionation, whereas the ankaramites and olivine basalts were sourced from shallower levels where they were allowed to fractionate and evolve before erupting at the surface. The dominantly higher proportions of plagioclase in the groundmasses of the ankaramites (Figs 4.2 & 4.32), and more so in the groundmasses of the olivine basalts (Figs 4.3 & 4.33), compared to the picrites (Figs 4.1 & 4.31) seem to support this. It can be further assumed therefore that the compositions of the picrites more closely reflect that of the primary mantle-derived melt compared to those of the

ankaramites and olivine basalts. The picritic magmas would have partially crystallised at depth and, on account of their high density, would have required high flux conditions to carry them directly to the surface. The virtual absence of picrites (and therefore of skeletal olivines) above the first palaeosol at Location 11 (Table 4.5) suggests then that by this point in the succession the magma flux had slowed to such an extent that it had become insufficient to carry such primitive magma to the surface. This is consistent with the change in architecture of the lava flows above the palaeosol at Location 11 already suggested to reflect a slowing of the magma flux caused by a reduction in the supply of the primary mantle-derived melt (Section 3.3.2). It is evident then that the picrites in the Dilb and Iyela sections show a similar stratigraphic distribution to picrites in other flood basalt provinces in that they are largely confined to the lower part of the succession.

4.5.3 Petrogenetic relations

Phase relations: Textural relations between the minerals in the lavas from each group indicate that olivine crystallised first, followed by clinopyroxene, titaniferrous magnetite and plagioclase respectively. This contrasts with the normal phase relations in tholeiitic flood basalts in which plagioclase crystallises before clinopyroxene and magnetite. The sequence of crystallisation seen in the Dilb and Iyela lavas is more consistent with that seen in ferropicrites and presumably reflects the high Fe and Ti, and low Al of the parental magma (Gibson et al. 2000). NiO contents of olivine phenocrysts notably higher than might be expected for olivines with such low Mg# (Fig. 4.47b), and the almost invariable abundance of chrome-spinel, titanomagnetite and ilmenite in the lavas (Fig. 4.58) do seem to signify a source high in Fe and Ti respectively. Furthermore, the below average Al_2O_3 contents of clinopyroxene phenocrysts (Fig. 4.52c), and the high Cr# of spinel inclusions in olivine phenocrysts (Fig. 4.62b) in the lavas compared to those in lavas from other plume-related provinces imply that the source was depleted in Al reflecting the presence of residual garnet.

Olivine phenocrysts: The variation in the composition and proportion of olivine phenocrysts in the Dilb and Iyela lavas suggest that they underwent variable degrees of fractionation at varying depths prior to eruption. Large, small and striated polyhedral, and elongate, olivines are present in most of the lavas from each lava group, and, as already mentioned, skeletal olivines are largely confined to the picrites (Tables 4.1 & 4.6). Despite the occurrence in selected lavas of polyhedral olivines with high Mg# (89 – 90) typical of xenocrystic mantle olivines (Table 4.9), the range

of CaO contents and the continuous compositional trends exhibited by the olivines from all three lava groups (Figs 4.44 - 4.46), suggest that they are cognate phenocrysts precipitated from basaltic or picritic magmas rather than accidental xenocrysts. Furthermore, the textural relations and compositions of the spinel inclusions (Section 4.4.5), the rarity of strain features such as kink bands within the olivines, and the presence of fragile elongate and skeletal morphologies unlikely to have survived prolonged transport, suggest that they are phenocrystic rather than xenocrystic. All olivine morphologies show variable degrees of rounding and embayment which generally suggest that they crystallised at depth and were subsequently transferred to more shallow levels where they were no longer in equilibrium with the ambient melt and were consequently resorbed. The dominantly flat zoning profiles shown by the majority of the olivine phenocryts (Fig. 4.48) suggest that most crystallised close to equilibrium conditions in which the olivine was able to continuously re-equilibrate with the melt whilst the bulk composition of the magma remained relatively constant, i.e. there was no opportunity for magmatic differentiation (Larsen & Pedersen, 2000). The sharp decline in Mg# seen in the thin rims and overgrowths around some of these otherwise unzoned phenocrysts in the ankaramites and olivine basalts suggests an abrupt change in equilibrium conditions giving rise to new growth of Fe-rich olivine during and after entrainment and eruption, either before or after iddingsitization. This shift in equilibrium conditions is likely to have occurred when partially crystallised magma was transferred, either directly to the surface, or to more shallow or near-surface depths where more evolved magma had fractionated for some time. In this respect the form of some of the zoning profiles may be considered to be indicative of magma mixing. It may be assumed that those phenocrysts with initially higher Mg# seen to show more pronounced differences between their core and rim compositions were sourced from greater depths than those with initially lower Mg# and less pronounced differences between their core and rim compositions. Furthermore, the composition of the Fe-rich olivine overgrowths may be considered more appropriately to reflect the composition of the most evolved melts erupted at the surface. In contrast to the dominantly flat profiles described above as representative of near equilibrium crystallisation, the more curved profiles with steepening gradients toward the rim seen in some of the olivines are indicative of simple fractional crystallisation (Larsen & Pedersen, 2000), suggesting that in some instances the olivine phenocrysts became separated from the melt and were thus prevented from reaching equilibrium. Such differentiation leading to the accumulation of olivine phenocrysts in reservoirs at varying depths might account for high proportions of olivine in many of the erupted lavas.

The dominance of unzoned or equilibrated olivines with variable Mg# implies that the majority of olivine phenocrysts had sufficient time to continuously re-equilibrate with the evolving melt at varying depths for some time prior to the influx of new parental magma from below, and before entrainment and ascent to the surface. It is likely then that the supply of parental magma was sporadic and occurred in pulses capable of displacing volumes of partially crystallised magma stalled, because of their high density, in crustal reservoirs, thereby forcing their continued ascent higher into the crust or onto the surface. Once displaced, it is probable that the partially crystallised magmas at varying levels rose rapidly to the surface. This is supported by the sparse occurrence in the lavas of olivine phenocrysts with linear zoning profiles, suggested by Maaloe & Hansen (1982) to be indicative of a slow ascent to the surface and the continuous re-equilibration by diffusional exchange between olivine and the melt at progressively shallower depths en-route.

The presence of large polyhedral olivines with Mg# as high as 89 – 90 in selected lavas from each lava group (Table 4.9) suggests that all the lavas originated from the same parent, but were sourced from derivative magmas at different depths where they were allowed to mix, equilibrate, and/or fractionate prior to eruption. In this sense none of the lavas are strictly representative of the primary mantle-derived magma. The highest Mg# olivines present in the lavas, however, may be considered to reflect the composition of the primary melt, which, assuming a partition coefficient of Fe^{2+} and Mg between olivine and liquid (K_D) of 0.3 (Ulmer, 1989), would have had an Mg# of at least 71 (at 1 atm - Table 4.14). Since, however, it is probable that these high Mg# olivines equilibrated at depth, and since it has been shown that K_D changes with pressure (Ulmer, 1989), it is likely that the Mg# of the primary melt was significantly greater than this lowest estimate. Recent geophysical evidence suggests that the thickness of the crust beneath the Ethiopian Plateau is near to 50 km (Mackenzie et al. 2004), and if it is assumed that olivine equilibration occurred at the base of the crust this thick prior to lithospheric attenuation (Section 2.3.2), the Mg# of the melt would have been as high as 75 (Table 4.14).

The sparse occurrence in the lavas of primary olivines might imply that most were left at depth. It is possible that the parent melt fractionated olivine with Mg# 89 – 90 at depth until it had evolved sufficiently to yield olivine with lower Mg# before entrainment and ascent to the surface as a partially crystallised magma charged mainly with accumulated later-formed olivine. Such magmas could erupt as picrites dominated by olivines with Mg# 83 – 84, or as ankaramites or olivine basalts

Table 4.14 Mg# for melts calculated from compositions of olivine phenocrysts from the Dilb and Iyela lavas

Picrites	**LP**	**SP**	**ST**	**E**	**SK**
Mg# of olivine	83.78	83.56	83.77	83.46	83.37
Mg# of melt at 1 atm	60.78	60.39	60.76	60.22	60.06
Mg# of melt at 0.5 Gpa	61.56	61.17	61.54	61.00	60.85
Mg# of melt at 1.2 Gpa	63.02	62.65	63.01	62.48	62.33
Ankaramites	**LP**	**SP**	**ST**	**E**	**OG**
Mg# of olivine	80.78	80.15	73.22	78.13	65.73
Mg# of melt at 1 atm	55.77	54.78	45.06	51.73	36.52
Mg# of melt at 0.5 Gpa	56.58	55.59	45.88	52.55	37.29
Mg# of melt at 1.2 Gpa	58.11	57.13	47.43	54.11	38.76
Olivine Basalts	**LP**	**SP**	**ST**	**E**	**OG**
Mg# of olivine	83.79	80.81	77.25	81.03	64.86
Mg# of melt at 1 atm	60.80	55.82	50.46	56.17	35.64
Mg# of melt at 0.5 Gpa	61.57	56.62	51.28	56.97	36.39
Mg# of melt at 1.2 Gpa	63.04	58.15	52.84	58.50	37.85
Highest Mg# olivine	**Picrites**	**Ankar.**	**Olv.Bsts**		
Mg# of olivine	89.17	89.92	89.20		
Mg# of melt at 1 atm	71.18	72.80	71.25		
Mg# of melt at 0.5 Gpa	71.85	73.44	71.91		
Mg# of melt at 1.2 Gpa	73.10	74.64	73.16		

$Mg\#_{(melt)} = 1 / (1 + ((1 - (Mg\#_{ol} / 100)) / (Mg\#_{ol} / 100)) / K_D^{Fe\text{-}Mg}{}_{ol\text{-}liq}) \times 100.$
$K_D^{Fe\text{-}Mg}{}_{ol\text{-}liq}$ = 0.3 for 1 atm, 0.31 for 0.5 GPa and 0.33 for 1.2 GPa (Ulmer, 1989)
These values are based on crustal thicknesses of 0, 20 km and 50 km respectively.
Average Mg# for all phenocryst types, and the highest values for each group are from Table 4.9. Mg# for overgrowths are averaged from values in Table 4.10.
Values in red represent the most realistic melt compositions calculated from the compositions of the later-formed elongate olivines at depths considered most reasonable for their crystallisation. LP - Large Polyhedral, SP - Small Polyhedral, ST - Striated, E - Elongate, SK - Skeletal and OG - fayalitic overgrowth

dominated by olivines with Mg# 79 – 81, depending on the time over which they had evolved. The abundance in the lavas of unzoned olivines with variable Mg#, however, suggests that it is more likely that pulses of primary magma containing variable amounts of primary olivines ascended through the crust and became stalled at varying depths where primary olivine became resorbed and new olivines were able to crystallise or re-equilibrate under lower pressure equilibrium conditions before eruption or transferral to more shallow depths. Each pulse of primary magma could mix with and/or displace partially crystallised magma stalled at varying depths, thereby changing its bulk composition and diversifying its olivine phenocryst population, as well as forcing its continued ascent higher into the crust where, in turn, it could mix with and displace partially crystallised magma stalled there. The more vigorous pulses of primary magma, perhaps laden with primary olivines, may have been capable of ripping through the stalled magmas to higher levels in the crust and in doing so may have entrained later-formed olivine phenocrysts en-route. Successive pulses of varying ferocity and frequency would over time have created

variably mixed magmas with an increasingly complex mix and range of olivine compositions at successively shallower depths. This may account for the greater range of olivine compositions in the ankaramites and olivine basalts compared to the picrites (Figs 4.43 – 4.45). The picrites contain a variety of olivine morphologies with a limited mix and range of compositions with consistently high Mg# and NiO contents, placing them in the high Mg# and high NiO fields to the right of the compositional divide in Figures 4.44 and 4.45 respectively. This implies that they were derived from partially crystallised mixed magmas which made their way from depth directly to the surface, and that their journey en-route was not punctuated by prolonged periods of shallow level fractionation. In addition to polyhedral olivines with similar Mg# to those seen in the picrites, the ankaramites and olivine basalts, on the other hand, contain olivine phenocrysts with markedly lower Mg# than any seen in the picrites, suggesting that they were derived from mixed magmas that evolved for some time at more shallow levels. It is notable, in particular, that all later-formed striated and elongate olivines in the ankaramites and olivine basalts have consistently low Mg# and NiO, placing them in the low Mg# and low NiO fields to the left the compositional divide in Figures 4.44 and 4.45 respectively, suggesting that they equilibrated at shallow or near-surface depths prior to eruption. Some have Mg# and NiO contents almost as low as those seen in the fayalitic olivine overgrowths (Table 4.10) implying they may have precipitated from the erupted melts along with or shortly before the overgrowths. The fact that most are both iddingsitized and overgrown with Fe-rich olivine, however, supports the assumption that they crystallised at shallow depths and were subsequently oxidized prior to eruption.

Since the majority of olivine phenocrysts in the lavas were inherited from depth they are unlikely to provide a reliable estimate of the Mg# of the magmas prior to eruption. The pre-eruptive Mg# for the lavas was instead estimated from the Mg# of the elongate and skeletal olivines as they are likely to have crystallised at later stage than any of the other phenocrysts. If the Mg# of the melt is taken as a proxy for the relative depth of olivine equilibration, it may be deduced from these estimates (shown in red in Table 4.14) that both the ankaramites and olivine basalts were derived from shallow seated magmas, whereas the picrites were derived from a significantly deeper level. Following this assumption, the distinction between a shallow and deep source for the respective lava types is perhaps an over-simplification, considering the continuous range of olivine compositions exhibited by the lavas (Fig. 4.44) that suggest olivine was able to crystallise and equilibrate over a range of depths before entrainment and eruption. Larsen & Pedersen (2000) propose that such a range of

olivine compositions may be generated in an open conduit system which allows the processes of equilibrium and fractional crystallisation, magma mixing, oxidation and partial to complete re-equilibration of olivine to operate together, simultaneously or at different times, at different levels between the source and the surface (Fig. 4.63).

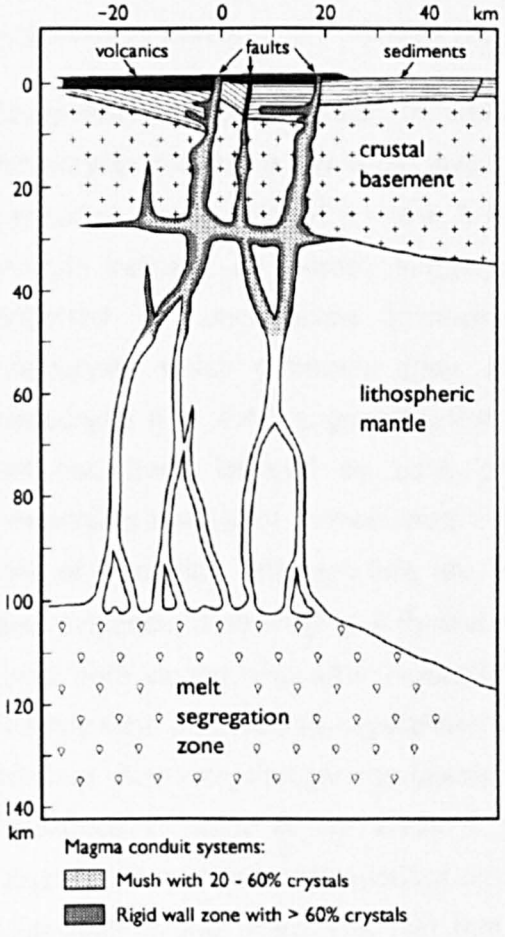

Asthenospheric mantle melts segregated at 140 - 100 km ascended through narrow dyke-like conduits developed along fractures in the lithospheric mantle and crust. The conduits became armoured with a rigid zone of > 60% olivine crystals thereby preventing the interior zone from being contaminated by the sidewalls. The crystal content of the interior zone may have varied between 20 and 60%, and the amount of crystals left behind in the conduits was probably dependent on the ascent velocity. It is envisaged that crystallisation began at a depth of around 45 km, and that some magma accumulated at the base of the crust, although most magma is likely to have ascended directly into the crust. High-Mg olivines (90 - 93) and chromites (66 - 77) precipitated at depth and less Mg-rich olivines (86 - 88) and chromites (< 69) precipitated at shallower levels. At high ascent rates high percentages of crystals were carried in suspension directly to the surface, and at low ascent rates only a few small crystals may have been erupted. Successive pulses of acending magma would lead to mixing of batches of magma at various stages of fractionation and equilibration at varying depths. Low-Mg olivines (78 -85) were able to crystallise in stagnating magma pockets. Most of the magma, however, passed so rapidly to the surface that equilibration was rarely complete. Resultant phenocryst assemblages were consequently dominated by mechanical mixtures of crystals from different batches of magma, some of which were picked up from the sidewalls during ascent. Magma batches that intruded laterally into the crystalline basement or into the sediments near the surface became contaminated and consequently fractionated sulphides and occasionally native iron.

Figure 4.63 Conceptual model of the conduit system for the volcanic rocks of the Vaigat Formation, West Greenland (Larsen & Pedersen, 2000)

This model may to some extent account for the variety of the olivine compositions seen in the ankaramites and olivine basalts, thereby suggesting that such a system may have operated at shallow levels beneath the Dilb and Iyela region, but it does not offer a viable explanation for the consistently high Mg# and NiO contents of the picritic phenocrysts. The main feature of the model is that as batches of magma ascend through the conduit system they are able to mix with earlier batches at varying stages of fractionation and equilibration, and entrain crystals from the conduit walls en-route to the surface. The absence in the picrites of olivine phenocrysts with Mg# as low as those seen in olivine phenocrysts in the ankaramites and olivine basalts, on the contrary, suggests, as previously inferred, that the picrites were

derived from magmas that ascended from depth directly to the surface unmodified by mixing and entrainment en-route. Also, it is possible, as inferred earlier, that the range of olivine compositions in the ankaramites and olivine basalts could have resulted from varying degrees of mixing, fractionation and equilibration in discreet reservoirs at varying depths rather than in a continuous conduit network as suggested by Larsen and Pedersen (2000).

Clinopyroxene phenocrysts: In addition to olivine, clinopyroxene is present as phenocrysts in all but a few of the lavas, and in the ankaramites it forms the dominant phenocryst phase (Figs 4.1 – 4.3 & 4.31 – 4.33). Textural relations between the minerals indicate, as already suggested, that it crystallised after olivine. This is supported by uncorrected microprobe analyses of selected clinopyroxene phenocrysts which generally show lower Mg# compared to coexisting olivine phenocrysts (Fig. 4.49) suggesting that they precipitated after the Mg content of the melt had been lowered by early crystallisation of olivine. The clinopyroxene phenocrysts are better formed than the olivine phenocrysts since they rarely show signs of resorption, although they are considerably more fragmented and commonly show evidence of strain (Fig. 4.8) which imply that they were continually moved and mixed both during and after crystallisation; this might suggest that many of the clinopyroxene phenocrysts crystallised in the ascending magmas. The most obvious evidence, however, that clinopyroxene crystallised after olivine is apparent from the occurrence in many of the lavas of large clinopyroxene phenocrysts containing inclusions of rounded and resorbed olivines which they have clearly engulfed during crystallisation (Fig. 4.9). The fact that these olivine inclusions show no signs of iddingsitization furthermore indicates that at least some clinopyroxene phenocrysts crystallised before the introduction of water into the melt near the surface. Microprobe analyses of the phenocrysts confirm inferences made from their extinction angles that in all the lavas they are, without exception, low pressure augites (Fig. 4.50a) and therefore may be assumed have crystallised together with more Fe-rich olivines during the later stages of fractionation at shallow depths. The absence in the lavas of low-Ca clinopyroxene or pigeonite, indicative of high pressure crystallisation, is a feature which distinguishes them from superficially similar lavas in other flood basalt provinces (Fig. 4.50b).

Although, at first-glance, the compositions of the clinopyroxene phenocrysts from all the lavas show remarkably consistent chemistry, on closer inspection there are discernable differences between the ankaramites and olivine basalts, and the picrites

(Fig. 4.51), which reflect similar differences in their petrogenesis to those inferred from olivine compositions in the discussion above. The relatively high Cr_2O_3, Al_2O_3 and Na_2O, and low MgO contents for clinoproxene phenocrysts in the picrites compared to those in the ankaramites and olivine basalts suggest that the phenocrysts in the picrites crystallised from melts with notably different compositions from those which the phenocrysts in the ankaramites and olivine basalt crystallised from. Relatively higher Cr_2O_3 contents, in particular, suggest that the picritic melts were less evolved than the ankaramitic and olivine basalt melts, and therefore more likely to have been derived from a deeper source, as proposed above. Marginally higher Ca and Na contents relative to Ti shown by most of the clinopyroxene phenocrysts in the picrites compared to most in the ankaramites and olivine basalts, furthermore, reveal that the picrites have an alkali affinity whereas the ankaramites and olivine basalts are more typically tholeiitic (Fig. 4.53b). The distinctive compositional trends shown by the clinopyroxene phenocrysts from the picrites and those from the other lava groups, indicated by the regression lines for the picrites and ankaramites from the Dilb Section in Figure 4.51, imply that melts from which they precipitated evolved separately, and in this sense it is unlikely that they did so in a conduit system similar to that described by Larsen & Pedersen (2000). It is likely therefore that the clinopyroxene phenocrysts in the ankaramites with alkaline affinities, high Cr contents, and high Mg# were inherited in the same way as the coexisting high Mg# olivines by mixing with the picritic magmas as described above. It is equally likely that similarly enriched inherited phenocrysts occur in the olivine basalts; their apparent absence from the presented data-set may therefore be attributable to the simple fact that such phenocrysts were not analysed. The cogenetic relationship between the clinopyroxene phenocrysts in all the lavas implied by such inheritance is evident from the near-perfect correlations between their Al and Si, and Al and Ti contents illustrated in Figures 4.54a and 4.54b respectively.

The common occurrence in all of the lavas of oscillatory zoned clinopyroxene phenocrysts (Fig. 4.11b), and normal zoning profiles which show a general decrease in SiO_2, CaO, MgO, Cr_2O_3 and NiO, and a corresponding increase in FeO, Al_2O_3, TiO_2, Na_2O and Fe_2O_3 (where present) from core to rim in such phenocrysts (Fig. 4.56), support the above assumption that clinopyroxene fractionated from progressively evolving melts at shallow or near-surface depths. The thin rims of the phenocrysts marked by same but more pronounced compositional variations are likely to represent continued fractionation following eruption of the lavas; the fact that the composition of these rims is not dissimilar to that of the clinopyroxene microlites

in the groundmass of the lavas would seem to confirm this (Table 4.11). In contrast, the antithetic peaks and troughs showing similarly shifts in composition in some of the zoning profiles are more likely to be attributed to mixing with more evolved magmas at shallow depths than solely to changes in pressure as a consequence of ascent. This is apparent from the fact that these profiles show similar but slightly more evolved compositional gradients after than before such peaks and troughs (CPX4 (01.03.24.09), Fig. 4.56). Such irregularities may also be related to changes in fO_2 associated with the introduction of water into the melt, particularly where they are accompanied by the sudden appearance in the profile of Fe_2O_3.

Plagioclase phenocrysts: Although the compositional variations across plagioclase phenocryts in the olivine basalts were not analysed, it is likely that the ocillatory zoning seen in some these phenocrysts (Fig. 4.10) can provide similar records of relative changes in temperature and pressure, magma mixing, oxidation and melt-evolution at shallow depths to those seen in the zoned clinopyroxenes described above. Strain features in these phenocrysts, like those in many of the clinopyroxene phenocrysts, also indicate that they were moved and mixed in the same way during their ascent to the surface. The longer slender plagioclase phenocrysts that occur agglomerated with these strained and zoned phenocrysts, on the other hand, are more likely, on account of their fragile almost acicular form, to have crystallised quickly at or near the surface and as a result were not strained and fragmented by ascent. This is consistent with the fact that the morphology and composition of these slender phenocrysts estimated from their extinction angles is not dissimilar to the larger plagioclase microlites present in the groundmass of some of the lavas. Differences in the range of extinction angles for two populations of plagioclase phenocrysts (Section 4.2.2) support the differences in their crystallisation history suggested by their morphological characteristics. The fact then that these differences were not more apparent from the microprobe analyses (Fig. 4.57a) may be attributable to the limited number of plagioclase analyses made.

Glomerocrysts: The most obvious petrographic evidence of mixing of partially crystallised magmas at various depths prior to eruption is apparent from the extraordinary variety of glomerocrysts present in almost all of the lavas (Fig. 4.11). Many glomerocrysts composed exclusively of olivine are likely to have agglomerated at depth (possibly as deep as the source tapped by the picrites), where they may have been fused by subsequent influxes of hot primary magma before being transferred to more shallow depths where they became resorbed and embayed (Fig.

4.11a), and sometimes agglomerated with lower Mg# olivines and/or clinopyroxenes, already crystallised, or yet to crystallise at such depths, to form secondary glomerocrysts (Fig. 4.11c). The fact that primary glomerocrysts of olivine often form the cores of secondary glomerocrysts of mixed mineralogy seems to supports this. Secondary glomerocrysts in which the olivine cores show no signs of iddingsitization (Fig. 4.11c) are likely to have agglomerated at depths below the penetration of meteoric-derived groundwater, whereas those in which the olivine cores are iddingsitized (Fig. 4.11d) are more likely to have agglomerated at shallower depths within the zone of groundwater penetration. Evidence of continued mixing and agglomeration at shallow or near-surface depths is apparent from the occurrence in selected olivine basalts of glomerocrysts containing plagioclase in addition to olivine (often replaced by iddingsite) and clinopyroxene (Fig. 4.11f). The formation of secondary glomerocrysts might not necessarily have involved a change in depth, as implied above, since olivine could have crystallised and agglomerated before the onset of clinopyroxene crystallisation at the same depth. Similarly, the formation of primary glomerocrysts was not, as implied above, necessarily confined to great depth; clear evidence of this is the abundance of glomerocrysts composed exclusively of low-pressure clinopyroxene (Figs 4.11 b & e).

Groundmass microlites: Textural relations between the microlites within the groundmass of the lavas suggest that plagioclase crystallised first, followed by clinopyroxene, apatite (where present) and Fe-Ti oxides respectively. In the final stages of cooling the interstices between the microlites were infilled with volcanic glass, which was subsequently devitrified. Attention has already been drawn to the difference in the ratios of plagioclase to clinoproxene in the groundmass of the picrites compared to those in the ankaramites and olivine basalts, and how this difference may relate to the differences in the source of the lava types (Section 4.5.2). There are, in addition, other notable differences in the mineralogy of the groundmasses of the three lava groups that similarly reflect significant differences in the respective compositions of the erupted melts that may be related to their source. For example, the almost invariable presence in the picrites, and general absence in the ankaramites and olivine basalts, of acicular ilmenite and spinel (Table 4.2) is evidence that the Ti content of the picritic melts arriving at the surface was significantly higher than that for ankaramitic and olivine basalt melts. This suggests, as previously implied, that the picrites were sourced from a deeper, less evolved source than the ankaramites and olivine basalts. Also, the presence of sanidine microlites in the groundmass of the picrites (Fig. 4.57) supports earlier inferences

made from the composition of clinopyroxene phenocrysts that the picrites were derived from a source with alkaline affinities, whereas the ankaramites and olivine basalts were derived from a source more typically tholeiitic (Fig. 4.53b). The common occurrence of apatite in the groundmass of the picrites (Fig. 4.35) and its relative absence in the ankaramites and olivine basalts furthermore indicate that the picritic melts were relatively enriched in phosphorus compared to the ankaramitic and olivine basalt melts.

The fine-grained nature of the groundmass in all of the lavas indicates that they cooled quickly once erupted at the surface. The rate of cooling would have been dependent on the thickness of the flows (Chapter 3), and the temperature, composition and consequent viscosity of the erupted melt. It may be assumed then, on the basis of their composition and the speed at which they were transferred from depth to the surface, that the eruption temperatures of the picrites were significantly hotter than those of the ankaramites and olivine basalts. The picrites must therefore have experienced greater degrees of cooling than the ankaramites and olivine basalts, although this is not directly reflected in the differences in the grain-size of the groundmasses of the different lava types (Tables 4.2 & 4.7) probably because of the variable thicknesses of individual flows. It is, however, to an extent reflected in the predominance in the picrites compared to the ankaramites and olivine basalts of skeletal and acicular forms of Fe-Ti oxide, and clinopyroxene microlites exhibiting hour-glass zoning suggested by Wass (1973) to be indicative of variable rates of supercooling.

Despite the fine grained nature of the groundmasses of the lavas, and the probable differences in their cooling regimes and the consequent differences in viscosity, features indicative of flow such as the alignment of elongate olivine phenocrysts (Fig. 4.6), and of plagioclase microlites (Fig. 4.14), are equally well developed in selected lavas from each group. The general uniformity of the mineralogy and texture of the groundmass in most of the lavas suggests that they were emplaced as discreet effusive units. In some of the lavas, however, there are mineralogical and textural variations in the groundmass that indicate that mixing of different lava types did at times occur and that in some instances fresh eruptions of lava were injected into previously erupted but still fluid flows on the surface (Fig. 4.19). This suggests, as implied from field evidence presented in Chapter 3, that many of the lavas were erupted in quick succession. Other similar variations in the texture and mineralogy observed in some of the lavas are more likely to be a result of internal differentiation

associated with the migration of volatiles through individual lava flows rather than mixing between lavas with different compositions. These differentiated regions, notably richer in Fe-Ti oxides and larger than average plagioclase microlites compared to the main groundmass (Fig. 4.38), are likely to be enriched in elements such as Fe, Mn, Ti, Na, K, P and many incompatible trace elements not removed by initial crystallisation of the host lava (Goff, 1996).

Volatile content: The presence of vesicles (Fig. 4.20) and associated features such as vesicle sheets (Fig. 4.17) and cylinders (Fig. 3.5, Location 9) are more common in the olivine basalts than in the picrites and ankaramites. This is more noticeable in the field than in thin section (Chapter 3), and is more likely to be a consequence of the higher volatile content of the olivine basalts compared to the picrites and ankaramites than a result of their respective differences in viscosity. The more pervasive effects of iddingsitization in the olivine basalts compared to the ankaramites and picrites indicate that their comparatively higher volatile content may be a result of the high water content of the magmas from which they were derived. It may be argued therefore that the olivine basalts were derived from shallow magmas within the zone of groundwater penetration, whereas the ankaramites were sourced from below this zone. Alternatively, both lava types may share the same source region within the zone of groundwater penetration but may be distinguished from each other by the length of time spent there fractionating and being oxidised before eruption.

Xenoliths: Xenoliths of extraneous origin, such as that seen in the field at Location 24 (Fig. 3.5), were not encountered in any of the hand specimens or thin sections of the sampled lavas. The inclusions interpreted as xenoliths in Figure 4.12 are likely to represent fragments of earlier formed lavas incorporated into the host lava either during ascent or during flow. The fact that these inclusions are not dissimilar to lavas that occur lower in the sequence may suggest that they represent fragments of such lavas that were broken off and incorporated into the host lava during its ascent to the surface. Equally, on account of their rounded form, they may represent fragments of earlier erupted lava swept up and rolled into the advancing host flow. Also, it cannot be discounted that they may represent differentiation features associated with volatile release within the lava.

Alteration: The effects of iddingsitization are seen in all of the lavas. Only a few glomerophyric olivines tightly encased within mosaics of clinopyroxene phenocrysts were armoured against its effects. Iddingsitization is a selective form of alteration in that it only affects minerals such as olivine which are particularly reactive under

hydrothermal and weathering conditions. The chemical changes involved in such alteration of olivine include the loss of Mg and Si, the oxidation and increase in Fe, and the addition of Al to form a composite mineral of variable composition commonly referred to as iddingsite (Delvigne et al. 1979). Reported analyses of iddingsite range from mixtures of orthopyroxene, maghemite, hematite, cristobalite and amorphous silica (Goff, 1996) to mixtures of goethite and layer silicates such as saponite or other forms of smectite (Eggleton, 1984). The mixtures of Fe-oxides and layer silicates tend to form as crystallographically parallel aggregates, and as a result iddingsite often inherits its structural orientation from the parent olivine (Brown & Stephen, 1959). This is evident from the straight extinction reminiscent of the parent olivines shown by iddingsite pseudomorphs in the Dilb and Iyela lavas.

Iddingsitization of olivines is a common feature of the lavas in many flood basalt provinces; however, its causes are either overlooked or are loosely attributed to weathering subsequent to the emplacement of the lavas. The presence of Fe-rich olivine overgrowths around iddingsitized olivines in the ankaramites and olivine basalts in the Dilb and Iyela sections, on the contrary, suggests that iddingsitization occurred at magmatic temperatures prior to eruption as a result of an increase in fO_2 associated with the introduction of water into the magma at shallow depths. Subsequent crystallisation of the fayalitic olivine overgrowths is likely to have occurred in the erupted lava following a dramatic drop in fO_2 associated with the rapid release of volatiles upon eruption (Fig. 4.64). This interpretation is in agreement with that proposed by Goff (1996) and Furgal & McMillan (2001) to explain iddingsitized olivines with faylalitic overgowths in basalts from the western United States and New Mexico respectively. Goff (1996) estimates eruption temperatures for the host-lavas from the western USA at ~ 1110 - 1235 °C, and it is proposed that iddingsitization of the constituent olivine phenocrysts occurred at oxygen fugacities of around 10^{-4}, when volatile contents were highest, just before eruption (Fig. 4.64). Since the olivine basalts from the Dilb Section show similar compositions to the host lavas analysed by Goff (1996) it may be expected that their cooling paths would be similar to the model shown in Figure 4.64. The cooling paths for the picritic and ankaramitic lavas from the Dilb Section might however be expected to lie someway to the right of this model because of their higher MgO contents which would give them respectively higher eruption temperatures. In a study of the fractionation processes and differentiated structures developed during the crystallisation of basalt in the 1959 Kilauea Iki lava lake, Hawaii, Helz (1987) estimates eruption temperatures as high as 1215 °C for picritic tholeiites similar in composition to the

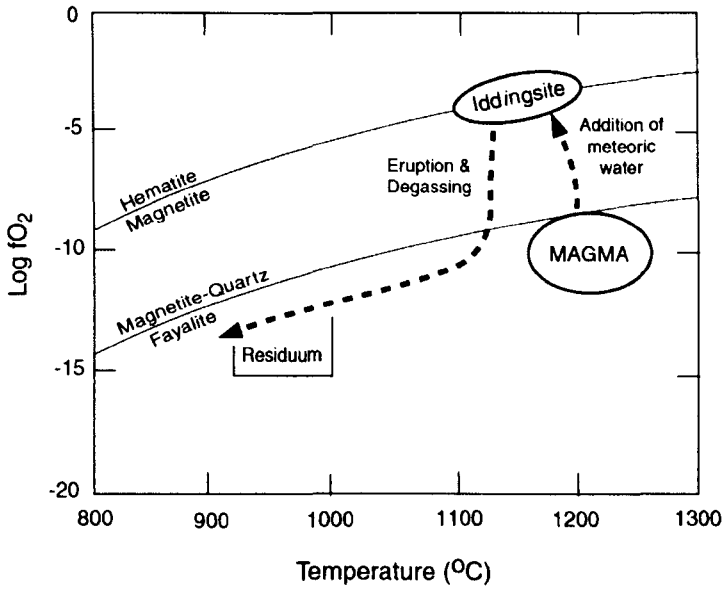

Figure 4.64 Plot of fO_2 versus temperature for diktytaxitic basalts containing vesicle cylinders and high temperature iddingsite. Introduction of meteoric water into the magma creates unusually high fO_2 so that olivine becomes altered to iddingsite. Following eruption, the fO_2 in the lava drops dramatically as volatiles are released. Thereafter, fO_2 in the differentiated liquids of vesicle cylinders and sheets parallel the QFM buffer with falling temperature (after Goff, 1996).

picrites from the Dilb Section. Low density melts generated during fractional crystallisation of these magmas formed at 1145 - 1160 °C and the segregation veins formed from this differentiate are estimated to have liquidus temperatures 1135 - 1105 °C. At temperatures between 1085 and 1070 °C, liquid compositions in the segregation veins begin to diverge from those in the host, and the liquidus temperatures for the most highly differentiated liquids derived from continued fractionation of these divergent liquids are estimated to be between 1085 1070 °C.

Goff (1996) and Furgal & McMillan (2001) propose that the source of the water responsible for raising the fO_2 of the magmas evident from the replacement of olivine by iddingsite and the unusually high volatile release in the cylinder-bearing lavas, was meteoric in origin. Either this water was drawn down into shallow seated chambers, or regions of fractured crust, where it could interact with the fractionating magma stalled there, or it may have simply represented the natural zone of groundwater penetration into which the magmas ascended. As a consequence the magma would have become relatively more oxidising at a late stage in its evolution just prior to eruption. Under these conditions, already formed olivine phenocrysts would no longer have been in equilibrium with ambient conditions in the magma chamber and would therefore have been partially or totally oxidised to iddingsite

depending on their degree of exposure to such conditions. It is notable in, the Dilb Section, that the the olivine phenocrysts in the olivine basalts are almost all entirely replaced with iddingsite, and as a consequence they appear as friable rusted brown pseudomorphs which are often partially removed by preferential weathering (Appendix 3.1). Iddingsitization of the olivines in the ankaramites and picrites, on the other hand, is confined to the rims of the crystals, and, in some cases, is barely evident in hand-specimen. It may be assumed then that the olivine basalts spent a significant amount of time equilibrating to conditions in the magma chamber before being erupted, and that the ankaramites and picrites either bypassed the magma chamber, or ripped quickly through it during their ascent to the surface. Even if the picrites, which represent the most unaltered of the lava types from the Dilb Section, did not pass through the magma chamber on their way to the surface, it is still likely that they were exposed to some level of oxidising conditions en route since, if water was able to make its way down to the magma chamber, then it was likely that the crust was saturated with meteoric water. This is evident from the fact that all the lavas, including the picrites, show some degree of iddingsitization. As a general rule, the more evolved lavas show higher degrees of iddingsitization to the extent that the degree of iddingsitization in the lavas may be used as a rough estimate of the relative amount of time they interacted with water in the magma chamber prior to eruption.

It is possible that some of the peaks and troughs observed in the zoning profiles of clinopyroxene phenocrysts described earlier, particularly those accompanied by in increase, or sudden appearance in the profile, of Fe_2O_3, may be associated with the same influxes of water into the magma responsible for the iddingsitization of the olivines. In the same respect it may be assumed that the iddingsite rims around olivines in the picrites are also of magmatic origin despite the fact that they are not overgrown with fayalitic olivine. This is supported by the fact the groundmass of the picrites, like that of the ankaramites and olivine basalts is not affected by weathering or by oxidation from hydrothermal activity at the surface that might otherwise account for the effects of iddingsitiztion in the picrites. The absence of fayalitic overgrowths in similarly iddingsitized basalts in New Mexico is attributed by Furgal & McMillan (2001) to the fact that their source magmas were too evolved to crystallise such overgrowths. The less evolved compositions of the picrites compared to the ankaramites and olivine basalts in the Dilb and Iyela sections discounts this as a possible explanation for the absence of fayalitic overgrowths in the picrites. Instead it is proposed that the high normative olivine contents of the picritic magmas were exhausted by the rapid crystallisation of skeletal olivine phenocrysts prior to iddingsitization so that the

erupted melts were incapable of further crystallisation of olivine necessary for the formation of the overgrowths.

The effects of serpentinization differ from those of iddingsitization in that they are only seen in selected lava flows and are often confined to localised areas within these lavas flows. Furthermore, whereas the effects of iddingsitization are confined to the phenocrysts, the effects of serpentinization are seen in the groundmass as well as in the phenocrysts of the lavas in which they occur (Section 4.3.2). It is likely therefore that serpentinization in the lavas was caused during eruptive events by the permeation of associated thermal waters into the already emplaced and variably cooled lavas immediately adjacent to the source of the eruption. The hydrothermal fluids responsible for the serpentinization were probably meteoric-derived groundwater either drawn into the magma and released as steam during eruption, or heated by the lava during its ascent and eruption on to the surface. Serpentinization is a relatively low temperature retrograde alteration process that, like iddingsitization, affects only those minerals such as olivine that particularly reactive under hydrothermal conditions. Experimental data and thermodynamic calculations indicate that olivine is unstable in the presence of water below 350°C at 300 bars (Chernosky et al. 1988), and as a result of its reaction with water at 300°C at such pressures olivine will irreversibly dissolve and transform to an assemblage of serpentine, brucite and magnetite (Normand et al. 2002). Most of the Fe in the olivine is incorporated separately into magnetite or hematite and so does not enter the structure of the serpentine (Deer et al. 1999). The effects of serpentinization in the Dilb and Iyela lavas are similar to iddingsitization in that they are generally confined to the margins of olivine phenocrysts (Fig. 4.21). In some cases the interior of the olivines have been serpentinized where the hydrothermal waters have been able to penetrate their structure along weakness opened up by iddingsitization. This gives the false impression that such phenocrysts were serpentinized prior to iddingsitization (Fig. 4.21b). In the olivine phenocrysts which have been less pervasively iddingsitized the remnant olivine within the iddingsite rims has been replaced by serpentinite to form secondary rims around the iddingsite (Fig. 4.21a). The separate growth of magnetite or hematite from the Fe liberated from the olivine during serpentinization is evident from the clusters of prismatic Fe-oxides often seen ungulfed in the altered margins of the phenocrysts (Fig. 4.21c).

Low temperature (< 200°C) hydrothermal activity associated with the permeation of late-stage fluids through the lavas after their emplacement is evident from the

widespread deposition of zeolites in vesicles and cavities (Fig. 4.20), and from the zeolitization of selected minerals in the groundmass of many of the lavas (Fig. 4.22). Zeolitization is typically associated with the waning stages of volcanic activity and is considered to be indicative of near-surface water-saturated conditions. Mammilated zeolitic crusts exhibiting growth rings (Fig. 4.20b) evident in some vesicles imply that such activity was recurrent rather than continuous, and in this respect it is likely to have occurred to one degree or another following each effusive event. The variety of types of zeolite encountered in lavas (Appendix 4.1), furthermore suggests that the temperature and composition of the hydrothermal fluids varied from one event to the next depending on the temperature, composition and water content of the lava, and the volume erupted.

4.5.4 Temperature and oxygen fugacity

References in this discussion to temperature, depth and oxygen fugacity have so far been relative, and have been loosely based on differences in mineral chemistry which may not necessarily be as meaningful as implied. It is, however, critical to obtain more quantifiable estimates of such parameters in order to make more realistic assumptions regarding the petrogenesis of the lavas. Accurate estimates of temperature are primarily important in determining the depth and pressure of crystallisation, which in turn are essential for the determination of oxygen fugacity. Oxygen fugacity ($fO2$) reflects the oxidation state of the magma, and together with temperature it can provide insight into processes such as metasomatism, degassing and assimilation that may have affected the magma during its ascent to the surface (Brandon & Draper, 1996; Ague, 1998; Frost & Ballhaus, 1998; Parkinson & Arculus, 1999). Moreover, these variables control the sequence of crystallisation and the composition of the resultant minerals. Such relationships have been explored in a variety of rock types by experimental work and a number of geothermometers and geobarometers have been developed from the results of such work.

Temperature: The most reliable and widely applied geothermometers for basaltic rocks use the partitioning of Mg and Fe^{2+} between coexisting olivine and glass (Roeder and Emslie, 1970; Ulmer, 1989) or the partitioning of Ca, Mg and Fe^{2+} between coexisting Ca-rich and Ca-poor pyroxenes (Lindsley, 1983; Davidson & Linsley, 1989), or the exchange of Fe^{2+}, Ti^{4+} and Fe^{3+} between ilmenite and titanomagnetite (Buddington & Lindsley, 1964). Unfortunately, because of the lack of fresh glass, coexisting orthopyroxene and suitable Fe-Ti oxide pairs these geothermometers could not be applied to the Dilb and Iyela lavas; consequently,

alternative geothermometers were used in an attempt to determine crystallisation temperatures for specific mineral phases within the lavas.

Temperatures for olivine crystallisation were calculated from the paired compositions of spinel inclusions and their host olivines using the Fe-Mg olivine-spinel exchange geothermometer described by Ballhaus et al. (1991). Details of these calculations for pressures of 0.001, 0.5 and 1.2 GPa are outlined in Appendix 4.6, and the temperatures obtained were compared with those calculated from the same paired compositions using the published software PTMAFIC (Soto & Soto, 1995). Consistently higher temperatures calculated using the spreadsheet in Appendix 4.6 compared to those calculated with PTMAFIC reportedly using the same method outlined by Ballhaus et al. (1991) are attributed to the use of modified equations for the calculation of selected molar fractions. PTMAFIC includes Mn and Zn in the calculation of molar fractions for Fe^{2+} and Mg, and Ti in the calculation of molar fractions for Al, Ti, Cr and Fe^{3+} for spinel, whereas the spreadsheet in Appendix 4.6 uses unmodified equations from Ballhaus et al. (1991a, 1991b & 1994) as shown (Appendix 4.6). Despite these differences, both versions show a similar increase in temperature with pressure of about 1.2 °C per kb, which amounts to a relatively insignificant difference of between 11 and 15 °C for near surface pressures compared to those beneath thick crust.

Temperature estimates for olivine crystallisation calculated by both methods show an unexpected general decrease with Mg# of the host olivines suggesting that the mineral pairs are not in equilibrium - as already been implied from the irregular variation in Mg# for the spinel inclusions and host olivines (Fig. 4.62). The low temperatures yielded by both methods may be attributed to faster re-equilibration rates for the spinel inclusions compared with their olivine hosts (Carmichael, 1967; Scowen et al. 1991). This is consistent with the idea that many of the olivine phenocrysts in the lavas were inherited from magmas that partially crystallised at deeper levels than the magmas from which the erupted lavas were derived. Unrealistically low crystallisation temperatures for clinopyroxene estimated relative to experimentally determined isotherms for 1 atm – 5 kb after Lindsley (1983) suggest the same may be true for many of the clinopyroxene phenocrysts. More realistic temperatures for clinopyroxene crystallisation are obtained using a single clinopyroxene geothermometer (Appendix 4.7.1). Temperatures calculated using this geothermometer are based on the Fe/Mg ratios of clinopyroxene in relation to a fixed molar fraction for Ca of 0.37. Such a fixed molar fraction for Ca is fairly

representative of the majority of phenocrysts (Appendix 4.7.1) and is relatively consistent with the limited range of Ca contents of the phenocrysts from the picrites and ankaramites over a temperature range between 1160 and 1230 °C. The lower temperatures (Temp. 1) exhibit a more realistic range than the higher temperatures (Temp. 2), and are more in-line with those calculated from normative compositions (Appendix 5.4) and with MELTS models generated from whole-rock geochemistry (Appendix 5.7). Discreet linear arrays shown by the variation of Si, Al and Ti with temperature for each group generally indicate higher crystallisation temperatures for the clinopyroxene phenocrysts from the picrites compared to the ankaramites and olivine basalts respectively, although the highest overall temperatures are for phenocrysts from the ankaramites (Figs 4.65c - e). If temperature is equated with depth, then the highest temperatures for the ankaramites (1229 °C) suggest that clinopyroxene crystallisation began in the ankaramites at deeper levels than in the picrites (1214 °C). This might be because the ankaramitic magmas were stalled at depth for long enough periods to allow for such crystallisation, whereas the picritic magmas ascended so quickly toward the surface that they were able to reach shallower levels where they were able to lose heat before clinopyroxene began crystallising. Alternatively, the ankaramitic phenocrysts which show the highest calculated temperatures may simply have been inherited from the picritic magmas. Crystallisation of clinopyroxene in the olivine basalts is likely (as indicated in Figure 4.65) to have begun at lower temperatures (1192 °C) at shallower levels than in the ankaramites and picrites.

The temperature variation with composition for the clinopyroxene phenocrysts from each lava group (Fig. 4.65) suggest that they either crystallised at varying depths and/or at varying stages of fractionation as the magma cooled prior to or after eruption. A relatively continuous record of such magmatic evolution is similarly reflected in the same co-variation in temperature and composition shown by temperature profiles from core to rim across selected clinopyroxene phenocrysts (Fig. 4.66) and their respective compositional zoning profiles (Fig. 4.56). In particular, the profile for CPX4 from the ankaramite 01.03.24.09 shows a similar range in temperature (1229 – 1156 °C) and composition from core to rim to that for the core compositions of all the phenocrysts from the ankaramites (Fig. 4.65). Similarly, the range in temperature and composition from core to rim shown by OP1 and CPX1 from the olivine basalt 01.03.24.06 can be seen to be remarkably concordant with that of the core compositions of all the phenocrysts from the olivine basalts. This suggests that these primary zoned phenocrysts continued to grow alongside new

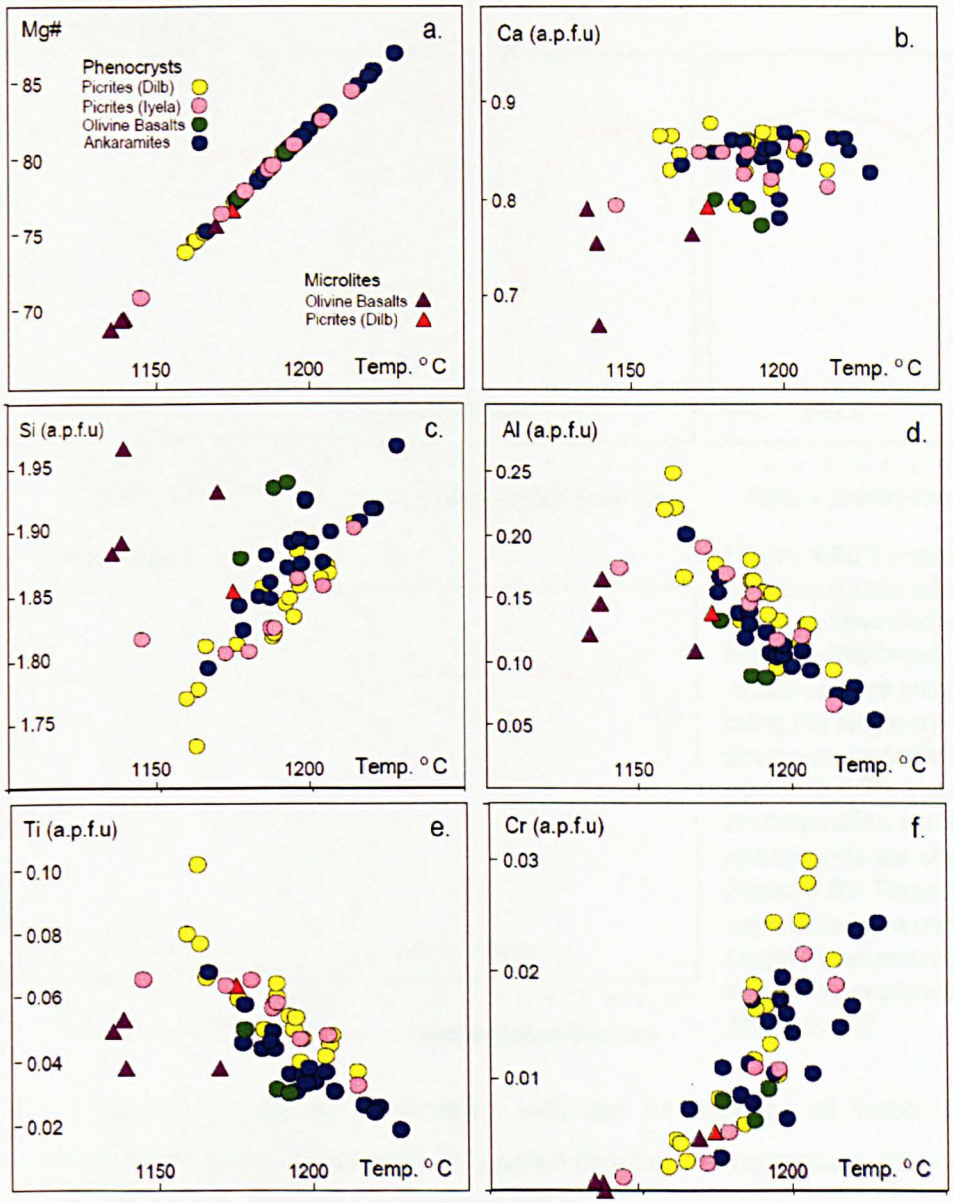

Figure 4.65 Compositional variation with temperature for clinopyroxene phenocrysts and groundmass microlites from the Dilb and Iyela lavas. Temperatures were calculated using the single clinopyroxene geothermometer shown in Appendix 4.7.

phenocrysts as the magma evolved. Moreover, the lower and more limited range in the temperature shown by both the zoning profiles and the core compositions of the phenocrysts from the olivine basalts compared to those from the ankaramites suggests that clinopyroxene crystallisation in the olivine basalts began at lower temperatures than in the ankaramites; it may therefore be assumed that the olivine basalts were sourced from shallower depths than the ankaramites, as previously implied. The pronounced temperature troughs seen in some of the profiles coincide with an increase in Al, Ti, Na and Fe^{3+} and an antithetic decrease in Mg, Ca, Si and Ni. The sudden drops in temperature coincident with the appearance of Fe_2O_3 in the

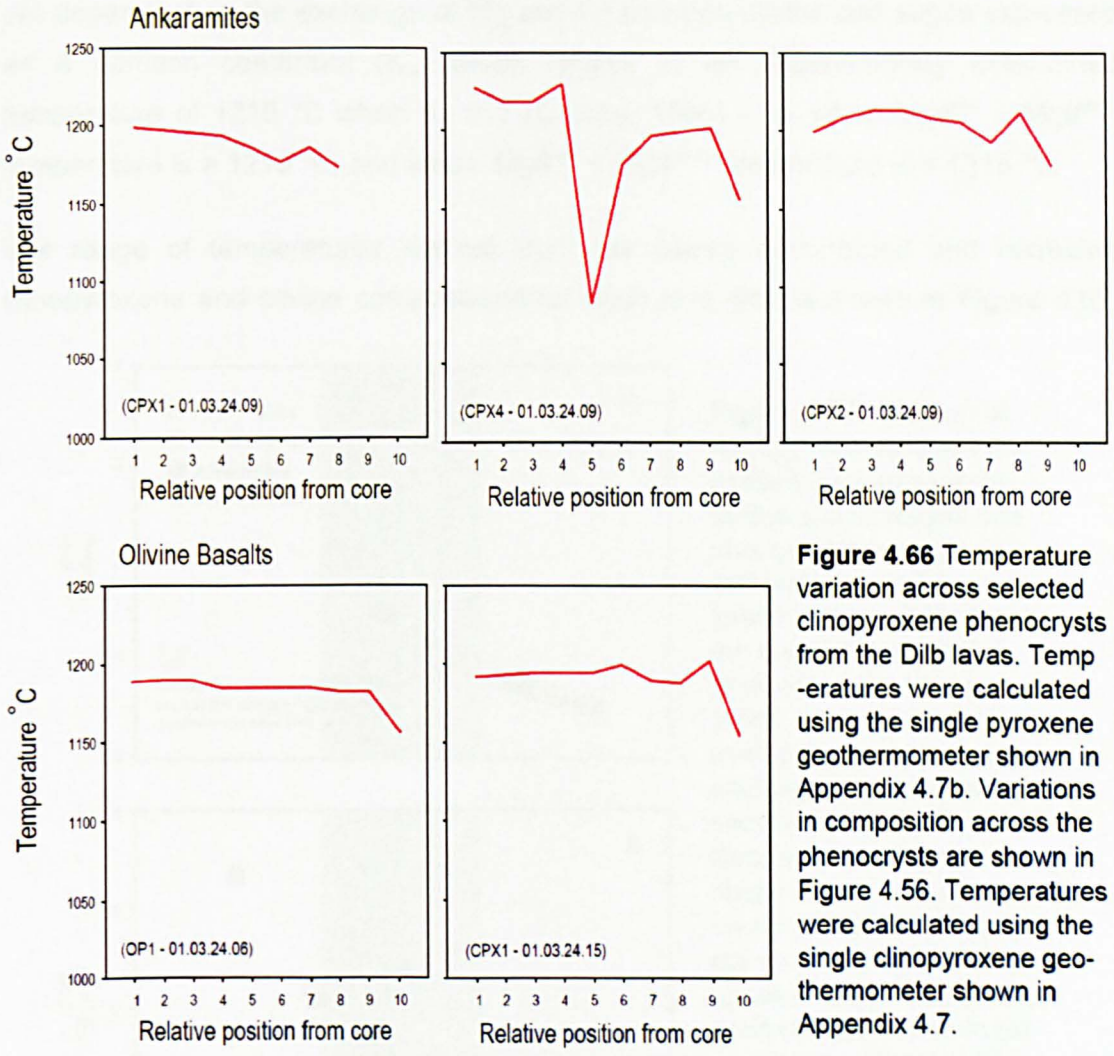

Figure 4.66 Temperature variation across selected clinopyroxene phenocrysts from the Dilb lavas. Temp -eratures were calculated using the single pyroxene geothermometer shown in Appendix 4.7b. Variations in composition across the phenocrysts are shown in Figure 4.56. Temperatures were calculated using the single clinopyroxene geo-thermometer shown in Appendix 4.7.

profiles, in particular, may be associated with the introduction of water into the magma and the consequent increase in oxygen fugacity. Temperature estimates for the groundmass clinopyroxene microlites may be assumed to be representative of erupted lavas. Those calculated from the microlites from the olivine basalts range from 1134 – 1168 °C whereas the only microlite analysed from the picrites yields a slightly higher temperature of 1174 °C.

Temperature estimates for the co-precipitation of olivine and clinopyroxene in the lavas were calculated using the olivine-augite geothermometer described by Loucks (1996). Olivine/clinopyroxene-pairs with the highest and lowest Mg# from each representative sample were selected to give the range of possible temperatures over which co-precipitation of these minerals occurred. Co-precipitation temperatures were calculated using both uncorrected and corrected clinopyroxene analyses to illustrate possible differences associated with the oxidation state of the magmas (Appendix 4.8.1). Temperatures calculated using the olivine-augite geothermometer

are dependent on the exchange of Mg and Fe between olivine and augite expressed as a partition coefficient (K_D) which relates to an experimentally determined temperature of 1218 °C when K_D = 1 (Loucks, 1996) - i.e. when $Mg\#^{(ol)} > Mg\#^{(cpx)}$ temperature is > 1218 °C, and when $Mg\#^{(ol)} < Mg\#^{(cpx)}$ temperature is < 1218 °C.

The range of temperatures derived from the paired uncorrected and corrected clinopyroxene and olivine compositions for each lava type is shown in Figure 4.67.

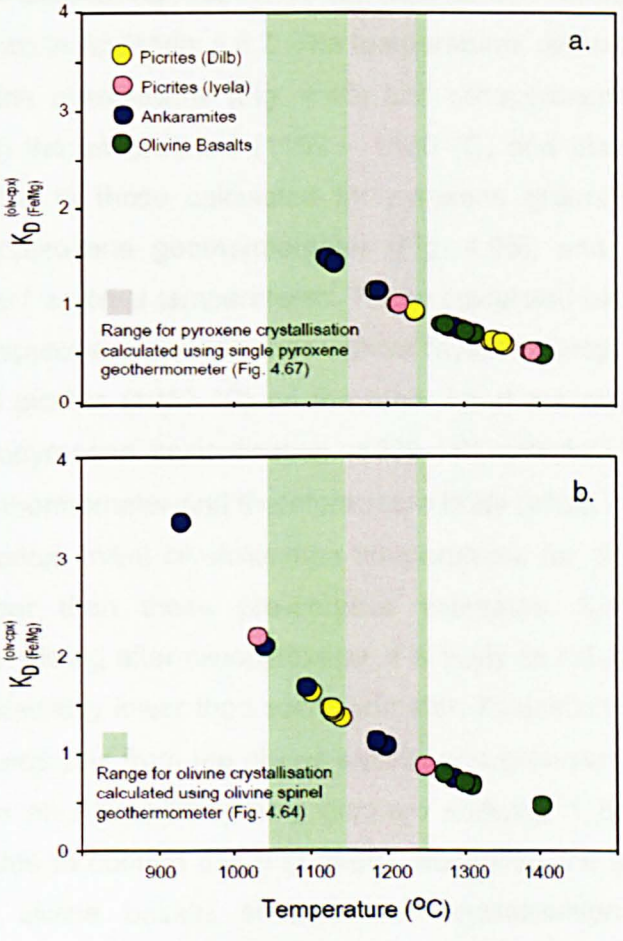

Figure 4.67 Variation of $K_{D\,(Fe/Mg)}^{(olv\text{-}cpx)}$ with temperature derived from co-existing olivine and clinopyroxene phenocrysts from the Dilb and Iyela lavas. Temperatures were calculated using the method illustrated in Appendix 4.8 (Loucks, 1996). Olivine-clinopyroxene pairs with the highest and lowest Mg# from each sample were selected to illustrate the temperature range of temperatures for each lava group. Temperatures calculated from the uncorrected clinopyroxene analyses are shown in (a), and those calculated from the corrected analyses are shown in (b).

Excessively high co-precipitation temperatures, particularly for the olivine basalts, may be attributed to the inappropriate compositional pairing of clinopyroxene phenocrysts with inherited olivine phenocrysts with higher Mg# than would be expected for coexisting olivine. Likewise, the excessively low temperatures (particularly those calculated from the corrected clinopyroxene analyses) may be attributed to inappropriate compositional pairing of olivine phenocrysts with inherited clinopyroxene phenocrysts with higher than ambient Mg#. In this sense the use of the olivine-augite geothermometer in determining accurate temperatures for the co-precipitation of olivine and clinopyroxene in lavas with such a mix of phenocrysts may

be considered inappropriate. It does, however, provide indirect evidence for mixed phenocryst assemblages.

The olivine-augite geothermometer may be more reliably used to estimate late-stage co-precipitation temperatures from the compositions of the rims of coexisting olivine and clinopyroxene since these are more likely to have crystallised from the same late-stage melts either just prior to, or immediately after, eruption. Such temperature estimates for representative samples for each of the lava types in the Dilb section are shown in Appendix 4.8.2. The temperatures derived from the compositions of fayalitic olivine overgrowths (Fig. 4.48) and clinopyroxene rims (Fig. 4.56) in phenocrysts from the ankaramites (1159 – 1160 °C) and olivine basalts (1130 – 1143 °C) are similar to those calculated for pyroxene groundmass microlites using the single clinopyroxene geothermometer (Fig. 4.65), and therefore may be considered to reflect eruptive temperatures. Those calculated using the compositions of the rims of clinopyroxenes and olivines without fayalitic overgrowths in the ankaramites (1227 °C) and picrites (1232 °C) on the other hand are close to the highest temperature for clinopyroxene crystallisation (1228 °C) calculated using the single clinopyroxene geothermometer and therefore more likely reflect crystallisation temperatures prior to eruption. Initial crystallisation temperatures for olivine must have been appreciably higher than these pre-eruptive estimates. Similarly, since plagioclase began crystallising after clinopyroxene, it is likely its initial crystallisation temperatures were appreciably lower than such estimates. Projection of the compositions of plagioclase phenocrysts from the olivine basalts and groundmass microlites from each lava type onto an Ab-An-Or ternary diagram showing 1 bar feldspar solvi (Nekvasil, 1992) seems to confirm this (Fig. 4.68). Moreover, the fact that the two phenocrysts from the olivine basalts show similar crystallisation temperatures to those of the groundmass microlites suggest that they crystallised in the erupted lava as previously suggested from textural evidence (Section 4.5.3).

Oxygen Fugacity: Since iron is the only major rock-forming element in basalts to exist in multiple valence states it is frequently used to assess fO_2. The most commonly used methods to quantify fO_2 utilize the ferric content of glasses (Sack et al. 1980; Kilinc et al. 1983; Kress & Carmichael, 1988) or coexisting Fe-Ti oxides (Sack & Ghiorso, 1991); however because of the absence of fresh glass and suitable coexisting Fe-Ti pairs in the Dilb and Iyela lavas such methods could not be used. Instead, the semi-empirical olivine-spinel oxygen geobarometer described by Ballhaus et al. (1991) was used to estimate fO_2. This geobarometer relies on the

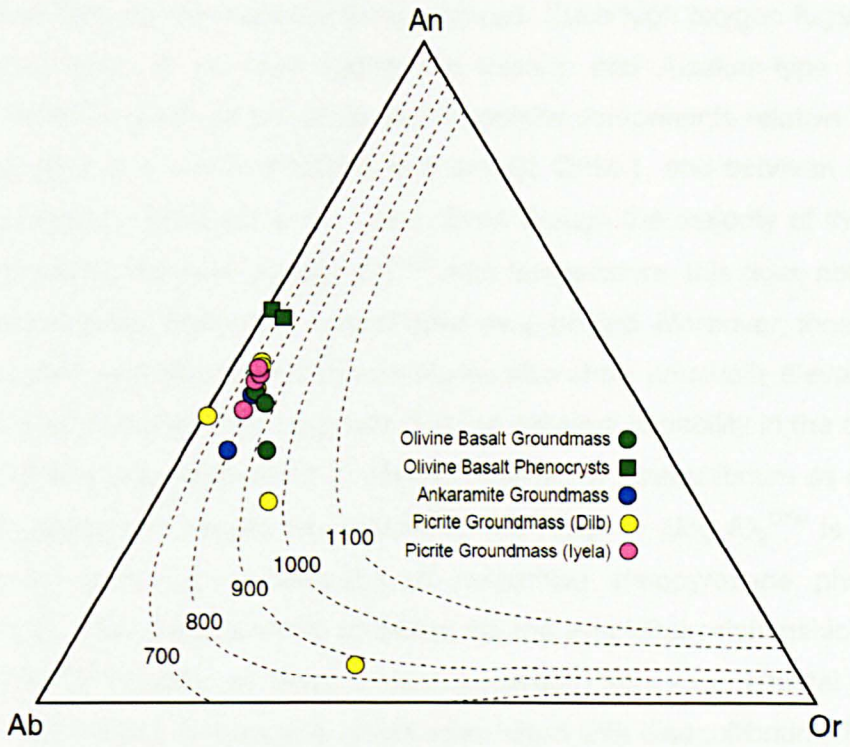

Figure 4.68 Ab-An-Or ternary diagram showing the compositions of feldspar phenocrysts and groundmass microlites for the Dilb and Iyela lavas relative to the 1 bar feldspar solvi (Nekvasil, 1992).

equilibrium between olivine, orthopyroxene, spinel and oxygen relative to the quartz-fayalite-magnetite buffer (QFM) widely used as a monitor of the oxidation state of the Earth's mantle; therefore, the calculated fO_2 represents the oxidation state of the magma at temperatures at which olivine and spinel equilibrated. In this sense, it is potentially more useful than the other geothermometers listed above since they all rely on the composition of groundmass components which record the final oxygen fugacity of the magma after the removal of previously crystallised phases at eruption rather than crystallisation temperatures.

Oxygen fugacities for representative samples of each lava type were calculated from the paired compositions of spinel inclusions and their host olivines for pressures of 1 atm, 0.5 GPa and 1.2 GPa respectively using the temperatures derived from the olivine-spinel geothermometer (Appendix 4.6). Although there is a discernable and consistent increase in fO_2 with pressure, this is relatively insignificant over the temperature range shown by the lavas; therefore, for convenience, fO_2 is referred here relative to the QFM buffer ($\Delta\log fO_2^{QFM}$) at a pressure of 1 atm. This effectively renders the calculated fO_2 virtually independent of pressure and temperature (Parkinson & Arculus, 1999). Generally, the lavas show an increase in fO_2 with temperature, and a range in fO_2 between 1 and 3.5 log-units above the QFM buffer

indicating that their source magmas were oxidised. Such high oxygen fugacities are generally only seen in primitive island arc basalts and Alaskan-type intrusives typically enriched in magnesiochromite and magnetite components relative to MORB - fO_2 for depleted and enriched MORB plot around QFM-1, and between QFM and QFM+1 respectively (Ballhaus et al. 1991). Even though the majority of the dataset shows a predictable increase in $\Delta\log fO_2^{QFM}$ with temperature, this does not coincide with an increase in the Mg# of the host olivines as expected. Moreover, those mineral pairs that yielded anomalously low temperatures also show unusually elevated fO_2 in relation to the QFM buffer. This suggests that the extreme variability in the calculated fO_2 is not real and may attributable to varying degrees of disequilibrium as described above for temperature. Despite this variability, the range in $\Delta\log fO_2^{QFM}$ is similar to that calculated from the composition of respective clinopyroxene phenocrysts (Appendix 4.9). This oxybarometer is based on the empirical relationship between fO_2 and the $Fe^{3+}/\sum Fe$ ratio of clinopyroxene generated from experimental data, and is therefore not subject to the same errors associated with disequilibrium. Therefore, even though the potential errors for both methods are large, the fact that most of the data plot above QFM+1 suggests at least that the majority of the olivine and clinopyroxene phenocrysts crystallised from oxidised magmas.

Higher overall fO_2 shown by the olivine-spinel pairs compared to the clinopyroxene phenocrysts implies that fO_2 was higher during the early stages of olivine crystallisation than it was during the later stages of fractionation when clinopyroxene crystallised. This suggests that the oxidising source was deep-seated. The fact that the clinopyroxene phenocrysts in the shallow-sourced olivine basalts contain little or no ferric iron (i.e. close to QFM), whereas those in the deeper-sourced picrites show the highest ferric iron contents (Fig. 4.55) and estimated fO_2 values (Appendix 4.9) (i.e. > QFM+1) seem to support this. It is still debatable whether or not the oxygen fugacity in the Dilb and Iyela lavas is related more to the composition of the magma than to its temperature (as is more often considered to be the case in theoretical studies). It is, however, likely that the range in fO_2 shown by the lavas reflects the mixing of magmas carrying phenocrysts that crystallised at varying depths from variably oxidised and evolved melts.

5. MAJOR AND TRACE ELEMENT COMPOSITIONS

5.1 Introduction

5.1.1 Rationale

The chemistry of magmatic rocks is fundamentally controlled by the composition and mineralogy of the primary melt source region, the type of melting process, the degree of partial melting, and the extent to which the primary melt has been modified en-route to the surface by a variety of high-level processes including fractional crystallisation, magma mixing and crustal contamination. The primary melt source region is best characterised by its radiogenic isotope composition since this is generally not modified by during partial melting and magmatic processes (Chapter 6). For similar reasons it may be argued that the concentration ratios of selected trace elements also reflect the composition of the source because of their highly incompatible behaviour (Hofmann, 1997). With reference to experimental work and theoretical models further constraints may be placed on the composition of the parent melt and the temperatures and pressures at which partial melting occurred using the major and trace element compositions of magmatic rocks. Similarly, trends in the major and trace element composition of a suite of magmatic rocks may also be used to identify evolutionary processes that have modified the primary magma prior to, and possibly after, eruption at the surface or cooling within the crust. Moreover, major- and trace-element chemistry may be used in conjunction with the mineral chemistry of cumulate phases in a suite of magmatic rocks to further constrain the nature and composition of the primary melt and how it may have been modified by magmatic processes. In addition, major- and trace-element compositions may be used to classify magmatic rocks so that they may be compared with those characteristic of similar or contrasting tectonic environments, and their commonly associated source regions.

The major and trace element contents of all the rocks from the sampled sections described in Chapter 3 were analysed by XRF and ICPMS respectively, but for the reasons outlined in Section 4.1.1, the presentation and interpretation of these analyses presented in this chapter is focused on the lavas from the Dilb and Iyela sections. This focus enables more rigorous constraints to be placed on the petrogenesis of the lavas described Chapter 4, both in terms of the nature and composition of the primary magma and the role of magmatic processes in generating the range of rock-types seen in these stratigraphically related sections.

5.1.2 Sample preparation

Prior to preparing the samples for major and trace element analysis, it was necessary to produce fine (< 60 μm) representative rock powders of all the rocks from the sampled sections. This was done following the procedure described in Appendix 5.1.1. Sample preparation for major element analysis by XRF involved the production of glass fusion discs and for trace element analysis by XRF the production of compressed powder pellets; both methods, together with the strategy adopted for analytical control, are described in Appendix 5.1.2 and 5.1.3 respectively. For trace element analysis by ICPMS, rock-powders were digested in a mixture of concentrated HF and HNO_3, refluxed in HNO_3 and subsequently dissolved in a 2% solution of HNO_3; this procedure, and the strategy adopted for analytical control, is described in Appendix 5.1.4.

5.1.3 Instrumentation and analysis

Major and selected trace element analyses by XRF were carried out on an ARL 8420+ dual goniometer wavelength dispersive XRF spectrometer at the Open University. A brief description of the technique, together with details of the analytical procedure, instrumentation, operating conditions, calibration and on-line data processing are given in Appendix 5.2.1. The raw and compiled analyses and associated percentage uncertainties and percentage errors calculated from the analyses of standard reference materials and procedural duplicates are presented in Supplements 2 and 3 as indicated in Appendix 5.2.1.

Trace element analyses by ICPMS were carried out on an Agilent 7500 Series inductively coupled plasma mass spectrometer at the Open University. A brief description of the technique, together with details of the analytical procedure, instrumentation, operating conditions, calibration and on-line data processing are given in Appendix 5.2.2. The raw and compiled analyses and associated percentage uncertainties and percentage errors calculated from the analyses of standard reference materials and procedural duplicates are presented in Supplement 4 as indicated in Appendix 5.2.2.

The trace element analyses determined by both analytical methods show almost perfect correlations, although the accuracy and precision between different elements, and between methods and reference materials, is variable (Supplement 4c). Generally however the analyses determined by ICPMS show better overall accuracy and precision for all elements compared to those determined by XRF. For this reason,

the trace element analyses determined by XRF were used for nothing more than an additional check on the procedural and analytical accuracy and precision for ICPMS. Major and trace element analyses for each section are compiled in sample number order according to rock-type in Appendix 5.3.1; those elements showing above 2% uncertainty or unreasonable percentage errors (generally taken as > ± 2 %) were not included. The percentage uncertainties and errors for all included major and trace element analyses are shown in Appendix 5.3.2 and 5.3.3 respectively – uncertainties (expressed as % rsd) are shown for both selected standards and procedural duplicates.

5.2 Major and trace element geochemistry

5.2.1 Classification

For the purposes of preliminary classification, all sampled rocks from each section are plotted on a variation diagram of total alkalis versus silica overlain with the widely used taxonomic framework of Le Maitre et al. (1989) (Fig. 5.1). As well as providing the basis on which the rock-types from each section were grouped, this diagram illustrates the broad and dispersed variation in the composition of the volcanic and intrusive rocks between the sections, and the relative coherence of the lavas of the Dilb and Iyela sections compared to those of the other sections. The distinction between the three lava groups from the Dilb and Iyela sections is clearly evident on a SiO_2 versus total alkalis diagram (Fig. 5.2a). The picrites (classified on the basis that they have > 12 % MgO and a phenocryst population dominated by olivine) and the olivine basalts (with < 12 % MgO) straddle the alkaline-tholeiitic compositional divide from the picrite to basalt field. The ankaramites (classified as such because of the dominance of clinopyroxene in the phenocrysts assemblage despite the fact they have > 12 % MgO), on the other hand, plot within the basalt field at an angle to the alkaline-tholeiitic divide on account of their relatively higher SiO_2 contents. The alkaline affinity shown here by the majority of the picrites was noted earlier from the compositions of their clinopyroxene phenocrysts (Fig. 4.53) and the presence of K-feldspars in their groundmass. Pik et al. (1998) report similar characteristics for the HT1 and HT2 basalts. Despite this, the Dilb and Iyela lavas together display a distinctive tholeiitic differentiation trend on an AFM diagram, particularly when seen in relation to the more evolved rhyolitic ignimbrites on top of the Dilb Section (Fig. 5.2b). This dominantly tholeiitic affinity is also evident from the normative compositions of the lavas (Fig. 5.3) as well as from the compositions of the clinopyroxene

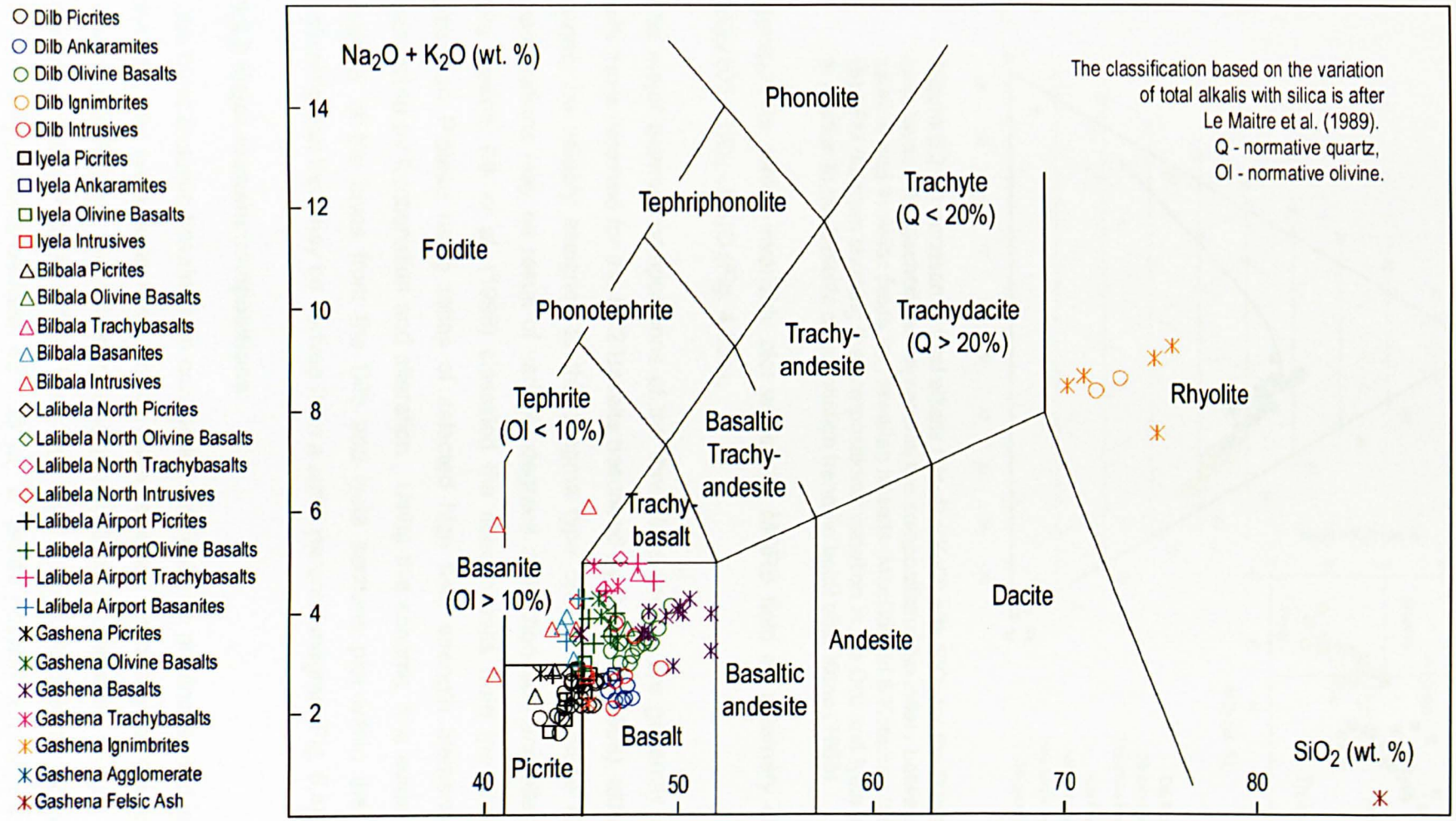

Figure 5.1 Classification of the volcanic, pyroclastic and intrusive rocks from the sampled sections

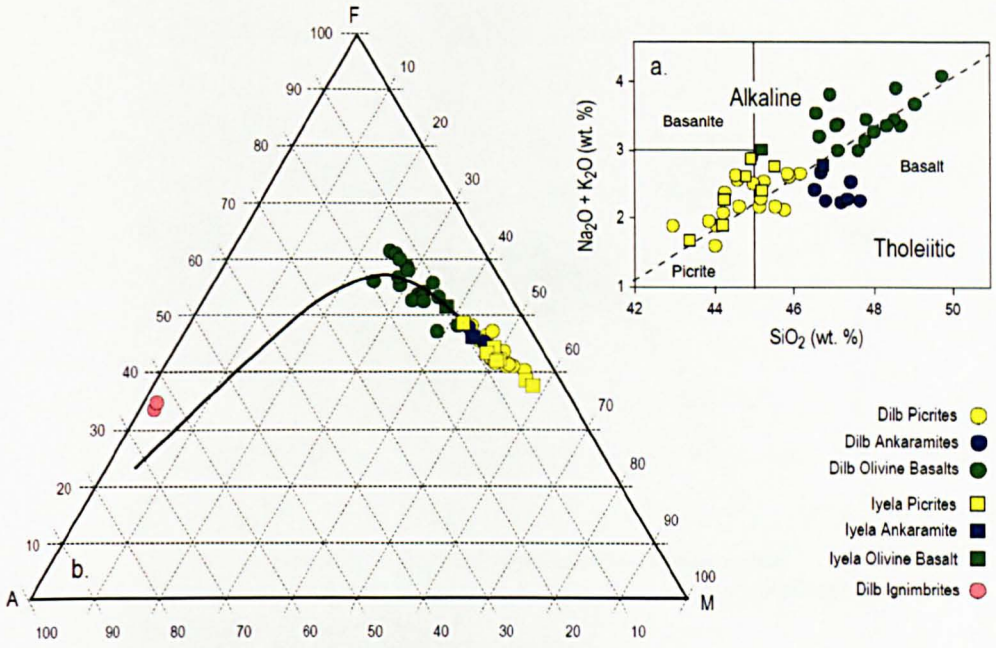

Figure 5.2 (a) Variation of total alkalis ($Na_2O + K_2O$) with SiO_2 for the Dilb and Iyela lavas - the dashed line represents the compositional boundary between the alkaline and tholeiitic fields for Hawaiian basalts (MacDonald & Katsura (1964). **(b)** AFM diagram showing the compositional variation in the Dilb and Iyela lavas in relation to the tholeiitc differentiation trend (in bold) after Kuno (1968).

phenocrysts, which invariably plot within the MORB field on a ternary diagram of $SiO_2/100$ - TiO_2 - Na_2O (Fig. 4.53a).

The major element compositions of the three lava groups are generally consistent with those reported for the HT2 Basalts described by Pik et al. (1998), although they cannot be reliably assigned to this magma type on this basis alone since such compositions may be result of variable degrees of fractionation and alteration. For this reason, Pik et al. (1998) classified the flood basalts from the north-western Ethiopian Plateau using ratios of selected high field strength elements typically unaffected by fractionation and alteration. Using this scheme, it is evident that the majority of the lavas from the Dilb and Iyela sections plot within the HT2 field indicating that they may be derived from a same parental magma (Fig. 5.4).

5.2.2 Major element compositions

Like most tholeiitic basalts from continental and oceanic provinces, and island arcs, the Dilb and Iyela lavas have similar major element chemistry to mid-ocean ridge basalts (MORB) but show higher concentrations of incompatible and LIL elements (including Ti and P, and K). They have high MgO contents between 6 - 22 wt. %, and limited SiO_2 contents between 43 - 50 wt. %. Broad positive correlations for Al_2O_3, Na_2O and K_2O with SiO_2 that mirror more significant negative correlations with MgO

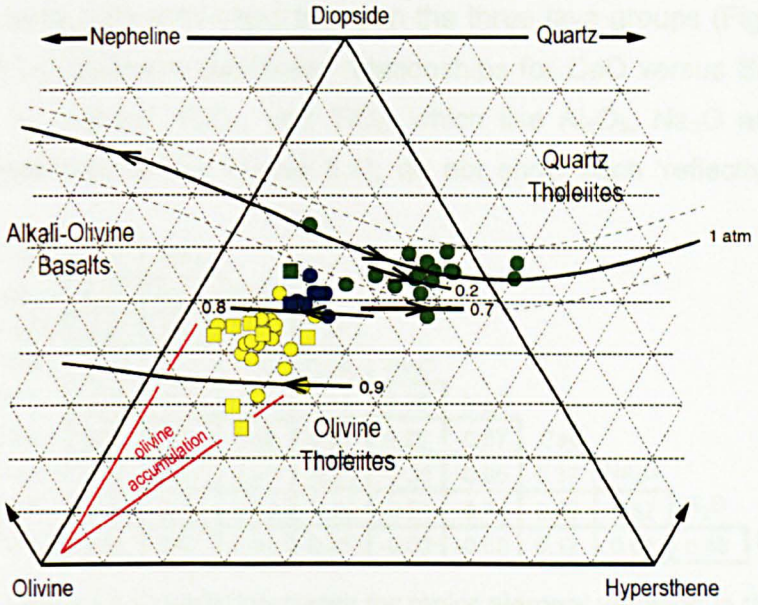

Key for Cotectics (represented by bold lines)
1 atm - compiled experimental dataset (Thompson et al. 2001)
0.2 and 0.8 Gpa - experimental data for MORB (Grove et al. 1992)
0.7 GPa - tholeiitic fractional crystallisation (Villiger et al. 2007)
0.9 GPa - experimental data for olivine tholeiites, alkali basalts and hawaiites (Thompson, 1982)

All cotectics are for the equilibrium assemblage olivine + plagioclase + clinopyroxene + basaltic melt except for the 9 kb cotectic which is for olivine + clinopyroxene = plagioclase

Figure 5.3 CIPW normative diopside, olivine, hypersthene, nepheline and quartz in the Dilb and Iyela lavas. Symbols are as in Figure 5.2. Normative compositions were calculated as described in Appendix 5.4. Cotectics for a range of pressures are shown by bold lines as indicated in the key, and the attached arrows indicate the directions of decreasing temperature. The 1 atm cotectic is the best-fit line through a compiled dataset, all of which falls within the dashed lines either side.

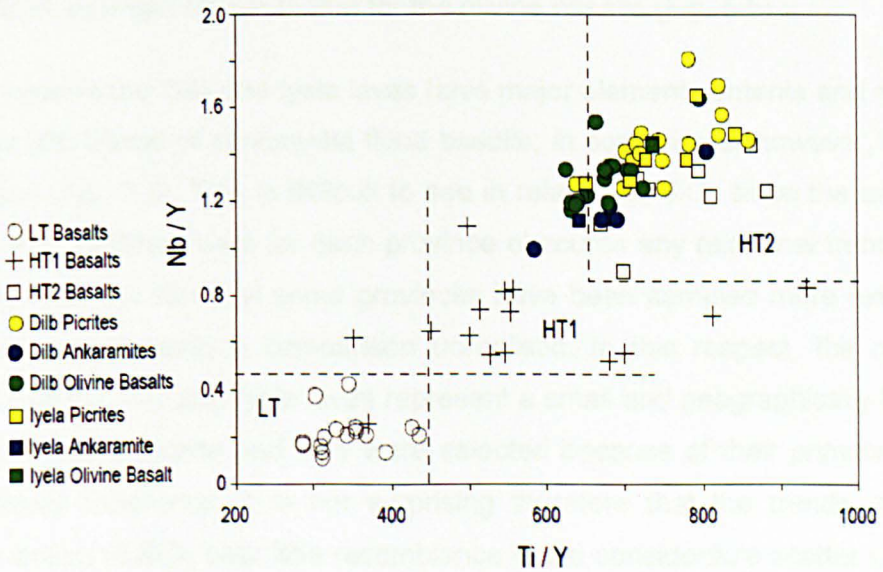

Figure 5.4 Nb/Y versus Ti/Y diagram showing the compositions of the Dilb and Iyela lavas in relation to the LT, HT1 and HT2 basalts from the north-western Ethiopian Plateau reported by Pik et al. (1998).

suggest colinearity both within and between the three lava groups (Fig. 5.5). This is evident also from antithetic curvilinear relationships for CaO versus SiO_2, and CaO versus MgO. In contrast, P_2O_5, and TiO_2, which like Al_2O_3, Na_2O and K_2O show strongly correlated behaviour (Table 5.1), do not show such 'reflective linearity' in

TiO_2	0.01	TiO_2								
Al_2O3	0.74	0.56	Al_2O3							
Fe_2O_3	-0.60	0.52	-0.22	Fe_2O_3						
MnO	-0.24	0.14	-0.17	0.64	MnO					
MgO	-0.73	-0.63	-0.96	0.10	0.06	MgO				
CaO	0.51	0.33	0.39	0.05	0.25	-0.57	CaO			
Na_2O	0.77	0.54	0.97	-0.26	-0.20	-0.95	0.37	Na_2O		
K_2O	0.69	0.39	0.72	-0.29	-0.21	-0.74	0.29	0.82	K_2O	
P_2O_5	0.09	0.87	0.63	0.35	-0.02	-0.63	0.17	0.62	0.46	P_2O_5

Table 5.1 Correlation matrix for major element variation in the Dilb and Iyela lavas

relation to SiO_2 and MgO. Instead, they are relatively constant with varying SiO_2 but negatively correlated with MgO. $Fe_2O_3^{(tot)}$ and MnO, on the other hand are relatively constant with respect to both SiO_2 and MgO. The olivine basalts generally show more scatter compared to the picrites and ankaramites for all major element variations, and this is most pronounced for $Fe_2O_3^{(tot)}$ and MnO. The SiO_2 plots are useful in that, unlike the MgO plots, they clearly distinguish the ankaramites from the picrites. This is best seen on the plots for Al_2O_3, Na_2O and K_2O where the ankaramites form a separate linear array which branches from the main trend for the entire suite at an angle similar to that for the olivine basalts (Fig. 5.5).

In many respects the Dilb and Iyela lavas have major element contents and relational trends that are typical of continental flood basalts; in some ways, however, they are quite unique (Fig. 5.6). This is difficult to see in relation to SiO_2 since the amount of scatter in the published data for each province obscures any relational trends which may exist. Also, the fact that some provinces have been sampled more extensively than others makes such a comparison unrealistic. In this respect, the reader is reminded that the Dilb and Iyela lavas represent a small and geographically localised part of their host province and they were selected because of their primitive nature and relational coherency. It is not surprising therefore that the trends described above in relation to SiO_2 bear little resemblance to the considerable scatter shown for the provinces represented in Figure 5.6. Major element trends in relation to MgO for the same provinces, however, show more pronounced linearity, particularly at higher MgO contents, and in this respect they are more easily compared with the trends

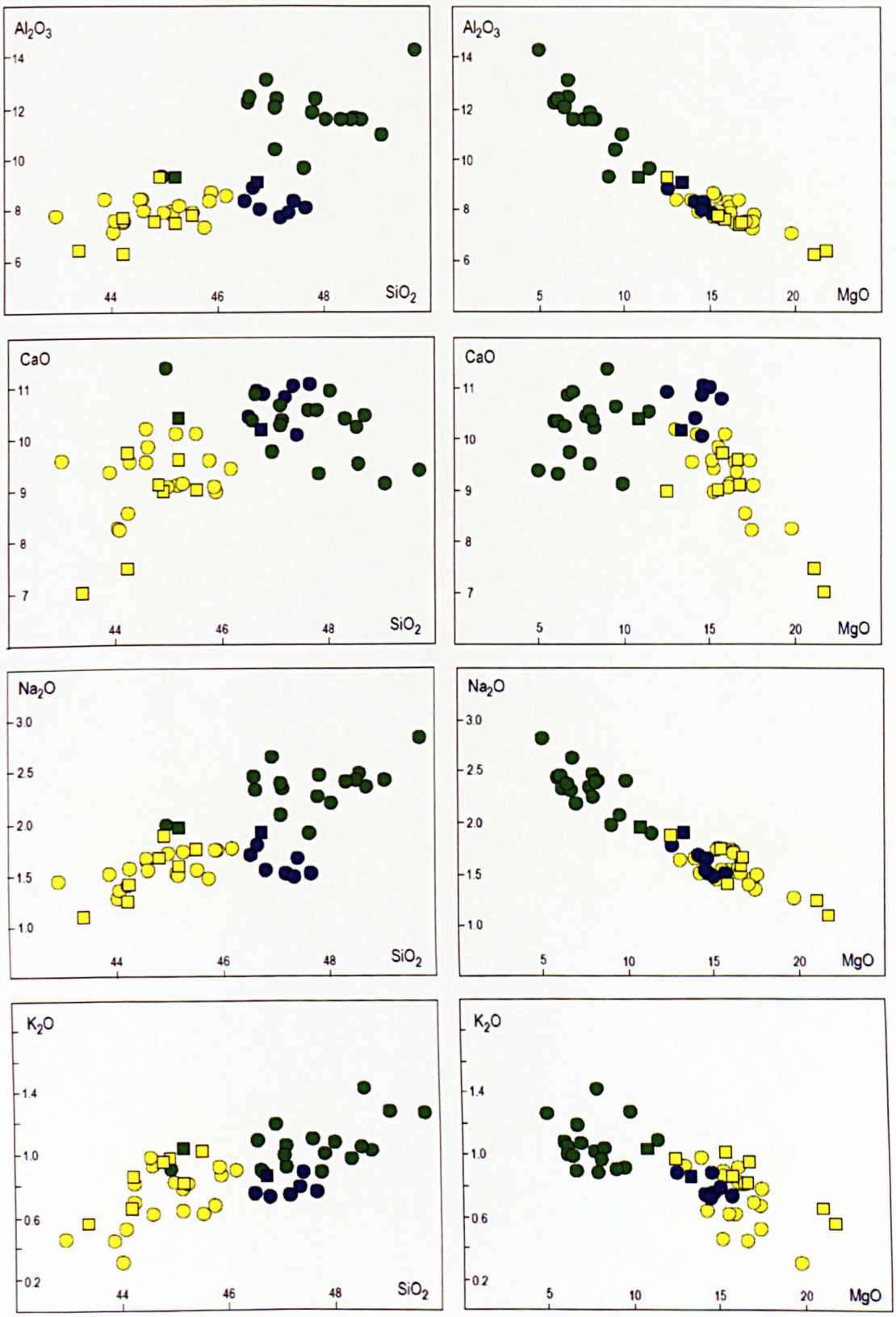

Figure 5.5 Major element variation in relation to SiO_2 and MgO. Values are in weight % and symbols are as in Figure 5.2. Correlation coefficients are listed in Table 5.1.

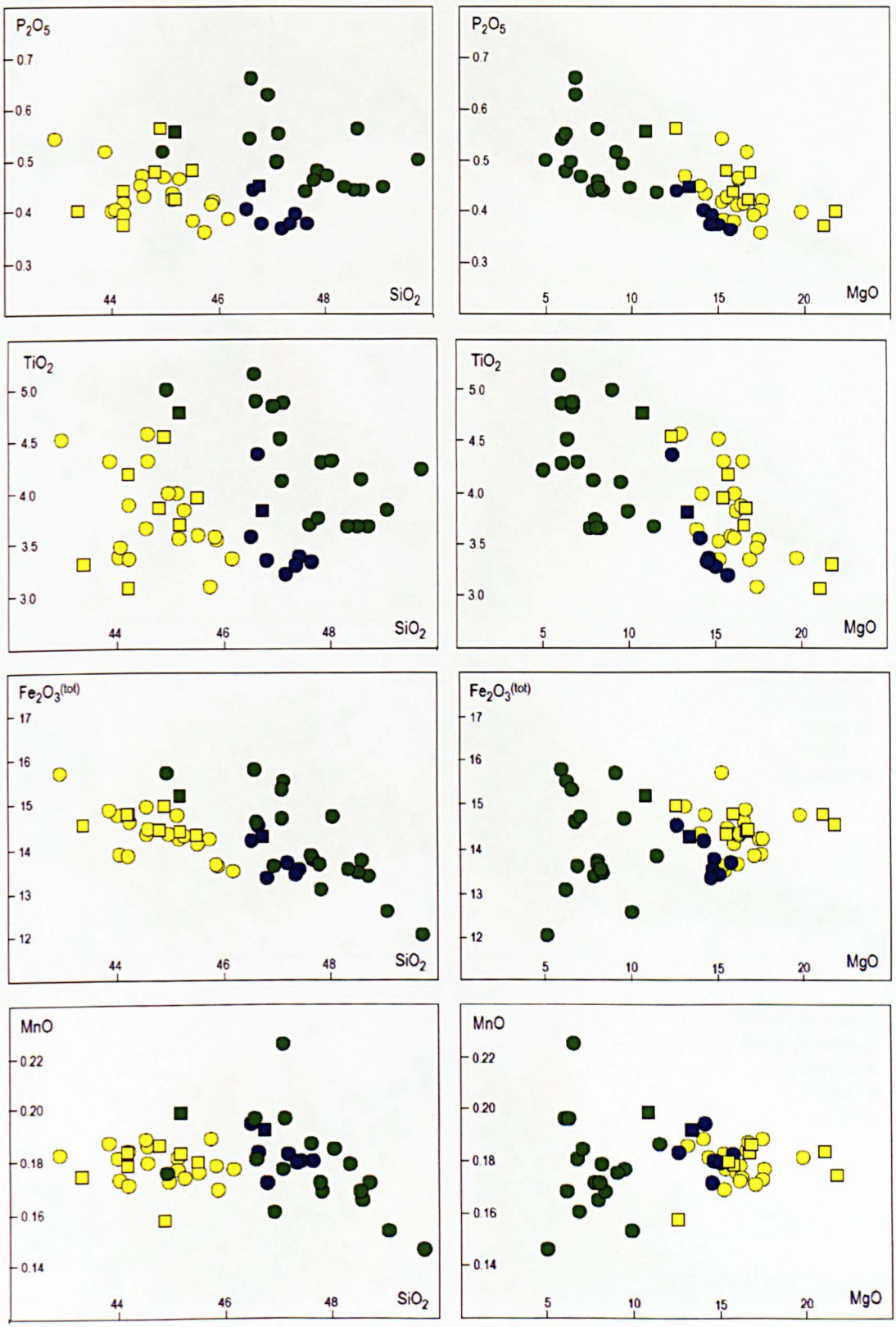

Figure 5.5 Continued.

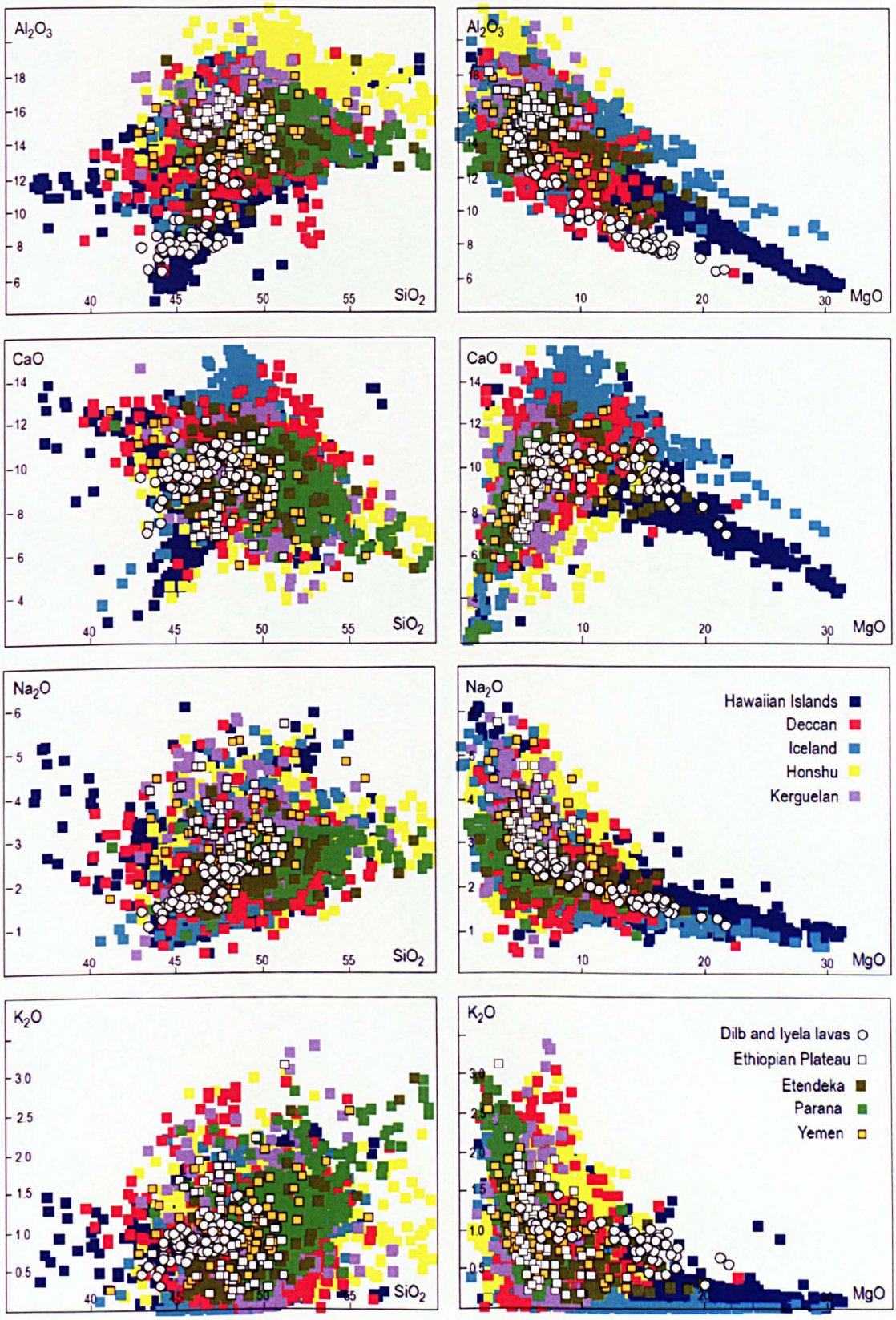

Figure 5.6 Variation of major element oxides with SiO_2 and MgO for the Dilb and Iyela lavas compared to that for similar and contrasting tectonic environments. Data for all provinces are from the GEOROC database - the compilation includes basalts, picrites and tholeiites only. Values are in weight percent.

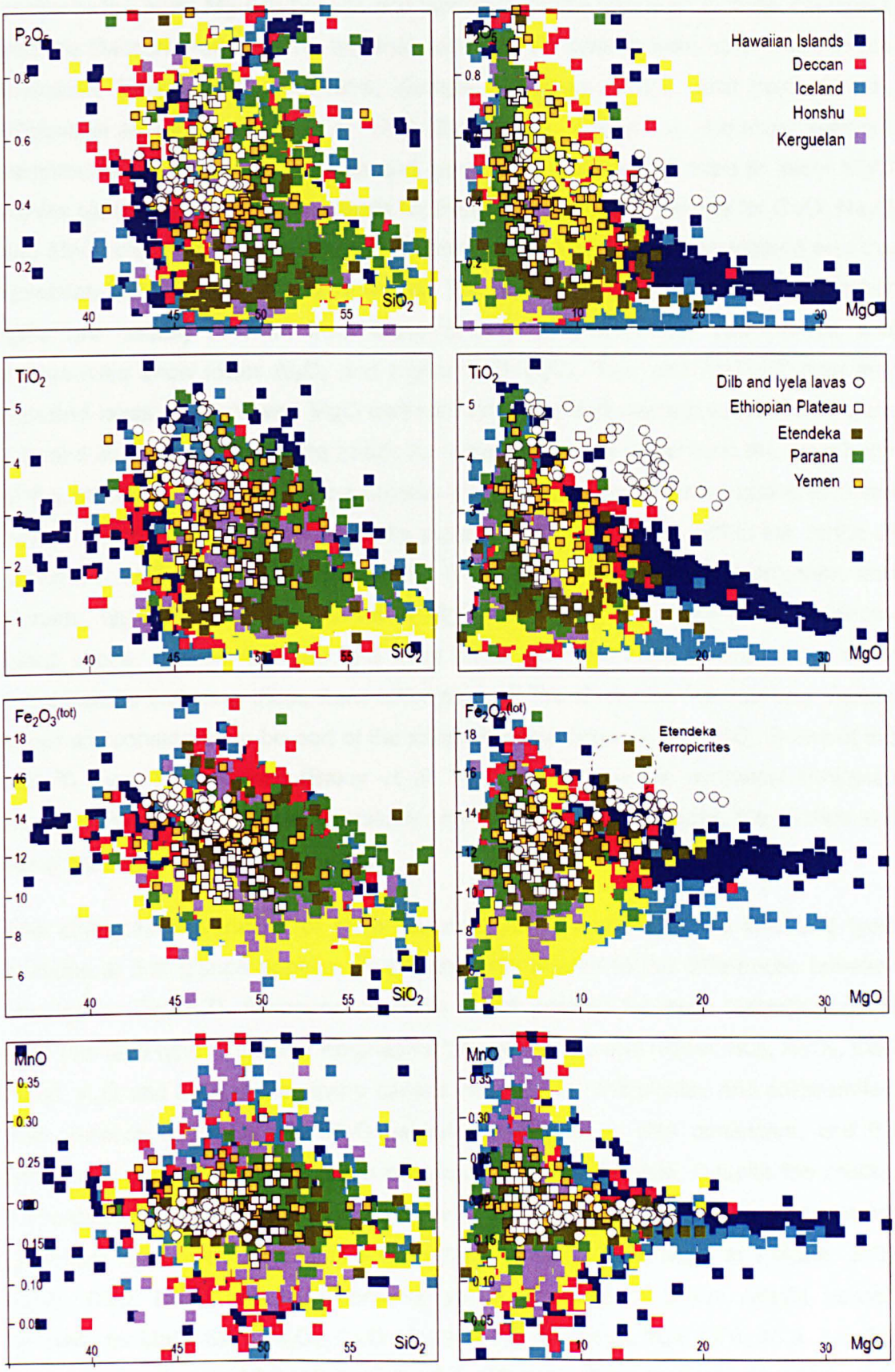

Figure 5.6 Continued.

described above. Such comparisons reveal that the Dilb and Iyela lavas are most similar to the more Mg-rich basalts and picrites from the Hawaiian Islands, Etendeka and the Deccan. Furthermore, together with data for basalts from other parts of the Ethiopian Plateau (Pik et al.1998, George & Rogers, 2002), and from Yemen, (Chiesa et al. 1989; Manetti et al. 1991; Baker et al. 1996 a - b), the major element variation trends shown by the Dilb and Iyela lavas may be extended to lower MgO values concordant with similar trends for these provinces. The trends for CaO, Na_2O and MnO which form discreet arrays sandwiched between those for Iceland and the Hawaiian Islands are particularly typical. The arrays for other oxides, on the other hand are notably different from those of any other province. The picrites and ankaramites show lower Al_2O_3 and higher K_2O, P_2O_5, TiO_2 and $Fe_2O_3^{(tot)}$ than any reported lavas of equivalent MgO content from the provinces represented in Figure 5.6, and as a consequence the trends for these oxides are offset from the main body of the compiled data. The olivine basalts have more typical concentrations of these oxides and plot slightly apart from the picrites and ankaramites within the range of provinces such as the Columbia River (not shown), the Parana, Kerguelan and Honshu, typified by basalts with lower MgO and higher SiO_2 than those provinces listed above. Overall, the Dilb and Iyela lavas are chemically different from other flood basalts including those from other parts of the Ethiopian Plateau and Yemen which are considered to be part of the same volcanic province (Fig. 5.6). Some of the high-Ti lavas from Yemen (Baker et al. 1996 a - b) and the northwest Ethiopian Plateau (Pik et al. 1998) are chemically similar to the olivine basalts; the picrites and the ankaramites are however unique.

The stratigraphic variation of major element concentrations in the Dilb and Iyela sections at first glance appears erratic and only related to the differences between lava-types (Fig. 5.7). Pronounced spikes in the profiles for each respective oxide from one lava type to another emphasise the lower MgO and higher TiO_2, Al_2O_3, CaO, Na_2O, K_2O and P_2O_5 of the olivine basalts compared to the picrites and ankaramites. The variation of Fe_2O_3 and MnO between lava-types is less consistent, and the profiles for these oxides are, as a consequence, less variable. Despite the relative fluctuations between the lava-types, there is a distinct change in the major element chemistry marked by an overall shift in the profiles to lower MgO and higher SiO_2, Al_2O_3, CaO, Na_2O and K_2O contents above 01.03.25.02. Mean weight percent contents for MgO, SiO_2, Al_2O_3, CaO, Na_2O and K_2O change from 14.8, 45.3, 8.4, 9.5, 1.7 and 0.8 below, to 10.9, 47.3, 10.2, 10.1, 2.0 and 1.0 respectively above this flow. The profiles for TiO_2, Fe_2O_3, MnO and P_2O_5 do not reflect this same shift in chemistry

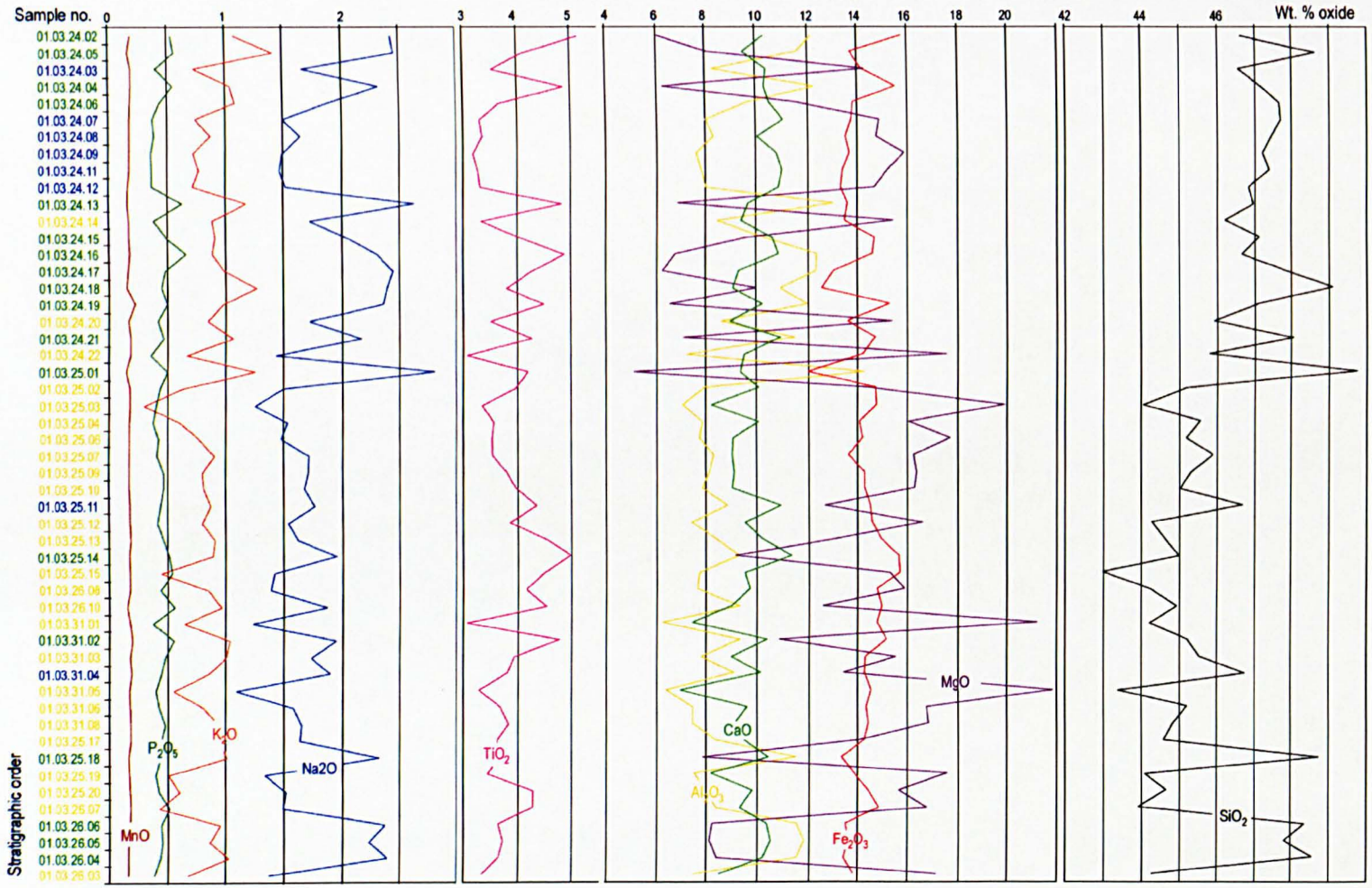

Figure 5.7 Stratigraphic variation of major element oxides for the Dilb and Iyela sections. Sample numbers are listed alongside the vertical axis, and lava-types are indicated by colour - yellow for picrites, blue for ankaramites and green for olivine basalts.

and there is no significant difference in the mean contents of these oxides above and below 01.03.25.02.

5.2.3 Trace element compositions

Like most flood basalts, the Dilb and Iyela lavas are enriched in incompatible elements compared to MORB and are depleted in heavy rare earth elements relative to middle and light rare earth elements. In these respects they are similar to Ocean Island Basalts (Fig. 5.8). More specifically, their trace element abundance profiles

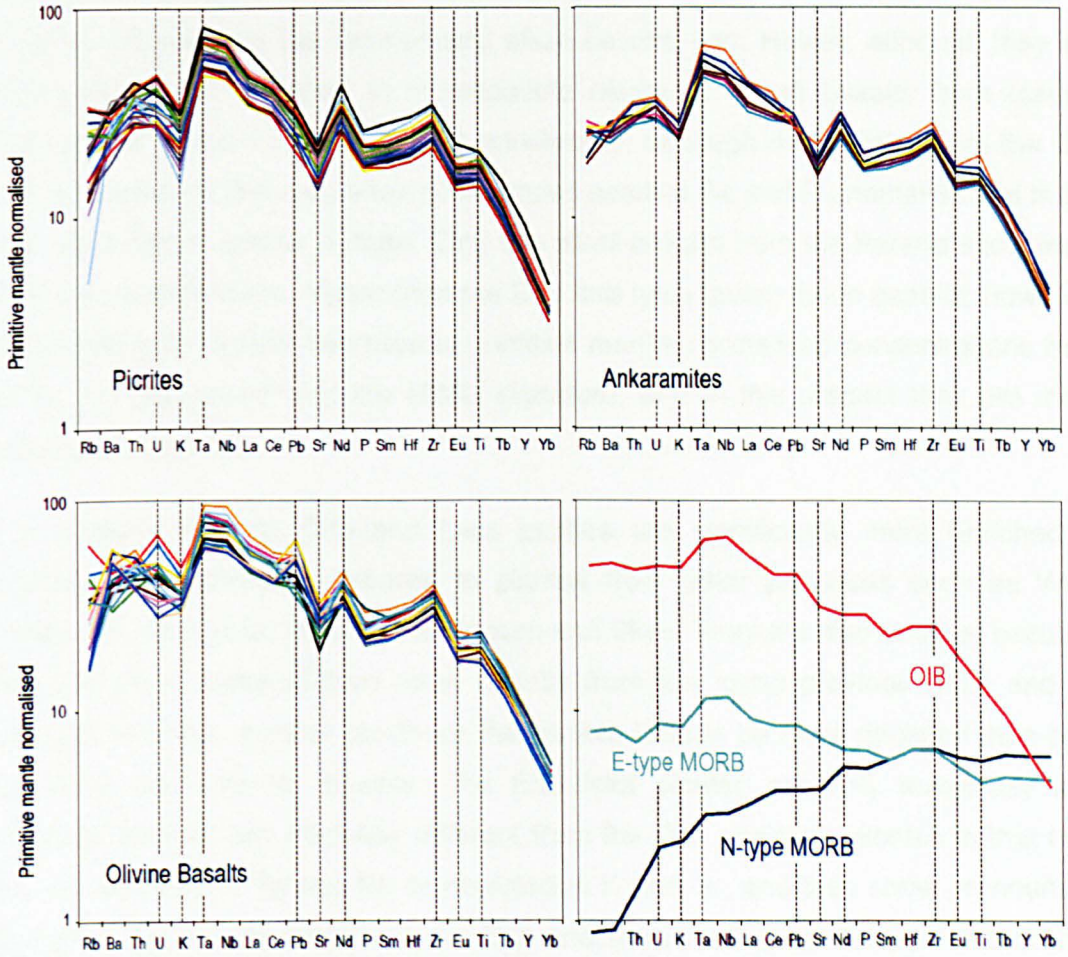

Figure 5.8 Primitive mantle-normalised trace element diagrams for the Dilb and Iyela lavas. Averaged compositions for ocean island basalts (OIB), E-type, and N-type mid-ocean ridge basalts (MORB) are shown for comparison (Sun & McDonough, 1989). Picrites 01.03.25.03 and 01.03.26.07 are not shown because they have anomalously high Ba and Pb. 01.03.25.03 also has anomalously low K and U (Appendix 5.3.1).

exhibit a HIMU signature characterised by an enrichment of Nb and Ta relative to Ba, and Rb, a general decrease in primitive mantle normalised concentrations from Nb to Cs, and a pronounced negative K anomaly indicative of LILE depletion (Willbold & Stracke, 2005). Such a signature is reported for the HT2 basalts from the NW

Ethiopian Plateau (Pik et al. 1999) and for uncontaminated high-Ti basalts from western Yemen (Baker et al. 1996). As with other continental flood basalts, however, the Dilb and Iyela lavas exhibit distinct differences from typical HIMU OIB, mainly associated with the variability in their abundances of mobile incompatible elements such as K, Rb, Sr, Ba, and Th, and with variably elevated concentrations of selected high field strength elements including Pb, Zr and Ti (Fig. 5.9). Unlike HIMU OIB, the trace element profiles of the Dilb and Iyela lavas, lack negative Pb anomalies, and show prominent negative Sr anomalies and less pronounced P and Eu troughs associated with antithetic peaks for Nd, Zr and Ti. In this sense they are similar to tholeiitic basalts from the Deccan and alkali basalts from Hawaii, although they are significantly more enriched in incompatible elements. Alkali basalts from Iceland show similar levels of trace element enrichment, although these differ from the Dilb and Iyela lavas in that they show pronounced positive Ba and P anomalies and much less significant K and Sr troughs. Only the alkali basalts from the Parana show trace element concentrations higher than the Dilb and Iyela lavas; these basalts, however, do not show the typical decrease in primitive mantle normalised concentrations from Nb to Cs characteristic of the HIMU signature, and in this respect they are more typical of EM basalts.

It is notable that the Dilb and Iyela picrites are significantly more enriched in incompatible elements compared to picrites from other provinces such as West Greenland, Etendeka, Iceland, the Deccan and Skye. They are also unusual because they are more enriched than other basalts from the same province (HT1 and LT Basalts), whereas in other provinces the picrites tend to be more depleted than both the alkali and tholeiitic basalts. The Etendeka picrites are only marginally less enriched but they are markedly different from the Dilb and Iyela picrites in that they are not enriched in Ta and Nb or depleted in K and Sr, and they show pronounced peaks for Ba and Pb. Moreover, the Dilb and Iyela picrites are unusual in that they are more alkaline yet less enriched in incompatible elements than the majority of olivine basalts, whereas in all other provinces the alkali basalts tend to be more enriched than the tholeiites.

Willbold & Stracke (2006) suggest that because La/Th and La/Sm ratios are relatively constant in OIB, La and Th represent a common 'anchor' for enrichment and depletion patterns of very incompatible elements (VICE) in OIB. Given this assumption, the degree of enrichment or depletion in the Dilb and Iyela lavas of VICE with respect to OIB may be illustrated by the ratios of these elements with La as a

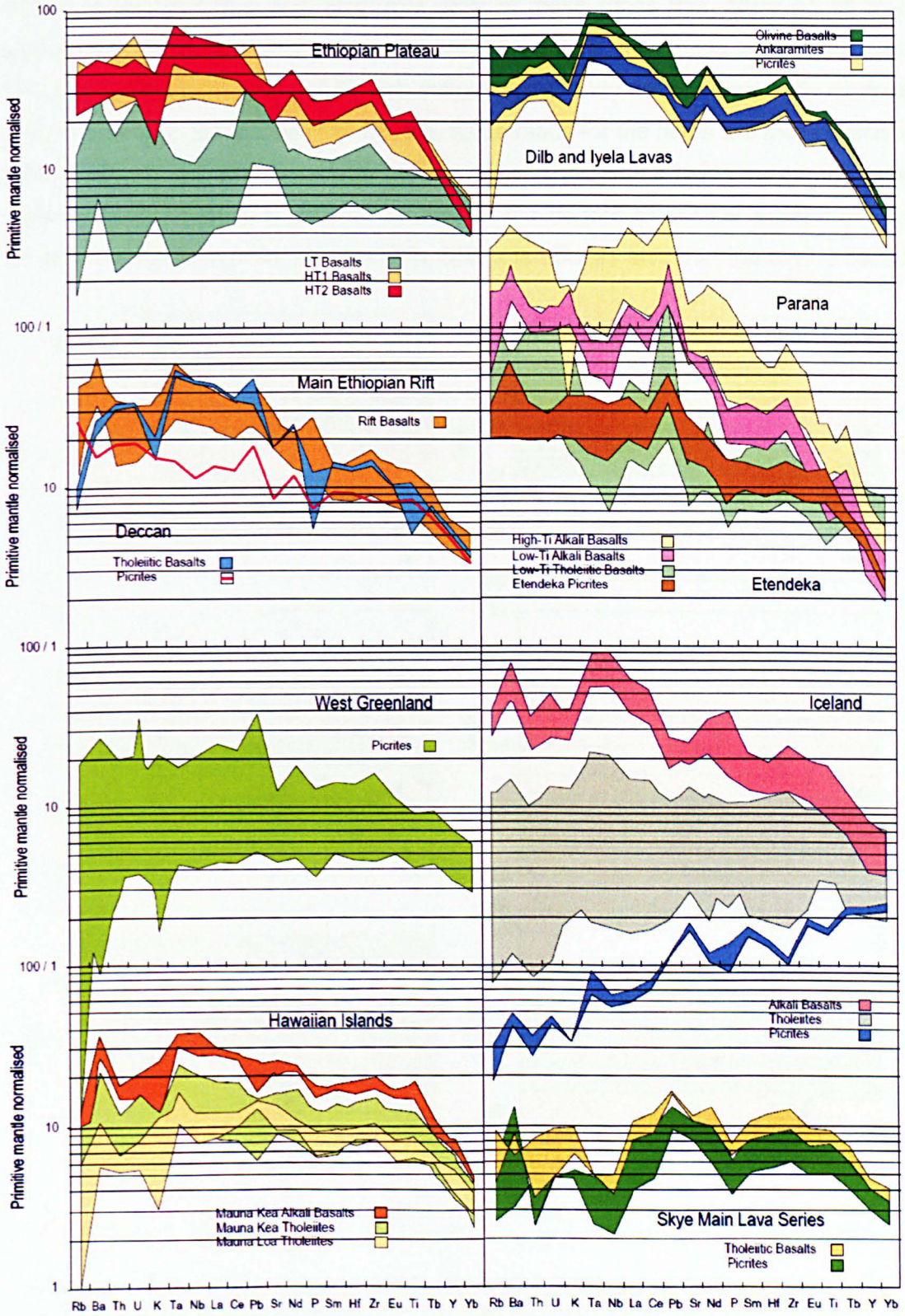

Figure 5.9 Comparison of trace element abundance profiles for the Dilb and Iyela lavas with representative profiles for selected volcanic provinces - the Ethiopian Plateau (Pik et al. 1999), Main Ethiopian Rift (Furman et al. 2006), Deccan, Skye and Etendeka (Gibson et al. 2000), Hawaiian Islands (Hofmann & Jochum, 1996), West Greenland (Lightfoot et al. 1997), Parana (Peate & Hawkesworth, 1996; Gibson et al. 1996), Iceland (Kokfelt et al. 2006). Concentrations are normalised to primitive mantle (Sun & McDonough, 1989).

reference element. It is apparent from plots of these ratios that, although all three lava groups have relatively consistent VICE/La ratios, they have marginally lower Th/La and U/La ratios than HIMU OIB indicating that they are comparatively depleted in Th and U (Fig. 5.10). The (Rb, Ba, Nb, K)/La ratios for the lavas are more typical of HIMU OIB with respectively similar mean values. Their Rb/La ratios are nevertheless more dispersed reflecting greater variation in the degree of relative enrichment and depletion of Rb than is for typical HIMU OIB. It is notable also that the olivine basalts

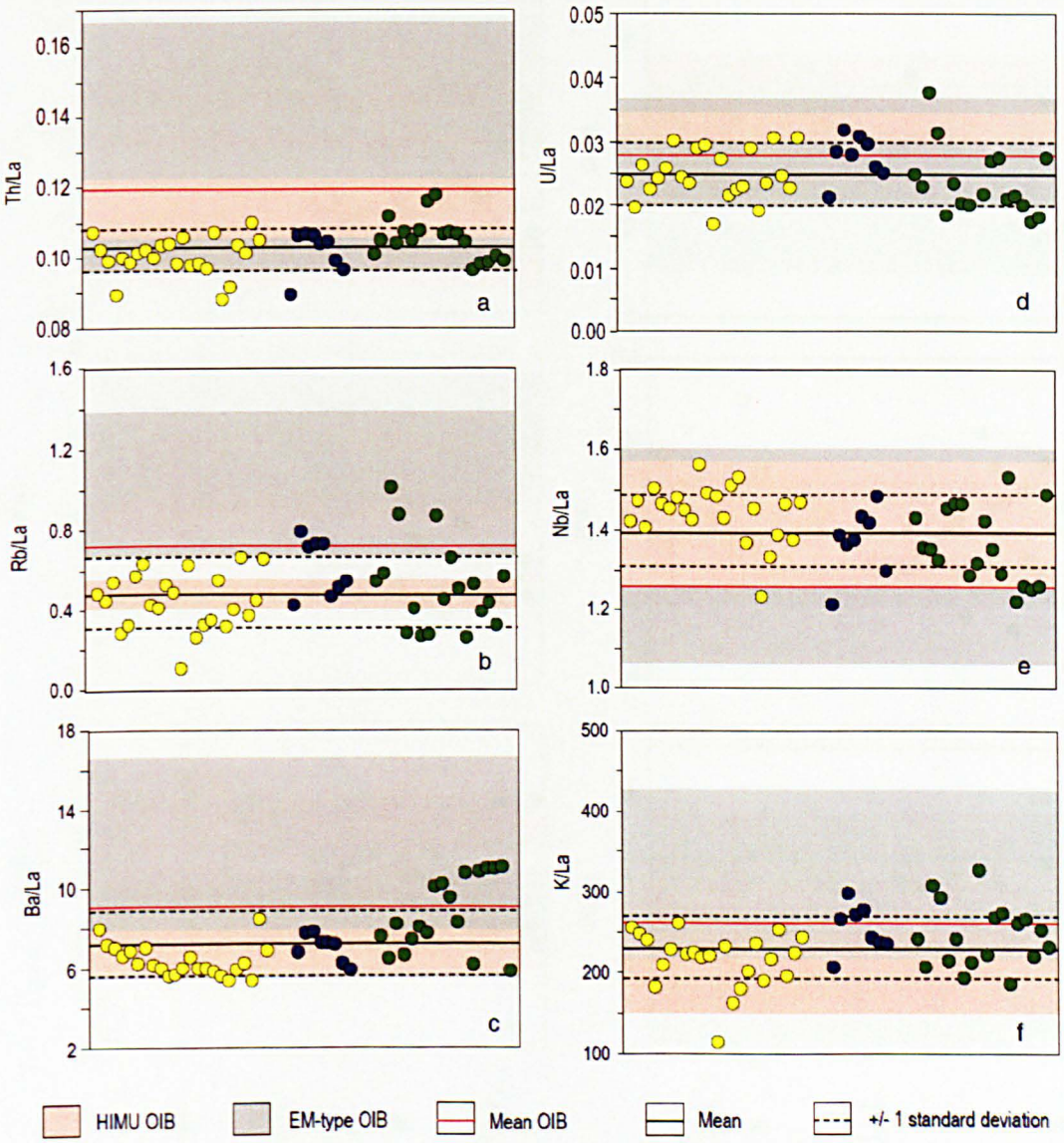

Figure 5.10 Ratios of very incompatible elements (VICE) and La for the Dilb and Iyela lavas in relation to HIMU and EM OIB. The field for HIMU basalts is constructed from the range of mean values for the islands of St. Helena, Mangaia, Rurutu and Tubuali. The EM basalt field encompasses EM1 and EM2 since both overlap and are more variable than that of HIMU. The EM field is constructed from the range of mean values for the islands of Gough, Tristan da Cunha, Pitcairn, representing EM1, and Marquesas -Tahuata, Marquesas-Ua Pou, Samoa-Malumalu, Samoa-Savali, Society-Tahaa, Society -Moorea, Society-Hauhine, Marquesas-Tahuata, and Azores-Sao Miguel representing EM2 (Willbold & Stracke, 2006).

show relatively higher Ba/La ratios than the picrites and ankaramites reflecting their elevated Ba contents evident from distinctive peaks for this element in their trace element profiles.

Ratios of elements considered to behave similarly during the generation of OIB show the same differences from HIMU OIB associated with the relative depletion of U (Fig. 5.11). In particular, their K/U and Nb/U ratios are, as a result, generally higher than

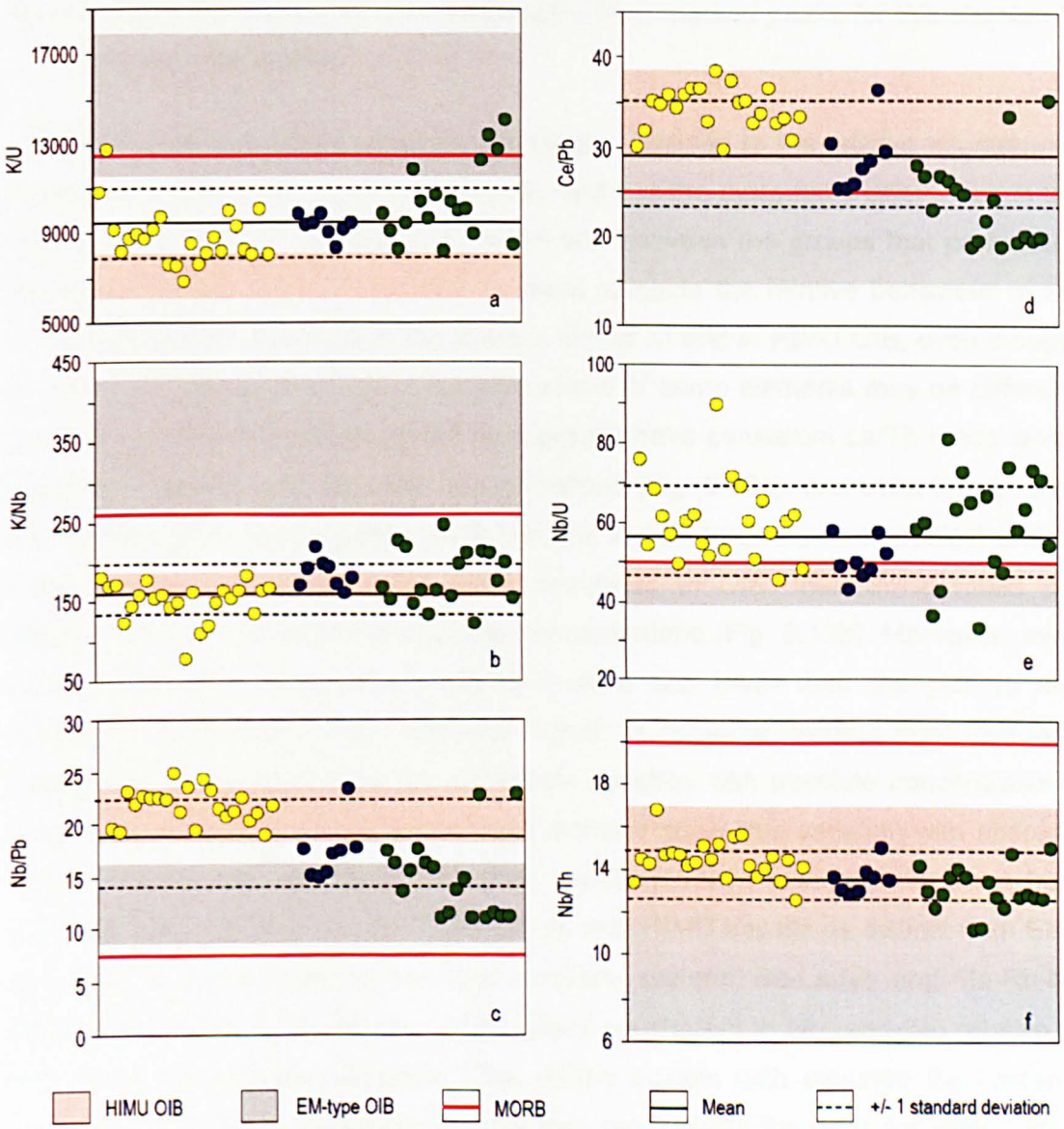

Figure 5.11 Selected ratios of elements thought to behave similarly during generation of OIB. Ratios for the Dilb and Iyela lavas are shown in relation to fields for HIMU and EM basalts, and average MORB compiled by Sun & McDonough (1989).

those typical for HIMU basalts with mean values plotting significantly above the respective fields for HIMU. The Nb/Th ratios, on the other hand are relatively consistent with those of HIMU OIB and therefore do not reflect the same degree of

depletion in Th evident in relation to La. The ankaramites and olivine basalts have generally higher K/Nb and lower Nb/Th ratios than the picrites reflecting their higher K and Th contents. These differences are also apparent in their trace element profiles from the less pronounced K troughs and shallower gradients in the general decrease in mantle normalised concentrations from Nb to Th compared to the picrites (Fig. 5.8). The ankaramites and olivine basalts have distinctly lower Ce/Pb and Nb/Pb ratios compared to the picrites reflecting their higher Pb contents, also evident (particularly in the case of the olivine basalts) from marked peaks for this element in their trace element profiles.

The differences between the groups are largely confined to the relative abundances of the more mobile incompatible elements, and it is the systematic differences in the relative behaviour of such elements within and between the groups that particularly differentiates them from typical OIB. In most respects the relative behaviour of the more incompatible elements in the lavas is similar to that in HIMU OIB, even though, as described above, the relative concentrations of some elements may be different. For example, like all OIB, the three lava groups have consistent La/Th ratios which show little variation with absolute concentrations (Fig. 5.12a), and even though they are depleted in Sr (evident from the Sr troughs in their trace element profiles) and as consequence have lower Sr/Nd ratios compared to OIB, their Sr/Nd ratios are likewise similar irrespective of absolute concentrations (Fig. 5.12b). Moreover, even though the Sr/Nd ratios of the olivine basalts are lower than the picrites and ankaramites because of their relatively higher Sr contents (evident from their less pronounced Sr troughs), they too show little variation with absolute concentrations. The Rb/Sr ratios of the three lava groups similarly show little variation with absolute concentrations, and like HIMU OIB their restricted range distinguishes them from EM1 and EM2 OIB (Fig. 5.12c). Their affinity with HIMU basalts as distinct from EM1 and EM2 is most evident from their similarly uniform Ba-La-Nb and Ba-Rb-Nb systematics (Figs. 5.12d and e) which reflect enrichment in Nb (and Ta) relative to other very incompatible elements. The olivine basalts with elevated Ba contents show slightly different systematics in that they plot outside the fields for HIMU within the fields for EM1, so that on the plot of Ba/Nb versus La/Nb they form a positively correlated linear array together with the ankaramites and picrites. Such a correlation is typical for OIB and it commonly used to illustrate the genetic relationship between HIMU and EM basalts (Weaver et al. 1991; Sun & McDonough, 1989).

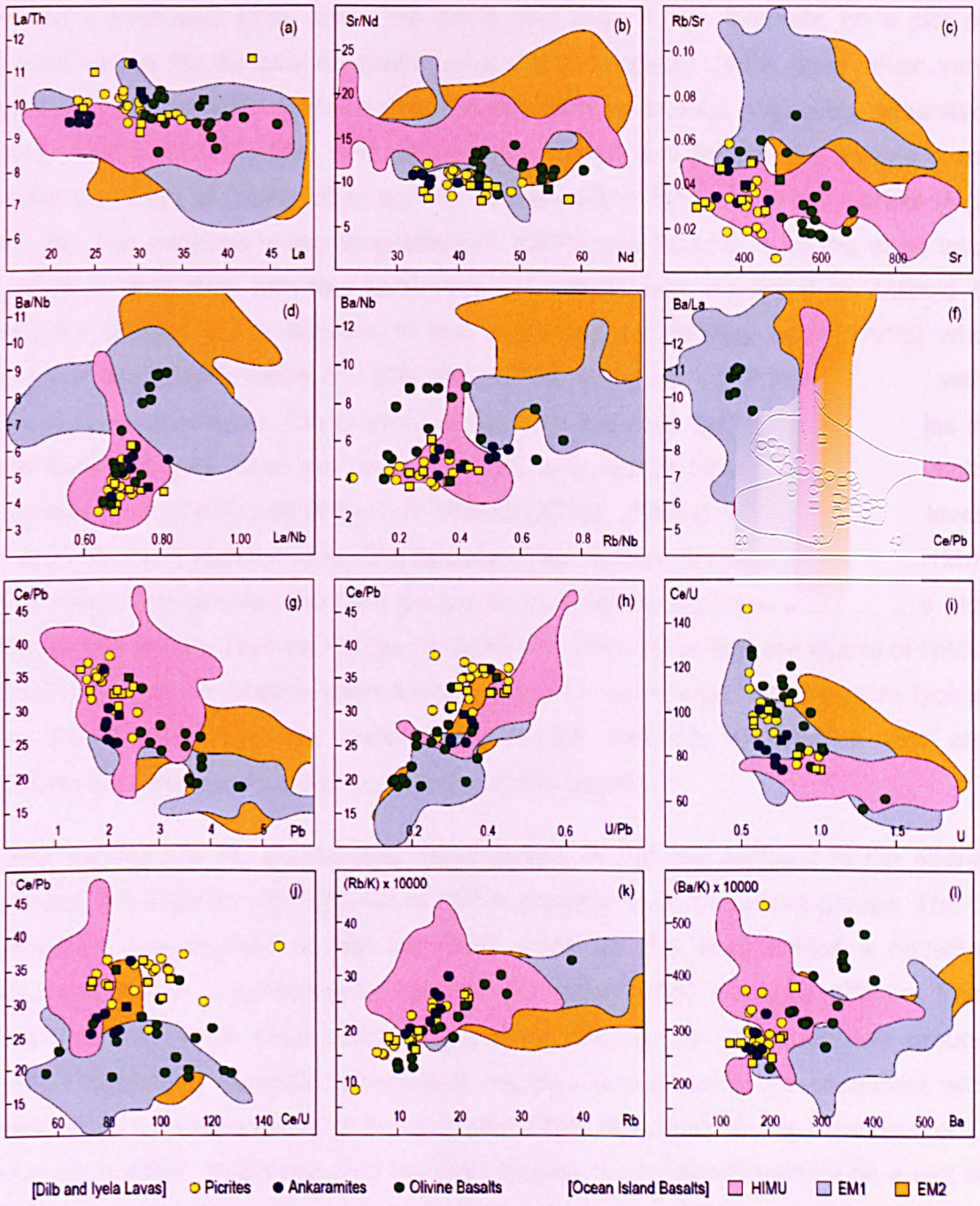

Figure 5.12 Similarities and differences in the relative behaviour of selected VICE for the Dilb and Iyela lavas with that for typical OIB. The fields for OIB were constructed around data from St. Helena, Rurutu, Raivavae, Mangaia and Tubai for HIMU; Tristan da Cunha, Pitcairn and Gough for EM1; and Samoa-Malumalu, Samoa-Savai'i, Society-Tahaa and Azores-Sao Miguel for EM2 (Willbold & Stracke, 2006).

It is the elevated Ba and Pb contents and the systematic relationship between these elements in the olivine basalts that most markedly distinguishes them from the picrites and ankaramites, and makes them similar to EM1 rather than HIMU basalts. This is particularly apparent on a plot of Ba/La versus Ce/Pb where the majority of olivine basalts define a tight negatively correlated array mainly within the EM1 field whereas the picrites and ankaramites together show a more dispersed though

similarly orientated array within the HIMU field (Fig. 5.12f). Similarly, on a plot of Ce/Pb versus Pb the olivine basalts show a wide range of Ce/Pb ratios which vary systematically with Pb concentration thereby defining a loose negatively correlated array mainly within the EM1 field, whereas the picrites and ankaramites show a more restricted range of Ce/Pb ratios and Pb concentrations typical of HIMU basalts (Fig. 5.12g). The negative relationship between Ce/Pb and Pb shown by the three lava groups is consistent with that shown for the OIB dataset presented by Willbold & Stracke (2006), but is contrary to that presented by Halliday et al. (1995) who suggest that Ce/Pb ratios for OIB and MORB show no significant variation with absolute concentration. The positive relationship between Ce/Pb and U/Pb ratios in the Dilb and Iyela lavas on the other hand is typical of OIB as reported by both Halliday et al. (1995) and Willbold & Stracke (2006), although the array for the lavas lies parallel and above that for OIB because their relative depletion in U (Fig. 5.12h). The distinction between the lava groups is nonetheless apparent since on this plot the picrites show a restricted range of Ce/Pb and U/Pb ratios that are typical of HIMU basalts, the olivine basalts show a wider range for such ratios that are more typical for EM basalts, and the ankaramites exhibit Ce-U-Pb systematics that are intermediate between the picrites and the olivine basalts.

Whereas Ba and Pb enrichments characteristic of EM are confined to the olivine basalts, the depletion of U relative to OIB is common to all three lava groups. The U depletion is systematic in that the Ce/U ratios for the lavas exhibit a negative relationship with U concentration, and in this respect they are quite different from HIMU basalts which have uniform Ce/U ratios (Fig. 5.12i). The three lava groups define discernibly separate sub-parallel negative arrays which are consistent with their relative differences in U concentration. This difference in the behaviour of U relative to other VICE compared to HIMU basalts is particularly evident on a plot of Ce/Pb versus Ce/U where the majority of data-points for all three groups fall outside the HIMU field (Fig. 5.12j). The only other significant difference in the relative behaviour of VICE in the Dilb and Iyela lavas compared to that in OIB is associated with the relative abundances of alkali and alkaline earth elements. Whereas in all OIB, the ratios between the alkali and alkaline earth elements are similar irrespective of absolute concentrations (Willbold & Stracke, 2006), such ratios in the Dilb and Iyela lavas exhibit systematic relationships with concentration both within and between the three lava groups. Their Rb/K ratios in particular are positively correlated with absolute concentration showing a well-defined linear array which extends at an angle from low values into the OIB (HIMU) field (Fig. 5.12k). On account of their lower Rb/K

Table 5.2 Correlation matrix for trace element variations in the Dilb and Iyela lavas

The numbers in brackets above each symbol represent the ionic charge for that element

Low Field Strength Elements

High Field Strength Elements

Transition Elements

Other Elements

| | [1] | | |

ratios, the olivine basalts define a discreet array beneath and sub-parallel to that of the picrites and ankaramites. This reflects the higher Rb and K contents of the olivine basalts evident in their trace element profiles from the less pronounced K troughs and shallower gradient in the general decrease in mantle-normalised concentrations from Nb to Rb compared to the other groups. The extremey low Rb contents and Rb/K ratios of the lavas (also apparent from pronounced negative anomalies for this element in the trace element profiles of some of the picrites and olivine basalts) are particularly unusual for OIB-type magmas. As with the Rb/K ratios, the Ba/K ratios of the three lava groups also appear to vary positively with concentration rather than showing consistently similar values typical of OIB (Fig. 5.12l).

The relative variation of VICE in the Dilb and Iyela lavas is generally systematic in that groups of elements with similar charge/size ratios and similar ionic radii show similar chemical behaviour. The degree of similarity in such behaviour across the three lava groups is to an extent evident from the correlation coefficients between different elements (Table 5.2), but these do not show differences in behaviour of specific elements between the lava groups. Similarly, as effectively as the trace element profiles and variation plots previously described in relation to OIB may highlight important compositional differences between the lava groups, they do not clearly show systematic differences or deviations from element-group behaviour that may be useful in identifying petrological processes. Such systematic differences are better illustrated on simple bivariate plots of VICE versus a reference or anchor element such as La (Fig. 5.13). Since La is a high field strength element (HFSE) it is expected to show highly correlated behaviour with other high field strength elements and less consistent behaviour with low field strength elements (LFSE). The plots in Figure 5.13 show that although this is generally the case, there are discernible differences in the behaviour of some elements between the lava groups. Although the HFSE Th, Ta, Nb and Ce all exhibit highly significant positive correlations with La, Th and Ce exhibit a common linearity between the lava groups whereas Ta and Nb show separate sub-parallel linear arrays for the olivine basalts, and the picrites and ankaramites. The lower arrays for the olivine basalts reflect their generally lower Ta/La and Nb/La ratios compared to the picrites and ankaramites - this is only marginally evident from the flatter trace element profiles of the olivine basalts compared to those of the picrites and ankaramites from Ce through to Ta. The similarity in behaviour of Ta and Nb in relation to La is supported by a highly significant correlation coefficient between these elements and by their consistent linearity between the lava groups (Fig. 5.13). In contrast, U, which is also a HFSE, is

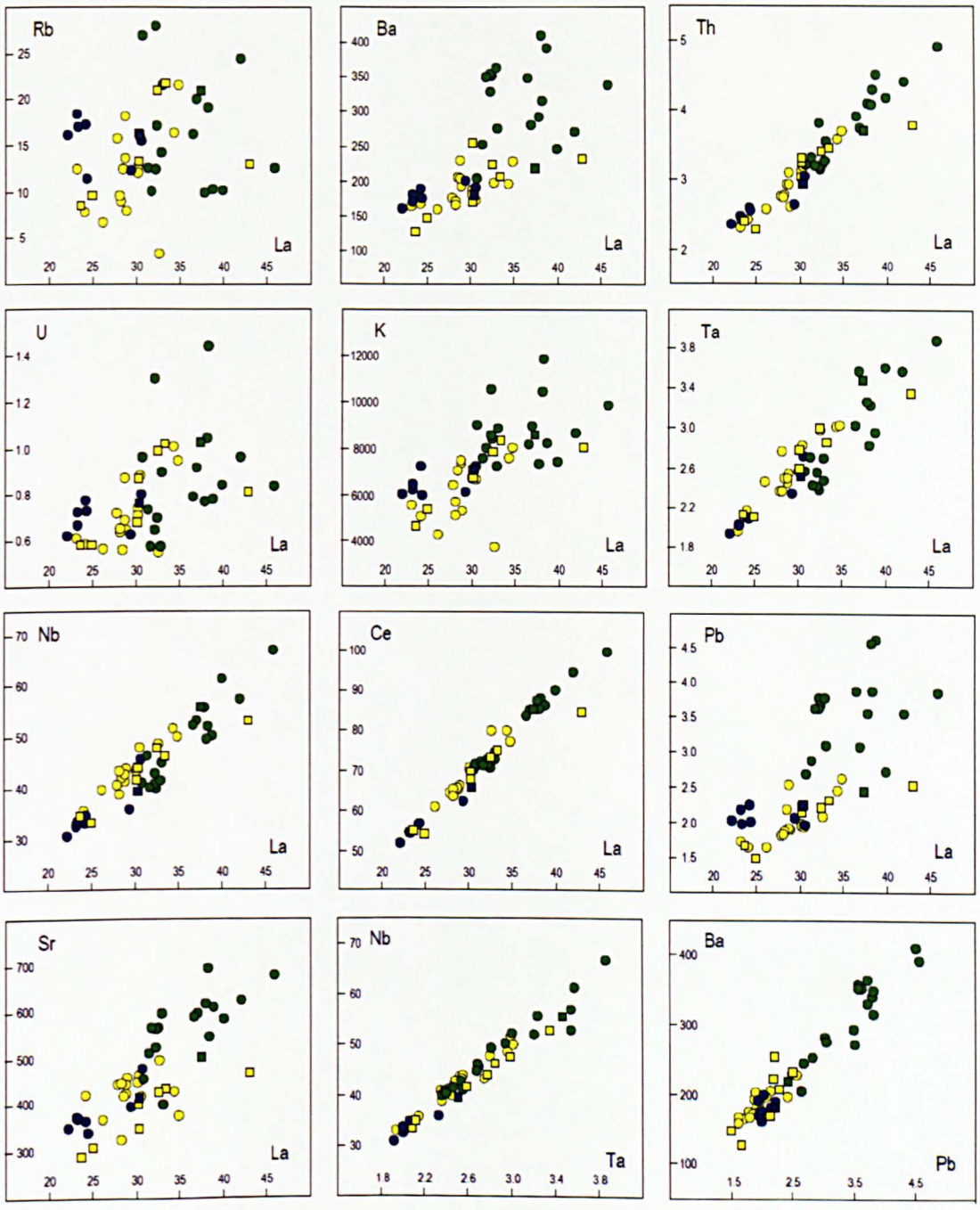

Figure 5.13 VICE versus La for the Dilb and Iyela lavas. Concentrations are in ppm.

poorly correlated with La, and shows dispersed behaviour for all three lava groups. Similarly, though as expected, the LFSE Rb, K and Sr are also poorly correlated with La, and as a result show equally dispersed distributions for all the lava groups. The other LFSE, Ba and Pb, however, although poorly correlated with La across the lava groups, show remarkably constrained linearity in relation to La for the picrites. It may also be argued that for both Ba and Pb versus La the ankaramites and olivine basalts together form a separate more steeply inclined but less constrained linear array than that of the picrites. Like Ta and Nb, this consistent behaviour of Ba and Pb in relation

to La is supported by a highly significant correlation coefficient between them and consistent linearity between the lava groups (Fig. 5.13).

Compared to their VICE, the Dilb and Iyela lavas show much less variability in the relative abundances of their moderately incompatible elements (MICE). The majority of MICE, including the rare earth elements (REE), are HFSE and as a result they show highly significant positive correlations with one another (Table 5.2). This is reflected in the dominantly parallel chondrite-normalised rare earth patterns for each lava group (Fig. 5.14). All three groups have similarly fractionated REE patterns

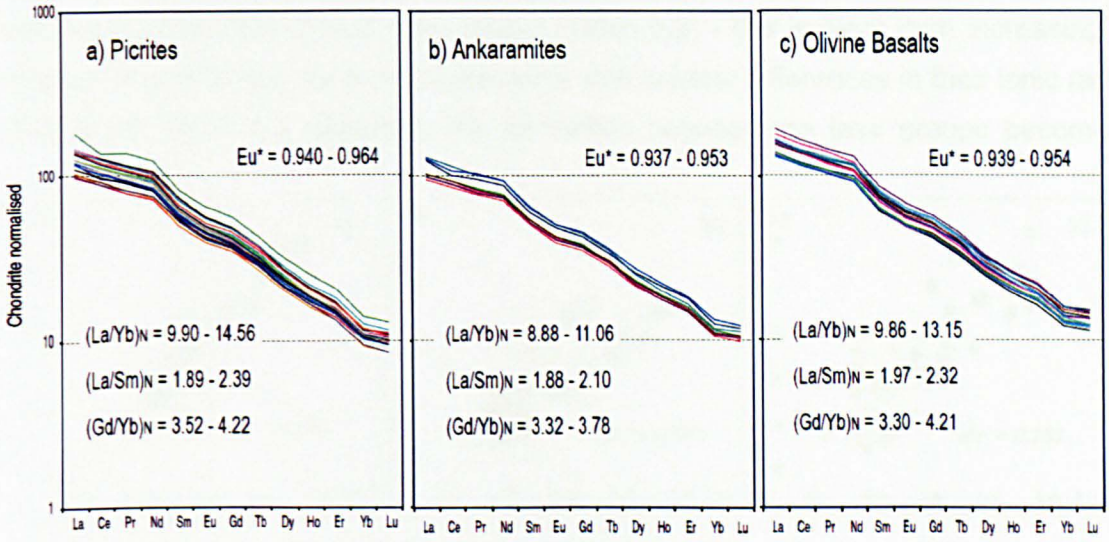

Figure 5.14 Chondrite-normalised REE patterns for the Dilb and Iyela lavas. Chondrite values are taken from Sun & McDonough (1989). $Eu^* = Eu_N / (Sm_N \times Gd_N)$. $_N$ indicates chondrite normalised.

showing strong enrichment of light rare earth elements (LREE) relative to heavy rare earth elements (HREE) with $(La/Yb)_N$ ratios of between 8.9 and 14.6, and slight Eu anomalies. The olivine basalts are generally more enriched than the picrites and ankaramites in REE, although the picrites show a slightly greater degree of enrichment of LREE relative to HREE (mean $(La/Yb)_N = 11.7$), and middle rare earth elements (MREE) relative to HREE (mean $(Gd/Yb)_N = 3.8$), compared to the ankaramites (mean$(La/Yb)_N = 9.5$, mean $(Gd/Yb)_N = 3.4$) and the olivine basalts (mean $(La/Yb)_N = 10.8$, mean $(Gd/Yb)_N = 3.5$). The olivine basalts on the other hand show greater relative enrichment of LREE over MREE (mean $(La/Sm)_N = 2.2$) compared to the picrites (mean $(La/Sm)_N = 2.1$) and the ankaramites (mean $(La/Sm)_N = 2$). Bivariate plots of these ratios are more effective in distinguishing the lava groups, one from another (Fig. 5.15).

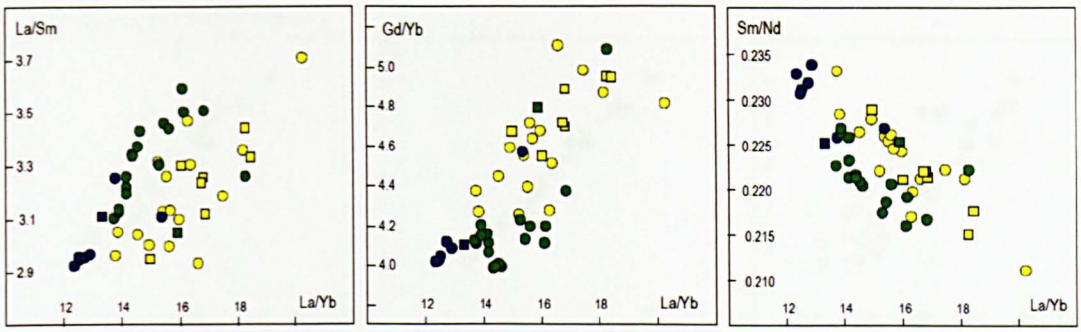

Figure 5.15 REE ratio plots for the Dilb and Iyela lavas.

As expected, the correlation coefficients between the REE decrease progressively with increasing difference in ionic radius (Table 5.2) - this is clear from increasingly dispersed data arrays for pairs of elements with greater differences in their ionic radii (Fig. 5.16). With this dispersal, the distinction between the lava groups becomes

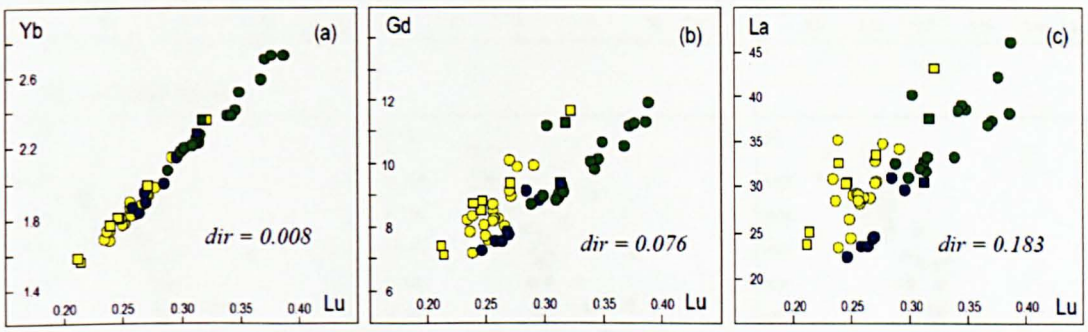

Figure 5.16 The relative behaviour in the Dilb and Iyela lavas of the REE pairs with different incompatibilities resulting from differences in ionic radii. dir = difference in ionic radius.

visible as the picrites form a separate steeper linear array to that of the ankaramites and olivine basalts. It is notable that these arrays, which appear to share a common origin, are similarly distributed to those for Ba and Pb versus La (Fig 5.13). Likewise they show a similar separation of the lava groups evident from the REE ratio plots (Fig. 5.15).

Correlations between the REE and other HFSE do not show the same consistent linear relationship with ionic radius as shown by the REE alone (Fig. 5.17a). Generally the HFSE (Nb, Ta, Ti, Hf and Ti) and P are better correlated with the MREE (Fig. 5.17b). The LFS VICE (Sr, Pb, K, Ba, Cs and Rb), which predictably show much lower correlations with the REE than the HFSE are better correlated with the HREE (Fig. 5.17c). As a group, the transition elements behave less coherently than the other element groups in relation to the REE. Whereas Ni, Co and Cr are negatively correlated with the REE, and better correlated with the HREE (Fig. 5.17d),

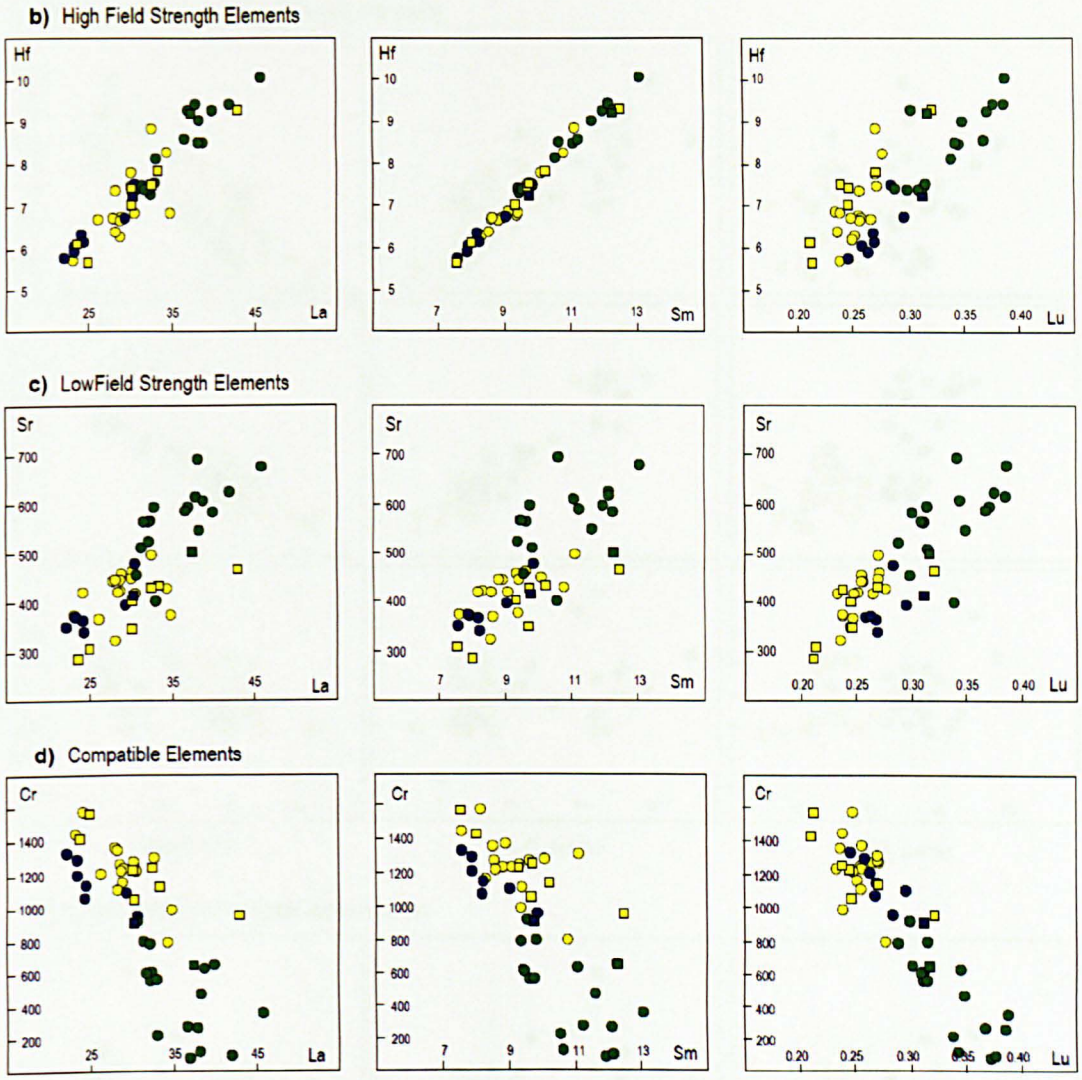

Figure 5.17 Relationship of REE with other trace elements for the Dilb and Iyela lavas. Bivariate plots of selected elements are included to illustrate the typical variation in the datasets for each lava group at varying correlation coefficients. Concentrations in ppm.

Zn and V are positively correlated and more so with the HREE. Sc on the other hand is negatively correlated with the LREE from La through to Nd, positively correlated with the MREE and HREE from Eu through to Lu, and better correlated with the HREE. Cu shows a weak positive relationship with the REE and is marginally better correlated with the MREE.

The relative variation of trace elements with respect to the major element fractionation indices, MgO, Al_2O_3 and SiO_2, and the associated distinction between the lava groups (Fig. 5.18) are consistent with that previously described for the major elements (Fig. 5.5). The incompatible elements show negative relations with MgO which are antithetic to positive relations with Al_2O_3, and the compatible elements show the reverse. The variation with SiO_2 is more dispersed, though it is generally

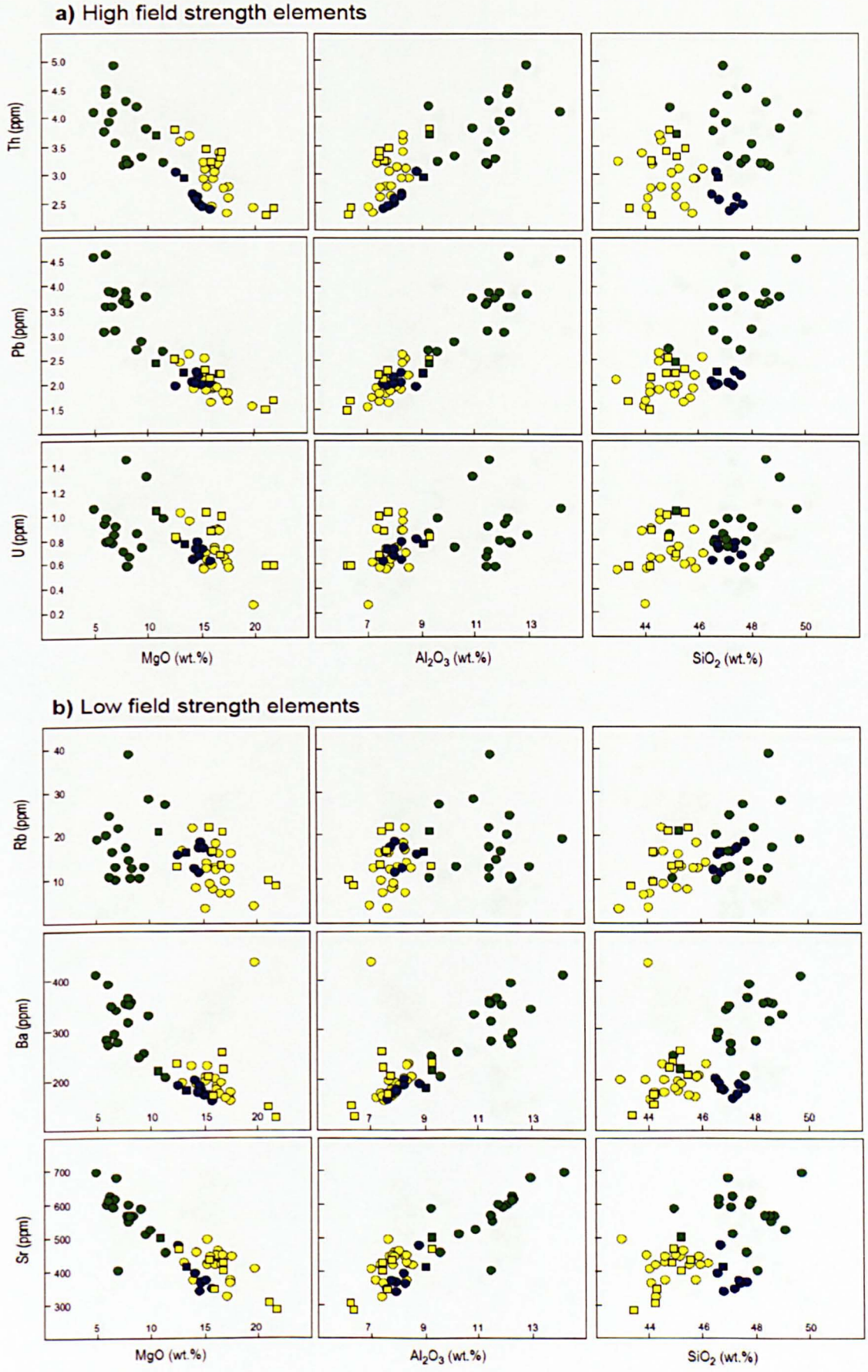

Figure 5.18 Trace element variation in relation to major element fractionation indices for the Dilb and Iyela lavas.

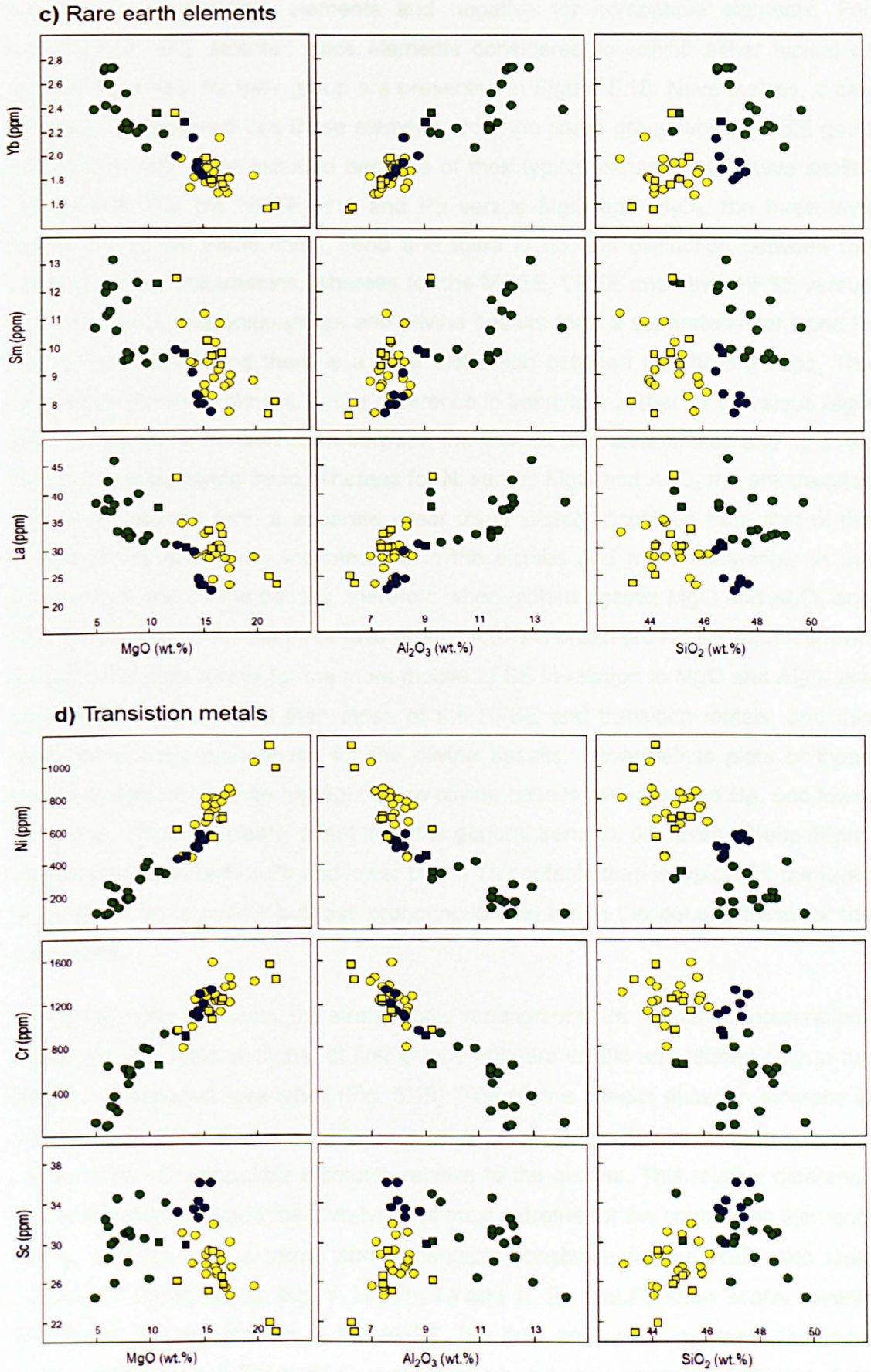

Figure 5.18 Continued

positive for incompatible elements and negative for compatible elements. For convenience, only selected trace elements considered to exhibit either typical or atypical behaviour for their group are presented in Figure 5.18. Nevertheless, it can generally be assumed that those elements from the same group which exhibit good correlations with those included because of their typical behaviour will have similar distributions. For the HREE (Yb) and Pb versus MgO and Al_2O_3, the three lava groups lie on the same linear trend and there is no real distinction between the picrites and the ankaramites, whereas for the MREE, LREE and other HFSE versus MgO and Al_2O_3, the ankaramites and olivine basalts form a separate linear trend to that of the picrites, and there is a clear distinction between the three groups. The compatible elements show a similar difference in behaviour in that for Cr versus MgO and Al_2O_3 there is no distinction between the picrites and ankaramites and all three groups lie on the same trend, whereas for Ni versus MgO and Al_2O_3 the ankaramites and olivine basalts form a separate linear trend slightly displaced from that of the picrites. Sc is dominantly incompatible in the picrites and more compatible in the ankaramites and olivine basalts, therefore when plotted against MgO and Al_2O_3 and SiO_2 the data array for the three lava groups forms a broad arc similar to that shown by CaO. The data arrays for the more mobile LFSE in relation to MgO and Al_2O_3 are generally more dispersed than those of the HFSE and transition metals, and this dispersal is most pronounced for the olivine basalts. Nevertheless plots of these elements against MgO do highlight those olivine basalts with elevated Ba, and lower Rb and U, which are clearly offset from the general trend for the lavas. These olivine basalts also show higher Pb and lower U and Th contents than is typical for the lavas as evident from a similar but less pronounced offset from the general trend for the entire suite.

As for the major elements, the stratigraphic variation of trace element concentrations in the Dilb and Iyela sections, at first glance appears erratic and related only to the differences between lava-types (Fig. 5.19). The olivine basalts show an increase in the concentration of incompatible elements and an antithetic decrease in the concentration of compatible elements relative to the picrites. This relative difference in concentration between the lava-types is most extreme for the compatible elements Cr, Ni, and Co, less extreme and remarkably consistent for the REE, and least extreme for the HFSE Zr, Nb, Y, Hf, Th, Ta and Ti. Ba and Pb show similar relative differences in concentration to the HFSE, but they are less consistent. The more mobile LFSE (Cs and Rb) and U behave similarly but much more unpredictably than all other trace elements. The ankaramites generally show similar behaviour to the

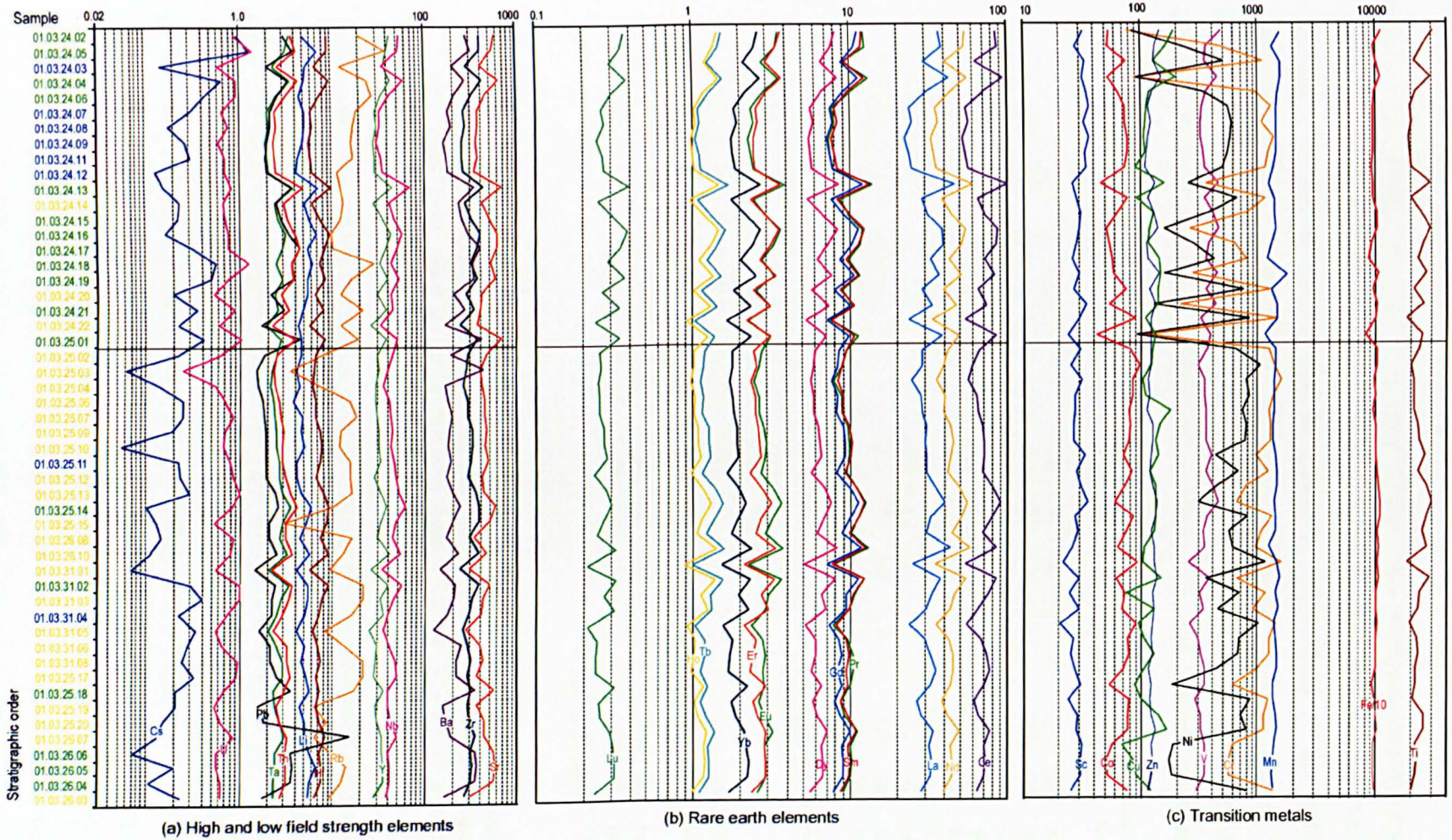

Figure 5.19 Stratigraphic variation in the concentration of trace elements in the Dilb and Iyela lavas. The sample numbers are listed alongside the vertical axis, and the different lava-types are indicated by colour - yellow for picrites, blue for ankaramites and green for olivine basalts. Concentrations are in ppm.

picrites although the relative differences in concentration compared to the olivine basalts are less pronounced.

Above 01.03.25.02 the profiles for most of the trace elements become more erratic despite the fact that above this horizon there are few picrites, and the section is dominated by olivine basalts and ankaramites. Regardless of the differences in variability between flows, almost all trace elements show a shift in the mean concentration above the 01.03.25.02, although the percentage difference in this shift varies for each element (Table 5.3). Generally the mean concentration of

a. Rare Earth Elements

Elem't	Mean below	Mean above	% diff.
La	31.2	32.0	2.46
Ce	69.9	72.2	3.20
Pr	9.83	9.97	1.42
Nd	43.7	44.2	1.03
Sm	9.73	9.86	1.35
Eu	2.90	2.95	1.51
Gd	8.90	9.16	2.75
Tb	1.27	1.32	4.44
Dy	6.28	6.69	6.16
Ho	1.11	1.20	7.69
Er	2.67	2.97	10.2
Yb	1.95	2.20	11.8
Lu	0.27	0.31	13.3

b. High Field Strength Elements

Elem't	Mean below	Mean above	% diff.
Th	3.09	3.38	8.64
U	0.73	0.82	11.3
Ta	2.68	2.67	-0.16
Nb	44.0	44.0	0.05
Hf	7.36	7.54	2.38
Zr	313	324	3.51
Ti	23332	23547	0.91
Y	31.7	34.6	8.57

c. Low Field Strength Elements

Elem't	Mean below	Mean above	% diff.
Cs	0.20	0.39	48.6
Rb	12.8	17.6	27.1
Ba	220	255	13.6
K	6495	7937	18.2
Pb	2.25	2.95	23.6
Sr	442	486	8.98

d. Transition Metals

Elem't	Mean below	Mean above	% diff.
Sc	28.2	30.8	8.45
Ti	23332	23547	0.91
V	337	374	9.79
Cr	1080	757	-42.8
Mn	1382	1382	0.02
Fe	100592	97226	-3.46
Co	74	64	-15.6
Ni	622	382	-62.7
Cu	117	130	9.60
Zn	123	125	1.71

e. Other Trace Elements

Elem't	Mean below	Mean above	% diff.
Li	5.04	5.36	5.88
P	1955	2006	2.56

Table 5.3 Mean concentration of trace elements above and below lava flow 01.03.25.02. Percentage differences between means are shown for comparison. The anomalous value for Pb shown by sample 01.03.26.07 was not included in the calculation of the mean. Concentrations are in ppm.

incompatible elements increases whereas that of the compatible elements decreases above 01.03.25.02. The percentage increase in the mean concentration for the REE above 01.03.25.02 is lowest for the MREE and highest for the HREE. The majority of other HFSE show relatively insignificant differences in the mean concentration above 01.03.25.02 (similar to those shown by the LREE and MREE) while the more mobile HFSE Th, U and Y show much more significant percentage increases in their mean concentration comparable with those shown by the equally mobile LFSE. The more mobile LFSE (Cs and Rb) show the largest percentage increases in concentration above 01.03.25.02. Of the transition metals, the compatible elements Ni and Cr show dramatic percentage decreases in concentration. Co too shows an appreciable

decrease, whereas Zn, Mn and Ti show only marginal and quite insignificant percentage increases in concentration above 01.03.25.02. Cu, Co, V and Sc on the other hand show significant percentage increases in concentration above this horizon comparable to those of the moderately mobile LFSE. What is perhaps more notable is that below this horizon the behaviour of Sc is generally concordant with the REE and antithetic to that of Cr, Ni and Co while above it is generally concordant with the behaviour of Cr, Ni and Co and antitheic to that the REE.

The variability in the mean concentration of trace elements above and below 01.03.25.02 is better illustrated by selected ratios (Fig. 5.20). This is perhaps more

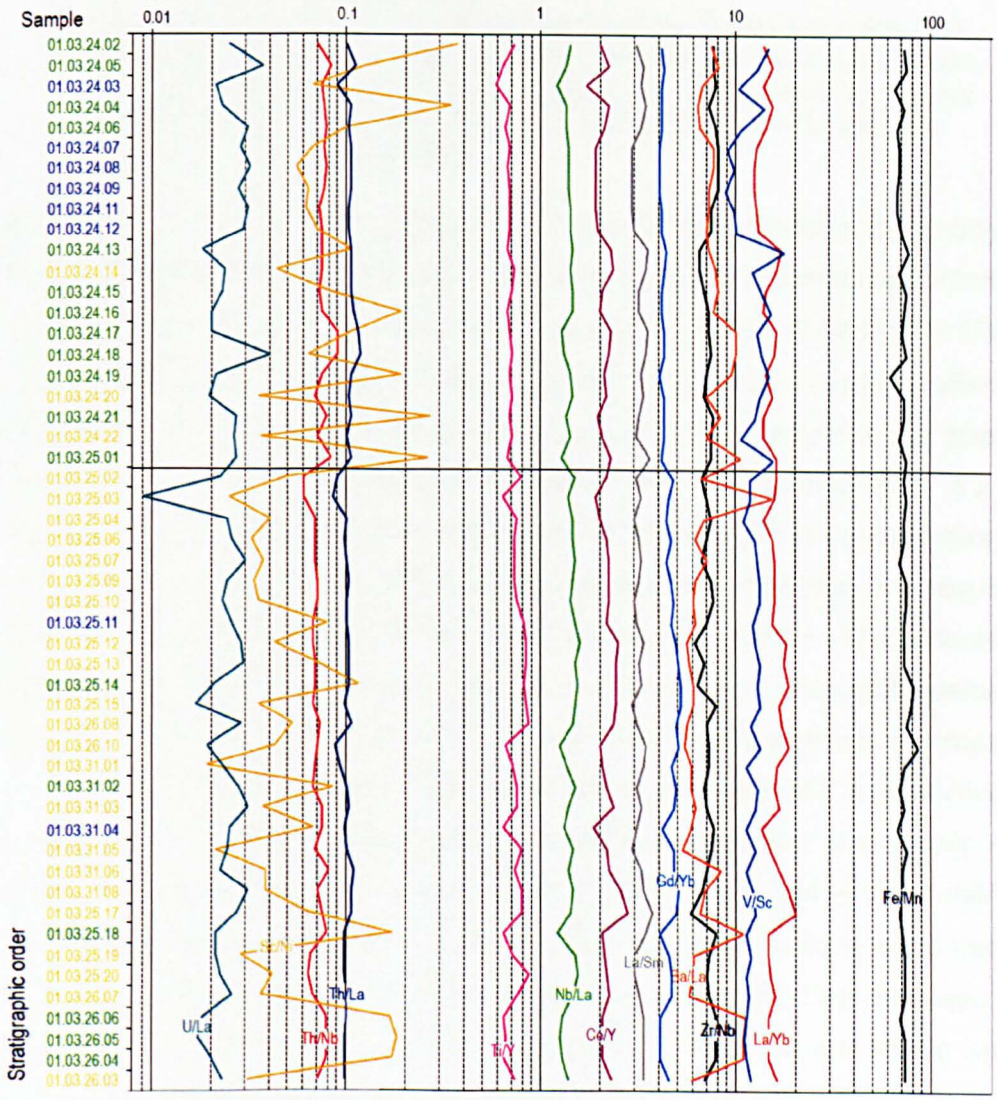

Figure 5.20 Stratigraphic variation of selected trace and major element ratios in the Dilb and Iyela lavas. The sample numbers are listed alongside vertical axis, and the different lava-types are indicated by colour - yellow for picrites, blue for ankaramites and green for olivine basalts. Concentrations are in ppm. Ti/Y = (Ti/Y) x 1000.

Ratio	Mean below	Mean above	% diff.
La/Yb	16.1	14.4	-11.5
La/Sm	3.20	3.22	0.5
Gd/Yb	4.59	4.15	-10.6
Th/Nb	0.07	0.08	8.3
Ba/La	7.08	7.90	10.4
Th/La	0.10	0.11	6.1
U/La	0.02	0.03	10.4
Nb/La	1.41	1.38	-2.6
Nb/Y	1.40	1.27	-10.3
Ce/Y	2.21	2.08	-6.5
Ti/Y	740	681	-8.6
Zr/Nb	7.14	7.42	3.7

a. HFS and LFS elements

Ratio	Mean below	Mean above	% diff.
Rb/Sr	0.03	0.04	21.1
Lu/Hf	0.04	0.04	11.2
Nd/Hf	5.94	5.85	-1.5
Sm/Nd	0.2	0.2	0.6
Ce/Pb	32.3	25.3	-27.7
U/Pb	0.34	0.29	-17
Th/U	4.42	4.19	-5.6

b. Parent/Daughter Ratios

Ratio	Mean below	Mean above	% diff.
Fe/Mn	72.9	70.6	-3.3
Sc/Ni	0.06	0.13	51.5
V/Sc	12.0	12.3	2.8

c. Transition Metals

Table 5.4 Mean ratios for selected trace elements above and below lava flow 01.03.25.02 . Percentage differences between the means are shown for comparative purposes.The anomalous value for Pb shown by sample 01.03.26.07 was not included in the calculation of the Ce/Pb and U/Pb ratios and their respective means.

apparent from the mean values presented in Table 5.4 than it is from the stratigraphic profiles. The ratios presented in Figure 5.20 were selected to compliment information from the primitive mantle normalised multi-element (Fig. 5.8) and REE plots (Fig 5.14) as well as to check for variations in those elements considered to be least affected by fractionation and alteration. The decrease in the La/Yb ratio indicates that above the 01.03.25.02 there is a discernable flattening of the REE profiles (Fig. 5.21a). A similar decrease in the Gd/Yb ratio and near to no change in the concentration of La and Sm and in the mean ratio between indicates that such flattening is a result of an increase in the concentration of HREE above the marked horizon. This reflects small differences in incompatibility of the REE as confirmed by comparable percentage differences shown by ratios of other HFSE with similar differences in incompatibility (eg. Ti/Y). The increase in the Th/Nb ratio above 01.03.25.02 is indicative of a shallowing of the gradient representing the general decrease in primitive mantle normalised concentrations from Nb to Cs (Fig. 5.21b). Enrichment of the mobile VICE (Ba, U and Th) above 01.03.25.02 is evident from the marked increase in the ratios of these elements with La as a reference or anchor-element. The decrease in the Nb/La ratio on the other hand shows that above 01.03.25.02 the Nb-Ta anomaly characteristic of HIMU basalts is not so pronounced. Percentage increases for Ce/Y and Nb/Y, and a percentage decrease for Zr/Nb, furthermore reflect a general increase in concentration of MICE relative to VICE above 01.03.25.02. The dramatic increase in the Sc/Ni ratio highlights the sudden drop in concentration of compatible elements relative to other transistion metals above 01.03.25.02. There is little

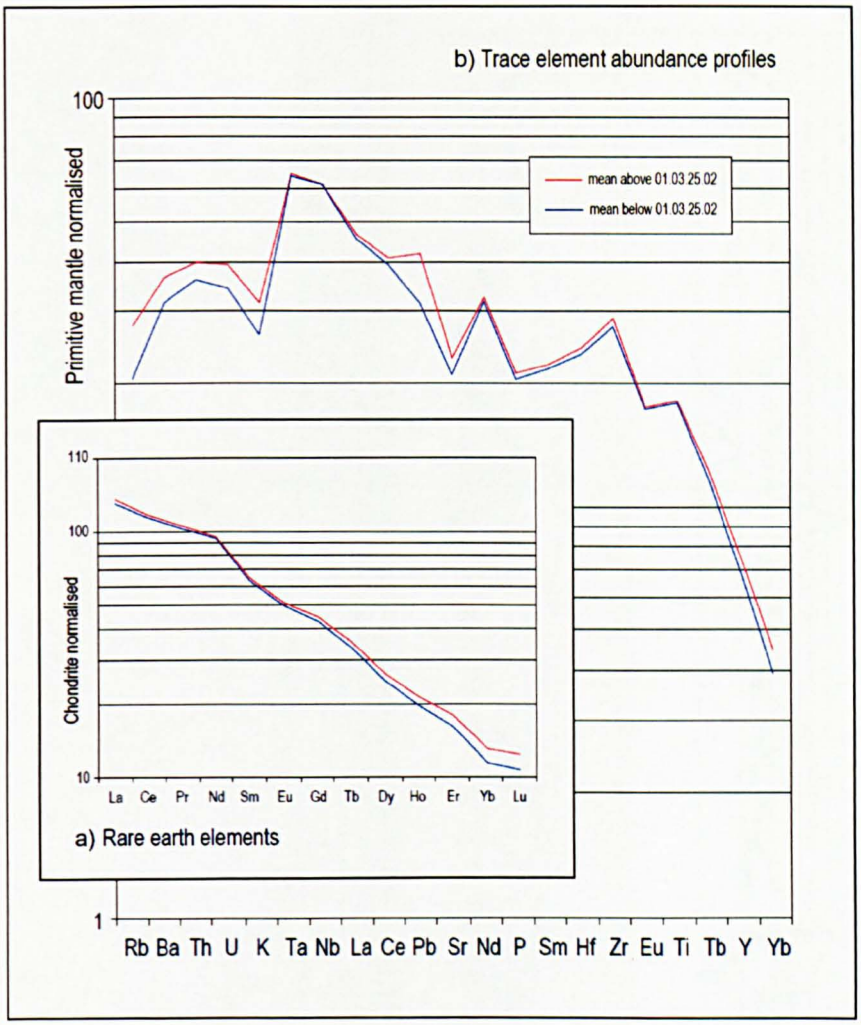

Figure 5.21 Mean trace element concentrations above and below 01.03.25.02. 01.03.26.07 was not included in the calculation of the means as its elevated Pb contents suggest that it is contaminated.

variation in the Fe/Mn ratio throughout the section, while the V/Sc ratio becomes more erratic above this horizon.

The stratigraphic variations in parent daughter ratios are shown in Figure 5.22 and the difference in their mean values above and below the palaeosol are presented in Table 5.4. Although there are slight differences in these ratios compared to those for OIB, the changes in their mean values above 01.03.25.02 are generally similar to those seen between HIMU and average OIB. Rb/Sr shows a marked increase, and Ce/Pb and U/Pb show a marked decrease, whereas Sm/Nd and Nd/Hf show little change, i.e. there is a shift to less HIMU-like and more EM-like ratios above 01.03.25.02. In contrast, Lu/Hf and Th/U show the opposite behaviour in that they become more similar to HIMU basalts above this horizon.

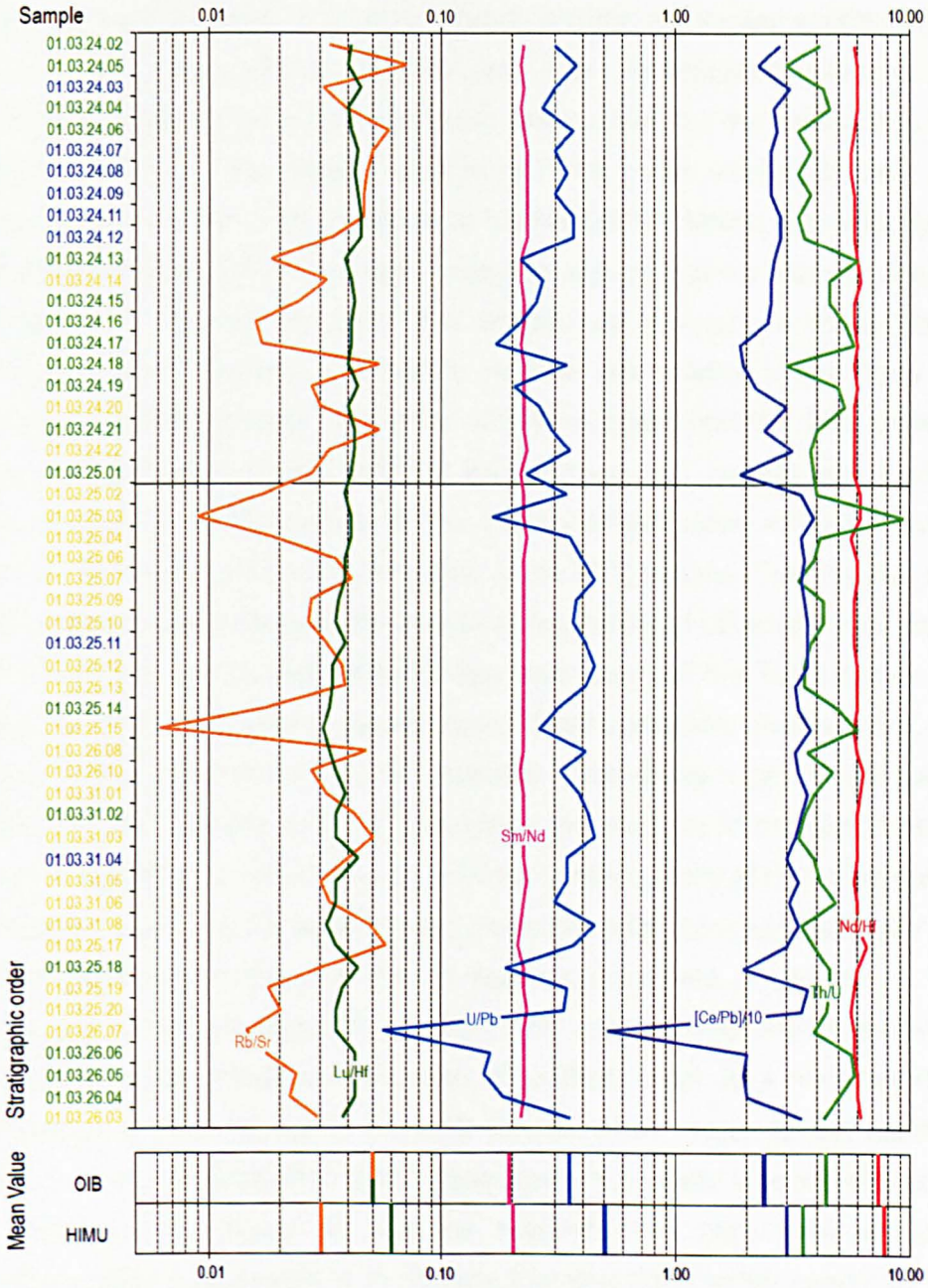

Figure 5.22 Stratigraphic variation of parent/daughter ratios of the Sr, Pb and Hf isotope decay systems for the Dilb and Iyela lava. The mean values for OIB an HIMU have been included for comparison (Willbold & Stracke, 2006). Sample numbers are listed alongside the vertical axis and the different lava-types are indicated by colour - yellow for picrites, blue for ankaramites and green for olivine basalts. Concentrations are in ppm.

5.3 Discussion

5.3.1 Chemistry, location and timing

The volcanic rocks from the Ethiopian Plateau and its counterpart in Yemen so far reported in the published literature exhibit considerable chemical and isotopic

diversity, and are therefore difficult to relate to a common primary source (Chapter 2). This is made more difficult by the fact that stratigraphic relations between documented sections on a regional scale are unclear, to the extent that temporal geochemical trends are largely conjectural. The most stratigraphically coherent sequence yet reported in the province is for the Simien Shield and underlying flood basalts (Kieffer et al. 2004); however it may be argued that the evolved nature of the flood basalts in this section make it of limited use in tracing a lineage back to a primary source composition, particularly as their age relative to the more primitive HT2 basalts is questionable. Pik et al. (1998) suggest that the HT2 basalts were emplaced contemporaneously with the more evolved LT basalts and Kieffer et al. (2004) suggest that the basalts of the Simien Shield were extruded onto a thin veneer of LT basalts prior to the eruption of the HT2 basalts. This implied shift from more to less evolved compositions over time is contrary to observations in other flood basalt provinces where picrites form the lower part of the flood basalt pile and thereby constitute the earliest outpourings of flood volcanism. Furthermore, although Pik et al (1998) suggest that the HT2 basalts in the eastern part of the plateau are underlain by HT1 basalts, the two lava types are nowhere in the region near to the Dilb and Iyela sections reported to be in direct contact. Many of the rocks reported for the Eastern Plateau by Pik et al. (1998) were collected from geographically separate localities some as far apart as the six sections described in Chapter 2. The HT1 basalts, reputed to constitute the bottom of the eastern section and lie beneath the HT2 basalts, were collected from north of Lalibela, near to a hundred kilometres north-west of where several of the HT2 basalts which make up the middle of the eastern section were collected from. Considering the lateral discontinuity of the lava flows described in Chapter 2, and the likelihood that they were extruded from localised centres, it is unrealistic to assume that lava flows so far apart may form part of the same volcanic sequence. Even if it was possible that this was the case, the incidence and effects of faulting and rotational slumping evident in the landscape would make it almost impossible to reliably relate sequences separated by such distances. Picrites are found in the northern part of the Eastern Plateau near to Lalibela, but they are rare, chemically quite different from those found in the Dilb and Iyela sections, and exhibit different field relations. Generally, they are more alkaline (Fig. 5.1) and tend to occur close in sequence to more evolved basanites, trachybasalts and felsic pyroclastics (Chapter 2), suggesting that they were erupted close to or shortly after the onset of bimodal volcanism. In an evolutionary sense, therefore, it may be assumed that they post date the picrites found in the Dilb and Iyela sections.

Some of the more picritic HT2 basalts that are assigned to the middle of the eastern section have coordinates that match points along the Dilb and Iyela sections. The sequence here is stratigraphically continuous and is capped by a series of rhyolitic ignimbrites which mark the onset of bimodal volcanism and the division between the lower (Ashangi and Aiba) the upper (Alaji) flood basalt formations (Chapter 2). This distinction between the lower and upper traps is recognised almost everywhere across the Ethiopian Plateau and is evident beneath the Simien Shield from the occurrence of felsic pyroclastics in the Lima Limo Section (Hofmann et al 1997; Rochette et al. 1998, Kieffer et al. 2004). It is more likely then that the HT2 basalts (here represented by the Dilb and Iyela lavas) predate, rather than post-date, the Simien volcanic pile. Furthermore it is as likely that they represent some of the earliest, uncontaminated and most primitive outpourings of flood volcanism in Afro-Arabian flood basalt province, since like picrites in other flood basalt provinces they occur in the central part of the province. Campbell & Davies (2006) suggest that such lavas are the products of initial melting in the heads of plumes and that they are rarely seen because they are centrally located and are covered by later flows. Early picrites are exposed in the Parana-Etendeka, Deccan, Emeishan, North Atlantic, Siberian and Karoo provinces, where the central regions have been deeply dissected by erosion.

It is clear that the major and trace element compositions of the Dilb and Iyela lavas are consistent with those reported for the HT2 basalts, and their Nb-Y-Ti systematics appear to support that they are related to the same parental magma (Fig. 5.4). They are subdivided both on the basis of their petrography and geochemistry, into three distinct groups. The presence in all three lava groups of highly fosteritic olivines (Fo_{90}) which are not in equilibrium with the whole rock compositions reveals that despite their primitive nature none of the lavas represent primary magmas. The picrites are the most primitive components of the sequence and are therefore probably the closest compositional analogues of the primary melt, and these are confined to the lower part of the section. The ankaramites, despite having MgO contents similar to the less Mg-rich picrites are on the other hand largely confined to the upper part of the section. The olivine basalts are more evolved with lower MgO contents and, although they occur at intervals throughout the section, they are mainly found in the upper part of the section. Major and trace element variations within and between the groups, as well as the chemistry of the inherited olivine phenocrysts, strongly suggest that all the lavas are cogenetically related and share a similar magmatic parent. Moreover, the broad stratigraphic variation in the geochemistry of the lavas reflects a

significant change in the nature the magmatism and style of volcanism leading up to the onset of bimodal volcanism.

5.3.2 Fractionation and partial melting

The classification of the three lava groups according to their major element compositions is consistent with the petrographic descriptions outlined in Chapter 4. Despite the mildly alkaline affinity shown mainly by the picrites, the Dilb and Iyela lavas (and the ignimbrites above) together exhibit a typical tholeiitic trend suggesting that they are cogenetically related through differentiation (Fig. 5.1). This trend is indicative of iron enrichment in the early stages of differentiation. The coherent variation of major element compositions in relation to MgO, Al_2O_3 and SiO_2 suggests that the lavas are related through the chemical evolution of a melt, and this is more likely to be a consequence of fractionation than partial melting since the petrology of the lavas and mineral chemistry of their phenocrysts are both indicative of low pressure conditions. The general trends shown by most major oxides reflect typical liquid lines-of-descent, and much of the scatter about these trends may be attributed to the accumulation of specific crystallising phases (Fig. 5.5). It cannot be discounted, however, that some of the scatter may also be attributed to the effects of polybaric crystallisation and variable degrees of partial melting, magma mixing and crustal contamination. The better constrained trends for MgO compared to SiO_2 suggest that olivine is the dominant fractionating phase and this is supported by the abundance of olivine phenocrysts in all of the lavas (Chapter 4). Moreover, the observed enrichment of Al_2O_3, CaO and the alkali oxides, constant $Fe_2O_3^{(tot)}$ and depletion of Ni, with falling MgO are all characteristic of olivine fractionation. Additional fractionation of spinel together with olivine is also reflected in the consistent depletion of Cr with falling MgO (Fig. 5.18d) as well as from the common occurrence of spinel inclusions within the olivine phenocrysts (Figs 4.1 - 4.3). Other fractionating phases have less influence on the overall compositional trends, although some are marked by discernable inflection points which seem to confirm the order of crystallisation (olivine ±spinel – clinopyroxene – titanomagnetite – plagioclase ± apatite) already inferred from petrographic examination (Section 4.5.3). The most obvious inflection occurs at about 10 % MgO and the pronounced depletion of CaO with falling MgO shown by the olivine basalts from this point suggests the involvement of a Ca-rich phase. It is likely that this is a result of clinopyroxene fractionation.

Relatively constant Al_2O_3, Na_2O and K_2O above 48 % SiO_2 also suggests late-stage involvement of plagioclase in the fractionating assemblage. The presence of

plagioclase phenocrysts in only those olivine basalts with over 48 % SiO_2 seems to confirm this. The depletion in $Fe_2O_3^{(tot)}$, MnO and TiO_2 marked by a steepening of this trend with falling MgO is indicative of the early crystallisation of titanomagnetite in addition to clinopyroxene prior to the crystallisation of plagioclase, as already inferred from the occurrence in some of the lavas of titanomagnetite phenocrysts agglomerated with olivine and clinopyroxene phenocrysts (Fig. 4.16). This early liquidus appearance of titaniferous magnetite prior to plagioclase is unusual for tholeiitic basalts, although it appears to be a common characteristic of ferropicrites (Hanski & Smolkin, 1995; Stone et al. 1995; Gibson et al. 2000). Continued depletion of $Fe_2O_3^{(tot)}$and MnO, and consistent TiO_2 with increasing SiO_2 above 48 % (close to the point entry of plagioclase) is indicative of the addition of magnetite to the fractionating assemblage and the onset of groundmass crystallisation. Microprobe analyses confirm that the Fe-Ti oxides in the groundmass of most of the lavas are predominantly magnetite (Section 4.4.5), and that there is a marked similarity in the composition of plagioclase phenocrysts and groundmass microlites. It is probable therefore that the majority of the lavas were erupted at temperatures at or just below those at which plagioclase began fractionating and that this is marked by the common inflection at about 7.5 % MgO and 48 % SiO_2. It has already been suggested on the strength of petrographic evidence and temperature estimates for phenocrysts and groundmass microlites that the plagioclase phenocrysts in the olivine basalts and one ankaramite may have crystallised after eruption (Section 4.5.4). Scarrow & Cox, (1995), suggest that such random occurrences of small amounts of plagioclase across a wide compositional range in the Skye Main Lava Series implies that a significant proportion of its lavas were erupted at temperatures just below that at which plagioclase began fractionating. Continued crystallisation of clinopyroxene along with plagioclase and magnetite with falling MgO and rising SiO_2 may be also inferred from the similarity between the compositions of the clinopyroxene phenocryst rims and groundmass microlites (Table 4.11). The late stage crystallisation of apatite, evident from the presence of distinctive micro-phenocrysts within the groundmass of selected lavas (Fig. 4.35) is not evident from compositional inflections like those of the other fractionating phases. This may be because its occurrence is limited to a few of the coarser grained picrites.

Bowen (1928) argued that liquid lines-of-descent are only realistic for suites of volcanic rocks that are aphyric or phenocryst-poor. Nevertheless, departures from typical fractionation trends exhibited by porphyritic rocks like the Dilb and Iyela lavas, and those from other provinces, may be attributed to the chemical composition and

amount of phenocrysts present so that general trends are still discernable (Cox et al. 1979). The general fractionation trends in relation to MgO and SiO_2 described above may therefore be compared to and are seen to be relatively consistent with those for other CFBs (Figs. 5.5 - 5.6). As previously noted, however, the Dilb and Iyela lavas are unique in that they exhibit exceptionally low Al_2O_3 and high K_2O, P_2O_5, Fe_2O_3 and TiO_2 compared with basalts of equivalent MgO contents from other provinces and their trends for these oxides are offset accordingly. They represent only part of the fractionation array (> 5 % MgO) typically shown by the datasets for basaltic lavas from other provinces, although when combined with data for basalts with < 5 % MgO from other parts of the province, this array may be similarly extended to more evolved compositions.

MELTS was used to test the reliability of the fractionation trends described above. This is a software package designed to thermodynamically model phase equilibria in magmatic systems over the temperature range 500 – 2000 °C and pressure range up to 2 GPa (Ghiorso & Sack, 1995; Asimow & Ghiorso, 1998). Brief descriptions of the software and the procedure followed are compiled in Appendix 5.7.1 & 2 respectively. Isobaric crystal fractionation models were calculated for selected picrites and ankaramites as well as for modelled derivative compositions at varying oxygen fugacity, pressure, water content and degree of crustal contamination. The majority of the models were calculated for anhydrous compositions with pressure set at 0.001 kb and oxygen fugacity set between QFM-1 and QFM+2 (Supplement 8a). Selected compositions were modelled at higher pressures up to 10 kb, and for some a nominal water content of 0.05 % was added to the starting composition. The fractionation curves for Al_2O_3, CaO, Na_2O, K_2O, P_2O_5, TiO_2 and $Fe_2O_3^{(tot)}$ versus SiO_2 and MgO for representative model calculations plotted together with the respective data for the lavas, and associated paragenesis diagrams are shown in Appendix 5.7.3 – 8. The composition and temperature of the melt at the points of entry and exit of each mineral in the crystallisation sequence are included with the paragenesis diagrams so that they may be related to inflections in the fractionation curves. Since the diagrams are abridged and only include phase changes, the reader is reminded that the temperature scale is not linear as in conventional paragenesis diagrams.

There are common features in the fractionation trends generated from the picrites and ankaramites using MELTS. The initial order of crystallisation for both compositions is generally similar with olivine crystallising first followed by spinel, clinopyroxene, plagioclase feldspar, whitlockite, and rhm (Fe-Ti) oxide respectively.

This is consistent with the order of crystallisation described for the lavas above, although whitlockite was not identified as part of the sequence. The points at which each respective mineral joins the crystallisation sequence are well marked by inflections in the fractionation curves for selected oxides versus MgO. Initial crystallisation of olivine is characterised by increasing Al_2O_3, CaO, Na_2O, P_2O_5, TiO_2, and near constant to marginally increasing K_2O and $Fe_2O_3^{(tot)}$ with falling MgO. The addition of spinel to the fractionating assemblage is not evident from the oxides shown. The onset of clinopyroxene fractionation on the other hand is marked by increased enrichment of Al_2O_3, Na_2O, K_2O, P_2O_5, TiO_2, and $Fe_2O_3^{(tot)}$ and depletion of CaO with a continued fall in MgO. It is generally the case for the picrites that olivine drops out of the crystallisation sequence before clinopyroxene joins, and this reflected in an initial enrichment of TiO_2 and a more pronounced downturn in the $Fe_2O_3^{(tot)}$ than seen in the ankaramites before the sharp rise in both these oxides following the onset of clinopyroxene fractionation. The sharp decline in TiO_2, and $Fe_2O_3^{(tot)}$ with continued MgO depletion is attributable to the progressive incorporation of Ti and Fe into the spinel structure as ulvospinel and magnetite respectively subsequent to the complete depletion of Cr; this is evident from the zero chromite content of spinel from this point, the increase in ulvospinel and the later increase in magnetite. The addition of plagioclase feldspar to the fractionating assemblage is roughly coincident with this change, and is marked by the progressive depletion of Al_2O_3 together with continued enrichment of Na_2O, K_2O, P_2O_5 and depletion of TiO_2, and $Fe_2O_3^{(tot)}$, and a shallowing in the depletion-gradient for CaO. At high oxygen fugacity (QFM+1 and above), orthopyroxene makes a short appearance in the crystallisation sequences for the ankaramites following the entry of plagioclase, but this is not evident from an inflection in the fractionation curve. A second clinopyroxene appears in some of the sequences of the picrites at this point, and although it is similar in composition to orthopyroxene it is not classed as such by the MELTS program. The sudden steepening of the depletion-gradient for CaO at lower MgO marks the addition of whitlockite to the fractionating assemblage - the gradual rounding of the profile for Na_2O from enrichment through to depletion concomitant with the decrease in Al_2O_3 and CaO from this point is a result of the progressive change in chemistry of clinopyroxene and feldspar with continued fractionation. The addition of rhm oxide to the fractionating assemblage close to this transition leads to a steepening in the depletion-gradients for TiO_2, and $Fe_2O_3^{(tot)}$ as MgO continues to fall, although this is not always apparent in the profile of the fractionation curves. When oxygen fugacity is high (> QFM) spinel generally drops out of the crystallisation sequence as rhm oxide enters, whereas at lower oxygen fugacity

(QFM-1) it continues to crystallise alongside rhm oxide. At lower temperatures (< 1000 °C) when the MgO content of the melt drops below 0.5 %, olivine rejoins the fractionating assemblage but at this stage it is fayalitic rather than forseritic in composition. At this point it is often joined by tridymite and quartz, and at higher oxygen fugacity, by orthoclase feldspar, sphene and rutile. The effect of these minerals on the fractionation curves is not as apparent as those described above and more often than not they are beyond the scale of the plots shown. It is notable that with the exception of rare occurrences of orthoclase feldspar in some of the picrites, none of these minerals are found in the Dilb and Iyela lavas. The absence of fayalitic olivine, which is commonly found in the groundmass of many flood basalts from other provinces, is particularly unusual.

The MgO content at each inflection can be matched with the coloured-coded bars on the paragenesis diagrams to give the temperature and composition of the melt when each mineral begins crystallising or when specific components of the minerals change in concentration or become exhausted. This reveals that for both the picrites and ankaramites, all minerals, with the exception of olivine and whitlockite begin crystallising at higher temperature and MgO content when oxygen fugacity is higher; olivine and whitlockite crystallise at higher MgO content but at lower temperature when oxygen fugacity is higher. The overall effect of this is that at higher oxygen fugacity there is a net shift in the fractionation curves to the right on the MgO plots and to the left on the SiO_2 plots. For both the unmodified picrite and ankaramite compositions, the fractionation curves generated at higher oxygen fugacity (up to QFM+2) show a better fit with the data for the Dilb and Iyela lavas. This strongly suggests that the lavas fractionated under oxidising conditions as already inferred from their mineral chemistry. Despite the improved fit at higher oxygen fugacity, the fractionation curves generated from the unmodified picrite compositions do not pass through data for the ankaramites and olivine basalts. The small shift in the curves after subtracting phenocrysts only marginally improves the fit, but not so that it could be suggested that all the lavas could be generated from by simple fractionation from the picrites (Appendix 5.7.3 & 5). Similarly, the fit cannot be improved by increasing the pressure (Appendix 5.7.6), adding water (Appendix 5.7.7) or by contaminating the picrites with small amounts of crustal material (Appendix 5.7.8). In contrast the fractionation curves generated from the unmodified ankaramite composition fit well with the olivine basalt data suggesting that the olivine basalts could at least be produced by fractionation from an ankaramitic source (Appendix 5.7.4). Moreover, since the curves generated from the respective phenocryst-subtracted composition

pass through those olivine basalts that are offset from the curves for the unmodified composition, it may be suggested that it is possible to produce the entire range of compositions shown by the olivine basalts from an ankaramitic source by simply varying its phenocryst content. Contrary to this however, the fractionation curves calculated from the phenocryst subtracted ankaramite compositions show a particularly poor fit with the data for the lavas.

The ankaramites and picrites are only differentiated from one another by the dominance of clinopyroxene phenocrysts, and in every other respect they are similar. This is supported by the fact that if only the clinopyroxene phenocrysts were subtracted from the ankaramites, the shift in the phenocryst-subtracted curves would bring them in-line with the picrites (Appendix 5.7.4 - 3). It may be concluded therefore in as much as it is possible to produce the olivine basalts from the ankaramites, it is possible to produce the ankaramites from the picrites. This does not however make the picrites primary. It is already stated on the strength of their mineral chemistry that they are not primary. It is likewise proposed that the presence of chemically identical olivines with Fo contents of 89 in some of the lavas from each group suggests that the lavas are all related and that the parent magma is likely to have been in equilibrium with these olivines. The fact that the fractionation curves, particularly those for elevated oxygen fugacity (QFM+1), generated from a theoretically modelled composition in equilibrium with olivine phenocrysts with a Fo content of 89 show a remarkably good fit with the data for the lavas adds considerable weight to this argument (Fig. 5.23). Model source compositions in equilibrium with Fo_{89} olivine were calculated for all samples with > 10 % MgO by either fractionating or accumulating olivine as necessary using the method outlined in Appendix 5.6, and the average of these was used as the starting composition for these curves. Of all the compositions modelled using MELTS, they show by far the best fit with all oxide distributions for the lavas. Moreover, the deviations from these trends are easily explained in terms of accumulation (Section 5.3.3). The order of crystallisation and the relative inflections in the fractionation curves and the differences between them calculated for different oxygen fugacities are similar to those already described above for the unmodified compositions. The only significant difference is that at QFM-1, feldspar begins crystallising before clinopyroxene. At QFM+1, the order of crystallisation and the MgO content at inflections marking the points of entry of the higher temperature fractionating minerals match well with the descriptions for the lavas above (Figs 5.23 a - d). The lower temperature minerals whitlockite, orthopyroxene, sphene, tridymite, quartz and fayalitic olivine included in this model, however, are not seen in the lavas.

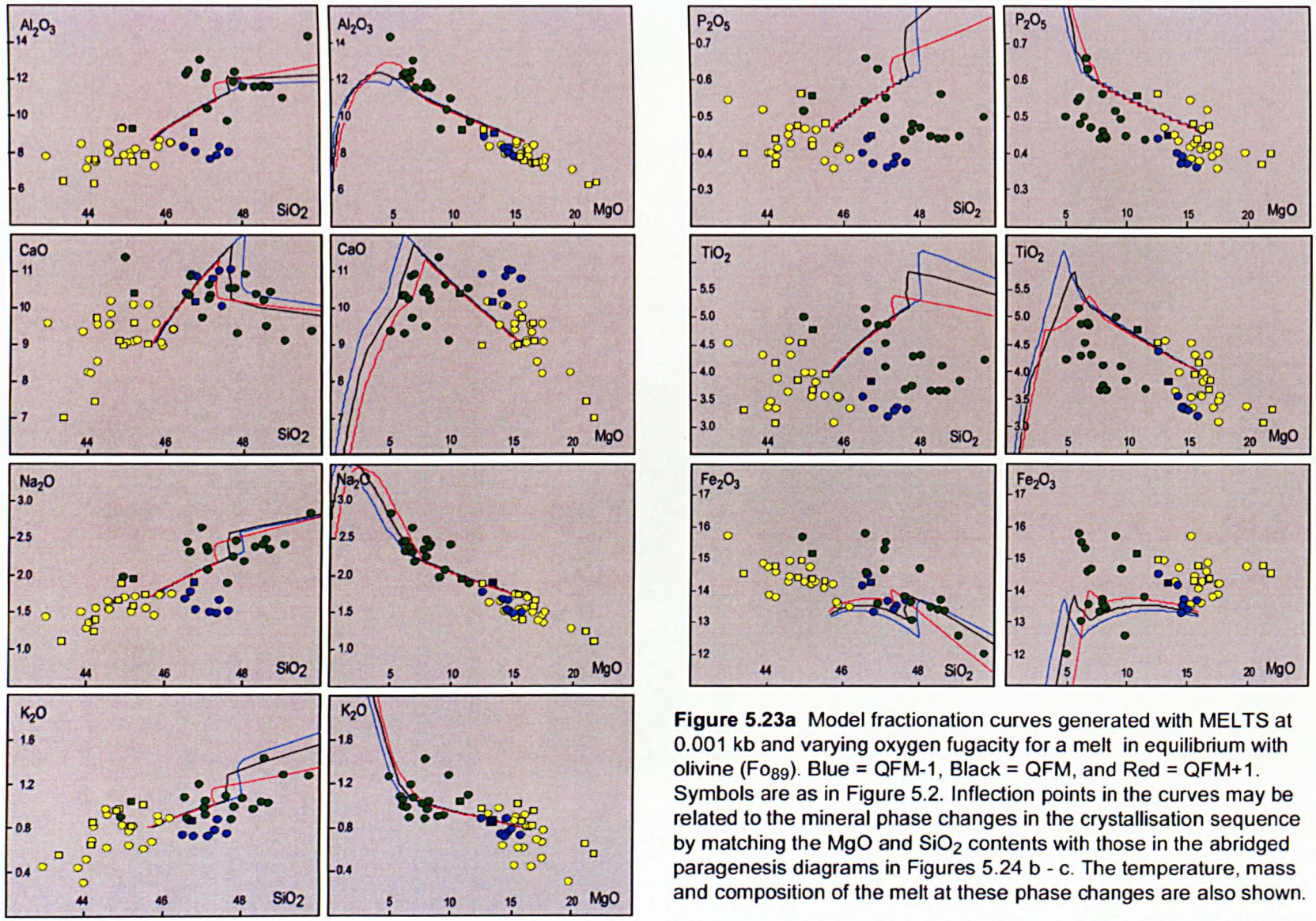

Figure 5.23a Model fractionation curves generated with MELTS at 0.001 kb and varying oxygen fugacity for a melt in equilibrium with olivine (Fo_{89}). Blue = QFM-1, Black = QFM, and Red = QFM+1. Symbols are as in Figure 5.2. Inflection points in the curves may be related to the mineral phase changes in the crystallisation sequence by matching the MgO and SiO_2 contents with those in the abridged paragenesis diagrams in Figures 5.24 b - c. The temperature, mass and composition of the melt at these phase changes are also shown.

Paragenesis Sample: Fo 89 Pressure: 0.001 kb Oxygen fugacity: QFM = -1

Temp. (C)	1384.18	1279.18	1129.18	1126.68	1086.68	1056.68	1054.18	976.68	974.18	876.68	874.18	839.18	836.68
liq mass (gm)	100.2	87.10	73.94	63.99	30.80	22.56	22.01	14.87	14.62	9.57	9.52	8.91	8.88
tephroite		0.002	0.002	0.004									
fayalite		0.106	0.148	0.251									
co-olivine		0.000	0.000	0.000									
ni-olivine		0.006	0.004	0.002									
monticellite		0.008	0.011	0.015									
forsterite		0.879	0.835	0.729									
chromite			0.535	0.245	0.108	0.000	0.000						
hercynite			-0.458	-0.353	-0.368	-0.254	-0.197						
magnetite			0.106	0.163	0.155	0.155	0.155						
spinel			0.678	0.510	0.472	0.305	0.237						
ulvospinel			0.139	0.435	0.633	0.795	0.806						
albite				0.367	0.395	0.482	0.540	0.543	0.616				
anorthite				0.620	0.590	0.490	0.418	0.414	0.224				
sanidine				0.013	0.015	0.028	0.042	0.043	0.160				
diopside					0.447	0.389	0.380	0.377	0.164	0.153	-0.219		
clinoenstatite					0.158	0.152	0.133	0.133	0.122	0.121	0.095		
hedenbergite					0.218	0.294	0.332	0.339	0.584	0.595	0.983		
alumino-buffonite					0.123	0.105	0.092	0.088	0.046	0.045	0.015		
buffonite					-0.028	-0.014	-0.006	-0.006	0.011	0.012	0.046		
essenite					0.064	0.055	0.047	0.047	0.047	0.047	0.048		
jadeite					0.018	0.020	0.022	0.022	0.026	0.026	0.032		
whitlockite													
geikielite							0.122	0.042	0.040	0.000	0.000	0.000	0.000
hematite							0.050	0.057	0.057	0.050	0.051	0.054	0.541
ilmenite							0.814	0.872	0.874	0.894	0.893	0.889	0.888
pyrophanite							0.014	0.028	0.028	0.056	0.056	0.058	0.058
albite								0.460	0.456	0.424	0.423	0.411	0.410
anorthite								0.066	0.064	0.032	0.031	0.026	0.026
sanidine								0.473	0.480	0.545	0.546	0.563	0.565
sphene													
SiO_2	45.71	46.53	48.02	47.96	56.18	61.82	62.31	69.61	69.84	76.44	76.51	77.40	77.44
TiO_2	4.01	4.61	5.37	5.85	4.29	3.43	3.26	1.53	1.50	0.74	0.73	0.52	0.51
Al_2O_3	8.70	10.01	11.59	12.11	11.77	11.06	11.00	9.13	9.02	5.85	5.78	4.91	4.86
$Fe_2O_3^{(tot)}$	13.21	13.38	12.55	13.16	8.89	6.12	5.97	3.89	3.85	1.94	1.94	1.84	1.83
Cr_2O_3	0.19	0.22	0.06	0.03	0.00	0.00	0.00	0.00	0.00	0.00	0.00	0.00	0.00
MnO	0.16	0.16	0.14	0.16	0.33	0.45	0.46	0.63	0.64	0.92	0.92	0.97	0.98
MgO	15.87	11.24	6.14	5.17	2.35	1.32	1.25	0.26	0.25	0.00	0.00	0.00	0.00
NiO	0.11	0.05	0.01	0.01	0.02	0.03	0.03	0.05	0.05	0.07	0.07	0.08	0.08
CaO	9.06	10.37	12.08	11.04	9.02	7.66	7.54	5.66	5.66	5.87	5.91	6.40	6.43
Na_2O	1.72	1.98	2.31	2.54	3.29	3.52	3.53	3.40	3.39	3.20	3.19	3.10	3.09
K_2O	0.81	0.93	1.09	1.26	2.48	3.29	3.36	4.60	4.57	3.44	3.41	3.02	2.99
P_2O_5	0.46	0.53	0.63	0.73	1.38	1.30	1.28	1.25	1.25	1.53	1.54	1.76	1.78

Olivine Feldspar Quartz
Spinel Whitlockite Sphene
Clinopyroxene Rhm oxide

Figure 5.23b Abridged paragenesis diagram for model fractionation calculated at QFM-1from theoretical melt in equilibrium with olivine Fo89. **Note:** the scale is not arithmetic.

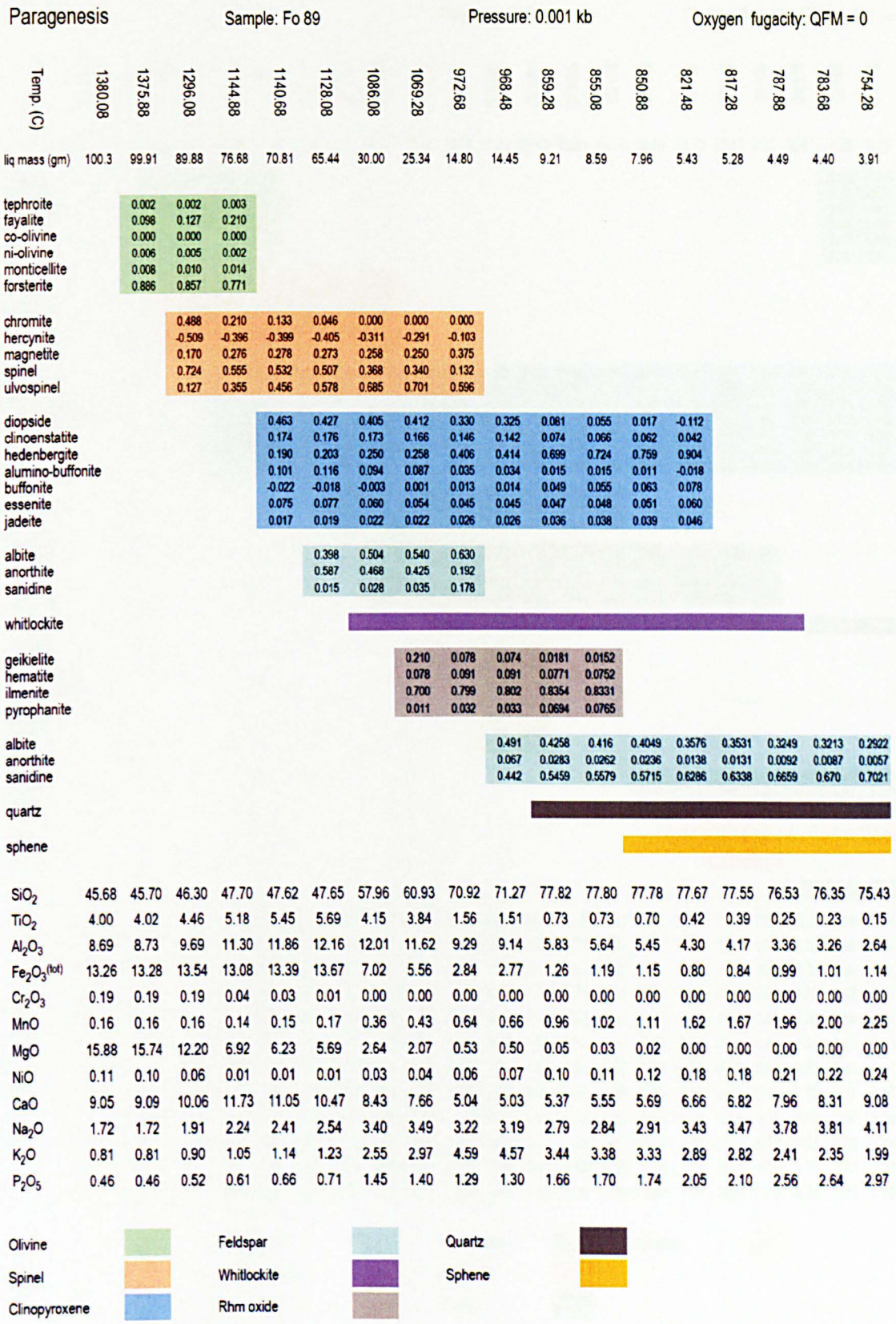

Figure 5.23c Abridged paragenesis diagram for model fractionation calculated at QFM-1 from theoretical melt in equilibrium with olivine Fo89. **Note:** the scale is not arithmetic.

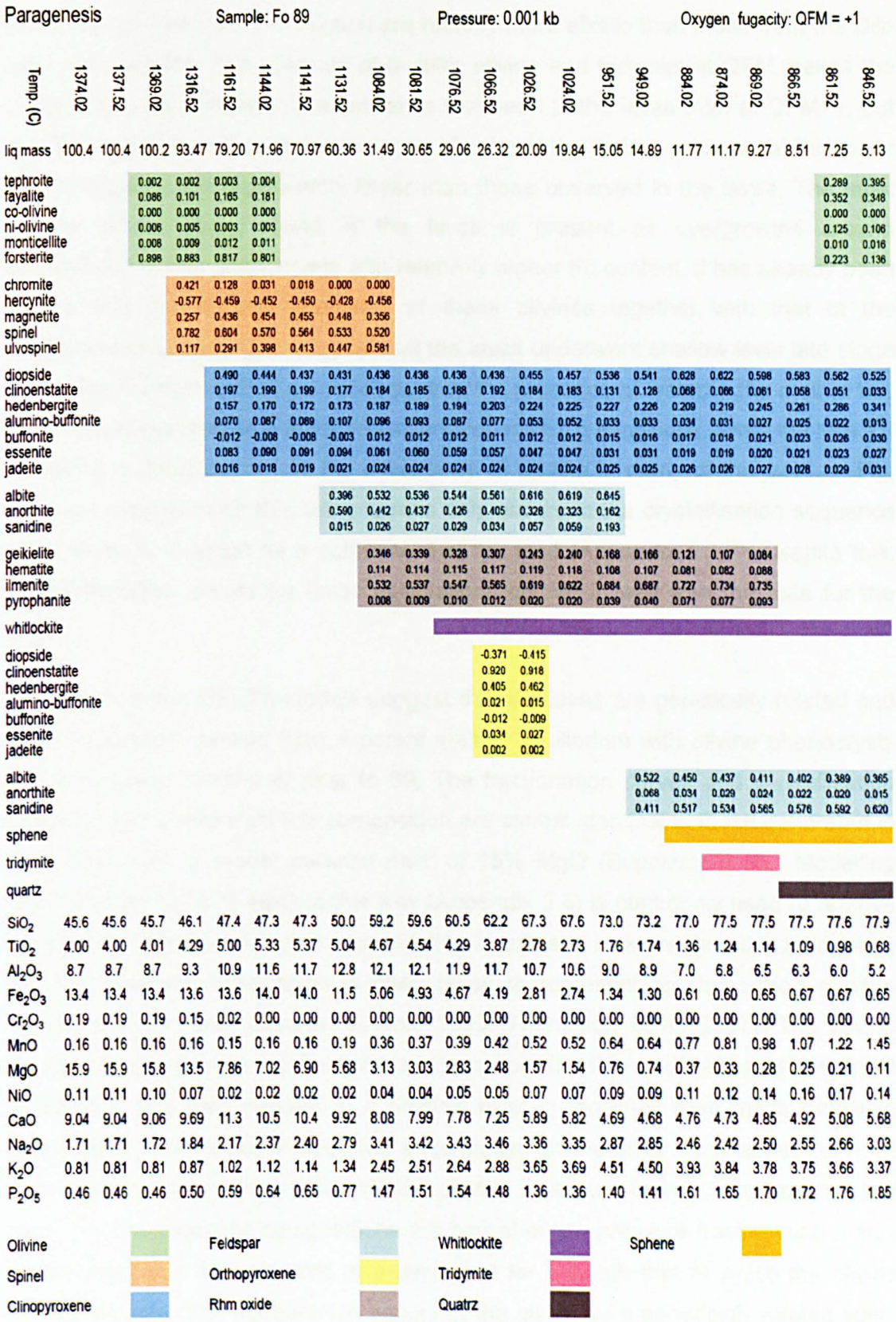

Figure 5.23d Abridged paragenesis diagram for model fractionation calculated at QFM+1 from theoretical melt in equilibrium with olivine Fo89. **Note:** the scale is not arithmetic.

Orthopyroxene is found in one of the picrites from the Bilbala Section, but, as already noted, the picrites from this section are notably more alkalic than those from the Dilb and Iyela sections. The absence of fayalitic olivine and tridymite at QFM makes the fractionation assemblage more similar to that seen in the lavas than at QFM+1, but the MgO contents of the melt at the point of entry of the various minerals at this lower oxygen fugacity are significantly lower than those observed in the lavas. The most fayalitic olivine (Fo_{60}) found in the lavas is present as overgrowths around iddingsitized olivine phenocrysts with relatively higher Fo content. It has already been argued that the mineral chemistry of these olivines together with that of the clinopyroxene phenocrysts suggest that the lavas underwent shallow level late stage fractionation under oxidising conditions, and the presence of water in the melt at this stage was suggested as a possible explanation for such conditions. From the MELTS modelling it would seem that the occurrence of apatite in many of the picrites (Fig. 4.35) is consistent with this since apatite only occurs in the crystallisation sequence when water is included as a component of the melt (Appendix 5.7.7). Despite this, the fractionation curves for these calculations do not fit well with the data for the lavas.

On the whole the MELTS models suggest that the lavas are genetically related and could have been derived from a parent melt in equilibrium with olivine phenocrysts with a forsterite content of near to 89. The fractionation curves and crystallisation sequence generated from this composition are almost identical to those generated in same way from a 'model parental melt' of 15% MgO (Supplement 8b). Modelling basaltic rocks to 15 % MgO in this way (Appendix 5.6) is commonly used to remove the effects of fractionation and accumulation in suites of rocks assumed to be related, and the resultant composition is often taken to represent an unmodified mantle-derived primary melt (Scarrow & Cox, 1995; Thompson et al. 2007). The olivine basalts represent the more fractionated lavas from the Dilb and Iyela sections and it is probable that they evolved at a shallow level in the crust from melts similar in composition to the ankaramites. The ankaramites on the other hand appear to have evolved from compositions similar to the picrites by accumulating clinopyroxene, and since the clinopyroxene compositions are typical of low pressure fractionation it may be assumed that this occurred at a depth not far beneath that at which the olivine basalts evolved. The fractionation history of the lavas, as a genetically related suite, is then likely to have been polybaric rather than isobaric as modelled here by MELTS. This has already been inferred from the mineral chemistry of the olivine phenocrysts in the lavas (Chapter 4). It is also evident from the distribution of the three lava types

on a plot of CIPW normative ol-di-hy-ne-qz (Fig. 5.3). Although this projection ignores plagioclase, it is useful for illustrating the crystallisation behaviour of olivine tholeiite suites such as the Dilb and Iyela lavas in relation to experimentally determined cotectics for equilibrium assemblages including olivine, plagioclase, clinopyroxene and basaltic melt. The olivine basalts plot along the 1 atm cotectic thereby supporting the view that the final stage of evolution of the lavas took place at low pressures. The ankaramites and picrites plot closer to the olivine apex either side of the 0.8 GPa cotectic suggesting they evolved at higher pressures. As the cotectic moves downwards on the normative plot it can be estimated that the ankaramites evolved at pressures between 0.6 – 0.8 GPa whereas the picrites evolved at pressures between 0.8 and 0.9 GPa. For some samples which have accumulated olivine and consequently elevated MgO contents, these estimates are unrealistically high; this is certainly the case for the picrites that plot below the 0.9 GPa cotectic. With decreasing MgO, the lavas together form a coherent trend toward quartz apex. The distribution is typical of olivine tholeiite magmas that have fractionated within the upper crust (Thompson, 1987) and is notably similar to that shown by the Horingbaai dykes of Southern Etendeka (Thompson et al. 2001). Like the more MgO rich Horingbaai dykes, the Dilb and Iyela ankaramites and picrites cluster together around the 0.8 GPa cotectic with the Etendeka ferropicrites and Fe-rich basalts (Gibson et al. 2000), but unlike these they do not contain aluminous clinopyroxene phenocrysts as additional evidence of high-pressure magmatic evolution. It is assumed from the absence of hydrous minerals in the lavas that the magmas were essentially dry. The presence of magmatic iddingsite and apatite however implies the late stage involvement of water as previously suggested. This may have been ground water drawn into the magma either during its ascent to the surface or whilst trapped in a shallow seated magma chamber (Chapter 4). With the evolution of the magmatic plumbing system and the establishment of shallow seated reservoirs or magma chambers, the associated fracturing of the crust would increase the likelihood of water interacting with the magma. This is supported by the presence of hydrous minerals such as hornblende and biotite in the rhyolitic ignimbrites at the top of the Dilb Section.

The distributions for trace elements in relation to MgO, Al_2O_3 and SiO_2 (noted earlier to resemble those for the major elements - Section 5.2.3) appear to similarly reflect an evolution for the lavas dominated by fractionation as described above. The majority of trace elements are generally incompatible in the main fractionating phases and hence show distinctive negative correlations with Mg which reflect their

increasing concentration in the melt during fractionation (Fig. 5.18). It follows then that the higher concentrations of incompatible trace elements in the olivine basalts compared to the picrites and ankaramites are a consequence of them being more evolved, having undergone greater degrees of fractionation (Fig. 5.8). The dominance of these more evolved lavas in the upper part of the section and the associated increase in mean concentration of VICE above 01.03.25.02 (Fig. 5.21) furthermore support the suggestion that over time there was an increasing tendency for volcanism to be sourced from shallow seated reservoirs in which the magma was able to fractionate for substantial periods before being erupted. In contrast, Ni and Cr are compatible in the main crystallising phases (dominantly olivine for Ni and spinel for Cr) and therefore show strong positive correlations with Mg which reflect their decreasing concentration in the melt during fractionation. This is evident from the low concentrations of these elements in the olivine basalts compared to the picrites and ankaramites, and from the dramatic decrease in their concentration in the section above 01.03.25.02 (Fig. 5.19 & Table 5.3d). Sc, is incompatible in olivine but compatible in clinopyroxene and consequently shows an arced trend in relation to Mg similar to that for CaO vs MgO reflecting its progressive depletion from the point at which clinopyroxene joins the fractionating assemblage (Fig. 5.18d). It may be assumed therefore that the elevated concentrations of Sc in the ankaramites are a result of accumulated clinopyroxene. Despite the fact there is no discernible inflection in the distribution of Sr in relation to the major element indices (Fig. 5.18b), and that plagioclase phenocrysts occur in only a few of the lavas, evidence for low-pressure plagioclase fractionation is apparent from the distinctive trough for Sr in the trace element profiles for all the lavas.

The respective trace element trends in relation to Mg are matched well by model curves for olivine fractionation calculated as in Appendix 5.8.1 from samples representative of the picrites and ankaramites (Fig. 5.24). As with the MELTS models, the better fit for those curves generated from the ankaramite compared to those generated from the picrite supports the proposition that the olivine basalts are produced from an ankaramitic rather than a picritic source. This is not the case for the mobile LFSE or large ion lithophile elements (LILE) such as Cs and Rb which show more scattered distributions compared to the HFSE and REE possibly as a result of late-stage fluid mobilisation (Figs. 5.24 a - c). Ba and Pb, which on the contrary show tightly constrained distributions, also do not conform to this typical behaviour for similar reasons. The distributions of HFSE on the other hand are controlled more by the composition of the source or by crystal-melt processes and

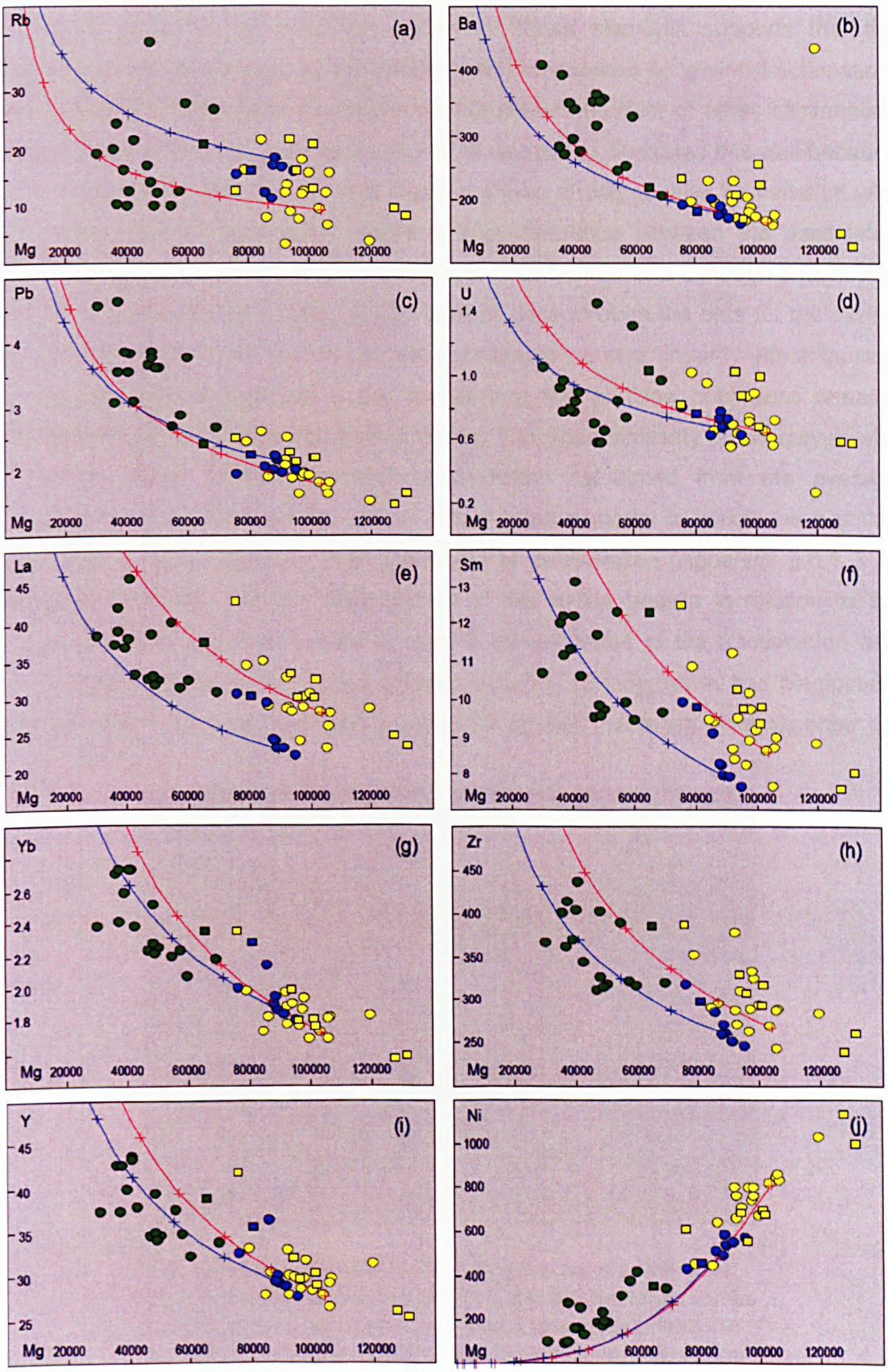

Figure 5.24 Distribution of selected trace elements in relation to Mg showing model curves for olivine fractionation generated from representative picritic and ankaramitic compositions. The red curve is for picrite 01.03.26.03, and the blue is for ankaramite 01.03.24.07. Concentrations are in ppm and symbols are as in Figure 5.2.

are therefore more likely to reflect the evolution of the lavas more reliably. The closeness of fit for the modelled curves for these elements supports that the evolution of the lavas was, as previously noted, dominated by olivine fractionation, although at the same time the curves do not show the effect of other fractionating phases (Figs 5.24 d - i). The distribution of Ni versus Mg illustrates this well because of its compatibility with olivine; as a result it shows strong positive co-variation with Mg during olivine fractionation. There is little difference between the associated olivine fractionation curves for the picrites and ankaramites, and although both fit well with the data for the both these groups, neither pass through the data for the olivine basalts (Fig. 5.24j). This may in part be a consequence of a 'linearity effect' caused by the assumption inherent in the model that the partition coefficient remains constant throughout the fractionation process. The close similarity of the curves with those for olivine fractionation and accumulation calculated from the average composition in equilibrium with olivine (Fo_{89}) using a model in which the partition coefficient is recalculated for each increment of fractionation (Appendix 5.6.1 & 2) suggests, however, that the displacement of the olivine basalts in relation to the model olivine fractionation curves is more a consequence of the fractionation and accumulation of additional mineral phases including clinopyroxene and plagioclase feldspar (Fig. 5.25). It is clear from the MELTS models that these minerals enter the

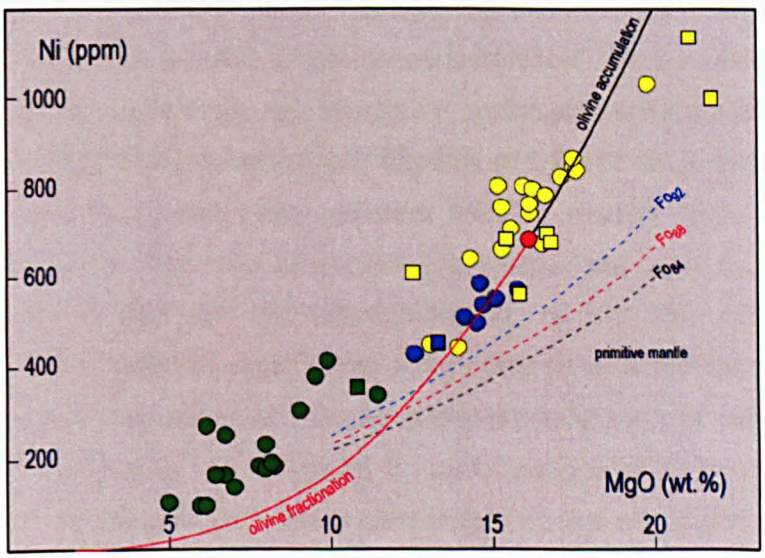

Figure 5.25 MgO (wt.%) versus Ni (ppm) for the Dilb lavas showing model olivine fractionation and accumulation curves calculated as in Appendix 5.6.1 and 2 respectively from the average composition for the lavas in equilibrium with olivine (Fo_{89}) (Appendix 5.6.4) - represented by the red circle. The dashed lines represent equilibrium melts for mantle olivine (Fo_{84} -Fo_{92}) calculated as in Appendix 5.6.5. Symbols are as in Figure 5.2.

crystallisation sequence at lower temperatures than olivine and the points at which they begin crystallising are marked by significant inflections in the fractionation curves. Therefore in order to test whether or not such inflections are sufficient to bring the fractionation curves more in line with the trace element distributions, a trace element fractionation model which uses data from the MELTS output files was developed (Appendix 5.8.2).

For selected compositions, the temperature, solid mass and remaining liquid mass for each fractionation increment were transferred from the respective melts-liquid.tbl files, and the mass of olivine, clinopyroxene and feldspar from the associated mineral.tbl files were totalled and recalculated as a proportion of one (Supplement 9b). For each increment of fractionation, the recalculated mineral proportions were used to calculate a bulk partition coefficient, which was used together with the normalised and recalculated liquid mass to calculate the concentration of each trace elements in the remaining liquid (Appendix 5.8.2). All calculations for this model are compiled in Supplement 9c. Since the partition coefficients for Mg vary more significantly with pressure, temperature and oxygen fugacity for clinopyroxene and feldspar than for olivine, Y was used as a fractionation index. Y is minimally affected by source heterogeneity and crustal contamination and is strongly correlated with Mg thus indicating that it behaves predictably during fractionation (Fig. 5.24i). It may also be a more reliable fractionation index than Mg because the Mg content of many of the lavas is elevated as a result of olivine accumulation. Fractionation curves were generated using this model from representative picritic and ankaramitic compositions for a pressure of 0.001 kb and an oxygen fugacity of QFM+1 since these parameters provided the best fit for the major element MELTS models (Fig. 5.26). Marked inflections at the points where clinopyroxene and plagioclase begin crystallising bring the curves more in line with the distributions for all but the very incompatible elements (Rb, Ba, U and Pb) which show a high degree of dispersal, particularly for the olivine basalts. The onset of clinopyroxene crystallisation is expressed by an increase in the gradient of the curves at Y concentrations of 37 ppm for the picrite and 33 ppm for the ankaramite - these concentrations are equivalent in the MELTS output data to 8.1 % and 9.6 % MgO, and temperatures of 1171 and 1199 °C respectively. The onset of plagioclase crystallisation is evident from a subsequent decrease in the gradient of the curves at Y concentrations of 44 ppm for the picrite and 41 ppm for the ankaramite – equivalent to 4.5 % and 4.8 % MgO, and 1121 and 1124 °C respectively. This is most noticeable for Sr which is compatible in plagioclase and therefore becomes progressively depleted at higher Y concentrations.

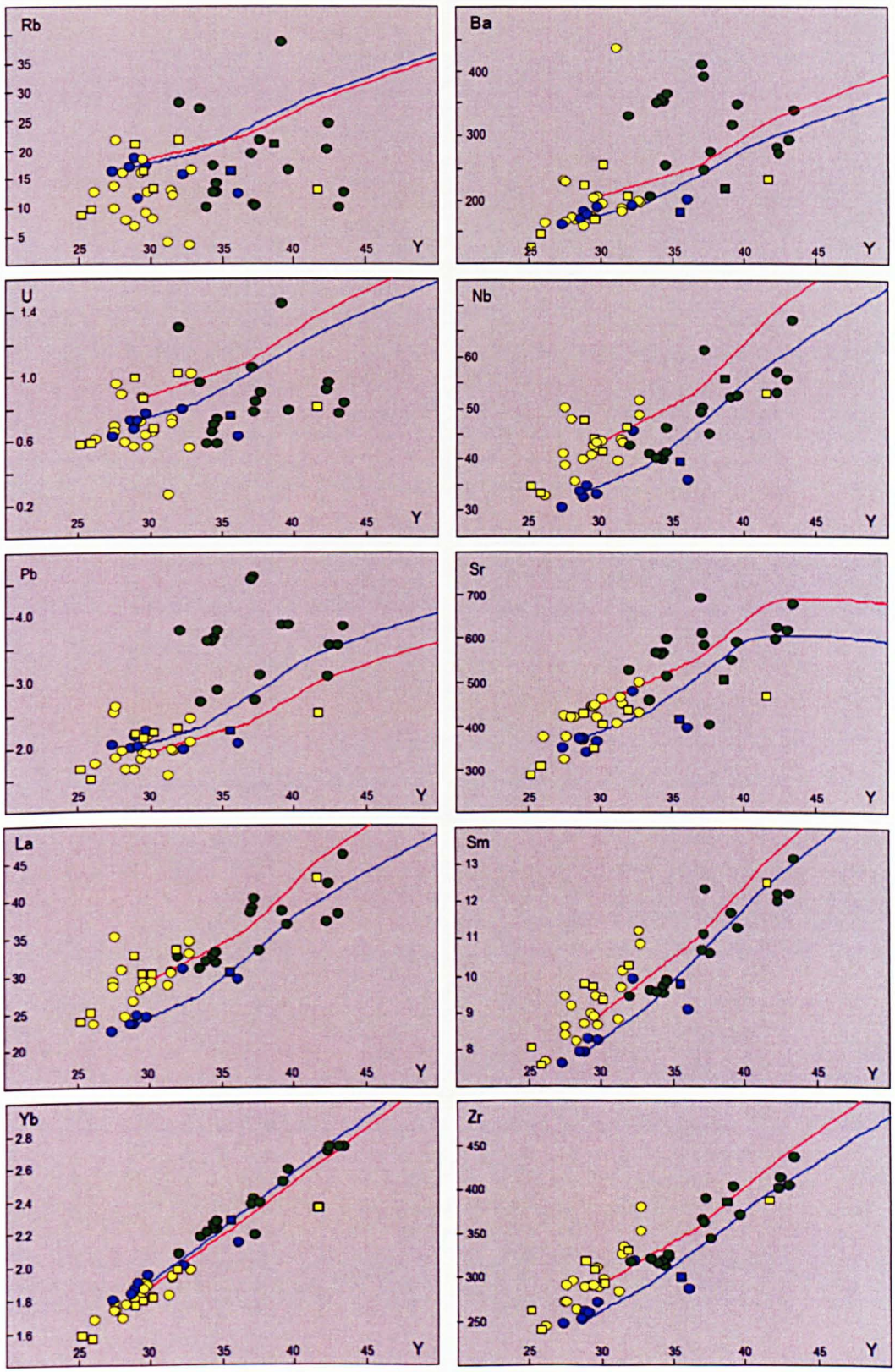

Figure 5.26 Distribution of selected trace elements in relation to Y showing model fractionation curves generated from selected picritic (01.03.25.07 - red) and ankaramitic (01.03.24.11 - blue) compositions using the liquid mass and proportion of crystallising minerals for each fractionation increment from the respective MELTS output files (Appendix 5.8.2). Concentrations are in ppm and symbols are as in Fig.5.2.

Olivine drops out of the crystallisation sequence at Y concentrations of 39 ppm (6.8 % MgO - 1146 °C) for the picrite and 37 ppm (7.3 % MgO - 1154 °C) for the ankaramite, although this is not evident from the curves. It is notable that, although the initial MgO content and temperature at which olivine begins crystallising in the picrite (16.3 % MgO - 1386 °C) is higher than in the anakramite (15.2 % MgO - 1344 °C), clinopyroxene and plagioclase begin crystallising at higher MgO contents and temperatures in the ankaramite than in the picrite. Moreover, it is evident from the major element MELTS models that this is a consistent difference between the two lava groups. Overall, the fit of the curves to the data is better for the middle and heavy rare earth elements and other HFSE elements such as Hf, Ti and Zr with similar degrees of incompatibility, Also, as with the previous fractionation models, the curves generated from the ankaramitic compositions generally show a better fit with the olivine basalts than those generated from the picritic compositions. This further supports the proposition that the olivine basalts are more likely produced from an ankaramitic rather than a picritic source. It is evident, however, that for some elements (Ba, La, Sr and Zr) the curves generated from the picrite in this model do pass through some of the olivine basalts, so it cannot be discounted that some may have been produced from a source not unlike the picrites.

On the strength of mineral chemistry and the data from the major element MELTS models, the above model assumes that fractionation occurred at low pressures in oxidising conditions with an oxygen fugacity of QFM + 1 or above. For similar reasons also it assumes that the observed trends are a result of fractionation. Chondrite-normalised REE ratio plots designed to illustrate the degree of REE fractionation however suggest that the observed trends may in part be a result of differences in partial melting (Fig. 5.27). Fractionation trends for olivine and clinopyroxene at varying oxygen fugacity, pressure and temperature were generated using the method described in Appendix 5.8.3 and are included on the REE ratio plots to illustrate a range of idealised scenarios. REE partition coefficients for clinopyroxene were calculated for the range of conditions shown using a predictive model for REE partitioning between clinopyroxene and anhydrous silicate melts developed by Wood & Blundy (1997) (Appendix 5.8.4), whereas those for olivine were kept the same regardless of the conditions. The REE ratios selected represent the gradient of sections of the chondrite-normalised REE patterns shown in Figure 5.15, i.e. $(La/Yb)_N$ for all REE, $(La/Sm)_N$ for the LREE and $(Gd/Yb)_N$ for the HREE. Since the partition coefficients increase by an order of magnitude from Lu to La in olivine and clinopyroxene, enrichment of LREE relative to HREE is often attributed to

a. Varying oxygen fugacity at fixed temperature (normative) and pressure (0.001 kb)

b. Varying pressure at fixed temperature (normative) and oxygen fugacity (Fe_2O_3 = 0.10)

c. Varying temperature at fixed pressure (0.001 kb) and oxygen fugacity (Fe_2O_3 = 0.10)

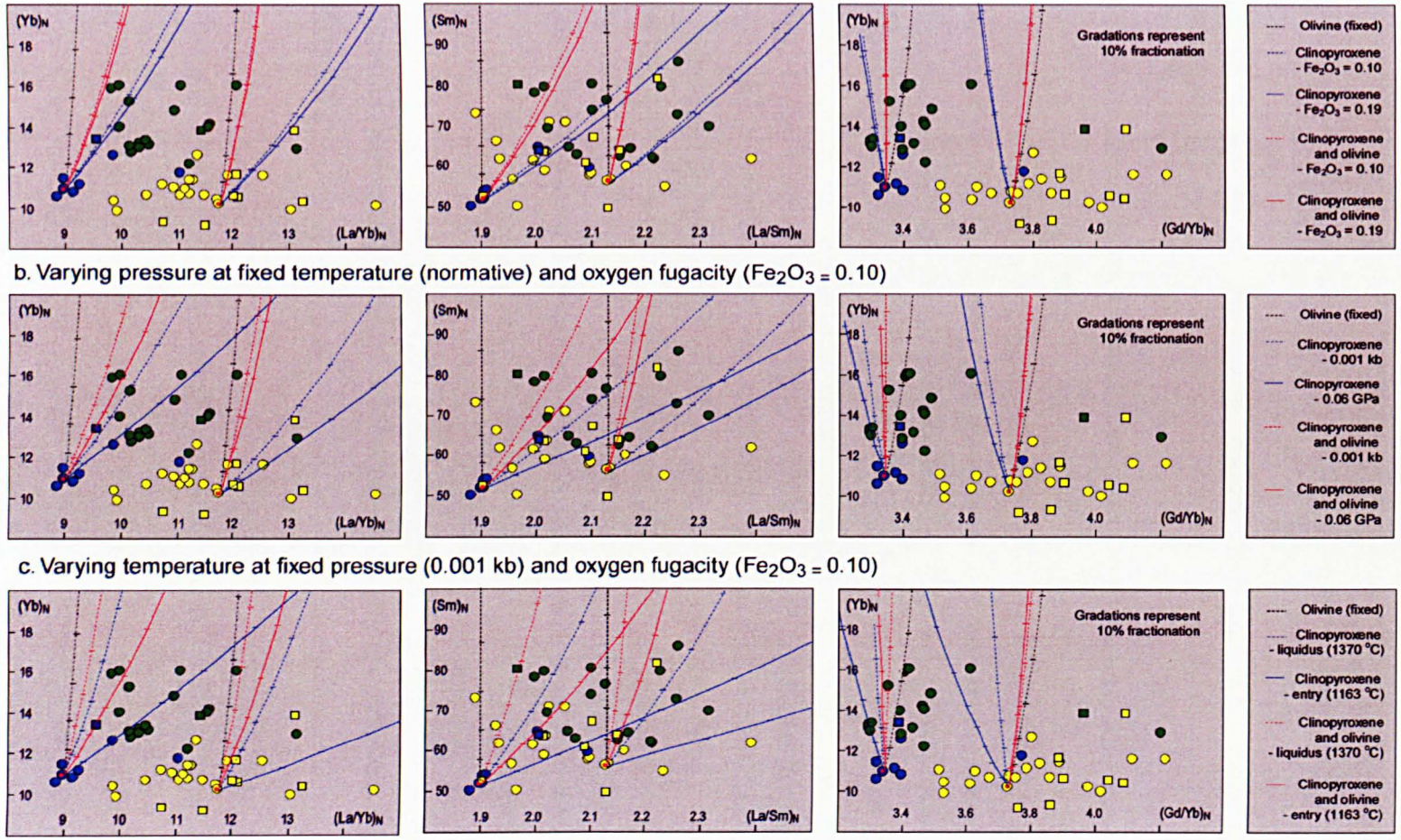

Figure 5.27 Chondrite normalised REE ratio plots showing the theoretical fractionation curves for olivine and clinopyroxene generated from representative picritic (01.03.26.03 - yellow origin) and ankaramitic (01.03.24.07 - blue origin) compositions over a range of conditions. The liquidus temperatures for both lavas calculated from their normative compositions (Appendix 5.4.2) are used where temperature is fixed.

the fractionation of these minerals. Strong enrichment of HREE relative to LREE marked by steep REE profiles for the three lava groups and the fractionation trends discussed so far would suggest that this is the case for the Dilb and Iyela suite. Such enrichment of LREE relative to HREE may however result from partial melting, and when lavas within a defined suite have originated from different degree partial melts, their REE ratios will vary so that when plotted one element against another, or against a fractionation index such as Mg or Y, they will form a trend identical to that for fractionation.

Generally it is thought that REE ratios such as $(La/Yb)_N$ and $(Gd/Yb)_N$ are minimally affected by fractional crystallisation, therefore they are often taken to reflect the composition of the source – this is considered to be particularly true for the HREE ratios. Moreover these ratios are initially determined by the degree of partial melting – or in other words by the percentage melt fraction from which the rock is sourced. Since the degree of incompatibility of the REE increases (albeit marginally) from Lu through to La, the relative proportion of heavy to light REE increases with partial melting. Consequently, REE ratios in which the heavier element is the denominator (like those used in Figure 5.27) will decrease as melt fraction increases. It is clear from Figure 5.27 that, with few exceptions, the olivine basalts have a restricted range of $(Gd/Yb)_N$ ratios (3.3 - 3.5) that is notably lower than that of the picrites and similar to that of the ankaramites, and that they plot along model fractionation curves that originate from an ankaramitic source. This seems to confirm that the olivine basalts evolved by fractional crystallisation from ankaramitic source. This is less discreetly defined from the LREE ratios since differences in the partition coefficients for these elements are not as pronounced as they are for the HREE and the data is more dispersed, and the lava groups are less well defined as a consequence.

In contrast, the ankaramites and picrites appear to not be related so much through fractional crystallisation, but instead represent different percentage melt fractions from the same source. The picrites have larger and more wide ranging $(La/Yb)_N$ and $(Gd/Yb)_N$ ratios than the ankaramites are therefore more likely to have been derived from smaller and more variable degrees of partial melting, although it cannot be discounted that such differences may be attributed to variable amounts of garnet in the source. The distinction between fractionation, and partial melting and/or variable amounts of garnet is particularly well illustrated on plots of the chondrite-normalised REE ratios used above against the major element fractionation indices MgO and

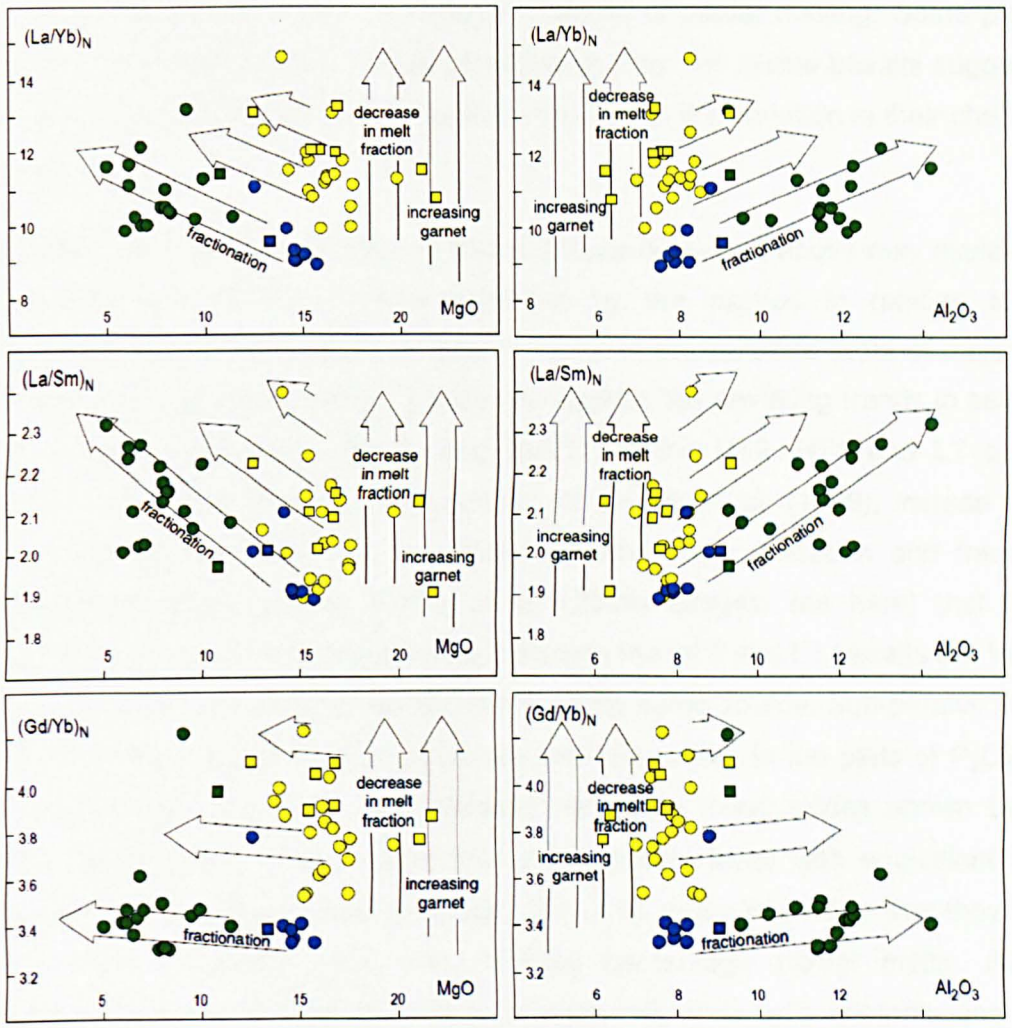

Figure 5.28 Distribution of chondrite-normalised REE ratios versus MgO and Al_2O_3. The arrows indicate the generalised trends for fractionation and partial melting. MgO and Al_2O_3 are in wt. %. Symbols are as in Figure 5.2.

Al_2O_3 (Fig. 5.28). On these plots the picrites and ankaramites exhibit a trend that is clearly dominated by variable degrees of partial melting, whereas the olivine basalts lie on what is dominantly a fractionation trend coincident with falling MgO and rising Al_2O_3. The model curves in Figure 5.27 indicate that the olivine basalts were generated from an ankaramitic source by between 10 and 40% fractional crystallisation of olivine and clinopyroxene in an oxidising environment (> QFM+1) at low pressure (< 0.06 GPa) and at temperatures considerably lower than the liquidus for olivine (1370 °C) – possibly lower than the temperature at which clinopyroxene began crystallising (1163 °C). This suggests that they evolved from an already partially crystallised source, as inferred earlier from the diversity of their phenocryst populations (Chapter 4). The restricted range of Al_2O_3 concentrations in the picrites and ankaramites (7 - 9 wt. %) suggests that there is little variation in the amount of garnet in the source and that the observed differences in the REE ratios for the lavas

are more likely to be a result of variable degrees of partial melting. Some picrites however plot on fractionation trends parallel to that for the olivine basalts suggesting that fractional crystallisation has at least contributed to the variation in their chemistry as a group.

The difference in genesis between the lava groups described above may explain the sub-parallel and deviating trends exhibited by the picrites in relation to the ankaramites and olivine basalts evident in many of the bivariate plots of major and trace elements described earlier. It may also explain the deviating trends in selected trace element distributions (Nb-Zr and Pb-Zr) for the HT2, HT1 and LT basalts described as scatter and left unaccounted for by Pik et al. (1999); instead these trends were vaguely attributed to 'processes other than alteration and fractional crystallisation. More recently Kieffer et al. (2004) suggest (as here) that these fundamental differences in geochemistry between the HT2 and LT basalts are largely a result of variable degrees of partial melting of the same source. Sub-parallel trends for the Dilb and Iyela lavas are particularly well developed in the plots of P_2O_5 and TiO_2 versus MgO (Fig. 5.5). The elevated trends for these oxides shown by the picrites, noted earlier to be higher than any reported lavas with equivalent MgO contents from other flood basalt provinces (Fig. 5.6), seem to confirm that they were derived from unusually small and variable percentage partial melts. Similar conclusions may be inferred from their exceptionally low Al_2O_3 contents and their deviating, and uniquely elevated, trends for K_2O and Fe_2O_3 (Fig. 5.5). It is moreover consistent with suggestion that the most enriched HT2 basalts which contain La contents 100 times greater than primitive mantle were derived from a source generated from less than 1% partial melting (Kieffer et al. 2004). The olivine basalts however, having evolved by fractional crystallisation from relatively larger percentage partial melts, have compositions that are more typical of flood basalts from other provinces (Fig. 5.6). This same line of reasoning led Kieffer et al. (2004) to suggest that the LT basalts when corrected for fractionation could have been derived from the same source as the HT2 basalts by 10 times more partial melting.

The distinction between fractionation and partial melting evident in the Dilb and Iyela lavas may be further inferred from the variable 'fractionation-orientated' EM signature of the olivine basalts compared to the relatively consistent HIMU signature of the picrites and ankaramites (Figs 5.10 - 12), and less so from the relative distributions of selected VICE (Fig. 5.14). It is most clearly defined on bivariate plots of REE ratios (Figs 5.15 & 27), REE pairs with increasing differences in ionic radii (Fig. 5.18) and

all except the more mobile trace elements versus MgO, Al_2O_3 (Figs 5.18 & 28) and Y (Fig. 5.26). Essentially, the differences in slope of the REE patterns for the picrites and ankaramites is mainly related to differences in partial melting whereas for the olivine basalts they are a result of variable degrees of fractionation (Fig. 5.16). Similarly the greater degree of enrichment of VICE in the olivine basalts compared to the picrites and ankaramites expressed in their trace element abundance profiles is largely attributable to greater degrees of fractional crystallisation (Fig. 5.8). The EM signature of the olivine basalts relative to the HIMU signature of the picrites and ankaramites is therefore assumed to be a consequence of this rather than of mixing with an enriched sub continental lithospheric mantle or crustal source as suggested by Pik et al (1999) for the more evolved HT1 and LT basalts (Section 5.3.4).

5.3.3 Mixing and accumulation

As SiO_2 is a major component of the main fractionating phases, its variation in relation to other major element oxides highlights accumulation trends that are not apparent in relation to MgO (Fig. 5.6). On the plots for Al_2O_3, Na_2O, K_2O, P_2O_5 and TiO_2 against SiO_2, the ankaramites in particular together define a discreet clinopyroxene accumulation trend at an angle to the main olivine fractionation trend. This is particularly apparent in relation to the MELTS model fractionation curves (Fig. 5.23a). Some of the picrites and olivine basalts with a high percentage of clinopyroxene phenocrysts also tend to show similarly aligned displacements tangential to the main fractionation trends. A plot of the Mg# of representative clinopyroxene phenocrysts from each lava group against the Mg# of their host rock appears to confirm that most are accumulative since all respective analyses plot below the line for theoretical equilibrium between the phenocrysts and melt at atmospheric pressure (Fig. 5.29). It also indicates that the majority of clinopyroxene phenocrysts in the lavas are not in equilibrium with the whole-rock compositions and have crystallised from less magnesian melts than suggested by the bulk rock chemistry. Pik et al. (1998) suggests that this is a feature that distinguishes some HT2 basalts from the LT, HT1 and other HT2 basalts which plot close to the equilibrium line (Fig. 5.29). Compositional differences between the clinopyroxene groundmass microlites in the olivine basalts and the majority of clinopyroxene phenocryst cores (Figs 4.51 - 55), on the contrary, suggest that the phenocrysts crystallised from a more magnesian melt than the groundmass. The similarity in the composition of some phenocryst rims and groundmass microlites suggest at least that the later formed phenocrysts may have been in equilibrium with the melt, and that the Mg# of the host lavas may be unusually elevated because of their olivine

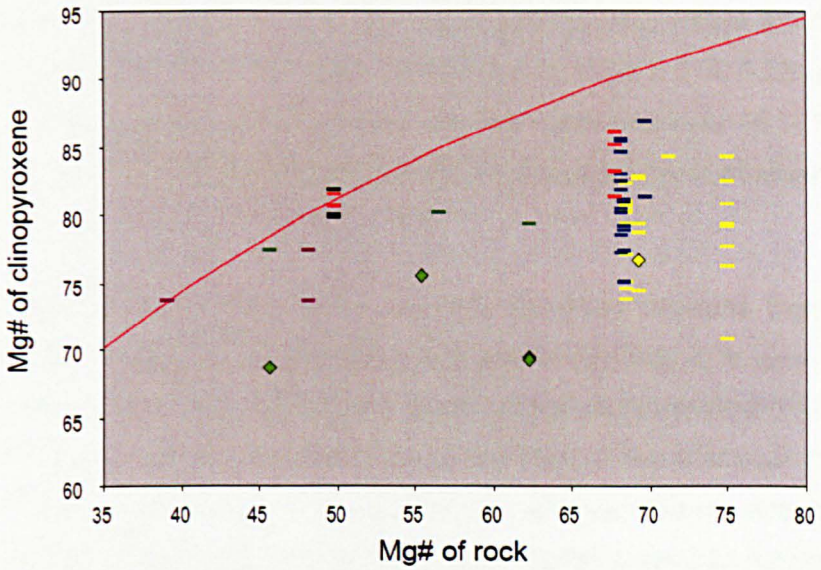

Figure 5.29 Mg# of clinopyroxene phenocrysts versus Mg# of their host rocks. Individual analyses are shown by short bars - yellow for picrites, blue for ankaramites and green for olivine basalts. Analyses of clinopyroxene groundmass microlites for the picrites and olivine basalts are represented respectively by yellow and green diamonds. Mg# = 100x(Mg/(Mg+Fe) with total Fe as FeO. The red line represents the theoretical equilibrium between phenocrysts and their host rocks at atmospheric pressures; this is calculated from $Mg\#^{(rock)} = 1/(1+((1-(Mg\#^{(cpx)}/100))/(Mg\#^{(cpx)}/100))/K_D)x100$ where the partition coefficient for Fe^{2+} and Mg between clinopyroxene and the melt (K_D) is 0.23 (Grove & Bryan, 1983). Black, purple and red bars represent clinopyroxene phenocrysts from the LT, HT1 and HT2 basalts respectively (Pik et al. 1998). Calculations in Supplement 10a.

phenocryst contents. Moreover, despite differences between the lava groups in the composition of their clinopyroxene phenocrysts that suggest each evolved from separate melts, all are without exception the products of shallow level fractionation. The compositional zoning evident in many of the phenocrysts indicates that as fractionation progressed equilibrium conditions changed and that often this was in response to magma mixing (Section 4.5.3). As useful as it is then to identify cumulative characteristics, the comparison of phenocryst compositions with a common theoretical equilibrium can be misleading, particularly when the phenocrysts exhibit compositional gradients from core to rim and when the composition of the host rock may be influenced by the accumulation of other fractionating phases.

Plagioclase accumulation is apparent from the clusters of phenocrysts that occur in some of the olivine basalts and in one ankaramite, and like clinopyroxene some exhibit compositional differences and zoning that are indicative of mixing and changing equilibrium conditions (Section 4.5.3). Accumulation trends for this phase

are best seen on the plots for Al_2O_3 and Na_2O against SiO_2 where the olivine basalts with > 48 % deviate from the main fraction trend (Figs 5.5 & 5.23a). Plagioclase phenocrysts are generally only present in the few lavas with over 48 % SiO_2 and their composition and morphology suggests that they are products of shallow level or even post-eruption crystallisation (Section 4.5.3).

The accumulation trends for olivine are less apparent because they are near to opposite to the trends for fractionation and partial melting; it is clear though from petrographic evidence that most of the lavas contain accumulated olivine. Individual microprobe analyses plotted as functions of the Mg# of the host rock reveal that the majority of olivine phenocrysts in the picrites and ankaramites are accumulative since they plot below the theoretical olivine-melt equilibria for pressures between 1 atm and 1.2 GPa (Fig. 5.30). The ranges in composition of olivine phenocrysts in the olivine

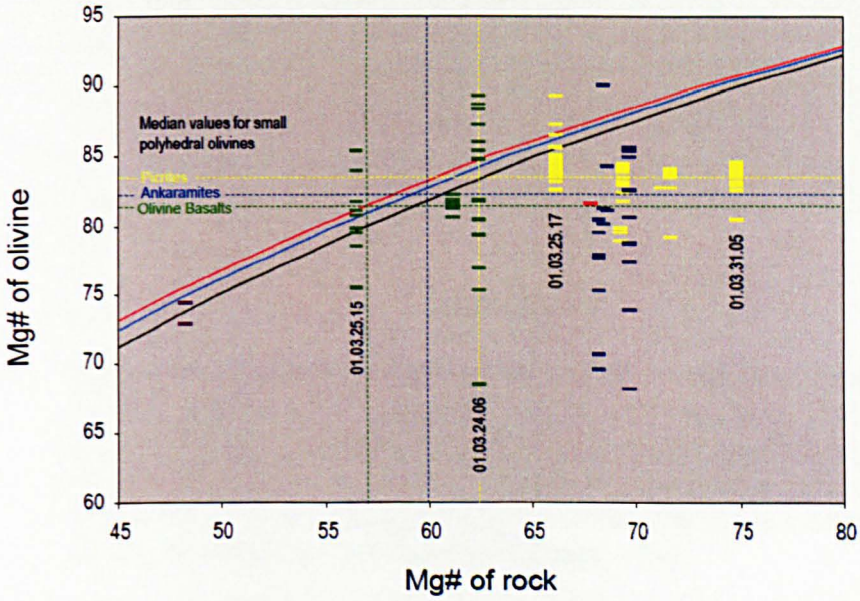

Figure 5.30 Mg# of olivine phenocrysts versus Mg# of their host rocks. Symbols and calculations (Supplement 10a.) are as in Figure 5.21. Curves for theoretical equilibrium between the phenocrysts and host rocks are calculated for pressures of 1 atm (red), 0.5 GPa (blue) and 1.2 GPa (black) using D values for Fe^{2+} and Mg between olivine and the melt of 0.30, 0.31 and 0.33 respectively (Ulmer, 1989). The fine dashed vertical lines are the equilibrium Mg# for each lava group - yellow for picrites, blue for ankaramites, and green for olivine basalts (Table 5.6).

basalts on the other hand straddle these equilibria suggesting that they contain some that are in equilibrium with the whole-rock composition. 01.03.25.15 contains three olivine phenocrysts which lie directly on equilibria implying that they crystallised in equilibrium conditions; these have Mg# of 81.0, 80.8 and 79.9 and estimated

equilibrium melt compositions with Mg# of 56.1 at 1 atm, 56.6 at 0.5 GPa and 56.4 at 1.2 GPa respectively. Following the procedure described by Thompson & Gibson (2000), these values plotted against 2nd order polynomial curves fitted through the distributions of MgO versus Mg# calculated using a range of Fe^{3+}/Fe^{2+} ratios for the lavas (Fig. 5.31) yield MgO contents for the melt of between 8.7 - 7.1 %, 8.9 - 7.2 %

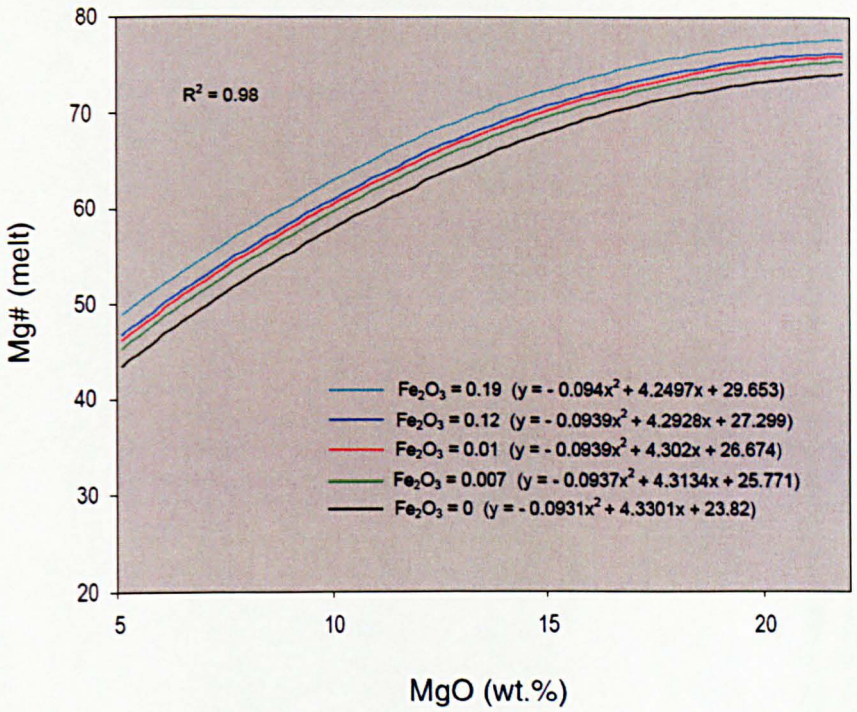

Figure 5.31 Least squares fit for MgO versus Mg# calculated for selected Fe^{3+}/ Fe^{2+} ratios for the Dilb and Iyela lavas. The datasets for all curves are hidden, the correlation coefficients are the same for each and the respective equations are shown alongside the key. The curves are 2nd order polynomials which were generated using Excel (Supplement 10a).

and 8.8 - 7.2 respectively (Table 5.5). By the same method, the equilibrium olivine phenocrysts with Mg# of 85.4 and 86.3 in the picrite 01.03.25 17 equate to equilibrium melt compositions with Mg# of 65.9 at 1.2 GPa and 65.5 at 1 atm, and MgO contents between 13.7 – 11.0 % and 13.4 - 10.8 % respectively, (depending on the Fe^{3+}/Fe^{2+} ratio). Those phenocrysts that plot above the equilibria are inherited from less evolved, genetically related higher magnesian melts; this is evident also from their mineral chemistry and textural relations (Section 4.5.3). Thompson et al. (2001) refer to such genetically inherited phenocrysts as macrocrysts to avoid confusion with the term xenocryst; however it is considered here that the term geneticryst is more appropriate since not all of the inherited olivine phenocrysts in the Dilb and Iyela lavas are large as the term macrocryst might imply. The most primitive geneticrysts with Mg# between 89 and 90 are large polyhedral crystals, and it is

Table 5.5 Calculated weight % MgO of equilibrium melt compositions for selected olivine phenocrysts from the Dilb and Iyela Lavas

Sample	Mg# (rock)	Mg# (olv)	Mg# (equilibrium melt)			MgO for set Fe_2O_3 at 1 atm					MgO for set Fe_2O_3 at 0.5 GPa					MgO for set Fe_2O_3 at 1.2 GPa					MgO for set Fe_2O_3 (Method 2)				
			0.3	0.31	0.33	0	0.07	0.1	0.12	0.19	0	0.07	0.1	0.12	0.19	0	0.07	0.1	0.12	0.19	0	0.07	0.1	0.12	0.19
Phenocrysts in equilibrium																									
01.03.25.17	66.1	86.3	65.5	66.2	67.6	13.4	12.5	12.3	11.8	10.8	13.9	12.9	12.7	12.2	11.2	14.8	13.8	13.6	13.1	12.0	14.2	13.7	12.7	12.4	11.4
01.03.25.17	66.1	85.4	63.7	64.5	65.9	12.4	11.4	11.3	10.8	9.9	12.8	11.9	11.7	11.2	10.3	13.7	12.7	12.5	12.0	11.0	13.1	12.2	11.7	11.4	10.4
01.03.24.06	62.4	84.7	62.4	63.2	64.6	11.6	10.8	10.6	10.2	9.3	12.1	11.2	11.0	10.6	9.7	12.9	12.0	11.8	11.3	10.4	11.7	10.8	10.4	10.2	9.2
01.03.24.15	56.5	81.0	56.1	56.9	58.4	8.7	8.1	8.0	7.7	7.1	9.0	8.3	8.2	7.9	7.3	9.7	8.9	8.8	8.4	7.8	9.6	8.8	8.5	8.3	7.5
01.03.24.15	56.5	80.8	55.8	56.6	58.1	8.6	7.9	7.9	7.5	7.0	8.9	8.2	8.1	7.8	7.2	9.5	8.8	8.7	8.3	7.7	9.4	8.7	8.3	8.1	7.4
01.03.24.15	56.5	79.7	54.1	54.9	56.4	8.0	7.4	7.4	7.1	6.7	8.3	7.7	7.6	7.3	6.8	8.8	8.2	8.1	7.8	7.2	8.7	8.0	7.7	7.5	6.8
High Mg# geneticrysts																									
01.03.24.08	68.4	89.9	72.8	73.4	74.6	18.7	17.6	17.4	16.8	15.6	19.3	18.1	17.9	17.3	16.1	20.3	19.1	18.9	18.3	17.0	18.3	17.0	16.5	16.1	14.9
01.03.25.17	66.1	89.2	71.2	71.9	73.1	17.4	16.3	16.1	15.6	14.4	18.0	16.8	16.6	16.1	14.9	19.0	17.8	17.6	17.0	15.8	18.2	17.0	16.6	16.2	14.9
01.03.24.06	62.4	89.2	71.3	72.0	73.2	17.5	16.4	16.2	15.6	14.5	18.1	16.9	16.7	16.1	15.0	19.1	17.9	17.7	17.1	15.9	17.5	16.3	15.8	15.5	14.2
Low Mg# phenocrysyts																									
01.03.24.06	62.4	68.5	39.5	40.2	41.8	6.0	6.2	6.5	6.5	7.2	5.9	6.1	6.4	6.4	7.0	5.9	6.0	6.2	6.2	6.7	3.9	3.5	3.4	3.3	2.9
01.03.24.08	68.4	68.2	39.2	40.0	41.5	6.0	6.3	6.5	6.6	7.3	5.9	6.2	6.4	6.4	7.1	5.9	6.0	6.2	6.2	6.7	3.7	3.4	3.2	3.1	2.8

Note:

The MgO contents for melt compositions in equilibrium with the olivine phenocrysts were calculated from the curves shown in Figure 5.32.

The figures in bold are those in equilibrium with the melt as indicated by the curves for theoretical equilibrium in Figure 5.31.

The figures for Method 2 were calculated as in Appendix 5.6.1 & 2 (calculations are included in Supplement 7). These were included for comparative purposes.

The figures in red calculated using Method 2 are unrealistic since the partitioning systematics used are not suitable for phenocrysts with such low Mg#.

proposed that these crystallised from the primary melt. Furthermore, since such primitive geneticrysts occur in all three lava groups it may be inferred that the magma for each lava group was linked either directly or indirectly to this primary melt. The theoretical composition of this parent source in equilibrium with the most primitive geneticrysts has an estimated Mg# of between 71.2 and 74.6, and a calculated MgO content of between 14.4 and 20.3 % depending on the pressure and Fe^{3+}/Fe^{2+} ratio (Table 5.5).

The variation in the MgO contents of the equilibrium melt with pressure and oxygen fugacity calculated in this way highlights the potential for error without reliable estimates for such parameters, particularly when the Mg# for the whole rock may be elevated as a result of olivine accumulation. As well as making determinations of the melt compositions unreliable, it makes the assessment of whether phenocrysts are accumulated or inherited speculative. For example, the olivine phenocryst with a Mg# of 86.34 in the picrite 01.03.25.17 yields MgO contents for the melt of between 14.8 and 10.8 % depending on the pressure and oxygen fugacity (indicated by the proportion of Fe_2O_3) (Table 5.5). Even if it is assumed that the Mg# for the bulk rock is correct (therefore placing the phenocryst in equilibrium at a pressure of 1 atm), the variation in the calculated MgO content of the melt still varies between 13.4 and 10.8 over the range of Fe^{3+}/Fe^{2+} ratios shown. If however the Mg# of the bulk rock is elevated because of accumulated olivine, the phenocryst is likely to be inherited rather than in equilibrium, and any calculation of the MgO content of the melt without prior knowledge of the pressures and oxygen fugacity during crystallisation would be tentative. This is likely to be the case for many of the Dilb and Iyela lavas. It is almost certainly the case for the olivine basalt 01.03.24.06 containing the equilibrium phenocryst with a Mg# of 84.7 which equates to a melt composition with a Mg# of 62.4 at 1 atm and an MgO content between 11.6 and 9.3 % depending on Fe^{3+}/Fe^{2+} ratio (Table 5.5). This phenocryst has a Mg# more typical of the picrites and since the sample has a high phenocryst content (10% Olivine and 15 % clinopyroxene - Fig. 4.3) it is likely that it is inherited rather than in equilibrium. For samples with > 10% MgO this incongruity may to an extent be avoided by plotting the Mg# for the fractionation-corrected compositions (Appendix 5.6.3 or 4). This is not an option for the majority of the olivine basalts which have lower MgO contents and more diverse phenocryst assemblages which make such modelling unreliable. If it were, the Mg# of the bulk rock for many samples would shift to lower values so that more of the phenocrysts would show as inherited rather than accumulated - this is more likely to affect the olivine basalts than the picrites and ankaramites since their olivine

phenocrysts already plot close to the equilibria. It would require an unrealistic shift in Mg# to bring the phenocrysts in the picrites and ankaramites to the left of the equilibria, therefore it may still be concluded that the majority in these lavas are accumulated.

The reliability of the above method in generating estimates of the MgO contents of equilibrium melts (and associated melt-temperatures) can be improved even with rough estimates of pressure and oxygen fugacity at which the olivine phenocrysts crystallised. The normative compositions of the lavas suggest that the olivine basalts evolved at near surface pressures whereas the ankaramites and picrites evolved at pressures of 0.6 - 0.8, and 0.8 - 0.9 GPa respectively. It has also been proposed that the primary melt ponded at the base of the crust. Tiberi et al. (2005, 2007) estimate the thickness of the crust beneath the Ethiopian Plateau to be near to 40 km, which is consistent with seismic receiver function estimates of ~ 44 km (Maguire et al. 2003; Dudga, et al. 2005, 2007; Dudga & Nyblade, 2006; Stuart et al. 2006); assuming an average crustal density of 2.74 g/cm^3 (Jentzsch et al. 2000), this equates to a pressure of about 1.2 GPa. Moreover, the mineral chemistry and MELTS modelling strongly suggest that the magmas which produced the lavas evolved in oxidising conditions, between QFM+1 and QFM+2 (equivalent to between 0.1 - 0.19 Fe_2O_3 - Kress & Carmichael, (1991)). This range in oxygen fugacity is typical of OIB-type magmas (Ballhaus, 1993). Using these parameters for pressure and oxygen fugacity, representative Mg#, MgO contents and temperatures of the equilibrium melts for the primary magma and the magmas for each lava group were calculated from the highest Mg# genticryst and the median Mg# of the small polyhedral olivine from each group respectively (Table 5.6). The median Mg# for the small polyhedral olivines from each group was selected as representative since these olivines are more likely to have crystallised directly from the ambient melt and are less likely than the larger polyhedral olivines to have been inherited from depth. The median values are plotted as fine dashed lines on Figure 5.30 together with the Mg# of the equilibrium melt for each group at the representative pressures taken from above. From these intersecting lines it is clear that the majority of the phenocrysts in the picrites have close to the representative Mg#, but their bulk-rock Mg# is elevated because of olivine accumulation. In contrast, the olivine phenocrysts in the olivine basalt 01.03.25.15 plot close to the representative Mg# for the group and are close to the equilibrium composition of the melt. The phenocrysts in the other two olivine basalts are close to the representative Mg# for the group, but are clearly accumulated like those in the picrites. Those that plot well above the representative Mg# for the group

Table 5.6 Characteristics of the primary and reservoir melts for the three lava groups from the Dilb and Iyela sections.

Pressure (kbar)		0.0	7.0	8.5	12.0	Proportion Fe_2O_3			Proportion Fe_2O_3			Proportion Fe_2O_3			Proportion Fe_2O_3		
Kd (olv-melt)		0.300	0.318	0.322	0.330	0.1	0.12	0.19	0.1	0.12	0.19	0.1	0.12	0.19	0.1	0.12	0.19
	Mg# (olv)	Mg# of equilibrium melt				MgO of melt at 1atm			MgO of melt at 7 kbar			MgO of melt at 8.5 kbar			MgO of melt at 12 kbar		
Primary melt	89.92	72.77	73.92	74.15	74.67	17.4	16.8	15.6	18.3	17.7	16.5	18.5	17.9	16.7	18.9	18.3	17.1
Picrites	83.78	60.74	62.13	62.42	63.06	9.8	9.4	8.6	10.5	10.0	9.2	10.6	10.2	9.3	10.9	10.5	9.6
Ankaramites	82.51	58.56	59.98	60.27	60.92	8.9	8.5	7.8	9.4	9.1	8.3	9.6	9.2	8.4	9.9	9.5	8.7
Olivine Basalts	81.55	56.97	58.40	58.70	59.36	8.3	7.9	7.3	8.8	8.4	7.8	8.9	8.5	7.9	9.2	8.8	8.1
	Mg# (olv)	Mg# of equilibrium melt				Temperature of melt			Temperature of melt			Temperature of melt			Temperature of melt		
Primary melt	89.92	72.77	73.92	74.15	74.67	1471	1458	1430	1493	1479	1451	1497	1483	1455	1507	1493	1465
Picrites	83.78	60.74	62.13	62.42	63.06	1298	1289	1271	1313	1304	1284	1317	1307	1287	1324	1314	1294
Ankaramites	82.51	58.56	59.98	60.27	60.92	1277	1268	1253	1290	1281	1264	1293	1284	1267	1300	1291	1273
Olivine Basalts	81.55	56.97	58.40	58.70	59.36	1263	1256	1242	1275	1267	1252	1278	1270	1254	1284	1276	1259

Explanation

1. Mg# of phenocrysts are median values for small polyhedral olivines for each lava group (Table 4.9), except that for the primary melt which is the phenocryst with the highest recorded Mg#
2. Mg# of the equilibrium melt is calculated from $Mg\#^{(rock)} = 1/(1+((1-(Mg\#^{(olv)}/100))/(Mg\#^{(olv)}/100)/Kd)x100$. Kd values are from Ulmer (1989) (Appendix 5.9.1). Bold figures are preferred values.
3. MgO content of the melt is interpolated from the least squares fit for MgO versus Mg# calculated for selected Fe^{3+}/Fe^{2+} ratios for the lava groups.
4. Temperature of the melt is calculated from the linear equation T = 22.892 x MgO + 1074 generated from experimental dat for KLB-1 (Hirose & Kushiro, 1993) - (Appendix 5.9.2).

are likely to have been inherited from the picritic magmas or magmas similar in composition. The olivine phenocrysts in the ankaramites show a wide range of Mg# which straddles the representative composition for the group. The bulk-rock Mg# values of the hosts however are much higher than the representative equilibrium melt; therefore it can be assumed that the olivines in these rocks are mainly accumulated.

It can be concluded as before (Section 4.5.3) that the restricted range in the composition of the olivine pheoncrysts in the picrites suggest that their magmas evolved from an already partially crystallised source at depth, and that they made their way rapidly to the surface thereafter. During this evolution it is likely that the picritic magmas further fractionated and accumulated olivine and were erupted as phenocryst charged lavas. The greater range in the composition of the olivine phenocrysts in the ankaramites and more so in the olivine basalts, suggests that these lavas evolved from magmas at respectively shallower levels and that mixing occurred between these and possibly the deeper-derived picritic magmas. Since all the lavas represented in Figure 5.30 contain olivine phenocrysts that span the equilibria it is likely that olivine crystallisation was polybaric. This is particularly apparent for the olivine basalt 01.03.25.15 which contains olivine phenocrysts in equilibrium with the melt at different pressures, and more so from the fact that the MgO contents of the equilibrium melt calculated from these phenocrysts for the different pressures are similar over the range of Fe_2O_3 contents shown (Table 5.5).

5.3.4 Source characteristics

The trace element and normative compositions of the lavas support that the picrites and ankaramites were generated at depth from variable degrees of partial melting of the same source, whereas the olivine basalts evolved by crystal fractionation at a shallow level from a magma similar in composition to the ankaramites. As noted earlier, the ankaramites are in fact picrites and are specifically classified according to dominance of clinopyroxene in their phenocryst assemblage. It is likely that they were derived from the same source as the picrites from relatively consistent but larger degree partial melts, and that they evolved for a longer period at a shallower level where they were able to accumulate clinopyroxene. The major and trace element models presented in Section 5.3.2 support that the olivine basalts cannot be generated by fractionation from the picrites, so it may be assumed that they are genetically related to the picrites only in the sense that, indirectly through the ankaramites, they share the same parental source (Fig. 5.32a). This is reflected in the relatively homogeneous trace element abundance profiles (Fig. 5.8) and REE

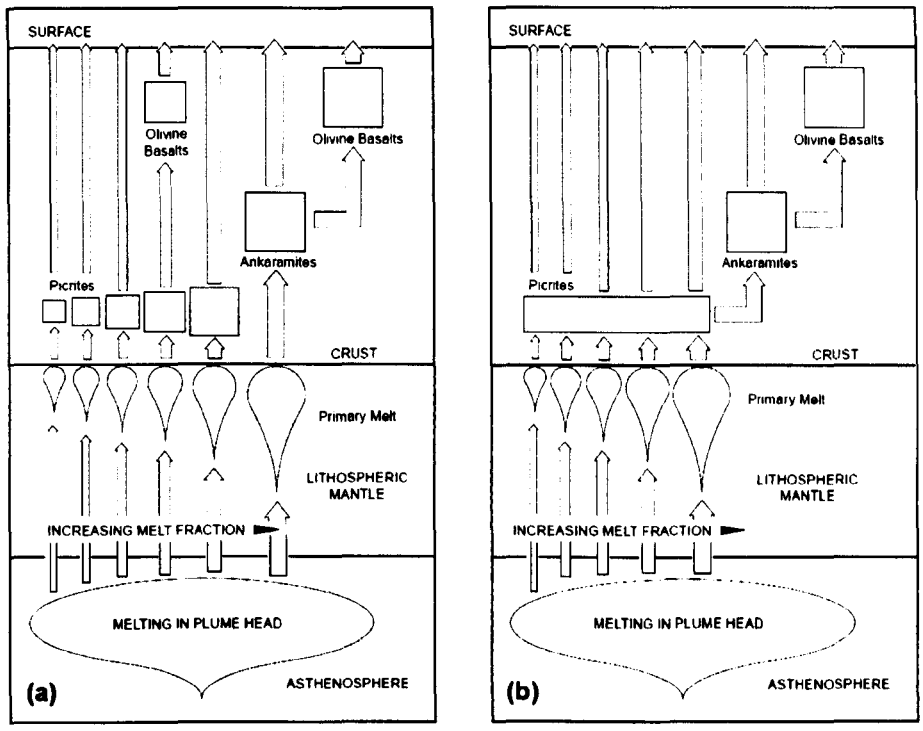

Figure 5.32 Petrogenetic models illustrating the relations between the three lava groups from the Dilb and Iyela sections. In **(a)** there is no link between the olivine basalt and picrite magmas, except via the source, whereas in **(b)** they are linked via the ankaramite magma. See text for further explanation.

patterns (Fig. 5.14) for the three lava groups. The slightly steeper overall gradient in the REE profiles for the picrites compared to the ankaramites and olivine basalts probably reflects the differences in their evolution described above, and the greater degree of enrichment of incompatible trace elements in the olivine basalts supports that these lavas are more fractionated. It cannot however be discounted that the few olivine basalts with higher Gd/Yb ratios (> 3.9) were generated by shallow level fractionation of picritic magmas (Figs 5.28 & 32a). Although the increasing diversity in the mix of olivine phenocryst compositions from the picrites through to the olivine basalts can be explained by this model, it may alternatively require that the magmas for the three groups were linked in some way. This is possible if the overall plumbing system allowed variable degree partial melts generated at different times to pass between them (Fig. 5.32b). Such a model is similar in principle to one described in Section 4.5.3 developed from the conceptual model of the conduit systems proposed for the volcanic rocks of the Vaigat Formation, West Greenland (Larsen & Pedersen, 2000).

It may be concluded then that the main compositional differences between the lava groups are attributable to variable degrees of partial melting, fractionation and

accumulation, and the depths at which these processes operated. Assuming an average crustal density of 2.74 g/cm^3, as above, the calculated depths at which the magmas evolved, estimated from the pressures indicated by the normative compositions of the lavas, are 31 km for the picrites, 26 km for the ankaramites and near surface for the olivine basalts. The respective MgO contents of the representative melts calculated as above are between 18.9 and 17.1 for the primary source, 10.6 and 9.3 for the picrites, 9.4 and 8.3 for the ankaramites and 8.3 and 7.3 for the olivine basalts, depending in the Fe_2O_3 content (Table 5.6). Melt temperatures calculated from these MgO contents using a linear equation generated from experimental data KLB-1 (Hirose & Kushiro, 1993) (Appendix 5.9.2) are between 1507 and 1465 °C for the primary melt, 1317 and 1287 °C for the picrites, 1290 and 1264 °C for the ankaramites, and 1263 and 1242 °C for the olivine basalts. These representative temperatures are plotted against depth on a pressure-temperature diagram constructed using experimental melt data for the peridotite KLB-1 (Figure 5.33). The temperatures for the primary melt over the range of Fe_2O_3 contents representative of fO_2 values between QFM+1 and QFM+2 are extrapolated back to the solidus along liquid adiabats of ~ 1 °C km^{-1} (McKenzie & Bickle, 1988) to give potential temperatures between 1450 and 1500 °C, and pressures of melting between 3.1 and 3.4 GPa at depths of between 95 and 110 km respectively. It is clear, however, on a plot of Fe^*_{15} versus Si_{15} (Fig. 5.34) that the Fe^*_{15} contents of the Dilb and Iyela lavas are too high to be simple isobaric melts of KLB-1 mantle at the temperatures and pressures shown, and therefore it is likely that these estimated potential temperatures, and pressures and depths of melting are too low. This is also the case for the picrites from West Greenland (Lightfoot et al. 1997) and the Parana-Etendeka province (Gibson et al. 2000; Thompson et al. 2001), and for the Fe-rich basalts from the Skye Main Lava Series (Scarrow & Cox, 1995) (Fig. 5.34). Such lavas require an Fe-rich mantle source such as HK-66 or PHN1611 (Scarrow & Cox, 1995; Scarrow et al. 2000; Gibson et al. 2000), or a contribution from deep-sourced Fe-rich melts generated by decompression melting of a peridotite source analogous to KLB-1 at high pressures (> 4 GPa) (Langmuir et al. 1992).

Extension of the liquid adiabats for the Dilb and Iyela primary melt to the experimentally determined solidus for the Fe-rich peridotite PHN1611 (Kushiro, 1996) (represented by the blue line in Figure 5. 34) gives higher potential temperatures between 1470 and 1520 °C and melting depths and pressures of 125 - 140 km, and 4 - 4.5 GPa respectively. These figures are relatively consistent with those proposed for the Parana-Etendeka ferropicrites (represented as red triangles in Figure 5.34),

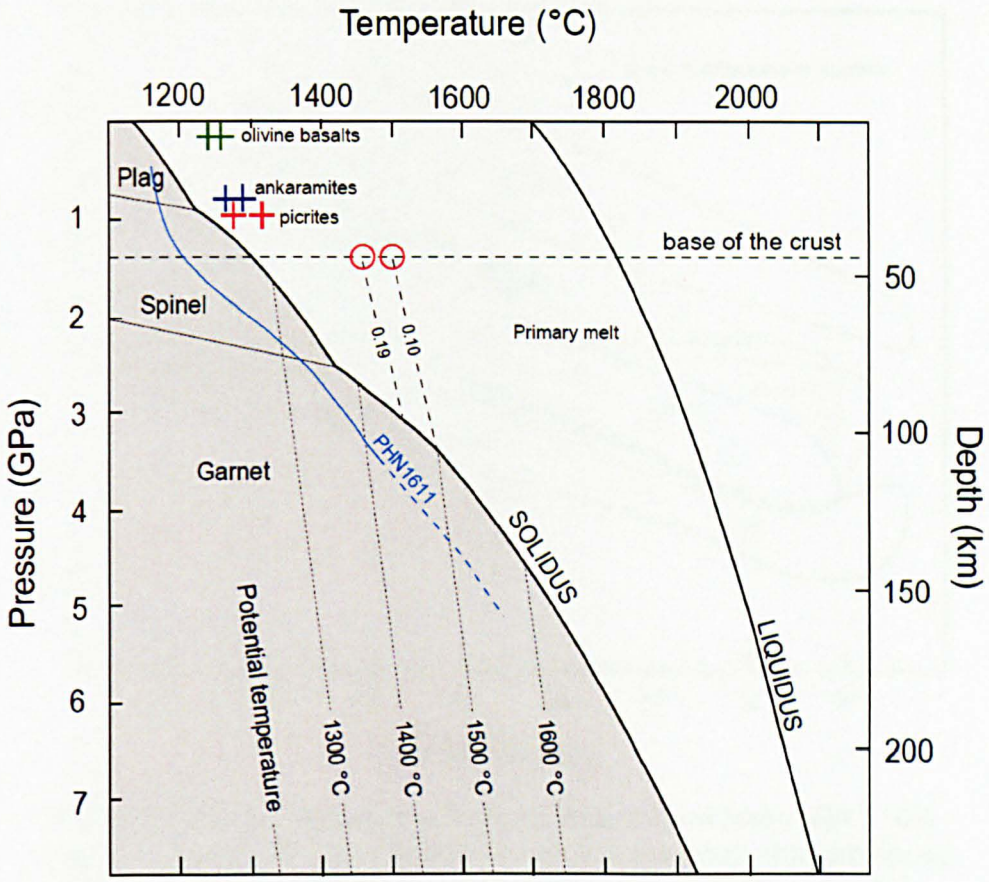

Figure 5.33 Anhydrous pressure-temperature diagram for mantle lherzolite KLB-1 (Takahashi et al. 1993; Herzberg & Zhang, 1996) showing the approximate temperature, depth and pressure at which the Dilb and Iyela magmas evolved. The dashed lines joining the open red circles (representing the pirimary melt) with the solidus are liquid adiabats for the range of Fe_2O_3 contents between 0.1 and 0.19; the pairs of crosses for the lava groups also indicate the differences in the respective melt temperatures over this range. The blue line is the solidus for the Fe-rich peridotite PHN1611. This is extrapolated to higher pressures as indicated by the dashed line.

which are estimated to have been generated by 10% melting of a source similar to PHN1611 at pressures of 45 – 35 kb and mantle potential temperatures near to 1550 °C (Gibson et al. 2000). Although these lavas have similar Fe^*_{15} to the Dilb and Iyela picrites, there are significant chemical differences between them that suggest that they were derived from primary magmas with quite different compositions. Even though the Fe_{15}-Si_{15} field for Dilb and Iyela picrites and ankaramites overlaps with that for the Etendeka ferropicrites, technically they are not ferropicrites because they have FeO* contents below 13 wt.% (FeO* = $Fe_2O_3^{(tot)}$ x 0.9); this is also apparent from their comparatively lower $Fe_2O_3^{(tot)}$ (Fig. 5.6). Their uniquely higher K_2O, P_2O_5 and TiO_2 and lower Al_2O_3 contents furthermore suggests that they were derived from higher temperature lower degree partial melts than the Parana-Etendeka ferropicrites.

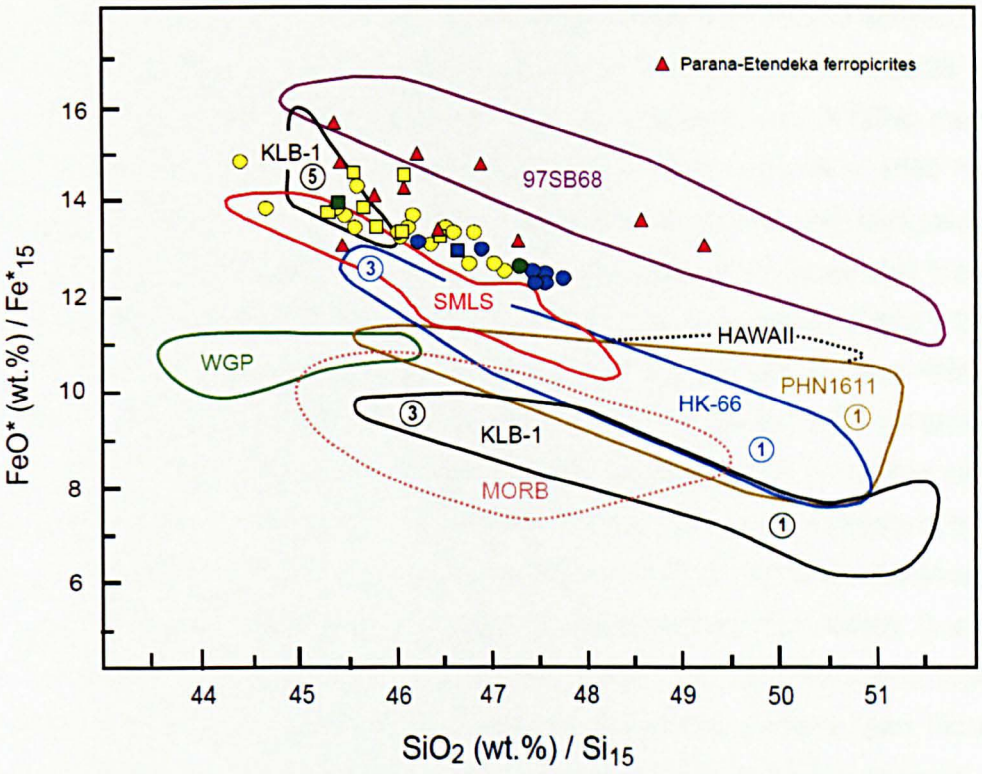

Figure 5.34 Fe^*_{15} versus Si_{15} for the Dilb and Iyela lavas with >10% MgO compared with picrites and Fe-rich basalts from other provinces, and glasses from anhydrous experimental melting studies of mantle peridotites (KLB-1, HK-66, PHN1611), and an uncontaminated ferro-picrite lava (97SB68) from the Parana-Etendeka. All rock-data have been fractionation-corrected to 15% MgO (Appendix 5.6) whereas all experimental data is not corrected. Pressures indicated by the circled numbers are in GPa. Sources are as follows: Parana-Etendeka ferro-picrites (Gibson et al. 2000); Skye Main Lava Series - SMLS (Scarrow & Cox, 1995);West Greenland Picrites - WGP (Lightfoot et al. 1997); MORB - basalts with > 10 wt. % MgO) (Lamont MORB database); HAWAII (Norman & Garcia, 1999); KLB-1 (Hirose & Kushiro, 1993; Takahashi et al. 1993; Herzberg & Zhang, 1996); HK-66 (Hirose & Kushiro, 1993); PHN1611 (Kushiro, 1996); 97SB68 (Tuff et al. 2005). Symbols for the Dilb and Iyela lavas are as in Figure 5.2.

More particularly, the presence of Fo_{90} olivine geneticrysts in the Dilb and Iyela lavas would require exceptionally high degrees of partial melting of a source such as PHN1611; this is not such an issue for the Parana-Etendeka ferropicrites since their olivine phenocrysts are significantly more Fe-rich (Fo_{85}) than those generally considered to be in equilibrium with anhydrous fertile peridotite (Fo_{90-92}).

Some authors argue that mantle plume heads composed only of peridotite are incapable of generating the huge volumes of melts seen in large igneous provinces, and that an eclogite or pyroxenite component is required (Cordery et al. 1997; Campbell, 1998; Takahashi et al. 1998; Yaxley, 2000; Leitch & Davies, 2001).

Following this reasoning, Tuff et al. (2005) suggests on the basis of anhydrous phase relations determined by experimental melting of the ferropicrite 97SB28, that the Parana-Etendeka ferropicrites were derived from high-pressure (5 GPa) melting of a garnet-pyroxenite source with a mantle potential temperature of ~ 1550 °C. It can however be argued that compositional constraints on the modal mineralogy make such a source implausible for both the Dilb and Iyela (D-I) lavas and the Parana-Etendeka (P-E) ferropicrites. High Ni contents in both the olivines (2360 - 2800 ppm for D-I and 3500 ppm for P-E) and bulk rock (357 - 925 ppm for D-I and ~700 ppm for P-E at 15 % MgO) suggest that the melts were in equilibrium with a mantle source with a high modal percentage olivine such as a peridotite or an olivine websterite, rather than with a clinopyroxene-rich mantle source such as an ecolgite or pyroxenite. This is consistent with the high FeO and low Na_2O contents of the lavas. Since clinopyroxene has lower FeO and higher Na_2O contents than olivine, a pyroxenite source would instead produce a melt with respectively low FeO and high Na_2O. Therefore, despite the differences in composition clearly evident from Figure 5.34, whereas PHN1611 and 97SB68 (as a proxy for a pyroxenite source) may be construed as a potential source for the Parana-Etendeka ferropicrites, neither are a likely source for the Dilb and Iyela lavas. Instead it is proposed here that the primary melts for the Dilb and Iyela lavas are derived from high-pressure (4 - 5 GPa) melting of an anhydrous mantle peridotite such as KLB-1 with potential temperatures in excess of 1600 °C (Fig. 5.33). The absence of high pressure pyroxenes, and SiO_2 contents for the lavas that are not unusually low, are, however, inconsistent with melting at such high pressure.

Melting at such high temperatures and pressures together with high Ni contents typically of the Dilb and Iyela picrites are indicative of melting within an ascending mantle plume. Arndt (1991) demonstrated that there is a systematic difference in the Ni contents of plume, arc and mid-ocean ridge basalts at a given MgO content, and that this difference is dependent on changes in the partition coefficient between olivine and silicate melt with temperature and pressure. When the mantle melts at high temperature and pressure, Ni strongly partitions into the melt, whereas at lower temperatures and pressures it will remain in the olivine. Temperatures in ascending plumes are hotter than ambient mantle, and because the ascent of plumes is restricted beneath thick lithosphere the range in temperature and pressure over which melting occurs is much smaller than for average adiabatically cooled mantle beneath mid-ocean ridges. Melting therefore both starts and finishes at higher temperatures in plumes than in normal upwelling mantle, and as a consequence

magmas derived from plumes have higher Ni contents than average MORB. The trace element distributions of the Dilb and Iyela lavas suggest that the partial melts from which they were originally derived were generated by melting of a HIMU-type OIB source, and the liquidus temperatures in excess of 1400 °C inferred from MELTS, and the high potential temperatures and pressures of melting estimated from the MgO content of the primary melt furthermore suggest that this took place within the asthenospheric mantle. The maximum MgO content of magmas that can be produced by adiabatic melting of normal upper mantle with an average potential temperature 1300 °C is 11% (Klein & Langmuir, 1987; McKenzie & Bickle, 1988). Since the MgO contents of the Dilb and Iyela picrites are well in excess of this, it can be assumed that melting occurred in an anomalously hot zone within the convecting mantle, possibly represented by the Afar mantle plume. It is possible to produce picrites by melting normal mantle at average temperature in the presence of water, which effectively reduces the liquidus temperature by about 100 °C (Green & Ringwood, 1968), and although this is an acceptable mechanism at subduction zones, it is unlikely for the Dilb and Iyela picrites since the absence of hydrous mineral suggest that the source magma was essentially anhydrous. This is contrary to the findings of Pik et al. (1998) and Kieffer et al. (2004) who report an abundance of phlogopite and amphibole in the HT2 basalts indicating that the magma may have had significant water contents. These minerals are only stable at low temperatures and pressures, so their presence in the deep-sourced HT2 basalts is enigmatic. Kieffer et al. (2004) suggest that the HT2 basalts were sourced from a deeper volatile-rich reservoir than the anhydrous LT basalts, even though this contradicts their assumption that the LT basalts were derived from higher degree partial melts of the same source as the HT2 basalts. It is suggested here, as previously, that the presence of hydrous minerals may instead be attributed to the interaction of the HT2 magmas with groundwater.

The primary partial melt generated in the hot head of the Afar plume is likely (because of its high density) to have ponded at the base of the crust where crystallisation of the high-Mg olivines (Fo_{90}) occurred. Crystallisation of the primary olivines would have effectively lowered the MgO content of the parent melt before it made its way into the crust. It is likely therefore that the primary olivines (Fo_{90}) were entrained and transferred to more shallow levels this lower density, less Mg-rich melt. The magmas for the picrites and ankaramites that formed higher in the crust were probably fed by this crystal-charged melt and so inherited some primary olivines together with the distinctive HIMU-type signature of the parent melt. Although primary

olivines are found in all three lava groups, they are rare; it may be assumed therefore that most remained trapped in the lower crust or at the Moho. This scenario is consistent with the origin for the HT2 Basalts proposed by Pik et al. (1998; 1999). The HIMU-signature is analogous to their C1 component representing the presumed composition of the Afar mantle plume during the Oligocene, and this is in accordance with the findings of Vidal et al. (1991), Schilling et al. (1992), Chazot & Bertrand (1993), Deniel et al. (1994) and Stewart & Rogers (1996). Baker et al. (1996b) report a similar HIMU trace element signature for the Oligocene flood basalts from the Yemen, but like Chazot & Bertrand (1993) and Volker et al. (1993) they consider this as distinct from an isotopically more depleted mantle source which may be more representative of the Afar plume. Similar characteristics exhibited by magmas derived from the Iceland plume are attributed to recycling of oceanic lithosphere and are interpreted accordingly as products from an immature HIMU mantle plume (Thirlwall et al. 1994).

To account for the less radiogenic Sr values of some of the LT, HT1 and Adigrat basalts Pik et al. (1999) also propose the existence of a depleted mantle (DM or PREMA) component (C2), which they suggest is located in the Arabian-Nubian lithospheric mantle. More recently, Bertrand et al. (2003) suggest that it is the HIMU rather than the DM signature that is inherited from the lithospheric mantle. They present trace element and isotopic evidence for a pervasive HIMU component in late Miocene to Plio-Quaternary basalts across the Arabian Plate, and suggest that this resides within the Arabian lithospheric mantle. It is discounted that the HIMU signature could be associated with the Afar plume since it extends beyond its topographic influence, and beyond the area characterized by high $^{3}He/^{4}He$ ratios (Ra > 9) which are considered to be a more specific geochemical signature for the plume (Pik et al. 2006). The HIMU-type signature is also common to all Cenozoic volcanism over North Africa and the East African Rift, and likewise can be ascribed to subcontinental lithospheric melts (Pik et al. 2006, Furman (2007). Following this logic, Rogers (2004, 2006) concludes that the uncontaminated melt from the Afar plume was rarely sampled except perhaps by the earliest outpourings of the flood basalts. Whether this is the case, however, would depend intrinsically on the nature of the interaction between the plume and the subcontinental lithospheric mantle (see below). The depleted component (C2) on the other hand is less widespread than the HIMU component and is focussed more within the influence of the Afar plume. The Oligocene flood basalts from the Ethiopian Plateau (Pik et al. 1999) and the Yemen (Baker et al. 1996b), and later Miocene to recent lavas from northern Ethiopia (Kieffer

et al. 2004), Afar (Deniel et al. 1994; Barrat et al. 1998); the Red Sea (Rogers, 1993; Volker et al. 1997) and Gulf of Aden (Schilling et al. 1992) all exhibit mixing between depleted mantle and HIMU components. Unlike Pik et al. (1999), Baker et al. (1996b) suggest that the two components are a result of melting of a heterogeneous plume and that the C2 component, which is close to PREMA, represents entrained isotopically depleted streaks within the plume. Schilling et al. (1992) and Volker et al. 1997), alternatively suggest that the depleted component simply represents ambient depleted asthenospheric mantle which progressively dilutes the HIMU signature by simple binary mixing over the course of continental breakup. Contrary to these general observations of compositional components within the influence of the Afar plume, Furman et al. (2006) and Furman (2007) suggest that the HIMU signature is not present in the Ethiopian Rift, and it is confined to within and south of the Turkana Depression. Instead they propose three end member compositions including a depleted mantle component interpreted as convecting upper mantle or MORB, an EM1 component inferred to be within the lower crust, and an EM2 component inferred to be within the upper crust. The latter two components are comparable with the C3 and C4 components interpreted by Pik et al. (1999) as upper and lower crust respectively. With the exception of perhaps the HT2 basalts and some Ti-rich basalts from the Yemen, the compositions of most of the Cenozoic volcanics throughout the Afro-Arabian (including the HT1 and LT basalts) are coloured by these crustal components, so much so that the signature for the Afar plume (if present) is diluted out of recognition.

The Dilb and Iyela lavas are the most primitive and possibly some of the earliest outpourings of flood basalts in the Afro-Arabian province yet reported, and were derived from partial melts generated by melting in the Afar Plume, they are the closest representations we have of its composition. As already pointed out in Section 5.2.3, the trace element abundance profiles for all three lava groups, exhibit distinctive HIMU-like signatures (Fig. 5.8), and their VICE compositions generally seem to reflect this (Figs 5.10 -12). Moreover, the strong negative correlation between Fe_{15} and Si_{15} exhibited by the lavas (Fig. 5.34) is a characteristic that has long been considered a distinguishing feature of OIB (Langmuir et al. 1992). It is nevertheless emphasised in Section 5.3.2 that there are some consistent differences which make the lavas not quite HIMU. In particular, their trace element profiles are different from those of HIMU basalts in that they do not show a negative Pb anomaly and they have pronounced peaks for Nd, Zr and Ti. Also, their relative concentrations of alkali and alkali earths reflected in their Rb/K ratios show conflicting trends

compared to OIB in general. In relation to La as an anchor element, all three lava groups are moreover depleted in U and Th with respect to typical HIMU basalts. A number of the olivine basalts exhibit greater degrees of depletion in these elements, but since these are accompanied by elevated Ba and Pb it is likely that they have been contaminated by crustal material. With the exception of these, the Dilb and Iyela lavas can be considered essentially uncontaminated, therefore the differences in their VICE compositions compared to HIMU basalts described above are probably source-related. Ratio plots of K/Nb and Ba/Nb versus Zr/Nb emphasise the compositional displacement of the Dilb and Iyela lavas relative to HIMU, and place them on a mixing trend between average sub-continental lithospheric mantle (SCLM) and depleted mantle (Fig. 5.35). The HIMU field lies slightly offset from this trend but

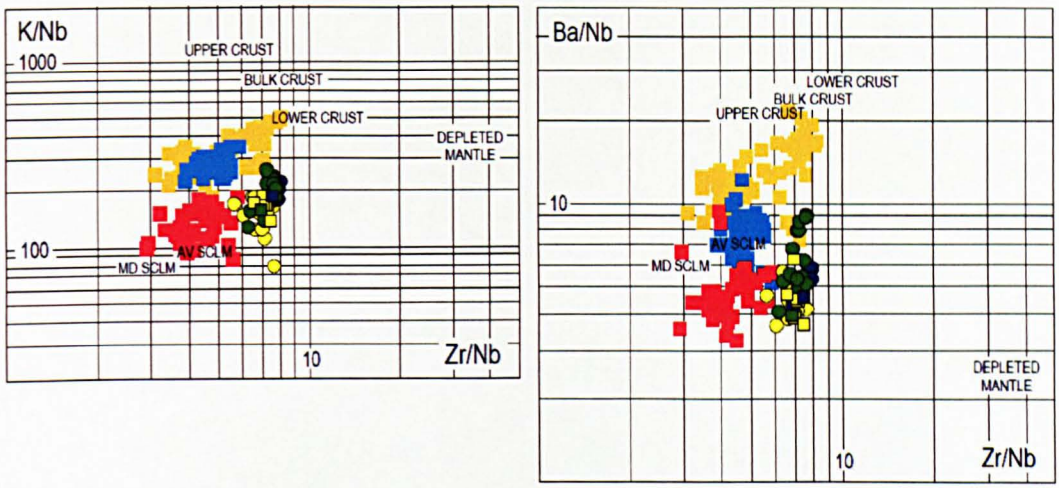

Figure 5.35 K/Nb and Ba/Nb versus Zr/Nb for the the Dilb and Iyela lavas compared with fields for HIMU (red), EM1 (blue) and EM2 (mustard), and values for continental crust, average (AV) and median (MD) subcontinental lithospheric mantle (SCLM), and depleted mantle. OIB data are from Willbold & Stracke (2006) as listed in Figure 5.12, average compositions for the crustal components are from Taylor & McLennan (1985), SCLM values are from McDonough (1990) and depleted mantle is average N-MORB value from Sun & McDonough (1989).

between the compositional field for the Dilb and Iyela lavas and the median value for SCLM. If the HIMU or C1 component is located in the lithospheric mantle as proposed by Bertrand et al. (2003), it may be inferred from Figure 5.35 that the depleted or C2 component is representative of the composition of the Afar plume, and that the primary melt inherited its HIMU-type signature from sub-continental lithospheric melting or metasomatic activity as a result of the interaction with the hot depleted melt from the plume. In such a scenario, if it is assumed that the Dilb and Iyela lavas and HT2 basalts represent the earliest outpourings of the flood basalts, it might be expected that they show the strongest HIMU signature inherited from the initial melting of this component. Similarly, the HT1 and LT basalts would be

expected to show a stronger depleted mantle signature as the HIMU component became progressively diluted by the interaction with the depleted melt from the plume. This is consistent with the progressively higher Y/Nb and Zr/Nb ratios for the Dilb and Iyela lavas, HT2, HT1 and LT basalts, which together plot along a well-defined trajectory from HIMU to N-MORB (Fig. 5.36). Equally, the increasing

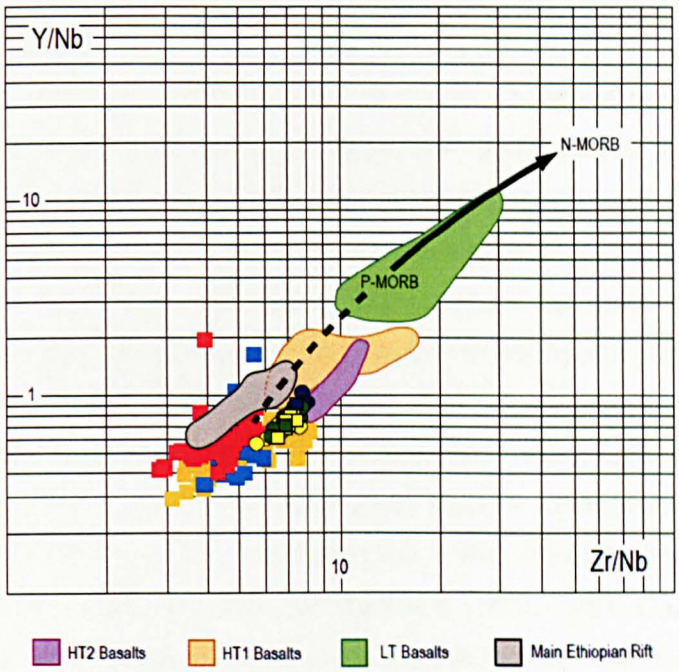

Figure 5.36 Y/Nb versus Zr/Nb for the Dilb and Iyela lavas compared with fields for HIMU (red), EM1 (blue) and EM2 (mustard), and selected lavas from Ethiopia. Sources: OIB (Willbold & Stracke (2006), HT2, HT1 & LT basalts (Pik et al. 1999), Ethiopian Rift (Furman et al. 2006). The trend between P-MORB and N-MORB delineates the field for South Atlantic MORB data from Humphris et al. (1985). This trend is extrapolated back to averge HIMU as shown by the dashed line.

depleted mantle signature evident at least from the trace element compositions may simply represent the progressive dilution of a HIMU-type plume-derived source by normal asthenospheric mantle as plume activity waned as (Schilling et al. 1992). The fact the basalts from the Main Ethiopian Rift plot at the other extreme of the array within the HIMU field however contradicts this simple scenario.

It is possible that melting within the plume did not occur until the lithosphere thinned sufficiently to allow for decompression and that the flood basalts (initially at least) were generated by melting of lithospheric peridotite as a result of conductive heat exchange with the plume (this might account for the elusive nature of the Afar Plume signature). Such a mechanism is proposed by Turner et al. (1996) for the generation

of the Parana flood basalts. They suggest that if the lithosphere is > 100 km thick and is composed of volatile-rich peridotite, a thickness of 1 – 2 km of flood basalts may be generated by lithospheric melting over a period of 10 – 15 Myr. Small volumes of alkaline basalts would precede the eruption of tholeiites, and eruption rates would increase as the lithosphere was thinned by thermal erosion. The migration of magmatism from the NW to SE accompanied by partial melting of increasingly ancient and depleted peridotite at progressively shallower levels is proposed to explain the shift from high-Ti/Y to low-Ti/Y lavas observed across the Parana. A similar mechanism may be invoked to explain the generation of the high- and low-Ti basalts described by Pik et al. (1998), but the high eruption rates for the Afro-Arabian flood basalts (1 km^3/yr) are generally inconsistent with the conductive heating model. Whereas other flood basalt provinces characterised by lower eruption rates and lithospheric geochemical signatures may be explained by this model (Duncan et al. 1984; Hawkesworth et al. 1984; Erlank et al. 1984; Hawkesworth et a. 1988; Hergt et al. 1991; Brewer et al. 1992; Hooper & Hawkesworth, 1993; Lightfoot et al. 1993), the higher eruption rates for the Afro-Arabian flood basalts, comparable with those for the Deccan (Duncan & Pyle, 1988; Courtilliot et al. 1988; Venkatesan et al. 1993; Baksi, 1994; Allegre et al. 1999) and Siberia (Renne & Basu, 1991; Campbell et al, 1992) can only be explained by rapid decompression melting within a mantle plume.

Rather than assigning specific temporally constrained compositions to various plume and lithospheric components Kieffer et al. (2004) suggest that the eruption of the different lava-types were synchronous and that the compositional variations across the Afro-Arabian volcanic province are a result of heterogeneities in the underlying Ethiopian superswell. In this respect they suggest the Ethiopian lavas are similar to those from French Polynesia associated with the Pacific superswell (Chauvel et al. 1992). They maintain that both suites of lavas are isotopically distinct from HIMU and that the Ethiopian lavas plot far from the end member EM1, EM2, DM and HIMU compositions near to the centre of the Polynesian field that encompasses the entire compositional field for all end members. The fact that picritic lavas comparable in composition to the HT2 basalts and the Dilb and Iyela picrites and ankaramites are generally confined to the base of flood basalt sequences in other flood basalt provinces conveniently appears to hold little credibility in this model.

The uncertainty of the stratigraphic order of the lava-types across the Ethiopian province makes much of this discussion purely conjectural, and this is exacerbated by uncertainties over the thickness of the lithospheric mantle and where the HIMU

and the DM components reside. Such uncertainties are arguably a legacy of reconnaissance or roadside geochemistry in Ethiopia. It is evident at least that the Dilb and Iyela lavas represent the most Mg/Ti-rich basaltic lavas yet reported from the Afro-Arabian flood basalt province, and that these dominantly picritic rocks are centrally located in the province near the base of the volcanic pile as reported for picrites in other provinces. Their chemistry moreover suggests that they evolved deep within the crust from partial melts that were generated at pressures in excess of 3 GPa, possibly within the asthenospheric mantle.

5.3.5 Constraints on melt generation

The strong depletion of HREE relative to LREE in all the Dilb and Iyela lavas (Fig. 5.14) suggests the presence of residual garnet in the source, and that melting was initiated within the garnet stability field at pressures in excess of 2.5 GPa. Such high

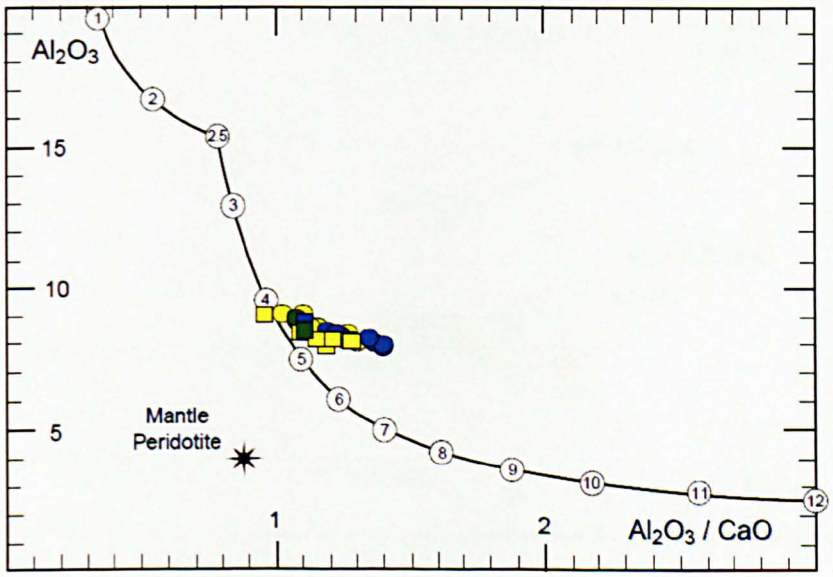

Figure 5.37 Al_2O_3 versus CaO/Al_2O_3 for the fractionation-corrected Dilb and Iyela lavas with > 10 % MgO compared with the experimentally determined solidus for KLB-1 over pressures between 1 and 12 GPa (Herzberg & Zhang, 1996). The solidus is indicatedby the bold curve and the pressures are indicated by the numbered circles along its length. The compositions for the lavas are from Appendix 5.6.3. Liquids formed along the solidus will have values of Al_2O_3 and CaO/Al_2O_3 indicated by the pressures in GPa. Symbols are as in Figure 5.2.

pressure melting is similarly implied by the limited range of Si_{15} for these lavas which places them at the high pressure end of the arrays for mantle analogues KLB-1 and HK-66 (Fig. 5.34). Low Al_2O_3 to CaO/Al_2O_3 ratios for the lavas more precisely imply

melting at considerable depth. This ratio is a more reliable estimate of melting depth than those based on FeO, MgO and SiO_2 since it is less affected by fractionation (Herzberg & Zhang, 1996). Al_2O_3 is a good indicator of depth in the garnet peridotite field because its content in the initial melt drops dramatically with increasing pressure; CaO on the other hand is less affected by changes in pressure, consequently the CaO/Al_2O_3 ratios for magmas on the solidus increase or decrease accordingly with pressure. The degree of partial melting and the amount of olivine fractionated can affect the Al_2O_3 content of magma, but for liquids on the solidus such factors will not affect the pressures estimated from CaO/Al_2O_3 (Herzberg, 1992, 1995). When compared to experimental data for KLB-1 (Herzberg and Zhang, 1996), the Al_2O_3 - CaO/Al_2O_3 ratios for the fractionation–corrected Dilb and Iyela lavas with > 10 % MgO imply melting at pressures between 4 and 5 GPa (Fig. 5.37). With reference to

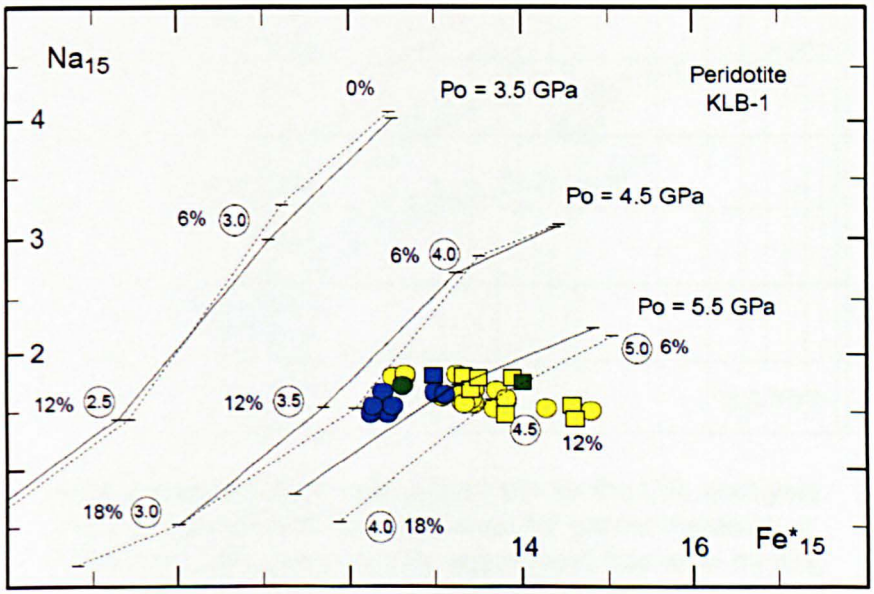

Figure 5.38 Variation of Fe^*_{15} and Na_{15} for the Dilb and Iyela lavas compared to model melting curves for KLB-1 calculated using the procedure of Langmuir et al. (1992) and the partition coefficients of Ulmer (1989). The solid line represents the curve for anhydrous polybaric batch (equilibrium) melting; the dashed line represents the curve for accumulated fractional melting. The circled numbers indicate pressure in GPa and the percentages alongside indicate the degree of melting. Po represents the initial pressure at which the ascending mantle intersects the solidus. The compositions for the lavas are from Appendix 5.6.3, and the symbols are as in Figure 5.2.

the P-T diagram for KLB-1 (Fig. 5.33) such pressures may be shown to be equivalent to depths of between 120 and 150 km and potential temperatures in excess of 1600 °C. The variation in Na_{15} and Fe^*_{15} for the lavas with > 10 % MgO compared to model

melting curves for KLB-1 suggests higher pressures between 4.5 and 5.5 GPa (implying depths of melting in excess of 150 km), and percentage melt fractions between 10 and 12 %, (Fig. 5.38). Such estimates (both for pressure and melt fraction) are likely to be unrealistically elevated because of the low Na_2O and high FeO contents of the lavas.

More reliable estimates of the melt fraction or percentage melting may be obtained from a comparison between the chondrite-normalised REE ratios for the lavas and model melting curves for garnet lherzolite (Fig. 5.39). Such a comparison may also

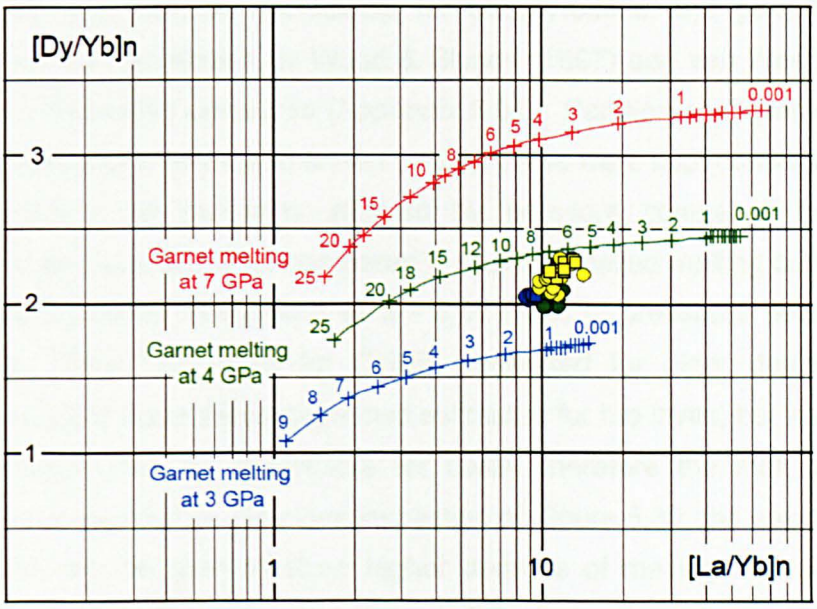

Figure 5.39 [Dy/Yb]n versus [La/Yb]n for the Dilb and Iyela lavas compared with melting curves for garnet lherzolite at 3, 4, and 7 GPa generated by aggregated fractional melting of a primitive mantle source. REE ratios for the lavas are for chondrite-normalised concentrations (n). Percentage melting is indicated by the figures along the melting curves.

be used to further constrain the pressure of melting within the garnet stability field. In order to generate a representative time-integrated starting composition εNd values were calculated from Nd isotope measurements for the HT2 basalts assuming an age of 30 Ma (Pik et al. 1999) (Appendix 5.9.3). εNd values between 5 and 7, and $^{143}Nd/^{144}Nd$ ratios higher than present-day CHUR indicate derivation from a depleted mantle source. Liew & McCulloch (1985) propose that LREE depletion from the chondritic reservoir occurred during a major episode of crustal genesis between 2.5 and 3 Ga, and they propose a linear evolution of $^{143}Nd/^{144}Nd$ in the depleted mantle since that time. Following this reasoning, the isotopic evolution of CHUR was modelled over a period of 2.5 Ga to give an initial ratio of 0.50939552 (Appendix

5.9.4). This initial ratio and a time of 2.5 Ga were used to calculate the $^{143}Nd/^{144}Nd$ ratio of the starting composition, which was generated by non-modal fractional melting of primitive mantle and modified by altering the degree of melting until εNd = 6 (Appendix 5.9.5). This composition derived from fractional melting of primitive mantle was then chondrite-normalised to give a starting composition for modelling melting. Partition coefficients and modal proportions of mineral in the source and melt were taken from Hauri & Hart (1995). Melting curves for [La/Yb]n versus [Dy/Yb]n at 3, 4 and 7 GPa were generated from the starting composition by non-modal aggregated fractional melting using mineral proportions for the source and melt from Walter (1998), and partition coefficients for clinopyroxene and garnet calculated using spreadsheets developed by Wood & Blundy (1997) and van Westrenen et al. (2001) for the respective pressures (Appendix 5.9.6). Partition coefficients for olivine and orthopyroxene are from Hauri & Hart (1995); these were kept constant since they are considered to be minimally affected by pressure compared to those for clinopyroxene and garnet. When compared to these modelled melting curves the Dilb and Iyela lavas may be interpreted as 3 - 6 % melts at pressures near to 4 GPa. Higher initial $^{143}Nd/^{144}Nd$ ratios for CHUR generated for older depleted mantle sources would yield lower percentage melt estimates for the lavas, but an age of 2.5 Ga is considered here as reasonable for DMM, therefore the melt percentages shown are taken as reliable. On close inspection of Figure 5.39, the ankaramites and olivine basalts can be seen to show higher degrees of melting at lower pressure compared to the picrites, as inferred from the discussion above. This is more apparent on a plot of REE ratios against Si_{15} for the lavas with > 10 % MgO where

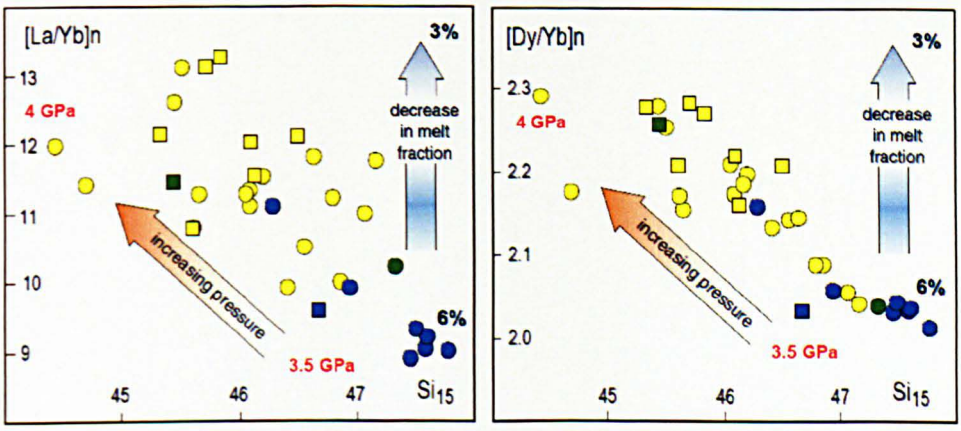

Figure 5.40 Pressure and melt fraction relations shown by chondrite normalised La/Yb and Dy/Yb ratios versus Si_{15} for the Dilb and Iyela lavas. Percentage melting is shown in bold black text and pressure of melting is shown in red (estimated from Figure 5.39) Symbols are as in Figure 5.2.

the ankaramites plot at the lower-pressure and lower-melt-fraction end of the compositional array (Fig. 5.40). Although the pressures estimated from Figure 5.39 are lower than those estimated from the CaO/Al_2O_3 ratios (Fig. 5.39), they are still sufficiently high to conclude that melting occurred beneath thick lithosphere prior to extension.

6. NOBLE GAS AND RHENIUM-OSMIUM ISOTOPE COMPOSITIONS

6.1 Introduction

6.1.1 Isotopes and the Afar Plume

It is a widely held notion that the Afar Plume contributed in some way to the voluminous eruptions which formed the Afro-Arabian flood basalt province 30 Ma ago. This may have been in the form of partial melts derived directly from melting in the head of the plume, or from lithospheric components mobilised by interaction either with partial melts from the plume or with heat from the plume itself (Section 5.3.4). The persistence of a plume-like feature interpreted to be the remnants of the Afar plume, evident today from seismic tomography as a lobate region of low velocity in the mantle below Afar (Ritsema et al. 1999) has encouraged numerous geochemical studies to focus on the search for a common plume-component in the products of Cenozoic to Recent volcanism across the province. Much of this work has involved the analysis of Sr, Nd and Pb isotopes and differences in the interpretation of these data have led to sometimes contradictory conclusions concerning the nature and composition of the Afar plume; as a result it remains a subject for debate.

Despite their OIB-type trace element signatures, inferred by some to be representative of a plume contribution, the lavas from the province exhibit variable and contrasting isotopic compositions (Figs 6.1 & 2). Moreover, the only lavas in East Africa with high $^{206}Pb/^{204}Pb$ ratios that approach HIMU-type isotopic compositions are those from the Kenyan Rift (south of the Turkana Depression) where they are ascribed to either a lithospheric (Paslick et al. 1995; Simonetti & Bell, 1995; Kalt et al. 1997; Rogers et al. 2000) or mantle (Cohen et al. 1984; Furman, 2007) component. Furman (2007), like Kieffer et al. (2004), argues that the primary source for these lavas, and for the Tertiary and Quaternary lavas further north from the Main Ethiopian Rift, Ethiopian Plateau, Yemen and Afar, lies within the chemically heterogeneous South African Superplume. Rogers et al. (2000) on the other hand argue that the isotopic differences between the lavas north and south of the Turkana Depression can only be explained by the existence of two separate mantle plumes. Although the basalts from both regions have similar $^{87}Sr/^{86}Sr$ ratios and have Nd and Pb isotopic compositions within the range of the global OIB database, the proposed composition for the Kenyan Plume (to the south) has a $^{143}Nd/^{144}Nd$ ratio significantly below that reported for the Afar Plume (to the north) represented by the HT2 basalts (Pik et al. 1999) which have isotopic compositions close to a common primitive mantle component variably referred to as FOZO (Hauri et al. 1994), PHEM (Farley et al.

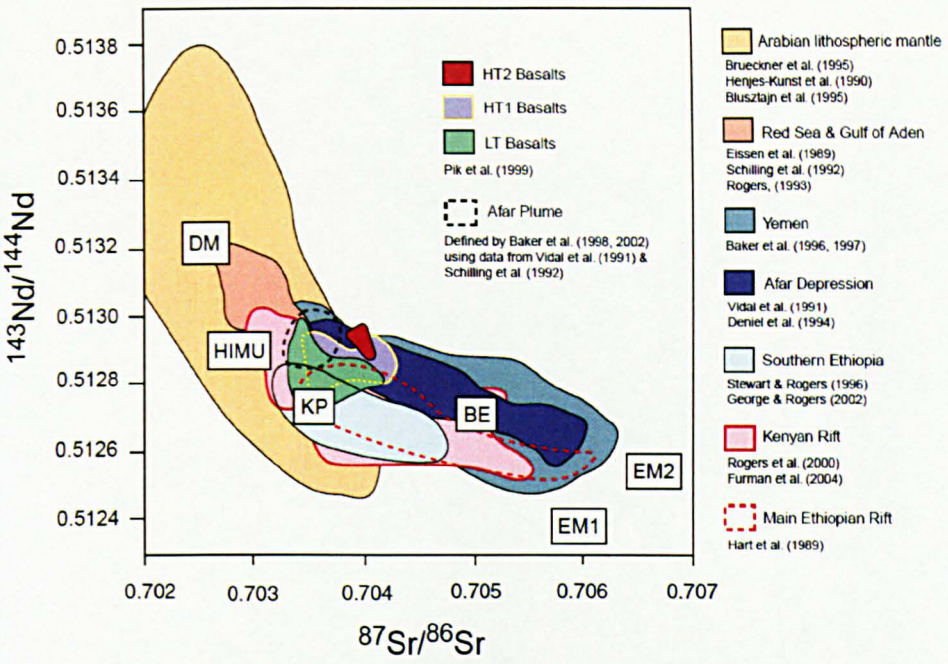

Figure 6.1 Compilation of Sr-Nd isotopic data from the Afro-Arabian volcanic province compared with typical values for depleted mantle (DM), high time-integrated U/Pb ratio (HIMU), and enriched mantle (EM1 & EM2). (KP) indicates the isotopic composition of the Kenyan plume estimated by Rogers et al. (2002). (BE) represents Bulk Earth.

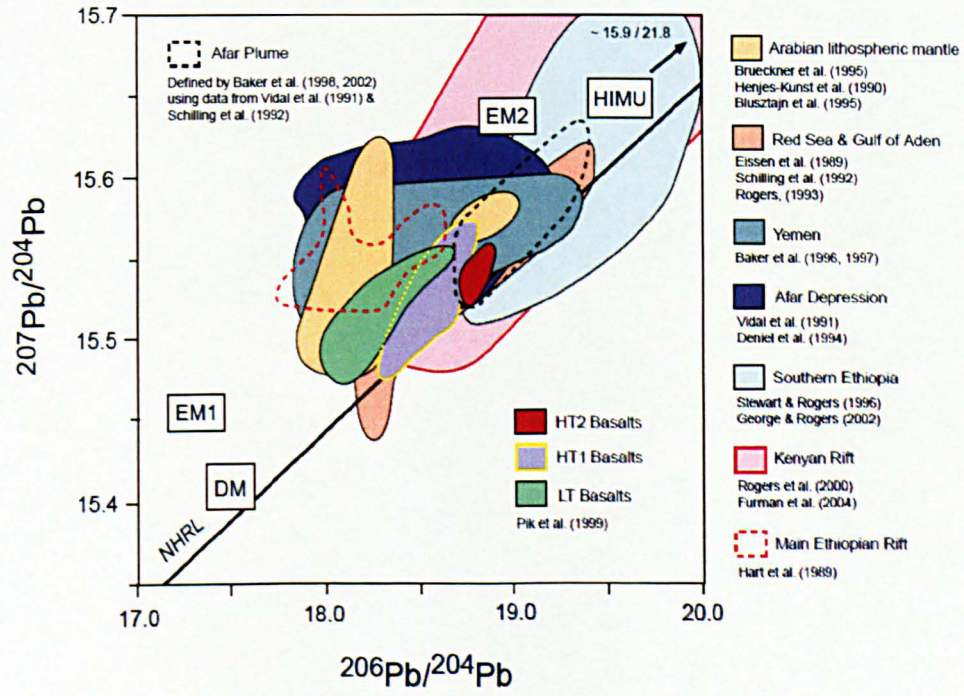

Figure 6.2 Compilation of Pb isotopic data from the Afro-Arabian volcanic province compared with typical values for depleted mantle (DM), high time-integrated U/Pb ratio (HIMU), and enriched mantle (EM1 & EM2). The line labelled NHRL is the northern hemisphere reference line from Hart (1984).

1992) or C (Hanan & Graham, 1996) (Fig. 6.1). This is consistent with the $^3He/^4He$ ratios for the two regions (Pik et al. 2006). The Kenyan Rift basalts have MORB-type $^3He/^4He$ ratios within the range of the continental upper mantle (R/R_a = 5 - 9), whereas the HT2 basalts have elevated $^3He/^4He$ ratios indicative of a deep primitive mantle component (R/R_a up to 19.6) (Fig. 6.3). The absence of elevated $^3He/^4He$

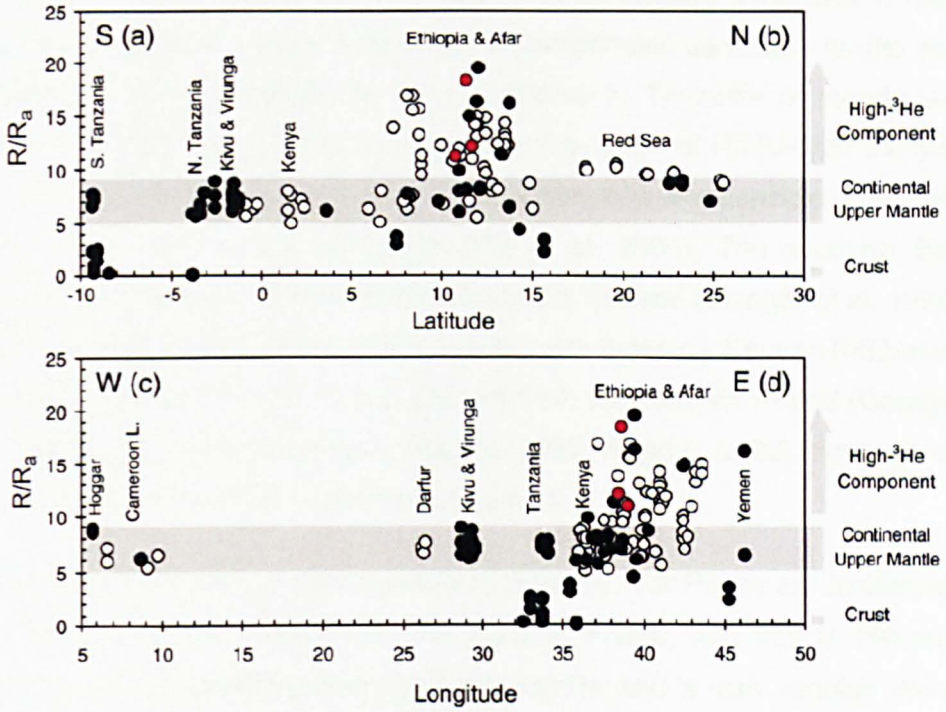

Figure 6.3 Distribution of helium isotopic ratios R/R_a (with R_a the ratio of atmosphere) over the African plate (Pik et al. (2006). Data are plotted as a function of their latitude and longitude. Open circles are data from Pik et al. (2006) and filled circles are data from Marty et al. (1993, 1996); Darling et al. (1995); Moreira et al. (1996); Scarsi & Craig (1996); Franz et al. (1999); Barfod et al. (1999). The black outlined red circles are data for the picrites from the Dilb and Bilbala sections.

ratios in the Kenyan Rift basalts is not consistent with an origin in the deep-sourced South African Superplume as proposed by Furman (2007) although it is suggested that this may reflect mixing between the deep mantle reservoir and crustal or lithospheric components with lower $^3He/^4He$ signatures. Even so, the MORB-type $^3He/^4He$ ratios of the Kenyan Rift basalts are typical of HIMU lavas worldwide. Hanyu & Kaneoka (1997) suggest that relatively low and uniform $^3He/^4He$ ratios are characteristic of the mantle source region for HIMU lavas and are generated from recycled oceanic crust and/or sediments present in this region. They propose an open-system evolution model where helium diffuses between the recycled material and the convecting upper mantle. Hanyu & Nakamura (2000) note that there is a positive correlation between $^3He/^4He$ ratios and εNd in Polynesian HIMU basalts and

suggest that this may be explained by simple binary mixing between MORB and a HIMU source. The higher $^{143}Nd/^{144}Nd$ ratios (closer to HIMU) of the Kenyan Rift basalts erupted through the Panafrican (Mozambique) mobile belt compared to those erupted through the reworked craton may similarly be attributed to such binary mixing regardless of whether the HIMU component is located within the upper mantle or within the lithosphere as inferred by Rogers et al. (2000). Wherever it resides, it seems that the shallow mantle is the most uncomplicated candidate for the source of these lavas. This is supported by the occurrence in Tanzania of mantle xenoliths reported by Cohen et al. (1984) to exhibit the full-range of HIMU-type compositions seen in the East African alkaline lavas; these xenoliths are considered to represent samples of the shallow mantle source (Pik et al. 2006). The southern Ethiopian basalts erupted between 45 and 35 Ma during the Eocene (Ebinger et al. 1993) have Sr and Nd isotopic compositions which overlap with those for Kenyan Rift basalts and are therefore considered also to be sourced from the Kenyan Plume (George et al. 1998; Rogers et a. 2000; George & Rogers, 2002; Rogers, 2006), although they do not exhibit such strong HIMU signatures (Figs 6.2 & 3).

The Oligocene to Recent basalts associated with the Afar Plume are isotopically less diverse than those associated with the Kenyan Plume, and this is interpreted to reflect a more homogeneous basement lithosphere and a less variable developing tectonic regime (Vidal et al. 1991; Schilling et al. 1992; Deniel et al. 1994; Rogers, 2006). Nevertheless, Baker et al. (1996b) and Pik et al. (1999) report that the trace element and Sr, Nd and Pb isotopic compositions of the flood basalts from Yemen and Ethiopia have been so substantially modified by fractionation, differing degrees of partial melting and by the interaction with a heterogeneous Pan-African crust that they lie outside the isotopic ranges of temporally and spatially appropriate mantle components identified in the region (i.e. Red Sea/Gulf of Aden MORB mantle, the Afar Plume and Pan-African lithospheric mantle). Consequently, the task of identifying a common primary source for these lavas (and for more recent lavas in the region) is somewhat cryptic since it is dependent on the interpretation of vectors leaning toward one component or another. Whereas the basalts from the Red Sea and Gulf of Aden spreading centres are dominated by high $^{143}Nd/^{144}Nd$ ratios and low $^{87}Sr/^{86}Sr$ ratios typical of MORB, those from Afar and the Yemen have overlapping fields characterised by lower $^{143}Nd/^{144}Nd$ ratios and higher $^{87}Sr/^{86}Sr$ ratios that extend to values beyond that for bulk earth (Fig. 6.1). These broad fields hide temporal and therefore stratigraphic variations in the isotopic ratios that reveal significant

evolutionary changes in the influence of various contributing components on the composition of the source.

Within the fields for the Afar Depression and the Yemen the older Miocene lavas generally trend toward lower $^{143}Nd/^{144}Nd$ ratios and higher $^{87}Sr/^{86}Sr$ ratios whereas the most recent lavas trend toward higher $^{143}Nd/^{144}Nd$ ratios and lower $^{87}Sr/^{86}Sr$ ratios near to FOZO or PHEM ($^{143}Nd/^{144}Nd$ ~0.5130, $^{87}Sr/^{86}Sr$ ~ 0.7035). A similar trend is apparent from the Pb isotopic compositions which show a younging trend toward higher $^{206}Pb/^{204}Pb$ within these fields (Fig. 6.2). Like the HT2 basalts which are taken to represent the earliest uncontaminated outpourings of flood basalts from the Afar Plume, the most recent lavas are characterized by high $^{3}He/^{4}He$ ratios indicative of a deep primitive mantle component (Hanan & Graham, 1996; Ellam & Stuart, 2004). It may be inferred therefore that the Sr, Nd and Pb isotopic variations described above for both regions are a consequence of the waning influence of the lithosphere and the increasing influence of the Afar Plume as Arabia drifted away from Africa following rifting and extension (Vidal et al. 1991, Deniel et al. 1994, Rogers, 2006). The persistence of the deep-sourced Afar plume component throughout this process from the onset of flood volcanism is evident from the high $^{3}He/^{4}He$ ratios in the Oligocene flood basalts from Ethiopia and Yemen, Miocene basalts from the Ethiopian shield volcanoes such as Ras Dashen, and Quaternary to Recent basalts from the Assal Rift (Djibouti) and Afar (Pik et al. 2006).

The trend toward elevated $^{206}Pb/^{204}Pb$ ratios for the younger lavas led Vidal et al. (1991), Schilling et al. (1992) and Deniel et al. (1994) to conclude that the Afar plume has a HIMU rather than a primitive mantle signature as inferred by Baker et al. (1996b, 1998) and Pik et al. (1999). The HIMU signature is a more a feature of the trace element compositions of the HT1 and HT2 basalts (Pik et al. 1999) and the high-Ti basalts from the Yemen (Baker et al. 1996 a & b) and it is argued that since it extends beyond the influence of the Afar Plume, it is a signature associated with the Afro-Arabian lithospheric mantle (Baker et al. 1998; Pik et a. 1999; Bertrand et al. 2003) (Section 5.3.4). Isotopically however the Oligocene high-Ti basalts from both sides of the Red Sea (including the picrites and ankaramites from the Dilb and Iyela sections) are similar to the modern Afar basalts with εNd values of +6 ($^{143}Nd/^{144}Nd$ ~ 0.5129) typical for primitive depleted mantle (Fig. 6.1) and high $^{3}He/^{4}He$ ratios (R/R_a ~ 18) (Pik et al. 2006). These features together with strongly fractionated REE patterns, low Al_2O_3 contents, and high TiO_2, MgO and FeO (as described for the Dilb and Iyela lavas – Chapter 5), are indicative of high temperature, high pressure

melting of a deep mantle derived source within the garnet stability field at pressures probably in excess of 4 GPa, beneath thick lithosphere, possibly within the convecting mantle. Moreover, the presence of highly forsteritic olivine phenocrysts in the Dilb and Iyela lavas suggests that the primary melts generated by such melting initially ponded and fractionated at the moho prior to further evolution within the crust. Subsequent melting of a heterogeneous enriched subcontinental lithospheric mantle as a result of the interaction with the hot depleted asthenospheric melts accompanied by lithospheric thinning through the Oligocene and Miocene produced magmas with hybrid elemental and isotopic compositions (PREMA + DM, EM1, EM2 and HIMU). These compositions are consistent with the range seen in mantle-derived xenoliths from Arabia (Brueckner et al.1988; Henjes-Kunst et al. 1990; Blusztajn et al. 1995; Baker et al. 1998), and East Africa (Cohen et al. 1984, Roger et al. 1999; Conticelli et al. 1999; Bedini et al. 1997; Bedini & Boudinier, 1999; Beccaluva et al. 2007, 2008; Ferrando et al. 2008).

$^{3}He/^{4}He$ ratios of with R/R_a of < 9 for spinel lhezlolite, harzburgite and websterite xenoliths from the Northern Ethiopian Plateau (Beccaluva et al. 2008) confirm that these lithospheric hybrid end-member components are distinct from the plume with its characteristic deep mantle high ^{3}He signature. Beccaluva et al. (2008) suggest that the chemistry of the Ethiopian xenoliths reflect complex asthenospheric-lithospheric interactions that occurred within the impact-zone of the plume where consequent lithospheric bulging and thinning was accompanied by pervasive refertilisation as a result of reactive percolation of sublithospheric subalkaline melts. Bedini et al. (1997) propose that this process of thermo-mechanical erosion of the lithospheric mantle occurred during the early stages of continental rifting. Pervasive infiltration of plume derived melt would have generated a regional-scale high porosity domain at the transition between adiabatic and conductive mantle. The impermeable nature of this domain to basaltic melts combined with melt-rock reactions at increasing melt mass would have led to the accumulation at the base of the lithosphere of hybridised melts which are proposed as a potential source for the flood basalts.

From a study of mantle xenoliths from the Yemen, Baker et al. (1998) conclude that the melts from the plume were carbonatitic and rich in volatiles and incompatible trace elements, and that these features are consistent with derivation from recycled oceanic crust. The presence of volatiles may have caused a lowering of the peridotite solidus which triggered extensive melting in the overlying lithospheric mantle and the

generation of abnormally large volumes of melt at close to ambient mantle temperatures. The initial melts from the plume may have been volatile-rich as suggested by Kieffer et al. (2004). This is supported in a recent study of the chemistry of mantle xenoliths from Ethiopia by Ferrando et al (2008) who suggest that there were two distinct metasomatic events associated with the emplacement of the Afar plume - first a pervasive modal metasomatism driven by water-rich fluids, and a second, a non-pervasive cryptic metasomatism probably related to the migration of melts.

Further hybridisation as a result of crustal contamination, most marked in the Oligocene to Miocene plateau basalts, is suggested to have taken place primarily at lower crustal levels prior to and during the initial stages of rifting (Hart et al. 1989; Pik et al. 1999; Baker et al. 1996). Pik et al. (1999) attribute the main chemical differences between the HT and LT basalts to crustal contamination. More recently however, Beccaluva et al. (2007, 2008) propose that such differences, which are geographically manifest, are a result of different degrees of metasomatism in the lithospheric mantle associated with differences in temperature across the head of Afar plume. It is suggested that the LT basalts (in the western Ethiopian Plateau) were generated in the outer zone of the plume by partial melting of moderately metasomatised lithospheric mantle at about 1200 °C, whereas the HT basalts (in the eastern Ethiopian Plateau) were generated in its core from mantle sources significantly more enriched by melts derived from the plume at 1500 °C.

The declining influence of lithospheric components following continental breakup between 4 and 5 Ma is reflected in the Pliocene basalts from Afar, which were dominantly derived from a PREMA-type reservoir (Hart et al. 1989). Continued extension and the opening of the Gulf of Aden and the Red Sea during the Holocene saw the formation of ocean crust and the appearance of depleted MORB-type mantle as the main source component for volcanism along the axial rift and associated sea-mounts and islands (Eissen et al. 1989; Rogers, 1993: Volkner et al. 1997; Antonini et al. 1998). In the Main Ethiopian Rift, where continental breakup was less advanced, volcanism remained hybridised (as today). With reference to U-series isotope analyses Rogers (2000) implies that melting within the Afar plume continues to contribute to volcanism in region. It is argued that the near vertical trends defined by variable $^{230}Th/^{232}Th$ with almost constant $^{238}U/^{232}Th$ ratios for recently erupted basalts from the Afar and the Kenyan Rift are indicative of dynamic melting in the convecting mantle beneath both these regions (Fig. 6.4).

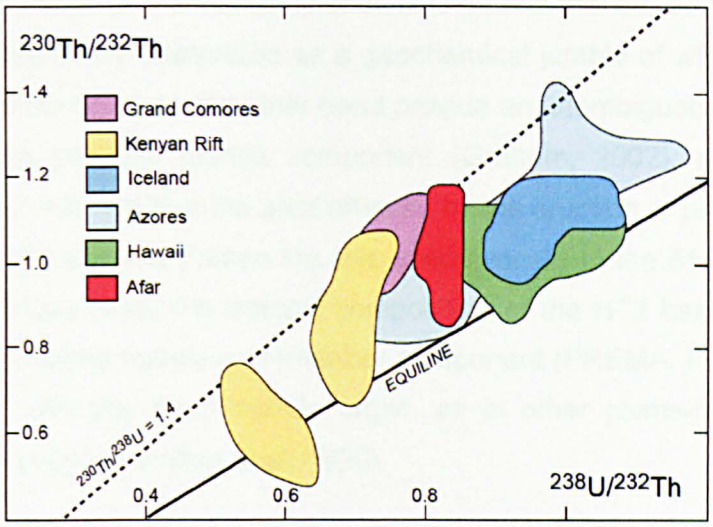

Figure 6.4 U-series equiline diagram of $^{230}Th/^{232}Th$ versus $^{238}U/^{232}Th$ for the Afar and Kenyan Rift basalts and selected OIB (Rogers, 2006). The activity of ^{238}U is arbitrarily set to 1 (i.e. $^{230}Th/^{238}U = 1$) representing secular equilibrium shown by the solid line or equiline. The dashed line represents the 40 % excess of ^{230}Th evident from the maximum deviation from the equiline shown by the $^{230}Th/^{232}Th$ ratios for the Afar basalts.

Hart et al. (1989) noted that the trends in the trace element chemistry and Sr, Nd and Pb isotopic composition of Cenozoic to Recent basaltic volcanism in Ethiopia (as described above) reflect chronological and tectonic controls on mantle melting, mantle reservoir evolution and associated lithospheric interactions that are common to many extensional regimes. Nevertheless, all sorts of alternative hypotheses based on loosely contextualised geochemical data have since been forwarded in an attempt to explain the geochemical evolution of the Afro-Arabian Province and the involvement of suggested end-member components. It has taken the advent of new and improved analytical techniques in noble gas geochemistry for faith to be placed again in detailed stratigraphically constrained geochemical studies such as that by Hart et al. (1989). Current consensus suggests that the most likely signature for the Afar plume is depleted primitive mantle (referred to as PREMA by Hart et al. 1989) and that this, as a common source component for flood volcanism and continued basaltic volcanism up to the present day, has been variously coloured by interaction with lithospheric mantle components. Still, attempts to resolve the contribution of various end-member components using the Nd, Sr, U and Pb isotopic compositions of the lavas from different regions remain ambiguous, particularly when their compositional fields show considerable overlap and when data is presented without consistent stratigraphic context. This is exacerbated by the lack of knowledge of the

nature and composition of the subcontinental lithospheric mantle, so much so that it has become conveniently interpreted as a geochemical jumble of whatever fits with theory. High $^{3}He/^{4}He$ ratios on the other hand provide an unambiguous signature of a deep undegassed primitive mantle component (Graham, 2002), and the limited distribution of such ratios within the area affected by the eruption of pre-rift Oligocene flood basalts in Ethiopia and Yemen link this unequivocally to the Afar plume (Pik et al. 2006). The unique Nd-Sr-Pb isotopic composition of the HT2 basalts compatible with a depleted primitive mantle end-member component (PREMA, FOZO, PHEM or C) is consistent with this deep mantle origin, as in other plume-related volcanic provinces such as Iceland (Hilton et al. 1999).

On the grounds of statistical bias, Anderson (1998, 2000a, 2001, 2004), Meibom & Anderson (2004) and Meibom et al. (2004) argue that high $^{3}He/^{4}He$ ratios are not necessarily indicative of deep mantle and are more likely to originate in the shallow mantle, although the reasoning behind this has been strongly and convincingly contested by Graham (2002). It is generally accepted that high $^{3}He/^{4}He$ ratios are indicative of undegassed primitive mantle and that this is most likely to reside in an unmixed lower mantle - this assumes that the mantle is layered. Recent tomographic studies, however, provide evidence that subducted material can pass through the 660 km discontinuity (van der Hilst et al. 1997), and numerical models of mantle convection show that neither the high viscosity of the lower mantle nor the phase change at the 660 km discontinuity can preserve layering or large scale heterogeneity in the deep mantle (van Keken & Ballentine, 1999; Hunt & Kellogg, 2001). This discounts the existence of a primordial lower mantle, and makes the preservation of significant reservoirs for primordial ^{3}He difficult to explain. Class & Goldstein (2005) propose that the high $^{3}He/^{4}He$ ratios in plumes reflect incomplete degassing of the deep Earth during continent and ocean crust formation, and that such ratios are inherited from pockets of undegassed mantle that have somehow remained isolated from mantle convection. Ballentine (2002) suggest also that the core cannot be ruled out as a source for ^{3}He in the mantle. Marty et al. (1996) nevertheless suggests that the high $^{3}He/^{4}He$ ratios associated with the Afar plume were inherited as a result of limited mass transfer of deep mantle material across the 660 km discontinuity together with efficient heat transfer and material upwelling above. This is consistent with the primitive mantle source and the tomographic images presented by Ritsema et al. (1999) in which the connection between the upper and lower mantle low velocity anomalies is not clear. It is also in agreement with models proposed for other plume-related volcanic provinces (Ellam & Stuart,

2004). Marty et al. (1996) estimate the contribution from the lower mantle to be < 5 % and in this respect it is envisaged that it would have had no discernable effect on the trace element and Nd, Sr and Pb isotopic compositions of the flood basalts which are dominated by mixing between upper mantle and lithospheric components.

6.1.2 Resolving the plume signature: noble gas and osmium isotopes

Noble gas isotopes: Primordial noble gases in mantle originate either from the solar nebula or from volatiles trapped in accreting material such as impacting meteorites during the early formation of the Earth, and these are still degassing from the mantle into the atmosphere today (Ballentine, 2002). It can be assumed therefore that, in addition to ^{3}He, primordial isotopes of other noble gases such as Ne, Ar and Xe are still present in undegassed mantle, and may be used like ^{3}He as tracers for deep mantle. Our understanding of the geochemical behaviour of these heavier noble gases is still largely tentative and the inherent difficulty in reproducing accurate and reliable isotopic measurements for them has meant that we have a limited data base to work with. Comprehensive reviews of our understanding of the geochemistry of noble gases in the mantle have been compiled by McDougall & Honda (1998), Farley & Neroda (1998) and Graham (2002). Unlike helium, which upon degassing escapes to space, the heavier noble gases remain for some time in the atmosphere and may be reincorporated into the geological cycle thus making the job of unravelling the contributions to measured isotopic compositions more complicated than for helium. Moreover, their low abundance in the mantle means that such exchange can result in a swamping of mantle-derived isotopic signatures by atmospheric compositions as a result of the recycling of atmosphere-derived gases back into the mantle and/or the interaction of lavas with the atmosphere during eruption. Atmospheric contamination can also be a problem during analysis, although such isobaric interference can usually be corrected for.

The reliability of analyses for all noble gases has however improved with the recent development of in-vacuo stepwise gas release methods by either incremental crushing or incremental heating. Despite such improvements, more sense has been made of the analyses for neon than for the other heavy noble gases partly because its geochemical behaviour can be related to that of helium. Terrestrial primordial neon and helium are thought to be solar in composition and to have been augmented over time by the coupled production of radiogenic ^{21}Ne and ^{4}He respectively from the decay of U and Th in the mantle. α particles generated during the production of ^{4}He and neutrons produced from particle collisions with other elements such as oxygen,

interact with ^{18}O and ^{24}Mg to produce ^{21}Ne. Therefore mantle Ne and He isotopic compositions are controlled by the ratios of (primordial $^{20}Ne+^{22}Ne$)/(U+Th) and (primordial ^{3}He)/([U+Th) respectively. If the coupled production of nucleogenic ^{21}Ne and radiogenic ^{4}He is assumed to be perfect, the $^{3}He/^{4}He$ ratio for any locality could be predicted from the slope on a Ne three-isotope diagram ($^{20}Ne/^{22}Ne$ versus $^{21}Ne/^{22}Ne$) (Honda et al. 1993). This is largely substantiated by the growing data-base of Ne isotope compositions for mantle-derived lavas, which when plotted on a Ne three-isotope diagram show progressively steeper trends for OIBs with higher $^{3}He/^{4}He$ ratios compared with MORB (Fig. 6.5). These steep trends reveal that the

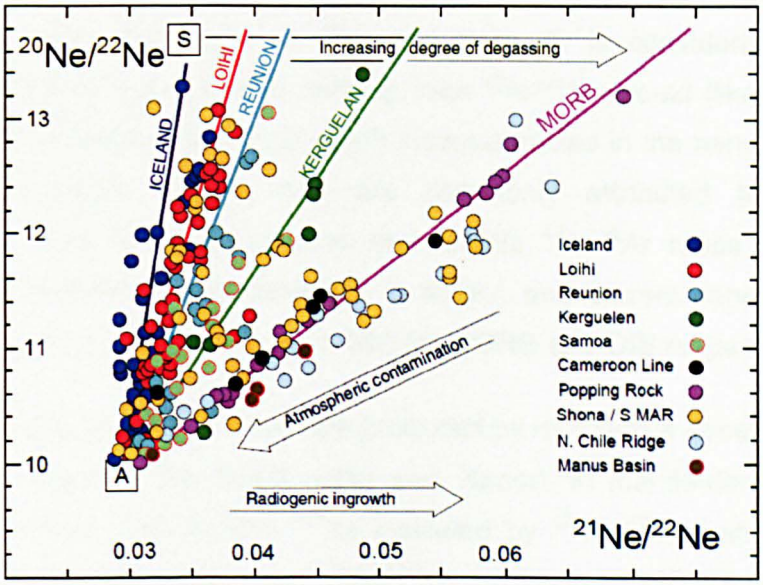

Figure 6.5 Ne three-isotope diagram showing Ne isotopic composition for selected volcanic provinces. $^{20}Ne/^{22}Ne$ with < 2 sigma above air are not included. S = solar neon, and A = air. Bold coloured lines represent mixing between air and mantle sources. $^{21}Ne/^{22}Ne$ ratios extrapolated to solar value = 0.035 for Iceland, 0.039 for Loihi, 0.043 for Reunion, 0.053 for Kerguelen and 0.075 for MORB (Graham, 2002).

mantle sources for OIB have less nucleogenic Ne (lower $^{21}Ne/^{22}Ne$) and radiogenic He (higher ^{4}He) than the source for MORB, which is evidently characterised by lower time-integrated $^{3}He/(U+Th)$ and $^{22}Ne/(U+Th)$ ratios. Such isotopic compositions for OIB together with significant enrichment in trace elements compared to MORB are indicative of an undegassed primitive mantle source. The trend lines for the range of OIB and MORB shown in Figure 6.5 all pass through the isotopic composition for air, and in this respect they represent mixing between the atmosphere and mantle sources with a solar $^{20}Ne/^{22}Ne$ ratio of 13.8 and varying $^{21}Ne/^{22}Ne$ ratios representing different degrees of radiogenic ingrowth.

The isotopic ratios for Ar, Kr and Xe in mantle derived lavas are less well constrained than Ne mainly because of the effect of atmospheric contamination, and are therefore currently limited in their usefulness as reliable tracers of mantle components. Nonetheless, Valbracht et al. (1997) propose that the significant correlation between low $^{38}Ar/^{36}Ar$ and elevated, non-atmospheric $^{20}Ne/^{22}Ne$ ratios in deep-erupted glassy basalts at Loihi, is evidence for a solar Ar component in the mantle (mean $^{38}Ar/^{36}Ar$ for solar wind = 0.175). These values are, however, not correlated with high $^{40}Ar/^{36}Ar$ as might be expected from binary mixing between air and mantle components (Kunz, 1999). Moreover, $^{40}Ar/^{36}Ar$ ratios do not correlate with $^{3}He/^{4}He$ as they should (Graham, 2002). ^{36}Ar and ^{38}Ar are primordial and ^{40}Ar is produced by radioactive decay of ^{40}K, and since Ar is considered to be more incompatible than K during mantle melting, high $^{40}Ar/^{36}Ar$ should (like high $^{3}He/^{4}He$) be indicative of undegassed mantle. Such inconsistencies in the behaviour of Ar are yet to be resolved, though they are commonly attributed to atmospheric contamination. It is at least accepted that mantle $^{40}Ar/^{36}Ar$ ratios are principally dependent on time-integrated variations in $K/^{36}Ar$, and current consensus assigns $^{40}Ar/^{36}Ar$ ratios of around 40,000 and 8,000 for MORB and OIB respectively (Fig. 6.7).

With nine isotopes, several of which are produced by radioactive decay, resolving the isotopic composition of the rarest noble gas, Xenon, in mantle-derived basalts is particularly complex. Still, excess ^{129}Xe indicated by $^{129}Xe/^{130}Xe$ ratios significantly higher than modern atmosphere (air $^{129}Xe/^{130}Xe$ = 2.17) in MORB are generally taken to indicate a mantle component (Staudacher & Allegre, 1982; Marty, 1989; Kunz et al. 1998; Moreira et al. 1998; Sarda et al. 2000). Less significant anomalies for $^{134}Xe/^{130}Xe$ and $^{136}Xe/^{130}Xe$ are also found in MORB. Graham (2002) suggests that excess ^{129}Xe in MORB is derived from extinct radioactivity of ^{129}I, whereas excess $^{131,132,134,136}Xe$ are fissiogenic after ^{238}U and extinct ^{244}Pu. Correlation of excess ^{136}Xe and ^{129}Xe in MORB (Fig. 6.8) is generally interpreted as mixing between air and a depleted mantle component. OIB show much smaller excesses in radiogenic and fissiogenic Xe compared to MORB (Hiyagon et al. 1992; Trieloff et al. 2000) and this may be attributed to differences in the relative fissiogenic contributions from ^{238}U and ^{244}Pu. In a steady state mantle OIBs with high $^{3}He/^{4}He$ ratios might be expected to have lower $^{136}Xe/^{130}Xe$ than MORBs because of the greater abundance of fissiogenic Xe from ^{238}U decay in the more degassed upper mantle (Porcelli & Wasserburg, 1995). However, a systematic lower angle trend for OIB for $^{136}Xe/^{130}Xe$ versus $^{129}Xe/^{130}Xe$ compared to MORB is not resolvable from the current data base. It is argued that there is a lower angle systematic trend for $^{129}Xe/^{130}Xe$ versus $^{20}Ne/^{22}Ne$

for OIB (represented only by Iceland and Loihi) compared to MORB, and that if this is extrapolated to a value for $^{20}Ne/^{22}Ne$ of 13.9, representative of solar Ne, the equivalent value of ~ 7.2 for $^{129}Xe/^{130}Xe$ might constitute evidence for excess ^{129}Xe in OIB mantle source regions (Fig. 6.9). If, on the other hand, Ne-B with a $^{20}Ne/^{22}Ne$ of 12.5 is taken as solar (Trieloff et al. 2000), the equivalent $^{129}Xe/^{130}Xe$ ratio is be close to air and therefore would not constitute excess ^{129}Xe. Ratios of the lighter Xe isotopes ($^{124,126,128}Xe$) may be more diagnostic of solar Xe, but generally the abundances of these nuclides are too low to measure. Excesses of these isotopes are correlated with excess ^{129}Xe and $^{20}Ne/^{22}Ne$ occur in mantle-derived CO_2 well gases from the south-western US and southern Australia; such excesses are yet to be found in basalts.

Isotopic measurements for Kr in basalts show little variation from air, therefore to-date it has been of little use in tracing mantle chemistry. The production of ^{83}Kr, ^{84}Kr and ^{86}Kr from spontaneous fission of ^{238}U is so low that it is yet to be measured in basalts.

There are few studies on the isotopic composition of the heavy noble gases for mantle-derived rocks from the Afro-Arabian volcanic province, and these are limited to the Red Sea region (Moreira et al. 1996; Hopp et al. 2004) and east of the Kenyan rift (Hopp et al 2007). Moreira et al. (1996) report solar Ne isotopic signatures and low $^{40}Ar/^{36}Ar$ ratios near to air, together with variable He isotopic ratios for submarine basalts from the Red Sea. They suggest that the observed isotopic systematics are a result of mixing between air, MORB and a plume-derived component similar in composition to that for Loihi. It is noted that whereas the contribution from plume-derived helium decreases with increasing distance from Afar (reaching MORB-like values in the northern Red Sea) the contribution from plume-related solar Ne remains relatively constant. Hopp et al. (2004) describe similar decoupling of He and Ne in ultramafic rocks from Zabargad Island and mantle xenoliths from Quaternary volcanic fields in Saudi Arabia within the Red Sea region. They attribute this to mixing between a deep-mantle, a pre-rift MORB-like, and a more radiogenic pre-rift lithospheric mantle component. It is suggested that the deep mantle component represents the Afar plume and that this contributed primordial noble gases to more radiogenic and nucleogenic lithospheric and asthenospheric components up to a distance of >1800 km from Afar as early as 20 Ma during the early stages of continental rifting. Similar mixing relations, evident from noble gas isotope systematics, are described for the lithospheric mantle beneath the Chyulu Hills east

of the Kenyan Rift (Hopp et al. 2007), but it is proposed here that the primitive mantle component is related to the Kenyan rather than the Afar plume. The noble gas isotopic compositions of two picrites from the eastern Ethiopian Plateau are presented as part of this thesis (Section 6.2.1) - one from the Bilbala Section, and one from the Dilb Section. These analyses were carried out to verify the high ^{3}He signatures reported for the HT2 basalts by Marty et al. (1996) and to test for the presence of other primordial noble gases which may characterise the Afar plume. The results of these analyses are discussed in relation to the existing data from the Red Sea in Section 6.3.

Osmium isotopes: Even though the isotopic composition of noble gases may indicate a source for the Afar plume in undegassed primitive mantle, uncertainties regarding the structure of the mantle place considerable ambiguity on where in the mantle this undegassed reservoir resides. Arguments in favour of an unlayered mantle that discount the existence of an undegassed reservoir in the lower mantle propose the core-mantle boundary as a potential source for primordial noble gases. The tentative connection between the lower mantle low velocity seismic anomaly originating at the core mantle boundary and the upper low velocity anomaly beneath Afar certainly does not rule this out as a possible source for the primordial noble gases presumed to be carried in the Afar plume. The accompanying presence in plume-derived lavas of other elemental or isotopic signatures indicative of a contribution from the core would strengthen this supposition. The Dilb and Iyela Lavas (including the picrites, ankaramites and olivine basalts), which are synonymous with the HT2 basalts and assumed to represent the earliest and least contaminated outpourings of flood volcanism in the Afro-Arabian province, would be the most likely hosts for such signatures linking the Afar plume to an origin at the core-mantle boundary.

Brandon et al. (1998, 1999) propose that coupled enrichments of $^{186}Os/^{188}Os$ and $^{187}Os/^{188}Os$ relative to chondritic upper mantle in picritic lavas from Hawaii are indicative of an evolved outer core component in the Hawaiian plume (Chapter 1). These are correlated with high $^{3}He/^{4}He$ ratios with $R/R_a > 30$ (Brandon et al. 1999), and are consistent with seismic evidence for a low velocity zone extending down to the core-mantle boundary beneath Hawaii (Ritsema et al. 1999; Ritsema & Allen, 2003; Lei & Zhao, 2006; Zhao, 2008). It is thought that during its formation, the Earth's core sequestered most highly siderophile elements (HSE) including Re, Pt and Os. The bulk-core is as a result considered to have chondritic Re/Os and Pt/Os

ratios and relative abundances of HSE concentrations about a factor of 10^3 higher than the upper mantle (Newsom & Sims, 1991). H5 ordinary chondrites (taken to represent the initial composition of the core by Walker et al. 1995) have Os concentrations of ~ 3000 ng/g and $^{187}Re/^{188}Os$ ratios near 0.402 (Luck & Allegre, 1983), whereas the upper mantle is estimated to have an Os concentration of 3.3 ng/g and $^{187}Re/^{188}Os$ ratio of 0.401 (Morgan, 1986). During crystallisation of the inner core and formation of the liquid outer core, however, fractionation of Re from Os and Os from Pt is likely to have led to supra-chondritic Re/Os and Pt/Os ratios and lower concentrations of HSE in the outer core. Modelling predicts a decrease in Os from 3000 to 1040 ng/g in the outer core with 5.5 % fractional crystallisation, which contrasts with upper mantle concentrations of 3 - 4 ng/g, reflecting HSE concentrations 300 to 400 times higher in the outer core compared to the mantle. Assuming an inner core with initial chondritic ratios of $^{187}Re/^{188}Os$ = 0.4224 and $^{190}Pt/^{188}Os$ = 0.001692, 5.5 % crystallisation produces outer core ratios of $^{187}Re/^{188}Os$ = 0.5303 and $^{190}Pt/^{188}Os$ = 0.00423. With crystallisation occurring within several hundred million years after core separation, the outer core would evolve to present day values of $^{187}Os/^{188}Os$ = 0.1372 and $^{186}Os/^{188}O$ = 0.119852 ($^{187}Os/^{188}Os$ = 0.1372 is equivalent to γOs = +8, where γOs is the percent deviation from the present-day chondrite average of $^{187}Os/^{188}Os$ = 0.1270). Plumes originating at the core mantle boundary should therefore show enrichments in $^{187}Os/^{188}Os$ and $^{186}Os/^{188}O$ reflecting the decay of ^{187}Re and ^{190}Pt to ^{187}Os and ^{186}Os respectively (Newsom & Sims, 1991; Smoliar et al. 1996). The large contrast in HSE concentrations between the outer core and the mantle mean that the entrainment of between 0.5 to 1 % of outer core are sufficient to significantly influence the Os isotopic composition of a plume (Brandon et al. 1998). Moreover, the Os isotopic composition inherited from such a contribution is likely to be preserved in plume-derived lavas since, unlike the relative abundances of HSE it is not modified by crystal-liquid fractionation processes. Supra-chondritic $^{187}Os/^{188}Os$ ratios alone, however, are not exclusively indicative of outer entrainment since such ratios may also be generated by recycling of 1- to 3- billion-year-old oceanic crust (Reisberg et al. 1993; Hauri & Hart, 1993; Shirey & Walker, 1998; Lassiter & Hauri, 1998; Schaefer et al. 2002). Coupled enrichments in $^{187}Os/^{188}Os$ and $^{186}Os/^{188}O$ on the other hand cannot be produced by recycling of ancient oceanic crust, and are therefore are taken as a more reliable indicator of a contribution from the core. In addition to Hawaii, coupled enrichments in $^{187}Os/^{188}Os$ and $^{186}Os/^{188}O$ have been reported for suphide ores from the Siberian flood basalt province (Walker et al. 1997) and for komatiites from Gorgona Island, and in each case these have been attributed to a chemical interaction between the outer core and

the lower mantle. Ravizza et al. (2001) propose that such coupled enrichments might alternatively be explained by the addition of ancient hydrothermally altered or metalliferous sediments, but this is unlikely because of the absence in the analysed samples from Hawaii, Siberia and Gorgona of elevated Mn and Fe contents that would be expected with a sedimentary input of this nature.

The absence of elevated $^{186}Os/^{188}O$ ratios in Icelandic picrites with the highest recorded $^{3}He/^{4}He$ ratios occurring above a low velocity seismic anomaly that can be traced to the core mantle boundary casts doubt on the consistency of Os as a tracer for the core (Brandon et al. 2007). The absence too of primordial tungsten isotopic signatures reflected by unradiogenic $^{182}W/^{184}W$ in the Hawaiian picrites and selected South African komatiites known to contain coupled excesses of ^{186}Os and ^{187}Os seems to discount a simple core-mantle mixing scenario (Schersten et al. 2004). Despite the moderate Mn contents of the samples from Hawaii, Siberia and Gorgona (Brandon et al. 2003), Schersten et al. (2004) suggest that such excesses are instead a result of recycling of surficial Mn sediments with high Pt/Os and Pt/Re ratios. Humayun et al. (2004) argue that coupling between $^{182}W/^{184}W$, ^{186}Os and ^{187}Os and Fe/Mn is not necessarily a prerequisite for core-mantle interaction. They suggest that W and Os can be decoupled by fractional crystallisation of immiscible Fe-FeS melts generated during metasomatism of the lower mantle caused by its interaction with the outer core. Since Fe is the dominant constituent of the core it must represent the main exchange across the core-mantle-boundary; this exchange (or flux) is likely to influence the Fe content, and therefore the density, of the mantle which Humayan et al. (2004) argue is resolvable by seismic tomography. They suggest from the analyses of Fe/Mn ratios for a series of Hawaiian lavas that there is an increase of 1 – 2 % in the mole fraction of iron in the mantle beneath Hawaii, which corresponds to a density anomaly of 0.5 % (equivalent to that observed in seismic tomography models of the Pacific superswell). This is consistent with the estimated contribution from the outer core calculated from the excess ^{187}Os and ^{186}Os in the Hawaiian lavas (Brandon et al. 1998, 1999), and largely discounts the involvement of recycled Mn-rich sediments.

Published Os isotopic analyses of the Afro-Arabian flood basalts are limited to $^{187}Os/^{188}Os$ ratios for one LT basalt and one HT2 basalt from the Ethiopian Plateau (Reisberg et al. 1998). The LT basalt has a low Os concentration (13 ppt) and an initial $^{187}Os/^{188}Os$ ratio of 0.151 reflecting crustal assimilation, whereas the HT2 basalt shows no sign of crustal contamination, is rich in Os (147 ppt), and has an

initial $^{187}Os/^{188}Os$ ratio of 0.127, close to that for primitive mantle. This is notably lower than most $^{187}Os/^{188}Os$ ratios measured in OIB. The HT2 basalt also has a $^{3}He/^{4}He$ ratio of R/R_a = 12.6 indicating derivation from an undegassed mantle source. $^{187}Os/^{188}Os$ ratios for a number of basaltic lavas from the Ethiopian rift were also analysed by Reisberg et al. (1998). Few of these show Os isotopic compositions indicative of direct derivation from a mantle source. Generally they exhibit greater degrees of crustal contamination than the flood basalts and together show a rough correlation between $^{187}Os/^{188}Os$ and osmium concentration (expressed as 1/[Os]) reflecting the fact that the more differentiated lavas with consequently lower concentrations of Os are more sensitive to the effects of crustal contamination. The $^{3}He/^{4}He$ ratios in the rift lavas are negatively correlated with the degree of crustal contamination, but are unrelated to the $^{187}Os/^{188}Os$ ratios since these are controlled by the Os concentration in the rock in addition to the proportion of assimilated crustal material. The osmium isotopic compositions for a series of representative lavas from the Dilb and Iyela sections, and for representative picrites from the Bilbala and North Lalibela sections lavas are presented in this thesis (Section 6.2.2). These analyses were carried out to test for a contribution from the outer-core and further refine the isotopic signature of the Afar plume. The data are discussed in relation to the presented noble gas isotopic compositions and existing Os isotopic data for the LT and HT2 basalts from the Ethiopian Plateau and basaltic lavas from the Main Ethiopian Rift in Section 6.3.

6.1.3 Sample preparation

Owing to the time-consuming sample preparation procedures for both noble gas and osmium isotopic analysis, it was not possible to analyse all the lavas and was therefore necessary to select representative samples. This was more critical for noble gas analysis since this was not an initially planned part of the thesis and the opportunity to analyse one or two samples arose at a late stage. The sample selection procedures are described together with the sample preparation for both analytical methods in the respective sub-sections below.

Noble Gases: For noble gas analysis it was necessary to separate at least 10 g of clean, unaltered olivine from each rock-sample to be analysed, and since the aim of the analysis was to identify a signature from the plume, this had to come from olivine-rich lavas with the most primitive compositions. 01.03.25.12 (from the Dilb Section - Appendix 3.1.1) and 01.03.27.12 (from the Bilbala Section - Appendix 3.1.3) were chosen on this basis. They are both minimally altered picrites with MgO contents of

16.6 and 17.6 % and estimated olivine phenocryst contents of 25 and 35 % respectively. All the lavas from the Dilb and Iyela sections are iddingsitized to one degree or another, and although the olivine phenocrysts 01.03.25.12 are thinly rimmed with iddingsite, this was considered to be easily removed during sample preparation. Although the olivine phenocrysts from 01.03.27.12 are not iddingsitized, they some show signs of chloritization, but again because this alteration is superficial it was likely to have been removed during sample preparation. Assuming a recovery rate of < 5 %, near to 200 g of each rock were split and coarsely crushed in a steel jaw crusher before being ground to < 1.5 mm in a steel disc mill. The milled samples were then washed and separated into various size-fractions by sieving. The majority of the groundmass was removed with a hand magnet, and thereafter with a magnetic separator. Olivine and pyroxene concentrates were initially recovered by magnetic separation. These were partially digested in HF and HCl to remove surface oxidation and any remaining groundmass before being further refined using heavy liquid gravimetry with methylene iodide. After washing, remaining impurities were removed by hand-picking under a binocular microscope. Illustrated details of the sample preparation procedure are shown in Appendix 6.1.1.

Rhenium-Osmium: Samples for rhenium-osmium isotope analysis were selected to represent the range of major and trace element compositions shown by the lavas, and to provide good stratigraphic coverage of the sampled sections to check for temporal variations in composition. Selected representative samples from the Bilbala and Lalibela North Section were also analysed to test for possible geographical variations in osmium isotope systematics. Samples were initially chosen on the basis of their variation in major and trace element compositions in relation to significant geochemical trends taken to reflect important petrogenetic processes that have clearly affected the evolution of the lavas; additional samples were selected to fill the gaps in the stratigraphic coverage (Appendix 6.2.1). The samples were analysed using isotope dilution therefore it was necessary to add known amounts of enriched spike to each sample. Two spike solutions were used, one enriched in ^{190}Os and the other in ^{185}Re. The volume of spike solution added to each sample was determined from their respective Ni contents using the method described in Appendix 6.2.2. Os and Re were liberated from the sample powders by digestion in inverse aqua-regia in Carius tubes at ~ 180 °C for 5 days. This digestion dissolves platinum-group minerals, metals and sulphides, and reacts with silicates to release most contained Re and Os. Re and Os are oxidised to their highest valences, therefore resulting in the complete chemical equilibrium of sample Re and Os with enriched isotopes of Re and Os

added for isotope dilution analysis. Os was subsequently extracted from the aqua regia with CCl4, taken up in HBr, dried down and purified by micro-distillation with CrO_3 in H_2SO_4, whereas the Re was retained in the aqua regia, dried down, re-dissolved in HNO_3, extracted with 3-methyl-1-butanol (iso-amylol), washed out with water and evaporated to a residuum. The purified Os and Re were loaded onto Pt filaments for analysis by N-TIMS. Further details of the sample preparation and loading procedures are described in Appendix 6.3.1 - 6.3.3.

6.1.4 Instrumentation and analysis

Noble gas analyses were carried out by Dr M Honda at the Research School of Earth Sciences at the Australian National University (ANU). The gases were extracted from the olivine separates by crushing and the isotopes of He, Ne, Ar, Kr and Xe were analysed using a VG5400 magnetic sector, single-focusing mass spectrometer. The specifications of the instrument and a description of the analytical procedure are given in Appendix 6.4.1. The results of these analyses are compiled in Appendix 6.6.1 – 6.6.3.

Rhenium-Osmium isotopic analyses were carried out at the Open University using a Thermo-Finnigan Triton multi-collector mass spectrometer in negative ionisation mode. A description of N-TIMS together with the specifications of the instrument, and the analytical procedure followed is given in Appendix 6.5.1. Reference is made in this appendix to specific details on the operation of the instrument (Appendix 6.5.2 – 6.5.4), and on the treatment of the output data (Appendix 6.5.5 – 6.5.9). The corrected results are tabulated in Appendix 6.7.1.

6.2 Isotopic compositions

6.2.1 Noble gases

With so few analyses for noble gas isotopes it was not possible to identify trends, and the data was instead used to highlight possible source signatures in relation to trends derived from already published data.

Helium: Results for $^3He/^4He$ range from 1.53×10^{-05} to 2.6×10^{-05}; this is equivalent to a range in R/R_a values from 11.0 to 18.7. For the picrite from the Bilbala section (01.03.27.12), it is notable that the larger size fraction (599 -1204 μm) has a significantly higher R/R_a value (18.7) than the finer size fraction (295 - 599 μm) (R/R_a = 12.3). The size fractions for the picrite from the Dilb section (01.03.25.12) were combined and yielded an R/R_a value of 11.0. When plotted as a function of latitude

and longitude these results can be seen to be consistent with published data compiled by Pik et al. 2006 (Fig. 6.3). The R/R_a values are higher than those reported by Hopp et al. (2004) for the northern Red Sea region (6.8 - 8.3 R/R_a), but are nowhere near as high as the highest values reported for Iceland and Hawaii (30 - 40 R/R_a).

Neon: Since the picrites analysed show enrichments in ^3He it is expected that they will have low $^{21}Ne/^{22}Ne$ ratios (Section 6.1.2). This is confirmed by the three-isotope diagram ($^{20}Ne/^{22}Ne$ vs $^{21}Ne/^{22}Ne$) in which the data plot along the mixing line between Loihi-type mantle and air (Fig. 6.6). The smaller size fraction for 01.03.27.12 plots

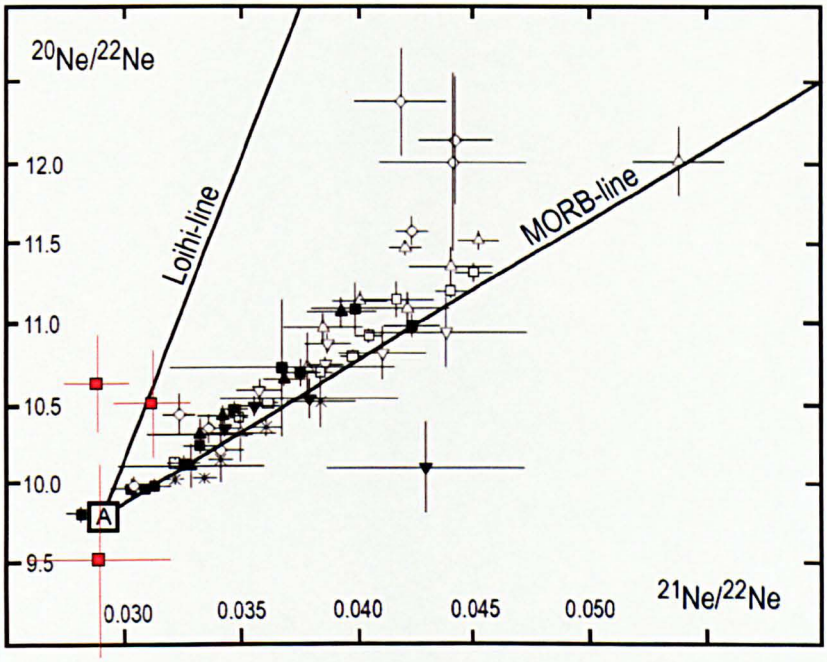

Figure 6.6 Three-isotope plot of $^{20}Ne/^{22}Ne$ versus $^{21}Ne/^{22}Ne$ for the Ethiopian lavas (red squares) compared with data for ultra-mafic rocks from Zabargad Island (triangles), mantle xenoliths from the Quaternary volcanic fields of Al Birk (black squares) and Jizan (asterisks), Saudi Arabia (Hopp et al. 2004) and basalt glasses from the Red Sea (diamonds) (Moreira et al. 1996). Uncertainties shown by 1σ error bars. Reference lines for MORB (Sarda et al. 1988; Moreira et al. 1998) and Loihi mantle sources (Honda et al. 1991; Valbracht et al. 1997; and Trieloff et al. 2000) are also shown for comparison.

close to the composition for air but with slightly lower $^{20}Ne/^{22}Ne$. Again, as with helium, this is in contrast with the data for ultramafic rocks and mantle xenoliths from the northern Red Sea region (Hopp et al. 2004) and the basalt glasses from the Red Sea (Moreira et al. 1996) which plot closer to the mixing line between MORB-mantle and air.

Argon: The Argon isotopic compositions for the two Ethiopian picrites are near atmospheric. The range of $^{38}Ar/^{36}Ar$ ratios from 0.184 to 0.192 is closer to air (0.188) than the solar wind (0.175). Similarly, on a plot of $^{40}Ar/^{36}Ar$ versus $^{20}Ne/^{22}Ne$ the picrites plot close to the value for air, although there is an indication of a possible trend toward OIB rather than MORB-type mantle compositions (Fig. 6.7).

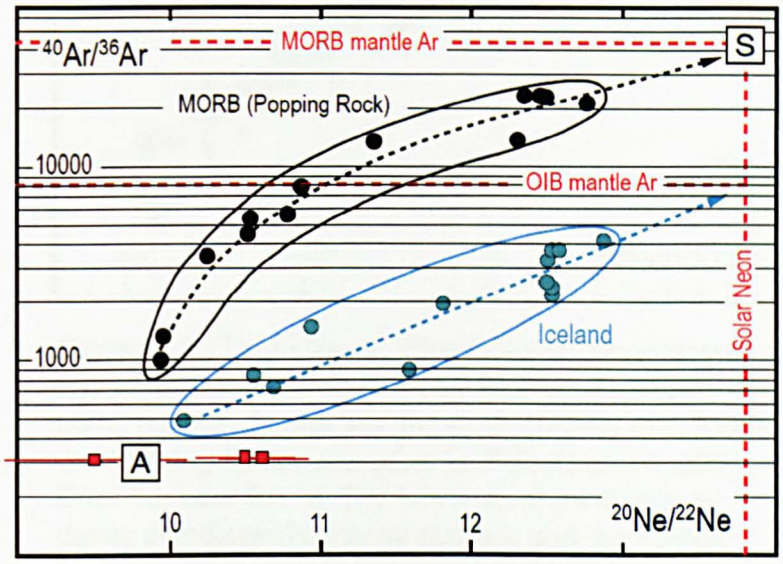

Figure 6.7 $^{40}Ar/^{36}Ar$ vs $^{20}Ne/^{22}Ne$ showing Ethiopian lavas (red squares) compared with data from MORB (Sarda et al. 1988; Moreira et al. 1998) and Iceland (Trieloff et al. 2000; Moreira et al. 2001). Extrapolated $^{40}Ar/^{36}Ar$ ratios for MORB and OIB determined from a solar $^{20}Ne/^{22}Ne$ ratio of 3.8 are indicated by the red dashed line (Graham, 2002).

Xenon: The xenon isotopic compositions of the picrites, like argon, are dominantly atmospheric (Fig. 6.8), though when plotted against $^{20}Ne/^{22}Ne$ ratios may be interpreted as leaning toward an OIB-type mantle composition (Fig. 6.9). Xenon isotopic analyses were not processed for the picrite from the Dilb section.

6.2.2 Osmium

The isotopic analyses for Re-Os are listed in Appendix 6.7.1. Many of the samples from the Bilbala and Lalibela North sections were not included because of unacceptable analytical errors. The results for duplicate analyses and standards are compiled in Appendix 6.7.2.

Measured Os concentrations for the picrites from the Dilb and Iyela sections are high with a range from 825 to 3143 ppt, whereas they are significantly lower for the olivine basalts with a range from 46 to 758 ppt. The more evolved basanite and trachybasalts from the Bilbala and Lalibela North sections respectively have

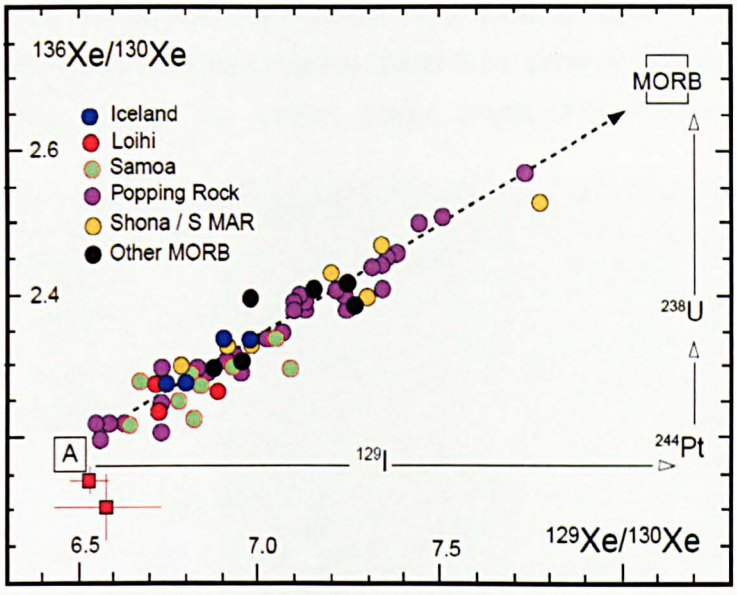

Figure 6.8 $^{136}Xe/^{130}Xe$ vs $^{129}Xe/^{130}Xe$ for the Ethiopian lavas (red squares) compared with data from Iceland, Loihi, Samoa, Shona and the south Mid-Atlantic Ridge, the Popping Rocks and other MORB (Graham, 2002). Error bars are for 1σ. The fine lines show trends for decay of indicated parental nuclide, and the dashed line represents mixing between MORB mantle and air.

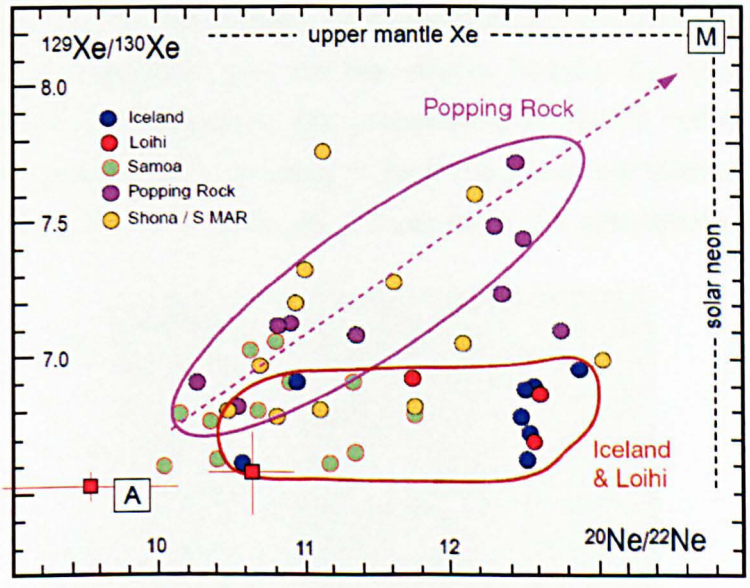

Figure 6.9 $^{129}Xe/^{130}Xe$ vs $^{20}Ne/^{22}Ne$ for the Ethiopian lavas (red squares) compared with data from Iceland, Loihi, Samoa, the Popping Rocks and the south Mid-Atlantic Ridge. The $^{129}Xe/^{130}Xe$ ratio for MORB extrapolated from a solar $^{20}Ne/^{22}Ne$ ratio of 3.8 is indicated by the black dashed line (Graham, 2002). The purple dashed line represents mixing between MORB-type mantle (M) and air (A).

consistently low Os concentrations (409 ppt for the basanite, and 123 –147 ppt for the trachybasalts); these are offset relative to the main body of data from the Dilb and Iyela sections (Fig. 6.10). The olivine basalt 01.03.24.06 has an elevated Os

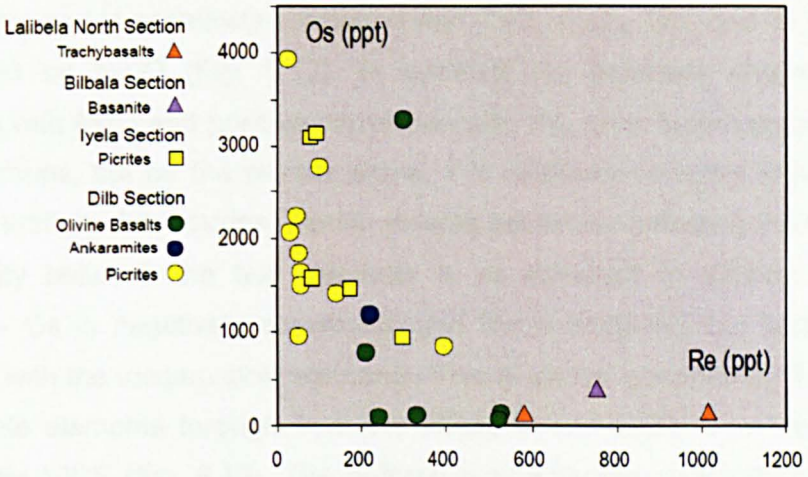

Figure 6.10 Os versus Re for the Ethiopian Plateau lavas

concentration of 3269 ppt and lies particularly off-line with the rest of the data. Re concentrations, on the other hand, are low for the picrites (31 – 298 ppt) and high for the olivine basalts and ankaramites (215 – 530 ppt). Consequently, there is a noticeable negative curvilinear relationship for Os and Re concentration between the lava –types, although for the picrites, Re concentrations are generally constant with increasing Os concentration and for the olivine basalts Os concentrations are relatively constant with increasing Re concentrations. Re-Os ratios increase with decreasing Os concentration defining a clear negative correlation between both variables (Fig. 6.11). This is generally a function of the differences in compatibility

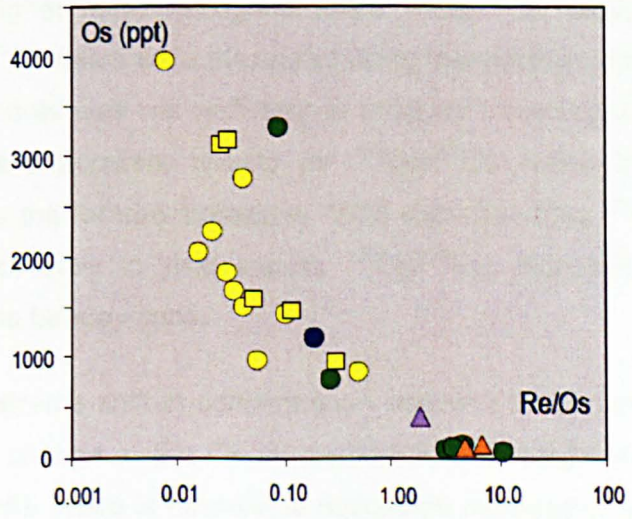

Figure 6.11 Os versus Re/Os for the Ethiopian Plateau lavas. Symbols are as in Figure 6.10.

between the two elements during fractionation and this is particularly clear from the behaviour of Os and Re in relation to the major and trace elements.

Os shows a strong positive correlation with MgO as a major index for olivine fractionation, and is negatively correlated with CaO, Al_2O_3, TiO_2 and all three alkalis - represented by Na_2O (Fig. 6.12). In contrast Re generally shows a negative correlation with MgO and positive correlation with the other major elements between the lava-groups, but for the picrites alone, it is relatively constant with variations in the concentration of the oxides. Similar inverse behaviour reflecting the differences in compatibility between the two elements is as apparent in relation to the trace elements - Os is negatively correlated, and Re is positively but less consistently correlated with the incompatible elements. This is almost consistently the case for all incompatible elements through from the HREE to the LREE and the more highly incompatible VICE (Fig. 6.13). The reverse is true for the compatible elements (Cr and Ni) which are positively correlated with Os and negatively correlated with Re (Fig. 6.14). It is notable (as with the major elements) that Re concentrations for the picrites are relatively constant with respect to variations in the concentration of other elements.

Regardless of their elemental concentrations, the picrites have remarkably consistent initial $^{187}Os/^{188}Os$ ratios ranging from 0.124685 to 0.126942. This range is just below the present day chondritic value of 0.1270, therefore they all have negative γOs values. A comparison of their measured and age-corrected values naturally shows that the initial ratios are less variable than for the measured ratios (Fig. 6.15). Some of the olivine basalts and the more evolved rocks from the Bilbala and Lalibela North sections show higher more radiogenic initial $^{187}Os/^{188}Os$ ratios (up to 0.156279). Although $^{186}Os/^{188}Os$ ratios were measured using the electron multiplier, the precision of the measurements was not sufficient to produce meaningful results. In order to obtain precise and accurate results for $^{186}Os/^{188}Os$ ratios it would have been necessary to use the faraday collectors. With sub-chondritic $^{187}Os/^{188}Os$ ratios, the samples were not likely to yield excess $^{186}Os/^{188}Os$, therefore they were not re-analysed using the faraday cups.

Apart form the extreme shift in concentration between lava-types, there is generally little discernable change in the Os concentration with height in the Dilb and Iyela sections (Fig. 6.16). There is however a noticeable increase in the Re concentration with time, and this is reflected also in a corresponding increase in the Re/Os and $^{187}Os/^{188}Os$ and $^{187}Re/^{185}Re$ ratios with height in the section.

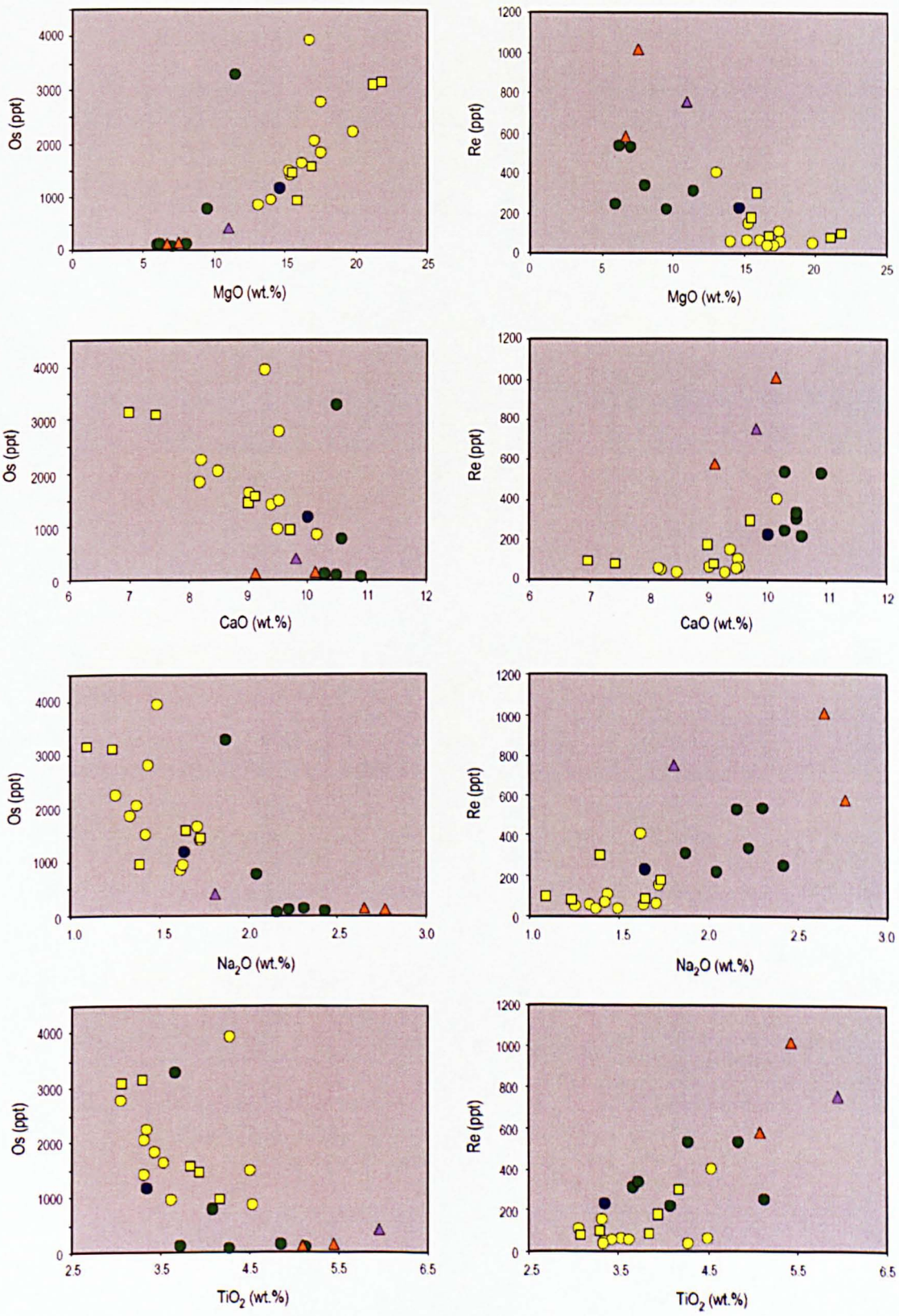

Figure 6.12 Os and Re concentration in relation to selected major element oxides for the Ethiopian Plateau lavas. Symbols are as in Figure 6.10.

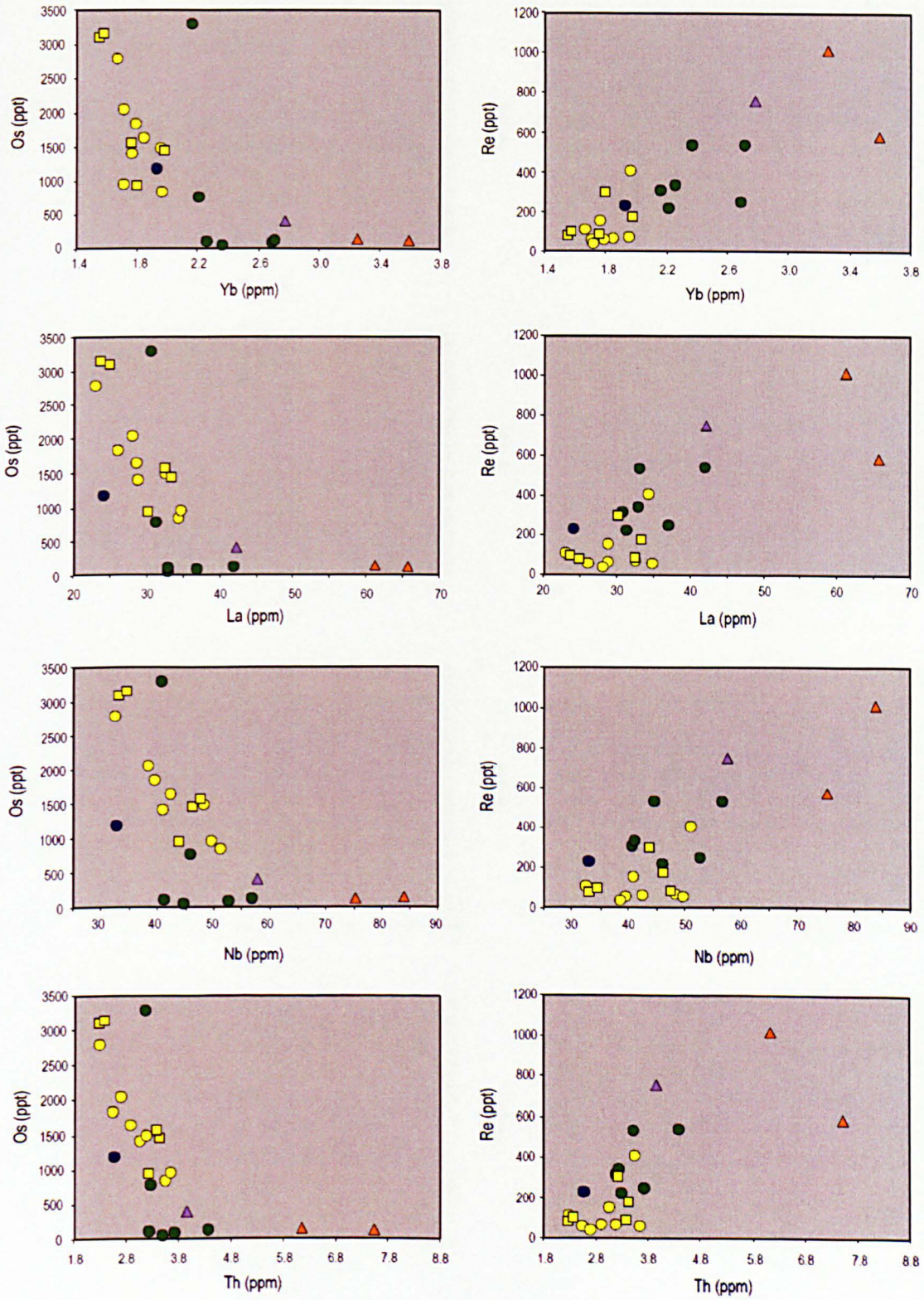

Figure 6.13 Os and Re concentration in relation to selected trace elements for the Ethiopian Plateau lavas. Representative elements for the HREE (Yb), LREE (La) and VICE (Nb and Th) are included for comparative purposes. Symbols are as in Figure 6.10.

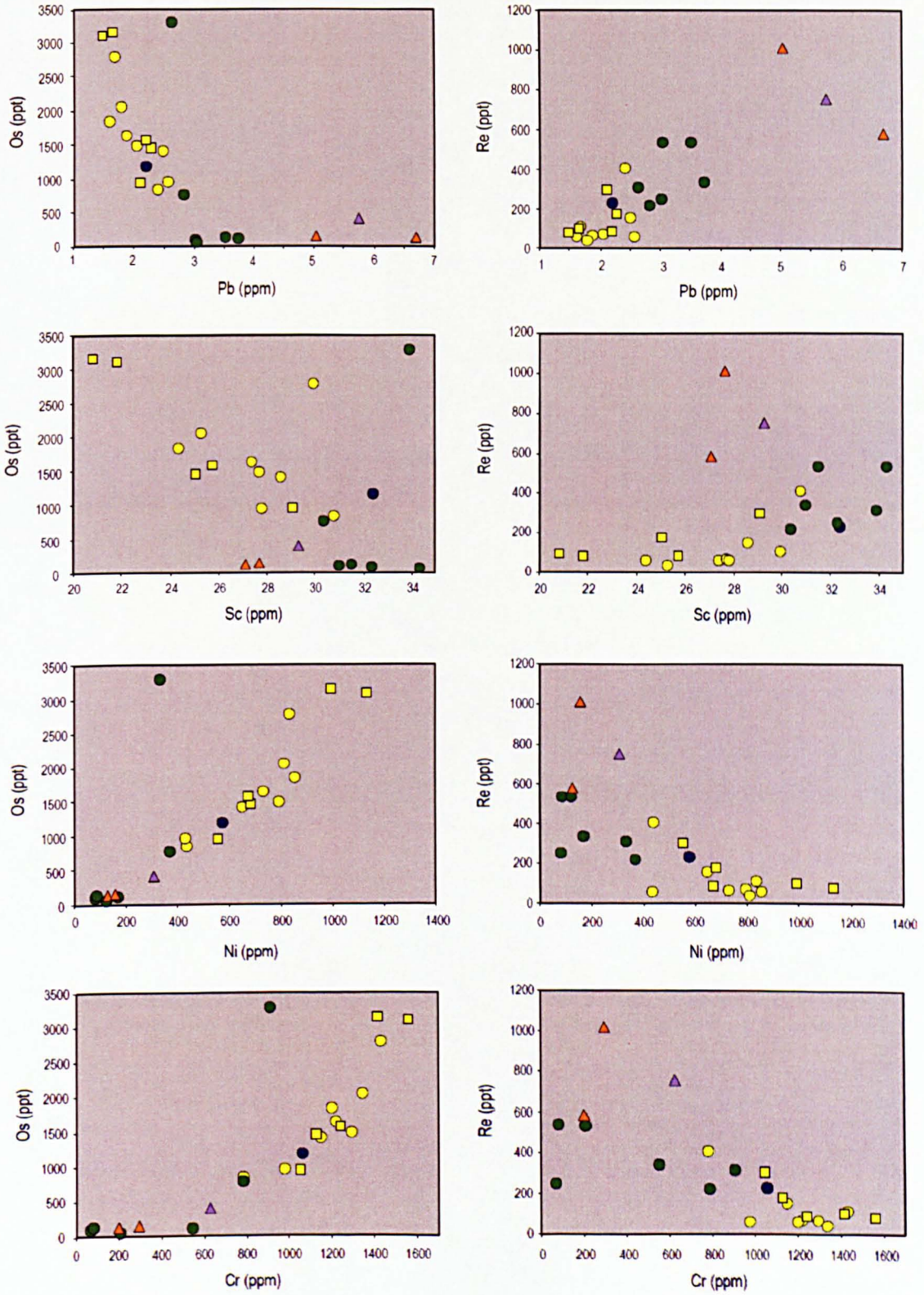

Figure 6.14 Os and Re concentration in relation to selected trace elements for the Ethiopian Plateau lavas. Representative elements for incompatible VICE (Pb) and partially incompatible (Sc) and compatible (Ni and Cr) transition elements are included for comparative purposes. Symbols are as in Figure 6.10.

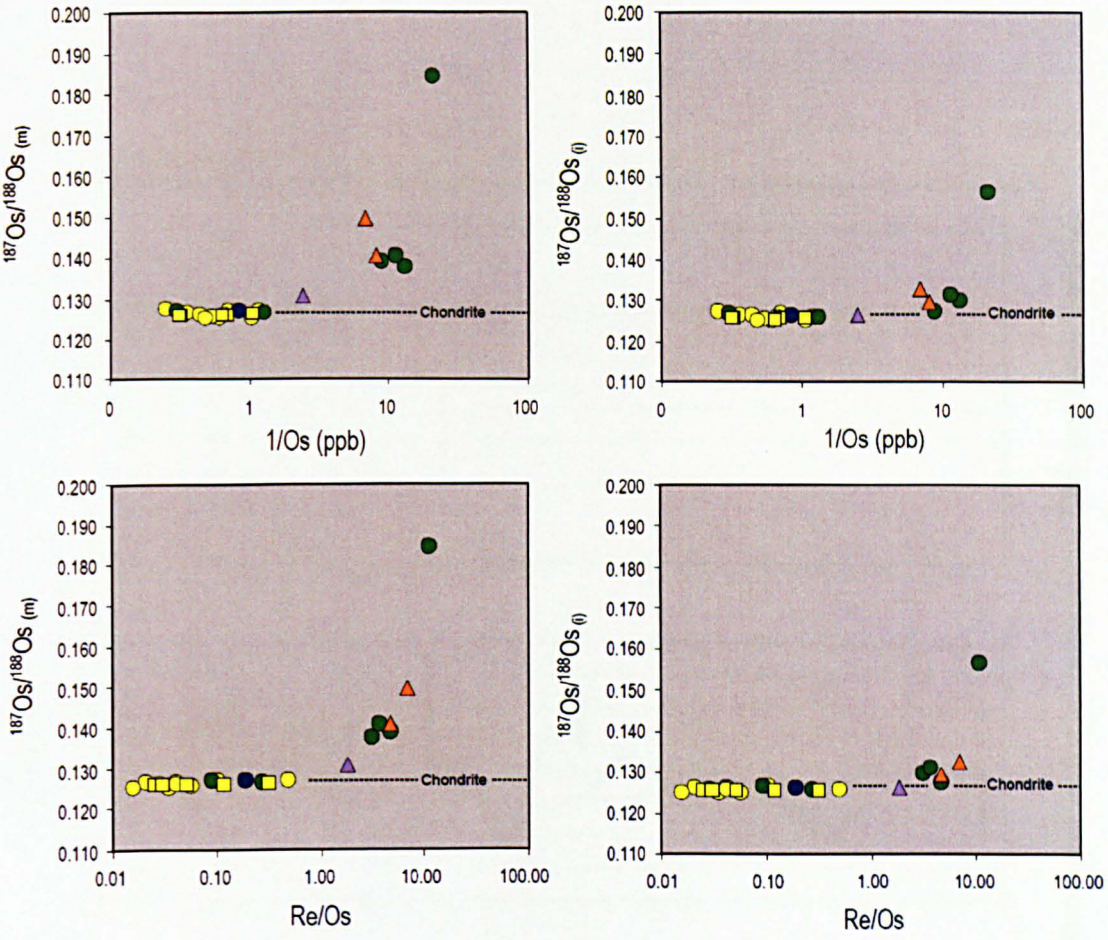

Figure 6.15 $^{187}Os/^{188}Os$ versus 1/Os (ppb) and Re/Os (ppb) for the Ethiopian Plateau lavas. The plots show the difference between the measured (m) and age corrected or initial ratios (i) for $^{187}Os/^{188}Os$. Symbols are as in Figure 6.10.

6.3 Discussion

6.3.1 Partitioning, concentration and composition

Helium in the source region of a primary melt becomes incorporated in olivine during crystallisation. Bubbles become preferentially nucleated on crystal surfaces and are subsequently trapped during crystal growth (Natland, 2003); the gas is therefore generally found in cavities or bubbles within olivine phenocrysts and is liberated during crushing. The fact that, for the olivine from the Bilbala picrite, the larger size-fraction yields an appreciably higher R/R_a value than the smaller size fraction suggests that the variability in the $^3He/^4He$ ratios for the picrites may be attributed to such He-loss during the initial crushing of the rock samples. The behaviour of the other noble gases during petrogenesis is likely to be similar to that of helium, therefore variations in their concentrations and isotopic ratios may similarly be partly attributable to variable degrees of gas-loss during crushing. Atmospheric contamination during sample preparation and analysis is possibly more of a problem

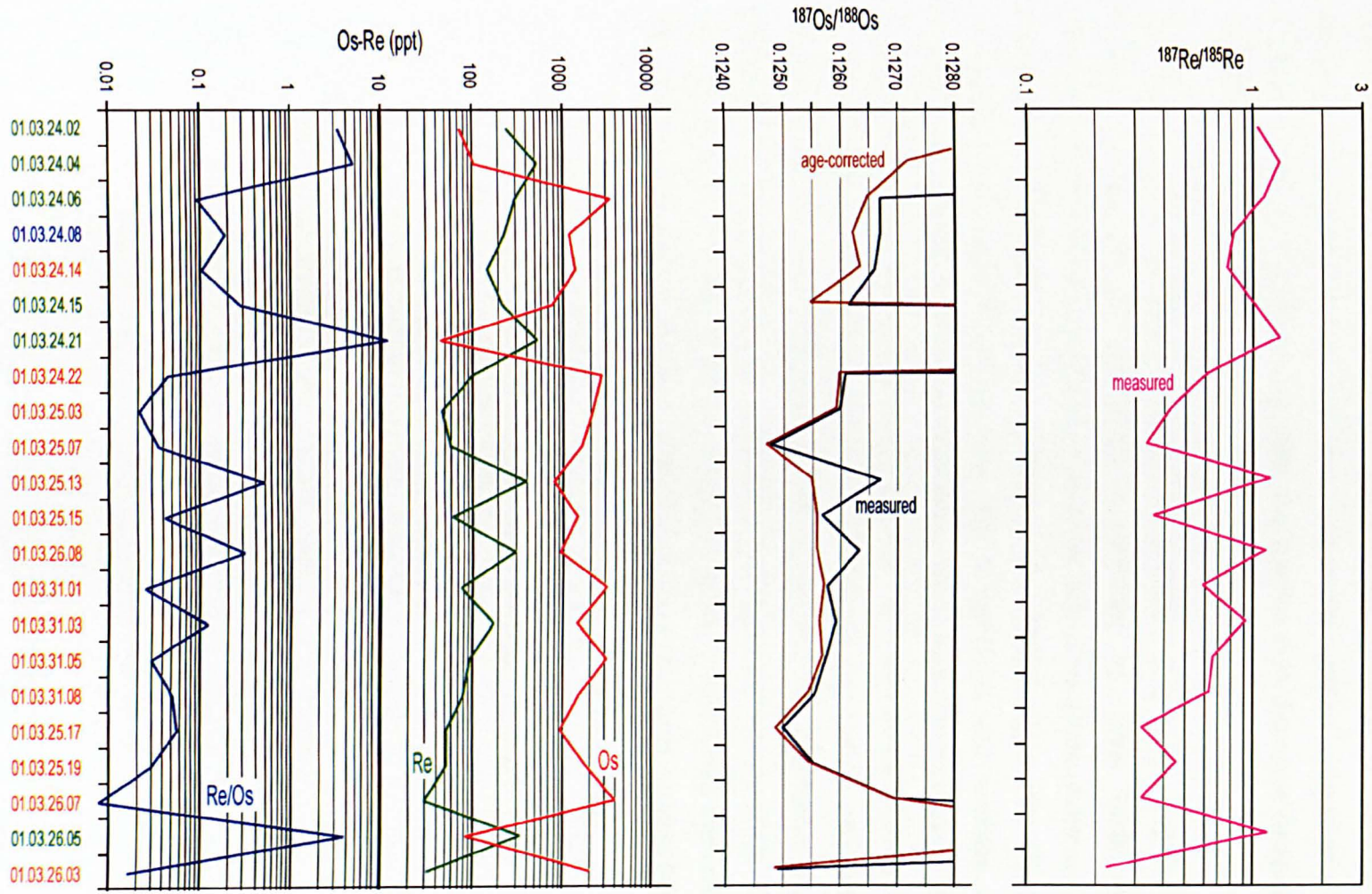

Figure 6.16 Stratigraphic variation in Re-Os concentration and isotopic ratios in the Dilb and Iyela section

with the heavier noble gases (Ne, Xe and Ar) since, unlike helium, they remain in the atmosphere at concentrations that can swamp their low abundances inherited from the mantle source. This may account for the more air-like Ne, Ar and Xe isotopic compositions for the larger olivine size-fraction from the Bilbala picrite (Figs 6.6 - 6.9). Higher concentrations of ^{4}He, ^{22}Ne and ^{130}Xe in this fraction compared to the other analysed fractions (including the smaller size fraction from the same sample) seem to support this (Appendix 6.6.1 - 6.6.3).

Significant positive correlations between Os and MgO (Fig. 6.12), and Ni (Fig. 6.14) strongly suggest that Os abundance is controlled by olivine fractionation. It is debatable whether the Os is present in sulphide inclusions within olivine or in discrete positions in its silicate structure. Burton et al. (2002) argue that Os is in fact incompatible in magmatic olivine and that it partitions into sulphide inclusions generated as a result of olivine crystallisation. Re is also incompatible in olivine, but unlike Os will preferentially partition into the melt. The high concentrations of osmium in the picrites may be taken to reflect an unusually Os-rich source, and although this might be indicative of a contribution to the plume from the core-mantle-boundary, it may equally be a feature of high pressure/temperature partitioning of Os. They have Os concentrations of over 1000 ppt, which are closer to komatiites than most CFBs, and markedly higher than those of OIBs (Fig. 6.17). Only picritic basalts from Siberia

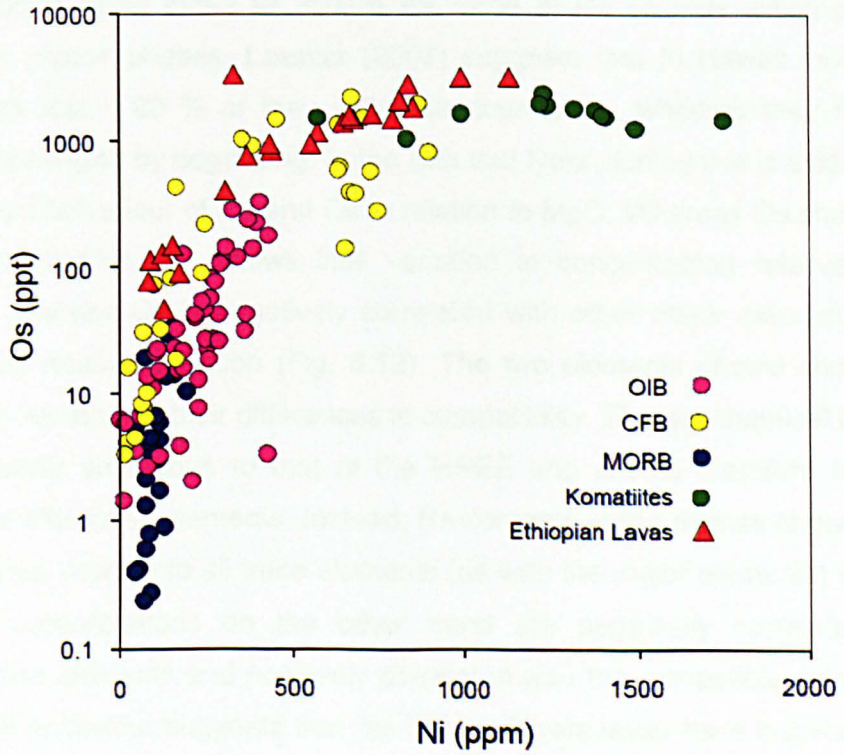

Figure 6.17 Os versus Ni for the Ethiopian Plateau lavas in relation to data for OIB, MORB, komatiites and other CFBs.

(Horan et al. 1995), West Greeenland (Schaefer et al. 2000a) and Komatiites from Munro Township (Walker et al. 1988) and Gorgona Island (Walker et al. 1991) have comparable Os concentrations for given MgO contents. Schaefer et al. (2000) suggest that such high concentrations in the West Greenland picrites are a result of high degrees of partial melting (> 25 %) where the melt becomes sulphur under-saturated and is able to effectively extract platinum group elements from the mantle because of the absence of sulphide in the melting residue. This, however, is an unlikely explanation for the elevated Os contents in the Dilb and Iyela picrites since they were generated from significantly lower degrees of partial melting (Fig. 5.39). The lower concentrations of Os in the olivine basalts are more typical for CFBs, and this is a likely result of them being more evolved. In this respect the high Os concentrations in the picrites (which are less evolved) may indeed be source-related. If this is the case then the Re concentrations should be correspondingly high, but instead they are consistently low in the picrites, and higher in the olivine basalts. Such low Re concentrations may be explained by degassing on eruption (Schaefer et al. 2000). This is a common feature of subaerial lavas and is a generally accepted explanation for the difference in Re concentrations between CFBs and MORB. Positive correlations between emplacement depth Re and Re/Yb in surface-to-submarine drill-cores of lavas from Mauna Kea reflect progressive loss of Re during subaerial and shallow marine degassing (Lassiter, 2003). The Re is released from the degassing lavas either as volatile Re oxide or Re chloride which partition into water-rich vapour phases. Lassiter (2003) suggests that In Hawaii most subaerial lavas have lost ~ 80 % of their initial Re abundance, whereas their Os contents remain unchanged by degassing. In the Dilb and Iyela picrites this is evident from the inconsistent behaviour of Re and Os in relation to MgO. Whereas Os shows a strong positive correlation, Re shows little variation in concentration relative to MgO - similarly, whereas Os is negatively correlated with other major element oxides, Re shows little relative variation (Fig. 6.12). The two elements should show antithetic behaviour because of their differences in compatibility. The geochemical behaviour of Re is broadly analogous to that of the HREE and should therefore be positively correlated with these elements. Instead, Re contents in the picrites show remarkably little variation relative to all trace elements (as with the major elements) (Figs 6.13 & 14). Os concentrations on the other hand are negatively correlated with the incompatible elements and positively correlated with the compatible elements. Such decoupled behaviour suggests that the Dilb and Iyela lavas have lost Re as a result of degassing, whereas Os concentrations have remained unchanged by the process. When seen in relation to generalised fields for MORB, OIB, CFB and komatiites, the

lavas are similarly correlated for Os versus Re/Os (Fig. 6.18) but for Re versus Yb (Fig. 6.19) they show consistently low Re concentrations relative to variations in Yb.

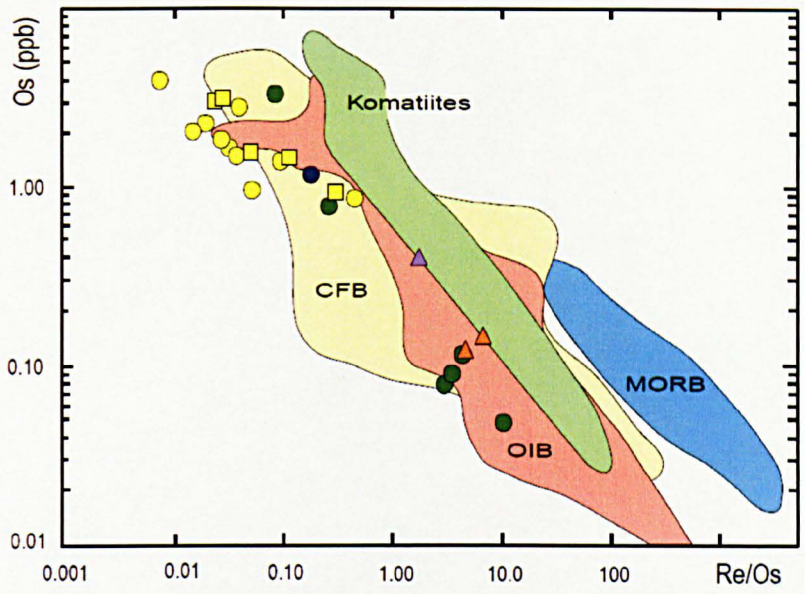

Figure 6.18 Os versus Re/Os for the Ethiopian lavas in relation to OIB, MORB, komatiites and other CFBs. Symbols are as in Figure 6.10.

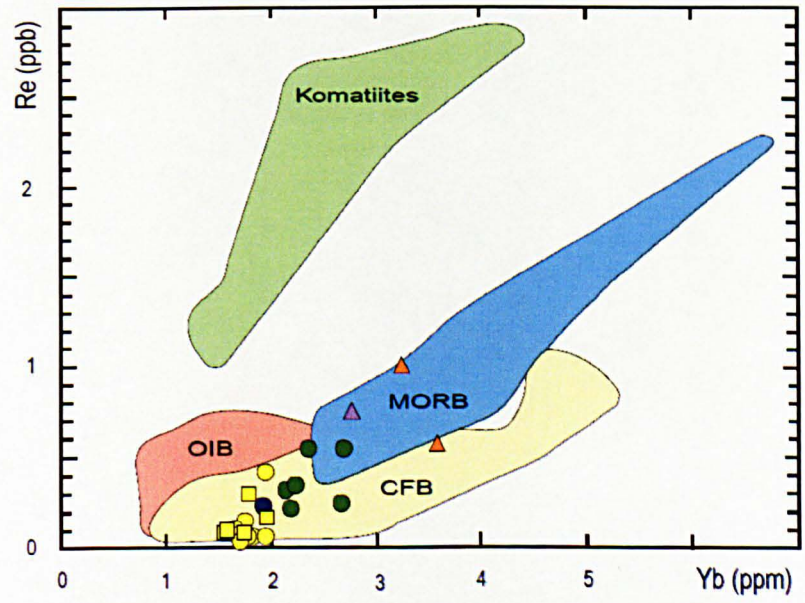

Figure 6.19 Re versus Yb for the Ethiopian lavas in relation to OIB, MORB, komatiites and other CFBs. Symbols are as in Figure 6.10.

Although such decoupling is largely a result of degassing, the low Re and Yb of the picrites may in part reflect the presence of residual garnet in the source as in the case for OIB. Unlike the Dilb and Iyela lavas however the low concentrations of Re in OIB are generally coincident with low concentrations of Os as a result of it

preferentially partitioning into sulphide in the mantle during melting (Morgan & Baedecker, 1983; Hart & Ravizza, 1996; Burton et al. 1999).

6.3.2 Crustal contamination

Highly variable and radiogenic Os isotope signatures and low Os concentrations in basalts are often indicative of crustal contamination (Widom et al. 1999). When crustal material melts and mixes with magma it becomes sulphur-satuarated, and as a result Os is rapidly depleted and the isotope ratio is disturbed. Moreover, the high Re concentrations and radiogenic Os isotope signatures (a consequence of high Re/Os ratios) of the crustal contaminant may colour the characteristics of the magma. Markedly lower Os and higher Re concentrations and elevated $^{187}Os/^{188}Os$ ratios for some of the olivine basalts from the Dilb section and the trachybasalts and basanite from the Lalibela North and Bilbala sections respectively suggest that these lavas have been affected by crustal contamination (Figs 6.12 - 6.15). This is more so evident from the positive correlation between $^{187}Os/^{188}Os$ and Re/Os shown by these more evolved lavas (Fig. 6.20). The gradient of this array is too steep to be a feature

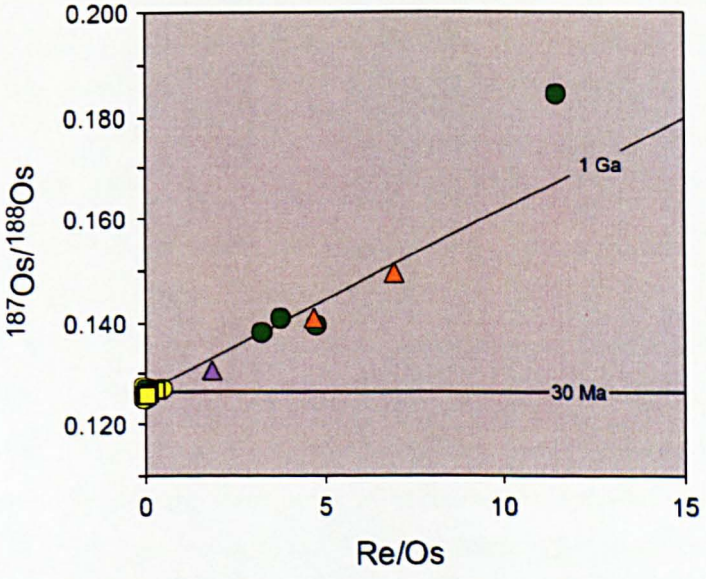

Figure 6.20 $^{187}Os/^{188}Os$ vs Re/Os for the Ethiopian Plateau lavas. Reference lines are shown for 30 Ma (age of eruption), and 1 Ga (representative age for the local continental basement). Symbols are as in Figure 6.10.

of post-eruptive radiogenic in-growth and more likely represents a mixing line between the uncontaminated magma and a crustal component, particularly since it lies along a 1 Ga reference line which corresponds to an age range of between 0.6 and 1.2 Ga for the Pan-African basement of NE Africa (Harris et al.1984). The

picrites and ankaramites can be considered essentially uncontaminated since they show more consistent Os isotopic compositions and more tightly constrained and predictable trends for Os and Re concentrations versus major and trace element concentrations compared to the more evolved contaminated lavas discussed above.

6.3.3 Origin within the mantle

Despite the variability in the helium isotopic compositions between samples and for different size fractions for the same sample, all analyses yield higher R/R_a values than are typical for normal asthenospheric mantle (MORB). The picrite from the Bilbala section has an R/R_a value of 18.6, which is close to the highest reported value of 20 for the HT2 basalts (Pik et al. 2006). This implies that the Afar plume was sourced from an undegassed part of the mantle. Lower R/R_a values for basalts in other parts of the province (Fig. 6.3) suggest that the HT2 basalts and the picrites from the Dilb and Iyela (and Bilbala) sections represent the least contaminated signature from the Afar plume. Solar-like Ne isotopic ratios for the picrites are also consistent with an origin in undegassed mantle. The Ne ratios, which plot along the Loihi line (Fig. 6.6), are typical of OIB which are generally considered to have an origin in the deep unmixed mantle (Graham, 2002). Hopp et al. (2004) report significant plume-like neon isotopic compositions for ultramafic rocks and mantle xenoliths from the northern Red Sea region, and they suggest that these imply mixing of a deep mantle component with pre-rift MORB-like and more radiogenic pre-rift lithospheric mantle components. They argue that, because the deep mantle plume component is likely to have a higher Ne/He ratio, its signature is more prominent in the Ne isotopes than in the He isotopes. In this respect, although the rocks from the northern Red Sea region have $^3He/^4He$ ratios close to MORB, the Ne isotopes indicate that the Afar plume contributed primordial noble gases to intrinsically more radiogenic and nucleogenic lithospheric and asthenospheric component up to a distance of 1800 km from its centre during the early stages of continental rifting ~ 20 Ma ago (Hopp et al. 2004). This may have occurred when the plume was flattened to its full extent upon impingement with the base of the lithosphere; however, the Ne isotopic array for the rocks from the northern Red Sea plots just to the left of the MORB mixing line whereas the Ne isotopic compositions of the Ethiopian picrites plot closer to the Loihi line implying that the two signatures are different.

The OIB-like Ne signature in the Dilb and Bilbala picrites is accompanied by high $^3He/^4He$ ratios and is therefore more likely to be representative of the plume. It is questionable whether or not the Ne isotopic compositions of the rocks from the

northern Red Sea are indicative of the same source. The fact that they plot along mixing lines between a localised MORB-type or SCLM component and a Loihi-type mantle component on a $^{21}Ne/^{22}Ne_E$ versus $^{4}He/^{3}He$ diagram might suggest that they are related (Fig. 6.21). Nevertheless, although they lie on the same modelled mixing

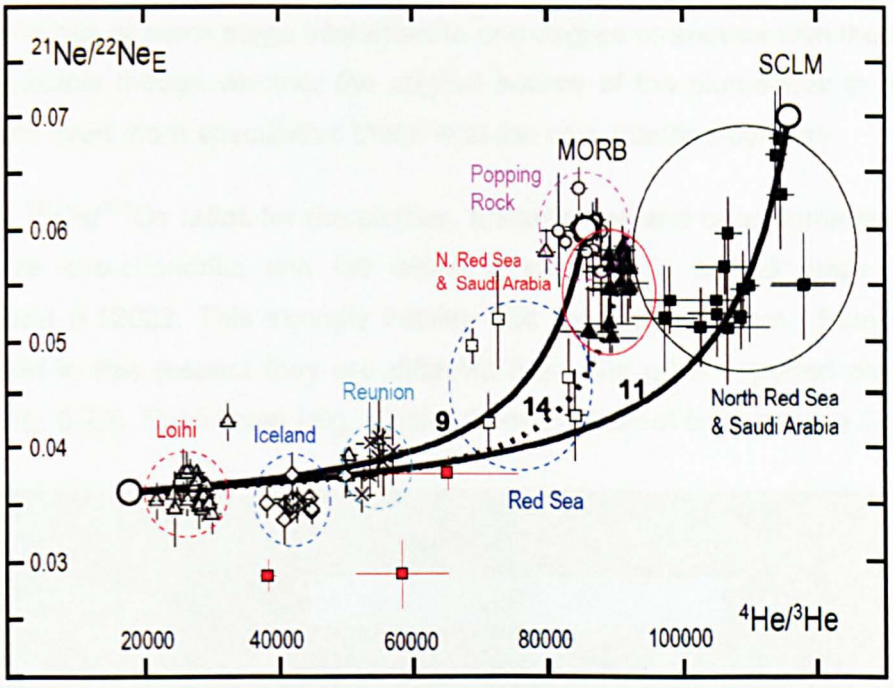

Figure 6.21 He-Ne isotope systematics. $^{21}Ne/^{22}Ne$ ratios extrapolated to a mantle end member $^{20}Ne/^{22}Ne = 12.5$ (Trieloff et al. 2000) versus $^{4}He/^{3}He$ ratios. Error bars are for 1σ. The data for the Ethiopian lavas (red squares) are compared to published data for Loihi (Honda et al. 1991; Valbracht et al. 1997; Trieloff et al. 2000), Iceland (Trieloff et al. 2000; Moreira et al. 2001), Reunion (Staudacher et al. 1997; Trieloff et al, 2002), Red Sea glasses (Moreira et al. 1996), normal MORB (Sarda et al. 1988; Moreira et al. 1998), and ultramafic rocks and mantle xenoliths from the North Red Sea and Saudi Arabia (Hopp et al. 2004). Calculated mixing lines (Langmuir et al. 1978) represent two-component mixing between Loihi-type mantle ($^{4}He/^{3}He = 18050$ (40 R_A), $^{21}Ne/^{22}Ne_E = 0.0362$), SCLM ($^{4}He/^{3}He = 116000$ (6.2 R_A), $^{21}Ne/^{22}Ne_E = 0.070$), MORB ($^{4}He/^{3}He = 86000$ (8.4 R_A), $^{21}Ne/^{22}Ne_E = 0.060$), and a Red Sea MORB-type component ($^{4}He/^{3}He = 92000$ (7.85 R_A), $^{21}Ne/^{22}Ne_E = 0.060$) - circled in red (Hopp et al. 2004). The numbers alongside the lines indicate the *r* values used in the mixing calculations. Calculations for extrapolated $^{21}Ne/^{22}Ne$ ratios are shown in Appendix 6.6.4.

lines as the Ethiopian picrites, their He-Ne isotope systematics are different in that they plot closer to the composition for MORB and SCLM. The sample from the Dilb section with an extrapolated $^{21}Ne/^{22}Ne$ ratio of 0.03787 (Appendix 6.6.4) is in line with the mixing trends and plots between the fields for Reunion and the northern Red Sea region, the two samples from the Bilbala section lie below the mixing lines. It is likely

that the Ne isotope ratios of the two off-line samples are lower as a result of contamination either during eruption or analysis, and realistically should also lie on the mixing line within the fields for Iceland and Reunion. It may at least be concluded that the Ethiopian picrites have helium and neon isotopic compositions that are consistent with a plume source in an undegassed region of the mantle, and that the rising plume has at some stage interacted to one degree or another with the SCLM. It is still debatable though whether the original source of the plume was in the lower mantle, and even more speculative that it is at the core mantle boundary.

The initial $^{187}Os/^{188}Os$ ratios for the picrites, ankaramites and uncontaminated olivine basalts are sub-chondritic and fall within a surprisingly limited range between 0.12569 and 0.12622. This strongly implies that they were sourced from depleted mantle, and in this respect they are different from any other reported plume-head picrites (Fig. 6.22). Such lavas (e.g. picrites from the Karoo) tend to have Os and Nd

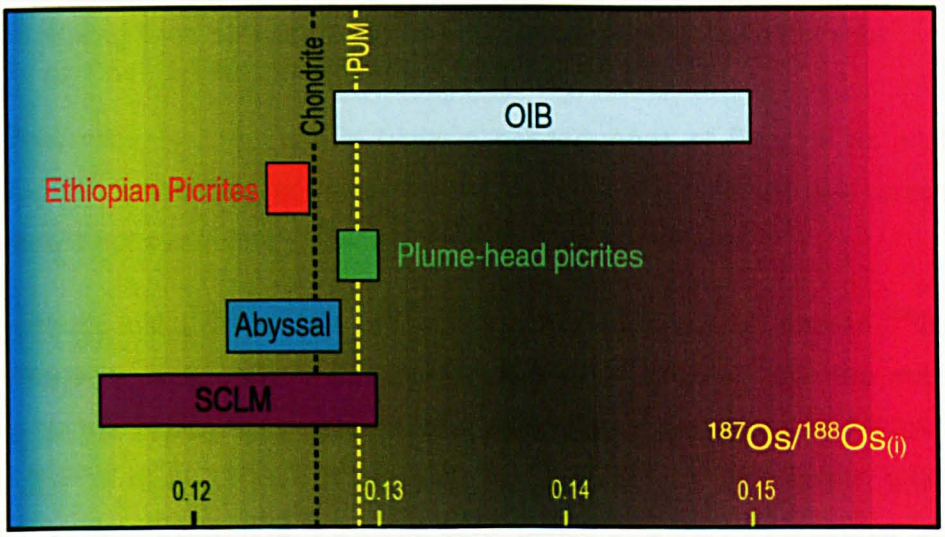

Figure 6.22 Range of $^{187}Os/^{188}Os$ ratios for the picrites from the Dilb and Iyela sections (red) compared to OIB, abyssal peridotites, SCLM, and plume-head picrites from other provinces. The dashed lines are for present day chondrite (black) and primitive upper mantle (yellow).

isotopic compositions which plot along mixing lines between OIB-type and lithospheric peridotite components, whereas those for the uncontaminated Dilb and Iyela lavas plot between the fields for MORB and OIB suggesting that they were derived from a source slightly less depleted than normal asthenospheric mantle (Fig. 6.23). This is consistent with the depleted primitive mantle component assigned to the Afar plume by Hart et al. (1989), Baker et al. (1996) and Pik et al. (1999). The measured and initial $^{187}Os/^{188}Os$ ratios for the uncontaminated lavas are similar, indicating that the age correction for the time of eruption at 30 Ma is minimal (Fig.

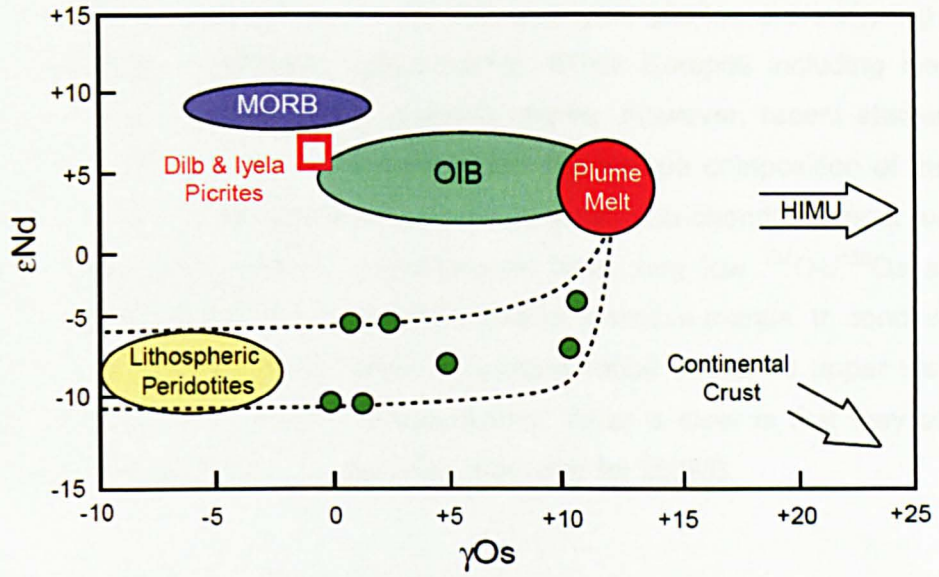

Figure 6.23 εNd versus γOs showing the approximate field for the Dilb and Iyela picrites compared to those for MORB, OIB, HIMU, lithospheric peridotites and continental crust. Data for picrites from the Karoo are also included for comparison since they plot along mixing lines between a plume melt and peridotites from the sub-continental lithospheric mantle (Ellam et al. 1992).

6.15). This minimal difference is partly a consequence of Re loss as a result of degassing (Section 6.3.1), but even if the lavas had not lost Re the age correction for 30 Ma would not significantly alter the initial Os isotopic ratios.

Sub-chondritic initial $^{187}Os/^{188}Os$ ratios suggest that there is no excess ^{186}Os in the lavas; therefore it is unlikely that the source has interacted with the outer core, contrary to the implications from seismic tomography presented by Ritsema et al. (1999), Gurnis et al. (2000), Nyblade et al. (2000 a - b), Montanger, (2007), and Ritsema & Allen (2002) (Fig. 1.6). The core mantle boundary as a source for mantle plumes remains a controversial issue. Luguet et al. (2008a) argue that elevated $^{186}Os/^{187}Os$ ratios do not necessarily reflect material flux from the metallic core and are more reasonably inherited from metasomatic sulphides derived from either pyroxenite or peridotite melts. Moreover, some of the first measurements of $^{186}Os/^{187}Os$ ratios which were quoted as evidence for a core contribution in the Hawaii (Brandon et al. 1999) and Gorgona Island (Brandon et al. 2003) melts have been discredited on the basis that they were not corrected for PtO_2 interferences (Luguet et al. 2008b). More recent finite frequency tomographic images presented by Nolet et al. (2003) and Montelli et al. (2004) also illustrate that the mantle upwelling beneath Afar is unlikely to extend any deeper than the 660 km discontinuity.

The Os isotopic compositions of the Dilb and Iyela picrites are intriguing because they are similar to depleted upper mantle. Other isotopes including He and Ne suggest an origin in the deeper unmixed mantle. However, recent studies of both MORB and OIB lavas, and estimates of the Os isotope composition of the mantle, indicate that there is no simple delineation between sub-chondritic upper mantle and more primitive lower mantle. Some plumes have very low $^{187}Os/^{188}Os$ and some MORB have values within error of estimates for primitive mantle. In conclusion then, although the Ethiopian lavas have Os isotope ratios similar to upper mantle their actual origin within the mantle is still elusive. What is clear is that they are from a source significantly more homogeneous than that for MORB.

7. CONCLUSIONS

7.1 Context

7.1.1 The Afro-Arabian flood basalt province

The Afro-Arabian flood basalt province is classified on the basis of its size and mode of melt generation as a large igneous province and represents the youngest example on the planet of mantle plume volcanism and incipient continental break-up. The region encompasses a complete record of magmatic activity from high-flux flood volcanism generated by melting in the hot head of the impacting Afar mantle plume during the Oligocene through the development of more sporadic low-flux bimodal and shield volcanism during the Miocene to the onset of continental rifting and sea-floor spreading from the Pliocene as plume activity gave way to normal asthenospheric or upper mantle convection. In this sense it charts the nature and evolution of the plume source responsible for a major continental flood basalt event and the manner in which it interacted with the lithosphere over the course of continental separation and the formation of a new ocean basin. Like other continental flood basalt provinces, the Afro-Arabian province comprises a great diversity of volcanic rocks which are variably fractionated and modified by magma mixing and crustal contamination, and, as much as this diversity allows us to unravel the processes that affected the evolution of the magmatism through time, the degree to which such processes have modified the magmas often obscures any signature of the source. In their search for the source most geochemical studies of the region have concentrated on recent volcanic rocks in the Main Ethiopian Rift and Afar and propose the involvement of the Afar mantle plume variably mixed with HIMU-like lithospheric mantle and depleted (DM and PREMA), and/or enriched (EM-like) mantle components (Furman et al. 2006). The few studies on the Oligocene flood basalts, which form the Ethiopian and Yemen plateaux and constitute the largest part of the province, reach similar conclusions but emphasise the additional role of crustal contamination in modifying the lavas (Baker et al. 1996b; Pik et al. 1999).

The HT2 basalts from the NW Ethiopian Plateau are essentially uncontaminated and their compositions are therefore interpreted to be close to that of the plume source, although they cannot be considered as representative of the primary magma since their elevated MgO contents are a consequence of olivine accumulation. They exhibit extreme OIB-like compositions which are quite unusual and isotopically close to a depleted primitive mantle end member component (PREMA, FOZO, PHEM or C) indicative of a deep mantle origin (Hart et al. 1989; Baker et al. 1996b; Pik et al.

1999). This is consistent with their high $^{3}He/^{4}He$ ratios (Pik et al. 2006) and seismic tomographic images for the mantle beneath Afar which show a deflected plume-like structure extending upward from the core-mantle boundary (Ritsema & Allen, 2003).

The HT2 basalts occur only in the eastern part of the NW Plateau suggesting that they are geographically rather than temporally constrained, although Pik et al. (1998, 1999) maintain that they are stratigraphically sandwiched between HT1 basalts within the high-Ti sub-province. The reliability of this stratigraphy is questionable since it is based on sampling laterally discontinuous lithological units, which are often displaced by faulting and slumping, over an area of hundreds of km^2. Over-lapping age data for different lavas within the same sequence and the lack of consistent marker horizons and unconformities, moreover, make such a generalised stratigraphy unreliable. It is further suggested by Pik et al. (1998) that the HT2 basalts were emplaced contemporaneously with the more evolved and contaminated LT basalts, and Kieffer et al. (2004) propose that the bimodal lava sequences of the Simien Shield were extruded onto a thin veneer of LT basalts prior to the eruption of the HT2 basalts. This implied shift from more to less evolved compositions over time is contrary to observations in other flood basalt provinces where picrites form the lower part of the flood basalt pile and are among the earliest outpourings of flood volcanism. It is also inconsistent with the established stratigraphy for the region in which the first ignimbrite marks the division between the lower tholeiitic basalts of the Aiba Formation and the upper bimodal alkaline volcanics of the Alaji Formation. This distinction between the lower and upper traps is recognised almost everywhere across the Ethiopian Plateau and is evident beneath the Simien Shield from the occurrence of felsic pyroclastics in the Lima Limo Section. Therefore, it seems more plausible that the HT2 basalts pre-date the Simien volcanic pile and are among the earliest, uncontaminated outpourings of flood volcanism in Afro-Arabian Province.

7.1.2 Lavas of the high-Ti sub-province.

The lavas of the high-Ti sub-province are not exclusively high Ti basalts. The sequences described in this thesis, on the contrary, display considerable lithological and chemical diversity both within and between sections. They comprise complex successions of variably porphyritic olivine-rich basalts, ankaramites and picrites, and more evolved trachybasalts, basanites, rhyolitic ignimbrites, agglomerates of variable composition and layers of silicic ash. The basaltic lava flow units vary in thickness from 1 to 30 m and in places are seen to pinch out and overlap. In contrast, the ignimbrite units are commonly tens of metres thick and laterally extensive, forming

prominent breaks of slope stretching tens of kilometres along the edges of the plateau. Such differences in lateral extent reflect differences in the nature of the volcanism. Whereas the geographically limited basalt flows are a feature of localised effusive fissure volcanism, the laterally extensive ignimbrite deposits are a feature of periodic explosive volcanism from isolated vents.

The Dilb and Iyela sections together constitute the only stratigraphically coherent sequence comprised exclusively of basaltic lavas and picrites. $^{40}Ar/^{39}Ar$ ages for selected lavas in the sequence (31 - 30 Ma) and for the ignimbrite at the top marking the base of the Alaji Formation (28.2 - 30.2 Ma) (Hofmann et al. 1995; Hofmann, 1997) place temporal constraints on the emplacement of the sequence that allow it to be related to other documented lava sequences elsewhere in the province. In the other sampled sections, picrites are rare and the lava sequences are not so clearly related stratigraphically because of their more sporadic exposure and the apparent presence of structural discontinuities. The fact that there are no reliable age data for these other sections also makes cross-correlation between sequences difficult. Moreover, the lavas and pyroclastic deposits in these other sections are petrographically and geochemically more diverse and not so obviously related compared with those in the Dilb and Iyela sections. Despite the fact that these sequences are located within the high-Ti sub-province, their clear bimodality suggests that they are part of the Alaji Formation and therefore younger than the Dilb and Iyela lavas which are analogous to the HT2 basalts.

7.1.3 Significance of the picrites

Picrites are rare in most flood basalt provinces. This has generally been ascribed to density trapping of the primary magma at the base of the crust where olivine is precipitated to form ultramafic cumulates, and only the evolved basaltic melts are erupted (Cox, 1980). The eruption of picrites therefore requires that a density trap does not exist, or is circumvented in some way (Larsen & Pedersen, 2000). It cannot be discounted, however, that the absence of picrites in many flood basalt successions may be attributable to the simple fact they are yet to be uncovered or, on account of their localised occurrence, are yet to be discovered. In provinces where picrites do occur, they are generally confined to the lower parts of the succession and show limited geographical extent, implying that they represent the initial outpourings of flood volcanism controlled by structural features linked at depth to a primary magmatic source. On the basis of their high Mg contents, they are interpreted to be products of partial melting in the hottest parts of the upwelling

mantle at temperatures significantly higher than the ambient mantle (McKenzie & Bickle, 1988; Campbell & Griffiths, 1990); therefore their composition may be assumed to be close to that of the primary mantle-derived melt. The localised occurrence of such an abundance of picrites in the Dilb and Iyela sections implies that the region was the structural focus for the earliest outpourings of the Ethiopian flood volcanics derived from partial melting in the convecting head of the Afar mantle plume.

7.2 The Dilb and Iyela lava sequence

7.2.1 Stratigraphic relations

The Dilb and Iyela sections expose an essentially unbroken sequence of near to 900 m of variably porphyritic, olivine-rich HT2 basalts belonging to the Aiba Formation. The lower part of the sequence below the first palaeosol is dominated by picrites which form compound flows indicative of a high magma-flux and continuous volcanism, whereas the upper part of the of the sequence above the palaeosol is dominated by olivine basalts which tend to form more simple flows separated by oxidised horizons and occasional thin palaeosols indicative of a lower magma-flux and more sporadic volcanism. The ignimbrite which caps the sequence marks the base of the Alaji Formation and the onset of bimodal volcanism. The both sections together provide a complete record from early conduit directed high-flux magmatism capable of carrying dense olivine-charged picritic melts to the surface, through to the development of shallow-level magma chambers where the low-flux magmas stalled, fractionated and mixed with other variably fractionated magmas and/or melted crust before erupting either explosively or effusively depending on the time between.

7.2.2 Petrography and mineral chemistry

The lavas are variably porphyritic and are unusual in that phenocrysts of plagioclase are rare and that the dominant phenocryst phases are either olivine or clinopyroxene. The virtual absence of aphyric lavas and the relative abundance of picritic basalts throughout the sequence similarly reflect their unusual character. They are divided into three distinct groups. The picrites are characterised by phenocryst assemblages dominated by olivine with subsidiary amounts of clinopyroxene, whereas the ankaramites are characterised by phenocryst assemblages dominated by clinopyroxene, with subsidiary amounts of olivine. Both these groups show a characteristic dominance of clinopyroxene over plagioclase in their groundmass assemblages, although this is less pronounced in the ankaramites than in the picrites.

The olivine basalts have a variable mix of phenocrysts, but are more so characterised by a dominance of plagioclase over clinopyroxene in their groundmasses, and by the occurrence of plagioclase phenocrysts in the more coarse-grained samples.

Textural relations between the minerals in the lavas from each group indicate that olivine crystallised first, followed by clinopyroxene, titaniferrous magnetite and plagioclase respectively. This contrasts with the normal phase relations in tholeiitic flood basalts in which plagioclase crystallises before clinopyroxene and magnetite. The sequence of crystallisation is more consistent with that seen in ferropicrites and presumably reflects the high Fe and Ti, and low Al of the parental magma (Gibson et al. 2000). NiO contents of olivine phenocrysts which are notably higher than might be expected for olivines with such low Mg#, and an abundance of chrome-spinel, titanomagnetite and ilmenite also signify a source high in Fe and Ti. The low Al_2O_3 contents of clinopyroxene phenocrysts and high Cr# of spinel inclusions in the olivine phenocrysts furthermore imply that the source was depleted in Al reflecting the presence of residual garnet.

The olivine phenocrysts exhibit a range of morphologies including large and small polyhedral, elongate, and skeletal crystals. These have a range of compositions which imply that the lavas were derived from partially crystallised magmas that stalled at varying depths where they were allowed to mix, equilibrate, and/or fractionate prior to eruption. This is supported the presence of variably resorbed and fragmented phenocrysts, and mineralogically diverse glomerocrysts. It is apparent that the ankaramite and olivine basalt magmas have undergone a greater degree of mixing compared to the picrites since they their olivine phenocrysts show a significantly more diverse range in compositions compared to those from the picrites. The presence of large polyhedral olivines with Mg# of 90 in selected lavas from each lava group suggests that the magmas were in some way linked to the same primary melt, and the sparse occurrence in the lavas of these primary olivines implies that most were left at depth. The clinopyroxene phenocrysts are without exception, low pressure augites and therefore may be assumed have crystallised together with more Fe-rich olivines during the later stages of fractionation at shallow depths, and the few plagioclase phenocrysts that occur in the olivine basalts are likely to have crystallised near to or at the surface.

Skeletal olivines, which are indicative of melts with high normative olivine contents, are almost entirely confined to the picrites. This suggests that the picrites were

derived from magmas with significantly higher normative olivine contents than those from which the ankaramites and olivine basalts were derived. In this respect it can be assumed that the picrites were sourced at depth and that their ascent to the surface was not punctuated by prolonged periods of shallow level fractionation, whereas the ankaramites and olivine basalts were sourced from shallower levels where they were allowed to fractionate and evolve before erupting at the surface. The dominantly higher proportions of plagioclase in the groundmasses of the ankaramites and more so in the groundmasses of the olivine basalts compared to the picrites seem to support this. It can be further assumed therefore that the compositions of the picrites more closely reflect that of the primary mantle-derived melt compared to those of the ankaramites and olivine basalts. The picritic magmas would have partially crystallised at depth and, on account of their high density, would have required high flux conditions to carry them directly to the surface. The virtual absence of picrites above the first palaeosol suggests then that by this point in the succession the magma flux had slowed to such an extent that it had become insufficient to carry such primitive magma to the surface. This is consistent with the change in architecture of the lava flows above the palaeosol.

The introduction of water into the magma at shallow levels is indicated by the pervasive effects of iddingsitization in all of the lavas, and this is confirmed by elevated oxygen fugacities calculated from the mineral chemistry of olivine and clinopyroxene phenocrysts. Crystallisation temperatures calculated from the mineral chemistry of the phenocrysts are > 1250 °C for olivine and 1160 – 1230 °C for clinopyroxene. These temperatures are consistent with those calculated with MELTS for clinopyroxene, but are low for olivine which begins crystallising between 1360 and 1400 °C.

The dominance of unzoned or equilibrated olivines with variable Mg# implies that the majority of olivine phenocrysts were able to continuously re-equilibrate with the evolving melt at varying depths for some time prior to the influx of new parental magma from below, and before entrainment and ascent to the surface. It is likely then that the supply of parental magma was sporadic and occurred in pulses capable of displacing volumes of partially crystallised magma stalled, because of their high density, in crustal reservoirs, thereby forcing their continued ascent higher into the crust or onto the surface. The common occurrence in all of the lavas of oscillatory zoned clinopyroxene phenocrysts support the assumption that clinopyroxene fractionated from progressively evolving melts at shallow or near-surface depths. The

thin Fe-rich rims of the clinopyroxene and olivine phenocrysts represent continued fractionation following eruption of the lavas; the fact that the composition of these rims in the clinopyroxene phenocrysts is not dissimilar to that of the clinopyroxene microlites in the groundmass of the lavas seem to confirm this. Shifts in composition in some of the clinopyroxene zoning profiles may be attributed to mixing with more evolved magmas at shallow depths rather than to changes in pressure as a consequence of ascent. Such irregularities may also be related to changes in fO_2 associated with the introduction of water into the melt, particularly where they are accompanied by the sudden increase in Fe_2O_3.

Oscillatory zoning seen in the few plagioclase phenocrysts that occur in the lavas provide similar records of relative changes in temperature and pressure, magma mixing, oxidation and melt-evolution at shallow depths to those seen in the zoned clinopyroxenes. Strain features in these phenocrysts, like those in many of the clinopyroxene phenocrysts also indicate that they were moved and mixed during their ascent to the surface. The longer slender plagioclase phenocrysts that occur agglomerated with these strained and zoned phenocrysts, on the other hand, are more likely, on account of their fragile almost acicular form, to have crystallised quickly at or near the surface and as a result were not strained and fragmented by ascent. This is consistent with the fact that the morphology and composition of these slender phenocrysts estimated from their extinction angles is not dissimilar to the larger plagioclase microlites present in the groundmass of some of the lavas.

Most of the lavas have been iddingsitized to one degree or another and the presence of fresh fayalitic olivine overgrowths around iddingsitized olivines suggest that this was a result of an increase in fO_2 associated with the introduction of water into the magma at shallow depths. Some of the lavas have also been serpentinized or zeolitized to varying degrees as a result of hydrothermal alteration associated with the emplacement of subsequent lava flows. Compared to flood basalts from other provinces, however, the Dilb and Iyela lavas are relatively unaltered, and this is largely because of their comparatively young age. Consequently, their major and trace element, and isotopic compositions are sufficiently pristine to reflect their petrogenesis.

7.2.3 Major element compositions

The Dilb and Iyela lavas are generally tholeiitic to transitional in composition and their geochemistry is consistent with their petrographic classification. Like most tholeiitic

basalts from continental and oceanic provinces, and island arcs, they have similar major element chemistry to MORB but show higher concentrations of incompatible and LILE (including Ti and P, and K) which reflect differences in the composition of their source. With the exception of two of the more evolved lavas, which are quartz normative, all are hypersthene normative. They have a relatively restricted range of SiO_2 contents (43 - 50%) and high TiO_2 contents (3 - 5%) and all plot within the field for the HT2 basalts. The picrites and ankaramites show lower Al_2O_3 and higher K_2O, P_2O_5, TiO_2 and $Fe_2O_3^{(tot)}$ than any reported lavas of equivalent MgO content from other flood basalt provinces, and in this sense they are unique. The transition from high-flux to low-flux magmatism and the first signs of crustal contamination are marked by a shift to lower MgO and higher SiO_2, Al_2O_3, CaO, Na_2O and K_2O contents above the first palaeosol. This shift in chemistry is not reflected in the oxides of the more incompatible elements, TiO_2, Fe_2O_3, MnO and P_2O_5 which are more indicative of the composition of the source. Together the lavas form a coherent suite which appears to be related through olivine fractionation and accumulation. The offset trends for most of the major element oxides relative to MgO and SiO_2 shown by the olivine basalts and ankaramites compared to the respective trends for the picrites are however more likely attributable to differences in partial melting. This is confirmed by model fractionation curves generated using MELTS. Whereas it is possible to produce the olivine basalts by fractional crystallisation of an ankaramitic source, and the ankaramites by clinopyroxene accumulation from a picritic source, it is not possible to produce the olivine basalts by fractional crystallisation from a picritic source. This confirms that the picrites are not primary melts.

It is more likely that the picrites as well as the ankaramites and olivine basalts evolved from a primary melt in equilibrium with olivine phenocrysts with a Fo content of 90 since these are the most primitive olivines found in the lavas from all three lava-groups. The MgO content of the primary melt calculated from the olivine phenocrysts with Mg# of 90 is between 17 and 18 % depending on the pressure (from crustal thickness) and oxygen fugacity expressed by the Fe^{3+}/Fe^{2+} ratio of the melt. This equates to a melt temperature between 1507 and 1465 °C. MgO contents of representative melts for the lava groups calculated similarly from the median value of their small polyhedral olivines are between 10.6 and 9.3 for the picrites, 9.4 and 8.3 for the ankaramites and 8.3 and 7.3 for the olivine basalts, depending on the pressure and Fe_2O_3 content of the melt. Melt temperatures calculated from these MgO contents are between 1317 and 1287 °C for the picrites, 1290 and 1264 °C for the ankaramites, and 1263 and 1242 °C for the olivine basalts. These temperatures

are similar to those calculated using MELTS. Normative compositions of the lavas suggest that the olivine basalts evolved at near surface pressures whereas the ankaramites and picrites evolved at pressures of 0.6 - 0.8, and 0.8 - 0.9 GPa respectively - equivalent to crustal thicknesses of between 26 and 31 km respectively. It is proposed that the primary melt ponded at the base of the crust with an estimated thickness of 50 km, and, therefore, it would have evolved at pressures of near to 1.2 GPa. MELTS modelling, and the mineral chemistry of the lavas, furthermore, strongly suggest that the magmas evolved in oxidising conditions between QFM+1 and QFM+2, equivalent to between 0.1 - 0.19 Fe_2O_3 - this typical of OIB-type magmas (Ballhaus, 1993).

The temperatures estimated for the modelled primary melt over the range of Fe_2O_3 contents representative of fO_2 values between QFM+1 and QFM+2 extrapolated back to the solidus for typical mantle peridotite (KLB-1) along liquid adiabats of ~ 1 °C km^{-1} (McKenzie & Bickle, 1988) give potential temperatures between 1450 and 1500 °C, and pressures of melting between 3.1 and 3.4 GPa at depths of between 95 and 110 km respectively. Such estimates are probably low since the Fe^*_{15} contents of the Dilb and Iyela lavas are too high to be simple isobaric melts of KLB-1 mantle. The lavas require an Fe-rich mantle source or a contribution from deep-sourced Fe-rich melts generated by decompression melting of a peridotite source analogous to KLB-1 at high pressures (> 4 GPa) (Langmuir et al. 1992). Extension of the liquid adiabats for the modelled primary composition in equilibrium with Fo 89 to the experimentally determined solidus for a Fe-rich peridotite (PHN1611) gives higher potential temperatures between 1470 and 1520 °C and melting depths and pressures of 125 - 140 km, and 4 - 4.5 GPa respectively. These figures are relatively consistent with those proposed for the Parana-Etendeka ferropicrites, which are estimated to have been generated by 10% melting of a source similar to PHN1611 at pressures of 45 – 35 kb and mantle potential temperatures near to 1550 °C (Gibson et al. 2000). Although these lavas have similar Fe^*_{15} to the Dilb and Iyela picrites, there are significant chemical differences between them that suggest that they were derived from primary magmas with quite different compositions. With FeO* contents below 13 wt. % the Dilb and Iyela lavas are not technically ferropicrites and their uniquely higher K_2O, P_2O_5 and TiO_2 and lower Al_2O_3 contents furthermore suggests that they were derived from higher temperature lower degree partial melts than the Parana-Etendeka ferropicrites. More particularly, the presence of Fo_{90} olivine phenocrysts in the Dilb and Iyela lavas would require exceptionally high degrees of partial melting of a source such as PHN1611.

Some authors argue that mantle plume heads composed only of peridotite are incapable of generating the huge volumes of melts seen in large igneous provinces, and that an eclogite or pyroxenite component is required. It can, however, be argued that compositional constraints on modal mineralogy make such a source implausible for both the Dilb and Iyela lavas. High Ni contents in both the olivines (2360 - 2800 ppm) and bulk rock (357 - 925 ppm at 15 % MgO), on the contrary, suggest that the primary melt was in equilibrium with a mantle source with a high modal percentage olivine such as a peridotite or an olivine websterite, rather than with a clinopyroxene-rich mantle source such as an ecolgite or pyroxenite. This is consistent with the high FeO and low Na_2O contents of the lavas. Since clinopyroxene has lower FeO and higher Na_2O contents than olivine, a pyroxenite source would instead produce a melt with respectively low FeO and high Na_2O. It is therefore proposed here that the primary melt for the Dilb and Iyela lavas was derived from high-pressure (4 - 5 GPa) melting of an anhydrous mantle peridotite such as KLB-1 with potential temperatures in excess of 1600 °C. This is consistent with the melting pressures and temperatures estimated from their CaO/Al_2O_3 - Al_2O_3 ratios which imply melting beneath thick (120 - 150 km) lithosphere prior to extension. Melting at such high temperatures and pressures, together with high Ni contents for the lavas are indicative of melting within an ascending mantle plume (Arndt, 1991).

7.2.4 Trace element compositions

Like most flood basalts, the Dilb and Iyela lavas are enriched in incompatible elements compared to MORB and depleted in heavy rare earth elements relative to middle and light rare earth elements, and in these respects they are similar to OIB. More specifically, their trace element abundance profiles exhibit a HIMU signature characterised by an enrichment of Nb and Ta relative to Ba, and Rb, a general decrease in primitive mantle normalised concentrations from Nb to Cs, and a pronounced negative K anomaly indicative of LILE depletion. As with other continental flood basalts, however, they exhibit distinct differences in the variability of their mobile incompatible element abundances compared to typical HIMU OIB. In contrast to trace element profiles for HIMU OIB those for the Dilb and Iyela lavas lack negative Pb anomalies, and show significant negative Sr anomalies and less pronounced P and Eu troughs associated with antithetic peaks for Nd, Zr and Ti. In this respect they are similar to tholeiitic basalts from the Deccan and alkali basalts from Hawaii, although they are significantly more enriched in incompatible elements. Alkali basalts from Iceland show similar levels of trace element enrichment, but differ from the Dilb and Iyela lavas in that they show pronounced positive Ba and P

anomalies and much less significant K and Sr troughs. Only the alkali basalts from the Parana show trace element concentrations higher than the Dilb and Iyela lavas, but these basalts do not show the typical decrease in primitive mantle normalised concentrations from Nb to Cs characteristic of the HIMU signature, and in this respect they are more typical of EM basalts. The level of enrichment in incompatible elements shown by the Dilb and Iyela picrites is particularly unusual since it is higher than the more evolved lavas from across the province. In all other flood basalts provinces where picrites occur they are generally depleted in incompatible elements relative to the more evolved lavas. This suggests that the original plume source of Dilb and Iyela picrites has been affected by the interaction with a secondary source-component enriched in incompatible elements.

The HIMU signature of the Dilb and Iyela lavas (and HT2 basalts) is analogous to the C1 component described by Pik et al. (1999) who propose that it represents the composition of the Afar mantle plume during the Oligocene. This is, however, discounted here as it extends beyond the topographic influence of the plume, and beyond the area characterised by high $^{3}He/^{4}He$ ratios which are considered to be a more indicative of the plume (Pik et al. 2006). Instead it is suggested that the HIMU-like signature of the lavas is inherited from the Arabian-Nubian lithospheric mantle and that the variations in VICE abundances of the lavas are unique to this component (Bertrand et al. 2003). Such compositional variations are emphasised on plots of K/Nb and Ba/Nb versus Zr/Nb which place the Dilb and Iyela lavas outside the field for HIMU OIB on a mixing trend between average sub-continental lithospheric mantle and a depleted mantle component analogous to the C2 component described by Pik et al. (1999). This component is less widespread than the HIMU component, is focused more within the area characterised by high $^{3}He/^{4}He$ ratios and is therefore more likely to represent the composition of the Afar plume rather than the SCLM as advocated by Pik et al. (1999). It is possible that the consistent depletion in U and Th shown by all of the lavas from the Dilb and Iyela sections is a characteristic from the plume that shows through the HIMU-like signature inherited from lithospheric mantle. Relative enrichments in LFSE (Cs, Rb, Ba K, Pb and Sr) seen only in the olivine basalts and ankaramites, on the other hand, are more a consequence of crustal contamination. This is evident from the increase in the concentrations of these elements coincident with a dramatic decrease in the concentration of compatible elements (Ni and Cr) and the shift from high to low-flux magmatism above the first palaeosol. Highly significant increases in the parent

daughter ratios Rb/Sr and Ce/Pb ratios above the palaeosol seem to confirm that this shift in chemistry is attributable to a contribution from crustal material.

The relative abundances of MICE in the lavas are less variable than to those of their VICE. This is reflected in the remarkably consistent, sub-parallel chondrite-normalised REE patterns for each lava group, and is likely to be related to a common source composition. All three groups have similarly fractionated REE patterns showing strong enrichment LREE relative to HREE reflecting the presence of residual garnet in the source. $(La/Yb)_N$ ratios range between 8.9 and 14.6, and there are only slight negative Eu anomalies (0.94 - 0.96) which signify minimal fractionation of plagioclase as evident from the petrology. Generally the olivine basalts are more REE-enriched and are more enriched in LREE relative to MREE compared to the picrites and ankaramites. The picrites, on the other hand, show a greater degree of enrichment of LREE and MREE relative to HREE compared to the ankaramites the olivine basalts. These differences reflect different degrees of partial melting within the garnet stability field. The picrites exhibit higher and more wide-ranging $(La/Yb)_N$ and $(Gd/Yb)_N$ ratios than the ankaramites and olivine basalts suggesting that were derived from respectively smaller and more variable degrees of partial melting, although it cannot be discounted that such differences may be attributed to variable amounts of garnet in the source. The degree of partial melting estimated from the [La/Yb]n and [Dy/Yb}n ratios for the lavas relative to model melting curves for garnet lherzolite varies between 3 and 6 % at pressures near to 4 GPa. This supports that melting occurred beneath thick lithosphere prior to lithospheric extension.

Strong negative correlations for the incompatible elements and positive correlations for the compatible elements with MgO imply an evolution for the lavas dominated by olivine fractionation. This is evident more from the linear trends for the ankaramites and olivine basalts, and from the higher concentrations of incompatible elements in the olivine basalts compared to the picrites and anakramites which reflect greater degrees of shallow-level fractionation. Similarly orientated trends for the picrites are more a reflection of differences in the degree of partial melting and olivine accumulation. Trace element modelling suggests that the evolution of the lavas is related through fractional crystallisation. REE modelling, however, reveals that whereas the picrites and ankaramites were derived from deep seated magmas generated by different degrees of partial melting of the same primary melt, the olivine basalts magmas evolved by crystal fractionation at a shallow level from a melt similar in composition to the ankaramites. Model fractionation curves for REE indicate that

the olivine basalt magmas evolved at low pressure (< 0.06 GPa) from an oxidised (> QFM+1) ankaramitic melt by 10 - 40% fractional crystallisation of olivine and clinopyroxene at temperatures considerably lower than the liquidus for olivine (1370 °C), and possibly lower than the temperature at which clinopyroxene began crystallising (1163 °C). Similarly, the anakramites are shown to have evolved at pressures of < 0.6 GPa from an oxidised (> QFM+1) melt by 10 - 20 % fractional crystallisation of olivine and clinopyroxene at < 1370 °C. In contrast, the variations in the REE ratios for the picrites suggest that the picritic magmas were derived from melts similar to that of the ankaramites but generated by different degrees of partial melting of primary melt, and that their ascent to the surface was not punctuated by prolonged periods of shallow level fractionation. The restricted range of Al_2O_3 concentrations in the picrites seems to confirm that such variations are unlikely to be a result of differences in the amount of garnet in the source and are indeed indicative of the degree of partial melting in the plume.

7.2.5 Sr, Nd, Pb and noble gas isotopic compositions

Despite their HIMU-type trace element signatures, the lavas from across the Afro-Arabian volcanic province exhibit contrasting range of isotopic compositions. The only lavas in East Africa with high $^{206}Pb/^{204}Pb$ ratios that approach HIMU-type isotopic compositions are associated with binary mixing between a lithospheric component and the Kenyan plume, which is considered isotopically and therefore physically distinct from the Afar plume (Rogers et al. 2000). Although both plumes have been assigned similar $^{87}Sr/^{86}Sr$ ratios and Nd and Pb isotopic compositions within the range of the global OIB database, the proposed composition for the Kenyan Plume has a $^{143}Nd/^{144}Nd$ ratio significantly below that reported for the Afar Plume - represented by the HT2 basalts (including the lavas from the Dilb and Iyela sections) which have isotopic compositions close to common primitive mantle (PREMA, FOZO, PHEM, C). This is consistent with the contrasting $^{3}He/^{4}He$ ratios for basalts from the regions within the influence of each plume (Pik et al. 2006). Whereas the Kenyan Rift basalts have MORB-type $^{3}He/^{4}He$ ratios within the range of the continental upper mantle (R/R_a = 5 - 9), the HT2 basalts have elevated $^{3}He/^{4}He$ ratios indicative of a deep primitive mantle component (R/R_a up to 19.6). The range of isotopic compositions exhibited by the HT1 and LT basalts and other more recent lavas from the Afro-Arabian volcanic province reflect the effects of crustal contamination, and the waning influence of the lithosphere and the increasing influence of the Afar plume as Arabia drifted away from Africa following rifting and extension. The HIMU signature observed in the flood basalts is attributed to a

metasomatic exchange between the lithospheric mantle and the impacting hot plume, and is more a feature of their trace element rather than isotopic compositions.

The plume component characterised by εNd values of +6 ($^{143}Nd/^{144}Nd$ ~ 0.5129) is evident only in the Oligocene flood basalts from the Ethiopian and Yemen plateaux and the modern Afar basalts (Pik et al. 1999; Baker et al. 1996b; Deniel et al. 1994), and it appears to be masked by lithospheric overprinting in the lavas between. Its persistence from the onset of flood volcanism through to present day volcanism is, however, evident from the high $^{3}He/^{4}He$ ratios in basaltic lavas of Oligocene, Miocene, Quaternary and Recent age from the Ethiopian Plateau and Afar. High $^{3}He/^{4}He$ ratios (1.53×10^{-05} to 2.6×10^{-05} - equivalent to R/R_a values from 11.0 to 18.7) in the picrites from the Dilb and Bilbala sections confirm the presence of this signature in the early flood basalts, and therefore support a source for the plume in an undegassed region of the mantle. The same can be concluded from the solar-like Ne isotopic ratios ($^{20}Ne/^{22}Ne$ = 10.4 - 10.6, $^{21}Ne/^{22}Ne$ = 0.029 - 0.031) for the picrites, which plot along the Loihi line representing mixing between air and OIB-type mantle. This OIB-like Ne signature in the picrites is consistent with high $^{3}He/^{4}He$ ratios and is therefore likely to be representative of the plume. Furthermore the $^{21}Ne/^{22}Ne_E$ - $^{4}He/^{3}He$ systematics for the picrites place them on a mixing line between a Loihi-type mantle component and the SCLM thereby substantiating the proposition that the composition of the plume has been metasomatically modified by the interaction with the SCLM. The contrasting air-like Ar and Xe isotopic compositions in the picrites are indicative of atmospheric contamination since they are not concordant with their He isotopic compositions.

7.2.6 Rhenium-osmium systematics

Os is incompatible in olivine but readily partitions into sulphide inclusions (such as spinel) and is therefore dominantly controlled by olivine fractionation (Burton et al. 2002), whereas Re, like other incompatible elements, preferentially partitions into the melt. The consistently low Re concentrations compared to variable Os concentrations in the picrites therefore suggests that the lavas have experienced Re-loss as a result of degassing on eruption. This is evident from the surprisingly small difference between their measured and age-corrected or initial $^{187}Os/^{188}Os$ ratios. Like the picrites from Siberia (Horan et al. 1995) and West Greenland (Schaefer et al. 2000a), the Dilb and Iyela picrites have Os concentrations of over 1000 ppt, which are closer to those for komatiites than most CFBs, and markedly higher than those for OIBs. Since their magmas were derived were derived from small degree partial melts, it is

probable such high Os concentrations reflect an unusually Os-rich source. The markedly lower Os and higher Re concentrations for the olivine basalts and the more evolved lavas from the Lalibela North and Bilbala sections, on the other hand, are attributable to crustal contamination. This is supported by their $^{187}Os/^{188}Os$ ratios relative to Re/Os which plot along a 1 Ga mixing line between the uncontaminated magma and a crustal component corresponding to an the Pan-African basement of NE Africa with an age-range of between 0.6 and 1.2 Ga (Harris et al. 1984). The influence of this crustal component is evident in the stratigraphy of the Dilb and Iyela sections from an increase in Os and decrease in Re concentrations, and the coincident increase in $^{187}Os/^{188}Os$ and $^{187}Re/^{185}Re$ ratios above the first palaeosol marking the shift from high to low-flux magmatism.

The initial $^{187}Os/^{188}Os$ ratios for the picrites, ankaramites and uncontaminated olivine basalts are sub-chondritic and fall within an unusually limited range between 0.12569 and 0.12622. This strongly implies that they were sourced from depleted mantle, and in this respect are different from any other reported plume-head picrites. Other plume-related picrites generally have Os and Nd isotopic compositions which plot along mixing lines between OIB-type and lithospheric peridotite components (Ellam et al. 1992), whereas those for the uncontaminated Dilb and Iyela lavas plot between the fields for MORB and OIB implying that they evolved from a source slightly less depleted than normal asthenospheric mantle. This is consistent with the depleted primitive mantle component previously assigned to the Afar plume and therefore discounts the HIMU-type component as a possible source for the plume thereby making its affinity with the SCLM more plausible.

Sub-chondritic initial $^{187}Os/^{188}Os$ ratios suggest that there is no excess ^{186}Os in the Dilb and Iyela lavas; it is unlikely, therefore, that the source of the plume has interacted with the outer core. This is contrary to the implications from seismic tomographic images of the mantle beneath Afar showing a plume-like low-velocity anomaly extending down to the core mantle boundary. It is also inconsistent with the proposition that deep-sourced mantle plumes contain coupled enrichments of $^{186}Os/^{188}Os$ and $^{187}Os/^{188}Os$ relative to chondritic upper mantle that are indicative of an evolved outer-core component. The core mantle boundary as a source for mantle plumes therefore remains a controversial issue, as does the source region of the Afar plume. Whereas the Os isotopic compositions of the Dilb and Iyela picrites imply an origin for the Afar plume in the depleted upper mantle, their He and Ne isotopic compositions imply an origin in the deeper unmixed mantle. Such conclusions

assume that the mantle is in some way stratified so that the lower part is unmixed, and that mantle plumes are dependent on a boundary-layer for their genesis. Recent seismic tomographic imaging of the mantle, however, suggests that this might not be the case. What is clear from the isotopic compositions of the Dilb and Iyela lavas is that the depleted-mantle-like composition of the Afar plume is significantly more homogeneous than that for MORB.

7.3 Model for the origin and petrogenesis of the Ethiopian flood basalts

7.3.1 Explanation

A model of petrogenesis for the Afro-Arabian flood basalts is developed in the next section from the observations and interpretations previously summarised in this chapter. To avoid unnecessary repetition, only a skeletal outline of the model is presented to accompany the schematic diagram in Figure 7.1.

7.3.2 The model

- Initiation of a wave-like instability at a thermal boundary-layer in an unmixed, undegassed region of the deep mantle characterised by primordial noble gas compositions. On reaching a critical Rayleigh number this instability develops into a plume which ascends through the mantle because of its lower density.

- Entrainment of material into the plume occurs mainly from below, but also from the surrounding mantle as a result of radial conduction Material is fed through the tail to the head, which enlarges as the plume matures.

- The plume-head flattens on reaching the base of the lithospheric mantle at a depth of 120 – 150 km.

- Temperature in the plume head ~ 200 °C higher than ambient mantle and lower pressure causes accelerated adiabatic melting.

- Partial melts of between 3 and 6 % are generated by melting of high Fe-Ti-Os, low Al depleted-mantle in the plume head at pressures of between 4 and 5 GPa and at temperatures of near to 1600 °C.

- The primary melts rise through the lithospheric mantle where they are metasomatically modified by the interaction with a HIMU-like component.

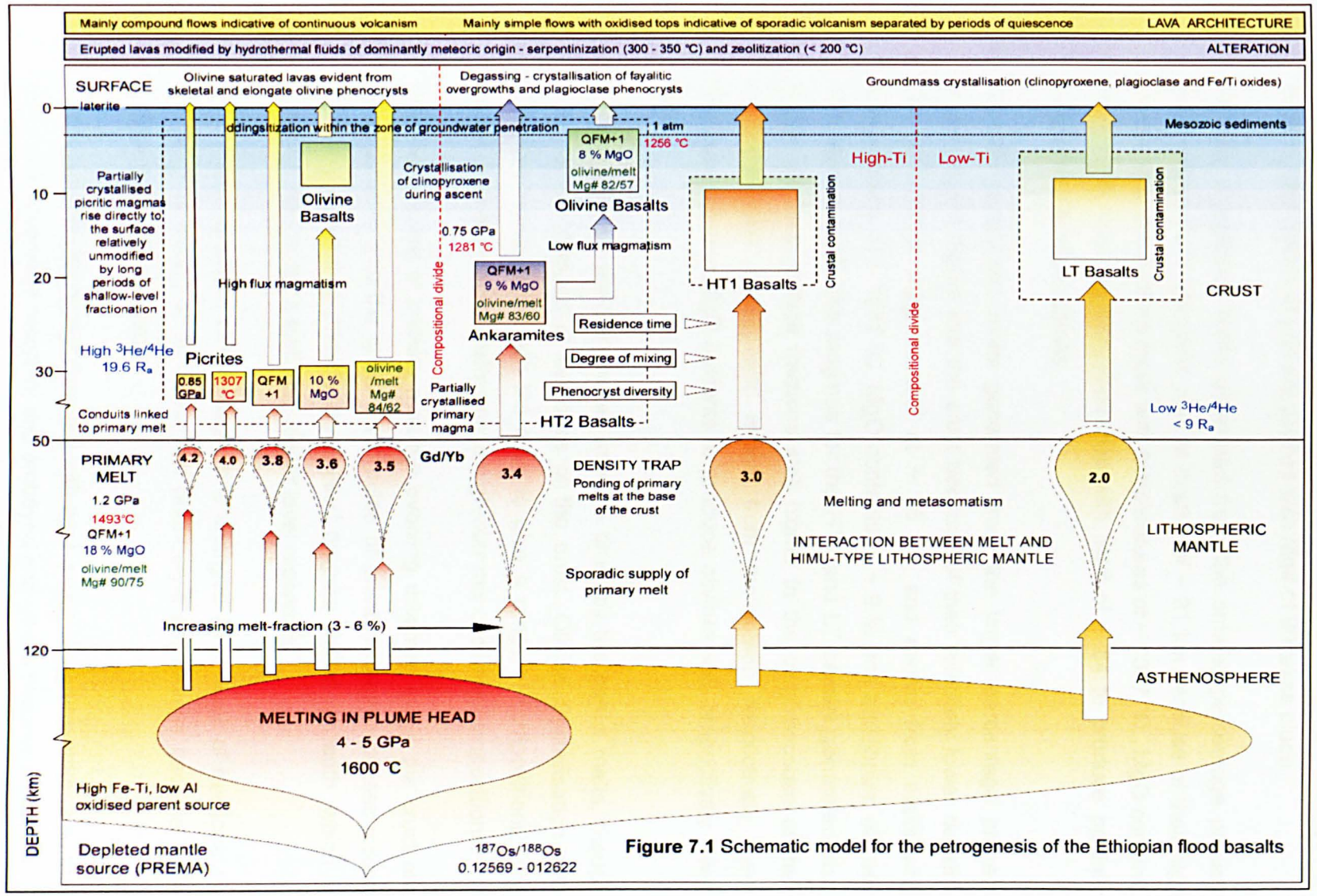

Figure 7.1 Schematic model for the petrogenesis of the Ethiopian flood basalts

- Modified primary melts with MgO contents between 17 and 18 % pond at the base of the crust (at a depth of ~ 50 km) because of their high density, and initial crystallisation of primary olivines with Mg# of 90 takes place.

- Partially crystallised melts generated from the smaller percentage primary melts ascend into the crust, stall at depths of ~ 31 km because of their high density and evolve from melts with temperatures of ~ 1307 °C, MgO contents of ~ 10 %, and equilibrium-olivines with Mg# of ~ 84 to produce partially crystallised picrite magmas.

- Partially crystallised melts generated from the larger percentage primary melts ascend higher into the crust because of their relatively lower density. The ankaramite magmas stall at ~ 26 km and evolve from melts with temperatures of ~ 1281 °C, MgO contents of ~ 9 % and equilibrium olivines with Mg# of ~ 83. The magmas for the HT1 and LT basalts generated from higher percentage melt fractions stall higher in the crust because of their relatively lower density and evolve from melts with respectively lower temperatures and MgO contents to produce olivines with respectively lower Mg#.

- Primary olivines are transported into the crust by the partial melts, though most remain trapped at the base of the crust. Olivine crystallisation also continues en-route through the crust to give a range of compositions. The higher level magmas therefore have a greater mix of olivine compositions.

- With each pulse of primary melt the evolving magmas within the crust are pushed higher into the crust. Each pulse of primary magma causes mixing and displacement of partially crystallised magma stalled at depth, which in turn displaces magma stalled in higher level reservoirs.

- The bulk-composition of the magmas is changed as a result of fractionation and magma mixing at all levels and phenocryst populations become more diverse toward the surface.

- Equilibrium conditions are changed with each pulse of primary magma so that phenocrysts become resorbed and embayed and others become zoned.

- High flux magmatism is necessary to move the picrite lavas and they ascend directly to the surface arriving as olivine-saturated lavas which produce skeletal and elongate olivine phenocrysts.

- With the shift to low-flux magmatism, the pulses of primary melt are less frequent or are slower. This allows the less dense lavas time to fractionate in the crust before being erupted on the surface.

- As the magma flux slows, crustal melting occurs and shallow-seated magma chambers develop so that the plumbing system changes from one exclusively of conduits to one punctuated by one or more reservoirs in which fractionation and crustal contamination of the magma can occur.

- The ankaramites are erupted at the surface after a period of low-pressure (0.7 GPa) fractionation in a mid-level magma chamber where clinopyroxene crystallises alongside olivine and is allowed to accumulate.

- The olivine basalts are erupted at the surface after a period of lower-pressure (1 atm) fractionation in a shallow-level magma chamber where plagioclase and clinopyroxene crystallise alongside fayalitic olivine. This magma chamber is fed by partially crystallised ankaramite magmas.

- The HT1 and LT basalts are erupted at the surface after longer periods of fractionation and crustal contamination in shallow-level magma chambers

- Percolation of meteoric groundwater into the shallow-level magma chambers causes an increase in the oxygen fugacity of the magmas leading to iddingzitization of the olivines.

- The picrite magmas which ascend directly to the surface experience smaller degrees of iddingsitization as they pass through the zone of groundwater penetration.

- Degassing during eruption leads to volatile loss (including Re and water vapour) and lower oxygen fugacity in the remaining melt, allowing the growth of fragile plagioclase phenocrysts and fayalitic olivine rims around iddingsitized olivine.

- Rapid crystallisation of the groundmass follows.

- The picrites erupt over long periods at low effusion rates and therefore produce thick compound flows with chaotically stacked flow-lobes, whereas the more evolved lavas erupt periodically at high effusion rates and tend to form thinner simple flows characterised by massive well-jointed bodies and scoriaceous tops.

- Some lavas are serpentinized or zeolitized as a result of the interaction with hydrothermal solutions produced during the emplacement of subsequent lavas.

- Breaks in volcanic activity allow the surface of the more evolved lavas to become oxidised, and long periods of quiescence are marked by palaeosol development.

7.3.3 Epilogue

The model described above is specific to the evolution and petrogenesis of the Ethiopian flood basalts but may be extended to include flood basalts from other parts of the Afro-Arabian volcanic province. It may be applied to other continental flood basalt provinces, but only in so far as the data fits. It would be impossible to develop a model to explain the petrogenesis of all seemingly similar provinces since the nature of their source components and the tectonic frameworks controlling their emplacement are all quite different. All flood basalts provinces are in this respect unique. What is unanimously applicable is the approach and reasoning behind the model. It is a synthesis of observations from field relations, stratigraphy, petrography, major and trace element, and isotopic compositions that gives context to our interpretations, and is limited only by these interpretations which are in essence limited by our current understanding of petrogenetic processes and the nature of the mantle.

REFERENCES

Abbate, E., and M. Sagri (1980), Volcanites of the Ethiopian and Somali Plateaus and major tectonic lines, in *Geodynamic Evolution of the Afro Arabian Rift System*, edited, pp. 219–227, Accademia Nazionale dei Lincei.

Abbate, E., et al. (1995), Strike-slip faults in a rift area - a transect in the Afar Triangle, East-Africa, *Tectonophysics*, *241*(1-2), 67-97.

Abbate, E., et al. (2002), Morphostructural development of the Eritrean rift flank (southern Red Sea) inferred from apatite fission track analysis, *Journal of Geophysical Research-Solid Earth*, *107*(B11), 0148-0227.

Abbott, D. H., and A. E. Isley (2002), The intensity, occurrence, and duration of superplume events and eras over geological time, *Journal of Geodynamics*, *34*(2), 265-307.

Abebe, T., et al. (1998), The Yerer-Tullu Wellel volcanotectonic lineament: a transtensional structure in central Ethiopia and the associated magmatic activity, *Journal of African Earth Sciences*, *26*(1), 135-150.

Abebe, B., et al. (2007), Quaternary faulting and volcanism in the main Ethiopian Rift, *Journal of African Earth Sciences*, *48*, 115-124.

Ackland, G. (2001), Quantum mechanical computer calculations of mineral structures, paper presented at Mantle materials, processes and products (VMSG Annual Conference), Mineralogical Society, Durham.

Acocella, V., and T. Korme (2002), Holocene extension direction along the Main Ethiopian Rift, East Africa, *Terra Nova*, *14*(3), 191-197.

Acocella, V., et al. (2003), Elliptic calderas in the Ethiopian Rift: control of pre-existing structures, *Journal of Volcanology and Geothermal Research*, *119*(1-4), 0377-0273.

Acocella, V. (2006), Regional and local tectonics at Erta Ale caldera, Afar (Ethiopia), *Journal of Structural Geology*, *28*(10), 1808-1820.

Acocella, V., et al. (2008), Structure of Tendaho Graben and Manda Hararo Rift: Implications for the evolution of the southern Red Sea propagator in Central Afar, *Tectonics*, *27*(4).

Acton, G. D., et al. (2000), The tectonic and geomagnetic significance of paleomagnetic observations from volcanic rocks from central Afar, Africa, *Earth and Planetary Science Letters*, *180*(3-4), 225-241.

Ague, J. J. (1998), Simple models of coupled fluid infiltration and redox reactions in the crust, *Contributions to Mineralogy and Petrology*, *132*(2), 180-197.

Alard, O., et al. (2002), New insights into the Re-Os systematics of sub-continental lithospheric mantle from in situ analysis of sulphides, *Earth and Planetary Science Letters*, *203*(2), 651-663.

Albarede, F. (1992), How deep do common basaltsic magmas from and differentiate, *Journal of Geophysical Research-Solid Earth*, *97*(B7), 10997-11009.

Al'Kadasi, M. (1995), Temporal and spatial evolution of the basal flows of the Yemen Volcanic Group (unpublished PhD thesis), Royal Holloway, London.

Allegre, C. J., and D. L. Turcotte (1986), Implications of a two-component marble-cake mantle, *Nature*, *323*(6084), 123-127.

Allegre, C. J., et al. (1999), Age of the Deccan traps using Re-187-Os-187 systematics, *Earth and Planetary Science Letters*, *170*(3), 197-204.

Almond, D. C. (1986a), The relation of Mesozoic-Cainozoic volcanism to tectonics in the Afro-Arabian dome, *Journal of Volcanology and Geothermal Research*, *28*(3-4), 225-246.

Almond, D. C. (1986b), Geological evolution of the Afro-Arabian dome, *Tectonophysics*, *131*(3-4), 301-332.

Al'Subbary, A. A. (1996), The sedimentology and stratigraphy of the Cretaceous-early Tertiary Tawilah group, western Yemen (unpublished PhD thesis), Royal Holloway London.

Althaus, T., et al. (2003), Noble gases in olivine phenocrysts from drill core samples of the Hawaii Scientific Drilling Project (HSDP) pilot and main holes (Mauna Loa and Mauna Kea, Hawaii), *Geochemistry Geophysics Geosystems*, *4*.

Amelung, F., et al. (2000), Ground deformation near Gada 'Ale Volcano, Afar, observed by Radar Interferometry, *Geophysical Research Letters*, *27*(19), 3093-3096.

Anderson, D. L., et al. (1992), Plate tectonics and hotspots - the third dimension, *Science*, *256*(5064), 1645-1651.

Anderson, D. L. (1994a), Superplumes or supercontinents, *Geology*, *22*(1), 39-42.

Anderson, D. L. (1994b), The sublithospheric mantle as the source for continental flood basalts - the case against the continental lithosphere and plume head reservoirs *Earth and Planetary Science Letters*, *123*(1-4), 269-280.

Anderson, D. L. (1994c), Komatiites and picrites - evidence that the plume source is depleted, *Earth and Planetary Science Letters*, *128*(3-4), 303-311.

Anderson, D. L. (1995), Lithosphere, asthenosphere and perisphere, *Reviews of Geophysics*, *33*(1), 125-149.

Anderson, D. L. (1998), The scales of mantle convection, *Tectonophysics*, *284*(1-2), 1-17.

Anderson, D. L. (2000a), The statistics of helium isotopes along the global spreading ridge system and the central limit theorem, *Geophysical Research Letters*, *27*(16), 2401-2404.

Anderson, D. L. (2000b), The thermal state of the upper mantle; no role for mantle plumes, *Geophysical Research Letters*, *27*(22), 3623-3626.

Anderson, D. L. (2000c), The statistics and distribution of helium in the mantle, *International Geology Review*, *42*(4), 289-311.

Anderson, D. L. (2001), A statistical test of the two reservoir model for helium isotopes, *Earth and Planetary Science Letters*, *193*(1-2), 77-82.

Anderson, D. L. (2002a), The case for irreversible chemical stratification of the mantle, *International Geology Review*, *44*(2), 97-116.

Anderson, D. L. (2002b), How many plates?, *Geology*, *30*(5), 411-414.

Anderson, D. L. (2003), Look again, *Astronomy and Geophysics*, *44*, 1.10-11.11.

Anderson, D. L. (2004), Simple scaling relations in geodynamics: the role of pressure in mantle convection and plume formation, *Chinese Science Bulletin*, *49*(19), 2017-2021.

Antonini, P., et al. (1998), A segment of sea-floor spreading in the central Red Sea: basalts from the Nereus Deep (23 degrees 00 '- 23 degrees 20 ' N), *Journal of African Earth Sciences*, *27*(1), 107-114.

Arai, S. (1994a), Compositional variation of olivine chromian spinel in Mg-rich magmas as a guide to their residual spinel peridotites, *Journal of Volcanology and Geothermal Research*, *59*(4), 279-293.

Arai, S. (1994b), Characterization of spinel peridotites by olivine spinel compositional relationships - review and interpretation, *Chemical Geology*, *113*(3-4), 191-204.

Argus, D. F., and R. G. Gordon (1991), No-net-rotational model of current plate velocities incorporationg plate motion model NUVEL-1, *Geophysical Research Letters*, *18*(11), 2039-2042.

Arndt, N. T. (1991), High Ni in Archean tholeiites, *Tectonophysics*, *187*(4), 411-419.

Arndt, N. T., and U. Christensen (1992), The role of lithospheric mantle in continental flood volcanism - thermal and geochemical constraints, *Journal of Geophysical Research-Solid Earth*, *97*(B7), 10967-10981.

Arndt, N. T., et al. (1993), Mantle and crustal contributions to continental flood volcanism, *Tectonophysics*, *223*(1-2), 39-52.

Arndt, N., et al. (2001a), The oldest continental and oceanic plateaus: geochemistry of basalts and komatiites of the Pilbara craton, Australia, in *Mantle plumes: their Identification through time*, edited by R. E. Ernst and K. L. Buchan, pp. 359-387, Geological Society of America.

Arndt, N. T., et al. (2001b), Hot heads and cold tails: the transition from tholeiitic flood basalts to alkaline shield volcanics in Ethiopia and Kerguelen, , paper presented at Magmatic rifted margins, Royal Holloway, Egham.

Asfaw, L. M., et al. (2004), Vertical deformation in the Main Ethiopian Rift: levelling results in its northern part, 1995-2004, paper presented at East African Rift Systems - Geodynamics, Resources and Environment, Geological Society Publishing House, Addis Ababa, Jun.

Asfaw, L. M., et al. (2006), Vertical deformation in the Main Ethiopian Rift: levelling results in its northern part, 1995-2004, *Afar Volcanic Province within the East African Rift System*, *259*, 185-190.

Asimow, P. D., and M. S. Ghiorso (1998), Algorithmic modifications extending MELTS to calculate subsolidus phase relations, *American Mineralogist*, *83*(9-10), 1127-1132.

Audin, J., et al. (1990), The 1928 - 1929 eruption of Kammourta volcano - evidence of tectonomagmatic activity in the Manda-Inakir Rift and comparison with the Asal Rift, Afar Depression, Republic of Djibouti, *Bulletin of Volcanology*, *52*(7), 551-561.

Audin, L., et al. (2001), Fault propagation and climatic control of sedimentation on the Ghoubbet Rift Floor: insights from the Tadjouraden cruise in the western Gulf of Aden, *Geophysical Journal International*, *144*(2), 391-413.

Audin, L., et al. (2004), Palaeomagnetism and K-Ar and $^{40}Ar/^{39}Ar$ ages in the Ali Sabieh area (Republic of Djibouti and Ethiopia): constraints on the mechanism of Aden ridge propagation into southeastern Afar during the last 10 Myr, *Geophysical Journal International*, *158*(1), 327-345.

Ayalew, D., et al. (1999), Geochemical and isotopic (Sr, Nd and Pb) characteristics of volcanic rocks from southwestern Ethiopia, *Journal of African Earth Sciences*, *29*(2), 381-391.

Ayalew, D., et al. (2002), Source, genesis, and timing of giant ignimbrite deposits associated with Ethiopian continental flood basalts, *Geochimica Et Cosmochimica Acta*, *66*(8), 1429-1448.

Ayalew, D., and G. Yirgu (2003), Crustal contribution to the genesis of Ethiopian plateau rhyolitic ignimbrites: basalt and rhyolite geochemical provinciality, *Journal of the Geological Society*, *160*, 47-56.

Ayalew, D., et al. (2004), Temporal compositional variation of syn-rift rhyolites along the western margin of the southern Red Sea and northern Main Ethiopian Rift, paper presented at East African Rift Systems: Geodynamics, Resources and Environment, Addis Ababa, Jun.

Ayalew, D., et al. (2006), Temporal compositional variation of syn-rift rhyolites along the western margin of the southern Red Sea and northern Main Ethiopian Rift, *Afar Volcanic Province within the East African Rift System*, *259*, 121-130.

Ayele, A., and O. Kulhanek (1997), Spatial and temporal variations of seismicity in the Horn of Africa from 1960 to 1993, *Geophysical Journal International*, *130*(3), 805-810.

Ayele, A., et al. (2004), Tectonic implication of the August, 2002 earthquake sequence at the western Danakil microplatein north-west Afar, paper presented at

The East African Rift System: Geodynamics, Resources and Environment, Addis Ababa.

Ayele, A., et al. (2007), The August 2002 earthquake sequence in north Afar: Insights into the neotectonics of the Danakil microplate, *Journal of African Earth Sciences*, *48*, 70-79.

Baker, M. B., et al. (1996), Petrography and petrology of the Hawaii Scientific Drilling Project lavas: Inferences from olivine phenocryst abundances and compositions, *Journal of Geophysical Research-Solid Earth*, *101*(B5), 11715-11727.

Baker, J., et al. (1996a), A brief Oligocene period of flood volcanism in Yemen: Implications for the duration and rate of continental flood volcanism at the Afro-Arabian triple junction, *Earth and Planetary Science Letters*, *138*(1-4), 39-55.

Baker, J. A., et al. (1996b), Sr-Nd-Pb isotopic and trace element evidence for crustal contamination of plume-derived flood basalts: Oligocene flood volcanism in western Yemen, *Geochimica et Cosmochimica Acta*, *60*(14), 2559-2581.

Baker, J. A., et al. (1997), Petrogenesis of quaternary intraplate volcanism, Sana'a, Yemen: Implications for plume-lithosphere interaction and polybaric melt hybridization, *Journal of Petrology*, *38*(10), 1359-1390.

Baker, J., et al. (1998), Metasomatism of the shallow mantle beneath Yemen by the Afar plume - Implications for mantle plumes, flood volcanism, and intraplate volcanism, *Geology*, *26*(5), 431-434.

Baker, J. A., et al. (2000), Resolving crustal and mantle contributions to continental flood volcanism, Yemen; constraints from mineral oxygen isotope data, *Journal of Petrology*, *41*(12), 1805-1820.

Baker, J. A., and K. K. Jensen (2004), Coupled ^{186}Os-^{187}Os enrichments in the Earth's mantle - core-mantle interaction or recycling of ferromanganese crusts and nodules?, *Earth and Planetary Science Letters*, *220*(3-4), 277-286.

Baksi, A. K. (1994), Geochronological studies on whole-rock basalts, Deccan Traps, India: evaluation of the timing of volcanism relative to the K-T boundary, *Earth and Planetary Science Letters*, *121*(1-2), 43-56.

Baksi, A. K. (2001), Search for a deep-mantle component in mafic lavas using a Nb-Y-Zr plot, *Canadian Journal of Earth Sciences*, *38*(5), 813-824.

Balestrieri, M. L., et al. (2005), Geomorphic development of the escarpment of the Eritrean margin, southern Red Sea from combined apatite fission-track and (U-Th)/He thermochronometry, *Earth and Planetary Science Letters*, *231*(1-2), 97-110.

Ballentine, C. J. (2002), Geochemistry - Tiny tracers tell tall tales, *Science*, *296*(5571), 1247-1248.

Ballhaus, C., et al. (1991a), High-pressure experimental calibration of the olivine-orthopyroxene-spinel oxygen geobarometer: implications for the oxidation state of the upper mantle, *Contributions to Mineralogy and Petrology*, *107*(1), 27-40.

Ballhaus, C., et al. (1991b), Erratum: High-pressure experimental calibration of the olivine-orthopyroxene-spinel oxygen geobarometer: implications for the oxidation state of the upper mantle (Vol. 107, pg 27, 1991), *Contributions to Mineralogy and Petrology*, *108*(3), 384-384.

Ballhaus, C. (1993), Redox states of the lithospheric and asthenospheric upper mantle, *Contributions to Mineralogy and Petrology*, *114*(3), 331-348.

Ballhaus, C., et al. (1994), Erratum: High-pressure experimental calibration of the olivine-orthopyroxene-spinel oxygen geobarometer: implications for the oxidation state of the upper mantle (Vol. 107, pg 27, 1991), *Contributions to Mineralogy and Petrology*, *118*(1), 109-109.

Ballhaus, C. (1995), Is the upper mantle metal-saturated?, *Earth and Planetary Science Letters*, *132*(1-4), 75-86.

Barberi, F., et al. (1975), Transistional basalt-pantellerite sequence of fractional crystallization, Boina Center (Afar Rift, Ethiopia), *Journal of Petrology*, *16*(1), 22-56.

Barberi, F., et al. (1980), Sr isotopic composition of Afar volcanics and its implication for mantle evolution, *Earth and Planetary Science Letters*, *50*(1), 247-259.

Barbieri, M., et al. (1995), Geochemistry of the volcanic basic rocks from the Bale Mountains (South-Eastern Ethiopia) - evidence of crustal contamination, *Chemie Der Erde-Geochemistry*, *55*(3), 205-216.

Barfod, D. N., et al. (1999), Noble gases in the Cameroon line and the He, Ne, and Ar isotopic compositions of high mu (HIMU) mantle, *Journal of Geophysical Research-Solid Earth*, *104*(B12), 29509-29527.

Barrat, J. A., et al. (1990), Mantle heterogeneity in north eastern Africa: evidence from Nd isotopic compositions and hydromagmaphile element geochemistry of basaltic rocks from the Gulf of Tadjoura and southern Red Sea regions, *Earth and Planetary Science Letters*, *101*(2-4), 233-247.

Barrat, J. A., et al. (1993), Magma genesis in an orogenic rifting zone: The Tadjoura Gulf (Afar Area), *Geochimica et Cosmochimica Acta*, *57*(10), 2291-2302.

Barrat, J. A., et al. (1998), Isotope (Sr, Nd, Pb, O) and trace-element geochemistry of volcanics from the Erta'Ale range (Ethiopia), *Journal of Volcanology and Geothermal Research*, *80*(1-2), 85-100.

Barrat, J. A., et al. (2003), Geochemistry of basalts from Manda Hararo, Ethiopia: LREE-depleted basalts in Central Afar, *Lithos*, *69*(1-2), 1-13.

Basaltic-Volcanism-Study-Project (1981), *Basaltic Volcanism on the Terrestrial Planets.*, Pergamon Press.

Bastow, I., et al. (2004), Upper mantle seismic structure of the northern Ethiopian rift: a region of incipient continental breakup, paper presented at The East African Rfit System: Geodynamics, Resources and Environment, Addis Ababa.

Bastow, I. D., et al. (2005), Upper-mantle seismic structure in a region of incipient continental breakup: northern Ethiopian rift, *Geophysical Journal International*, *162*(2), 479-493.

Bastow, I. D., et al. (2008), Upper mantle seismic structure beneath the Ethiopian hot spot: Rifting at the edge of the African low-velocity anomaly, *Geochemistry Geophysics Geosystems*, *9*.

Basu, A. R., et al. (1993), Early and late alkali igneous pulses and a high ^{3}He plume origin for the Deccan flood basalts, *Science*, *261*(5123), 902-906.

Basu, A. R., et al. (1995), High ^{3}He plume origin and temporal-spatial evolution of the Siberian flood basalts, *Science*, *269*(5225), 822-825.

Basu, A. R., et al. (1998), Melting of the Siberian mantle plume, *Geophysical Research Letters*, *25*(12), 2209-2212.

Beattie, P., et al. (1991), Partition coefficients for olivine-melt and orthopyroxene-melt systems, *Contributions to Mineralogy and Petrology*, *109*(2), 212-224.

Beattie, P., et al. (1993), Partition coefficients for olivine-melt and orthopyroxene-melt systems (Vol. 109, pg 212, 1991), *Contributions to Mineralogy and Petrology*, *114*(2), 288-288.

Beccaluva, L., et al. (1989), Clinopyroxene composition of ophiolite basalts as petrogenetic indicator, *Chemical Geology*, *77*(3-4), 165-182.

Beccaluva, L., et al. (2007), Intracratonic asthenosphere upwelling and lithosphere rejuvenation beneath the Hoggar swell (Algeria): evidence from HIMU metasomatised lherzolite mantle xenoliths, *Earth and Planetary Science Letters*, *260*(3-4), 482-494.

Beccaluva, L., et al. (2008), The role of HIMU metasomatic components in the North African lithospheric mantle: petrological evidence from the Gharyan lherzolite xenoliths, NW Libya, *Geological Society, London, Special Publications*, *293*(1), 253-277.

Bedini, R. M., et al. (1997), Evolution of LILE-enriched small melt fractions in the lithospheric mantle: a case study from the East African Rift, *Earth and Planetary Science Letters*, *153*(1-2), 67-83.

Bedini, R. M., and J. L. Bodinier (1999), Distribution of incompatible trace elements between the constituents of spinel peridotite xenoliths: ICP-MS data from the East African Rift, *Geochimica et Cosmochimica Acta*, *63*(22), 3883-3900.

Bellahsen, N., et al. (2003), Why did Arabia separate from Africa? Insights from 3-D laboratory experiments, *Earth and Planetary Science Letters*, *216*(3), 365-381.

Bellahsen, N., et al. (2006), Fault reactivation and rift localization: northeastern Gulf of Aden margin, *Tectonics*, *25*(1).

Bellieni, G., et al. (1984), High-TiO_2 and low-TiO_2 flood basalts from the Parana Plateau, Brazil: petrology and geochemical aspects bearing on their mantle origin, *Neues Jahrbuch Fur Mineralogie-Abhandlungen*, *150*(3), 273-306.

Bellieni, G., et al. (1986), Petrology and mineralogy of Miocene fissural volcanism of the East Kenya Plateau, *Neues Jahrbuch Fur Mineralogie-Abhandlungen*, *154*(2), 153-178.

Bellieni, G., et al. (1986), Petrogenetic aspects of acid and basaltic lavas from the Parana Plateau, Brazil: geological, mineralogical and petrochemical relationships, *Journal of Petrology*, *27*(4), 915-944.

Bendick, R., et al. (2006), Distributed Nubia-Somalia relative motion and dike intrusion in the Main Ethiopian Rift, *Geophysical Journal International*, *165*(1), 303-310.

Benoit, M. H., et al. (2006), Mantle transition zone structure and upper mantle S velocity variations beneath Ethiopia: evidence for a broad, deep-seated thermal anomaly, *Geochemistry Geophysics Geosystems*, *7*.

Benoit, M. H., et al. (2006), Crustal thinning between the Ethiopian and East African plateaus from modeling Rayleigh wave dispersion, *Geophysical Research Letters*, *33*(13).

Benoit, M. H., et al. (2006), Upper mantle P-wave speed variations beneath Ethiopia and the origin of the Afar hotspot, *Geology*, *34*(5), 329-332.

Berhe, S. M., et al. (1987), Geology, geochronology and geodynamic implications of the Cenozoic magmatic province in W and SE Ethiopia, *Journal of the Geological Society*, *144*, 213-226.

Bernstein, S., et al. (2006), Ultra-depleted, shallow cratonic mantle beneath West Greenland: dunitic xenoliths from Ubekendt Ejland, *Contributions to Mineralogy and Petrology*, *152*(3), 335-347.

Bertrand, H., et al. (2003), Implications of widespread high-mu volcanism on the Arabian Plate for Afar mantle plume and lithosphere composition, *Chemical Geology*, *198*(1-2), 47-61.

Betton, P. J., and L. Civetta (1984), Sr and Nd isotopic evidence for the heterogeneous nature and development of the mantle beneath Afar, Ethiopia, *Earth and Planetary Science Letters*, *71*(1), 59-70.

Beyth, M. (1974), Precambrian block-faulting, Ethiopia, *Geological Magazine*, *111*(5), 446-447.

Beyth, M. (1991), Smooth and rough propagation of spreading, southern Red Sea - Afar Depression, *Journal of African Earth Sciences*, *13*(2), 157-171.

Bilham, R., et al. (1999), Secular and tidal strain across the main Ethiopian rift, *Geophysical Research Letters*, *26*(18), 2789-2792.

Birck, J. L., and C. J. Allegre (1994), Contrasting Re-Os magmatic fractionation in planetary basalts, *Earth and Planetary Science Letters*, *124*(1-4), 139-148.

Bird, J. M., et al. (1999), Osmium and lead isotopes of rare Os-Ir-Ru minerals: derivation from the core-mantle boundary region?, *Earth and Planetary Science Letters*, *170*(1-2), 83-92.

Blake, S., and B. C. Bruno (2000), Modelling the emplacement of compound lava flows, *Earth and Planetary Science Letters*, *184*(1), 181-197.

Blandford, W. T. (1869), Geology of Ethiopia, *Journal of the Geological Society of London*, *25*, 401-406.

Blusztajn, J., et al. (1995), Trace element and isotopic characteristics of spinel peridotite xenoliths from Saudi Arabia, *Chemical Geology*, *123*(1-4), 53-65.

Boccaletti, M., et al. (1991), The Marda Fault: a remnant of an incipient aborted rift in the Palaeo-African Arabian plate, *Journal of Petroleum Geology*, *14*(1), 79-92.

Boccaletti, M., et al. (1998), Quaternary oblique extensional tectonics in the Ethiopian Rift (Horn of Africa), *Tectonophysics*, *287*(1-4), 97-116.

Boccaletti, M., et al. (1999), Plio-Quaternary volcanotectonic activity in the northern sector of the Main Ethiopian Rift: relationships with oblique rifting, *Journal of African Earth Sciences*, *29*(4), 679-698.

Bonatti, E., et al. (1984), Geology of the Red Sea transitional region (22° - 25° N), *Oceanologica Acta*, *7*(4), 385-398.

Bonatti, E. (1985), Punctiform initiation of sea-floor spreading in the Red Sea during transition from continental to an oceanic rift, *Nature*, *316*(6023), 33-37.

Bonavia, F. F., and J. Chorowicz (1992), Northward expulsion of the Pan-African of north-east Africa guided by a re-entrant zone of the Tanzania Craton, *Geology*, *20*(11), 1023-1026.

Bonavia, F. F., et al. (1995), Have wet and dry Precambrian crust largely governed Cenozoic intraplate magmatism from Arabia to East Africa, *Geophysical Research Letters*, *22*(17), 2337-2340.

Bondre, N. R., et al. (2004), Morphology and emplacement of flows from the Deccan Volcanic Province, India, *Bulletin of Volcanology*, *66*(1), 29-45.

Bonini, M., et al. (1997), Successive orthogonal and oblique extension episodes in a rift zone: laboratory experiments with application to the Ethiopian Rift, *Tectonics*, *16*(2), 347-362.

Bonini, M., et al. (2001), Dynamics of magma emplacement in centrifuge models of continental extension with implications for flank volcanism, *Tectonics*, *20*(6), 1053-1065.

Bonini, M., et al. (2005), Evolution of the Main Ethiopian Rift in the frame of Afar and Kenya rifts propagation, *Tectonics*, *24*(1).

Bosworth, W., et al. (1992), Integration of East African paleostress and present-day stress data: implications for continental stress-field dynamics, *Journal of Geophysical Research-Solid Earth*, *97*(B8), 11851-11865.

Bosworth, W. (1994), A model for the 3-dimensional evolution of continental rift basins, north-east Africa, *Geologische Rundschau*, *83*(4), 671-688.

Bosworth, W., and M. R. Strecker (1997), Stress field changes in the Afro-Arabian rift system during the Miocene to Recent period, *Tectonophysics*, *278*(1-4), 47-62.

Bosworth, W., et al. (2005), The Red Sea and Gulf of Aden basins, *Journal of African Earth Sciences*, *43*(1-3), 334-378.

Bowen, N. L. (1928), *The Evolution of the Igneous Rocks*, Princetown University Press.

Brandon, A. D., et al. (1998), Coupled ^{186}Os and ^{187}Os evidence for core-mantle interaction, *Science*, *280*(5369), 1570-1573.

Brandon, A. D., et al. (1999), ^{186}Os-^{187}Os systematics of Hawaiian picrites, *Earth and Planetary Science Letters*, *174*(1-2), 25-42.

Brandon, A. D., et al. (2000), ^{190}Pt-^{186}Os and ^{187}Re-^{187}Os systematics of abyssal peridotites, *Earth and Planetary Science Letters*, *177*(3-4), 319-335.

Brandon, A. D., et al. (2003), ^{186}Os-^{187}Os systematics of Gorgona Island komatiites: implications for early growth of the inner core, *Earth and Planetary Science Letters*, *206*(3-4), 411-426.

Brandon, A. D., et al. (2005), Platinum-Osmium isotope evolution of the Earth's mantle, *Geochimica et Cosmochimica Acta*, *69*(10), A392-A392.

Brandon, A. D., et al. (2006), Platinum-osmium isotope evolution of the Earth's mantle: Constraints from chondrites and Os-rich alloys, *Geochimica et Cosmochimica Acta*, *70*(8), 2093-2103.

Brandon, A. D., et al. (2007), ^{186}Os and ^{187}Os enrichments and high-$^{3}He/^{4}He$ sources in the Earth's mantle: Evidence from Icelandic picrites, *Geochimica et Cosmochimica Acta*, *71*, 4570-4591.

Branney, M. J., and P. Kokelaar (2003), Pyroclastic Density Currents and the Sedimentation of Ignimbrites, *Geological Society of London, Memoir 27*

Brazier, R. A., et al. (2008), Local magnitude scale for the Ethiopian Plateau, *Bulletin of the Seismological Society of America*, *98*(5), 2341-2348.

Brenan, J. M., et al. (2000), Diffusion of osmium in pyrrhotite and pyrite: implications for closure of the Re-Os isotopic system, *Earth and Planetary Science Letters*, *180*(3-4), 399-413.

Brenan, J. M., et al. (2005), An experimental study of the solubility and partitioning of iridium, osmium and gold between olivine and silicate melt, *Earth and Planetary Science Letters*, *237*(3-4), 855-872.

Brenan, J. M. (2008), Re-Os fractionation by sulfide melt-silicate melt partitioning: a new spin, *Chemical Geology*, *248*(3-4), 140-165.

Brewer, T. S., et al. (1992), Coats Land dolerites and the generation of Antarctic continental flood basalts, *Geological Society, London, Special Publications*, *68*(1), 185-208.

Bristow, J. W. (1984), Picritic rocks of the north Lebombo and south-east Zimbabwe, *Special Publication of the Geological Society of South Africa*, *13*, 105–123.

Brotzu, P., et al. (1981), Basaltic volcanism in the northern sector of the Main Ethiopian Rift, *Journal of Volcanology and Geothermal Research*, *10*(4), 365-382.

Brown, G. M., et al. (1957), Pyroxenes from the early and middle stages of fractionation of the Skaergaard intrusion, East Greenland *Mineral Magazine*, *31*, 511-543.

Brown, G., and I. Stephen (1959), A structural study of iddingsite from New South Wales, Australia, *American Mineralogist*, *44*, 251-260.

Brown, G. M., and E. A. Vincent (1963), Pyroxenes from the late stages of fractionation of the Skaergaard intrusion, East Greenland, *Journal of Petrology*, *4*(2), 175.

Brueckner, H. K., et al. (1988), Zabargad and the isotopic evolution of the sub-Red Sea mantle and crust, *Tectonophysics*, *150*(1-2), 163-176.

Brueckner, H. K., et al. (1995), A Pan-African origin and uplift for the gneisses and peridotites of Zabargad Island and Red Sea; a Nd, Sr, Pb and Os isotope study, *Journal of Geophysical Research-Solid Earth*, *100*(B11), 22283-22297.

Bryan, S., et al. (2002), Silicic volcanism: an undervalued component of large igneous provinces and volcanic rifted margins, in *Volcanic Rifted Margins*, edited by M. A. Menzies, et al., pp. 99–120, Geological Society of America.

Bryan, S. (2007), Silicic large igneous provinces, *Episodes*, *30*(1), 20-31.

Bryan, S. E., and R. E. Ernst (2008), Revised definition of large igneous provinces (LIPs), *Earth-Science Reviews*, *86*(1-4), 175-202.

Buck, W. R. (2004), The role of magma in the development of the Afro-Arabian Rift System, paper presented at East African Rift Systems: Geodynamics, Resources and Environment, Addis Ababa, Jun.

Buck, W. R. (2006), The role of magma in the development of the Afro-Arabian Rift System, *Afar Volcanic Province within the East African Rift System*, *259*, 43-54.

Buddington, A. F., and D. H. Lindsley (1964), Iron-Titanium Oxide Minerals and Synthetic Equivalents, *J. Petrology*, *5*(2), 310-357.

Bultitude, R. J., and D. H. Green (1971), Experimental study of crystal-liquid relationships at high pressures in olivine nephelinite and basanite compositions, *Journal of Petrology*, *12*, 121–147.

Burgi, P. Y., et al. (2002), Field temperature measurements at Erta'Ale Lava Lake, Ethiopia, *Bulletin of Volcanology*, *64*(7), 472-485.

Burton, K. W., et al. (1999), Osmium isotope disequilibrium between mantle minerals in a spinel-lherzolite, *Earth and Planetary Science Letters*, *172*(3-4), 311-322.

Burton, K. W., et al. (2002), The compatibility of rhenium and osmium in natural olivine and their behaviour during mantle melting and basalt genesis, *Earth and Planetary Science Letters*, *198*(1-2), PII S0012-0821X(0002)00518-00516.

Calais, E., et al. (2006), Kinematics of the East African Rift from GPS and earthquake slip vector data, *Afar Volcanic Province within the East African Rift System*, *259*, 9-22.

Camp, V. E., and M. J. Roobol (1989), The Arabian continental alkali basalt province: Part 1. Evolution of Harrat Rahat, Kingdom of Saudi Arabia, *Geological Society of America Bulletin*, *101*(1), 71-95.

Camp, V. E., and M. J. Roobol (1991), Topographic and volcanic asymmetry around the Red Sea: constraints on rift models - comment, *Tectonics*, *10*(3), 649-652.

Camp, V. E., et al. (1991), The Arabian continental alkali basalt province: Part 2. Evolution of Harrats Khaybar, Ithnayn and Kura, Kingdom of Saudi Arabia, *Geological Society of America Bulletin*, *103*(3), 363-391.

Camp, V. E., et al. (1992), The Arabian continental alkali basalt province: Part 3. Evolution of Harrat Kishb, Kingdom of Saudi Arabia, *Geological Society of America Bulletin*, *104*(4), 379-396.

Campbell, I. H., and R. W. Griffiths (1990), Implications of mantle plume structure for the evolution of flood basalts, *Earth and Planetary Science Letters*, *99*(1-2), 79-93.

Campbell, I. H., et al. (1992), Synchronism of the Siberian Traps and the Permo-Triassic boundary, *Science*, *258*(5089), 1760-1763.

Campbell, I. H. (1998), The mantle's chemical structure: insights from the melting products of mantle plumes, in *The Earth's Mantle: Composition, Structure and Evolution*, edited by I. N. S. Jackson, pp. 259-310, Cambridge University Press.

Campbell, I. H. (2005), Large igneous provinces and the mantle plume hypothesis, *Elements*, *1*(5), 265-269.

Campbell, I. H., and G. F. Davies (2006), Do mantle plumes exist?, *Episodes*, *29*(3), 162-168.

Canil, D., and H. S. C. O'Neill (1996), Distribution of ferric iron in some upper-mantle assemblages, *Journal of Petrology*, *37*(3), 609-635.

Carmichael, I. S. E. (1967), The iron–titanium oxides of salic volcanic rocks and their associated ferromagnesian silicates, *Contributions to Mineralogy and Petrology*, *14*, 36–64.

Caroff, M., et al. (1997), From alkali basalt to phonolite in hand-size samples: vapor-differentiation effects in the Bouzentes lava flow (Cantal, France), *Journal of Volcanology and Geothermal Research*, *79*(1-2), 47-61.

Caroff, M., et al. (2000), Segregation structures in vapor-differentiated basaltic flows, *Bulletin of Volcanology*, *62*(3), 171-187.

Casey, M., et al. (2006), Strain accommodation in transitional rifts: extension by magma intrusion and faulting in Ethiopian rift magmatic segments, *Afar Volcanic Province within the East African Rift System*, *259*, 143-163.

Chalmers, J. A., et al. (1995), Widespread Paleocene volcanism around the northern North-Atlantic and Labrador Sea – evidence for a large, hot, early plume-head, *Journal of the Geological Society*, *152*, 965-969.

Chase, C. G. (1978), Plate kinematics: Americas, East Africa and the rest of the World, *Earth and Planetary Science Letters*, *37*(3), 355-368.

Chauvel, C., et al. (1992), HIMU - EM: The French-Polynesian connection, *Earth and Planetary Science Letters*, *110*(1-4), 99-119.

Chazot, G., et al. (1991), Tertiary magmatism in South Yemen and the Red Sea rifting - evolution of transistional magmas controlled by fractional crystallisation and crustal contamination, *Comptes Rendus De L Academie Des Sciences Serie Ii*, *312*(3), 249-255.

Chazot, G., and H. Bertrand (1993), Mantle sources and magma-crust interactionsduring early Red Sea - Gulf of Aden rifting in southern Yemen - elemental and Sr, Nd and Pb isotope evidence, *Journal of Geophysical Research-Solid Earth*, *98*(B2), 1819-1835.

Chazot, G., and H. Bertrand (1995), Genesis of silicic magmas during Tertiary continental rifting in Yemen, *Lithos*, *36*(2), 69-83.

Chazot, G., et al. (1997), Oxygen isotopic composition of hydrous and anhydrous mantle peridotites, *Geochimica et Cosmochimica Acta*, *61*(1), 161-169.

Chernet, T., et al. (1998), New age constraints on the timing of volcanism and tectonism in the northern Main Ethiopian Rift-southern Afar transition zone (Ethiopia), *Journal of Volcanology and Geothermal Research*, *80*(3-4), 267-280.

Chernosky, J. V., et al. (1988), Stability, phase-relations and thermodynamic properties of chlorite and serpentine group minerals, *Reviews in Mineralogy*, *19*, 295-346.

Chessex, R., et al. (1975), Evolution of the Ali Sabieh (T.F.A.I.) in the light of K/Ar age determinations, in *Afar Depression of Ethiopia*, edited by A. Pilger and A. Rosler, pp. 221-227, Schweizerbart, Stuttgart.

Chiesa, S., et al. (1989), The Yemen trap series - genesis and evolution of a continental flood basalt province, *Journal of Volcanology and Geothermal Research*, *36*(4), 337-350.

Chorowicz, J., et al. (1994), Northwest to north-northwest extension direction in the Ethiopian rift deduced from the orientation of extension structures and fault-slip analysis, *Geological Society of America Bulletin*, *106*(12), 1560-1570.

Chorowicz, J., et al. (1998), The Tana basin, Ethiopia: intra-plateau uplift, rifting and subsidence, *Tectonophysics*, *295*(3-4), 351-367.

Chorowicz, J., et al. (1999), Left-lateral strike-slip tectonics and gravity induced individualisation of wide continental blocks in the western Afar margin, *Eclogae Geologicae Helvetiae*, *92*(1), 149-158.

Chorowicz, J. (2005), The East African rift system, *Journal of African Earth Sciences*, *43*(1-3), 379-410.

Christiansen, R. L., et al. (2002), Upper-mantle origin of the Yellowstone hotspot, *Geological Society of America Bulletin*, *114*(10), 1245-1256.

Chu, D. H., and R. G. Gordon (1999), Evidence for motion between Nubia and Somalia along the southwest Indian ridge, *Nature*, *398*(6722), 64-67.

Civetta, L., et al. (1975), Structural meaning of east-central Afar volcanism, Ethiopia, *Journal of Geology*, *83*(3), 363-373.

Clarke, D. B. (1970), Tertiary basalts of Baffin Bay: Possible primary magma from the Mantle, *Contributions to Mineralogy and Petrology*, *25*(3), 203-224.

Clarke, D. B., and A. K. Pedersen (1976), Tertiary volcanic province of West Greenland, in *Geology of Greenland*, edited by A. Escher and W. S. Watt, pp. 365–387, Geological Survey of Greenland.

Class, C., et al. (1998), The process of plume-lithosphere interactions in the ocean basins: the case of Grande Comore, *Journal of Petrology*, *39*(5), 881-903.

Class, C., and S. L. Goldstein (2005), Evolution of helium isotopes in the Earth's mantle, *Nature*, *436*(7054), 1107-1112.

Class, C., et al. (2005), Grand Comore Island: A well-constrained "low $^{3}He/^{4}He$" mantle plume, *Earth and Planetary Science Letters*, *233*(3-4), 391-409.

Coblentz, D. D., and M. Sandiford (1994), Tectonic stresses in the African plate: constraints on the ambient lithospheric stress state, *Geology*, *22*(9), 831-834.

Coffin, M. F., and O. Eldholm (1992), Volcanism and continental break-up; a global compilation of large igneous provinces, in *Magmatism and the causes of continetal break-up*, edited by B. C. Storey, et al., pp. 17 - 30, The Geological Society of London.

Coffin, M. F., and O. Eldholm (1994), Large igneous provinces: crustal structure, dimensions, and external consequences, *Reviews of Geophysics*, *32*(1), 1-36.

Coffin, M. F., and O. Eldholm (Eds.) (2001), *Large igneous provinces: progenitors of some ophiolites?*, 59-70 pp.

Cohen, R. S., et al. (1984), Isotope geochemistry of xenoliths from East Africa: implications for development of mantle reservoirs and their interaction, *Earth and Planetary Science Letters*, *68*(2), 209-220.

Coleman, R. G., et al. (1983), Cenozoic volcanic rocks of Saudi Arabia, U.S. Geological Survey

Coleman, R. G., and A. V. McGuire (1988), Magma systems related to the opening of the Red Sea, *Tectonophysics*, *150*(1-2), 77-100.

Coleman, R. G., et al. (1992), A-type granite and the Red Sea opening, *Tectonophysics*, *204*(1-2), 27-40.

Collet, B., et al. (1999), Altimetric anomalies in the Afro-Arab zone, *Eclogae Geologicae Helvetiae*, *92*(3), 275-284.

Collet, B., et al. (2000), Orientation of absolute African plate motion revealed by tomomorphometric analysis of the Ethiopian dome, *Geology*, *28*(12), 1147-1149.

Conticelli, C., et al. (1999), Petrology and geochemistry of ultramafic xenoliths and host lavas from the Ethiopian Volcanic Province; an insight into the upper mantle under eastern Africa, *Acta Vulcanologica*, *11*, 143-159

Cordery, M. J., et al. (1997), Genesis of flood basalts from eclogite-bearing mantle plumes, *Journal of Geophysical Research-Solid Earth*, *102*(B9), 20179-20197.

Cornwell, D. G., et al. (2004), Northern Main Ethiopian Rift crustal structure from new high-precision gravity data, paper presented at International Conference on East African Rift Systems - Geodynamics, Resources and Environment, Addis Ababa, ETHIOPIA, Jun.

Cornwell, D. G., et al. (2006), Northern Main Ethiopian Rift crustal structure from new high-precision gravity data, *Afar Volcanic Province within the East African Rift System*, *259*, 307-321.

Corti, G., et al. (2001), Centrifuge models simulating magma emplacement during oblique rifting, *Journal of Geodynamics*, *31*(5), 557-576.

Corti, G. (2008), Control of rift obliquity on the evolution and segmentation of the main Ethiopian rift, *Nature Geoscience*, *1*(4), 258-262.

Coulie, E., et al. (2003), Comparative K-Ar and Ar/Ar dating of Ethiopian and Yemenite Oligocene volcanism: implications for timing and duration of the Ethiopian traps, *Earth and Planetary Science Letters*, *206*(3-4), 477-492.

Courtillot, V., et al. (1984), Episodic spreading and rift propagation: new paleogamgnetic and geochronologic data from the Afar nascent passive margin, *Journal of Geophysical Research*, *89*(NB5), 3315-3333.

Courtillot, V., et al. (1988), Deccan flood basalts and the Cretaceous Tertiary boundary, *Nature*, *333*(6176), 843-846.

Courtillot, V., et al. (1999), On causal links between flood basalts and continental breakup, *Earth and Planetary Science Letters*, *166*(3-4), 177-195.

Courtillot, V., et al. (2003), Three distinct types of hotspots in the Earth's mantle, *Earth and Planetary Science Letters*, *205*(3-4), 295-308.

Courtillot, V., and P. Olson (2007), Mantle plumes link magnetic superchrons to phanerozoic mass depletion events, *Earth and Planetary Science Letters*, *260*(3-4), 495-504.

Cox, K. G., et al. (1965), Geology of the Nuanetsi igneous province, *Philosophical Transactions of the Royal Society of London Series a-Mathematical and Physical Sciences*, *257*(1078), 71-&.

Cox, K. G., et al. (1979), *The Interpretation of Igneous Rocks*, George Allen & Unwin.

Cox, K. G. (1980), A model for flood vulcanism, *Journal of Petrology*, *21*(4), 629-650.

Cox, K. G., et al. (1984), Petrogenesis of the basic rocks of the Lebombo, in *Petrogenesis of the Volcanic Rocks of the Karoo Province*, edited by A. J. Erlank, pp. 149–169, Geological Society of South Africa.

Cox, K. G., and C. J. Hawkesworth (1984), Relative contribution of crust and mantle to flood-basalt magmatism, Mahabaleshwar area, Deccan traps, *Philosophical Transactions of the Royal Society of London Series a-Mathematical Physical and Engineering Sciences*, *310*(1514), 627-641.

Cox, K. G., and C. J. Hawkesworth (1985), Geochemical stratigraphy of the Deccan traps at Mahabaleshwar, Western Ghats, India, with implications for open system magmatic processes, *Journal of Petrology*, *26*(2), 355-377.

Cox, K. G., and C. W. Devey (1987), Fractionation processes in Deccan Traps magmas - comments, *Journal of Petrology*, *28*(1), 235-238.

Cox, K. G., and C. Mitchell (1988), Importance of crystal settling in the differentiation of Deccan trap basaltic magmas, *Nature*, *333*(6172), 447-449.

Craig, H., and J. E. Lupton (1978), Helium isotope variations: evidence for mantle plumes at Yellowstone, Kilauea and the Ethiopian Rift Valley, *Transactions-American Geophysical Union*, *59*(12), 1194-1194.

Creaser, R. A., et al. (1991), Negative thermal ion mass spectrometry of osmium, rhenium and irridium, *Geochimica Et Cosmochimica Acta*, *55*(1), 397-401.

Crough, S. T. (1983), Hotspot swells, *Annual Review of Earth and Planetary Sciences*, *11*, 165-193.

Cserepes, L., and D. A. Yuen (2000), On the possibility of a second kind of mantle plume, *Earth and Planetary Science Letters*, *183*(1-2), 61-71.

d'Acremont, E., et al. (2005), Structure and evolution of the eastern Gulf of Aden conjugate margins from seismic reflection data, *Geophysical Journal International*, *160*(3), 869-890.

d'Acremont, E., et al. (2006), Structure and evolution of the eastern Gulf of Aden: insights from magnetic and gravity data (Encens-Sheba MD117 cruise), *Geophysical Journal International*, *165*(3), 786-803.

Daly, E., et al. (2008), Crustal tomographic imaging of a transitional continental rift: the Ethiopian rift, *Geophysical Journal International*, *172*(3), 1033-1048.

Darling, W. G., et al. (1995), The origin of hydrothermal and other gases in the Kenya Rift Valley, *Geochimica et Cosmochimica Acta*, *59*(12), 2501-2512.

Dauteuil, O., et al. (2001), Propagation of an oblique spreading centre: the western Gulf of Aden, *Tectonophysics*, *332*(4), 423.

Davidson, A., and D. C. Rex (1980), Age of volcanism and rifting in south-western Ethiopia, *Nature*, *283*(5748), 657-658.

Davidson, A. (1983), Reconnaissance geology and geochemistry of parts of Illubabor, Kefa, Gemu Gofa and Sidamo, Ethiopia, *Ministry of Mines and Energy, Ethiopian Institute of Geological Surveys, Bulletin*, *2*.

Davidson, P. M., and D. H. Lindsley (1989), Thermodynamic analysis of pyroxene-olivine-quartz equilibria in the system CaO-MgO-FeO-SiO_2, *American Mineralogist*, *74*(1-2), 18-30.

Davis, P. M., and P. D. Slack (2002), The uppermost mantle beneath the Kenya dome and relation to melting, rifting and uplift in East Africa, *Geophysical Research Letters*, *29*(7).

Davison, I., et al. (1994), Geological evolution of the south-eastern Red Sea rift margin, Republic of Yemen, *Geological Society of America Bulletin*, *106*(11), 1474-1493.

Dawson, J. B., et al. (1997), Ultrabasic potassic low-volume magmatism and continental rifting in north-central Tanzania: association with enhanced heat flow, *Geologiya I Geofizika*, *38*(1), 67-77.

de Souza, C. R., and S. A. Drury (1998), A neoproterozoic supra-subduction terrane in northern Eritrea, NE Africa, *Journal of the Geological Society*, *155*, 551-566.

Debayle, E., et al. (2001), Seismic evidence for a deeply rooted low-velocity anomaly in the upper mantle beneath the northeastern Afro/Arabian continent, *Earth and Planetary Science Letters*, *193*(3-4), 423-436.

Deer, W. A., et al. (1999), *An introduction to the rock-forming minerals*, 2nd ed., Longman.

Deller, M. E. A. (2006), Facies discrimination in laterites using Landsat Thematic Mapper, ASTER and ALI data: examples from Eritrea and Arabia, *International Journal of Remote Sensing*, *27*(12), 2389-2409.

Delvigne, J., et al. (1979), Olivines, their pseudomorphs and secondary products, *Pedologie*, *29*, 247-309.

DeMets, C., et al. (1990), Current plate motions, *Geophysical Journal International*, *101*(2), 425-478.

DeMets, C., et al. (1994a), Effect of recent revisions to the geomagnetic reversal time-scale on estimates of current plate motion, *Geophysical Research Letters*, *21*(20), 2191-2194.

DeMets, C., et al. (1994b), Location of the Africa-Austalia-India triple junction and motion between the Australian and Indian plates - results from an aeromagnetic investigation of the Central Indian and Carlsberg Ridges, *Geophysical Journal International*, *119*(3), 893-930.

Deniel, C., et al. (1994), Temporal evolution of mantle sources during continental rifting - the volcanism of Djibouti (Afar), *Journal of Geophysical Research-Solid Earth*, *99*(B2), 2853-2869.

Deniel, C., et al. (2000), Crustal control in the genesis of Plio-Quaternary bimodal magmatism of the Main Ethiopian Rift: geochemical and isotopic (Sr, Nd, Pb) evidence - reply, *Chemical Geology*, *168*(1-2), 5-7.

Desissa, M. (2004), Stratigraphy, morphology and structure of the Geba Rift basin, Witete Block (southwestern Ethiopia) from high frequency magneto-telluric data, paper presented at East African Rift Systems: Geodynamics, Resources and Environment, Addis Ababa.

Dixon, T. H., et al. (1989), Topographic and volcanic asymmetry around the Red Sea: constraints on rift models, *Tectonics*, *8*(6), 1193-1216.

Dixon, E. (2000), Noble gas geochemistry of Iceland basalts (unpublished PhD thesis), The Australian National University, Canberra.

Doglioni, C., et al. (2003), Rift asymmetry and continental uplift, *Tectonics*, *22*(3).

Donaldson, C. H. (1976), Experimental investigation of olivine morphology, *Contributions to Mineralogy and Petrology*, *57*(2), 187-213.

Drever, H. I., and R. Johnston (1957), Crystal growth of forsteritic olivine in magmas and melts, *Transactions of the Royal Society, Edinburgh*, *63*, 289-315.

Droop, G. T. R. (1987), A general equation for estimating Fe3+ concentrations in ferromagnesian silicates and oxides from microprobe analyses using stoichiometric criteria, *Mineralogical Magazine*, *51*(361), 431-435.

Drury, S. A., et al. (1994), Structures related to Red Sea evolution in northern Eritrea, *Tectonics*, *13*(6), 1371-1380.

Drury, S. A., et al. (2006), A comment on "Geomorphic development of the escarpment of the Eritrean margin, southern Red Sea from combined apatite fission-track and (U-Th)/He thermochronometry" by Balestrieri, M.L. et al. [Earth Planet. Sci. Lett. 231 (2005) 97-110], *Earth and Planetary Science Letters*, *242*(3-4), 428-432.

Dugda, M. T., et al. (2005), Crustal structure in Ethiopia and Kenya from receiver function analysis: Implications for rift development in eastern Africa, *Journal of Geophysical Research-Solid Earth*, *110*(B1).

Dugda, M. T., and A. A. Nyblade (2006), New constraints on crustal structure in eastern Afar from the analysis of receiver functions and surface wave dispersion in Djibouti, *Afar Volcanic Province within the East African Rift System*, *259*, 239-251.

Dugda, M. T., et al. (2007), Thin lithosphere beneath the Ethiopian plateau revealed by a joint inversion of Rayleigh wave group velocities and receiver functions, *Journal of Geophysical Research-Solid Earth*, *112*(B8).

Duncan, A. R., et al. (1984), Regional geochemistry of the Karoo Igneous Province, in *Petrogenesis of the volcanic rocks of the Karoo Province*, edited by A. J. Erlank, pp. 355-388, Geological Society of South Africa.

Duncan, R. A., and D. G. Pyle (1988), Rapid eruption of the Deccan flood basalts at the Cretaceous/Tertiary boundary, *Nature*, *333*, 841 - 843.

Dyar, M. D., et al. (1996), Crystal chemistry of Fe^{3+},H and D/H in mantle-derived augite from Dish Hill: implications for alteration during transport, in *Mineral spectroscopy: a tribute to Roger G. Burns*, edited by M. D. Dyar, et al., pp. 273-289, The Geochemical Society.

Eagles, G., et al. (2002), Kinematics of the Danakil microplate, *Earth and Planetary Science Letters*, *203*(2).

Ebinger, C. J., et al. (1993), Late Eocene: recent volcanism and faulting in the southern Main Ethiopian Rift, *Journal of the Geological Society*, *150*, 99-108.

Ebinger, C. J., and A. Ibrahim (1994), Multiple episodes of rifting in Central and East Africa - a re-evaluation of gravity data, *Geologische Rundschau*, *83*(4), 689-702.

Ebinger, C. J., and N. J. Hayward (1996), Soft plates and hot spots: views from Afar, *Journal of Geophysical Research-Solid Earth*, *101*(B10), 21859-21876.

Ebinger, C., et al. (1997), Rifting Archaean lithosphere: the Eyasi-Manyara-Natron rifts, East Africa, *Journal of the Geological Society*, *154*, 947-960.

Ebinger, C. J., et al. (2000), Rift deflection, migration, and propagation: linkage of the Ethiopian and eastern rifts, Africa, *Geological Society of America Bulletin*, *112*(2), 163-176.

Ebinger, C. J., and M. Casey (2001), Continental breakup in magmatic provinces: an Ethiopian example, *Geology*, *29*(6), 527-530.

Ebinger, C., et al. (2004), Incipient continental breakup in the northern Ethiopian rift: no need for detachment faults, paper presented at The East African Rift System: Geodynamics, Resources and Environment, Addis Ababa.

Ebinger, C. J., et al. (2008), Capturing magma intrusion and faulting processes during continental rupture: seismicity of the Dabbahu (Afar) rift, *Geophysical Journal International*, *174*(3), 1138-1152.

Eggins, S. M., et al. (1997), A simple method for the precise determination of >=40 trace elements in geological samples by ICPMS using enriched isotope internal standardisation, *Chemical Geology*, *134*(4), 311-326.

Eggleton, R. A. (1984), Formation of iddingsite rims on olivine: a transmission electron-microscope study, *Clays and Clay Minerals*, *32*(1), 1-11.

Eissen, J. P., et al. (1989), Petrology and geochemistry of basalts from the Red Sea axial rift at 18° north, *Journal of Petrology*, *30*(4), 791-839.

Ellam, R. M. (1992), Lithospheric thickness as a control on basalt geochemistry, *Geology*, *20*(2), 153-156.

Ellam, R. M., et al. (1992), Evidence from Re-Os isotopes for plume-lithosphere mixing in Karoo flood-basalt genesis, *Nature*, *359*(6397), 718-721.

Ellam, R. M., and F. M. Stuart (2004), Coherent He-Nd-Sr isotope trends in high $^{3}He/^{4}He$ basalts: implications for a common reservoir, mantle heterogeneity and convection, *Earth and Planetary Science Letters*, *228*(3-4), 511-523.

Erlank, A. J., et al. (1984), Geochemistry and petrogenesis of the Etendeka volcanic rocks from SWA, Namibia, in *Petrogenesis of the Volcanic Rocks of the Karoo Province*, edited by A. J. Erlank, pp. 195-245, Geological Society of South Africa.

Ernst, R. E., and K. L. Buchan (1997), Giant radiating dyke swarms: their use in identifying pre-Mesozoic large igneous provinces and mantle plumes, in *Large Igneous Provinces: Continental, Oceanic, and Planetary Volcanism*, edited by J. Mahoney and M. Coffin, pp. 297- 333, American Geophysical Union.

Ernst, R. E., and K. L. Buchan (Eds.) (2001), *Large mafic magmatic events through time and links to mantle plume heads*, 483-575 pp.

Ernst, R. E., and K. L. Buchan (2002), Maximum size and distribution in time and space of mantle plumes: evidence from large igneous provinces (vol 34, pg 309, 2002), *Journal of Geodynamics*, *34*(5), 711-714.

Ernst, R. E., and K. L. Buchan (2003), Recognizing mantle plumes in the geological record, *Annual Review of Earth and Planetary Sciences*, *31*, 469-523.

Ernst, R. E. (2007), Mafic-ultramafic Large Igneous Provinces (LIPs): Importance of the pre-mesozoic record, *Episodes*, *30*(2), 108-114.

Esser, B. K., and K. K. Turekian (1993), The osmium isotopic composition of continental crust, *Geochimica et Cosmochimica Acta*, *57*(13), 3093-3104.

Ewart, A., et al. (1998a), Etendeka volcanism of the Goboboseb Mountains and Messum Igneous Complex, Namibia. Part I: geochemical evidence of early cretaceous tristan plume melts and the role of crustal contamination in the Parana-Etendeka CFB, *Journal of Petrology*, *39*(2), 191-225.

Ewart, A., et al. (1998b), Etendeka volcanism of the Goboboseb Mountains and Messum Igneous Complex, Namibia. Part II: voluminous quartz latite volcanism of the Awahab Magma System, *Journal of Petrology*, *39*(2), 227-253.

Ewart, A., et al. (2004a), Petrology and geochemistry of early cretaceous bimodal continental flood volcanism of the NW Etendeka, Namibia. Part 1: Introduction, mafic lavas and re-evaluation of mantle source components, *Journal of Petrology*, *45*(1), 59-105.

Ewart, A., et al. (2004b), Petrology and geochemistry of early cretaceous bimodal continental flood volcanism of the NW Etendeka, Namibia. Part 2: Characteristics and petrogenesis of the high-Ti latite and high-Ti and low-Ti voluminous quartz latite eruptives, *Journal of Petrology*, *45*(1), 107-138.

Falloon, T. J., et al. (2007), The application of olivine geothermometry to infer crystallization temperatures of parental liquids: implications for the temperature of MORB magmas, *Chemical Geology*, *241*(3-4), 207-233.

Fantozzi, P. L. (1996), Transition from continental to oceanic rifting in the Gulf of Aden: Structural evidence from field mapping in Somalia and Yemen, *Tectonophysics*, *259*(4), 285-311.

Farley, K. A., et al. (1992), Binary mixing of enriched and undegassed (primitive-questionable) mantle components (He, Sr, Nd) in Samoan lavas, *Earth and Planetary Science Letters*, *111*(1), 183-199.

Farley, K. A., and E. Neroda (1998), Noble gases in the Earth's mantle, *Annual Review of Earth and Planetary Sciences*, *26*, 189-218.

Farnetani, C. G., and M. A. Richards (1994), Numerical investigations of the mantle plume initiation model for flood basalt events, *Journal of Geophysical Research-Solid Earth*, *99*(B7), 13813-13833.

Faure, G. (1986), *Principles of isotope geology. 2nd ed.*, Wiley, New York.

Favela, J., and D. L. Anderson (2000), Extensional tectonics and global volcanism, *Problems in Geophysics for the New Millennium*, 463-498.

Fei, Y. (2001), Phase transformations in the Earth's mantle and mantle heterogeneity, paper presented at Mantle materials, processes and products (VMSG Annual Conference), Mineralogical Society, Durham.

Ferrando, S., et al. (2008), Composition and thermal structure of the lithosphere beneath the Ethiopian plateau: evidence from mantle xenoliths in basanites, Injibara, Lake Tana Province, *Mineralogy and Petrology*, *93*(1-2), 47-78.

Fitton, J. G. (1997), X-ray fluorescence spectrometry, in *Modern analytical geochemistry*, edited by R. Gill, pp. 87-115, Longman.

Fitton, J. G., et al. (1997), Thermal and chemical structure of the Iceland plume, *Earth and Planetary Science Letters*, *153*(3-4), 197-208.

Fodor, R. V., et al. (1998), Isotopic and trace-element indications of lithospheric and asthenospheric components in Tertiary alkalic basalts, northeastern Brazil, *Lithos*, *43*(4), 197-217.

Ford, C. E., et al. (1983), Olivine liquid equilibria - temperature, pressure and composition dependence of the crystal-liquid cation partition coefficients for Mg, Fe^{2+}, Ca and Mn, *Journal of Petrology*, *24*(3), 256-265.

Foulger, G. (2002), Plumes, or plate tectonic processes?, *Astronomy & Geophysics*, *43*(6), 19-23.

Foulger, G. R., and D. L. Anderson (2005), A cool model for the Iceland hotspot, *Journal of Volcanology and Geothermal Research*, *141*(1-2), 1-22.

Foulger, G. R., et al. (2005a), A source for Icelandic magmas in remelted Iapetus crust, *Journal of Volcanology and Geothermal Research*, *141*(1-2), 23-44.

Foulger, G. R., et al. (Eds.) (2005b), *Plates, Plumes, And Paradigms*, Geological Society of America.

Foulger, G. R., and D. M. Jurdy (2007), *Plates, Plumes and Planetary Processes*, Geological Society of America.

Fournier, M., et al. (2001), Reappraisal of the Arabia-India-Somalia triple junction kinematics, *Earth and Planetary Science Letters*, *189*(3-4), 103-114.

Fournier, M., et al. (2007), Segmentation and along-strike asymmetry of the passive margin in Socotra, eastern Gulf of Aden: are they controlled by detachment faults?, *Geochemistry Geophysics Geosystems*, *8*.

Fournier, M., and C. Petit (2007), Oblique rifting at oceanic ridges: Relationship between spreading and stretching directions from earthquake focal mechanisms, *Journal of Structural Geology*, *29*(2), 201-208.

Fram, M. S., and C. E. Lesher (1997), Generation and polybaric differentiation of East Greenland early tertiary flood basalts, *Journal of Petrology*, *38*(2), 231-275.

Francis, D. (1985), The Baffin Bay lavas and the value of picrites as analogues of primary magmas, *Contributions to Mineralogy and Petrology*, *89*(2-3), 144-154.

Francis, D. (1995), The implications of picritic lavas for the mantle sources of terrestrial volcanism, *Lithos*, *34*(1-3), 89-105.

Franz, G., et al. (1999), Plume related alkaline magmatism in central Africa - the Meidob Hills (W Sudan), *Chemical Geology*, *157*(1-2), 27-47.

Frost, B. R., and C. Ballhaus (1998), Comment on "Constraints on the origin of the oxidation state of mantle overlying subduction zones: An example from Simcoe, Washington, USA", *Geochimica et Cosmochimica Acta*, *62*(2), 329-331.

Fuchs, K. (1997), Synopsis SFB 108 - stress and stress release in the lithosphere, *Tectonophysics*, *275*(1-3), 1-13.

Fujimaki, H., et al. (1984), Partition coefficients of Hf, Zr and REE between phenocrysts and groundmasses: proceedings of the fourteenth lunar and planetary science conference, Part 2, *Journal of Geophysical Research*, *89*, Supplement B662-B672.

Furgal, S. A., and N. J. McMillan (2001), Magmatic iddingsite: changes in H2O in magma chambers prior to eruption, paper presented at 2001 Annual National Meeting, Geological Society of America, Boston, Massachusetts

Furman, T., et al. (2004a), Heads and tails: 30 million years of Afar plume, paper presented at East African Rift Systems: Geodynamics, Resources and Environment, Addis Ababa, Jun.

Furman, T., et al. (2004b), East African Rift System (EARS) plume structure: insights from quaternary mafic lavas of Turkana, Kenya, *Journal of Petrology*, *45*(5), 1069-1088.

Furman, T., et al. (2006), Heads and tails: 30 million years of Afar plume, *Afar Volcanic Province within the East African Rift System*, *259*, 95-119.

Furman, T., et al. (2006), Tertiary mafic lavas of Turkana, Kenya: Constraints on East African plume structure and the occurrence of high-mu volcanism in Africa, *Journal of Petrology*, *47*(6), 1221-1244.

Furman, T. (2007), Geochemistry of East African Rift Basalts: an overview, *Journal of African Earth Sciences*, *48*, 147-160.

Gaetani, G. A., et al. (1998), MELTS, *Science*, *282*(5395), 1834-1835.

Gangopadhyay, A., et al. (2005), Re-Os systematics of komatiites and komatiitic basalts at Dundonald Beach, Ontario, Canada: evidence for a complex alteration history and implications of a late-Archean chondritic mantle source, *Geochimica et Cosmochimica Acta*, *69*(21), 5087-5098.

Garcia, M. O., et al. (1995), Olivine-rich submarine basalts from the southwest rift zone of Mauna Loa Volcano: implications for magmatic processes and geochemical evolution, *Geophysical Monograph, American Geophysical Union*, *92*, 219–239.

Garcia, M. O. (1996), Petrography and olivine and glass chemistry of lavas from the Hawaii Scientific Drilling Project, *Journal of Geophysical Research-Solid Earth*, *101*(B5), 11701-11713.

Garfunkel, Z., and M. Beyth (2006), Constraints on the structural development of Afar imposed by the kinematics of the major surrounding plates, *Afar Volcanic Province within the East African Rift System*, *259*, 23-42.

Garland, C. R. (1974), Precambrian block-faulting, Ethiopia, *Geological Magazine*, *111*(5), 447-448.

Gashawbeza, E. M., et al. (2004a), Shear-wave splitting in Ethiopia: Precambrian mantle anisotropy slightly modeified by Neogene rifting, paper presented at East African Rift Systems: Geodynamics, Resources and Environment, Addis Ababa.

Gashawbeza, E. M., et al. (2004b), Shear-wave splitting in Ethiopia: Precambrian mantle anisotropy locally modified by Neogene rifting, *Geophysical Research Letters*, *31*(18).

Gasparon, M., et al. (1993), Genesis of the Pliocene to Recent bimodal mafic-felsic volcanism in the Debre Zeyt area, Central Ethiopia: volcanological and geochemical connstraints, *Journal of African Earth Sciences*, *17*(2), 145-165.

Gass, I. G. (1970), Evolution of volcanism in junction area of Red Sea, Gulf of Aden and Ethiopian rifts, *Philosophical Transactions of the Royal Society of London Series a-Mathematical and Physical Sciences*, *267*(1181), 369-&.

Gaulier, J. M., and P. Huchon (1991), Tectonic evolution of Afar triple junction, *Bulletin De La Societe Geologique De France*, *162*(3), 451-464.

George, R. (1997), Thermal and tectonic controls on magmatism in the Ethiopian Province (unpublished PhD thesis), The Open University, Milton Keynes.

George, R., et al. (1998), Earliest magmatism in Ethiopia: evidence for two mantle plumes in one flood basalt province, *Geology*, *26*(10), 923-926.

George, R. M., and N. W. Rogers (2002), Plume dynamics beneath the African plate inferred from the geochemistry of the Tertiary basalts of southern Ethiopia, *Contributions to Mineralogy and Petrology*, *144*(3), 286-304.

Ghebreab, W. (1998), Tectonics of the Red Sea region reassessed, *Earth-Science Reviews*, *45*(1-2), 1-44.

Ghebreab, W., and C. J. Talbot (2000), Red Sea extension influenced by Pan-African tectonic grain in eastern Eritrea, *Journal of Structural Geology*, *22*(7), 931-946.

Ghebreab, W., et al. (2002), Constraints for timing of extensional tectonics in the western margin of the Red Sea in Eritrea, *Earth and Planetary Science Letters*, *200*(1-2).

Ghiorso, M. S., and R. O. Sack (1995), Chemical mass-transfer in magmatic processes IV. A revised and internally consistent thermo-dynamic model for the intepolation and extrapolation of liquid-solid equilibria in magmatic systems at elevated temperatures and pressures, *Contributions to Mineralogy and Petrology*, *119*(2-3), 197-212.

Gibson, S. A., et al. (1995), High-Ti and low-Ti mafic potassic magmas: key to plume-lithosphere interactions and continental flood-basalt genesis, *Earth and Planetary Science Letters*, *136*(3-4), 149-165.

Gibson, S. A., et al. (1996), High-Ti and low-Ti mafic potassic magmas: key to plume-lithosphere interactions and continental flood-basalt genesis (vol 136, pg 149, 1995), *Earth and Planetary Science Letters*, *141*(1-4), 325-341.

Gibson, S. A., et al. (1997), Late Cretaceous rift-related upwelling and melting of the Trindade starting mantle plume head beneath western Brazil, *Contributions to Mineralogy and Petrology*, *126*(3), 303-314.

Gibson, S. A., et al. (1999), The limited extent of plume-lithosphere interactions during continental flood-basalt genesis: geochemical evidence from Cretaceous magmatism in southern Brazil, *Contributions to Mineralogy and Petrology*, *137*(1-2), 147-169.

Gibson, S. A., et al. (2000), Ferropicrites: geochemical evidence for Fe-rich streaks in upwelling mantle plumes, *Earth and Planetary Science Letters*, *174*(3-4), 355-374.

Gibson, S. A. (2002), Major element heterogeneity in Archean to Recent mantle plume starting-heads, *Earth and Planetary Science Letters*, *195*(1-2), 59-74.

Gibson, S. A., et al. (2005), Melt-generation processes associated with the Tristan mantle plume: constraints on the origin of EM-1, *Earth and Planetary Science Letters*, *237*(3-4), 744-767.

Gibson, S. A., et al. (2006), Timescales and mechanisms of plume-litho sphere interactions: $^{40}Ar/^{39}Ar$ geochronology and geochemistry of alkaline igneous rocks from the Parana-Etendeka large igneous province, *Earth and Planetary Science Letters*, *251*(1-2), 1-17.

Gill, R. C. O., et al. (1992), Tertiary picrites in West Greenland: melting at the periphery of a plume?, *Geological Society, London, Special Publications*, *68*(1), 335-348.

Girdler, R. W. (1970), Structure and evolution of Red Sea and nature of Red Sea, Gulf of Aden and Ethiopian Rift junction, *Tectonophysics*, *10*(5-6), 579-&.

Girdler, R. W., and T. C. Southren (1987), Structure and evolution of the northern Red Sea, *Nature*, *330*(6150), 716-721.

Girdler, R. W. (1991), The Afro-Arabian rift system: an overview, *Tectonophysics*, *197*(2-4), 139-153.

Girdler, R. W. (1991), The case for ocean crust beneath the Red Sea, *Tectonophysics*, *198*(2-4), 275-278.

Goff, F. (1996), Vesicle cylinders in vapor-differentiated basalt flows, *Journal of Volcanology and Geothermal Research*, *71*(2-4), 167-185.

Graham, D. W., et al. (1992a), Helium isotope geochemistry of some volcanic rocks from saint Helena, *Earth and Planetary Science Letters*, *110*(1-4), 121-131.

Graham, D. W., et al. (1992b), Helium isotope geochemistry of mid-ocean ridge basalts from the South-Atlantic, *Earth and Planetary Science Letters*, *110*(1-4), 133-147.

Graham, D. W., et al. (1998), Helium isotope composition of the early Iceland mantle plume inferred from the tertiary picrites of West Greenland, *Earth and Planetary Science Letters*, *160*(3-4), 241-255.

Graham, D. W. (2002), Noble gas isotope geochemistry of mid-ocean ridge and ocean island basalts: characterization of mantle source reservoirs, *Reviews in Mineralogy and Geochemistry*, *47*(1), 247-317.

Green, T. H., and A. E. Ringwood (1968), Crystallization of basalt and andesite under high pressure hydrous conditions, *Earth and Planetary Science Letters*, *3*(5), 481.

Greenough, J. D., et al. (1999), Evidence for volatile-influenced differentiation in a layered alkali basalt flow, Penghu Islands, Taiwan, *Bulletin of Volcanology*, *60*(6), 412-424.

Griffiths, R. W., and I. H. Campbell (1991), Interaction of mantle plume heads with the Earth's surface and the onset of small-scale convection, *Journal of Geophysical Research-Solid Earth*, *96*(B11), 18295-18310.

Grove, T. L., and W. B. Bryan (1983), Fractionation of pyroxene-phyric MORB at low pressure: an experimental study, *Contributions to Mineralogy and Petrology*, *84*(4), 293-309.

Grove, T. L., et al. (1992), Fractionation of mid-ocean ridge basalt (MORB), in *Mantle flow and melt generation at mid-ocean ridges*, edited by J. P. Morgan, et al., pp. 281–310, American Geophysical Union, Washington, DC.

Gurnis, M., et al. (2000), Constraining mantle density structure using geological evidence of surface uplift rates: the case of the African Superplume, *Geochemistry Geophysics Geosystems*, *1*.

Haileab, B., et al. (2004), Gombe group basalts and initiation of Pliocene deposition in the Turkana depression, northern Kenya and southern Ethiopia, *Geological Magazine*, *141*(1), 41-53.

Halliday, A. N., et al. (1995), Incompatible trace elements in OIB and MORB and source enrichment in the sub-oceanic mantle, *Earth and Planetary Science Letters*, *133*(3-4), 379-395.

Hanan, B. B., and D. W. Graham (1996), Lead and helium isotope evidence from oceanic basalts for a common deep source of mantle plumes, *Science*, *272*(5264), 991-995.

Hansen, U., et al. (1993), Dynamical consequences of depth-dependent thermal expansivity and viscosity on mantle circulations and thermal structure, *Physics of The Earth and Planetary Interiors*, *77*(3-4), 205-223.

Hansen, H., and T. F. D. Nielsen (1999), Crustal contamination in Palaeogene East Greenland flood basalts: plumbing system evolution during continental rifting, *Chemical Geology*, *157*(1-2), 89-118.

Hansen, U. (2001), The fluid dynamics of plumes, paper presented at Mantle materials, processes and products (VMSG Annual Conference), Mineralogical Society, Durham.

Hanski, E. J., and V. F. Smolkin (1995), Iron-enriched and LREE-enriched mantle source for early Proterozoic intraplate magmatism as exemplified by the Pechenga ferropicrites, Kola Peninsula, Russia, *Lithos*, *34*(1-3), 107-125.

Hanyu, T., and I. Kaneoka (1997), The uniform and low $^{3}He/^{4}He$ ratios of HIMU basalts as evidence for their origin as recycled materials, *Nature*, *390*(6657), 273-276.

Hanyu, T., and E. Nakamura (2000), Constraints on HIMU and EM by Sr and Nd isotopes re-examined, *Earth Planets and Space*, *52*(1), 61-70.

Harris, N. B. W., et al. (1984), Crustal evolution in northeast and east-Africa from model Nd ages, *Nature*, *309*(5971), 773-776.

Hart, S. R. (1984), The DUPAL anomaly: a large-scale anomaly in the southern hemisphere, *Nature*, *309*, 753-756.

Hart, W. K., et al. (1989), Basaltic volcanism in Ethiopia: constraints on continental rifting and mantle interaction, *Journal of Geophysical Research-Solid Earth and Planets*, *94*(B6), 7731-7748.

Hart, S. R., et al. (1992), Mantle plumes and entrainment - isotopic evidence, *Science*, *256*(5056), 517-520.

Hart, S. R., and G. E. Ravizza (1996), Os partitioning between phases in lherzolite and basalt, in *Earth processes: reading the isotopic code*, edited by S. R. Hart and A. Basu, pp. 123–134, American Geophysical Union.

Hauri, E. H., and S. R. Hart (1993), Re-Os isotope systematics of HIMU and EMII oceanic island basaltsfrom the South-Pacific Ocean, *Earth and Planetary Science Letters*, *114*(2-3), 353-371.

Hauri, E. H., et al. (1994), Fluid dynamic and geochemical aspects of entrainment in mantle plumes, *Journal of Geophysical Research-Solid Earth*, *99*(B12), 24275-24300.

Hauri, E. H., and S. R. Hart (1995), Constaints on melt migration from mantle plumes: a trace element study of peridotite xenoliths from Savaii, western Samoa (Vol. 99, pg 24301, 1994), *Journal of Geophysical Research-Solid Earth*, *100*(B2), 2003-2003.

Hauri, E. H., et al. (1996), Osmium isotope systematics of drilled lavas from Mauna Loa, Hawaii, *Journal of Geophysical Research-Solid Earth*, *101*(B5), 11793-11806.

Hauri, E. H., and S. R. Hart (1997), Rhenium abundances and systematics in oceanic basalts, *Chemical Geology*, *139*(1-4), 185-205.

Hauri, E. H. (2002), Osmium isotopes and mantle convection, *Philosophical Transactions of the Royal Society of London Series A -Mathematical Physical and Engineering Sciences*, *360*(1800), 2371-2382.

Hawkesworth, C. J., et al. (1984), The role of continental lithosphere in the generation of the Karoo volcanic rocks: evidence from combined Nd-and Sr-isotope studies, in *Petrogenesis of the Volcanic Rocks of the Karoo Province*, edited by A. J. Erlank, Geological Society of South Africa.

Hawkesworth, C. J., et al. (1988), Lithosphere remobilisation during Paraná CFB magmatism, in *Oceanic and continental lithosphere: similarities and differences*, edited by M. A. Menzies and K. G. Cox, pp. 205–223, Journal of Petrology.

Hawkesworth, C. J., et al. (1995), Magma differentiation and mineralisation in the Siberian continental flood basalts, *Lithos*, *34*(1-3), 61-88.

Hawkesworth, C., et al. (1999), Mantle processes during Gondwana break-up and dispersal, *Journal of African Earth Sciences*, *28*(1), 239-261.

Hayward, N. J., and C. J. Ebinger (1996), Variations in the along-axis segmentation of the Afar Rift system, *Tectonics*, *15*(2), 244.

Hebert, H., et al. (2001), Lithospheric structure of a nascent spreading ridge inferred from gravity data: The western Gulf of Aden, *Journal of Geophysical Research-Solid Earth*, *106*(B11), 26345-26363.

Helz, R. T. (1987), Differentiation behavior of Kilauea Iki lava lake, Kilauea Volcano, Hawaii: an overview of past and current work, in *Magmatic processes physiochemical principles: Special Publication of the Geochemical Society*, edited by B. O. Mysen, pp. 241-258.

Henjes-Kunst, F., et al. (1990), Evolution and composition of the lithospheric mantle underneath the western Arabian peninsula: constraints from Sr-Nd isotope systematics of mantle xenoliths, *Contributions to Mineralogy and Petrology*, *105*(4), 460-472.

Henjes-Kunst, F., and R. Altherr (1992), Metamorphic petrology of Xenoliths from Kenya and northern Tanzania and implications for geotherms and lithospheric structures, *Journal of Petrology*, *33*(5), 1125-1156.

Hergt, J. M., et al. (1991), The petrogenesis of Mesozoic Gondwana low-Ti flood basalts, *Earth and Planetary Science Letters*, *105*(1-3), 134-148.

Herzberg, C. (1992), Depth and degree of melting of komatiites, *Journal of Geophysical Research-Solid Earth*, *97*(B4), 4521-4540.

Herzberg, C. (1995), Generation of plume magmas through time: An experimental perspective, *Chemical Geology*, *126*(1), 1-16.

Herzberg, C., and J. Z. Zhang (1996), Melting experiments on anhydrous peridotite KLB-1: Compositions of magmas in the upper mantle and transition zone, *Journal of Geophysical Research-Solid Earth*, *101*(B4), 8271-8295.

Herzberg, C., and M. J. O'Hara (1998), Phase equilibrium constraints on the origin of basalts, picrites, and komatiites, *Earth-Science Reviews*, *44*(1-2), 39-79.

Herzberg, C., and M. J. O'Hara (2002), Plume-associated ultramafic magmas of phanerozoic age, *Journal of Petrology*, *43*(10), 1857-1883.

Herzberg, C. (2004), Partial crystallization of mid-ocean ridge basalts in the crust and mantle, *Journal of Petrology*, *45*(12), 2389-2405.

Herzberg, C., et al. (2007), Temperatures in ambient mantle and plumes: constraints from basalts, picrites, and komatiites, *Geochemistry Geophysics Geosystems*, *8*.

Hill, R., and P. Roeder (1974), Crystallization of spinel from basaltic liquid as a function of oxygen fugacity, *Journal of Geology*, *82*(6), 709-729.

Hill, R. I. (1991), Starting plumes and continental break-up, *Earth and Planetary Science Letters 104*, 398-416.

Hilton, D. R., et al. (1999), Extreme $^{3}He/^{4}He$ ratios in northwest Iceland: constraining the common component in mantle plumes, *Earth and Planetary Science Letters*, *173*(1-2), 53-60.

Hirose, K., and I. Kushiro (1993), Partial melting of dry peridotites at high pressures: Determination of compositions of melts segregated from peridoties using aggregates of diamond, *Earth and Planetary Science Letters*, *114*(4), 477-489.

Hirschmann, M. M., et al. (1998), Calculation of peridotite partial melting from thermodynamic models of minerals and melts. I. Review of methods and comparison with experiments, *Journal of Petrology*, *39*(6), 1091-1115.

Hiyagon, H., et al. (1992), Noble gases in submarine glasses from mid-ocean ridges and Loihi Seamount: constraints on the early history of the Earth, *Geochimica Et Cosmochimica Acta*, *56*(3), 1301-1316.

Hofmann, C., et al. (1995), $^{40}Ar/^{39}Ar$ dating of Ethiopian traps, *Terra Abstracts*, *7*, 159.

Hofmann, A. W., and K. P. Jochum (1996), Source characteristics derived from very incompatible trace elements in Mauna Loa and Mauna Kea basalts, Hawaii Scientific Drilling Project, *J. Geophys. Res.*, *101*, 11831–11839.

Hofmann, A. W. (1997), Mantle geochemistry: The message from oceanic volcanism, *Nature*, *385*(6613), 219-229.

Hofmann, C., et al. (1997), Timing of the Ethiopian flood basalt event and implications for plume birth and global change, *Nature*, *389*(6653), 838-841.

Holbrook, W. S., et al. (2001), Mantle thermal structure and active upwelling during continental breakup in the North Atlantic, *Earth and Planetary Science Letters*, *190*(3-4), 251-266.

Holm, P. M., et al. (1988), Tertiary picrites of West Greenland: petrogenetic implications of trace element and Sr-Nd isotope geochemistry, *Chemical Geology*, *70*(1-2), 49-49.

Holm, P. M., et al. (1993), The Tertiary picrites of West Greenland: contributions from Icelandic and other sources, *Earth and Planetary Science Letters*, *115*(1-4), 227-244.

Hon, K., et al. (1994), Emplacement and inflation of pahoehoe sheet flows: observations and measurements of active lava flows on Kilauea volcano, Hawaii, *Geological Society of America Bulletin*, *106*(3), 351-370.

Honda, M., et al. (1991), Possible solar noble gas component in Hawaiian basalts, *Nature*, *349*(6305), 149-151.

Honda, M., et al. (1993), Noble gases in submarine pillow basalt glasses from Loihi and Kilauea, Hawaii: a solar component in the Earth, *Geochimica et Cosmochimica Acta*, *57*(4), 859-874.

Hooper, P. R. (1990), The timing of crustal extension and the eruption of continental flood basalts, *Nature 345*, 246-249.

Hooper, P. R., and C. J. Hawkesworth (1993), Isotopic and geochemical constraints on the origin and evolution of the Columbia River Basalt, *Journal of Petrology*, *34*(6), 1203-1246.

Hopp, J., et al. (2004), Neon isotopes in mantle rocks from the Red Sea region reveal large-scale plume-lithosphere interaction, *Earth and Planetary Science Letters*, *219*, 61-76.

Hopp, J., et al. (2007), Noble gas compositions of the lithospheric mantle below the Chyulu Hills volcanic field, Kenya, *Earth and Planetary Science Letters*, *261*, 635-648.

Horan, M. F., et al. (1995), Osmium and neodymium isotopic constraints on the temporal and spatial evolution of Siberian flood basalt sources, *Geochimica et Cosmochimica Acta*, *59*(24), 5159-5168.

Huchon, P., and K. Khanbari (2003), Rotation of the syn-rift stress field of the northern Gulf of Aden margin, Yemen, *Tectonophysics*, *364*(3-4), 147-166.

Hughes, G. W., and Z. R. Beydoun (1992), The Red Sea Gulf of Aden - biostratigraphy, lithostratigraphy and paleoenvironments, *Journal of Petroleum Geology*, *15*(2), 135-156.

Humayun, M., et al. (2004), Geochemical evidence for excess iron in the mantle beneath Hawaii, *Science*, *306*(5693), 91-94.

Humphris, S. E., et al. (1985), Petrological and geochemical variations along the Mid-Atlantic Ridge between 46° S and 32° S: influence of the Tristan da Cunha mantle plume, *Geochimica et Cosmochimica Acta*, *49*(6), 1445-1464.

Hunt, D. L., and L. H. Kellogg (2001), Quantifying mixing and age variations of heterogeneities in models of mantle convection: Role of depth-dependent viscosity, *Journal of Geophysical Research-Solid Earth*, *106*(B4), 6747-6759.

Ibrahim, K. M., and A. Al-Malabeh (2006), Geochemistry and volcanic features of Harrat El Fahda: A young volcanic field in northwest Arabia, Jordan, *Journal of Asian Earth Sciences*, *27*(2), 147-154.

Ilani, S., et al. (2001), New K-Ar ages of basalts from the Harrat Ash Shaam volcanic field in Jordan: implications for the span and duration of the upper-mantle upwelling beneath the western Arabian plate, *Geology*, *29*(2), 171-174.

Isley, A. E., and D. H. Abbott (2002), Implications of the temporal distribution of high-Mg magmas for mantle plume volcanism through time, *Journal of Geology*, *110*(2), 141-158.

Ismail-Zadeh, A., et al. (2006), Three-dimensional forward and backward numerical modeling of mantle plume evolution: effects of thermal diffusion, *Journal of Geophysical Research-Solid Earth*, *111*(B6).

Ito, E., and E. Takahashi (1987), Melting of peridotite at upper most lower-mantle conditions, *Nature*, *328*, 514-517.

Ivanov, A. V., et al. (2008), Low-ti melts from the southeastern Siberian Traps Large Igneous Province: Evidence for a water-rich mantle source?, *Journal of Earth System Science*, *117*(1), 1-21.

Izzeldin, A. Y. (1987), Seismic, gravity and magnetic surveys in the central part of the Red Sea: their interpretation and implications for the structure and evolution of the Red Sea, *Tectonophysics*, *143*(4), 269.

Jacques, E., et al. (1999), Relocation of M >= 2 events of the 1989 Dobi seismic sequence in Afar: evidence for earthquake migration, *Geophysical Journal International*, *138*(2), 447-469.

Jarvis, K. E. (1997), Inductively coupled plasma-mass spectrometry (ICP-MS), in *Modern analytical geochemistry: an introduction to quantitative chemical analysis techniques for earth, environmental and materials scientists*, edited by R. Gill, pp. 171-187, Longman.

Jentzsch, G., et al. (2000), Three dimensional inversion of gravity data from the Main Ethiopian Rift, *Physics and Chemistry of the Earth Part a-Solid Earth and Geodesy*, *25*(4), 365-373.

Jerram, D. A., and M. Widdowson (2003), The anatomy of Continental Flood Basalt Provinces: geological constraints on the processes and products of flood volcanism, paper presented at Conference on mantle plumes - physical process, chemical signatures, biological effects, Cardiff, Wales, Sep 11.

Jestin, F., and P. Huchon (1992), Kinematics and deformation of the Red Sea - Gulf of Aden-Ethiopian Rift triple junction since Oligocene, *Bulletin De La Societe Geologique De France*, *163*(2), 125-133.

Jestin, F., et al. (1994), The Somalia plate and the east African rift system: present day kinematics, *Geophysical Journal International*, *116*(3), 637-654.

Johannsen, A. (1931), *A descriptive petrology of the igneous rocks*, University of Chicago Press, Chicago.

Jones, P. W., and D. C. Rex (1974), New dates from Ethiopian Plateau volcanics, *Nature*, *252*(5480), 218-219.

Jones, P. W. (1976), Age of the lower flood basalts of Ethiopian Plateau, *Nature*, *261*(5561), 567-569.

Jones, S. M., and N. White (2003), Shape and size of the starting Iceland plume swell, *Earth and Planetary Science Letters*, *216*(3), 271-282.

Jones, J., et al. (2006), Seismic characteristics of variable convection at Erta 'Ale lava lake, Ethiopia, *Journal of Volcanology and Geothermal Research*, *153*(1-2), 64-79.

Juch, D. (1975), Geology of the Southeastern escarpment of Ethiopia between 39° and 42° long. E, in *Afar depression of Ethiopia*, edited by A. Pilger and A. Rosler, pp. 310–316, Schweizerbart, Stuttgart.

Kabeto, K., et al. (2001), Mantle sources and magma-crust interactions in volcanic rocks from the northern Kenya rift: geochemical evidence, *Lithos*, *56*(2-3), 111-139.

Kabeto, K., et al. (2004), Geology and geochemistry of Maichew volcanics, northwestern Ethiopian Plateau, paper presented at East African Rift System: Geodynamics, Resources and Environment, Addis Ababa.

Kalt, A., et al. (1997), Nd, Sr, and Pb isotopic evidence for diverse lithospheric mantle sources of East African Rift carbonatites, *Tectonophysics*, *278*(1-4), 31-45.

Kampunzu, A. B., et al. (2000), Geochemistry and tectonic setting of mafic igneous units in the Neoproterozoic Katangan basin, Central Africa: implications for Rodinia break-up, *Gondwana Research*, *3*(2), 125-153.

Karason, H., and R. D. van der Hilst (2000), Constraints on mantle convection from seismic tomography, in *The History and Dynamics of Global Plate Motion*, edited by M. R. Richards, et al., pp. 277-288, American Geophysical Union.

Karason, H., and R. D. van der Hilst (2001), Tomographic imaging of the lowermost mantle with differential times of refracted and diffracted core phases (PKP, P-diff), *Journal of Geophysical Research-Solid Earth*, *106*(B4), 6569-6587.

Kazmin, V., and C. R. Garland (1973), Evidence of Precambrian block-faulting in western margin of Afar Depression, Ethiopia, *Geological Magazine*, *110*(1), 55-57.

Kazmin, V. G. (1991), The position of continental flood basalts in rift zones and its bearing on models of rifting, *Tectonophysics*, *199*(2-4), 375-387.

Kazmin, V. G., and A. F. Byakov (2000), Magmatism and crustal accretion in continental rifts, *Journal of African Earth Sciences*, *30*(3), 555-568.

Keays, R. R., and P. C. Lightfoot (2007), Siderophile and chalcophile metal variations in Tertiary picrites and basalts from West Greenland with implications for the sulphide saturation history of continental flood basalt magmas, *Mineralium Deposita*, *42*(4), 319-336.

Kebede, F., and O. Kulhanek (1991), Recent seismicity of the East African Rift system and its implications, *Physics of the Earth and Planetary Interiors*, *68*(3-4), 259-273.

Keir, D., et al. (2005), Variations in late syn-rift melt alignment inferred from shear-wave splitting in crustal earthquakes beneath the Ethiopian rift, *Geophysical Research Letters*, *32*(23).

Keir, D., et al. (2006), Strain accommodation by magmatism and faulting as rifting proceeds to breakup: seismicity of the northern Ethiopian rift, *Journal of Geophysical Research-Solid Earth*, *111*(B5).

Keir, D., et al. (2006), Local earthquake magnitude scale and seismicity rate for the Ethiopian rift, *Bulletin of the Seismological Society of America*, *96*(6), 2221-2230.

Keller, W. R., et al. (2000), Resolution of tomographic models of the mantle beneath Iceland, *Geophysical Research Letters*, *27*(24), 3993-3996.

Keller, G. R., et al. (2004), A preliminary analysis of crustal structure variations along the Ethiopian Rift, paper presented at The East African Rift System: Geodynamics, Resources and Environment, Addis Ababa.

Keller, R. A., et al. (2004), Cretaceous-to-recent record of elevated $^{3}He/^{4}He$ along the Hawaiian-Emperor volcanic chain, *Geochemistry Geophysics Geosystems*, *5*.

Kellogg, L. H., et al. (1999), Compositional stratification in the deep mantle, *Science*, *283*, 1881-1888.

Kellogs, K. S., and R. L. Reynolds (1983), Opening of the Red Sea: constraints from a paleomagnetic study of the As Sarat volcanic field, southwestern Saudi Arabia, *Geophysical Journal of the Royal Astronomical Society 74*, 649–665.

Kendall, J. M., et al. (2005), Magma-assisted rifting in Ethiopia, *Nature*, *433*(7022), 146-148.

Kendall, J. M., et al. (2006), Mantle upwellings, melt migration and the rifting of Africa: insights from seismic anisotropy, *Afar Volcanic Province within the East African Rift System*, *259*, 55-72.

Kenea, N. H., et al. (2001), Late Oligocene volcanism and extension in the southern Red Sea Hills, Sudan, *Journal of the Geological Society*, *158*, 285-294.

Kennan, P. S., et al. (1990), The Segatu Ridge dyke swarm, Ethiopian rift margin: revised age and new Sr isotopic data, *Journal of African Earth Sciences*, *11*(1-2), 39-42.

Kent, R. W., et al. (1998), Emplacement of Hebridean Tertiary flood basalts: evidence from an inflated pahoehoe lava flow on Mull, Scotland, *Journal of the Geological Society*, *155*, 599-607.

Kent, R. W., and J. G. Fitton (2000), Mantle sources and melting dynamics in the British palaeogene igneous province, *Journal of Petrology*, *41*(7), 1023-1040.

Kent, A. J. R., et al. (2002), Contamination and melt aggregation processes in continental flood basalts: constraints from melt inclusions in Oligocene basalts from Yemen, *Earth and Planetary Science Letters*, *202*(3-4), PII S0012-0821X(0002)00823-00823.

Kent, A. J. R., et al. (2004), Mantle heterogeneity during the formation of the North Atlantic Igneous Province: Constraints from trace element and Sr-Nd-Os-O isotope systematics of Baffin Island picrites, *Geochemistry Geophysics Geosystems*, *5*.

Keranen, K., et al. (2004), Three-dimensional seismic imaging of a protoridge axis in the Main Ethiopian rift, *Geology*, *32*(11), 949-952.

Keranen, K., and S. L. Klemperer (2008), Discontinuous and diachronous evolution of the Main Ethiopian Rift: implications for development of continental rifts, *Earth and Planetary Science Letters*, *265*(1-2), 96-111.

Kerr, A. C., et al. (1995), Depleted geochemical signatures: no paradox for plume theories, *Geology*, *23*(9), 843-846.

Kerr, A. C., et al. (1996), The geochemistry and tectonic setting of late Cretaceous Caribbean and Colombian volcanism, *Journal of South American Earth Sciences*, *9*(1-2), 111-120.

Kerr, A. C., and N. T. Arndt (2001), A note on the IUGS reclassification of the high-Mg and picritic volcanic rocks, *Journal of Petrology*, *42*(11), 2169-2171.

Kerr, A. C. (2005), Oceanic LIPs: The kiss of death, *Elements*, *1*(5), 289-292.

Kerr, A. C., and J. J. Mahoney (2007), Oceanic plateaus: Problematic plumes, potential paradigms, *Chemical Geology*, *241*(3-4), 332-353.

Kersten, F., et al. (2007), Geochemistry of quaternary lavas from the Main Ethiopian Rift:constraints on continental breakup and rifting, *Geochimica et Cosmochimica Acta*, *71*(15), A479-A479.

Kersten, F., et al. (2008), Magma generation in the Main Ethiopian Rift (MER) and Afar, *Geochimica et Cosmochimica Acta*, *72*(12), A466-A466.

Keszthelyi, L., et al. (1999), Application of recent studies on the emplacement of basaltic lava flows to the Deccan Traps, in *Memoirs of the Geological Society of India: Deccan Volcanic Province*, edited by K. V. Subbarao, pp. 485-520.

Khalil, S. M., and K. R. McClay (2002), Extensional fault-related folding, northwestern Red Sea, Egypt, *Journal of Structural Geology*, *24*(4).

Kidane, T., et al. (1999), Paleomagnetic and geochronological identification of the Reunion subchron in Ethiopian Afar, *Journal of Geophysical Research-Solid Earth*, *104*(B5), 10405-10419.

Kidane, T., et al. (2002), New paleomagnetic result from the Ethiopian flood basalts in the Abbay (Blue Nile) and Kessem gorges, *Earth and Planetary Science Letters*, *203*(1), 353-367.

Kidane, T., et al. (2003), New paleomagnetic and geochronologic results from Ethiopian Afar: block rotations linked to rift overlap and propagation and determination of a similar to 2 Ma reference pole for stable Africa, *Journal of Geophysical Research-Solid Earth*, *108*(B2).

Kidane, T., et al. (2006), Palaeomagnetic constraints on continental break-up processes: observations from the Main Ethiopian Rift, *Afar Volcanic Province within the East African Rift System*, *259*, 165-183.

Kiefer, W. S., and L. H. Kellogg (1998), Geoid anomalies and dynamic topography from time-dependent, spherical axisymmetric mantle convection, *Physics of the Earth and Planetary Interiors*, *106*(3-4), 237-256.

Kieffer, B., et al. (2001), A petrological and geochemical study of the transistion from tholeiitic flood basalts to alkaline sheild volcanics in Ethiopia and Kerguelan, paper presented at Magmatic rifted margins, Royal Holloway, Egham.

Kieffer, B., et al. (2004), Flood and shield basalts from Ethiopia: magmas from the African superswell, *Journal of Petrology*, *45*(4), 793-834.

Kilinc, A., et al. (1983), The ferric-ferrous ratio of natural silicate liquids equilibrated in air, *Contributions to Mineralogy and Petrology*, *83*(1-2), 136-140.

King, S. D., and D. L. Anderson (1995), An alternative mechanism of flood basalt formation, *Earth and Planetary Science Letters*, *136*(3-4), 269-279.

King, S. D., and D. L. Anderson (1998), Edge-driven convection, *Earth and Planetary Science Letters*, *160*(3-4), 289-296.

King, S. D., and J. Ritsema (2000), African Hot spot volcanism: small scale convection in the upper mantle beneath cratons, *Science*, *290*, 1137 - 1140.

Kinzler, R. J., and T. L. Grove (1992), Primary magmas of mid-ocean ridge basalts: experiments and methods, *Journal of Geophysical Research-Solid Earth*, *97*(B5), 6885-6906.

Klein, E. M., and C. H. Langmuir (1987), Global correlations of ocean ridge basalt chemistry with axial depth and crustal thickness, *Journal of Geophysical Research-Solid Earth and Planets*, *92*(B8), 8089-8115.

Kohn, et al. (2001), Ordering hydroxyl defects in hydrous wadsleyite, paper presented at Mantle materials, processes and products (VMSG Annual Conference), Mineralogical Society, Durham.

Kokfelt, T. F., et al. (2006), Combined trace element and Pb-Nd-Sr-O isotope evidence for recycled oceanic crust (upper and lower) in the Iceland mantle plume, *Journal of Petrology*, *47*(9), 1705-1749.

Korenaga, J., and T. H. Jordan (2001), Effects of vertical boundaries on infinite Prandtl number thermal convection, *Geophysical Journal International*, *147*(3), 639-659.

Korenaga, J., et al. (2002), Methods for resolving the origin of large igneous provinces from crustal seismology, *Journal of Geophysical Research-Solid Earth*, *107*(B9).

Korme, T., et al. (1997), Volcanic vents rooted on extension fractures and their geodynamic implications in the Ethiopian Rift, *Journal of Volcanology and Geothermal Research*, *79*(3-4), 205-222.

Korme, T., et al. (2004), The role of pre-existing structures in the origin, propagation and architecture of faults in the main Ethiopian rift, *Gondwana Research*, *7*(2), 467-479.

Kreemer, C., et al. (2003), An integrated global model of present-day plate motions and plate boundary deformation, *Geophysical Journal International*, *154*(1), 8-34.

Kress, V. C., and I. S. E. Carmichael (1988), Stoichiometry of the iron oxidation reaction in silicate melts, *American Mineralogist*, *73*(11-12), 1267-1274.

Kress, V. C., and I. S. E. Carmichael (1991), The compressibility of silicate liquids containing Fe_2O_3 and the effect of composition, temperature, oxygen fugacity and pressure on their REDOX states, *Contributions to Mineralogy and Petrology*, *108*(1-2), 82-92.

Krienitz, M. S., et al. (2007), Magma genesis and mantle dynamics at the Harrat Ash Shamah volcanic field (Southern Syria), *Journal of Petrology*, *48*(8), 1513-1542.

Krishnamurthy, P., and K. G. Cox (1977), Picrite basalts and related lavas from Deccan traps of western India, *Contributions to Mineralogy and Petrology*, *62*(1), 53-75.

Krishnamurthy, P., and K. G. Cox (1980), A potassium-rich alkalic suite from the Deccan traps, Rajpipla, India, *Contributions to Mineralogy and Petrology*, *73*(2), 179-189.

Krishnamurthy, P., et al. (1999), Mineralogical and chemical studies on alkaline and basaltic rocks of Kutch, Gujarat, India. Deccan Volcanic Province, *Geological Society of India, Memoir 43*, 757–784.

Krishnamurthy, P., et al. (2000), Olivine compositions in picrite basalts and the Deccan volcanic cycle, *Journal of Petrology*, *41*(7), 1057-1069.

Kumar, A. R., and G. Mohan (2005), Mantle discontinuities beneath the Deccan volcanic province, *Earth and Planetary Science Letters*, *237*(1-2), 252-263.

Kuno, H. (1968), Differentiation of basalt magmas, in *Basalts: The Poldervaart treatise on rocks of basaltic composition*, edited by H. H. Hess and A. Poldervaart, pp. 623-688, Interscience, New York.

Kunz, K., et al. (1975), Potassium-argon age determinations of the trap basalt of the southeastern part of the Afar Rift, in *Afar depression of Ethiopia*, edited by A. Pilger and A. Rosler, pp. 370-374, Schweizerbart, Stuttgart.

Kunz, J., et al. (1998), Plutonium-fission xenon found in Earth's mantle, *Science*, *280*(5365), 877-880.

Kunz, J. (1999), Is there solar argon in the Earth's mantle?, *Nature*, *399*(6737), 649-650.

Kurz, M. D., et al. (1982), Helium isotopic systematics of ocan islands and mantle heterogeneity, *Nature*, *297*, 43-46.

Kurz, M. D. (1993), Mantle heterogeneity beneath oceanic islands: some inferences from isotopes, *Philosophical Transactions of the Royal Society of London Series A - Mathematical Physical and Engineering Sciences*, *342*(1663), 91-103.

Kurz, M. D., et al. (1996), Helium isotopic evolution of Mauna Kea Volcano: first results from the 1 km drill core, *Journal of Geophysical Research-Solid Earth*, *101*(B5), 11781-11791.

Kurz, M. D., and D. Geist (1999), Dynamics of the Galapagos hotspot from helium isotope geochemistry, *Geochimica et Cosmochimica Acta*, *63*(23-24), 4139-4156.

Kurz, T., et al. (2004), Deformation, distribution and type in the Main Ethiopian Rift, paper presented at The East African Rift: Geodynamics, Resources and Environment, Addis Ababa.

Kurz, T., et al. (2007), Deformation distribution and type in the Main Ethiopian Rift (MER): A remote sensing study, *Journal of African Earth Sciences*, *48*, 100-114.

Kushiro, I. (1996), Partial melting of fertile mantle peridotite at high pressures: an experimental study using aggregates of diamond, in *Earth Processes: reading the isotopic code*, edited by A. Basu and S. R. Hart, pp. 109-122, American Geophysical Union.

Lahitte, P., et al. (2003a), New age constraints on the timing of volcanism in central Afar, in the presence of propagating rifts, *Journal of Geophysical Research-Solid Earth*, *108*(B2).

Lahitte, P., et al. (2003b), Silicic central volcanoes as precursors to rift propagation: the Afar case, *Earth and Planetary Science Letters*, *207*(1-4), 103-116.

Langmuir, C. H., et al. (1978), General mixing equation with applications to Icelandic basalts, *Earth and Planetary Science Letters*, *37*(3), 380-392.

Langmuir, C. H., et al. (1992), Petrological systematics of mid-ocean ridge basalts: constraints on melt generation beneath ocean ridges, in *Mantle flow and Melt Generation at Mid-Ocean Ridges*, edited by J. P. Morgan, et al., pp. 183-280, American Geophysical Union, Washington DC.

Langmuir, C. H., and D. W. Forsyth (2007), Mantle melting beneath mid-ocean ridges, *Oceanography*, *20*(1), 78-89.

Larsen, L. M., et al. (1999), Trans-Atlantic correlation of the Palaeogene volcanic successions in the Faeroe Islands and East Greenland, *Journal of the Geological Society*, *156*, 1081-1095.

Larsen, L. M., and A. K. Pedersen (2000), Processes in high-mg, high-T magmas: Evidence from olivine, chromite and glass in palaeogene picrites from West Greenland, *Journal of Petrology*, *41*(7), 1071-1098.

Larsen, L. M., et al. (2003), Alkali picrites formed by melting of old metasomatized lithospheric mantle: Manitdlat member, Vaigat Formation, Palaeocene of West Greenland, *Journal of Petrology*, *44*(1), 3-38.

Larson, R. L. (1991), Geological consequences of superplumes, *Geology*, *19*, 963-966.

Lassiter, J. C., and E. H. Hauri (1998), Osmium-isotope variations in Hawaiian lavas: evidence for recycled oceanic lithosphere in the Hawaiian plume, *Earth and Planetary Science Letters*, *164*(3-4), 483-496.

Lassiter, J. C. (2003), Rhenium volatility in subaerial lavas: constraints from subaerial and submarine portions of the HSDP-2 Mauna Kea drillcore, *Earth and Planetary Science Letters*, *214*(1-2), 311-325.

Lassiter, J. C. (2006), Constraints on the coupled thermal evolution of the Earth's core and mantle, the age of the inner core, and the origin of the $^{186}Os/^{188}Os$ "core signal" in plume-derived lavas, *Earth and Planetary Science Letters*, *250*(1-2), 306-317.

Le Bas, M. J. (2000), IUGS reclassification of the high-Mg and picritic volcanic rocks, *Journal of Petrology*, *41*(10), 1467-1470.

Le Maitre, R. W., et al. (1989), *A Classification of Igneous Rocks and Glossary of Terms: Recommendations of the International Union of Geological Sciences Subcommission on the Systematics of Igneous Rocks*, Oxford: Blackwell Scientific.

Le Pichon, X., and J. M. Gaulier (1988), The rotation of Arabia and the Levant fault system, *Tectonophysics*, *153*(1-4), 271-294.

Lei, J. S., and D. P. Zhao (2006), A new insight into the Hawaiian plume, *Earth and Planetary Science Letters*, *241*(3-4), 438-453.

Leitch, A. M., and G. F. Davies (2001), Mantle plumes and flood basalts: enhanced melting from plume ascent and an eclogite component, *Journal of Geophysical Research-Solid Earth*, *106*(B2), 2047-2059.

Lemaux, J., et al. (2002), Location of the Nubia-Somalia boundary along the Southwest Indian Ridge, *Geology*, *30*(4), 339-342.

Leroy, S., et al. (2004), From rifting to spreading in the eastern Gulf of Aden: a geophysical survey of a young oceanic basin from margin to margin, *Terra Nova*, *16*(4), 185-192.

Leterrier, J., et al. (1982), Clinopyroxene composition as a method of identification of the magmatic affinities of paleovolcanic series, *Earth and Planetary Science Letters*, *59*(1), 139-154.

Levitte, D., et al. (1974), Reconnaisance geology of the Amaro Horst, Southern Ethiopian Rift, *Geological Society of America Bulletin*, *85*(3), 417-422.

Liew, T. C., and M. T. McCulloch (1985), Genesis of granitoid batholiths of Peninsular Malaysia and implications for models of crustal evolution: evidence from a Nd---Sr isotopic and U---Pb zircon study, *Geochimica et Cosmochimica Acta*, *49*(2), 587-600.

Lightfoot, P. C., et al. (1990), Source differentiation of the Deccan Trap lavas - implications of geochemical and mineral chemical variations, *Journal of Petrology*, *31*(5), 1165-1200.

Lightfoot, P. C., et al. (1993), Remobilization of the continental lithosphere by a mantle plume: major element, and Sr isotope, Nd isotope and Pb isotope evidence from picritic and tholeiitic lavas of the Norilsk district, Siberia Trap, Russia, *Contributions to Mineralogy and Petrology*, *114*(2), 171-188.

Lightfoot, P. C., et al. (1997), Geochemistry of tertiary tholeiites and picrites from Qeqertarssuaq (Disko Island) and Nuussuaq, West Greenland with implications for the mineral potential of comagmatic intrusions, *Contributions to Mineralogy and Petrology*, *128*(2-3), 139-163.

Lindsley, D. H. (1983), Pyroxene thermometry, *American Mineralogist*, *68*(5-6), 477-493.

Long, P. E., and B. J. Wood (1986), Structures, textures and colling histories of Columbia River basalt flows, *Geological Society of America Bulletin*, *97*(9), 1144-1155.

Long, P. E., and B. J. Wood (1987), Structures, textures and colling histories of Columbia River basalt flows - reply, *Geological Society of America Bulletin*, *99*(6), 887-888.

Lorand, J. P., et al. (2003), Platinum-group elements and melt percolation processes in Sidamo spinel peridotite xenoliths, Ethiopia, East African Rift, *Chemical Geology*, *196*(1-4), 57-75.

Loucks, R. R. (1996), A precise olivine-augite Mg-Fe exchange geothermometer, *Contributions to Mineralogy and Petrology*, *125*(2-3), 140-150.

Lucas, H., et al. (1989), Iron in kimberlitic ilmenites and chromian spinels: a survey of analytical techniques, *Special Publication, Geological Society of Australia,*, *14*, 311-320.

Lucassen, F., et al. (2008), Nd, Pb, and Sr isotope composition of Late Mesozoic to Quaternary intra-plate magmatism in NE-Africa (Sudan, Egypt): HIMU signatures from the mantle lithosphere, *Contributions to Mineralogy and Petrology*, *156*(6), 765-784.

Lucazeau, F., et al. (2008), Persistent thermal activity at the Eastern Gulf of Aden after continental break-up, *Nature Geoscience*, *1*(12), 854-858.

Luck, J. M., and C. J. Allegre (1983), ^{187}Re-^{187}Os systematics in meteorites and cosmochemical consequences, *Nature*, *302*(5904), 130-132.

Luck, J. M., and C. J. Allegre (1991), Osmium isotopes in Ophiolites, *Earth and Planetary Science Letters*, *107*(2), 406-415.

Luguet, A., et al. (2007), Residual platinum-group minerals from highly depleted harzburgites of the Lherz massif (France) and their role in HSE fractionation of the mantle, *Geochimica et Cosmochimica Acta*, *71*(12), 3082-3097.

Luguet, A., et al. (2008a), Enriched Pt-Re-Os isotope systematics in plume lavas explained by metasomatic sulfides, *Science*, *319*(5862), 453-456.

Luguet, A., et al. (2008b), $^{184}Os/^{188}Os$ and $^{186}Os/^{188}Os$ measurements by negative thermal ionisation mass spectrometry (N-TIMS): effects of interfering element and mass fractionation corrections on data accuracy and precision, *Chemical Geology*, *248*(3-4), 342-362.

Luth, R. W., and D. Canil (1993), Ferric iron in mantle-derived pyroxenes and a new oxybarometer for the mantle, *Contributions to Mineralogy and Petrology*, *113*(2), 236-248.

Lyle, P. (2000), The eruption environment of multi-tiered columnar basalt lava flows, *Journal of the Geological Society*, *157*, 715-722.

Maaloe, S., and B. Hansen (1982), Olivine phenocrysts of hawaiian olivine tholeiite and oceanite, *Contributions to Mineralogy and Petrology*, *81*(3), 203-211.

Macdonald, G. A., and T. Katsura (1964), Chemical Composition of Hawaiian Lavas1, *J. Petrology*, *5*(1), 82-133.

MacKenzie, G. D., et al. (2004), Evidence for crustal structure on the evolution of the Main Ethiopian Rift, paper presented at The East African Rift System: Geodynamics, Resources and Environment, Addis Ababa.

Mackenzie, G. D., et al. (2005), Crustal velocity structure across the Main Ethiopian Rift: results from two-dimensional wide-angle seismic modelling, *Geophysical Journal International*, *162*(3), 994-1006.

Maguire, P. K. H., et al. (2004), Crustal structure of the northern Main Ethiopian Rift from the EAGLE controlled-source survey: a snapshot of incipient lithospheric break-up, paper presented at The East African Rift System: Geodynamics, Resources and Environment, Addis Ababa, ETHIOPIA, Jun.

Maguire, P. K. H., et al. (2006), Crustal structure of the northern Main Ethiopian Rift from the EAGLE controlled-source survey; a snapshot of incipient lithospheric break-up, *Afar Volcanic Province within the East African Rift System*, *259*, 269-292.

Mahatsente, R., et al. (1999), Crustal structure of the Main Ethiopian Rift from gravity data: 3-dimensional modeling, *Tectonophysics*, *313*(4), 363-382.

Mahatsente, R., et al. (2000), Three-dimensional inversion of gravity data from the main Ethiopian Rift, *Journal of African Earth Sciences*, *31*(2), 451-466.

Mahoney, J. J., et al. (1985), Origin of contemporaneous tholeiitic and K-rich alkalic lavas: a case study from the northern Deccan Plateau, India, *Earth and Planetary Science Letters*, *72*(1), 39-53.

Mahoney, J., et al. (1992), South western limits of Indian Ocean ridge mantle and the origin of low $^{206}Pb/^{204}Pb$ mid-ocean ridge basalt - isotope systematics of the central south-west Indian ridge (17° E - 50° E), *Journal of Geophysical Research-Solid Earth*, *97*(B13), 19771-19790.

Mahoney, J. J., et al. (1995), Geochemical characteristics of lavas from Broken Ridge, the Naturaliste Plateau and southern-most Kerguelan Plateau - Cretaceous plateau volcanism in the south-east Indian Ocean, *Chemical Geology*, *120*(3-4), 315-345.

Mahoney, J. J., et al. (2000), Geochemistry of flood basalts of the Toranmal section, northern Deccan Traps, India: implications for regional Deccan stratigraphy, *Journal of Petrology*, *41*(7), 1099-1120.

Makovicky, M., et al. (1986), Experimental studies on the solubility and distribution of platinum group elements in base-metal sulphides in platinum deposits, in *Metallogeny of basic and ultrabasic rocks*, edited by M. J. Gallagher, et al., pp. 415–425.

Makris, J., et al. (1991), The gravity field of the Red Sea and East Africa, *Tectonophysics*, *198*(2-4), 369-381.

Makris, J., and C. H. Henke (1992), Pull-apart evolution of the Red Sea, *Journal of Petroleum Geology*, *15*(2), 127-134.

Manetti, P., et al. (1991), Magmatism of the eastern Red Sea margin in the northern part of Yemen from Oligocene to present, *Tectonophysics*, *198*(2-4), 181-202.

Manighetti, I., et al. (1997), Propagation of rifting along the Arabia-Somalia plate boundary: The Gulfs of Aden and Tadjoura, *Journal of Geophysical Research-Solid Earth*, *102*(B2), 2681-2710.

Manighetti, I., et al. (1998), Propagation of rifting along the Arabia-Somalia plate boundary: Into Afar, *Journal of Geophysical Research-Solid Earth*, *103*(B3), 4947-4974.

Manighetti, I., et al. (2001a), Slip accumulation and lateral propagation of active normal faults in Afar, *Journal of Geophysical Research-Solid Earth*, *106*(B7), 13667-13696.

Manighetti, I., et al. (2001b), Strain transfer between disconnected, propagating rifts in Afar (vol 106, pg 13,613, 2001), *Journal of Geophysical Research-Solid Earth*, *106*(B11), 26775-26786.

Manighetti, I., et al. (2001c), Strain transfer between disconnected, propagating rifts in Afar, *Journal of Geophysical Research-Solid Earth*, *106*(B7), 13613-13665.

Marques, L. S., et al. (1999), Mantle source compositions of the Parana Magmatic Province (southern Brazil): evidence from trace element and Sr-Nd-Pb isotope geochemistry, *Journal of Geodynamics*, *28*(4-5), 439-458.

Marty, B. (1989), Neon and xenon isotopes in MORB: implications for the earth-atmosphere evolution, *Earth and Planetary Science Letters*, *94*(1-2), 45-56.

Marty, B., et al. (1993), He, Ar, Sr, Nd and Pb isotopes in volcanic-rocks from Afar: evidence for a primitive mantle component and constraints on magamtic sources, *Geochemical Journal*, *27*(4-5), 219-228.

Marty, B., et al. (1996), Helium isotopic variations in Ethiopian plume lavas: Nature of magmatic sources and limit on lower mantle contribution, *Earth and Planetary Science Letters*, *144*(1-2), 223-237.

Marty, B., et al. (1998), Helium isotopes in early tertiary basalts, northeast Greenland: evidence for 58Ma plume activity in the north Atlantic Iceland volcanic province, *Geology*, *26*(5), 407-410.

Mazzarini, F., et al. (2004), Strain rate and bimodal volcanism in the continental rift: Debre Zeyt volcanic field, northern MER, Ethiopia, *Journal of African Earth Sciences*, *39*(3-5), 415-420.

Mazzarini, F. (2007), Vent distribution and crustal thickness in stretched continental crust: the case of the Afar Depression (Ethiopia), *Geosphere*, *3*, 152-162.

McCanta, M. C., et al. (2004), Iron partitioning between basaltic melts and clinopyroxene as a function of oxygen fugacity, *American Mineralogist*, *89*(11-12), 1685-1693.

McDonough, W. F. (1990), Constraints on the composition of the continental lithospheric mantle, *Earth and Planetary Science Letters*, *101*(1), 1-18.

McDonough, W. F., and S. S. Sun (1995), The composition of the Earth, *Chemical Geology*, *120*(3-4), 223-253.

McDougall, I., et al. (1992), A reappraisal of the geomagnetic polarity time-scale to 4 Ma using data from the Turkana Basin, East Africa, *Geophysical Research Letters*, *19*(23), 2349-2352.

McDougall, I., and M. Honda (1998), Primordial solar noble gas component in the Earth: consequences for the origin and evolution of the Earth and its atmosphere, in *The Earth's mantle: composition, structure and evolution*, edited by I. Jackson, pp. 159-187, Cambridge university Press, Cambridge.

McDougall, I., and R. T. Watkins (2006), Geochronology of the Nabwal Hills: a record of earliest magmatism in the northern Kenyan Rift Valley, *Geological Magazine*, *143*(1), 25-39.

McGuire, A. V., et al. (1992), Mineral standards for electron microprobe analysis of oxygen, *American Mineralogist*, *77*(9-10), 1087-1091.

McHone, J. G. (2000), Non-plume magmatism and rifting during the opening of the central Atlantic Ocean, *Tectonophysics*, *316*(3-4), 287-296.

McKenzie, D., and M. J. Bickle (1988), The volume and composition of melt generated by extension of the lithosphere, *Journal of Petrology*, *29*(3), 625-679.

McKenzie, J. M., et al. (2001), A geochemical survey of spring water from the main Ethiopian rift valley, southern Ethiopia: implications for well-head protection, *Hydrogeology Journal*, *9*(3), 265-272.

McKenzie, J. M., et al. (2003), Response to comments on article entitled 'A geochemical survey of spring water from the main Ethiopian rift valley, southern

Ethiopia: implications for well-head protection' by McKenzie et al., Hydrogeology Journal (2001) 9 : 265-272, *Hydrogeology Journal*, *11*(2), 316-317.

Meibom, A., et al. (2003), Are high $^{3}He/^{4}He$ ratios in oceanic basalts an indicator of deep-mantle plume components?, *Earth and Planetary Science Letters*, *208*(3-4), 197-204.

Meibom, A., and D. L. Anderson (2004), The statistical upper mantle assemblage, *Earth and Planetary Science Letters*, *217*(1-2), 123-139.

Meisel, T., et al. (1996), Re-Os, Sm-Nd, and rare earth element evidence for Proterozoic oceanic and possible subcontinental lithosphere in tectonized ultramafic lenses from the Swiss Alps, *Geochimica et Cosmochimica Acta*, *60*(14), 2583-2593.

Meisel, T., et al. (2001), Osmium isotopic compositions of mantle xenoliths: A global perspective, *Geochimica et Cosmochimica Acta*, *65*(8), 1311-1323.

Melluso, L., et al. (1995), Constraints on the sources of the Deccan Traps from the petrology and geochemistry of the basalts of Gugarat state (Western India), *Journal of Petrology*, *36*(5), 1393-1432.

Menzies, M. A., et al. (1992), The timing of magmatism, uplift and crustal extension: preliminary observations from Yemen, in *Magmatism and the causes of continental break-up*, edited by B. Storey, et al., pp. 293-304, Geological Society, London.

Menzies, M., et al. (1997), Volcanic and nonvolcanic rifted margins of the Red Sea and Gulf of Aden: Crustal cooling and margin evolution in Yemen, *Geochimica Et Cosmochimica Acta*, *61*(12), 2511-2527.

Menzies, M., et al. (2001), Cenozoic plume evolution and flood basalts in Yemen: A key to understanding older examples, *Mantle Plumes: Their Identification through Time*(352), 23-36.

Menzies, A. H., et al. (2003), Re-Os systematics of diamond-bearing eclogites from the Newlands kimberlite, *Lithos*, *71*(2-4), 323-336.

Merla, G., et al. (1979), Geological map of Ethiopia and Somalia (Explanatory Notes), Consiglio Nationale delle Richerche, Italy.

Meshesha, D., and R. Shinjo (2007), Crustal contamination and diversity of magma sources in the northwestern Ethiopian volcanic province, *Journal of Mineralogical and Petrological Sciences*, *102*(5), 272-290.

Meshesha, D., and R. Shinjo (2008), Rethinking geochemical feature of the Afar and Kenya mantle plumes and geodynamic implications, *Journal of Geophysical Research-Solid Earth*, *113*(B9).

Meyer, W., et al. (1975), Tectonic evolution of the northern part of the Main Ethiopian Rift, in *Afar depression of Ethiopia*, edited by A. Pilger and A. Rosler, pp. 374–395, Schweizerbart, Stuttgart.

Mickus, K., et al. (2007), Gravity analysis of the main Ethiopian rift, *Journal of African Earth Sciences*, *48*, 59-69.

Mitchell, D. J. W., et al. (1992), Tectonostratigraphic framework and hydrocarbon potential of the Red Sea, *Journal of Petroleum Geology*, *15*(2), 187-209.

Mock, C., et al. (1999), $^{40}Ar/^{39}Ar$ thermochronology of the Ethiopian and Yemeni basements: reheating related to the Afar plume?, *Tectonophysics*, *314*(4), 351-372.

Mohr, P. (1983), Ethiopian flood basalt province, *Nature*, *303*(5918), 577-584.

Mohr, P. (1987), Patterns of faulting in the Ethiopian Rift Valley, *Tectonophysics*, *143*(1-3), 169-179.

Mohr, P. A., and B. Zanettin (1988), The Ethiopian flood basalt province, in *Continental flood basalts*, edited by J. D. Macdougall, Kluwer Academic, Dordrecht.

Momme, P., and J. R. Wilson (2002), The Kraemer Island macrodyke, East Greenland: solidification of a flood basalt conduit, *Geological Magazine*, *139*(2), 171-190.

Montagner, J. P. (2000), Seismic plume detection in Africa at different scales, paper presented at Penrose Conference: Volcanic Rifted Margins, Geological Society of America, Royal Holloway, University of London.

Montagner, J. P., et al. (2007), Mantle upwellings and convective instabilities revealed by seismic tomography and helium isotope geochemistry beneath eastern Africa, *Geophysical Research Letters*, *34*(21).

Montelli, R., et al. (2004), Finite-Frequency Tomography Reveals a Variety of Plumes in the Mantle, *Science*, *303*(5656), 338-343.

Morbidelli, L., et al. (1975), Ethiopian southern plateau and related escarpment: K/Ar ages of the main volcanic events (Main Ethiopian Rift from 8°10' to 9°.00' lat. north, in *Afar depression of Ethiopia*, edited by A. Pilger and A. Rosler, pp. 362-369, Schweizerbart, Stuttgart.

Moreira, M., et al. (1996), Rare gas systematics in Red Sea ridge basalts, *Geophysical Research Letters*, *23*(18), 2453-2456.

Moreira, M., et al. (1998), Rare gas systematics in popping rock: Isotopic and elemental compositions in the upper mantle, *Science*, *279*(5354), 1178-1181.

Moreira, M., et al. (1999), Helium and lead isotope geochemistry of the Azores Archipelago, *Earth and Planetary Science Letters*, *169*(1-2), 189-205.

Moreira, M., and M. D. Kurz (2001), Subducted oceanic lithosphere and the origin of the HIMU basalt helium isotopic signature, *Earth and Planetary Science Letters*, *189*(1-2), 49-57.

Morgan, W. J. (1971), Convection plumes in the lower mantle, *Nature*, *230*(5288), 42-43.

Morgan, J. W., and P. A. Baedecker (1983), Elemental composition of sulphide particles from an ultramafic xenolith and the siderophile content of the upper mantle, paper presented at Lunar and Planetary Sciences Conference 14

Morgan, J. W. (1986), Ultramafic xenoliths: clues to the Earth's late accretionary history, *Journal of Geophysical Research-Solid Earth and Planets*, *91*(B12), 2375-2387.

Mulugeta, G., and W. Ghebreab (2001), Modeling heterogeneous stretching during episodic or steady rifting of the continental lithosphere, *Geology*, *29*(10), 895-898.

Mulugeta, G., et al. (2007), Emplacement mechanisms for Continental Flood Basalts and implications for plume activity during incipient continental breakup, *Journal of African Earth Sciences*, *48*(2-3), 137-146.

Murphy, M. S., et al. (2000), Secondary upwelling instabilities developed in high Rayleigh number convection: possible applications to hot spots, *Visual Geosciences*, *5*(4), 1-10.

Nasir, S. (1992), The lithosphere beneath the north-western part of the Arabian plate, Jordan: evidence from xenoliths and geophysics, *Tectonophysics*, *201*(3-4), 357-370.

Nasir, S., and A. Safarjalani (2000), Lithospheric petrology beneath the northern part of the Arabian Plate in Syria: evidence from xenoliths in alkali basalts, *Journal of African Earth Sciences*, *30*(1), 149-168.

Nasir, S., et al. (2006), Geochemistry and petrology of Tertiary volcanic rocks and related ultramafic xenoliths from the central and eastern Oman Mountains, *Lithos*, *90*(3-4), 249-270.

Nataf, H. C. (2000), Seismic imaging of mantle plumes, *Annual Review of Earth and Planetary Sciences*, *28*, 391-417.

Natland, J. H. (2003), Capture of Helium and Other Volatiles during the Growth of Olivine Phenocrysts in Picritic Basalts from the Juan Fernandez Islands, *J. Petrology*, *44*(3), 421-456.

Natland, J. H., and E. L. Winterer (2005), Fissure control on volcanic action in the Pacific, in *Plumes, Plates, and Paradigms*, edited by G. R. Foulger, et al., Geological Society of America.

Nekvasil, H. (1992), Ternary feldspar crystallization in high-temperature felsic magmas, *American Mineralogist*, *77*(5-6), 592-604.

Neumann van Padang, M. (1963), Arabia and the Indian Ocean. Catalog of Active Volcanoes of the World, *IAVCEI*, *16*, 39-41.

Newsom, H. E., and K. W. W. Sims (1991), Core formation during the early accretion of the Earth, *Science*, *252*(5008), 926-933.

Ni, S. D., et al. (1999), Low-velocity structure beneath Africa from forward modeling, *Earth and Planetary Science Letters*, *170*(4), 497-507.

Nicholls, J., and M. Z. Stout (1988), Picritic Melts in Kilauea: evidence from the 1967-1968 Halemaumau and Hiiaka Eruptions, *J. Petrology*, *29*(5), 1031-1057.

Nielsen, T. F. D. (1981), The ultramafic cumulate series, Gardiner Complex, East Greeland: cumulates in a shallow level magma chamber of a nephelinitic volcano, *Contributions to Mineralogy and Petrology*, *76*(1), 60-72.

Nisbet, E. G., et al. (1993), Constaining the potential temperture of the Archean mantle: review of the evidence from komatiites, *Lithos*, *30*(3-4), 291-307.

Nolet, G., et al. (2003), Finite frequencey tomography shows a variety of plumes, *Geophysical Research Abstracts, Vol. 5*

Nolet, G., et al. (2007), Mantle plume tomography, *Chemical Geology*, *241*(3-4), 248-263.

Norman, M. D., and M. O. Garcia (1999), Primitive magmas and source characteristics of the Hawaiian plume: petrology and geochemistry of shield picrites, *Earth and Planetary Science Letters*, *168*(1-2), 27-44.

Normand, C., et al. (2002), Hydrothermal alteration of olivine in a flow-through autoclave: nucleation and growth of serpentine phases, *American Mineralogist*, *87*(11-12), 1699-1709.

Nusbaum, R. L., et al. (1993), The distribution of earthquakes and volcanoes along the the East African rift system, *Episodes*, *16*(4), 427-432.

Nyblade, A. A. (2000), New seismic evidence for a mantle plume beneath East Africa, paper presented at Penrose Conference: Volcanic Rifted Margins, Geological Society of America, Royal Holloway, University of London.

Nyblade, A. A., et al. (2000a), Seismic evidence for a deep upper mantle thermal anomaly beneath east Africa, *Geology*, *28*(7), 599-602.

Nyblade, A. A., et al. (2000b), Mantle transition zone thickness beneath Afar: implications for the origin of the Afar hotspot, *Geophysical Journal International*, *142*(2), 615-619.

Nyblade, A. A., and R. A. Brazier (2002), Precambrian lithospheric controls on the development of the East African rift system, *Geology*, *30*(8), 755-758.

O'Connor, J. M., et al. (2001a), En echelon volcanic elongate ridges connecting intraplate Foundation Chain volcanism to the Pacific-Antarctic spreading center (Vol. 189, pg 93, 2001), *Earth and Planetary Science Letters*, *192*(4), 631-+.

O'Connor, J. M., et al. (2001a), En echelon volcanic elongate ridges connecting intraplate Foundation Chain volcanism to the Pacific-Antarctic spreading center, *Earth and Planetary Science Letters*, *189*(1-2), 93-102.

Oganov, A. R., et al. (2001), The elastic constants of $MgSiO_3$ perovskite at pressures and temperatures of the Earth's mantle, *Nature*, *411*(6840), 934-937.

Oganov, A. R., et al. (2001), Ab initio molecular dynamics study of $MgSiO_3$ perovskite: from wave-functions to high-P/T elasticity and interpretation of seismic tomography paper presented at Mantle materials, processes and products (VMSG Annual Conference), Mineralogical Society, Durham.

O'Hara, M. J., and C. Herzberg (2002), Interpretation of trace element and isotope features of basalts: relevance of field relations, petrology, major element data, phase equilibria, and magma chamber modeling in basalt petrogenesis, *Geochimica et Cosmochimica Acta*, *66*(12), 2167-2191.

Omar, G. I., and M. S. Steckler (1995), Fission-track evidence on the initial rifting of the Red Sea: two pulses, no propagation, *Science*, *270*(5240), 1341-1344.

O'Neill, H. S. C. (1987), Quartz-fayalite-iron and quartz-fayalite-magnetite equilibria and the free energy of formation of fayalite (Fe_2SiO_4) and magnetite (Fe_3O_4), *American Mineralogist*, *72*(1-2), 67-75.

Oppenheimer, C., and P. Francis (1997), Remote sensing of heat, lava and fumarole emissions from Erta'Ale volcano, Ethiopia, *International Journal of Remote Sensing*, *18*(8), 1661-1692.

Oppenheimer, C., and P. Francis (1998), Implications of longeval lava lakes for geomorphological and plutonic processes at Erta 'Ale volcano, Afar, *Journal of Volcanology and Geothermal Research*, *80*(1-2), 101-111.

O'Reilly, S. Y., et al. (2008), Taking the pulse of the Earth: linking crustal and mantle events, *Australian Journal of Earth Sciences*, *55*(6-7), 983-995.

Orihashi, Y., et al. (1998), Dispersion of the Afar plume: Implications from the spatiotemporal distribution of the late Miocene to recent volcanics, southwestern Arabian Peninsula, *Gondwana Research*, *1*(2), 221-234.

Orihashi, Y., et al. (2001), Primordial helium isotope signature from Plio-Quaternary alkaline basalts in Yemen, *Island Arc*, *10*(2), 145-157.

Overstreet, W. C., et al. (1977), Tertiary laterite of the As Sarat Mountains, Asir province, Kingdom of Saudi Arabia, *Mineral Resources Bulletin, Saudi Arabia Director General Mineral Resources*, *21*, 1-30.

Pan, M., et al. (2002), An analysis of the Ethiopian Rift Valley GPS campaigns in 1994 and 1999, *Journal of Geodynamics*, *33*(3).

Park, Y., and A. A. Nyblade (2006), P-wave tomography reveals a westward dipping low velocity zone beneath the Kenya Rift, *Geophysical Research Letters*, *33*(7).

Park, Y., et al. (2007), Upper mantle structure beneath the Arabian Peninsula and northern Red Sea from teleseismic body wave tomography: implications for the origin of Cenozoic uplift and volcanism in the Arabian Shield, *Geochemistry Geophysics Geosystems*, *8*.

Park, Y., et al. (2008), S wave velocity structure of the Arabian Shield upper mantle from Rayleigh wave tomography, *Geochemistry Geophysics Geosystems*, *9*.

Parkinson, I. J., and R. J. Arculus (1999), The redox state of subduction zones: insights from arc-peridotites, *Chemical Geology*, *160*(4), 409-423.

Paslick, C., et al. (1995), Enrichment of the continental lithosphere by OIB melts: isotopic evidence from the volcanic province of northern Tanzania, *Earth and Planetary Science Letters*, *130*(1-4), 109-126.

Patterson, D. B. (1992), Noble gas geochemistry of selected basalts and basaltic andesites, New Zealand, Tonga-Keradec and Vanatu (unpublished PhD thesis), The Australian National University, Canberra.

Pawley, A. R., et al. (2001), The stability of 10-angstrom phase in the Earth's mantle, paper presented at Mantle materials, processes and products (VMSG Annual Conference), Mineralogical Society, Durham.

Pearce, J. A., and J. R. Cann (1973), Tectonic setting of basic volcanic rocks determined using trace element analyses, *Earth and Planetary Science Letters*, *19*(2), 290-300.

Pearce, J. A. (1983), The role of sub-continental lithosphere in magma genesis at destructive plate margins, in *Continental basalts and mantle xenoliths*, edited by C. Hawkesworth and M. J. Norry, pp. 230-249, Shiva, Nantwich.

Peate, D. W., and C. J. Hawkesworth (1996), Lithospheric to asthenospheric transition in Low-Ti flood basalts from southern Parana, Brazil, *Chemical Geology*, *127*(1-3), 1-24.

Peate, D. W., et al. (1999), Petrogenesis and stratigraphy of the high-Ti/Y Urubici magma type in the Parana flood basalt province and implications for the nature of 'Dupal'-type mantle in the South Atlantic region, *Journal of Petrology*, *40*(3), 451-473.

Peate, D. W., et al. (2003), The Prinsen af Wales Bjerge formation lavas, East Greenland: the transition from tholeiitic to alkalic magmatism during Palaeogene continental break-up, *Journal of Petrology*, *44*(2), 279-304.

Peate, I. U., et al. (2005), Volcanic stratigraphy of large-volume silicic pyroclastic eruptions during Oligocene Afro-Arabian flood volcanism in Yemen, *Bulletin of Volcanology*, *68*(2), 135-156.

Peccerillo, A., et al. (1998), The Precambrian rocks from Southern Ethiopia: petrology, geochemistry and their interaction with the Recent volcanism from the Ethiopian Rift Valley, *Neues Jahrbuch Fur Mineralogie-Abhandlungen*, *173*(3), 237-262.

Peccerillo, A., et al. (2003), Relationships between mafic and peralkaline silicic magmatism in continental rift settings: a petrological, geochemical and isotopic study of the Gedemsa volcano, central Ethiopian rift, *Journal of Petrology*, *44*(11), 2003-2032.

Peccerillo, A., et al. (2007), Petrogenesis of silicic peralkaline rocks in the Ethiopian rift: Geochemical evidence and volcanological implications, *Journal of African Earth Sciences*, *48*, 161-173.

Phipps-Morgan, J., and W. J. Morgan (1999), Two-stage melting and the geochemical evolution of the mantle: a recipe for mantle plum-pudding, *Earth and Planetary Science Letters*, *170*(3), 215-239.

Piccirillo, E. M., et al. (1979), Geodynamic evolution from plateau to rift: major and trace element geochemistry of the central eastern Ethiopian plateau volcanics, *Neues Jahrbuch fur Geologie und Palaontologie*, *258*, 139-179.

Pik, R., et al. (1998), The northwestern Ethiopian Plateau flood basalts. Classification and spatial distribution of magma types, *Journal of Volcanology and Geothermal Research*, *81*(1-2), 91-111.

Pik, R., et al. (1999), Isotopic and trace element signatures of Ethiopian flood basalts: evidence for plume-lithosphere interactions, *Geochimica et Cosmochimica Acta*, *63*(15), 2263-2279.

Pik, R., et al. (2003), Stability of the Upper Nile drainage network (Ethiopia) deduced from (U-Th)/He thermochronometry: implications for uplift and erosion of the Afar plume dome, *Earth and Planetary Science Letters*, *215*(1-2), 73-88.

Pik, R., et al. (2006), How many mantle plumes in Africa? The geochemical point of view, *Chemical Geology*, *226*(3-4), 100-114.

Pik, R., et al. (2008), Timing of East African Rift development in southern Ethiopia: implication for mantle plume activity and evolution of topography, *Geology*, *36*(2), 167-170.

Polet, J., and D. L. Anderson (1995), Depth extent of cratonas as inferred from tomographgic studies, *Geology*, *23*(3), 205-208.

Porcelli, D. R., et al. (1992), Isotopic relationships of volatile and lithosphile trace elements in continental ultramafic xenoliths, *Contributions to Mineralogy and Petrology*, *110*(4), 528-538.

Porcelli, D., and G. J. Wasserburg (1995), Mass- transfer of helium, neon, argon and xenon through a steady-state upper mantle, *Geochimica et Cosmochimica Acta*, *59*(23), 4921-4937.

Pyle, D. M. (1999), Widely dispersed Quaternary tephra in Africa, *Global and Planetary Change*, *21*(1-3), 95-112.

Ravizza, G., et al. (2001), Re-Os systematics and platinum-group element distribution in metalliferous sediments from the Troodos ophiolite, *Earth and Planetary Science Letters*, *188*(3-4), 369-381.

Reisberg, L., et al. (1993), Os isotope systematics in ocean island basalts, *Earth and Planetary Science Letters*, *120*(3-4), 149-167.

Reisberg, L., et al. (1998), Os isotopic results from rift and flood basalts of Ethiopia and Djibouti, paper presented at Goldschmidt Conference, Toulouse.

Reisberg, L., et al. (2004), Reliability of Os model ages in pervasively metasomatized continental mantle lithosphere: a case study of Sidamo spinel peridotite xenoliths (East African Rift, Ethiopia), *Chemical Geology*, *208*(1-4), 119-140.

Renne, P. R., and A. R. Basu (1991), Rapid Eruption of the Siberian Traps Flood Basalts at the Permo-Triassic Boundary, *Science*, *253*(5016), 176-179.

Renne, P. R., et al. (1999), Chronostratigraphy of the Miocene-Pliocene Sagantole Formation, Middle Awash Valley, Afar rift, Ethiopia, *Geological Society of America Bulletin*, *111*(6), 869-885.

Revillon, S., et al. (2000), Geochemical study of ultramafic volcanic and plutonic rocks from Gorgona Island, Colombia: the plumbing system of an oceanic plateau, *Journal of Petrology*, *41*(7), 1127-1153.

Revillon, S., et al. (2002), Heterogeneity of the Caribbean plateau mantle source: Sr, O and He isotopic compositions of olivine and clinopyroxene from Gorgona Island, *Earth and Planetary Science Letters*, *205*(1-2), 91-106.

Rex, D. C., et al. (1971), Age of the Ethiopian flood basalts, *Nature*, *230*(5292), 282-&.

Rhodes, M., and J. H. Davies (2001), Tomographic imaging of multiple mantle plumes in the uppermost lower mantle, *Geophysical Journal International*, *147*(1), 88-92.

Ricard, Y., and N. Coltice (2004), Geophysical and geochernical models of mantle convection: Successes and future challenges, *State of the Planet: Frontiers and Challenges in Geophysics*, *150*, 59-68.

Riisager, J., et al. (1999), Paleointensity results from Ethiopian basalts: implications for the Oligocene geomagnetic field strength, *Geophysical Journal International*, *138*(2), 590-596.

Riisager, P., et al. (2005), Paleomagnetism and $^{40}Ar/^{39}Ar$ geochronology of Yemeni Oligocene volcanics: Implications for timing and duration of Afro-Arabian traps and geometry of the Oligocene paleomagnetic field, *Earth and Planetary Science Letters*, *237*(3-4), 647-672.

Ritsema, J., et al. (1999), Complex shear wave velocity structure imaged beneath Africa and Iceland, *Science*, *286*(5446), 1925-1928.

Ritsema, J., and H. van Heijst (2000), New seismic model of the upper mantle beneath Africa, *Geology*, *28*(1), 63-66.

Ritsema, J., and R. M. Allen (2003), The elusive mantle plume, *Earth and Planetary Science Letters*, *207*(1-4), 1-12.

Robertson-Research (1993), Red Sea/Gulf of Aden Hydrocarbon Study Project.

Robinson, J. A. C., et al. (1998), The beginning of melting of fertile and depleted peridotite at 1.5 GPa, *Earth and Planetary Science Letters*, *155*(1-2), 97-111.

Rochette, P., et al. (1998), Magnetostratigraphy and timing of the Oligocene Ethiopian traps, *Earth and Planetary Science Letters*, *164*(3-4), 497-510.

Roeder, P. L., and R. F. Emslie (1970), Olivine-liquid equilibrium, *Contributions to Mineralogy and Petrology*, *29*(4), 275.

Roger, S., et al. (1997), Active or passive rifting in Ethiopia? Contribution from the study of peridotitic xenoliths from the Tana lake area, *Comptes Rendus De L Academie Des Sciences Serie Ii Fascicule a-Sciences De La Terre Et Des Planetes*, *324*(12), 1009-1016.

Roger, S., et al. (1999), An insight on the nature, composition and evolution of the lithospheric mantle beneath the north-western Ethiopian Plateau; the ultrabasic xenoliths from the Tana Lake Province, *Acta Vulcanologica 11*, 161-168

Rogers, N. W. (1993), The isotope and trace element geochemistry of basalts from the volcanic islands of the southern Red Sea, *Geological Society, London, Special Publications*, *76*(1), 455-467.

Rogers, N., et al. (2000), Two mantle plumes beneath the east African rift system: Sr, Nd and Pb isotope evidence from Kenya Rift basalts, *Earth and Planetary Science Letters*, *176*(3-4), 387-400.

Rogers, N. W. (2004), Basaltic magnatism and the geodynamics of the East African rift system, paper presented at East African Rift Systems: Geodynamics, Resources and Environment, Addis Ababa, Jun.

Rogers, N. W. (2006), Basaltic magmatism and the geodynamics of the East African Rift System, in *The Afar Volcanic Province within the East African Rift System*, edited by G. Yirgu, et al., Geological Society of London.

Rollinson, H. (1998), *Using geochemical data: evaluation, presentation, interpretation*, Longman.

Romanowicz, B. (1995), A global tomographic model of shear attenuation in the upper mantle, *Journal of Geophysical Research-Solid Earth*, *100*(B7), 12375-12394.

Rooney, T., et al. (2007), Lithospheric modification during crustal extension in the Main Ethiopian Rift, *Journal of Geophysical Research-Solid Earth*, *112*(B10).

Rooney, T., et al. (2008), Multi-component isotopic mixing in the Ethiopian Rift: modeling plume contributions to recent magmatism, *Geochimica et Cosmochimica Acta*, *72*(12), A804-A804.

RoyBarman, M., et al. (1996), Os isotopes in orogenic lherzolite massifs and mantle heterogeneities, *Chemical Geology*, *130*(1-2), 55-64.

Roy-Barman, M., and C. J. Allegre (1994), $^{187}Os/^{186}Os$ ratios of mid-ocean ridge basalts and abyssal peridotites, *Geochimica Et Cosmochimica Acta*, *58*(22), 5043-5054.

Roy-Barman, M., and C. J. Allegre (1995), $^{187}Os/^{186}Os$ in oceanic island basalts: tracing oceanic crust recycling in the mantle, *Earth and Planetary Science Letters*, *129*(1-4), 145-161.

Roy-Barman, M., et al. (1998), Osmium isotopic compositions and Re-Os concentrations in sulfide globules from basaltic glasses, *Earth and Planetary Science Letters*, *154*(1-4), 331-347.

Sack, R. O., et al. (1980), Ferric–ferrous equilibria in natural silicate liquids at 1 bar, *Contributions to Mineralogy and Petrology*, *75*, 369–376.

Sack, R. O., and M. S. Ghiorso (1991), An internally consistent model for the thermodynamic properties of Fe-Mg titanomagnetite-aluminate spinels, *Contributions to Mineralogy and Petrology*, *106*(4), 474-505.

Saif, S. I., and S. M. A. Shah (1992), Geochemical characteristics of the Cenozoic basaltic rocks, north-western Saudi Arabia, *Journal of African Earth Sciences*, *14*(2), 173-181.

Sarda, P., et al. (1988), Neon isotopes in submarine basalts, *Earth and Planetary Science Letters*, *91*(1-2), 73-88.

Sarda, P., et al. (2000), Rare gas systematics on the southernmost Mid-Atlantic Ridge: constraints on the lower mantle and the Dupal source, *Journal of Geophysical Research-Solid Earth*, *105*(B3), 5973-5996.

Saunders, A. D., et al. (1992), Consequences of plume lithosphere interactions, in *Magmatism and the Causes of Continental Break-Up*, edited by B. C. Storey, et al., pp. 41-59, Geological Society, London.

Saunders, A. D. (2005), Large igneous provinces: origin and environmental consequences, *Elements*, *1*(5), 259-263.

Saunders, A. D., et al. (2005), A mantle plume origin for the Siberian traps: uplift and extension in the West Siberian Basin, Russia, *Lithos*, *79*(3-4), 407-424.

Saunders, A. D., et al. (2007), Regional uplift associated with continental large igneous provinces: the roles of mantle plumes and the lithosphere, *Chemical Geology*, *241*(3-4), 282-318.

Scarrow, J. H., and K. G. Cox (1995), Basalts generated by decompressive adiabatic melting of a mantle plume: a case study from the Isle of Skye, N W Scotland, *Journal of Petrology*, *36*(1), 3-22.

Scarrow, J. H., et al. (2000), Major element records of variable plume involvement in the North Atlantic Province tertiary flood basalts, *Journal of Petrology*, *41*(7), 1155-1176.

Scarsi, P., and H. Craig (1996), Helium isotope ratios in Ethiopian Rift basalts, *Earth and Planetary Science Letters*, *144*(3-4), 505-516.

Schaefer, B. F. (2000), Re-Os isotope separation and analysis at the Open University, *Unpublished Guide: Department of Earth Sciences, The Open University*.

Schaefer, B. F., et al. (2000a), Deep mantle plume osmium isotope signature from West Greenland Tertiary picrites, *Earth and Planetary Science Letters*, *175*(1-2), 105-118.

Schaefer, B. F., et al. (2000b), Re-Os isotope characteristics of postorogenic lavas: implications for the nature of young lithospheric mantle and its contribution to basaltic magmas, *Geology*, *28*(6), 563-566.

Schaefer, B. F., et al. (2002), Evidence for recycled Archaean oceanic mantle lithosphere in the Azores plume, *Nature*, *420*(6913), 304-307.

Schaefer, C. J., and S. A. Kattenhorn (2004), Characterization and evolution of fractures in low-volume pahoehoe lava flows, eastern Snake River Plain, Idaho, *Geological Society of America Bulletin*, *116*(3-4), 322-336.

Schersten, A., et al. (2004), Tungsten isotope evidence that mantle plumes contain no contribution from the Earth's core, *Nature*, *427*(6971), 234-237.

Schilling, J. G., et al. (1992), Nd-Sr-Pb isotopic variations along the Gulf of Aden: evidence for Afar mantle plume continental lithosphere interaction, *Journal of Geophysical Research-Solid Earth*, *97*(B7), 10927-10966.

Schmidt, G., et al. (2000), Are highly siderophile elements (PGE, Re and Au) fractionated in the upper mantle of the earth? New results on peridotites from Zabargad, *Chemical Geology*, *163*(1-4), 167-188.

Schultz, R. A., et al. (2008), Emplacement conditions of igneous dikes in Ethiopian Traps, *Journal of Volcanology and Geothermal Research*, *178*(4), 683-692.

Scowen, P. A. H., et al. (1991), Re-equilibration of chromite within Kilauea lava-lake, Hawaii, *Contributions to Mineralogy and Petrology*, *107*(1), 8-20.

Sebai, A., et al. (2006), Anisotropic structure of the African upper mantle from Rayleigh and Love wave tomography, *Physics of the Earth and Planetary Interiors*, *155*(1-2), 48-62.

Self, S., et al. (1996), A new model for the emplacement of Columbia River Basalts as large, inflated pahoehoe lava flow fields, *Geophysical Research Letters*, *23*(19), 2689-2692.

Self, S., et al. (1998), The importance of pahoehoe, *Annual Review of Earth and Planetary Sciences*, *26*, 81-110.

Sella, G. F., et al. (2002), REVEL: a model for Recent plate velocities from space geodesy, *Journal of Geophysical Research-Solid Earth*, *107*(B4).

Shaw, J. E., et al. (2003), Petrogenesis of the largest intraplate volcanic field on the Arabian plate (Jordan): a mixed lithosphere-asthenosphere source activated by lithospheric extension, *Journal of Petrology*, *44*(9), 1657-1679.

Shaw, J. E., et al. (2007), The geochemistry of the Arabian lithospheric mantle: a source for intraplate volcanism?, *Journal of Petrology*, *48*(8), 1495-1512.

Shen, J. J. S., and H. J. Yang (2004), Sources and genesis of the Chinkuashih Au-Cu deposits in northern Taiwan: constraints from Os and Sr isotopic compositions of sulfides, *Earth and Planetary Science Letters*, *222*(1), 71-83.

Sheth, H. C. (1999), Flood basalts and large igneous provinces from deep mantle plumes: fact, fiction, and fallacy, *Tectonophysics*, *311*(1-4), 1-29.

Sheth, H. C. (2007), Large igneous provinces (LIPs): definition, recommended terminology, and a hierarchical classification, *Earth-Science Reviews*, *85*(3-4), 117-124.

Shimizu, N. (1990), The oscillatory trace element zoning of augite phenocrysts, *Earth-Science Reviews*, *29*(1-4), 27-37.

Shirey, S. B., and R. J. Walker (1995), Carius tube digestion for low blank rhenium-osmium analysis, *Analytical Chemistry*, *67*(13), 2136-2141.

Shirey, S. B., and R. J. Walker (1998), The Re-Os isotope system in cosmochemistry and high-temperature geochemistry, *Annual Review of Earth and Planetary Sciences*, *26*, 423-500.

Sicilia, D., et al. (2008), Upper mantle structure of shear-waves velocities and stratification of anisotropy in the Afar hotspot region, *Tectonophysics*, *462*(1-4), 164-177.

Simonetti, A., and K. Bell (1995), Nd, Pb and Sr isotopic data from the Mount Elgon volcano, Eastern Uganda- Western Kenya: implications for the origin and evolution of nephelinite lavas, *Lithos*, *36*(2), 141-153.

Simonetti, A., et al. (1996), Diopside phenocrysts from nephelinite lavas, Napak volcano, eastern Uganda: evidence for magma mixing, *The Canadian Mineralogist*, *34*, 411-421.

Sleep, N. H. (1990), Hotspots and mantle plumes - some phenomenology, *Journal of Geophysical Research-Solid Earth and Planets*, *95*(B5), 6715-6736.

Smith, W. H. F., and D. T. Sandwell (1997), Global sea floor topography from satellite altimetry and ship depth soundings, *Science*, *277*(5334), 1956-1962.

Smith, A. D., and C. Lewis (1999), The planet beyond the plume hypothesis, *Earth-Science Reviews*, *48*(3), 135-182.

Smith, A. D. (2003), Intraplate volcanism: concepts, problems and proofs, *Astronomy & Geophysics*, *44*(2), 8-9.

Smith, A. D. (2003), Critical evaluation of Re-Os and Pt-Os isotopic evidence on the origin of intraplate volcanism, *Journal of Geodynamics*, *36*(4), 469-484.

Smoliar, M. I., et al. (1996), Re-Os ages of group IIA, IIIA, IVA, and IVB iron meteorites, *Science*, *271*(5252), 1099-1102.

Smoliar, M. I., et al. (1997), Rhenium-osmium isochron for IA meteorites: further refinement of the rhenium-187 decay constant, *Meteoritics & Planetary Science*, *32*(4), A122-A123.

Snow, J. E., and L. Reisberg (1995), Os isotopic systematics of the MORB mantle: results from altered abyssal peridotites, *Earth and Planetary Science Letters*, *133*(3-4), 411-421.

Snow, J. E., and L. Reisberg (1995), Os isotopic systematics of the MORB mantle: results from altered abyssal peridotites (Vol. 133, pg 411, 1995), *Earth and Planetary Science Letters*, *136*(3-4), 723-733.

Snow, J. E., and G. Schmidt (1999), Proterozoic melting in the northern peridotite Massif, Zabargad Island: Os isotopic evidence, *Terra Nova*, *11*(1), 45-50.

Soto, J. I., and M. Soto (1995), PTMAFIC: software for thermometry, barometry and activity calculations in mafic rocks using an IBM-compatible computer, *Computers & Geosciences*, *21*(5), 619-652.

Souriot, T., and J. P. Brun (1992), Faulting and block rotation in the Afar Triangle, East Africa - the Danakil crank-arm model, *Geology*, *20*(10), 911-914.

Spath, A., et al. (2000), The petrology of the Chyulu Hills Volcanic Province, southern Kenya, *Journal of African Earth Sciences*, *31*(2), 337-358.

Spath, A., et al. (2001), Plume-lithosphere interaction and the origin of continental rift-related alkaline volcanism - the Chyulu Hills Volcanic Province, southern Kenya, *Journal of Petrology*, *42*(4), 765-787.

Stamps, D. S., et al. (2008), A kinematic model for the east African rift, *Geophysical Research Letters*, *35*(5).

Staudacher, T., and C. J. Allegre (1982), Terrestrial xenology, *Earth and Planetary Science Letters*, *60*(3), 389-406.

Staudacher, T., et al. (1990), Noble gas systematics of Reunion Island, Indian Ocean, *Chemical Geology*, *89*(1-2), 1-17.

Steckler, M. S., and G. I. Omar (1994), Controls on erosional retreat of the uplifted rift-flanks at the Gulf of Suez and northern Red Sea, *Journal of Geophysical Research-Solid Earth*, *99*(B6), 12159-12173.

Stewart, K., and N. Rogers (1996), Mantle plume and lithosphere contributions to basalts from southern Ethiopia, *Earth and Planetary Science Letters*, *139*(1-2), 195-211.

Stone, W. E., et al. (1995), Origin of Archean ferropicrites: geochemical constraints from the Boston Creek flow, Abiti Greenstone Belt, Ontario, Canada, *Chemical Geology*, *121*(1-4), 51-71.

Storey, B. C., et al. (Eds.) (1992), *Magmatism and the causes of continetal break-up*, The Geological Society of London.

Storey, B. C. (1995), The role of mantle plumes in continental break-up: case histories from Gonwanaland, *Nature 377*, 301-308.

Stracke, A., et al. (2003), Theistareykir revisited, *Geochemistry Geophysics Geosystems*, *4*.

Stuart, F. M., et al. (2000), Constraints on mantle plumes from the helium isotopic composition of basalts from the British Tertiary Igneous Province, *Earth and Planetary Science Letters*, *177*(3-4), 273-285.

Stuart, G. W., et al. (2006), Crustal structure of the northern Main Ethiopian Rift from receiver function studies, *Afar Volcanic Province within the East African Rift System*, *259*, 253-267.

Sturm, R. (2002), PX-NOM - an interactive spreadsheet program for the computation of pyroxene analyses derived from the electron microprobe, *Computers & Geosciences*, *28*(4).

Sun, S. S., and W. F. McDonough (1989), Chemical and isotope systematics of oceanic basalts: implications for mantle composition and processes, in *Magmatism in ocean basins*, edited by A. D. Saunders and M. J. Norry, pp. 313-345, Geological Society of London.

Tadesse, T. (1996), Structure across a possible intra-oceanic suture zone in the low-grade Pan-African rocks of northern Ethiopia, *Journal of African Earth Sciences*, *23*(3), 375-381.

Tadesse, T., et al. (1999), Geochemistry of low-grade metavolcanic rocks from the Pan-African of the Axum area, northern Ethiopia, *Precambrian Research*, *96*(1-2), 101-124.

Tadesse, S., et al. (2003), Geology and mineral potential of Ethiopia: a note on geology and mineral map of Ethiopia, *Journal of African Earth Sciences*, *36*(4), 273-313.

Tadesse, S. (2004), Genesis of the shear zone-related gold vein mineralization of the Lega Dembi Gold, Adola gold field, southern Ethiopia, *Gondwana Research*, *7*(2), 481-488.

Takahahshi, E., et al. (1998), Origin of the Columbia River basalts: melting model of a heterogeneous plume head, *Earth and Planetary Science Letters*, *162*(1-4), 63-80.

Takahashi, E., and E. Ito (1987), Mineralogy of mantle peridotite along a model geotherm up to 700 km depth, in *High-Pressure Research in Mineral Physics*, edited by M. H. Manghnani and Y. Syono, pp. 427-437, American Geophysical Union.

Takahashi, E., et al. (1993), Melting of a peridotite KLB-1 to 6.5 GPa and the origin of basaltic magmas, *Philosophical Transactions of the Royal Society London*, *342*, 105-120.

Talbot, C. J., and W. Ghebreab (1997), Red Sea detachment and basement core complexes in Eritrea, *Geology*, *25*(7), 655-658.

Tapponnier, P., et al. (1990), Bookshelf faulting and horizontal block rotations between over-lapping rifts in southern Afar, *Geophysical Research Letters*, *17*(1), 1-4.

Taylor, S. R., and S. M. McLennan (1985), *The continental crust: its composition and evolution*, Blackwell Scientific Publications, Oxford.

Tesfaye, S., et al. (2003), Early continental breakup boundary and migration of the Afar triple junction, Ethiopia, *Geological Society of America Bulletin*, *115*(9), 1053-1067.

Tesfaye, S. (2005), Fault population investigation and estimating magnitude of extension in Guma Graben, Central Afar, Ethiopia, *Journal of African Earth Sciences*, *41*(5), 437-444.

Tesfaye, D. B., et al. (2008), Evolution of the Southern Ethiopian Rift System: constrained from geochronological and geochemical data of mafic lavas of Amaro and Yabello areas, *Geochimica et Cosmochimica Acta*, *72*(12), A942-A942.

Thirlwall, M. F., et al. (1994), Interaction between the continental lithosphere and the Iceland Plume: Sr-Nd-Pb isotope geochemistry of Tertiary basalts, NE Greenland, *Journal of Petrology*, *35*(3), 839-879.

Thirlwall, M. (1997), Thermal ionisation mass spectrometry (TIMS), in *Modern analytical geochemistry: an introduction to quantitative chemical analysis techniques for earth, environmental and materials scientists*, edited by R. Gill, pp. 135-153, Longman.

Thompson, R. N. (1974), Some high pressure pyroxenes, *Mineralogical Magazine*, *39*(307), 768-787.

Thompson, R. N. (1982), Magmatism of the British Tertiary Volcanic Province, *Scottish Journal of Geology*, *18*, 49-107.

Thompson, R. N. (1987), Phase-equilibria constraints on the genesis and magmatic evolution of oceanic basalts, *Earth-Science Reviews*, *24*(3), 161-210.

Thompson, R. N., and S. A. Gibson (1994), Magmatic expression of lithospheric thinning across continental rifts, *Tectonophysics*, *233*(1-2), 41-68.

Thompson, R. N., and S. A. Gibson (2000), Transient high temperatures in mantle plume heads inferred from magnesian olivines in Phanerozoic picrites, *Nature*, *407*(6803), 502-506.

Thompson, R. N., et al. (2001), Early Cretaceous basalt and picrite dykes of the southern Etendeka region, NW Namibia: Windows into the role of the Tristan mantle plume in Parana-Etendeka magmatism, *Journal of Petrology*, *42*(11), 2049-2081.

Thompson, R. N., et al. (2007), Origin of CFB magmatism: multi-tiered intracrustal picrite-rhyolite magmatic plumbing at Spitzkoppe, western Namibia, during early Cretaceous Etendeka magmatism, *Journal of Petrology*, *48*(6), 1119-1154.

Thy, P. (1995), Experimental constraints on the evolution of transitional and mildly alkaline basalts - crystallisation of spinel, *Lithos*, *36*(2), 103-114.

Tiberi, C., et al. (2005), Inverse models of gravity data from the Red Sea-Aden-East African rifts triple junction zone, *Geophysical Journal International*, *163*(2), 775-787.

Tiberi, C., et al. (2007), Crustal geometry of the northeastern Gulf of Aden passive margin: localization of the deformation inferred from receiver function analysis, *Geophysical Journal International*, *168*(3), 1247-1260.

Tomlinson, K. Y., and K. C. Condie (2001), Archean mantle plumes: evidence from greenstone belt geochemistry, in *Mantle Plumes: Their Identification through Time*, edited by R. E. Ernst and K. L. Buchan, pp. 341-357, Geological Society of America.

Tommasini, S., et al. (2005), The Ethiopian subcontinental mantle domains: geochemical evidence from Cenozoic mafic lavas, *Mineralogy and Petrology*, *84*(3-4), 259-281.

Touchard, Y., et al. (2003), High-resolution magnetostratigraphic and biostratigraphic study of Ethiopian traps-related products in Oligocene sediments from the Indian Ocean, *Earth and Planetary Science Letters*, *206*(3-4), PII S0012-0821X(0002)01084-01081.

Trieloff, M., et al. (2000), The nature of pristine noble gases in mantle plumes, *Science*, *288*(5468), 1036-1038.

Trieloff, M., et al. (2002), Noble gas systematics of the Reunion mantle plume source and the origin of primordial noble gases in Earth's mantle, *Earth and Planetary Science Letters*, *200*(3-4), PII S0012-0821X(0002)00639-00638.

Trua, T., et al. (1999), Crustal control in the genesis of Plio-Quaternary bimodal magmatism of the Main Ethiopian Rift (MER): geochemical and isotopic (Sr, Nd, Pb) evidence, *Chemical Geology*, *155*(3-4), 201-231.

Tuff, J., et al. (2005), Experimental constraints on the role of garnet pyroxenite in the genesis of high-Fe mantle plume derived melts, *Journal of Petrology*, *46*(10), 2023-2058.

Tuff, J., and S. A. Gibson (2007), Trace-element partitioning between garnet, clinopyroxene and Fe-rich picritic melts at 3 to 7 GPa, *Contributions to Mineralogy and Petrology*, *153*(4), 369-387.

Turner, S., et al. (1994), Magmatism and continental break-up in the south Atlantic: high-precision $^{40}Ar/^{39}Ar$ geochronology, *Earth and Planetary Science Letters*, *121*(3-4), 333-348.

Turner, S., and C. Hawkesworth (1995), The nature of the sub-continental mantle: constraints from the major-element composition of continental flood basalts, *Chemical Geology*, *120*(3-4), 295-314.

Turner, S., et al. (1996), Mantle plumes, flood basalts, and thermal models for melt generation beneath continents: assessment of a conductive heating model and application to the Parana, *Journal of Geophysical Research-Solid Earth*, *101*(B5), 11503-11518.

Turner, S. P., et al. (1999), Petrogenesis of an 800 m lava sequence in eastern Uruguay: insights into magma chamber processes beneath the Parana flood basalt province, *Journal of Geodynamics*, *28*(4-5), 471-487.

Ukstins, I. A., et al. (2002), Matching conjugate volcanic rifted margins: $^{40}Ar/^{39}Ar$ chrono-stratigraphy of pre- and syn-rift bimodal flood volcanism in Ethiopia and Yemen, *Earth and Planetary Science Letters*, *198*(3-4).

Ukstins-Peate, I., et al. (2003), Correlation of Indian Ocean tephra to individual Oligocene silicic eruptions from Afro-Arabian flood volcanism, *Earth and Planetary Science Letters*, *211*(3-4), 311-327.

Ukstins-Peate, I., et al. (2008), Extreme geochemical heterogeneity in Afro-Arabian Oligocene tephras: Preserving fractional crystallization and mafic recharge processes in silicic magma chambers, *Lithos*, *102*(1-2), 260-278.

Ulmer, P. (1989), The dependence of the Fe^{2+}- Mg cation partitioning coefficient between olivine and basaltic liquid on the pressure, temperature and composition : an experimental study to 30 Kbars, *Contributions to Mineralogy and Petrology*, *101*(3), 261-273.

Ulmer, et al. (2001), Stability of hydrous phases in the upper mantle: inconsistencies related to the intepretation of high-pressure experiments containing hydrous fluid paper presented at Mantle materials, processes and products (VMSG Annual Conference), Mineralogical Society, Durham.

Valbracht, P. J., et al. (1997), Noble gas systematics of deep rift zone glasses from Loihi Seamount, Hawaii, *Earth and Planetary Science Letters*, *150*(3-4), 399-411.

van der Hilst, R. D., et al. (1997), Evidence for deep mantle circulation fromglobal tomography, *Nature*, *386*, 578-584.

van der Hilst, R. D., and H. Karason (1999), Compositional heterogeneity in the bottom 1000 kilometers of Earth's mantle: toward a hybrid convection model, *Science*, *283*(5409), 1885-1888.

van der Hilst, R. D., and M. V. de Hoop (2005), Banana-doughnut kernels and mantle tomography, *Geophysical Journal International*, *163*(3), 956-961.

van der Hilst, R. D., and M. V. de Hoop (2006), Reply to comment by R. Montelli, G. Nolet and F. A. Dahlen on 'Banana-doughnut kernels and mantle tomography', *Geophysical Journal International*, *167*(3), 1211-1214.

van Keken, P. E. (1997), Evolution of starting mantle plumes: comparison between laboratory and numerical models, *Earth and Planetary Science Letters*, *148*, 1-14.

van Keken, P. E., and C. J. Ballentine (1998), Whole-mantle versus layered mantle convection and the role of a high-viscosity lower mantle in terrestrial volatile evolution, *Earth and Planetary Science Letters*, *156*(1-2), 19-32.

van Keken, P. E., and C. J. Ballentine (1999), Dynamical models of mantle volatile evolution and the role of phase transitions and temperature-dependent rheology, *Journal of Geophysical Research-Solid Earth*, *104*(B4), 7137-7151.

van Keken, P. E., et al. (2001), A dynamical investigation of the heat and helium imbalance, *Earth and Planetary Science Letters*, *188*(3-4), 421-434.

van Keken, P. E., et al. (2002), Mantle mixing: the generation, preservation, and destruction of chemical heterogeneity, *Annual Review of Earth and Planetary Sciences*, *30*, 493-525.

van Westrenen, W., et al. (2001), A predictive thermodynamic model of garnet-melt trace element partitioning, *Contributions to Mineralogy and Petrology*, *142*(2), 219-234.

Vandamme, D., and V. Courtillot (1992), Paleomagnetic constraints on the structure of the Deccan Traps, *Physics of the Earth and Planetary Interiors*, *74*(3-4), 241-261.

Venkatesan, T. R., et al. (1993), Did Deccan volcanism pre-date the Cretaceous-Tertiary transition?, *Earth and Planetary Science Letters*, *119*(1-2), 181-189.

Vidal, P., et al. (1991), Changes of mantle sources in the course of a rift evolution - the Afar case, *Geophysical Research Letters*, *18*(10), 1913-1916.

Villiger, S., et al. (2007), Equilibrium and fractional crystallization experiments at 0.7 GPa; the effect of pressure on phase relations and liquid compositions of tholeiitic magmas, *Journal of Petrology*, *48*(1), 159-184.

Volkening, J., et al. (1991), Osmium isotope ratio determinations by negative thermal ionization mass spectrometry, *International Journal of Mass Spectrometry and Ion Processes*, *105*(2), 147-159.

Volker, F., et al. (1993), Submarine basalts from the Red Sea: new Pb, Sr and Nd isotopic data, *Geophysical Research Letters*, *20*(10), 927-930.

Volker, F., et al. (1997), Quaternary volcanic activity of the southern Red Sea: new data and assessment of models on magma sources and Afar plume lithosphere interaction, *Tectonophysics*, *278*(1-4), 15-29.

Walker, R. J., et al. (1988), Comparative Re-Os, Sm-Nd and Rb-Sr isotope and trace element systematics for Archean komatiite flows from Munro Township, Abitibi belt, Ontario, *Earth and Planetary Science Letters*, *87*(1-2), 1-12.

Walker, R. J., et al. (1991), Re-Os isotopic constraints on the origin of volcanic rocks, Gorgona Island, Columbia: Os isotopic evidence for ancient heterogeneities in the mantle, *Contributions to Mineralogy and Petrology*, *107*(2), 150-162.

Walker, R. J., et al. (1995), ^{187}Os enrichment in some plumes: evidence for core-mantle interaction, *Science*, *269*(5225), 819-822.

Walker, R. J., et al. (1997a), Applications of the ^{190}Pt-^{186}Os isotope system to geochemistry and cosmochemistry, *Geochimica et Cosmochimica Acta*, *61*(22), 4799-4807.

Walker, R. J., et al. (1997b), Re-Os systematics of Early Proterozoic ferropicrites, Pechenga Complex, northwestern Russia: Evidence for ancient ^{187}Os-enriched plumes, *Geochimica et Cosmochimica Acta*, *61*(15), 3145-3160.

Walker, R. J., and W. E. Stone (2001), Os isotope constraints on the origin of the 2.7 Ga Boston Creek Flow, Ontario, Canada, *Chemical Geology*, *175*(3-4), 567-579.

Walker, R. J., et al. (2002), Comparative $^{187}Re/^{187}Os$ systematics of chondrites: implications regarding early solar system processes, *Geochimica et Cosmochimica Acta*, *66*(23), PII S0016-7037(0000)01003-01007.

Walker, R. J., et al. (2002), The osmium isotopic composition of convecting upper mantle deduced from ophiolite chromites, *Geochimica et Cosmochimica Acta*, *66*(2), 329-345.

Walker, R. J., et al. (2004), Low abundances of highly siderophile elements in the lunar mantle: evidence for prolonged late accretion, *Earth and Planetary Science Letters*, *224*(3-4), 399-413.

Walker, R. J., et al. (2005), $^{187}Os/^{186}Os$ systematics of Os-Ir-Ru alloy grains from southwestern Oregon, *Earth and Planetary Science Letters*, *230*(1-2), 211-226.

Walter, M. J. (1998), Melting of garnet peridotite and the origin of komatiite and depleted lithosphere, *Journal of Petrology*, *39*(1), 29-60.

Wass, S. Y. (1973), Origin and petrogenetic significance of hour-glass zoning in titaniferous clinopyroxenes, *Mineralogical Magazine*, *39*(302), 133-144.

Watson, J. S. (1996), Fast, simple method of powder pellet preparation for x-ray fluorescence analysis, *X-ray Spectrometry*, *25*, 173–174.

Weaver, B. L. (1991), The origin of ocean isalnd basalt end-member compositions: Trace element and isotopic constraints, *Earth and Planetary Science Letters*, *104*(2-4), 381-397.

Webb, P. J., and J. S. Watson (1996), A user's guide to sample preparation for x-ray fluorescence analysis of geological materials, *Unpublished Guide: Department of Earth Sciences, The Open University*

West, W. D. (1958), The petrography and petrogenesis of forty eight flows of Deccan trap penetrated by borings in Western India, *Transactions of the National Institute of Science, India 4*, 1–56.

Whaler, K. A., and S. Hautot (2006), The electrical resistivity structure of the crust beneath the northern Main Ethiopian Rift, *Afar Volcanic Province within the East African Rift System*, *259*, 293-305.

White, R. S., et al. (1995), The temperature of the Iceland plume and origin of outward-propagating v-shaped ridges, *Journal of the Geological Society*, *152*, 1039-1045.

White, R. S., and D. McKenzie (1995), Mantle plumes and flood basalts, *Journal of Geophysical Research-Solid Earth*, *100*(B9), 17543-17585.

White, W. M. (1995), Geochemical tracers of mantle processes, *Reviews of Geophysics*, *33*, 19-24.

White, R. V., and A. D. Saunders (2005), Volcanism, impact and mass extinctions: incredible or credible coincidences?, *Lithos*, *79*(3-4), 299-316.

Wiart, P., and C. Oppenheimer (2000), Largest known historical eruption in Africa: Dubbi volcano, Eritrea, 1861, *Geology*, *28*(4), 291-294.

Wiart, P. A. M. (2000), Quaternary volcanism of northeast Afar, Cambridge.

Wiart, P. A. M., et al. (2000), Eruptive history of Dubbi volcano, northeast Afar (Eritrea), revealed by optical and SAR image interpretation, *International Journal of Remote Sensing*, *21*(5), 911-936.

Wiart, P., and C. Oppenheimer (2005), Large magnitude silicic volcanism in north Afar: the Nabro Volcanic Range and Ma'alalta volcano, *Bulletin of Volcanology*, *67*(2), 99-115.

Widom, E., et al. (1999), Os Isotope Systematics in the Canary Islands and Madeira: Lithospheric Contamination and Mantle Plume Signatures, *J. Petrology*, *40*(2), 279-296.

Wignall, P. B. (2001), Large igneous provinces and mass extinctions, *Earth-Science Reviews*, *53*(1-2), 1-33.

Wignall, P. (2005), The link between large igneous province eruptions and mass extinctions, *Elements*, *1*(5), 293-297.

Wilkinson, J. F. G., and H. D. Hensel (1988), The petrology of some picrites from Mauna-Loa and Kilauea volcanoes, Hawaii, *Contributions to Mineralogy and Petrology*, *98*(3), 326-345.

Willbold, M., and A. Stracke (2006), Trace element composition of mantle end-members: Implications for recycling of oceanic and upper and lower continental crust, *Geochemistry Geophysics Geosystems*, *7*.

Williams, L. A. J. (1982), Physical aspects of magmatism in continental rifts, in *Continental and oceanic rifts*, edited by G. Palmason, pp. 193-222, American Geophysical Union, Washington, DC.

Wilson, M. (1993), Geochemical signatures of oceanic and continental basalts: a key to mantle dynamics, *Journal of the Geological Society*, *150*, 977-990.

Wilson, M. (2000), *Igneous petrogenesis: a global tectonic appraoch*, Kluwer Academic.

Wolde, B. (1989), Cenozoic volcanism and rift development in Ethiopia, *Journal of African Earth Sciences*, *8*(1), 99-105.

Wolde, B. (1996), Spatial and temporal variations in the compositions of Upper Miocene to Recent basic lavas in the northern main Ethiopian rift: implications for the causes of Cenozoic magmatism in Ethiopia, *Geologische Rundschau*, *85*(2), 380-389.

Woldegabriel, G., et al. (1990), Geology, Geochronology and rift-basin development in the central sector of the Main Ethiopia Rift, *Geological Society of America Bulletin*, *102*(4), 439-458.

Woldegabriel, G., et al. (1991), Age of volcanism and rifting in the Burji-Soyoma area, Amaro Horst, Southern Main Ethiopian Rift: geochronological and biochronological data, *Journal of African Earth Sciences*, *13*(3-4), 437-447.

Woldegabriel, G., et al. (2001), Geology and palaeontology of the Late Miocene Middle Awash valley, Afar rift, Ethiopia, *Nature*, *412*(6843), 175-178.

Woldegabriel, G., et al. (2005), Correlation of Plio-Pleistocene Tephra in Ethiopian and Kenyan rift basins: temporal calibration of geological features and hominid fossil records, *Journal of Volcanology and Geothermal Research*, *147*(1-2), 81-108.

Woldetinsae, G., and H. J. Gotze (2005), Gravity field and isostatic state of Ethiopia and adjacent areas, *Journal of African Earth Sciences*, *41*(1-2), 103-117.

Wolfenden, E. (2003), Evolution of the southern Reds Sea Rift: Birth of a magmatic margin (unpublished PhD thesis), 238 pp, Royal Holloway, London.

Wolfenden, E., et al. (2004), Evolution of the northern Main Ethiopian rift: birth of a triple junction, *Earth and Planetary Science Letters*, *224*(1-2), 213-228.

Wolfenden, E., et al. (2005), Evolution of a volcanic rifted margin: Southern Red Sea, Ethiopia, *Geological Society of America Bulletin*, *117*(7-8), 846-864.

Wood, B. J., and J. D. Blundy (1997), A predictive model for rare earth element partitioning between clinopyroxene and anhydrous silicate melt, *Contributions to Mineralogy and Petrology*, *129*(2-3), 166-181.

Wooden, J. L., et al. (1993), Isotopic and trace-element constraints on mantle and crustal contributions to Siberian continental flood basalts, Norilsk area, Siberia, *Geochimica Et Cosmochimica Acta*, *57*(15), 3677-3704.

Wyllie, P. J. (1981), Plate tectonics and magma genesis, *Geol. Rundsch.*, *70*, 128-153.

Xia, Q. X., et al. (2004), The trace element and Re-Os isotopic geochemistry of mantle-derived peridotite xenoliths from Hannuoba: nature and age of SCLM beneath the area, *Acta Petrologica Sinica*, *20*(5), 1215-1224.

Xiao, L., et al. (2004), Distinct mantle sources of low-Ti and high-Ti basalts from the western Emeishan large igneous province, SW China: implications for plume-lithosphere interaction, *Earth and Planetary Science Letters*, *228*(3-4), 525-546.

Xu, Y. G., et al. (2001), Petrologic and geochemical constraints on the petrogenesis of Permian-Triassic Emeishan flood basalts in southwestern China, *Lithos*, *58*(3-4), 145-168.

Xu, J. F., et al. (2007), Os, Pb, and Nd isotope geochemistry of the Permian Emeishan continental flood basalts: insights into the source of a large igneous province, *Geochimica et Cosmochimica Acta*, *71*(8), 2104-2119.

Xu, Y. G., et al. (2007), Identification of mantle plumes in the Emeishan Large Igneous Province, *Episodes*, *30*(1), 32-42.

Yang, H. J., et al. (1996), Evolution of Mauna Kea volcano: inferences from lava compositions recovered in the Hawaii Scientific Drilling Project, *Journal of Geophysical Research-Solid Earth*, *101*(B5), 11747-11767.

Yang, H. J., et al. (1996), Experiments and models of anhydrous, basaltic olivine-plagioclase-augite saturated melts from 0.001 to 10 kbar, *Contributions to Mineralogy and Petrology*, *124*(1), 1-18.

Yaxley, G. M. (2000), Experimental study of the phase and melting relations of homogeneous basalt plus peridotite mixtures and implications for the petrogenesis of flood basalts, *Contributions to Mineralogy and Petrology*, *139*(3), 326-338.

Yirgu, G., et al. (2004), The Afar volcanic province within the East African Rift System: introduction, paper presented at East African Rift Systems: Geodynamics, Resources and Environment, Addis Ababa, Jun.

Yirgu, G., et al. (2006), The Afar volcanic province within the East African Rift System: introduction, *Afar Volcanic Province within the East African Rift System*, *259*, 1-6.

Yuen, D. A., et al. (1995), Non-equilibrium effects of core-cooling and time-dependent internal heating on mantle flush events, *Nonlinear Processes in Geophysics*, *2*, 206-221.

Zanettin, B., and Justin-Visentin (1974), The volcanic succession in Central Ethiopia, the volcanism of western Afar and Ethiopian Rift margin, *Memorie del Instituto di Geologia e Mineraloga dell Universita di Padova 31*, 1-19.

Zanettin, B., and E. Justin-Visentin (1975), Tectonical and volcanological evolution of the Western Afar Margin, Ethiopia, in *Afar Depression of Ethiopia*, edited by A. Pilger and A. Rosler, pp. 300–309, Schweizerbart, Stuttgart.

Zanettin, B., et al. (1978a), The evolution of the Chencha escarpment and the Ganjuli graben (Lake Abaya) in the Southern Ethiopian Rift, *Neues Jahrbuch für Geologie und Palaontologie*, *8*, 473-490.

Zanettin, B., et al. (1978b), Volcanic succession, tectonics and magmatology in central Ethiopia, in *Atti e Memorie dell' Accademia Patavina di Scienze Lettere (1977-78)*, edited by V. Arti, pp. 1–19.

Zanettin, B., et al. (1980a), Migration of the Ethiopian Continental Rifts in the course of the Tertiary Evolution of the Afro-Arabian Rift System, paper presented at Geodynamic Evolution of the Afro-Arabian Rift System, Accademia Nazionale dei Lincei, Rome.

Zanettin, B., et al. (1980b), Correlations among Ethiopian volcanic formations with special references to the chronological and stratigraphic problems of the 'Trap Series', paper presented at Geodynamic Evolution of the Afro-Arabian Rift System, Accademia Nazionale dei Lincei.

Zanettin, B., et al. (2006), New radiometric age of volcanic rocks in the central Eritrean plateau (from Asmara to Adi Quala): considerations on stratigraphy and correlations, *Journal of African Earth Sciences*, *45*(2), 156-161.

Zanettin, B., et al. (2006), Stratigraphy and evolution of the trachy-rhyolitic volcanism of the Senafe area (Eastern Eritrean Plateau), *Journal of African Earth Sciences*, *45*(4-5), 478-488.

Zhang, S. X., and D. A. Yuen (1995), The influences of lower mantle viscosity stratification on 3D spherical-shell mantle convection, *Earth and Planetary Science Letters*, *132*(1-4), 157-166.

Zhang, Z. C., and F. S. Wang (2002), Geochemistry of two types of basalts in the Emeishan basaltic province: evidence for mantle plume-lithosphere interaction, *Acta Geologica Sinica-English Edition*, *76*(2), 229-237.

Zhang, Z. C., et al. (2008), Re-Os isotopic compositions of picrites from the Emeishan flood basalt province, China, *Earth and Planetary Science Letters*, *276*(1-2), 30-39.

Zhao, D. (2001), Seismic structure and origin of hotspots and mantle plumes, *Earth and Planetary Science Letters*, *192*(3), 251-265.

Zhao, D. P. (2004), Global tomographic images of mantle plumes and subducting slabs: insight into deep Earth dynamics, *Physics of the Earth and Planetary Interiors*, *146*(1-2), 3-34.

Zindler, A., and S. Hart (1986), Chemical geodynamics, *Annual Review of Earth and Planetary Sciences*, *14*, 493-571.

Zumbo, V., et al. (1995a), $^{40}Ar/^{39}Ar$ chronology of Tertiary magmatic activity in southern Yemen during the early Red Sea-Aden rifting, *Journal of Volcanology and Geothermal Research*, *65*(3-4), 265-279.

Zumbo, V., et al. (1995b), First $^{40}Ar/^{39}Ar$ dating on early Pliocene to Plio-pleistocene magmatic events of the Afar, Republic of Djibouti, *Journal of Volcanology and Geothermal Research*, *65*(3-4), 281-295.